

$$\langle \psi | \psi \rangle = 1, \quad \langle 0 | 0 \rangle = 1, \quad \langle \psi | 0 \rangle = \langle 0 | \psi \rangle = 0$$

$$V(-) = \sum_{\mathbf{k}} V_{\mathbf{k}} \exp(-i\omega_{\mathbf{k}} t) \quad Q = \{Q_{\mathbf{k}}\}_{\mathbf{k}} = \{ \langle \delta | \psi(-) \rangle \}$$

$$T = \sum_{\mathbf{k}} T_{\mathbf{k}} \quad \langle \mathbf{k} | H F \rangle = 0 \quad \langle \mathbf{k} | H F \rangle = |\mathbf{k}\rangle \quad T = T_1 + T_2 + T_3 + \dots$$

$$\langle \mathbf{k} | H F \rangle = \langle \mathbf{k} | H F \rangle \quad \langle \mathbf{k} | H F \rangle = \langle \mathbf{k} | H F \rangle$$

$$Q(\mathbf{k}) = \int_0^{\infty} \langle H F | U(t) | CC(t) \rangle dt$$

$$A_{\mathbf{k}} = \langle \mathbf{k} | [H_0, T_{\mathbf{k}}] | CC(t) \rangle$$

$$E^{\mathbf{k}} = \langle \mathbf{k} | [H_0, T_{\mathbf{k}}] | CC(t) \rangle$$

$$L_{\mathbf{k}} = \langle \mathbf{k} | [H_0, T_{\mathbf{k}}] | CC(t) \rangle$$

$$E^{\mathbf{k}} = \langle \mathbf{k} | [H_0, T_{\mathbf{k}}] | CC(t) \rangle$$

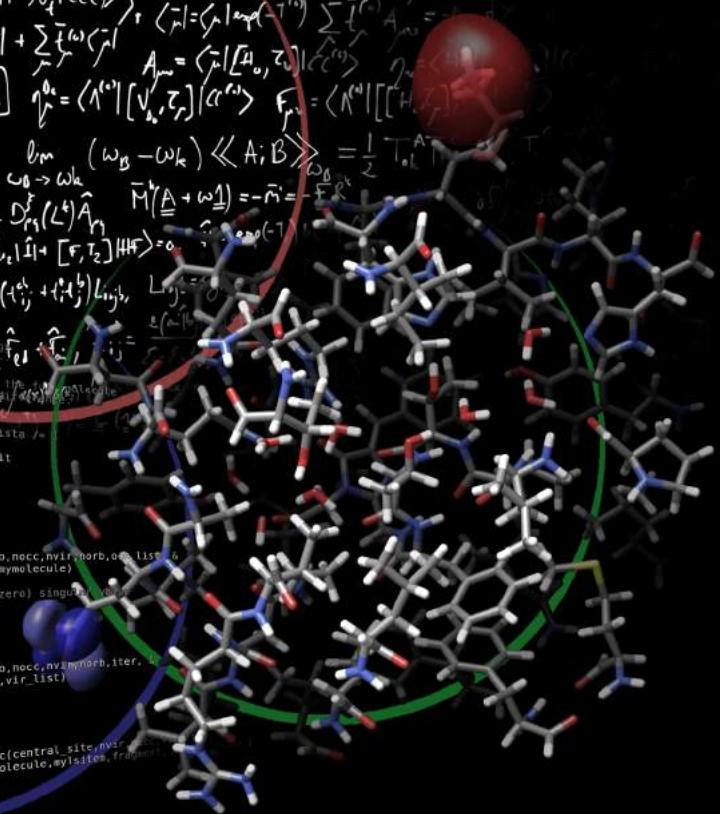
```

! The XOS converged or stopped by including the excitation
! by investigating the excitation
lofec = lofec_data%iexc
lofec_data%conv(iexc) = .false.
ista = lofec_data%iter ! in case of restart ista /=
oldx = 0.0 real8
xos_opt_loop: do iter=ista,DECInfo%lofec%maxit

! Get new XOS and initialize fragment
!-----
lofec_data%iter = iter
select case(DECInfo%lofec%istat)
case(5)
  call lofec_set_orbital_space2(nato,nfco,nocc,nvir,norb,occ_list,
    & vir_list,OccOrbitals,virOrbitals,mymolecule)
case(6)
  ! include all NTOs with positive (non-zero) singular values
  occ_list(1:nfco:nocc) = .true.
  vir_list(1:nocc) = .true.
  ! or quit
  if (iter=3) exit xos_opt_loop
case default
  call lofec_set_orbital_space1(nato,nfco,nocc,nvir,norb,iter,
    & track_ntos,priority_list,occ_list,vir_list)
end select

! initialize fragment
!-----
! atomic_fragment_init orbital_specific(central_site,nvir,
  occ_list,OccOrbitals,virOrbitals,mymolecule,mysites,fragment)

```



COUPLED CLUSTER THEORY FOR LARGE MOLECULES

Pablo Baudin

PhD Thesis

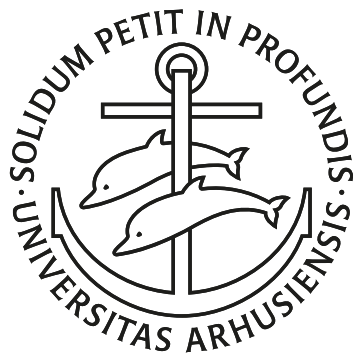
Coupled Cluster Theory for Large Molecules

PABLO BAUDIN

*qLEAP Center for Theoretical Chemistry,
Department of Chemistry,
Aarhus University,
Denmark*

March 1, 2017





CONTENTS

| | |
|--|------------|
| Contents | iii |
| Preface | vii |
| List of papers | x |
| List of abbreviations | xii |
| 1 Introduction | 1 |
| 2 Electronic-structure theory | 5 |
| 2.1 The electronic Schrödinger equation | 6 |
| 2.2 Hartree–Fock theory | 8 |
| 2.3 Coupled cluster theory | 10 |
| 2.3.1 The coupled cluster singles and doubles model: CCSD | 12 |
| 2.4 Coupled cluster perturbation theory | 15 |
| 2.4.1 The second-order Møller–Plesset model: MP2 | 16 |
| 2.4.2 The second-order approximate coupled cluster singles and doubles model: CC2 | 18 |
| 2.4.3 The coupled cluster singles and doubles with perturbative triples model: CCSD(T) | 19 |
| 2.5 Electronic transitions | 20 |
| 2.5.1 Response theory for exact states | 22 |
| 2.5.2 Excitation energies and oscillator strengths for CC models | 27 |
| 3 Local CC methods for ground states | 31 |
| 3.1 Introduction | 32 |
| 3.2 The Divide–Expand–Consolidate scheme | 33 |
| 3.2.1 Energy partitioning | 34 |
| 3.2.2 Atomic fragment optimization | 36 |

| | | |
|----------|---|-----------|
| 3.2.3 | Pair fragment screening | 38 |
| 3.2.4 | Parallelism strategy | 41 |
| 3.3 | Selected review of the state-of-the-art | 43 |
| 3.3.1 | Direct local CC methods | 44 |
| 3.3.2 | Cluster-in-molecule | 47 |
| 3.3.3 | The incremental scheme | 49 |
| 3.4 | Conclusion | 50 |
| 4 | Local CC methods for electronic transitions | 53 |
| 4.1 | Introduction | 54 |
| 4.2 | A local framework for calculating excitation energies | 54 |
| 4.2.1 | Mixed orbital space | 55 |
| 4.2.2 | XOS optimization | 56 |
| 4.2.3 | Numerical illustrations | 58 |
| 4.2.4 | Generalized NTOs | 59 |
| 4.2.5 | Treatment of multiple states | 62 |
| 4.3 | Selected review of the state-of-the-art | 63 |
| 4.3.1 | Direct local CC methods | 63 |
| 4.3.2 | The incremental scheme | 65 |
| 4.3.3 | Multilevel CC theory | 66 |
| 4.4 | Conclusion and perspective | 67 |
| 5 | Summary | 69 |
| 5.1 | English | 70 |
| 5.2 | Dansk | 71 |
| | References | 74 |
| A | CCS and CC2 working equations | 81 |
| A.1 | Overview | 82 |
| A.1.1 | The CC2 effective Jacobian | 83 |
| A.2 | Right-hand-side for the ground state Lagrangian multipliers | 85 |
| A.3 | Right linear transformation | 86 |
| A.3.1 | Part A | 87 |
| A.3.2 | Part B | 89 |
| A.3.3 | Summary | 92 |
| A.4 | Left linear transformation | 93 |
| A.5 | Right-hand-side of the transition Lagrangian multipliers | 94 |
| A.5.1 | Part A | 94 |
| A.5.2 | Part B | 95 |
| A.5.3 | Part C | 96 |

| | | |
|----------|--|------------|
| A.5.4 | Part D | 97 |
| A.5.5 | Part E | 98 |
| A.5.6 | Summary | 99 |
| A.6 | Transition strengths | 100 |
| A.6.1 | Introducing the ξ one-particle CC2 density matrix | 100 |
| A.6.2 | Introducing the η one-particle CC2 density matrix | 102 |
| A.6.3 | Summary | 105 |
| A.7 | CCS equations for transition strengths | 105 |
| A.7.1 | Ground state equations | 106 |
| A.7.2 | CCS Jacobian | 106 |
| A.7.3 | The CCS ground state multipliers | 106 |
| A.7.4 | The CCS transition moment multipliers | 107 |
| A.7.5 | The CCS transition moments | 107 |
| A.8 | Expressions for Fock matrices | 108 |
| A.9 | Commutator relations | 110 |
| A.9.1 | Relation 1 | 110 |
| A.9.2 | Relation 2 | 110 |
| A.9.3 | Relation 3 | 110 |
| A.9.4 | Relation 4 | 111 |
| B | Scientific papers | 113 |
| B.1 | The Divide–Expand–Consolidate coupled cluster scheme | 115 |
| B.2 | Orbital spaces in the Divide–Expand–Consolidate coupled cluster method | 129 |
| B.3 | Efficient linear-scaling second-order Møller–Plesset perturbation theory: The Divide–Expand–Consolidate RI-MP2 model | 147 |
| B.4 | Linear-scaling coupled cluster with perturbative triple excitations: The Divide–Expand–Consolidate CCSD(T) model | 159 |
| B.5 | Massively parallel and linear-scaling algorithm for second-order Møller– Plesset perturbation theory applied to the study of supramolecular wires | 171 |
| B.6 | LoFEx — A local framework for calculating excitation energies: Illus- trations using RI-CC2 linear response theory | 181 |
| B.7 | A local framework for calculating coupled cluster singles and doubles excitation energies (LoFEx-CCSD) | 193 |
| B.8 | CC2 oscillator strengths within the local framework for calculating ex- citation energies (LoFEx) | 205 |
| B.9 | Simplified Natural transition Orbital Framework for Large-scale coupled- cluster Excitation energy calculations (SNOFLEX) | 219 |

PREFACE

The present dissertation describes my work as a PhD student at the qLEAP center for theoretical chemistry, located in the department of chemistry of Aarhus university, Denmark. I joined the qLEAP center first as a research assistant in September 2013 and started my PhD under the supervision of Poul Jørgensen and Kasper Kristensen in February 2014.

The way I tried to write this thesis is to make it possible for people with different backgrounds to get insights about my work as a PhD student. The introduction should be general enough for a non-scientific reader to get an idea of what quantum chemistry and electronic-structure theory are about and a very broad introduction to the goal of my research. Chapter 2 has been designed to introduce some of the most important concepts in electronic-structure theory which correspond to the starting point of my work. This chapter and the following have been written for interested readers with a strong mathematical background and some knowledge of quantum mechanics. Chapters 3 and 4 present the theoretical methods developed (in part) during my PhD with emphasis on the fundamental ideas rather than the technical details. Some of the most important results are also presented in those chapters. All in all, this thesis should provide a strong introduction to my work as a PhD student and hopefully enable the reader to understand the scientific papers listed below and collected as appendices.

Miscellaneous

Atomic units (a.u.) are used throughout this thesis unless stated otherwise. A brief comparison of the atomic unit system and the international system (S.I.) is given in table 1 for the units relevant to this thesis.

The theory developments presented in parts of chapters 3 and 4 and in the scientific articles gathered in appendix B have been implemented in the LSDALTON program.^{1,2}

All molecular and orbital graphical representations have been generated using the

Table 1: The atomic unit (a.u.) system compared to the international system (S.I.). Abbreviations: kilogram (kg), Coulomb (C), second (s), Joule (J), meter (m).

| Symbol | Quantity | Value in a.u. | Value in S.I. units |
|---------|------------------------------------|---------------|-----------------------------|
| m_e | Electron mass | 1 | 9.110×10^{-31} kg |
| e | Elementary charge | 1 | 1.602×10^{-19} C |
| t | Time | 1 | 2.419×10^{-17} s |
| \hbar | Planck's constant, ($2\pi\hbar$) | 2π | 6.626×10^{-34} J·s |
| a_0 | Bohr radius (length) | 1 | 5.292×10^{-11} m |
| E_H | Hartree (energy) | 1 | 4.360×10^{-18} J |

USCF Chimera package.³ Chimera is developed by the Resource for Biocomputing, Visualization, and Informatics at the University of California, San Francisco (supported by NIGMS P41-GM103311).

Funding

The research leading to these results has received funding from the European Research Council under the European Unions Seventh Framework Programme (FP/2007-2013)/ERC Grant Agreement no. 291371

This research used resources of the Oak Ridge Leadership Computing Facility at Oak Ridge National Laboratory, which is supported by the Office of Science of the Department of Energy under Contract DE-AC05-00OR22725.

Acknowledgments

The completion of this work would not have been possible without the help and support of many people. I would like to thank my main supervisor Poul Jørgensen who let me join his team and taught me so many things. His passion and his dedication to science are very inspiring. Poul is always available to help one understand something and to explain things as many times as necessary. I am very proud to be one of the many students he supervised. Many thanks to Kasper Kristensen who took the role of a co-supervisor and helped me in every step of the way. His attention to details and his skeptical mind were often the key to identify and solve scientific issues. I really appreciated our strong and daily collaboration. I would also like to thank Lene Conley, who was of precious help, in particular when I first came to Aarhus and had to deal with a lot of paper work. Thanks a lot to Kasper Kristensen, Filip Pawłowski, Thomas Kjærgaard, and Ian Godtliebsen, for proofreading this thesis and to Prof. Andreas Köhn, Prof. Stephan P. A. Sauer and Prof. Ove Christiansen for accepting

to evaluate the quality of my work.

One of the many wonderful sides of being part of the theoretical group at Aarhus university is that one can always knock on the next door and ask for help. I would thus like to thank the whole theoretical group with special thanks to Thomas Kjærgaard, Patrick Ettenhuber, Filip Pawłowski, Janus J. Eriksen and Ian Godtliebsen for their help and advice. Thanks also to Ove Christiansen, Jeppe Olsen, Frank Jensen and Thomas B. Pedersen for their teaching and for very interesting discussions. The social environment is also exceptional in the group; many thanks to Kasper, Dima, Ian, Patrick, Thomas (Integralo), Yang, Janus, Carolin, Sergio, Dalibor (Daliburb), Simon (2.0), Filip, American Patrick, Sven, Bo, Ida, Mads, Niels, Andreas, Emil, Diana, Gunnar, Tilmann, and to the biomodelling group for some memorable parties.

Along the years, my passion for science was initiated and inspired by many people who are therefore part of the journey that led to this work. Thanks to my brother Maël and my uncle Benoît who probably triggered the process. Thanks also to some very inspiring lecturers and supervisors, M. Chrysos, T. Cauchy, M. E. Casida, and A. M. J. Sánchez de Merás.

Enfin, j'aimerais remercier mes parents pour m'avoir constamment supporté et encouragé et le reste de ma famille ainsi que mes amis pour tout les bons moments partagés ensemble. J'ai une pensée particulière pour mes grands-parents, Christiane, Marie-Paule et Michel qui ont toujours pris grand soin de moi.

Pablo Baudin
Aarhus, March 1, 2017

A handwritten signature in black ink, reading "Baudin" with a stylized flourish underneath.

List of papers

The following scientific articles have been written during my PhD studies and are attached as appendices to this thesis together with a short description of my own contributions to each paper.

Articles related to chapter 3:

Appendix B.1 — Ref. 4

The Divide–Expand–Consolidate coupled cluster scheme

T. Kjærgaard, P. Baudin, D. Bykov, K. Kristensen, and P. Jørgensen.

Manuscript submitted to *WIREs Comput. Mol. Sci.* (2017).

Appendix B.2 — Ref. 5

Orbital spaces in the Divide–Expand–Consolidate coupled cluster method

P. Etenhuber, P. Baudin, T. Kjærgaard, P. Jørgensen, K. Kristensen.

J. Chem. Phys. **144**, 164116 (2016).

Appendix B.3 — Ref. 6

Efficient linear-scaling second-order Møller–Plesset perturbation theory: The Divide–Expand–Consolidate RI-MP2 model

P. Baudin, P. Etenhuber, S. Reine, K. Kristensen, T. Kjærgaard.

J. Chem. Phys. **144**, 054102 (2016).

Appendix B.4 — Ref. 7

Linear-scaling coupled cluster with perturbative triple excitations: The Divide–Expand–Consolidate CCSD(T) model

J. J. Eriksen, P. Baudin, P. Etenhuber, K. Kristensen, T. Kjærgaard, P. Jørgensen.

J. Chem. Theory Comput. **11**, 2984 (2015).

Appendix B.5 — Ref. 8

Massively parallel and linear-scaling algorithm for second-order Møller–Plesset perturbation theory applied to the study of supramolecular wires

T. Kjærgaard, P. Baudin, D. Bykov, J. J. Eriksen, P. Etenhuber, K. Kristensen, J. Larkin, D. Liakh, F. Pawłowski, A. Vose, Y. M. Wang, and P. Jørgensen.

Comput. Phys. Commun. **212**, 152 (2017).

Articles related to chapter 4:

Appendix B.6 — Ref. 9

LoFEx — A local framework for calculating excitation energies: Illustrations using RI-CC2 linear response theory

P. Baudin, K. Kristensen.

J. Chem. Phys. **144**, 224106 (2016).

Appendix B.7 — Ref. 10

A local framework for calculating coupled cluster singles and doubles excitation energies (LoFEx-CCSD)

P. Baudin, D. Bykov, D. Liakh, P. Ettehuber, and K. Kristensen.

Mol. Phys. **MQM2016**, 1 (2017).

Appendix B.8 — Ref. 11

CC2 oscillator strengths within the local framework for calculating excitation energies (LoFEx)

P. Baudin, T. Kjærgaard, and K. Kristensen.

Manuscript submitted to *J. Chem. Phys.* 1 (2017).

Appendix B.9 — Ref. 12

Simplified Natural transition Orbital Framework for Large-scale coupled-cluster Excitation energy calculations (SNOFLEx)

P. Baudin, and K. Kristensen.

Manuscript in preparation, (2017).

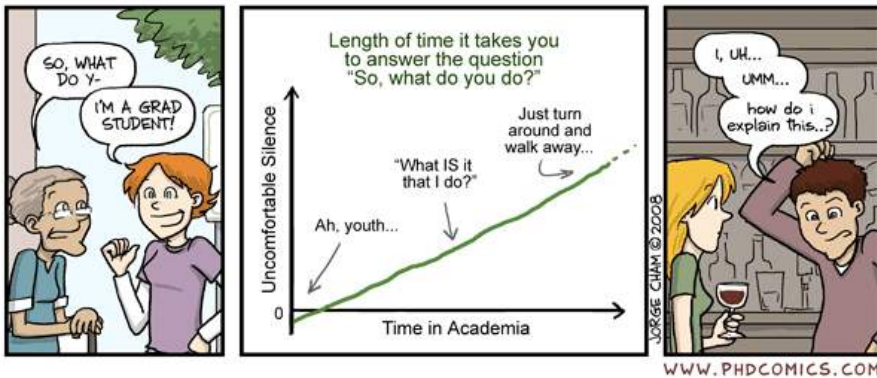
List of abbreviations

| | |
|--------------|---|
| a.u. | atomic units |
| Å | Ångström (length unit) |
| ADC(2) | algebraic diagrammatic construction to second-order (model) |
| AO | atomic orbital |
| AOS | amplitude orbital space (DEC) |
| aug-cc-pVDZ' | augmented cc-pVDZ basis without diffuse functions on hydrogen atoms (basis set) |
| B3LYP | Becke 3-parameter, Lee–Yang–Parr (DFT functional) |
| BCH | Baker–Campbell–Hausdorff (expansion) |
| BO | Born–Oppenheimer (approximation) |
| BP | Boughton–Pulay (criterion) |
| CAMB3LYP | Coulomb-attenuating method B3LYP (DFT functional) |
| CC | coupled cluster (theory) |
| cc-pVDZ | correlation-consistent polarized valence double- ζ (basis set) |
| CC2 | second-order approximate CCSD (model) |
| CC3 | iterative approximate CCSDT (model) |
| CCPT | CC perturbation theory |
| CCS | CC singles (model) |
| CCSD | CC singles and doubles (model) |
| CCSD(T) | CCSD with perturbative triples (model) |
| CCSDR(3) | perturbative triples corrections to CCSD excitation energies (model) |
| CCSDT | CCSD with triples (model) |
| CIM | cluster-in-molecule (approach) |
| CIS | configuration-interaction singles (model) |
| CIS(D') | approximate CIS(D) (model) |
| CIS(D) | doubles correction to CIS excitation energies (model) |
| CISD | CIS with doubles (model) |
| CMO | canonical MO |
| CPP | complex polarization propagator (approach) |
| DEC | divide–expand–consolidate (approach) |
| DF | density-fitting (approximation) |
| DFT | density-functional-theory |

| | |
|-------------|--|
| ECC2 | extended CC2 (model) |
| EOM-CC | equation-of-motion CC (approach) |
| EOM-MBPT(2) | equation-of-motion many-body perturbation theory to second-order (model) |
| EOS | energy orbital space (DEC) |
| eV | electron volt (energy unit) |
| FCI | full configuration-interaction (model) |
| FM | fourth central moments (of orbitals) |
| FOT | fragment optimization threshold (DEC) |
| HF | Hartree–Fock (model) |
| LMO | local MO |
| LoFEx | local framework for calculating excitation energies |
| MLCC | multilevel CC (approach) |
| MLCC3 | multilevel CC3 (model) |
| MO | molecular orbital |
| MP n | n -order Møller–Plesset theory (model) |
| NTO | natural transition orbital |
| ON | occupation number (vector) |
| ONIOM | our own n-layered integrated molecular orbital and molecular mechanics (approach) |
| OSV | orbital-specific virtual |
| OSV-DIP | OSV dipole-dipole (pair-energy) |
| PAO | projected AO |
| PNO | pair natural orbital |
| RI | resolution-of-the-identity (approximation) |
| SM | second central moments (of orbitals) |
| SNOFLE x | simplified natural transition orbital framework for large-scale coupled-cluster excitation energy calculations |
| SOPPA | second-order polarization propagator approximation (model) |
| SVD | singular-value-decomposition (matrix) |
| TDDFT | time-dependent DFT (approach) |
| TDHF | time-dependent HF (model) |
| UV | ultra-violet (light) |
| XOS | excitation orbital space (LoFEx and SNOFLE x) |

CHAPTER
ONE

INTRODUCTION



Most of the matter around us (except for dark matter and dark energy) is made of atoms, including ourselves, all the living beings, the air, the earth, but also the other planets and the stars like the sun. An atom is roughly 100 000 times smaller than a human cell which is already 100 000 times smaller than the human body. Atoms are made of even smaller particles called electrons, protons and neutrons. The protons and neutrons form the atomic nucleus which is positively charged and interact with the electrons (negatively charged) through the electromagnetic force (see figure 1.1). The electromagnetic force is also responsible for the interactions between the atoms which can be arranged in infinitely many combinations to form the molecules and *in fine*, the macroscopic objects that surround us. Even though we are made of atoms, the laws of physics that we are used to (classical mechanics), do not seem to apply at the atomic scale (10^{-10} m) which instead is governed by quantum mechanics.

One of the fundamental equations of quantum mechanics is the (time-dependent) Schrödinger equation,

$$H\Phi = i\partial_t\Phi, \quad (1.1)$$

which can be used to describe the behavior of objects like atoms and molecules. The two important quantities in eq. (1.1) are the Hamiltonian H and the wave-function Φ . The Hamiltonian is a mathematical operator associated with the energy of the system considered. It is used to describe both the energy resulting from the motion of the particles (the kinetic energy) and the interactions between those particles (the potential energy). The wave-function, on the other hand, is a mathematical object that can be used to represent the distribution of the particles in the system. Unfortunately, it is impossible to solve eq. (1.1) exactly for atoms and molecules of practical interest. A whole part of theoretical or quantum chemistry is therefore concerned with the design of tools in the form of mathematical models and computer programs that provide approximate solutions to eq. (1.1) and help chemists in their everyday tasks by substituting some of the chemical or physical experiments with *in silico* experiments, *i.e.*, computer simulations or calculations.

In many cases the systems to be described by the Schrödinger equation are “stable” in time and their wave-function can be factorized (*i.e.*, separated) into a time-dependent and a time-independent part. This form of the wave-function leads to the time-independent Schrödinger equation,

$$H\Psi = E\Psi, \quad (1.2)$$

where E is the energy of the system in the stationary state described by the time-independent wave-function Ψ and subject to the physical interactions contained in the Hamiltonian H . In the case of molecular systems, and when relativistic effects and external perturbations are ignored, the Hamiltonian can be decomposed into the following contributions, (see also figure 1.1).

- The kinetic operator for all nuclei, T_N ,

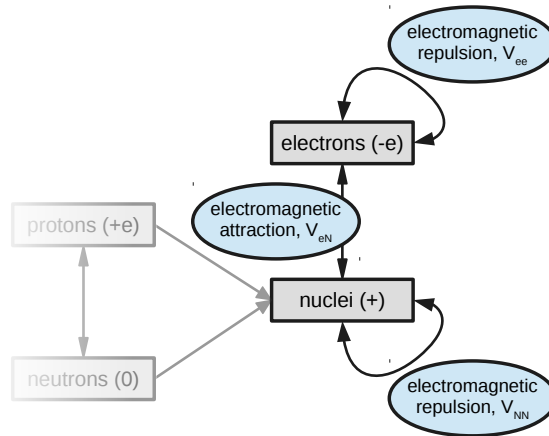


Figure 1.1: Schematic representation of the particles and the interactions present in atoms and molecules. The double-headed arrows represent interactions and the charges of the particles are given in parentheses.

- the kinetic operator for all electrons, T_e ,
- the electrostatic potential attraction between electrons and nuclei, V_{eN} ,
- the electrostatic potential repulsion between electrons, V_{ee} ,
- and, the electrostatic potential repulsion between nuclei, V_{NN} .

Note that we do not consider the interaction between protons and neutrons inside the nuclei. Instead, we take the nuclei to be point charges of masses and charges corresponding to the number of protons and neutrons they contain.

Even though it is now time-independent, eq. (1.2) is still too complicated to be applied to molecules containing several atoms since the motion of a given particle (electron or nucleus) is affected by the instantaneous position of all the others. To reduce the complexity of eq. (1.2), we introduce one of the most important approximation in chemistry, the Born–Oppenheimer (BO) approximation, which consists in decoupling the motion of electrons and nuclei based on the difference between their masses. Since the nuclei are much heavier than the electrons, it can usually be assumed that the electrons will adapt almost instantaneously to the displacement of the nuclei and their respective motion can thus be decoupled. The wave-function is then written as a product of a nuclear and an electronic part, $\Psi = \Psi_N \Psi_e$, and the impact of the nuclear motion on the electronic wave-function is neglected. This leads to two new Schrödinger equations, one for the nuclei and one for the electrons. In this thesis we will focus on the electronic Schrödinger equation,

$$H_e \Psi_e = E_e \Psi_e, \quad (1.3)$$

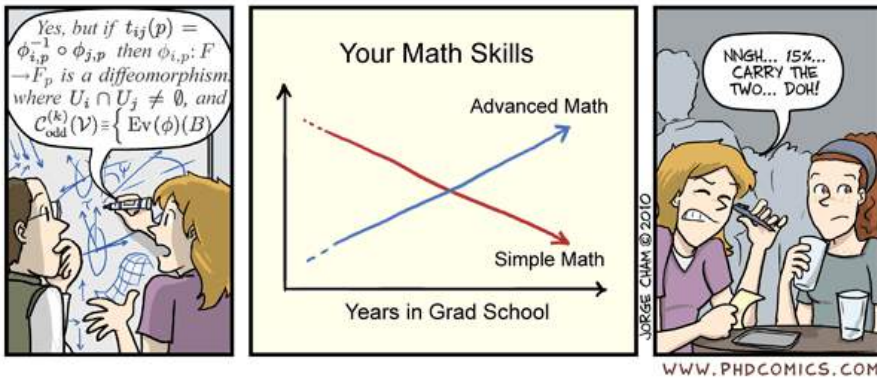
$$H_e = T_e + V_{eN} + V_{ee} + V_{NN} \quad (1.4)$$

where the position of the nuclei are fixed at a given molecular geometry due to the BO approximation and therefore the inter-nuclear interaction V_{NN} is just an additive constant.

It is evident that the complexity of eq. (1.3) increases with the number of electrons since it results in more and more interactions to consider at the same time. In the past hundred years, (since the beginning of quantum mechanics), physicists and chemists have designed a wide range of models to solve the electronic Schrödinger equation in which the complexity of the solutions (the computational complexity) is usually correlated with the quality or the accuracy of those solutions. For that reason, very accurate solutions to the electronic Schrödinger equations have only been obtained for rather small molecules.

As a PhD student, my goal was to contribute to the design of new accurate models that solve the electronic Schrödinger equation for systems as large as proteins, *i.e.*, from a few hundreds to a few thousands atoms. In the following chapter, some of the fundamental concepts of molecular electronic-structure theory which are relevant to this work are summarized, while an overview of the methods developed (partly) during my PhD is given in chapters 3 and 4.

ELECTRONIC-STRUCTURE THEORY



The content of this chapter is based on Ref. 13, except for section 2.5 for which adequate references are given therein.

2.1 The electronic Schrödinger equation

In this thesis we consider solutions to the time-independent electronic Schrödinger equation. Using Dirac's bra-ket notation we have,

$$H |\Psi\rangle = E |\Psi\rangle, \quad (2.1)$$

where we have omitted the e subscripts for clarity [compared to eq. (1.3)], *i.e.*, E is the electronic energy, Ψ is the electronic wave-function and H is the non-relativistic molecular electronic Hamiltonian under the BO approximation. In the second-quantization formalism the spin-free molecular Hamiltonian is given by,

$$H = \sum_{pq} h_{pq} E_{pq} + \frac{1}{2} \sum_{pqrs} g_{pqrs} e_{pqrs} + h_{\text{nuc}}, \quad (2.2)$$

where

$$E_{pq} = a_{p\alpha}^\dagger a_{q\alpha} + a_{p\beta}^\dagger a_{q\beta} \quad (2.3)$$

is a singlet excitation operator. $a_{q\sigma}$ annihilates an electron of spin σ from a spatial molecular orbital (MO) ϕ_q , while $a_{p\sigma}^\dagger$ creates an electron of spin σ in MO ϕ_p (in this thesis only real MOs are considered). Those elementary operators are called creation and annihilation operators and they follow the anti-commutation relations required to satisfy Pauli's exclusion principle (*i.e.*, the change of sign of the wave-function under exchange of two electrons). The two-electron singlet excitation operator can then be written as,

$$e_{pqrs} = E_{pq} E_{rs} - \delta_{qr} E_{ps}, \quad (2.4)$$

where δ_{qr} is the Kronecker function. The one- and two-electron integrals used in the definition of the Hamiltonian in eq. (2.2) are given by,

$$h_{pq} = \int \phi_p(\mathbf{r}) \left(-\frac{1}{2} \nabla^2 - \sum_I \frac{Z_I}{r_I} \right) \phi_q(\mathbf{r}) d\mathbf{r}, \quad (2.5a)$$

$$g_{pqrs} = \iint \phi_p(\mathbf{r}_1) \phi_q(\mathbf{r}_1) \frac{1}{r_{12}} \phi_r(\mathbf{r}_2) \phi_s(\mathbf{r}_2) d\mathbf{r}_1 d\mathbf{r}_2, \quad (2.5b)$$

$$h_{\text{nuc}} = \frac{1}{2} \sum_I \sum_{J \neq I} \frac{Z_I Z_J}{R_{IJ}}, \quad (2.5c)$$

where Z_I , r_I , and R_{IJ} denote the nuclear charge, the electron-nuclear distance and the inter-nuclear distance, respectively, while r_{12} corresponds to the inter-electron distance. By comparison with eq. (1.4), we note that, T_e and V_{eN} are included in h_{pq} , V_{ee} corresponds to g_{pqrs} , while V_{NN} is equivalent to h_{nuc} .

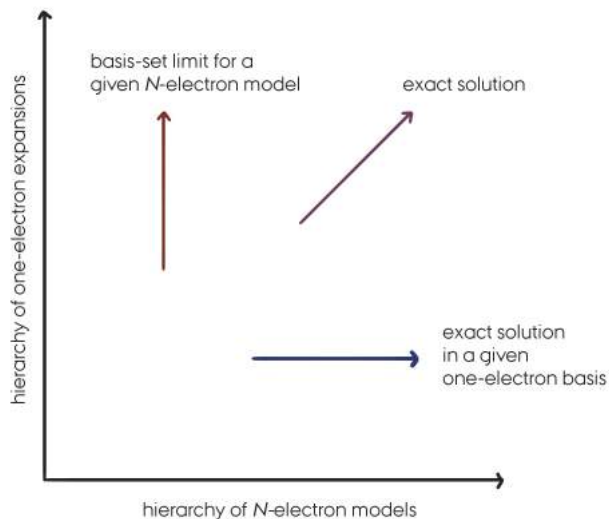


Figure 2.1: The systematic approach to the exact solution of the Schrödinger equation by successive improvements in the one- and N -electron spaces. (Replicated from Figure 5.1 in Ref. 13).

The spatial MOs are usually expressed as a linear combination of basis functions χ_μ ,

$$\phi_p(\mathbf{r}) = \sum_{\mu} C_{\mu p} \chi_{\mu}, \quad (2.6)$$

where $C_{\mu p}$ is an MO coefficient. In practice the basis sets $\{\chi_\mu\}$ often consist of a finite number of atomic orbitals (AOs), *i.e.*, one-electron functions centered on the atoms that resemble the solutions of the Schrödinger equation for the hydrogen atom. In a given basis set, the full configuration-interaction (FCI) wave-function provides a solution to eq. (2.1),

$$|\text{FCI}\rangle = \sum_I C_I |I\rangle, \quad (2.7)$$

where $|I\rangle$ is a Slater determinant or, in second-quantization, an occupation number (ON) vector, which specifies whether zero, one, or two electrons are occupying a given MO ϕ_p . The summation in eq. (2.7) runs over all ON vectors available within a given basis set.

To arrive at the exact solution to the electronic Schrödinger equation, one must consider a FCI expansion in a complete (*i.e.*, infinite) basis set. This cannot be achieved in practice and we usually introduce errors in both the one-electron space (size of the basis set) and the N -electron space (number of electronic configurations or ON vectors). In this thesis we will only discuss approximations in the N -electron

Table 2.1: Index conventions used to denote orbitals. For molecular orbitals, the occupancy is defined with respect to the optimized Hartree–Fock state.

| | |
|--------------------------------|---|
| $p, q, r, s \dots$ | Molecular orbitals of unspecified occupancy. |
| $i, j, k, l \dots$ | Occupied molecular orbitals. |
| $a, b, c, d \dots$ | Virtual or unoccupied molecular orbitals. |
| $\mu, \nu, \sigma, \rho \dots$ | Atomic orbitals, <i>i.e.</i> , basis functions. |

space, keeping in mind that for approaching the exact solution systematically, it is important to improve the description in both spaces (see figure 2.1).

2.2 Hartree–Fock theory

The FCI solution to the Schrödinger equation is tractable only for systems containing a small amount of electrons and using relatively small basis sets. For practical purposes approximate N -electron models have to be designed. The Hartree–Fock (HF) model is one of the cornerstones of electronic-structure theory and even though it is now rarely used as a target model (because it is too inaccurate), it serves as a starting point to some of the most successful approximations. HF is an independent-particle model, *i.e.*, it describes each electron as moving in the average electrostatic field generated by the other electrons and the nuclei. Additionally, the HF wave-function is constructed such that it satisfies Pauli’s exclusion principle. In this thesis, we consider only closed-shell systems, *i.e.*, molecules in which all MOs are either empty or occupied by two electrons in a HF description. This definition leads, to the following parametrization of the HF wave-function,

$$|\text{HF}\rangle = \left(\prod_i a_{i\alpha}^\dagger a_{i\beta}^\dagger \right) |\text{vac}\rangle, \quad (2.8)$$

where index i is used for denoting occupied MOs (see table 2.1 for index conventions), while $|\text{vac}\rangle$ denotes the vacuum state in which all MOs are empty. The HF energy can then be obtained as the expectation value of the Hamiltonian for a system described by the (normalized) HF wave-function,

$$E_{\text{HF}} = \langle \text{HF} | H | \text{HF} \rangle. \quad (2.9)$$

In electronic-structure theory, the variational principle states that finding the solution to the time-independent Schrödinger equation is equivalent to finding the stationary points of the following energy functional,

$$E[\tilde{\Psi}] = \frac{\langle \tilde{\Psi} | H | \tilde{\Psi} \rangle}{\langle \tilde{\Psi} | \tilde{\Psi} \rangle}. \quad (2.10)$$

From eq. (2.8), we see that the HF wave-function is determined by the set of occupied MOs, *i.e.*, by the MO coefficients in eq. (2.6). Using the variational principle it is thus apparent that the HF wave-function can be optimized by finding the set of MOs that minimize the HF energy in eq. (2.9) and get as close as possible to the exact energy with a single electronic configuration. In other words, the HF wave-function is required to satisfy the following condition,

$$E_{\text{HF}}(\boldsymbol{\kappa}) = \min_{\boldsymbol{\kappa}} \langle \widetilde{\text{HF}} | \exp(\boldsymbol{\kappa}) H \exp(-\boldsymbol{\kappa}) | \widetilde{\text{HF}} \rangle \quad (2.11)$$

where $|\widetilde{\text{HF}}\rangle$ is a guess for the HF wave-function and $\boldsymbol{\kappa}$ is a singlet anti-Hermitian one-electron operator that performs unitary transformations among the MOs,

$$\boldsymbol{\kappa} = \sum_{ai} \kappa_{ai} (E_{ai} - E_{ia}). \quad (2.12)$$

The optimization condition in eq. (2.11) can be written as,

$$\left. \frac{\partial E_{\text{HF}}(\boldsymbol{\kappa})}{\partial \kappa_{ai}} \right|_{\boldsymbol{\kappa}=0} = 2 \langle \text{HF} | [E_{ai}, H] | \text{HF} \rangle = 0, \quad (2.13)$$

where the optimized HF wave-function is given by $|\text{HF}\rangle = \exp(-\boldsymbol{\kappa}^{\text{HF}}) |\widetilde{\text{HF}}\rangle$ and the parameters κ_{ai}^{HF} satisfy the optimization condition in eq. (2.13). Instead of expressing the HF wave-function by performing a rotation of the original (guessed) MOs, the $\boldsymbol{\kappa}$ operator can be used to transform directly the elementary operators,

$$a_{p\sigma}^\dagger \equiv \exp(-\boldsymbol{\kappa}) a_{p\sigma}^\dagger \exp(\boldsymbol{\kappa}). \quad (2.14)$$

From now on we will assume that the MOs are expressed in the optimized HF basis (unless specified otherwise).

One important result of HF theory is the Brillouin theorem, which can be derived directly from eq. (2.13),

$$\langle \text{HF} | H E_{ai} | \text{HF} \rangle = 0. \quad (2.15)$$

It implies that the HF state does not interact with singly-excited electronic configurations. As a consequence, one cannot improve on the HF ground state energy by optimizing a linear combination of the HF states with all singly-excited states, as it is done in the configuration-interaction singles (CIS) model ($E_{\text{CIS}} = E_{\text{HF}}$).

Canonical HF theory

As discussed at the beginning of this section, the HF approximation is an independent-particle model. This suggests that the HF wave-function can be obtained by solving a set of effective one-electron Schrödinger equations. Indeed, in canonical HF theory, the optimized MOs are obtained as eigenvectors of an effective one-electron Hamiltonian

called the Fock operator,

$$F = \sum_{pq} F_{pq} E_{pq}, \quad (2.16)$$

$$F_{pq} = h_{pq} + \sum_i (2g_{pqii} - g_{piiq}), \quad (2.17)$$

$$= \epsilon_p \delta_{pq}, \quad (2.18)$$

where the eigenvalues ϵ_p are called orbital energies and are obtained from,

$$F a_{p\sigma}^\dagger |\text{vac}\rangle = \epsilon_p a_{p\sigma}^\dagger |\text{vac}\rangle. \quad (2.19)$$

A diagonalization of the Fock matrix is sufficient to satisfy the HF optimization condition in eq. (2.13) but it is not necessary. Only a block-diagonal form of the Fock matrix ($F_{ai} = F_{ia} = 0$) is required. This flexibility in the optimized HF orbitals (invariance with respect to rotations among orbitals of same occupancy) can be used to impose specific properties on the optimized MOs. For example, it can be interesting to generate localized MOs, as we will see in chapter 3.

Correlation energy

In HF theory, only electrons of parallel spin are correlated through Pauli's exclusion principle, which means that most of the electronic correlation effects are neglected. For a given basis set, the concept of *correlation energy* is thus defined as the difference between the “exact” (FCI) energy and the HF energy,

$$E_{\text{FCI}}^{\text{corr}} = E_{\text{FCI}} - E_{\text{HF}}. \quad (2.20)$$

The electronic correlation effects can be divided into two categories, (i) the static correlation effects, which arise when the HF state does not provide a qualitatively good approximation to the FCI solution due to the fact that more than one electronic configuration is required to qualitatively describe the system and (ii) the dynamic correlation effects which originate from the instantaneous repulsion of electrons through the Coulomb potential. In wave-function based methods, the treatment of static correlation requires the use of multi-configurational methods and will not be covered in this thesis.

2.3 Coupled cluster theory

In order to improve on the HF approximation and recover some of the correlation energy, one has to consider additional electronic configurations (*i.e.*, ON vectors) by performing excitations from the HF reference wave-function. If one targets the FCI energy, the linear parametrization of eq. (2.7) is appropriate. However, due to the

extreme computational scaling of the FCI method with the system size, intermediate descriptions are usually more appealing. In the truncated configuration-interaction (CI) method, one only considers a subset of excited configurations, *e.g.*, all singly and doubly excited configurations (CISD),

$$|\text{CISD}\rangle = |\text{HF}\rangle + \sum_{\mu_1} C_{\mu_1} |\mu_1\rangle + \sum_{\mu_2} C_{\mu_2} |\mu_2\rangle, \quad (2.21)$$

where the indices μ_i denote electronic configurations in which i electrons have been “excited” from occupied to virtual HF orbitals. However, a linear parametrization of the wave-function comes with undesirable features. For example, the correlation energy converges slowly to the FCI limit when the level of truncation is increased and it lacks *size-extensivity*, *i.e.*, at a given level of truncation, the recovery of the FCI correlation energy decreases with the number of electrons when it should be constant.

To avoid those issues, the coupled cluster (CC) wave-function is written in a product form, usually *via* an exponential parametrization,¹⁴

$$|\text{CC}\rangle = \exp(T) |\text{HF}\rangle, \quad (2.22)$$

where T is the so-called cluster operator which performs all possible excitations from the HF reference configuration,

$$T = \sum_i^N T_i. \quad (2.23)$$

N denotes the number of electrons in the system, while i corresponds to the excitation level, such that,

$$T_1 = \sum_{ai} t_i^a E_{ai}, \quad (2.24a)$$

$$T_2 = \frac{1}{2!} \sum_{aibj} t_{ij}^{ab} E_{ai} E_{bj}, \quad (2.24b)$$

$$T_i = \frac{1}{i!} \sum_{\mu_i} t_{\mu_i} \tau_{\mu_i}, \quad (2.24c)$$

Splitting the cluster operator into the different levels of excitation allows one to define a hierarchy of CC models. Including only the T_1 operator corresponds to the CC model, T_1 and T_2 to the CCSD model, T_1 , T_2 , and T_3 to the CCSDT model, *etc.* Such a hierarchy of CC models provides a fast and systematic way to converge to the FCI limit, while ensuring size-extensivity of the correlation energy at each level of truncation. Those attractive features are due to the definition of the exponential function used to parametrize the CC wave-function,

$$\exp(T) = 1 + T + \frac{1}{2!} T^2 + \frac{1}{3!} T^3 + \dots \quad (2.25)$$

Indeed, if only single and double excitations are included in the cluster operator (*i.e.*, for the CCSD model), all higher excitations will still be included in the CC wave-function through disconnected terms like $\frac{1}{2}T_1T_2$ or $\frac{1}{2}T_2T_2$.¹⁵ Those disconnected terms are the key to achieve size-extensivity as well as fast convergence to the FCI limit.

If the cluster operator is not truncated, the CC and FCI wave-functions are equivalent and the following CC Schrödinger equations are satisfied,

$$H|\text{CC}\rangle = E_{\text{CC}}|\text{CC}\rangle, \quad (2.26)$$

$$\exp(-T)H\exp(T)|\text{HF}\rangle = E_{\text{CC}}|\text{HF}\rangle. \quad (2.27)$$

In contrast to HF theory, the variational method cannot be used to optimize the CC wave-function efficiently. Instead, the CC amplitudes are obtained by projecting the CC Schrödinger equation in eq. (2.27) against the set of excited configurations $|\mu_i\rangle = \tau_{\mu_i}|\text{HF}\rangle$,

$$\langle\mu_i|\exp(-T)H\exp(T)|\text{HF}\rangle = 0, \quad (2.28)$$

where the projection manifolds $|\mu_i\rangle$ correspond to all configuration accessible by applying the truncated cluster operator T linearly to the HF state. Eq. (2.28) constitutes a set of non-linear equations which couple the amplitudes.

Once the CC amplitudes have been optimized from eq. (2.28), the CC energy can be obtained by projecting eq. (2.27) against the HF state,

$$E_{\text{CC}} = \langle\text{HF}|\exp(-T)H\exp(T)|\text{HF}\rangle, \quad (2.29a)$$

$$= E_{\text{HF}} + E_{\text{CC}}^{\text{corr}}, \quad (2.29b)$$

$$= E_{\text{HF}} + \sum_{aijb} (t_i^a t_j^b + t_{ij}^{ab}) L_{iajb}, \quad (2.29c)$$

where $L_{iajb} = 2g_{iajb} - g_{ibja}$. The expression for the CC correlation energy in eq. (2.29c) is the same for all standard CC models, which means that triple amplitudes t_{ijk}^{abc} and amplitudes of higher excitation level affect the CC energy only by coupling with the singles and doubles amplitudes through eq. (2.28).

2.3.1 The coupled cluster singles and doubles model: CCSD

The CCSD approximation is the first model of the standard CC hierarchy to introduce correlation effects. As such, it is a widely used approximation and we now introduce the working equations for the optimization of the CCSD amplitudes.

As mentioned previously, in the CCSD model, the cluster operator includes only single T_1 and double T_2 excitations. Eq. (2.28) can thus be divided into a singles amplitude equation,

$$\Omega_{\mu_1}^{\text{CCSD}} = \langle\mu_1|\exp(-T_2)\tilde{H}\exp(T_2)|\text{HF}\rangle = 0, \quad (2.30)$$

and a doubles amplitude equation,

$$\Omega_{\mu_2}^{\text{CCSD}} = \langle \mu_2 | \exp(-T_2) \tilde{H} \exp(T_2) | \text{HF} \rangle = 0, \quad (2.31)$$

where we have introduced the CCSD vector functions $\Omega_{\mu_1}^{\text{CCSD}}$ and $\Omega_{\mu_2}^{\text{CCSD}}$ as well as the similarity-transformed Hamiltonian,¹⁶

$$\tilde{H} = \exp(-T_1) H \exp(T_1), \quad (2.32)$$

where the similarity transformation can be applied directly to the elementary operators $a_{p\sigma}^\dagger$ and $a_{p\sigma}$ in the same way as in HF theory [see eq. (2.14)] such that the integrals in the T_1 -transformed Hamiltonian are now expressed in terms of T_1 -transformed MOs,

$$\tilde{H} = \sum_{pq} \tilde{h}_{pq} E_{pq} + \frac{1}{2} \sum_{pqrs} \tilde{g}_{pqrs} e_{pqrs} + h_{\text{nuc}}, \quad (2.33)$$

where the MO integrals can be directly generated from their counter-part in the AO basis $\{\chi_\mu\}$, as,

$$\tilde{h}_{pq} = \sum_{\mu\nu} X_{\mu p} Y_{\nu q} h_{\mu\nu} \quad (2.34a)$$

$$\tilde{g}_{pqrs} = \sum_{\mu\nu\sigma\rho} X_{\mu p} Y_{\nu q} X_{\sigma r} Y_{\rho s} g_{\mu\nu\sigma\rho}, \quad (2.34b)$$

and the transformation matrices \mathbf{X} and \mathbf{Y} are given by,

$$\begin{aligned} X_{\mu i} &= C_{\mu i} & X_{\mu a} &= C_{\mu a} - \sum_i C_{\mu i} t_i^a \\ Y_{\mu i} &= C_{\mu i} + \sum_a C_{\mu a} t_i^a & Y_{\mu a} &= C_{\mu a} \end{aligned} \quad (2.35)$$

where the \mathbf{C} matrix is directly obtained from the solution of the HF problem and performs transformations from AOs to HF MOs.

Using the Baker–Campbell–Hausdorff (BCH) expansion of the similarity-transformed Hamiltonian, eqs. (2.30) and (2.31) may be rewritten as,

$$\Omega_{\mu_1}^{\text{CCSD}} = \langle \mu_1 | \tilde{H} + [\tilde{H}, T_2] | \text{HF} \rangle = 0, \quad (2.36a)$$

$$\Omega_{\mu_2}^{\text{CCSD}} = \langle \mu_2 | \tilde{H} + [\tilde{H}, T_2] + \frac{1}{2} [[\tilde{H}, T_2], T_2] | \text{HF} \rangle = 0, \quad (2.36b)$$

where the BCH expansion naturally stops after a few terms due to rank-reduction and the fact that the Hamiltonian is a two-electron operator [see Ref. 13 for more details]. From eqs. (2.36a) and (2.36b) it is now possible to derive the CCSD working equations. The singles vector function can be written as,

$$\Omega_{ai}^{\text{CCSD}} = \Omega_{ai}^{A1} + \Omega_{ai}^{B1} + \Omega_{ai}^{C1} + \Omega_{ai}^{D1} \quad (2.37)$$

where,

$$\Omega_{ai}^{A1} = \sum_{cdk} u_{ki}^{cd} \tilde{g}_{adkc} \quad (2.38a)$$

$$\Omega_{ai}^{B1} = - \sum_{ckl} u_{kl}^{ac} \tilde{g}_{kilc} \quad (2.38b)$$

$$\Omega_{ai}^{C1} = \sum_{ck} u_{ik}^{ac} \tilde{F}_{kc} \quad (2.38c)$$

$$\Omega_{ai}^{D1} = \tilde{F}_{ai}, \quad (2.38d)$$

while the doubles vector function is given by,

$$\Omega_{aibj}^{\text{CCSD}} = \Omega_{aibj}^{A2} + \Omega_{aibj}^{B2} + P_{ij}^{ab} (\Omega_{aibj}^{C2} + \Omega_{aibj}^{D2} + \Omega_{aibj}^{E2}) \quad (2.39)$$

where,

$$\Omega_{aibj}^{A2} = \tilde{g}_{aibj} + \sum_{cd} t_{ij}^{cd} \tilde{g}_{acbd} \quad (2.40a)$$

$$\Omega_{aibj}^{B2} = \sum_{kl} t_{kl}^{ab} \left(\tilde{g}_{kilj} + \sum_{cd} t_{ij}^{cd} \tilde{g}_{kcld} \right) \quad (2.40b)$$

$$\Omega_{aibj}^{C2} = -\frac{1}{2} \sum_{ck} t_{kj}^{bc} \left(\tilde{g}_{kiac} - \frac{1}{2} \sum_{dl} t_{li}^{ad} \tilde{g}_{kdlc} \right) - \sum_{ck} t_{ki}^{bc} \left(\tilde{g}_{kjac} - \frac{1}{2} \sum_{dl} t_{lj}^{ad} \tilde{g}_{kdlc} \right) \quad (2.40c)$$

$$\Omega_{aibj}^{D2} = \frac{1}{2} \sum_{ck} u_{jk}^{bc} \left(\tilde{L}_{aikc} + \frac{1}{2} \sum_{dl} u_{il}^{ad} \tilde{L}_{ldkc} \right) \quad (2.40d)$$

$$\Omega_{aibj}^{E2} = \sum_c t_{ij}^{ac} \left(\tilde{F}_{bc} - \sum_{dkl} u_{kl}^{bd} \tilde{g}_{ldkc} \right) - \sum_k t_{ik}^{ab} \left(\tilde{F}_{kj} + \sum_{cdl} u_{lj}^{cd} \tilde{g}_{kdlc} \right), \quad (2.40e)$$

and where we have introduced the following intermediates,

$$u_{ij}^{ab} = 2t_{ij}^{ab} - t_{ij}^{ba}, \quad (2.41a)$$

$$\tilde{L}_{pqrs} = 2\tilde{g}_{pqrs} - \tilde{g}_{psrq}, \quad (2.41b)$$

$$\tilde{F}_{pq} = \tilde{h}_{pq} + \sum_i (2\tilde{g}_{pqi} - \tilde{g}_{pii}), \quad (2.41c)$$

$$P_{ij}^{ab} X_{ij}^{ab} = X_{ij}^{ab} + X_{ji}^{ba}. \quad (2.41d)$$

An analysis of the explicit expressions of the CCSD vector functions shows that the term with the highest computational scaling is the second term in eq. (2.40a), *i.e.*,

$$\Omega_{aibj}^{A2.2} = \sum_{cd} t_{ij}^{cd} \tilde{g}_{acbd}, \quad (2.42)$$

which scales as $\mathcal{O}(O^2V^4) \sim \mathcal{O}(N^6)$ where O and V denote the number of occupied and virtual orbitals, respectively, while N is used as a generic measure of the size of the system. Performing a similar analysis on the next approximation in the CC hierarchy would reveal that the CCSDT model scales as $\mathcal{O}(N^8)$. The lack of intermediates

between the CCSD and CCSDT models is problematic as it puts severe limits on the problems that can be treated, both in terms of size of the molecules and in terms of accuracy of the results. As we will show in the next section, a combination of CC theory with Møller–Plesset perturbation theory can be used to design such intermediate models and extend the applicability of the CC hierarchy.

2.4 Coupled cluster perturbation theory

In Møller–Plesset perturbation theory, the electronic molecular Hamiltonian in eq. (2.2) is partitioned into a zero-order Hamiltonian chosen to be the Fock operator and a perturbation,

$$H = F + \Phi + h_{\text{nuc}}, \quad (2.43)$$

where the perturbation Φ is often referred to as the fluctuation potential and corresponds to the difference between the true Coulomb potential,

$$g = \frac{1}{2} \sum_{pqrs} g_{pqrs} e_{pqrs} \quad (2.44)$$

and the effective one-electron Fock potential,

$$V = \sum_{pq} \sum_i (2g_{pqii} - g_{piii}) E_{pq}, \quad (2.45)$$

$$\Phi = H - F - h_{\text{nuc}} \quad (2.46a)$$

$$= g - V. \quad (2.46b)$$

As in CC theory, we assume the solution to the zero-order Schrödinger equation to be available, *i.e.*, the HF wave-function and the orbital energies are known,

$$H^{(0)} |\Psi^{(0)}\rangle = E^{(0)} |\Psi^{(0)}\rangle, \quad (2.47)$$

$$F |\text{HF}\rangle = 2 \sum_i \epsilon_i |\text{HF}\rangle. \quad (2.48)$$

where we have assumed a canonical representation of the Fock operator (see section 2.2).

To arrive at the CC perturbation theory (CCPT) main equations, the exact wave-function is parametrized with the CC *ansatz* in eq. (2.22), and the Møller–Plesset partitioning of the Hamiltonian is introduced in the projected CC equations [eqs. (2.28) and (2.29a)],

$$E = E^{(0)} + \langle \text{HF} | \exp(-T) \Phi \exp(T) | \text{HF} \rangle + h_{\text{nuc}}, \quad (2.49a)$$

$$\epsilon_{\mu_i} t_{\mu_i} = - \langle \mu_i | \exp(-T) \Phi \exp(T) | \text{HF} \rangle, \quad (2.49b)$$

where, ϵ_{μ_i} denotes a combination of orbital energies (*e.g.*, $\epsilon_{aibj} = \epsilon_a - \epsilon_i + \epsilon_b - \epsilon_j$). One can then consider a Lagrangian, in which the energy in eq. (2.49a) is calculated subject to the constraints in eq. (2.49b),

$$\begin{aligned} \mathcal{L}(\mathbf{t}, \bar{\mathbf{t}}) = & E^{(0)} + \langle \text{HF} | \exp(-T) \Phi \exp(T) | \text{HF} \rangle + h_{\text{nuc}} \\ & + \sum_i \sum_{\mu_i} \bar{t}_{\mu_i} \epsilon_{\mu_i} t_{\mu_i} + \sum_i \sum_{\mu_i} \bar{t}_{\mu_i} \langle \mu_i | \exp(-T) \Phi \exp(T) | \text{HF} \rangle, \end{aligned} \quad (2.50)$$

where the Lagrangian multipliers are denoted \bar{t}_{μ_i} . We note that ensuring the following variational condition,

$$\mathcal{L}_{\mu_i} = \frac{\partial \mathcal{L}}{\partial t_{\mu_i}} = 0, \quad (2.51)$$

is equivalent to solving eq. (2.49b) and thus determines the CCPT amplitudes. An additional condition is then required to determine the Lagrangian multipliers, and we ensure that the Lagrangian is also variational with respect to the amplitudes,

$$\bar{\mathcal{L}}_{\mu_i} = \frac{\partial \mathcal{L}}{\partial t_{\mu_i}} = 0. \quad (2.52)$$

In order to obtain expressions for CCPT energies and wave-function parameters, the Lagrangian is expanded in orders of the fluctuation potential, and the variational conditions in eqs. (2.51) and (2.52) are solved to each order separately,

$$\mathcal{L}_{\mu_i}^{(0)} = \mathcal{L}_{\mu_i}^{(1)} = \mathcal{L}_{\mu_i}^{(2)} = \dots = 0 \quad (2.53a)$$

$$\bar{\mathcal{L}}_{\mu_i}^{(0)} = \bar{\mathcal{L}}_{\mu_i}^{(1)} = \bar{\mathcal{L}}_{\mu_i}^{(2)} = \dots = 0 \quad (2.53b)$$

which yields the perturbed amplitudes and multipliers,

$$t_{\mu_i} = t_{\mu_i}^{(0)} + t_{\mu_i}^{(1)} + t_{\mu_i}^{(2)} \dots \quad (2.54a)$$

$$\bar{t}_{\mu_i} = \bar{t}_{\mu_i}^{(0)} + \bar{t}_{\mu_i}^{(1)} + \bar{t}_{\mu_i}^{(2)} \dots \quad (2.54b)$$

This specific formulation of CCPT leads to expressions that satisfy Wigner's $2n + 1$ rule, which states that the energy to order $2n+1$ may be calculated from the amplitudes to order n and lower. In addition, a similar rule can be derived for the multipliers of order n and lower, which then determine the energy to order $2n + 2$.

2.4.1 The second-order Møller–Plesset model: MP2

Considering the zero- and first-order energies in the Møller–Plesset series, leads to the HF energy, $E^{(0)} + E^{(1)} = E_{\text{HF}}$. Therefore, to start recovering some of the correlation energy, one has to consider the energy at least up to second-order in the fluctuation potential. This is done in the second-order Møller–Plesset (MP2) model,¹⁷

$$E_{\text{MP2}} = E^{(0)} + E^{(1)} + E^{(2)} \quad (2.55a)$$

$$= E_{\text{HF}} + E^{(2)}. \quad (2.55b)$$

The $2n + 1$ and $2n + 2$ rules imply that to obtain the second-order contributions to the energy one has to determine the zero-order amplitudes and multipliers as well as the first-order amplitudes. From the variational conditions in eq. (2.53), it can be shown that the zero-order amplitudes and multipliers vanish and only the first-order amplitudes are then needed to determine the MP2 energy,

$$t_{\mu_i}^{(1)} = -\frac{\langle \mu_i | \Phi | \text{HF} \rangle}{\epsilon_{\mu_i}}. \quad (2.56)$$

Because of the Brillouin theorem in eq. (2.15) and since the fluctuation potential is a two-electron operator, only doubles amplitudes enter in first-order, and eq. (2.56) becomes,

$$t_{ij}^{ab(1)} = \frac{g_{ajib}}{\epsilon_i - \epsilon_a + \epsilon_j - \epsilon_b}. \quad (2.57)$$

From the second-order terms in the CCPT Lagrangian in eq. (2.50) we then obtain an expression for the MP2 correlation energy,

$$E_{\text{MP2}}^{\text{corr}} = \langle \text{HF} | [\Phi, T_2^{(1)}] | \text{HF} \rangle \quad (2.58a)$$

$$= \sum_{ajib} t_{ij}^{ab(1)} L_{iajb}, \quad (2.58b)$$

which is equivalent to the CC expression of the correlation energy in eq. (2.29c) where the singles amplitudes are zero.

The MP2 model is one of the simplest models to include electronic correlation effects and it is extensively used since it recovers most of the CCSD correlation energy at a lower computational cost [MP2 scales as $\mathcal{O}(N^5)$ while CCSD scales as $\mathcal{O}(N^6)$]. It is also a non-iterative model, *i.e.*, the MP2 amplitudes in eq. (2.57) can be obtained directly from integrals and orbital energies, while the optimization of the CCSD amplitudes relies on iterative procedures. However, the accuracy of the MP2 results is limited and in order to reach higher accuracy it is important to include effects from connected single as well as triple excitations. Calculating the third or fourth order corrections to the energy in the Møller–Plesset series through the MP3 or MP4 models is not as effective as in the MP2 case and can lead to convergence problems.^{13,18,19} In the CCSD model presented in section 2.3.1, the effects of single excitations usually improves on the MP2 description but still lacks the relaxation effects of connected triple excitations which are important to achieve high accuracy.

In section 2.4.3 we introduce the so-called CCSD(T) model, which constitutes an intermediate between the CCSD and CCSDT models based on perturbation theory while in the next section we briefly present an alternative second-order model designed for the calculation of frequency-dependent molecular properties.

2.4.2 The second-order approximate coupled cluster singles and doubles model: CC2

Due to Brillouin’s theorem, the MP2 model does not include effects from single excitations. This becomes problematic in the derivation of frequency-dependent molecular properties in the framework of response theory (see section 2.5). To circumvent this issue, the CC2 model was introduced as a second-order approximation to the CCSD energy in which the singles are treated as zero-order parameters (instead of second-order).²⁰ The CC2 singles equations are therefore equivalent to the ones in the CCSD model [see eq. (2.36a)],

$$\Omega_{\mu_1}^{\text{CC2}} = \langle \mu_1 | \tilde{H} + [\tilde{H}, T_2] | \text{HF} \rangle = 0, \quad (2.59)$$

while the CC2 doubles amplitude equations are approximated to be correct to first-order in the fluctuation potential and eq. (2.36b) therefore becomes,

$$\Omega_{\mu_2}^{\text{CC2}} = \langle \mu_2 | \tilde{H} + [F, T_2] | \text{HF} \rangle = 0. \quad (2.60)$$

This approximated form of the doubles equations leads to a closed-form of the doubles amplitudes similar to MP2 but where the two-electron integrals are now expressed in the T_1 -transformed basis,

$$t_{ij}^{ab} = \frac{\tilde{g}_{aibj}}{\epsilon_i - \epsilon_a + \epsilon_j - \epsilon_b}. \quad (2.61)$$

While the MP2 model is non-iterative, the CC2 equations have to be solved iteratively since the singles and doubles amplitudes couple through eqs. (2.59) and (2.60). However, the CC2 model, like MP2, scales as $\mathcal{O}(N^5)$ with the system size and its energy is correct to second-order in the fluctuation potential.

In order to complete the hierarchy of CCPT models for the calculation of frequency-dependent molecular properties, the CC3 model has also been introduced as an intermediate between the CCSD and CCSDT models.²¹ We therefore end-up with the following set of iterative models, ordered according to increasing accuracy and computational scaling,

$$\begin{array}{cccccc} \text{CCS} < & \text{CC2} < & \text{CCSD} < & \text{CC3} < & \text{CCSDT} \dots \\ \mathcal{O}(N^4) & \mathcal{O}(N^5) & \mathcal{O}(N^6) & \mathcal{O}(N^7) & \mathcal{O}(N^8) \end{array}$$

We note that other CC models have been designed for the calculation of excitation energies. For second-order models we can mention the equation-of-motion second-order many-body perturbation theory EOM-MBPT(2),^{22,23} the algebraic diagrammatic construction ADC(2),²⁴ and the second-order polarization propagator approximation (SOPPA)^{25,26} models. A series of triples corrected models, such as CCSDR(3),²⁷ have also been designed for the calculation of excitation energies.^{28–30}

2.4.3 The coupled cluster singles and doubles with perturbative triples model: CCSD(T)

The hierarchy of CCPT models presented in the previous section is well adapted to calculate frequency-dependent properties. However, for ground-state energies or static molecular properties, the CC2 and CC3 models can be replaced by the MP2 and CCSD(T) models, respectively, which are more attractive since they rely on non-iterative procedures.

In the CCSD(T) model, a standard CCSD calculation is performed, as described in section 2.3.1, providing the CCSD singles and doubles amplitudes as well as the CCSD correlation energy. A triples correction to the CCSD energy, $E_{(T)}^{\text{corr}}$, can then be calculated based on perturbation theory,

$$E_{\text{CCSD(T)}}^{\text{corr}} = E_{\text{CCSD}}^{\text{corr}} + E_{(T)}^{\text{corr}}. \quad (2.62)$$

In contrast with the CC3 or CCSDT models, in the (T) correction, the triples do not couple back to relax the CCSD amplitudes. This lack of coupling is important to ensure that the (T) correction can be calculated using a non-iterative procedure.

From the CCPT Lagrangian formalism summarized at the beginning of this section, it can be shown that the CCSD energy is correct to third-order in the fluctuation potential. The CCSD energy can thus be corrected by calculating higher order terms from the CCPT expansion. In the CCSD(T) model, this is done by considering the fourth- and fifth-order contributions to the CCPT Lagrangian in eq. (2.50) and keeping only those terms that include connected triples and that are projected against the singly and doubly excited manifolds, *i.e.*,

$$E_T^{(4)} = \sum_{\mu_2} \bar{t}_{\mu_2}^{(1)} \langle \mu_2 | [\Phi, T_3^{(2)}] | \text{HF} \rangle \quad (2.63a)$$

$$E_T^{(5)} = \sum_{i=1,2} \sum_{\mu_i} \bar{t}_{\mu_i}^{(2)} \langle \mu_i | [\Phi, T_3^{(2)}] | \text{HF} \rangle, \quad (2.63b)$$

where the connected triples contained in the cluster operator $T_3^{(2)}$ are given by,

$$t_{ijk}^{abc(2)} = P_{ijk}^{abc} \frac{\sum_d t_{ij}^{ad(1)} g_{ckbd} - \sum_l t_{il}^{ab(1)} g_{cklj}}{\epsilon_i - \epsilon_a + \epsilon_j - \epsilon_b + \epsilon_k - \epsilon_c} \quad (2.64)$$

$$P_{ijk}^{abc} X_{ijk}^{abc} = X_{ijk}^{abc} + X_{ikj}^{acb} + X_{jik}^{bac} + X_{jki}^{bca} + X_{kij}^{cab} + X_{kji}^{cba}. \quad (2.65)$$

Finally, both the first- and second-order Lagrangian multipliers as well as the first-order amplitudes are replaced by the CCSD singles and doubles amplitudes,

$$E_{(T)}^{\text{corr}} = \sum_{i=1,2} \sum_{\mu_i} t_{\mu_i} \langle \mu_i | [\Phi, *T_3^{(2)}] | \text{HF} \rangle, \quad (2.66)$$

where we have inserted an asterisk to underline that the first-order doubles amplitudes in eq. (2.64) are also replaced by the CCSD amplitudes. After some algebraic manipulations, we arrive at the final (T) working equations,

$$E_{(T)}^{\text{corr}} = E^{[4]} + E^{[5]} \quad (2.67)$$

$$E^{[4]} = 2 \sum_{aibj} (2t_{ij}^{ab} - t_{ji}^{ab}) *T_{ij}^{ab} \quad (2.68)$$

$$E^{[5]} = 2 \sum_{ai} t_i^a *T_i^a \quad (2.69)$$

where we have used square brackets to underline that those contributions are not strictly equivalent to eq. (2.63). We have also introduced the following intermediates,

$$*T_i^a = \sum_{cdkl} (*t_{ikl}^{acd(2)} - *t_{lki}^{acd(2)}) L_{kcld} \quad (2.70)$$

$$\begin{aligned} *T_{ij}^{ab} = & \sum_{cdk} (*t_{ijk}^{acd(2)} L_{bckd} - *t_{kji}^{acd(2)} g_{kdbc}) \\ & - \sum_{ckl} (*t_{ikl}^{abc(2)} L_{kjl c} - *t_{lki}^{abc(2)} g_{kjl c}). \end{aligned} \quad (2.71)$$

The (T) correction to the CCSD energy has shown to be very efficient at recovering the effects of connected triples and the CCSD(T) model is often described as the gold standard of quantum chemistry. Finally, we note that the equations presented in this section differ from the original ones.³¹ They are however equivalent and will become convenient in our description of local CC methods in chapter 3.

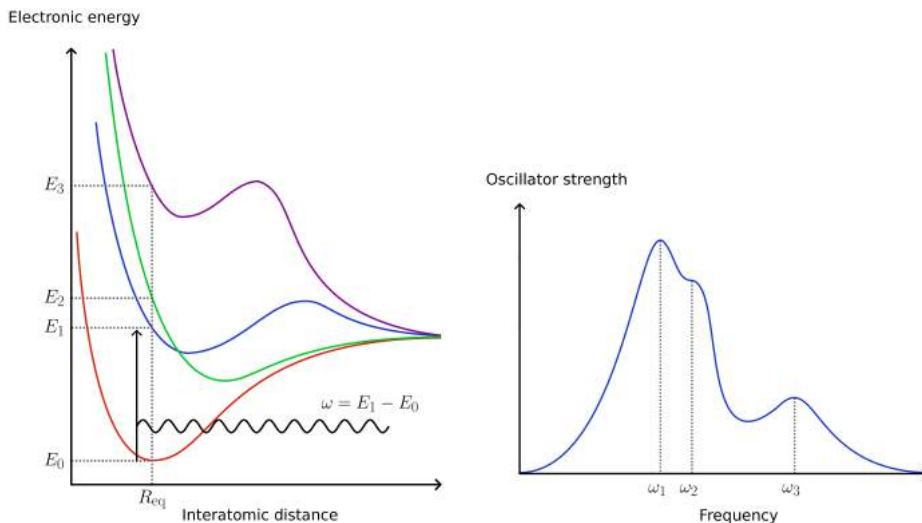
We have now introduced several models of electronic-structure theory that allows to solve the Schrödinger equation with different levels of approximations and different computational costs. In the following and last section of this chapter, we consider how molecular properties can be extracted from solutions of the Schrödinger equation and in particular, how electronic transitions can be described by those solutions.

2.5 Electronic transitions

The exact solutions to the time-independent electronic Schrödinger equation for molecules in their equilibrium geometry lead to a spectrum of energies and states,

$$H |\Psi_m\rangle = E_m |\Psi_m\rangle. \quad (2.72)$$

So far we have been discussing the solution corresponding to the lowest possible energy of a system, *i.e.*, the ground state energy E_0 . An isolated system in its ground state will stay indefinitely in that state. However, a transition from the ground state to a state of higher energy, *i.e.*, an excited state can occur if the right amount of energy is transferred to the system. This excitation energy is usually transferred by light in the



(a) Electronic energy levels and transitions.

(b) Typical UV-visible absorption spectrum.

Figure 2.2: (a): Cartoon representation of an electronic excitation from the ground state to the first excited state of a diatomic molecule by absorption of a single photon. R_{eq} refers to the equilibrium inter-atomic distance for the molecule in its electronic ground state (the energy levels associated with other degrees of freedom such as vibrations, rotations, *etc.* are neglected). (b): Cartoon representation of the corresponding absorption spectrum.

ultra-violet (UV) and visible regions of the electromagnetic spectrum. All electronic transitions are not equally likely to happen and knowing the excitation energy as well as the probability associated with a given transition (the transition strength) leads to absorption spectra that can be compared with experiments and give information about, *e.g.*, the color of a given compound. The processes involved in such light-matter interactions are illustrated in figure 2.2.

The concept of oscillator strength is often used to evaluate the electronic transition probability. It can be derived from time-dependent perturbation theory under the electric dipole approximation (in the length gauge),³²

$$f_{0m} = \frac{2}{3}\omega_m \sum_{i=x,y,z} \langle \Psi_m | \theta_i | \Psi_0 \rangle \langle \Psi_0 | \theta_i | \Psi_m \rangle, \quad (2.73)$$

where we have introduced the excitation energy from the ground state to the m -th excited state, $\omega_m = E_m - E_0$, as well as the electric dipole operator,

$$\theta_i = \sum_{pq} \theta_{pq}^i E_{pq}, \quad (2.74)$$

$$\theta_{pq}^i = - \int \phi_p(\mathbf{r}) r_i \phi_q(\mathbf{r}) d\mathbf{r}, \quad (2.75)$$

where r_i denotes one of the Cartesian components of the position operator.

The calculation of excitation energies is a difficult task which can in general not be achieved using the machinery developed in the previous sections. One important complication is that many excited states have multi-configurational character, *i.e.*, a single HF configuration does not provide a qualitative description of the states in question.^{33,34} This issue has been bypassed in the context of response theory where excitation energies as well as molecular properties can be computed without explicitly calculating the excited state wave-functions. Instead, the isolated system is considered in its ground state and is perturbed (in the sense of perturbation theory) by an external field. Molecular properties are then obtained as response functions, *i.e.*, the response of the system to the perturbation. Excitation energies and oscillator strengths then arise as side-products of the response functions.

In the next sections we summarize how excitation energies and oscillator strengths are calculated in response theory, first for exact states and then for CC models. Most of the following content is based on Refs. 35 and 36.

2.5.1 Response theory for exact states

The goal of response theory is to calculate molecular properties that can be compared with experiments. In quantum mechanics, physical properties or observables are associated with Hermitian operators and in general, only the average value of a series of measurements is predictable. A Hermitian time-independent operator V_A is therefore associated with a given property and the average value of interest is given by the expectation value of V_A ,

$$\langle V_A \rangle (t) = \langle \Phi(t) | V_A | \Phi(t) \rangle, \quad (2.76)$$

where $|\Phi(t)\rangle$ is a solution to the time-dependent Schrödinger equation,

$$\mathcal{H}(t) |\Phi(t)\rangle = i\partial_t |\Phi(t)\rangle. \quad (2.77)$$

Response theory therefore aims at calculating the expectation values of Hermitian operators. The Hamiltonian in eq. (2.77) can often be decomposed into a time-independent part H , taken to be the electronic molecular Hamiltonian in eq. (2.2) and a time-dependent perturbation $V(t)$,

$$\mathcal{H}(t) = H + V(t). \quad (2.78)$$

In the development of response theory for exact state, it is assumed that the solutions to the time-independent problem in eq. (2.72) are known. In addition, the perturbation is required to be periodic in time with period T and frequency $\omega = 2\pi/T$. The perturbation describes the interaction of the molecule with, *e.g.*, an electromagnetic

radiation, and it can be written as a Fourier expansion,

$$V(t) = \sum_A \varepsilon_A V_A \exp(-i\omega_A t), \quad (2.79)$$

where ε_A is the perturbation strength associated with the time-independent Hermitian operator V_A . The frequency of the perturbation ω_A , should not be confused with the excitation energy ω_m .

The quasi-energy

Without loss of generality, the time-dependent wave-function $|\Phi(t)\rangle$ can be expressed as a product of a phase-factor $e^{-i\mathcal{F}(t)}$ and a regular time-periodic wave-function $|\Phi_R(t)\rangle$,

$$|\Phi(t)\rangle = e^{-i\mathcal{F}(t)} |\Phi_R(t)\rangle. \quad (2.80)$$

The real phase $\mathcal{F}(t)$ can be separated into a time-periodic part $\mathcal{F}_T(t)$ and a part linear in time $\mathcal{Q}t$,

$$\mathcal{F}(t) = \mathcal{F}_T(t) + \mathcal{Q}t, \quad (2.81)$$

$$|\Phi(t)\rangle = e^{-i\mathcal{F}_T(t)} e^{-i\mathcal{Q}t} |\Phi_R(t)\rangle. \quad (2.82)$$

Inserting the expression for $|\Phi(t)\rangle$ in eq. (2.77) leads to the following eigenvalue problem, satisfied at each time t ,

$$\left(\mathcal{H}(t) - \dot{\mathcal{F}}_T(t) - i\partial_t \right) |\Phi_R(t)\rangle = \mathcal{Q} |\Phi_R(t)\rangle, \quad (2.83)$$

where the dot in $\dot{\mathcal{F}}_T(t)$ denotes differentiation with respect to time. The time-periodic phase $\mathcal{F}_T(t)$ is not uniquely defined and depends on the parametrization of $|\Phi(t)\rangle$. However, we can get rid of this term by considering eq. (2.83) in a composite Hilbert space³⁷ where the standard (spatial) inner-product $\langle f(t)|g(t)\rangle$ is augmented with time-averaging,

$$\left\{ \langle f(t)|g(t)\rangle \right\}_T = \frac{1}{T} \int_0^T \langle f(t)|g(t)\rangle dt. \quad (2.84)$$

We also recall that for a time-periodic function $f(t)$ of period T ,

$$\left\{ \dot{f}(t) \right\}_T = 0. \quad (2.85)$$

The operator $\mathcal{H}(t) - i\partial_t$ can be shown to be Hermitian in the composite Hilbert space and eq. (2.83) thus corresponds to a Hermitian eigenvalue problem in that space ($\dot{\mathcal{F}}_T(t)$

is real). By projecting eq. (2.83) against $\langle \Phi_R(t) |$ in the composite Hilbert space we arrive at,

$$\mathcal{Q} = \left\{ \langle \Phi_R(t) | \mathcal{H}(t) - i\partial_t | \Phi_R(t) \rangle \right\}_T \quad (2.86)$$

where we have used that the regular wave-function is time-periodic and normalized, $\langle \Phi_R(t) | \Phi_R(t) \rangle = 1$ and that $\mathcal{F}_T(t)$ is also time-periodic. As we will see below, in absence of perturbation, the quantity \mathcal{Q} reduces to the energy of the system and it is therefore called the quasi-energy. As for the energy in the time-independent case (see section 2.2), the following time-dependent variational principle can be formulated for the quasi-energy,

$$\begin{aligned} \delta \mathcal{Q} = & \left\{ \langle \delta \Phi_R(t) | \mathcal{H}(t) - i\partial_t | \Phi_R(t) \rangle \right\}_T \\ & + \left\{ \langle \Phi_R(t) | \mathcal{H}(t) - i\partial_t | \delta \Phi_R(t) \rangle \right\}_T = 0, \end{aligned} \quad (2.87)$$

which can be derived from eq. (2.83) by considering a time-periodic perturbation $\delta \Phi_R(t)$, for which $\langle \Phi_R(t) + \delta \Phi_R(t) | \Phi_R(t) + \delta \Phi_R(t) \rangle = 1$. The quasi-energy is thus stable with respect to first-order variations of the regular wave-function. Since eq. (2.83) corresponds to a Hermitian eigenvalue problem in the composite Hilbert space, finding the wave-functions $|\Phi_R(t)\rangle$ that satisfy $\delta \mathcal{Q} = 0$ is therefore equivalent to finding the eigenvalues and eigenvectors of eq. (2.83).¹³

It is now interesting to consider eq. (2.86) in the absence of perturbations, $\mathcal{H} \equiv H$. The time-dependent wave-function can then be parametrized as,

$$|\Phi(t)\rangle = e^{-i\phi} e^{-iE_m t} |\Psi_m\rangle, \quad (2.88)$$

where E_m and $|\Psi_m\rangle$ are the eigenvalues and eigenvectors solutions to the time-independent Schrödinger equation and ϕ is an undetermined time-independent phase. By turning off the perturbation in the Hamiltonian we have therefore induced the following changes in the wave-function,

$$|\Phi_R(t)\rangle \rightarrow |\Psi_m\rangle \quad (2.89)$$

$$\mathcal{F}_T(t) \rightarrow \phi \quad (2.90)$$

$$\mathcal{Q} \rightarrow E_m \quad (2.91)$$

which is also consistent with a substitution in eq. (2.86),

$$\mathcal{Q} = \left\{ \langle \Psi_m | H | \Psi_m \rangle \right\}_T = \langle \Psi_m | H | \Psi_m \rangle = E_m. \quad (2.92)$$

In other words, the quasi-energy indeed reduces to the energy of the system in absence of perturbation, hence the name.

As stated previously, physical properties are related to expectation values of Hermitian operators, it is thus important for the following to see how the quasi-energy can

be related to such quantities. Let us then consider the derivative of the quasi-energy with respect to a given perturbation strength,

$$\frac{dQ}{d\varepsilon_A} = \left\{ \langle \Phi_R(t) | \frac{\partial \mathcal{H}(t)}{\partial \varepsilon_A} | \Phi_R(t) \rangle \right\}_T + \delta Q \quad (2.93)$$

$$= \left\{ \langle \Phi_R(t) | V_A | \Phi_R(t) \rangle \exp(-i\omega_A t) \right\}_T, \quad (2.94)$$

where we have used the variational principle for the quasi-energy with the variation,

$$|\delta \Phi_R(t)\rangle = \left| \frac{\partial \Phi_R(t)}{\partial \varepsilon_A} \right\rangle. \quad (2.95)$$

This relation between the expectation value of a Hermitian operator V_A and the derivative of the quasi-energy is important to understand how molecular properties arise from response theory.

Response functions

In the case of a time-independent perturbation,

$$V = \sum_A V_A \varepsilon_A, \quad (2.96)$$

the quasi-energy in eq. (2.86) becomes the energy of the perturbed system $E_0(\varepsilon)$. Where the perturbation could be a distortion of the molecular structure or an electrostatic field. The perturbed energy can then be expanded in orders of the perturbation strengths,

$$E_0(\varepsilon) = E_0 + \sum_A E_0^{(A)} \varepsilon_A + \frac{1}{2} \sum_{A,B} E_0^{(A,B)} \varepsilon_A \varepsilon_B + \mathcal{O}(\varepsilon^3), \quad (2.97)$$

where,

$$E_0^{(A)} = \left. \frac{dE_0(\varepsilon)}{d\varepsilon_A} \right|_{\varepsilon=0} \quad (2.98)$$

describes the first-order response of the system to the external perturbation and,

$$E_0^{(A,B)} = \left. \frac{d^2 E_0(\varepsilon)}{d\varepsilon_A d\varepsilon_B} \right|_{\varepsilon=0} \quad (2.99)$$

is the second-order response to the perturbation *etc.* Depending on the perturbation, the response functions ($E_0^{(A)}$, $E_0^{(A,B)}$...) can then be attributed to different static (time-independent) molecular properties.^{38,39}

In analogy to the time-independent case, the quasi-energy can also be expanded in orders of the perturbation strengths,

$$Q(\varepsilon) = E_0 + \sum_A Q^{(A)} \varepsilon_A + \frac{1}{2} \sum_{A,B} Q^{(A,B)} \varepsilon_A \varepsilon_B + \mathcal{O}(\varepsilon^3). \quad (2.100)$$

Introducing the established notation in the field, we have that the first-order molecular properties,

$$\mathcal{Q}^{(A)} = \left. \frac{d\mathcal{Q}(\varepsilon)}{d\varepsilon_A} \right|_{\varepsilon=0} = \langle V_A \rangle_0 = \langle \Psi_0 | V_A | \Psi_0 \rangle \quad (2.101)$$

are frequency-independent and correspond to the ground state expectation value of the perturbation. The second-order properties,

$$\mathcal{Q}^{(A,B)} = \left. \frac{d^2\mathcal{Q}(\varepsilon)}{d\varepsilon_A d\varepsilon_B} \right|_{\varepsilon=0} = \langle \langle V_A; V_B \rangle \rangle_{\omega_B} \quad (2.102)$$

correspond to the linear response functions and in the well-known sum-over-states representation we have,

$$\langle \langle V_A; V_B \rangle \rangle_{\omega_B} = P(A, B) \sum_{m \neq 0} \frac{\langle \Psi_0 | V_A | \Psi_m \rangle \langle \Psi_m | V_B | \Psi_0 \rangle}{\omega_B - \omega_m}, \quad (2.103)$$

with the frequency condition, $\omega_A + \omega_B = 0$, and where we have introduced the permutation operator,

$$P(A, B)f(A, B) = f(A, B) + f(B, A). \quad (2.104)$$

Higher order response functions can also be derived, but only the linear response function is of interest in this thesis.

Excitation energies and oscillator strengths

It is easy to see in eq. (2.103) that excitation energies can be identified from the poles of the linear response function, *i.e.*, whenever $\omega_B = \omega_m$. Additionally, if the Hermitian operators V_A and V_B are chosen to be the components of the electric dipole operator, the linear response function then corresponds to frequency-dependent polarizabilities, and its residues give transition strengths,

$$\lim_{\omega \rightarrow \omega_m} (\omega - \omega_m) \langle \langle \theta_i, \theta_j \rangle \rangle_{\omega} = \langle \Psi_0 | \theta_i | \Psi_m \rangle \langle \Psi_m | \theta_j | \Psi_0 \rangle = S_{0m}^{\theta_i, \theta_j}. \quad (2.105)$$

Which can be directly related to the oscillator strength in eq. (2.73),

$$f_{0m} = \frac{2}{3} \omega_m \sum_{i=x,y,z} S_{0m}^{\theta_i, \theta_i}. \quad (2.106)$$

We have now shown how excitation energies and oscillator strengths can be obtained from response theory as side products (poles and residues) of the linear response function. In the next section we summarize how the response formalism can be applied to CC theory for the calculation of excitation energies and oscillator strengths.

2.5.2 Excitation energies and oscillator strengths for CC models

In the previous section we have not assumed any specific parametrization of the regular time-periodic wave-function $|\Phi_R(t)\rangle$. The only requirement was that the optimized wave-function satisfies the variational principle for the quasi-energy in eq. (2.87).

In order to apply the response formalism to CC theory, it is important that when the perturbation is turned off, the quasi-energy and the regular wave-function both reduce to the unperturbed CC ground state energy and wave-function as given in section 2.3, respectively.

Let us then write the CC time-dependent wave-function as,

$$|\text{CC}(t)\rangle = e^{-i\mathcal{F}_T(t)} e^{-i\mathcal{Q}t} |\text{CC}_R(t)\rangle \quad (2.107)$$

$$= N(t) e^{-i\mathcal{F}_T(t)} e^{-i\mathcal{Q}t} e^{T(t)} |\text{HF}\rangle. \quad (2.108)$$

The cluster operator $T(t)$ is now time-dependent in the CC amplitudes $t_\mu(t)$ and $N(t)$ is a time-periodic normalization factor due to the fact that the CC wave-functions is not unit-normalized but intermediate normalized,

$$\langle \text{HF} | \text{CC}_I(t) \rangle = 1, \quad (2.109)$$

$$|\text{CC}_I(t)\rangle = e^{T(t)} |\text{HF}\rangle. \quad (2.110)$$

The equivalent form of the projected CC equations in eqs. (2.28) and (2.29a) in the time-dependent regime and in the composite Hilbert space are then given by,

$$\mathcal{Q}_{\text{CC}} = \left\{ \langle \text{HF} | e^{-T(t)} (\mathcal{H}(t) - i\partial_t) e^{T(t)} | \text{HF} \rangle \right\}_T, \quad (2.111)$$

$$\left\{ \langle \mu | e^{-T(t)} (\mathcal{H}(t) - i\partial_t) e^{T(t)} | \text{HF} \rangle \right\}_T = 0. \quad (2.112)$$

Note that due to time-periodicity and time-averaging both the phase and the normalization factors are eliminated from eqs. (2.111) and (2.112). However, as in the time-independent case (see section 2.3), the time-dependent CC wave-function does not satisfy a variational principle for the CC quasi-energy in eq. (2.111), *i.e.*, $\delta\mathcal{Q}_{\text{CC}}$ is in general different from zero. The strategy developed in section 2.5.1 for variational models can thus not be directly applied to the CC quasi-energy. However, this difficulty can be bypassed by considering a CC quasi-energy Lagrangian,

$$\begin{aligned} \mathcal{L}_{\text{CC}} = & \left\{ \langle \text{HF} | e^{-T(t)} (\mathcal{H}(t) - i\partial_t) e^{T(t)} | \text{HF} \rangle \right\}_T \\ & + \sum_{\mu} \left\{ \bar{t}_{\mu}(t) \langle \mu | e^{-T(t)} (\mathcal{H}(t) - i\partial_t) e^{T(t)} | \text{HF} \rangle \right\}_T. \end{aligned} \quad (2.113)$$

By construction, the CC quasi-energy Lagrangian is variational with respect to the Lagrange multipliers $\bar{t}_{\mu}(t)$, and we require that it is also stationary with respect to

Table 2.2: Expressions for intermediate tensors used in CC response theory. The zero-order parameters T and t_μ correspond to the ground state and are determined as detailed in section 2.3, while \bar{t}_μ denotes the ground state Lagrangian multipliers determined from eq. (2.125).⁴⁰

| | | |
|-----------------------|---|--|
| η_μ | $= \frac{\partial \mathcal{Q}_{CC}^{(0)}}{\partial t_\mu} = \frac{\partial E_{CC}}{\partial t_\mu}$ | $= \langle \text{HF} [H, \tau_\mu] \text{CC} \rangle$ |
| η_μ^A | $= \frac{\partial^2 \mathcal{L}_{CC}^{(2)}}{\partial t_\mu^A \partial \varepsilon_A}$ | $= \langle \Lambda [V_A, \tau_\mu] \text{CC} \rangle$ |
| ξ_μ^A | $= \frac{\partial^2 \mathcal{L}_{CC}^{(2)}}{\partial \bar{t}_\mu^A \partial \varepsilon_A}$ | $= \langle \mu \exp(-T) V_A \text{CC} \rangle$ |
| $F_{\mu\nu}$ | $= \frac{\partial^2 \mathcal{L}_{CC}^{(2)}}{\partial t_\mu^A \partial t_\nu^B}$ | $= \langle \Lambda [[H, \tau_\mu] \tau_\nu] \text{CC} \rangle$ |
| $J_{\mu\nu}$ | $= \frac{\partial^2 \mathcal{L}_{CC}^{(2)}}{\partial \bar{t}_\mu^A \partial t_\nu^B}$ | $= \langle \mu \exp(-T) [H, \tau_\nu] \text{CC} \rangle$ |
| $\langle \Lambda $ | $= \langle \text{HF} + \sum_\nu \bar{t}_\nu \langle \nu \exp(-T)$ | |
| $ \text{CC} \rangle$ | $= \exp(T) \text{HF} \rangle$ | |

the CC amplitudes,

$$\frac{\partial \mathcal{L}_{CC}}{\partial \bar{t}_\mu(t)} = 0, \quad (2.114)$$

$$\frac{\partial \mathcal{L}_{CC}}{\partial t_\mu(t)} = 0. \quad (2.115)$$

For optimized parameters, the Lagrangian in eq. (2.113) is equivalent to the quasi-energy and it can therefore be used to determine response functions in the same way as for variational models.

The CC linear response function is then given by,

$$\langle \langle V_A; V_B \rangle \rangle_{\omega_B} = \mathcal{L}_{CC}^{(A,B)} = \left. \frac{d^2 \mathcal{L}_{CC}(\varepsilon)}{d\varepsilon_A d\varepsilon_B} \right|_{\varepsilon=0} \quad (2.116)$$

$$= \frac{1}{2} C^{\pm\omega} P(A, B) \sum_\mu (\eta_\mu^A + \frac{1}{2} \sum_\nu F_{\mu\nu} t_\nu^A) t_\mu^B, \quad (2.117)$$

with the frequency condition, $\omega_A + \omega_B = 0$, and where the symmetrization operator,

$$C^{\pm\omega} f(\omega_A, \omega_B) = f(\omega_A, \omega_B) + f(-\omega_A, -\omega_B)^* \quad (2.118)$$

is necessary in CC theory to ensure the correct symmetry of the response functions. t_ν^A and t_μ^B are the Fourier components of the expanded time-dependent CC amplitudes and the other intermediates (η^A and \mathbf{F}) are given in table 2.2.

An analysis of the linear response function in eq. (2.117) shows that its poles (*i.e.*, the CC excitation energies) correspond to the eigenvalues of the CC Jacobian matrix,⁴⁰

$$\mathbf{J}\mathbf{R}^m = \omega_m \mathbf{R}^m, \quad (2.119a)$$

$$\mathbf{L}^m \mathbf{J} = \mathbf{L}^m \omega_m, \quad (2.119b)$$

where the right (\mathbf{R}) and left (\mathbf{L}) eigenvectors can be different since the CC Jacobian matrix \mathbf{J} , defined in table 2.2, is in general not symmetric. This means that CC excitation energies as defined in response theory are not guaranteed to be real. However, whenever HF theory provides a good reference electronic configuration, the CC Jacobian is nearly symmetric and real CC excitation energies are obtained.

CC transition strengths, obtained as residues of the CC linear response function are given by,⁴⁰

$$S_{0m}^{A,B} = \frac{1}{2} \left[T_{0m}^A T_{m0}^B + (T_{0m}^B T_{m0}^A)^* \right], \quad (2.120)$$

where the left and right transition moments can be written as,

$$T_{m0}^A = \sum_{\mu} L_{\mu}^m \xi_{\mu}^A, \quad (2.121)$$

$$T_{0m}^A = \sum_{\mu} (\eta_{\mu}^A R_{\mu}^m + \bar{M}_{\mu}^m \xi_{\mu}^A), \quad (2.122)$$

where we have introduced the transition moments Lagrangian multipliers \bar{M}_{μ}^m which can be determined from the following response equation,

$$\bar{\mathbf{M}}^m (\omega_m \mathbf{1} + \mathbf{J}) + (\mathbf{R}^m)^T \mathbf{F} = 0. \quad (2.123)$$

We note that the oscillator strength corresponding to a transition from the ground state to the m -th excited state can be obtained directly as,

$$f_{0m} = \frac{2}{3} \omega_m \sum_{i=x,y,z} S_{0m}^{\theta_i, \theta_i}, \quad (2.124)$$

where we have set V_A and V_B to be components of the electric dipole operator.

Summary and other approaches

To summarize, for the calculation of CC excitation energies, the ground state time-independent CC amplitudes have to be obtained as detailed in section 2.3. Indeed, the ground state amplitudes are required to calculate the CC Jacobian matrix (see table 2.2) which needs to be diagonalized to obtain the CC excitation energies. If only the excitation energies are desired then only one (right or left) of the eigenvalue problems in eq. (2.119) has to be solved.

For the calculation of CC transition strengths, more response equations have to be solved. The $\boldsymbol{\eta}^A$ and \mathbf{F} tensors for example depend on the ground state Lagrangian

multipliers which are obtained from the following linear equation,

$$\bar{\mathbf{t}}\mathbf{J} + \boldsymbol{\eta} = 0, \quad (2.125)$$

where $\boldsymbol{\eta}$ is also given in table 2.2. The optimization of the transition moment Lagrangian multipliers from eq. (2.123) is also required, and both the right and left Jacobian eigenvectors in eq. (2.119) are needed.

The formalism and equations presented here are applicable to all standard CC models such as the CCS and CCSD models but also to CCPT models like the CC2 model presented in section 2.4.2. The working equations for the calculation of excitation energies and oscillator strengths at the CC2 level are derived in details in appendix A.

Finally, we note that CC excitation energies identical to the one obtained from linear response theory can be obtained through the equation-of-motion (EOM)-CC formalism.^{22,23,41,42} In EOM-CC theory, the excited states are parametrized from the ground state as a linear expansion,

$$|\Psi_m^{\text{EOM-CC}}\rangle = \sum_{\mu} R_{\mu}^m \tau_{\mu} |\text{CC}\rangle = \exp(T) \sum_{\mu} R_{\mu}^m \tau_{\mu} |\text{HF}\rangle, \quad (2.126)$$

where the ground state $|\Psi_0^{\text{EOM-CC}}\rangle = |\text{CC}\rangle$ is recovered by taking $\tau_0 = \mathbf{1}$. Inserting $|\Psi_m^{\text{EOM-CC}}\rangle$ in the time-independent Schrödinger equation in eq. (2.72) and projecting against $\langle\mu| \exp(-T)$ leads to,

$$\sum_{\nu} \langle\mu| \exp(-T) H \exp(T) |\nu\rangle R_{\nu}^m = E_m^{\text{CC}} \sum_{\nu} \langle\mu|\nu\rangle R_{\nu}^m \quad (2.127)$$

$$\sum_{\nu} \left(\langle\mu| \exp(-T) H \exp(T) |\nu\rangle - E_0^{\text{CC}} \delta_{\mu\nu} \right) R_{\nu}^m = (E_m^{\text{CC}} - E_0^{\text{CC}}) R_{\mu}^m \quad (2.128)$$

where it can then be shown that eq. (2.128) is equivalent to the right Jacobian eigenvalue problem in eq. (2.119a),

$$\sum_{\nu} J_{\mu\nu} R_{\nu}^m = \omega_m R_{\mu}^m, \quad (2.129)$$

$$J_{\mu\nu} = \langle\mu| \exp(-T) H \exp(T) |\nu\rangle - E_0^{\text{CC}} \delta_{\mu\nu}. \quad (2.130)$$

CC excitation energies obtained from EOM-CC or linear response approaches are thus identical. However, the calculation of molecular properties and transition strengths differs between the two formalisms. In this work, we use expressions for the oscillator strengths derived from response theory since EOM-CC expressions⁴¹ have been shown to lack size-intensivity.^{43,44}

CHAPTER
THREE

LOCAL CC METHODS FOR GROUND STATES



3.1 Introduction

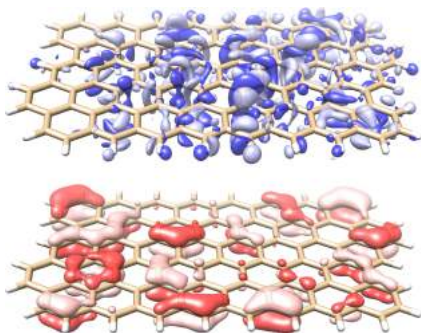
Single reference CC theory, as described in section 2.3, is well established in electronic-structure theory and is very successful for the calculation of energies and molecular properties of relatively small systems dominated by a single electronic configuration. However, the computational scaling of the CC models with the system size prohibits its application to large systems. For example, one of the largest conventional CCSD(T) calculation, *i.e.*, with an $\mathcal{O}(N^7)$ scaling, was performed on a cluster of 20 water molecules,⁴⁵ while, for the MP2 model, which scales as $\mathcal{O}(N^5)$, a conventional calculation was reported on two nanographene sheets ($C_{150}H_{30}$)₂.⁴⁶ Both of these calculations relied on massively parallel implementations which ran on super-computers and everyday applications of those models are generally targeting much smaller molecules. In order to perform high accuracy CC calculations on molecular systems containing several hundred atoms like proteins, it is thus crucial to design new theoretical models with lower computational requirements.

The dynamical correlation effects described in CC calculations can be divided into two contributions, (i) the Coulomb hole, which is a short-range effect and corresponds to the electrostatic repulsion of electrons, and (ii) dispersion effects, which can be classically interpreted as (induced-) dipole interactions and have a more long-range character. Dispersion forces are well known to decay as R^{-6} with the inter-dipole distance R , and all the correlation effects can thus be considered of local nature.⁴⁷ The locality of dynamic correlation suggests that a linear-scaling formulation of CC methods should be possible for large enough systems and finding the optimal way to design such models is one of the most important challenges of modern electronic-structure theory.⁴⁸

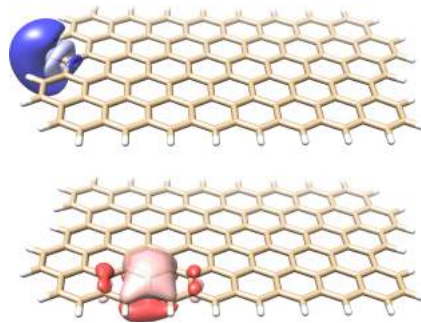
CC theory is most commonly formulated in terms of HF canonical molecular orbitals (CMOs) which are in general delocalized over the whole system [see figure 3.1(a)] and thus prevents the introduction of local approximations. As mentioned in section 2.2, canonical HF theory corresponds to a specific solution of the HF optimization condition in which the Fock matrix is diagonal. However, only the occupied-virtual and virtual-occupied blocks of the Fock matrix are required to be zero and this flexibility in the occupied-occupied and virtual-virtual blocks of the Fock matrix can be used to generate local orbitals. To this end, different procedures have been suggested, including, *e.g.*, Pipek-Mezey⁴⁹ and Boys^{50,51} strategies. The general idea is to define a localization function that describes in some way the locality of orbitals and to minimize that function subject to orthogonality constraints. For example, the Boys localization function corresponds to the sum of the orbitals' second central moment,

$$\xi_1^{\text{SM}} = \sum_p \langle \phi_p | (\mathbf{r} - \langle \phi_p | \mathbf{r} | \phi_p \rangle)^2 | \phi_p \rangle. \quad (3.1)$$

As an extension to the Boys localization function, powers of the second⁵² and fourth⁵³



(a) Virtual (top) and occupied (bottom) canonical molecular orbitals.



(b) Virtual (top) and occupied (bottom) local molecular orbitals.

Figure 3.1: Comparison of canonical and localized Hartree–Fock molecular orbitals for a graphene sheet ($C_{106}H_{28}$) in a cc-pVDZ basis. The local orbitals have been obtained *via* minimization of the square of the second central orbital moments (the least local orbitals have been plotted). A contour value of 0.02 a.u. was used.

central moments have proven to result in more homogeneous and more local orbitals [see figure 3.1(b)],⁵⁴

$$\xi_m^{\text{SM}} = \sum_p \langle \phi_p | (\mathbf{r} - \langle \phi_p | \mathbf{r} | \phi_p \rangle)^2 | \phi_p \rangle^m, \quad (3.2a)$$

$$\xi_m^{\text{FM}} = \sum_p \langle \phi_p | (\mathbf{r} - \langle \phi_p | \mathbf{r} | \phi_p \rangle)^4 | \phi_p \rangle^m. \quad (3.2b)$$

While localized occupied orbitals have been available for several decades, the generation of local virtual orbitals has been more problematic and it is only recently that new minimization algorithms have solved this issue.⁵⁵ As an alternative to orthogonal localized virtual orbitals, non-orthogonal orbitals have been introduced in the context of local CC methods. We can for example mention projected atomic orbitals (PAOs),⁵⁶ orbital-specific virtuals (OSVs),⁵⁷ and pair natural orbitals (PNOs).^{58,59}

In this chapter, we consider some of the state-of-the-art local CC methods with particular emphasis on the divide–expand–consolidate (DEC) scheme which is the central concept of the work described in the articles attached in appendices B.1 to B.5.

3.2 The Divide–Expand–Consolidate scheme

This section was used as a first draft for part of the manuscript in appendix B.1.

DEC is a massively parallel and linear-scaling algorithm designed for the calculation of CC energies and properties of large molecular systems. It takes advantage of the locality of correlation effects *via* localized and orthogonal occupied and virtual HF

orbitals and a partitioning of the energy into independent fragment contributions. In the following sections we summarize the overall DEC strategy when combined with the MP2, CCSD, and CCSD(T) models.

3.2.1 Energy partitioning

For standard CC models like CCSD, CCSDT, *etc.*, the CC correlation energy is given by,

$$E_{\text{CC}}^{\text{corr}} = \sum_{aibj} (t_i^a t_j^b + t_{ij}^{ab}) L_{iajb} \quad (3.3a)$$

$$= \sum_{aibj} E_{ij}^{ab}. \quad (3.3b)$$

If a basis of local orbitals is used in eq. (3.3a), both the integrals and the amplitudes will reflect the locality of correlation effects and for large systems, many contributions to $E_{\text{CC}}^{\text{corr}}$ can be discarded.^{47,48} For the integrals we have,

$$g_{iajb} = \iint \phi_i(\mathbf{r}_1) \phi_a(\mathbf{r}_1) \frac{1}{r_{12}} \phi_j(\mathbf{r}_2) \phi_b(\mathbf{r}_2) d\mathbf{r}_1 d\mathbf{r}_2, \quad (3.4)$$

where for local orbitals, the charge distribution $\phi_i \phi_a$ vanishes as the distance between the two orbitals increases, *i.e.*, a two-electron integral g_{iajb} is non-vanishing if orbital a is close to i and orbital b is close to j .⁵ The amplitudes are directly affected by the decay of the integrals, since the most important contribution to the doubles amplitudes is proportional to g_{iajb} [see eq. (2.57)].

The first step in setting up the main equations of the DEC scheme is to assign each orbital to its closest atomic site (denoted as $P, Q, R \dots$), based on the distance between the center of charge of the orbital and the positions of the nuclei. We denote the set of occupied (virtual) orbitals assigned to atomic site P as \underline{P} (\overline{P}), see also figure 3.2. This orbital assignment is then used to partition the energy into atomic fragment (E_P) and pair fragment (E_{PQ}) contributions,

$$E_{\text{DEC}}^{\text{corr}} = \sum_P [E_P + \sum_{Q>P} E_{PQ}], \quad (3.5)$$

$$E_P = \sum_{ij \in \underline{P}} \sum_{ab} E_{ij}^{ab}, \quad (3.6a)$$

$$E_{PQ} = \left(\sum_{\substack{i \in \underline{P} \\ j \in \underline{Q}}} + \sum_{\substack{i \in \overline{Q} \\ j \in \overline{P}}} \right) \sum_{ab} E_{ij}^{ab}. \quad (3.6b)$$

This formulation of the CC correlation energy is still exact but is now well suited for local approximations. Indeed, we can now use the decaying behavior of the charge distributions described above to restrict the summation over virtual indices in eq. (3.6)

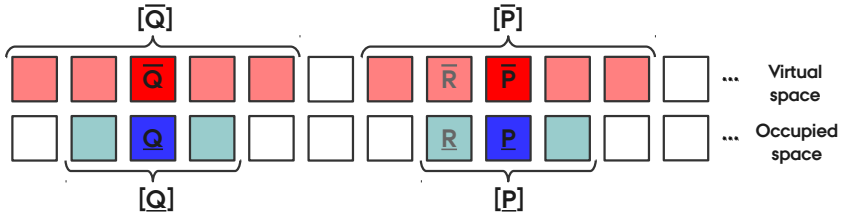


Figure 3.2: Schematic illustration of the different orbital spaces defined in a DEC calculation for a linear molecule.

such that only non-vanishing contributions are included. Of course the exact behavior of the integrals and amplitudes cannot be known beforehand and the important set of virtual orbitals associated to a given pair of occupied orbitals is thus unknown. However, due to the locality of correlation effects, including the virtual orbitals closest to atom P is a natural choice. We thus denote a set of virtual orbitals assigned to atomic sites in the vicinity of site P as $[\bar{P}]$ (see figure 3.2) and the final formulation for the DEC fragment energies becomes,

$$E_P = \sum_{ij \in P} \sum_{ab \in [\bar{P}]} E_{ij}^{ab} \quad (3.7a)$$

$$E_{PQ} = \left(\sum_{\substack{i \in P \\ j \in Q}} + \sum_{\substack{i \in Q \\ j \in P}} \right) \sum_{ab \in [\bar{P}] \cup [\bar{Q}]} E_{ij}^{ab}. \quad (3.7b)$$

We now see that, eqs. (3.5) and (3.7) provide a way to calculate the CC correlation energy that scales quadratically with the system size, assuming that the set of virtual orbitals in $[\bar{P}]$ corresponds to a small fraction of the total orbital space for all sites P . However, the pair fragment energies E_{PQ} are expected to describe dispersion forces and to decay as R_{PQ}^{-6} with the inter-atomic distance, which can be understood from a multipole analysis of the integrals g_{iajb} whenever the two charge distributions, $\phi_i \phi_a$ and $\phi_j \phi_b$, are not overlapping.⁶⁰ The number of pair fragment energy contributions can therefore be truncated such that it scales linearly in the limit of large systems, which renders eq. (3.5) *a priori* linear-scaling.

Let us now illustrate how this formulation can be extended to non-standard CC models such as the MP2 and CCSD(T) models. The DEC-MP2 model is trivially obtained by setting the singles amplitudes to zero,

$$E_{ij}^{ab} \equiv t_{ij}^{ab} L_{iajb}, \quad (3.8)$$

while, for the CCSD(T) model, we split the DEC energy into a CCSD contribution given by eq. (3.5) and a (T) correction which is further divided into the fourth- and a fifth-order terms presented in section 2.4.3. From eq. (2.68), we see that the fourth-

order term can be partitioned in analogy with the standard CC energy,

$$E_P^{[4]} = 2 \sum_{ij \in \underline{P}} \sum_{ab \in [\overline{P}]} (2t_{ij}^{ab} - t_{ji}^{ab}) * T_{ij}^{ab} \quad (3.9a)$$

$$E_{PQ}^{[4]} = 2 \left(\sum_{\substack{i \in \underline{P} \\ j \in \underline{Q}}} + \sum_{\substack{i \in \underline{Q} \\ j \in \underline{P}}} \right) \sum_{ab \in [\overline{P}] \cup [\overline{Q}]} (2t_{ij}^{ab} - t_{ji}^{ab}) * T_{ij}^{ab}, \quad (3.9b)$$

while for the fifth-order term, we chose the following partitioning,⁷

$$E_P^{[5]} = 2 \sum_{i \in \underline{P}} \sum_{a \in \overline{P}} t_i^a * T_i^a \quad (3.10a)$$

$$E_{PQ}^{[5]} = 2 \left(\sum_{\substack{a \in \overline{P} \\ i \in \underline{Q}}} + \sum_{\substack{a \in \overline{Q} \\ i \in \underline{P}}} \right) t_i^a * T_i^a. \quad (3.10b)$$

Note that the equations for the fifth-order contributions do not contain any reference to the virtual spaces $[\overline{P}]$ and are therefore exact whenever the singles amplitudes and the (T) intermediates are calculated in the complete orbital space. For further considerations regarding the formulation of DEC for the MP2 and CCSD(T) models, we refer to appendices B.3 and B.4, respectively.

3.2.2 Atomic fragment optimization

In the previous section, we have presented expressions for calculating the correlation energy of various CC models in a basis of local MOs. The DEC energy expressions are expected to yield linear-scaling algorithms provided that, (i) the virtual spaces $[\overline{P}]$ can be significantly reduced compared to the complete virtual space, (ii) the number of pair fragment energies E_{PQ} to be calculated can be reduced to scale linearly with the system size.

In this section we will consider how the virtual spaces $[\overline{P}]$ can be obtained to ensure error control in the fragment energies, while the screening of pair fragments [point (ii)] will be considered in section 3.2.3.

In order to understand how the fragment energies can be calculated and how the orbital spaces can be optimized we introduce the energy orbital space (EOS), *i.e.*, the space in which the atomic fragment energy is calculated in eq. (3.7a),

$$P_{\text{EOS}} \equiv \underline{P} \cup [\overline{P}]. \quad (3.11)$$

The CC amplitudes used in the DEC energy expression for a given fragment E_P are required to couple with the amplitudes used in all the surrounding fragments. Therefore, it is not possible to simply solve the CC amplitude equation in P_{EOS} without introducing additional coupling errors.

This coupling errors can be corrected by solving the CC amplitude equations in an extended space called the amplitude orbital space (AOS),

$$P_{\text{AOS}} \equiv [P] \cup [\bar{P}], \quad (3.12)$$

where, by analogy with the virtual spaces, $[P]$ denotes the set of occupied orbitals assigned to atomic sites in the vicinity of center P (see figure 3.2). Note that the coupling effects in the virtual space have been considered by implicit expansion of space $[\bar{P}]$ used in eq. (3.11) which thus implies $P_{\text{EOS}} \subset P_{\text{AOS}}$. Assuming $[P]$ and $[\bar{P}]$ to be known, the calculation of the atomic fragment energy E_P can be performed as follows,

1. Solve the CC amplitude equations in the restricted space, P_{AOS} .
2. Extract the CC amplitudes from P_{AOS} to P_{EOS} .
3. Calculate the two-electron integrals in P_{EOS} .
4. Use the CC amplitudes and integrals in P_{EOS} to calculate the atomic fragment energy using eq. (3.7a).

The strategy used in DEC to obtain the spaces $[P]$ and $[\bar{P}]$ leading to atomic and pair fragment energies of predefined accuracy can be divided into two steps: a fragment expansion step, followed by a fine-tuning reduction step. Let us consider the fragment energy E_P and the determination of the optimal spaces $[P]$ and $[\bar{P}]$. In the fragment expansion, a list of all the local molecular orbitals is dressed based on an estimation of the importance of each orbital to the unknown fragment energy E_P . Due to the locality of correlation effects, the distance between a given orbital and the atomic site P is an obvious choice to build the list but other measurements such as the numerical overlap of the orbitals or the Fock matrix elements could be used. Primary spaces ($[P]$ and $[\bar{P}]$) are then set up by considering a minimal number of (occupied and virtual) orbitals from the priority list. The fragment energy associated with those spaces is then calculated according to the recipe outlined above. The orbital spaces are then expanded based on the priority list and an improved fragment energy is calculated. This process is repeated until the difference between the last two fragment energies is below a user-defined threshold, the so-called fragment optimization threshold (FOT). The fragment expansion procedure is illustrated in the left part of figure 3.3.

In principle, the fragment expansion could be performed for all atomic fragments and the expanded spaces could be used for the pair fragment calculations, *i.e.*, building the pair equivalent of the AOS as,

$$PQ_{\text{AOS}} \equiv P_{\text{AOS}} \cup Q_{\text{AOS}}, \quad (3.13a)$$

solving the CC amplitude equations in PQ_{AOS} and calculating the pair fragment energies using eq. (3.7b). However, it is clear that the pair fragment orbital spaces can

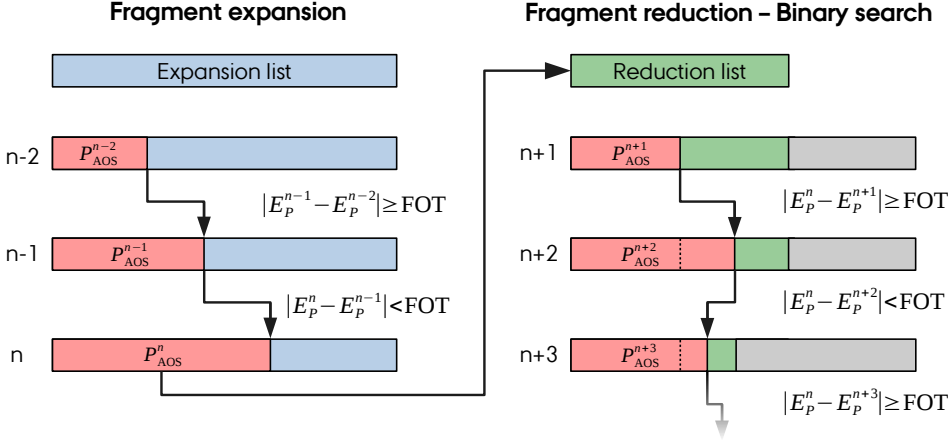


Figure 3.3: Illustration of the fragment optimization procedure, E_P is the atomic fragment energy associated to atomic site P , P_{AOS} denotes the space in which the CC amplitude equations are solved and the FOT is a user-defined threshold.

become significantly larger than the atomic fragment spaces and many more pair fragments than atomic fragments have to be considered. This two factors indicate that any reduction in the size of the pair fragment orbital spaces will result in significant computational savings in the total DEC calculation. Furthermore, in order to avoid false convergence in the fragment expansion (*i.e.*, converging to artificially too small orbital spaces) many orbitals need to be added to the fragment in each step of the expansion. As a consequence, the fragment expansion results in large orbital spaces and atomic fragment energies with error much smaller than the FOT. The large orbital spaces then propagate to the pair fragment energy calculations which become unpractical. A fragment reduction strategy is therefore employed on the expanded orbital spaces by relying on a binary search algorithm to remove unimportant orbitals without introducing errors larger than the FOT. The determination of the fragment orbital spaces is summarized in figure 3.3 and is considered in greater details in appendix B.2.

Finally, we note that for DEC-CCSD or DEC-CCSD(T) calculations (*i.e.*, when the targeted correlation energy is the CCSD or CCSD(T) correlation energy), the fragment optimization can be performed at the MP2 level, while only the fragment energies in the reduced orbital spaces are calculated at the targeted level of theory.

3.2.3 Pair fragment screening

As mentioned before, the DEC partitioning of the CC correlation energy is expected to lead to a linear-scaling algorithm whenever the number of pair fragments scales linearly with the system size. We now illustrate, how an efficient screening strategy allows for a linear-scaling number of pairs to be calculated.

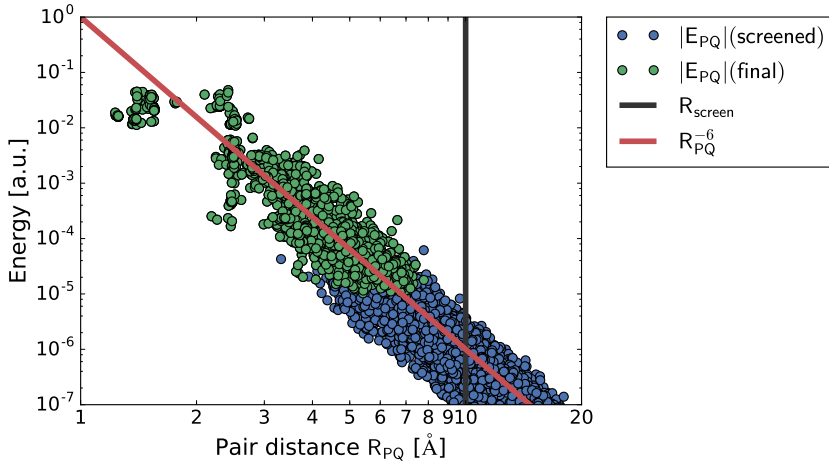


Figure 3.4: Decay of the MP2 pair fragment energies $|E_{PQ}|$ with the pair distance R_{PQ} for the titin-I27_{SS} molecule (392 atoms) using a cc-pVDZ basis set (3772 basis functions). The expected R_{PQ}^{-6} pair decay is also plotted. The pair fragment energies are separated into the calculated “final” pairs (in green) and the pairs screened away by the pair screening procedure (in blue). The molecular geometry was taken from Ref. 61.

The simplest way to reduce the number of pair fragment energies is to use a real-space cut-off, *i.e.*, if the distance between two atomic site R_{PQ} is greater than a distance threshold, *e.g.*, $R_{\text{screen}} = 10 \text{ \AA}$, then the corresponding pair fragment is screened away and the pair energy E_{PQ} is not calculated. Two issues arise with such strategy, (i) the number of pair fragment energies calculated is independent of the FOT and in order to converge to the standard CC correlation energy, both the FOT and R_{screen} would have to be tuned, (ii) the pair fragment energies for a given pair distance can spread over several orders of magnitude (see figure 3.4), hence, a significant number of the pairs included with a real-space threshold are less relevant than some of the pairs screened away. Those issues can be bypassed by considering a pair screening strategy based on an estimation of the pair fragment energies.

In DEC, we therefore calculate pair energy estimates at the MP2 level and using minimal orbital spaces in eq. (3.7b). The orbital spaces are chosen such that the pair energy estimates E_{PQ}^{esti} recover 80-95% of the “exact” MP2 pair fragment energies, while being very cheap in terms of computational efforts. Once the pair energy estimates have been calculated, the screening strategy proceeds as follows.

1. Order all pair energy estimates associated with a given site P ,

$$|E_{P1}^{\text{esti}}| \leq |E_{P2}^{\text{esti}}| \cdots \leq |E_{PN}^{\text{esti}}|, \quad (3.14)$$

where N is the total number of atomic sites in the molecule.

2. Sum-up the estimated contributions in the list until it adds up to the FOT, *i.e.*, find the atomic index I_P such that,

$$\max_{I_P} \left(\frac{1}{2} \sum_{Q=1}^{I_P} |E_{PQ}^{\text{esti}}| \right) \leq \text{FOT} \quad (3.15)$$

3. All pairs E_{PQ} for which $Q \leq I_P$ are then screened away and not calculated.
4. Repeat points 1 to 3 for all atomic sites.

This procedure has been designed to ensure that the error introduced by screening the pairs associated to a given atomic site would not exceed the FOT. For example, the energy contribution of a given atomic site to the DEC correlation energy can be written as,

$$\mathcal{E}_P = E_P + \frac{1}{2} \sum_{Q \neq P} E_{PQ}, \quad \forall Q > I_P. \quad (3.16)$$

It now becomes apparent that the DEC algorithm allows for an error of the order of $2 \cdot \text{FOT}$ for each site P , *i.e.*, $1 \cdot \text{FOT}$ in the atomic fragment energy E_P , *via* the fragment optimization procedure and another $1 \cdot \text{FOT}$ for the pair energies E_{PQ} discarded by the pair screening procedure. Therefore, the absolute error made in the final DEC correlation energy is expected to grow linearly with the number of sites in the system, thus yielding a size-intensive recovery of the CC correlation energy. This error analysis of the pair screening procedure relies on two assumptions, (i) the pair energy estimates provide a qualitative approximation of the actual pair fragment energies, (ii) the errors in the final pair fragment energies E_{PQ} are negligible compared to the FOT. While the first assumption is covered by the typical recovery of the pair energy estimates (80-95%), the second assumption is also generally satisfied whenever the pair fragment orbital spaces are constructed as union of the atomic fragment spaces, as suggested in section 3.2.2.

In figure 3.4, we have plotted the decay of MP2 pair fragment energies with the pair distance R_{PQ} for the titin-I27_{SS} molecule taken from Ref. 61, (FOT= 10^{-4} a.u.). The

Table 3.1: MP2 correlation energy $E_{\text{MP2}}^{\text{corr}}$ (a.u.) and recovery of the correlation energy (%) from DEC and conventional calculations on a linear alkane chain $\text{C}_{48}\text{H}_{98}$. Time-to-solution is also reported. See appendix B.3 for computational details.

| FOT (a.u.) | $E_{\text{MP2}}^{\text{corr}}$ (a.u.) | Recovery (%) | Time (hours) |
|------------|---------------------------------------|--------------|--------------|
| 10^{-3} | -9.0848 | 99.11 | 2 |
| 10^{-4} | -9.1541 | 99.87 | 6 |
| 10^{-5} | -9.1646 | 99.98 | 23 |
| 0 (full) | -9.1660 | 100.0 | 55 |

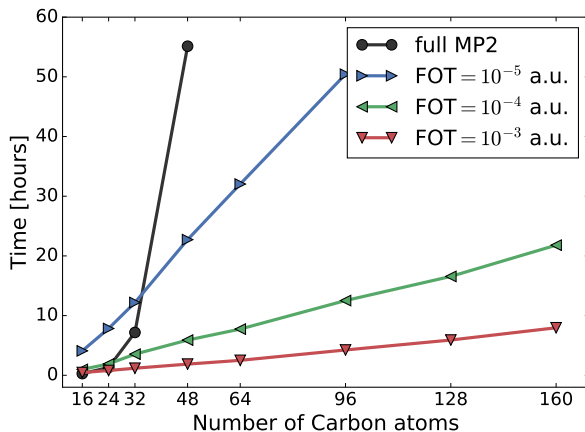


Figure 3.5: Timings of the DEC-MP2 and canonical MP2 algorithms for alkane chains of increasing length. See appendix B.3 for computational details.

plot shows the difference between the calculated pairs and the pairs that are screened away by the procedure outlined above. In the titin-I27_{SS} example, only about 13% of all the pair fragment energies have to be calculated, which represents significant savings and allows for a linear-scaling algorithm. The linear-scaling and error control features of the DEC-MP2 algorithm are also illustrated in figure 3.5 and table 3.1 for linear alkane chains.

3.2.4 Parallelism strategy

As we can see in figure 3.5, the DEC algorithm presented so far, scales linearly with the system size for large enough systems, *i.e.*, when the orbital spaces are saturated for a given FOT and when the number of pair fragments that survive the screening procedure grows linearly. However, due to the coupling effects in the amplitudes, the orbital spaces can become very large. As a consequence, a large amount of recalculation is required by the DEC strategy (the fragments overlap) and performing all the atomic and pair fragment calculations in series will result in a linear-scaling algorithm with a huge prefactor. In other words, the crossover of the time-to-solution between the DEC algorithm and a standard CC implementation will only occur for (very) large systems. Those observations are however dependent on the type of system considered and, as we can see in figure 3.5, the DEC-MP2 algorithm performs remarkably well even for linear chains of moderate size. Nonetheless, the range of application of the DEC scheme can be significantly extended by realizing that the atomic fragment and pair fragment energy calculations are completely independent of each other and can therefore be performed in parallel. This feature makes the DEC algorithm particularly well suited for super-computers and future architectures with many computing units.

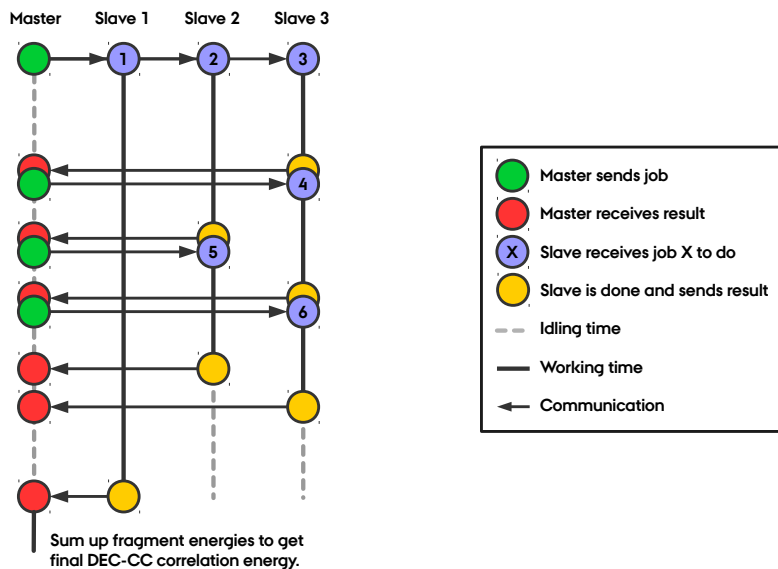


Figure 3.6: Coarse-grained parallelization of the DEC algorithm exemplified with four computing units and six fragment energies to be calculated.

In this section, we introduce the parallelization strategy used in DEC and summarize the different steps involved in a DEC calculation.

The DEC algorithm has been designed with three different levels of parallelization (coarse-, medium-, and fine-grained). The coarse-grained parallelization takes advantage of the independence of the fragment energy calculations, which can therefore be performed at the same time on different computing units. The medium- and fine-grained parallelizations are not specific to DEC and are designed to accelerate the solution of the CC amplitude equations inside each fragment energy calculation. In the following, we therefore focus exclusively on the coarse-grained level of parallelization and we refer to Ref. 62 and appendices B.3 and B.5 for more details.

At the coarse-grained level, the available computing units are divided into a *master* process, driving the DEC calculation and a set of *slaves*, executing the work. Assuming the fragment optimization has already been performed, the master starts by constructing a joblist where each job (an atomic or pair fragment energy calculation) is ordered based on an estimation of the workload (the size of the fragment orbital space). The master then communicates to each slave the information necessary to calculate a given fragment energy, starting with the largest fragments. Once every slave has a fragment energy to calculate, the master waits for the results from the slaves, and distributes the remaining jobs on the list as the slaves become available. When all the jobs have been distributed, the master waits for all the slaves to finish and to send their results. Finally, the master calculates the correlation energy based

on eq. (3.5). The coarse-grained parallelization of DEC is illustrated in figure 3.6.

Since a DEC calculation encompass three levels of parallelization, it is assumed that each slave in the procedure described above, has access to a subset of computing units which can be used at the medium- and fine-grained levels. The number of computing units allocated to each slave is then determined on-the-fly, based on the workload of the current job. This is important in order to minimize the idling time of all the computing units. Such a parallelism strategy allows the DEC algorithm to efficiently utilize several thousand computer nodes as demonstrated in appendices B.3 and B.5.

A typical DEC calculation can be summarized as follows.

1. Perform a conventional HF calculation on the whole system.
2. Localize the HF orbitals, for example, using a minimization of ξ_2^{SM} [see eq. (3.2a)].
3. Assign all localized orbitals to atomic sites, *i.e.*, set up \underline{P} , \underline{Q} , $\underline{R}\dots$ and \overline{P} , \overline{Q} , $\overline{R}\dots$
4. Perform the atomic fragment optimization procedure at the MP2 level, as illustrated in figure 3.3. All the atomic fragments are distributed to all the computing units.
5. Calculate the estimated MP2 pair fragment energies E_{PQ}^{esti} for all pairs (a real-space conservative threshold can also be used for very large systems, *e.g.*, $R_{\text{screen}} = 30 \text{ \AA}$).
6. Perform the atomic fragment and pair fragment energy calculations at the targeted CC level using the coarse-grained parallelization strategy (see figure 3.6).
7. Collect all the fragment energies and calculate the final DEC-CC correlation energy using eq. (3.5).

Note that point 6 is usually the time-dominating step in a DEC calculation and that in the case of a DEC-MP2 calculation only the pair fragment energies are calculated in that step since the atomic fragment energies are already known from the fragment optimization procedure.

3.3 Selected review of the state-of-the-art

In order to compare the DEC algorithm with other reduced scaling local CC methods, we now present a brief and non-exhaustive review of some of these methods. In particular, we focus on the following three strategies, the direct local CC methods, the cluster-in-molecule (CIM) approach, and the incremental scheme.

3.3.1 Direct local CC methods

In this section we briefly summarize the direct local CC methods in which the CC amplitude equations are solved only once for the whole system. For such models, a reduction in computational scaling is achieved by formulating the CC equations in a local basis in which a reduction of the number of wave-function parameters (the CC amplitudes) is possible.

The direct local CC methods employ localized orthogonal MOs for the occupied space [*e.g.*, Boys orbitals in eq. (3.1)], while the virtual space is usually spanned by non-orthogonal virtual orbitals. In the family of direct local CC methods, several strategies have been reported and they mainly differ in their choice of orbitals for the virtual space. Let us first present the common features of the direct methods using a generic non-orthogonal virtual basis (\check{a} , \check{b} , \check{c} ...) and then discuss the specificities of each method, including the choice of virtual orbitals.

The basic idea of the direct methods is to set up local domains of virtual orbitals, denoted $[i]$, for each localized occupied orbital i . The determination of the orbital domains is dependent on the choice of orbitals for the virtual space and they will therefore be discussed together. Pair domains $[ij]$, can then be defined as the union of the single domains, $[ij] = [i] \cup [j]$ and characterized as strong, weak, or distant pairs. While distant pairs are usually discarded, weak pairs can be computed at a lower level of theory than the targeted level (*e.g.*, MP2 instead of CCSD) and only strong pairs are calculated at the targeted level of theory. The characterization of the pairs can be done based on real-space cut-offs or preferably calculating estimates of the pair energies based on multipole expansions,^{63,64}

$$E_{ij}^{\text{OSV-DIP}} = \frac{8}{(R_{ij})^6} \sum_{\check{a} \in [i]} \sum_{\check{b} \in [j]} \frac{[\langle \phi_i | \mathbf{r} | \phi_{\check{a}} \rangle \cdot \langle \phi_j | \mathbf{r} | \phi_{\check{b}} \rangle]^2}{F_{ii} - \epsilon_{\check{a}} + F_{jj} - \epsilon_{\check{b}}}, \quad (3.17)$$

where a semi-canonical approach is used in the denominator, *i.e.*, the off-diagonal elements of the occupied Fock matrix have been neglected and the virtual orbitals have been canonicalized in the orbital domains. Once the orbital and pair domains have been defined and the strong pairs identified, the cluster operators can be written as,

$$T_1 = \sum_i \sum_{\check{a} \in [i]} t_i^{\check{a}} E_{\check{a}i}, \quad T_2 = \frac{1}{2} \sum_{ij} \sum_{\check{a}\check{b} \in [ij]} t_{ij}^{\check{a}\check{b}} E_{\check{a}i} E_{\check{b}j}, \quad (3.18)$$

and the CC amplitude equations become,

$$\Omega_i^{\check{a}} = 0, \quad \forall \check{a} \in [i], \quad (3.19a)$$

$$\Omega_{ij}^{\check{a}\check{b}} = 0, \quad \forall \check{a}, \check{b} \in [ij], \quad \forall i, j \in \{\text{strong pairs}\}. \quad (3.19b)$$

The non-orthogonality of the virtual space makes the computation of the CC vector function significantly more complicated and involve intensive book-keeping. We also

note that the CC equations above can be generalized to include triple excitations by introducing triples domains $[ijk]$.^{65–68} Let us now consider the details regarding the choice of the non-orthogonal virtual orbitals.

Projected atomic orbitals

As we mentioned in chapter 2, the basis sets $\{\chi_\mu\}$ used to build MOs are often constructed from non-orthogonal atomic orbitals which are by definition localized on the atomic sites. It then seems natural to try to transfer this locality to the virtual space by projecting the virtual CMOs on the set of AOs to obtain projected atomic orbitals (PAOs),^{56,65}

$$|\check{a}_\mu\rangle = \sum_a |a\rangle \langle a|\mu\rangle. \quad (3.20)$$

The PAOs \check{a}_μ can now be used in direct local CC methods as a set of non-orthogonal and redundant localized virtual orbitals. In PAO-based methods, the orbital domains $[i]$ are usually defined by considering a set of atoms $\{A\}$ where orbital i has a large Löwdin or Mulliken charge. The PAOs that are localized on atoms present in the set are then included in the orbital domain. The set of atoms $\{A\}$ can be fixed directly by a threshold (*i.e.*, all atoms where orbital i has a charge larger than τ_{charge} are included in the set) or using a Boughton–Pulay completion criterion,⁶⁹

$$BP^i = 1 - |(\phi_i - \tilde{\phi}_i)^2|, \quad (3.21)$$

where $\tilde{\phi}_i$ is expanded in the AOs assigned to the atoms present in the current set $\{A\}$ which is increased iteratively until $BP^i > \tau_{BP}$.

Successful local CC methods based on PAOs have been designed for the MP2,⁷⁰ CCSD, and CCSD(T) models.⁶⁵ However, the size of the (pair) domains grow quickly with the required accuracy and it seems that the community is now moving away from those methods.⁶⁴ Nonetheless, PAOs still play an important role in local CC methods as we will discuss below.

Orbital-specific virtuals

In order to reduce the size of the orbital domains, it is possible to generate a set of virtual orbitals that are not designed to be local but to efficiently describe correlation effects. To that end, orbital-specific virtuals (OSVs) can be generated by diagonalizing the MP2 diagonal pair density matrix,⁵⁷

$$\mathbf{D}^{(i)} \mathbf{U}^{(i)} = \mathbf{n}^{(i)} \mathbf{U}^{(i)}. \quad (3.22)$$

$$D_{ab}^{(i)} = 2 \sum_c t_{ii}^{ac} t_{ii}^{bc}. \quad (3.23)$$

The transformation from canonical virtual orbitals to OSVs is then given by,

$$|\check{a}_i\rangle = \sum_a U_{a\check{a}_i}^{(i)} |a\rangle. \quad (3.24)$$

Using OSVs, the MP2 pair correlation function,

$$E_{ij} = \sum_{\check{a}, \check{b} \in [ij]} t_{ij}^{\check{a}\check{b}} L_{i\check{a}j\check{b}}, \quad (3.25)$$

converges significantly faster than with PAOs, for a given number of virtual orbitals included in the pair domains $[ij]$.⁷¹ This observation suggests that the dimension of the virtual space can be reduced by employing OSVs compared to PAOs. In OSV-based local CC methods, the domains $[i]$ can thus be chosen either by ensuring that the error in the MP2 pair correlation function is below a given threshold or by including a subset of OSVs with the largest eigenvalues $n_{\check{a}_i}^{(i)}$. Linear-scaling implementation of the MP2,^{57,72} CCSD,⁷¹ and CCSD(T)⁶⁷ methods employing OSVs for the virtual space have been reported.

Pair natural orbitals (PNOs)

The virtual space can be further compressed by considering pair natural orbitals (PNOs), which can be seen as a generalization of OSVs for pairs of occupied orbitals. Instead of considering the MP2 diagonal pair density matrix, the complete pair density matrix is built for all strong pairs,^{58,59,73}

$$D_{ab}^{(ij)} = \frac{1}{1 + \delta_{ij}} \sum_c (\bar{t}_{ij}^{ac} t_{ij}^{bc} + \bar{t}_{ij}^{ca} t_{ij}^{cb}) \quad (3.26)$$

$$\bar{t}_{ij}^{ab} = 4t_{ij}^{ab} - 2t_{ij}^{ba}. \quad (3.27)$$

A diagonalization of the pair density matrix then yields the transformation matrices required to generate PNOs,

$$\mathbf{D}^{(ij)} \mathbf{U}^{(ij)} = \mathbf{n}^{(ij)} \mathbf{U}^{(ij)}, \quad (3.28)$$

$$|\check{a}_{ij}\rangle = \sum_a U_{a\check{a}_{ij}}^{(ij)} |a\rangle. \quad (3.29)$$

We note that PNOs usually provide an even more compact representation of the virtual space than OSVs for a comparable accuracy and that diagonal PNOs are equivalent to OSVs, $|\check{a}_{ii}\rangle \equiv |\check{a}_i\rangle$. Both orbital and pair domains can then be constructed directly by considering an energy based threshold for the pair correlation function in eq. (3.25) or by selecting the PNOs directly based on their eigenvalues.

In the above formulation both OSVs and PNOs require the optimization of the MP2 amplitudes which scale as $\mathcal{O}(N^5)$, with the system size. Such scaling is not

acceptable in the context of local CC methods and the usage of OSVs or PNOs seems to be compromised. However, it is possible to use the PAO domains defined previously to generate approximated MP2 amplitudes for a specific pair of localized occupied orbitals,⁶³

$$t_{ij}^{\check{a}\check{b}} = \frac{g_{\check{a}i\check{b}j}}{F_{ii} - \epsilon_{\check{a}} + F_{jj} - \epsilon_{\check{b}}}, \quad \forall \check{a}, \check{b} \in [ij]_{\text{PAO}}, \quad \forall i, j \in \{\text{strong pairs}\} \quad (3.30)$$

Using the amplitudes in eq. (3.30) to generate OSVs and PNOs removes the described bottlenecks without significant impact on the final set of virtual orbitals.

PNO-based local CC methods have become more and more popular in recent years and very efficient implementation have been reported for the MP2,^{74,75} CCSD,⁶³ and CCSD(T)^{66,68,76} models. In order to achieve linear-scaling for all operations, a framework has been developed^{74,76} to take advantage of the sparsity of the matrices and to facilitate the extensive book-keeping required by PNO methods. One of the key components of direct local CC methods is the use of density-fitting (DF) approximations for the two-electron integrals. In DF techniques like the resolution-of-the-identity^{77,78} or Cholesky decomposition,^{79,80} the four-center two-electron integrals are factorized into three-center coefficients,

$$g_{aibj} = \sum_I B_{ai}^I B_{bj}^I, \quad (3.31)$$

where the auxiliary index I runs over all non-redundant pairs of basis functions which scale linearly with the system size. Factorization techniques like DF have become very common in electronic-structure programs (*e.g.*, to reduce the computational and storage requirements of two-electron integrals) and are crucial for PNO-based methods in which a very large number of integral transformations is performed.⁶³

All in all, direct local CC methods can provide an accurate way of calculating CC correlation energies in a linear-scaling fashion. The price to pay for the compactness of the wave-function which leads to the reduction of the computational effort is a much more complex CC residual optimization routine. While such complexity is not compatible with embarrassingly parallel implementations, some parallel performances can be achieved by relying on more important communication phases.⁶⁴ We also note that the disk/memory requirements of the direct method scales linearly with the system size which can become problematic for very large systems.

3.3.2 Cluster-in-molecule

Let us now discuss a local CC method closely related to DEC, the cluster-in-molecule (CIM) approach. DEC and CIM rely on the same basic idea, namely, achieving linear-scaling by partitioning the CC correlation energy expression into a sum of fragment or cluster contributions. In CIM the partitioning of the energy is done at the orbital

level,

$$E_{CC}^{\text{corr}} = \sum_i E_i, \quad (3.32)$$

where E_i is the correlation energy of the cluster associated with occupied orbital i ,

$$E_i = \sum_{j \in \{\underline{i}\}} \sum_{ab \in \{\bar{i}\}} (t_i^a t_j^b + t_{ij}^{ab}) L_{iajb}. \quad (3.33)$$

This formulation is of course valid only when the occupied and virtual orbital spaces have been localized in some way and the spaces $\{\underline{i}\}$ and $\{\bar{i}\}$ thus denote a subset of occupied and virtual orbitals spatially close to orbital i . In the latest version of CIM by Li *et al.*,⁸¹ the construction of the clusters, *i.e.*, of the spaces $\{\underline{i}\}$ and $\{\bar{i}\}$, can be summarized as follows.

1. Localize the occupied space using the Boys localization function in eq. (3.1).
2. For a given occupied orbital i , construct the extended occupied space $\{\underline{i}\}$ using a distance cutoff, *i.e.*, include all orbitals j such that $R_{ij} < \tau_{\text{CIM}}$.
3. The set of basis functions $\{i\}_\chi$ used to describe the MOs in $\{\underline{i}\}$ are then determined using the Boughton–Pulay completion criterion, [see eq. (3.21)].
4. The virtual space $\{\bar{i}\}$ consists of PAOs obtained by projecting the occupied space of the full molecule out of the AOs included in the cluster,

$$|\check{a}_\mu\rangle = \left(1 - \sum_i^{\text{full}} |i\rangle \langle i|\right) |\mu\rangle, \quad \forall \mu \in \{i\}_\chi. \quad (3.34)$$

5. Finally, linear dependencies in the PAO basis are removed and a set of pseudo-canonical virtual orbitals can be obtained by diagonalizing the Fock matrix in the PAO space.

Once the clusters have been determined, standard CC calculations can be performed to obtain all the cluster energies using eq. (3.33). As in the DEC framework, all the cluster or fragment calculations are independent and can be performed in parallel. However, we note that in this formulation, the determination of the size of the clusters is fixed by the real-space cutoff, τ_{CIM} , which is therefore independent of the chemical environment and can lead to results of different quality for different systems. Another major difference with the DEC scheme concerns the balance between the description of the Coulomb hole and dispersion effects. Indeed, in CIM both effects are expected to be covered inside a given cluster (the clusters do not interact) which suggests that very large clusters might be required to describe dispersion effects properly.

Alternative formulations of CIM have been proposed to circumvent those potential problems. For example, Kállay and coworkers⁸² have combined the CIM energy

partitioning with approximated MP2 natural orbitals to determine the orbital spaces of the clusters. In this approach, primary spaces are generated based on the strategy outlined above in which a conservative distance cutoff is used. MP2 amplitudes are then calculated in the primary spaces in order to compute the following occupied and virtual density matrices,

$$D_{jk}^{(i)} = \sum_{ab} (2t_{ji}^{ab}t_{ki}^{ab} - t_{ji}^{ab}t_{ki}^{ba}) \quad (3.35a)$$

$$D_{ab}^{(i)} = \frac{1}{2} \sum_{cj} (3t_{ij}^{ca}t_{ij}^{cb} + t_{ij}^{ac}t_{ij}^{bc} - t_{ij}^{ca}t_{ij}^{bc} - t_{ij}^{ac}t_{ij}^{cb}), \quad (3.35b)$$

which are then diagonalized to provide a set of natural occupied and virtual orbitals. In the same spirit as for PNOs, the final occupied, $\{i\}$ and virtual, $\{\bar{i}\}$ spaces are then defined by keeping the natural orbitals with eigenvalues above a given threshold. Such a strategy allows for a more compact and more rigorous determination of the orbital spaces in each cluster and has been applied to the calculation of CCSD(T) correlation energies.⁸²

In a more recent work⁸³ the CIM partitioning of the CC correlation energy has been modified to include distant pairs explicitly and therefore correct for dispersion effects. To that end, primary orbital spaces are build based on localized occupied orbitals and PAOs using a procedure similar to the one described previously. Those primary spaces are then used to calculate pair correlation energies E_{ij} based on multipole expansions up to fourth-order (see eq. (3.17) for the first-order expression and Ref. 60 for higher orders). Each pair ij is then characterized as strong or distant based on the value of E_{ij} . The extended spaces $\{i\}$ are then formed by considering all occupied orbitals j that interact strongly with orbital i . The virtual spaces $\{\bar{i}\}$ are then made of PAOs, in line with the previously outlined strategy. Finally, the cluster energies are evaluated in the extended spaces using eq. (3.33) and the total correlation energy is given by,

$$E_{CC}^{\text{corr}} = \sum_i [E_i + \sum_{i < j} E_{ij}], \quad \forall j \in \{\text{distant pairs}\}, \quad (3.36)$$

where the pair correlation energies E_{ij} are only calculated based on multipole expansions. So far this strategy has only been reported at the MP2 level.⁸³

3.3.3 The incremental scheme

The incremental scheme, originally introduced by Stoll in Ref. 84 for the calculation of the correlation energy of crystals was later applied to CC theory. It can be seen as another local CC method based on a partitioning of the CC correlation energy (like DEC and CIM). As in the CIM approach, the incremental scheme relies on occupied orbitals localized using the Boys localization function and PAOs for the virtual space. The occupied orbital space is then divided into single domains \mathbb{S} that are determined

based on a connectivity matrix,

$$C_{ij} = \begin{cases} 10^8 & \text{if } R_{ij} \leq \tau \text{ and } fR_{ij}^{-1} \geq 10^8 \\ fR_{ij}^{-1} & \text{if } R_{ij} \leq \tau \text{ and } fR_{ij}^{-1} < 10^8 \\ 0 & \text{if } R_{ij} > \tau \end{cases} \quad (3.37)$$

where R_{ij} denotes the distance between the center of charge of orbitals i and j , τ is a distance threshold and f is a constant stretching factor. Once the connectivity matrix is known, the single domains \mathbb{S} are built by joining together a fix number of occupied orbitals which share large values in the connectivity matrix. We note that, the number of single domains is defined such that each occupied orbital is assigned to a unique domain. The virtual orbitals to consider in the domains are then determined as a subset of PAOs based on the Boughton–Pulay completion criterion in eq. (3.21). Pair domains \mathbb{D} , triple domains \mathbb{T} , *etc.*, are then defined as the union of single domains. Finally, the CC correlation energy is expressed as a many-body expansion,

$$E_{CC}^{\text{corr}} = \sum_{\mathbb{S}} \Delta E_{\mathbb{S}}^{\text{corr}} + \frac{1}{2} \sum_{\mathbb{D}} \Delta E_{\mathbb{D}}^{\text{corr}} + \frac{1}{3!} \sum_{\mathbb{T}} \Delta E_{\mathbb{T}}^{\text{corr}} + \dots, \quad (3.38)$$

where the exact correlation is recovered whenever the largest domain includes the complete orbital space. To obtain computational savings, the expansion can then be truncated to a given order (*e.g.*, second-order) and the domain’s contribution to the correlation energy are then given by,

$$\Delta E_{\mathbb{S}}^{\text{corr}} = E_{\mathbb{S}}^{\text{corr}}, \quad (3.39a)$$

$$\Delta E_{\mathbb{D}}^{\text{corr}} = E_{\mathbb{D}}^{\text{corr}} - \Delta E_{\mathbb{S}_1}^{\text{corr}} - \Delta E_{\mathbb{S}_2}^{\text{corr}}, \quad (3.39b)$$

where we have assumed $\mathbb{D} = \mathbb{S}_1 \cup \mathbb{S}_2$ and the energy contribution of a given domain \mathbb{X} is obtained by correlating all electrons in that domain,

$$E_{\mathbb{X}}^{\text{corr}} = \sum_{aibj \in \mathbb{X}} (t_i^a t_j^b + t_{ij}^{ab}) L_{iajb}. \quad (3.40)$$

In the incremental scheme, the accuracy is therefore controlled in two different ways, (i) by changing the order of the expansion in eq. (3.38), and (ii) by changing the number of occupied orbitals included in the single domains. We note that this measure is not dependent on the chemical environment of the orbitals which thus limits potential error control. Various flavors and applications of the incremental scheme have been reported, including the calculation of MP2, CCSD, and CCSD(T) ground state energies.^{85–87}

3.4 Conclusion

In this chapter we have presented some of the most important and recent developments in local CC methods with emphasis on the DEC scheme which is at the center of the

articles attached in appendices B.1 to B.5. A number of other methods have been developed with the aim of reducing the cost of CC calculations. However, for clarity, only the methods most closely related to the DEC scheme have been discussed here.

Enabling CC calculations on large molecules is a very active field and, as described in the previous sections, some remarkable advances have already been achieved. DEC stands out of the other local CC methods in two main points, (i) the DEC algorithm has been designed for super-computers and in that sense it is targeting the computers of tomorrow, (ii) the usage of local orthogonal virtual orbitals is specific to DEC and enables a number of attractive features such as the compatibility with conventional CC implementations (inside the fragments) and the calculation of molecular gradients.^{88,89} At this point, the application of the DEC-CCSD and DEC-CCSD(T) models to very large systems has not been possible due to size of the (pair) fragments. In order to remove those limitations, more approximations have to be introduced, such as relying on PNOs inside the fragments or performing a reduction of the pair fragments with a lower level CC model as it is done for the atomic fragments.

One aspect of electronic-structure calculation that lies outside the scope of this thesis is the convergence of the calculations with respect to the one-electron basis sets. Nonetheless, it is important to mention that most of the local CC methods, (including DEC),⁹⁰ have been developed in connection with explicitly correlated techniques to enable faster convergence to the complete basis set limit.

CHAPTER
FOUR

LOCAL CC METHODS FOR ELECTRONIC
TRANSITIONS



4.1 Introduction

The electronic ground state correlation energy—which was at the center of the previous chapter—is a size-extensive property, *i.e.*, it scales together with the size of the system.^{91,92} This indicates that any algorithm that attempts to calculate correlation energies has to scale at least linearly with the system size, as described in chapter 3. In contrast, transition properties, such as excitation energies and oscillator strengths, are size-intensive quantities, *i.e.*, they are independent of the system size.^{43,93} For electronic transitions localized to a small part of a molecule, it should therefore be possible to calculate the associated transition properties with a computational cost that is independent of the system size.

However, electronic transitions are not necessarily local and it is common to have transitions that are delocalized over many atomic sites.⁹⁴ In addition, the character of a given transition (*i.e.*, how it modifies the electronic density) cannot be known in advance. It is therefore not straightforward to apply the local approximations presented in the previous chapter to obtain accurate CC transition properties for all kinds of electronic transitions.⁹⁵ Until now, the calculation of transition properties of large molecules has thus been dominated by more affordable alternatives to CC response theory, such as time-dependent density-functional-theory (TDDFT).³³ The limitations of DFT methods are well known^{96–98} and it is therefore important to extend the applicability of CC response calculations to larger molecules.

The development of approximations to CC theory for the calculation of transition properties has become more and more active in the past 15 years. In the next sections, we briefly review some of those recent developments with emphasis on the LoFEx strategy which is presented in detail in the articles attached in appendices B.6 to B.8.

4.2 A local framework for calculating excitation energies

In this section, we present a local framework for calculating excitation energies denoted LoFEx. The main strategy of LoFEx is to generate a reduced set of orthogonal MOs designed for the description of a specific electronic transition. A standard CC calculation carried out in that reduced space should then result in an accurate CC excitation energy and oscillator strength. In LoFEx the reduction of the computational effort thus follows straightforwardly from the reduction of the occupied and the virtual orbital spaces.

4.2.1 Mixed orbital space

As pointed out previously, one important issue encountered when designing reduced scaling methods for calculating excitation energies is that the character of a given transition is *a priori* unknown. However, this information can often be obtained from low-level computational models such as CIS, and the concept of natural transition orbitals (NTOs) can be used to compress that information. NTOs are obtained by performing a singular-value-decomposition (SVD) of the one-particle transition density matrix \mathbf{b} ,^{99,100}

$$b_{ai} = \langle \Psi_m | E_{ai} | \Psi_0 \rangle, \quad (4.1)$$

where Ψ_0 and Ψ_m denote the electronic ground and excited states and are typically obtained from the HF and CIS methods, respectively. The transformation matrices from CMOs to NTOs are then given by the following eigenvalue problems,

$$\begin{aligned} \mathbf{D}^{o,\text{CIS}} \mathbf{U}^o &= \mathbf{n}^o \mathbf{U}^o & D_{ij}^{o,\text{CIS}} &= \sum_a b_{ai} b_{aj} \\ \mathbf{D}^{v,\text{CIS}} \mathbf{U}^v &= \mathbf{n}^v \mathbf{U}^v & D_{ab}^{v,\text{CIS}} &= \sum_i b_{ai} b_{bi} \end{aligned} \quad (4.2)$$

where the eigenvalues in the diagonal matrices \mathbf{n}^o and \mathbf{n}^v give an estimation of the importance of a given NTO to describe the transition associated with the matrix \mathbf{b} . In addition, the NTOs' eigenvalues have the following properties,

$$\begin{aligned} n_p^o &= n_p^v > 0 & 1 \leq p \leq N_o \\ n_p^v &= 0 & N_o < p \leq N_v \end{aligned} \quad (4.3)$$

where N_o (N_v) denotes the number of occupied (virtual) orbitals and we have assumed $N_o < N_v$. Most of the transitions of interest are dominated by single-electron replacements and for such transitions, the eigenvalues corresponding to pairs of NTOs are generally such that one of them is much larger than the others. In those cases, one pair of NTOs is therefore describing most of the transition effects and we have,

$$n_1 \simeq 1 \quad \sum_{p=2}^{N_o} n_p \ll 1. \quad (4.4)$$

NTOs have been almost exclusively used as a post-processing tool, *i.e.*, to analyze the character of electronic transitions described by a given wave-function (*e.g.*, CIS or TDDFT).^{100–103} In LoFEx however, we suggest to use CIS-NTOs to design a reduced orbital space in which a conventional CC calculation of transition properties can be performed. The CIS model, like HF, formally scales with the fourth power of the system size, but by employing adequate screening techniques, it is possible to achieve near linear-scaling,¹⁰⁴ and CIS-NTOs can therefore be generated for large systems.

CIS-NTOs provide the most compact description of the excitation described by the CIS transition density matrix. However, they do not contain any information about

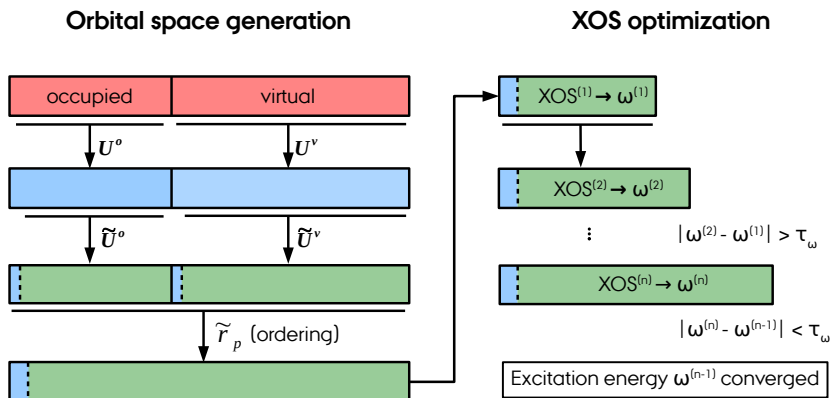


Figure 4.1: Summary of the LoFEx algorithm. The matrices \mathbf{U}^o and \mathbf{U}^v transform the occupied and virtual canonical molecular orbitals (CMOs in red) to natural transition orbitals (NTOs in blue). The dominant pair of NTOs is preserved, while the remaining orbitals are transformed to a local basis (LMOs in green) *via* the $\tilde{\mathbf{U}}^o$ and $\tilde{\mathbf{U}}^v$ matrices. The mixed orbital space is ordered according to \tilde{r}_p in eq. (4.5). Standard CC calculations are then performed on reduced excitation energy spaces (XOSs) of increasing dimensions until the excitation energy is converged.

correlation effects. For that reason, choosing a reduced set of orbitals for the correlated CC calculation as a subset of CIS-NTOs is likely to result in large and unpredictable errors.

In LoFEx, we therefore use the dominant pair of CIS-NTOs (the one with the largest singular-value) to obtain information about the main character of the targeted transition and the rest of the orbital space is localized, to enable an efficient description of correlation effects. After the CIS eigenvalue problem has been solved for all the transitions of interest, such a mixed orbital space (NTO/LMO) can be generated for each transition as depicted in the left part of figure 4.1.

4.2.2 XOS optimization

The mixed orbital space detailed in the previous section constitutes a set of orthogonal orbitals particularly well adapted to describe a specific transition. So far, the orbital space has not been reduced and a standard CC calculation in that space would be as expensive as in the complete canonical basis. In order to reduce the dimension of the mixed orbital space, the orbitals are ordered based on an estimated measure of their importance to describe the electronic transition of interest. Due to the locality of correlation effects, we use the effective distance \tilde{r}_p between a given LMO p and the

dominant pair of NTOs,

$$\tilde{r}_p = \min_A \left(\frac{r_{Ap}}{Q_A^{\text{CIS-NTO,o}}}, \frac{r_{Ap}}{Q_A^{\text{CIS-NTO,v}}} \right), \quad (4.5)$$

where index A denotes atomic sites, r_{Ap} corresponds to the distance between the center of charge of a local orbital p and atomic center A , and $Q_A^{\text{CIS-NTO,o}}$ and $Q_A^{\text{CIS-NTO,v}}$ are the Löwdin atomic charges (with values between 0 and 1) of the dominating occupied and virtual NTOs on center A , respectively. This effective distance is thus small if the center of orbital p is close to an atom where one (or both) of the CIS-NTOs have a large Löwdin charge. In other words, the smaller \tilde{r}_p is, the more important orbital p is expected to be to describe the targeted transition.

It is now possible to select a subset of orbitals with the smallest values \tilde{r}_p and to perform a standard CC calculation in that space to obtain the corresponding excitation energy and oscillator strength. This reduced space is denoted the excitation orbital space (XOS) and the CC response equations presented in section 2.5 and in appendix A can be solved in the XOS without further complications. For the CC2 model, it is however advantageous to move to a pseudo-canonical representation by diagonalizing the Fock matrix in the XOS such that expressions with orbital energies remain valid. In figure 4.2(b), we have plotted the convergence of the lowest CC2 excitation energy of dodecanoic acid with the size of the XOS. We see that, as expected, increasing the size of the XOS based on eq. (4.5) results in a smooth and fast convergence of the targeted excitation energy. However, it is not possible to know in advance how many orbitals should be included in the XOS to provide excitation energies with a controlled and limited error. To circumvent this problem, an optimization of the XOS is performed in which the XOS is increased iteratively until the variation in the excitation energy is below an energy threshold τ_ω [see figure 4.1 (right)].

From figure 4.1, we note that the last CC calculation in the XOS optimization is used to provide a reference value for the excitation energy $\omega^{(n-1)}$ calculated in the previous step, *i.e.*, $\omega^{(n-1)}$ can be considered converged to the desired accuracy. In general, it is of course more appropriate to report the values corresponding to $\omega^{(n)}$ since they are expected to be more accurate. However, for the calculation of CCSD excitation energies and CC2 oscillator strengths, the optimization of the XOS can be performed based on the CC2 excitation energy only, while the more expensive parts of the calculation (*i.e.*, the response equations for the CC2 oscillator strength or the solution of the CCSD eigenvalue problem) can be performed only once in the converged space (XOS $^{(n-1)}$). Such a strategy will result in more important computational savings with limited effects on the quantities of interest (see appendices B.7 and B.8 for more details).

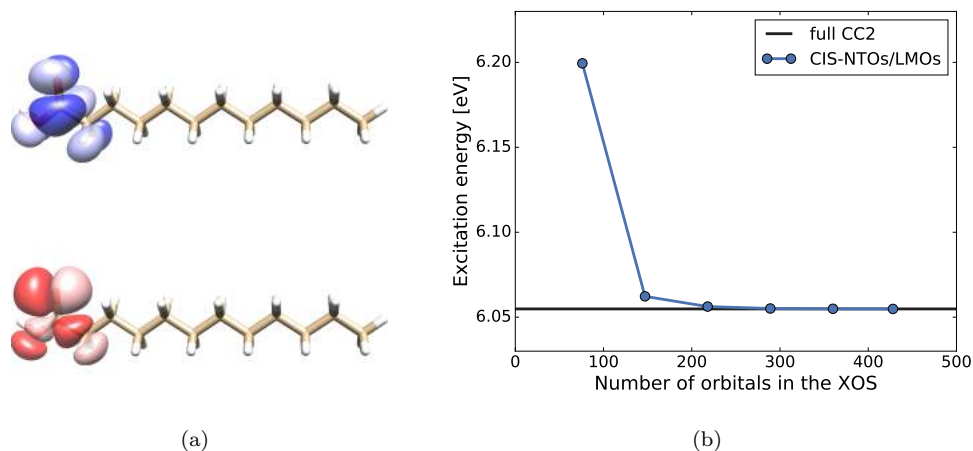


Figure 4.2: Left: virtual (top) and occupied (bottom) dominant CIS natural transition orbitals for the lowest transition of dodecanoic acid. A contour value of 0.02 a.u. was used. Right: Convergence of the lowest CC2 excitation energy of dodecanoic acid with the size of the excitation energy space (XOS) using a mixed orbital space (CIS-NTOs/LMOs).

4.2.3 Numerical illustrations

In the articles in appendices B.6 to B.8, we have shown that LoFEx can indeed be used to obtain accurate CC2 and CCSD excitation energies as well as CC2 oscillator strengths at a reduced computational cost. For example, we have calculated the lowest excitation energy and oscillator strength of the bivalirudin molecule (293 atoms and 4255 basis functions) at the CC2 level. The targeted transition is localized to a small part of the molecule and thus constitutes a best case scenario for LoFEx. In fact, LoFEx proved to be faster than TDDFT in that particular case (see table 4.1 and appendix B.8). For the calculation of CCSD excitation energies, computational savings are expected to be even more important due to the higher scaling of CCSD compared to CC2.¹⁰ However, the errors in the CCSD excitation energies depend on the quality of the CC2 optimized XOSs and larger errors are expected whenever the CC2 and CCSD models differ significantly (*e.g.*, for Rydberg states^{105,106}).

In table 4.2, we have reported a few representative results obtained with LoFEx when targeting CC2 excitation energies and oscillator strengths. In terms of accuracy, the results presented in table 4.2 are very satisfactory and confirm the black-box character of LoFEx with a strong error control. On the other hand, the computational savings obtained with LoFEx compared to conventional CC2 calculations are very system and transition dependent. Important speed-ups can be obtained (*e.g.*, 34 for met-enkephalin) but a reduction of the computational cost is not guaranteed. For example, the 11-cis-retinal molecule has a strongly delocalized electronic-structure

Table 4.1: Comparison of LoFEx and TDDFT/CAMB3LYP calculations of the lowest excitation energy ω and oscillator strength f of bivalirudin in an aug-cc-pVDZ' basis (293 atoms and 4255 basis functions). Timings are also reported. See appendix B.8 for computational details.

| Method | ω (eV) | f | Time (hours) |
|----------------|---------------|-------|--------------|
| CC2-LoFEx | 4.82 | 0.028 | 157 |
| TDDFT/CAMB3LYP | 5.01 | 0.029 | 205 |

Table 4.2: Lowest CC2 excitation energy ω and oscillator strength f obtained from LoFEx in an aug-cc-pVDZ' basis. The errors δ and speed-ups compared to conventional CC2 calculations are also reported. See appendix B.8 for computational details.

| System | ω (eV) | $\delta\omega$ (eV) | f | δf | Speed-up |
|----------------|---------------|---------------------|-------|------------|----------|
| 11-cis-retinal | 2.14 | 0.00 | 1.384 | 0.000 | 0.61 |
| Leupeptin | 4.27 | 0.01 | 0.001 | 0.000 | 3.37 |
| Latanoprost | 5.08 | 0.00 | 0.001 | 0.000 | 16.8 |
| Met-enkephalin | 4.78 | 0.00 | 0.024 | 0.002 | 34.0 |

which leads to the delocalized electronic transition represented by the dominant pair of CIS-NTOs in figure 4.3(a). In such a case, the complete set of LMOs has to be included in the XOS to properly correlate the dominant pair of CIS-NTOs, which prevents any computational savings with LoFEx (see table 4.2). This result is even more evident from figure 4.3(b) (blue curve), where a calculation of the lowest excitation energy of 11-cis-retinal is performed in a reduced mixed orbital space, which is progressively increased by adding LMOs based on eq. (4.5).

4.2.4 Generalized NTOs

In order to obtain computational savings even for systems with delocalized electronic transitions, such as 11-cis-retinal, we have investigated the possibility to generate NTOs that include information about the electronic correlation effects. If the CC2 Jacobian eigenvalue problem has been solved for the entire molecule we can consider a generalization of the CIS density matrices in eq. (4.2) as,

$$D_{ij}^{o,CC2} = \sum_a R_{ai} R_{aj} + \frac{1}{2} \sum_{abk} R_{ik}^{ab} R_{jk}^{ab}, \quad (4.6a)$$

$$D_{ab}^{v,CC2} = \sum_i R_{ai} R_{bi} + \frac{1}{2} \sum_{ijc} R_{ij}^{ac} R_{ij}^{bc}, \quad (4.6b)$$

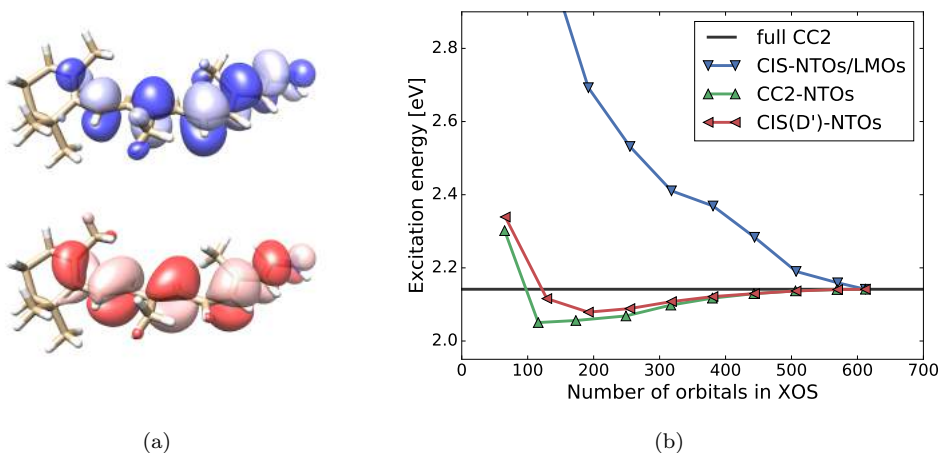


Figure 4.3: Left: virtual (top) and occupied (bottom) dominant CIS natural transition orbitals for the lowest transition of 11-cis-retinal. A contour value of 0.02 a.u. was used. Right: Convergence of the lowest CC2 excitation energy of 11-cis-retinal with the size of the excitation energy space (XOS) using different sets of orbitals.

where \mathbf{R} denotes the CC2 right excitation vector. The doubles part of the vector can be computed on-the-fly as,¹⁰⁷

$$R_{ij}^{ab} = \frac{\bar{g}_{aibj}}{\epsilon_i - \epsilon_a + \epsilon_j - \epsilon_b + \omega^{\text{CC2}}}, \quad (4.7)$$

where the two-electrons integrals are modified with the singles ground state and excitation amplitudes (see appendix A for details). By solving an eigenvalue problem for $\mathbf{D}^{o,\text{CC2}}$ and $\mathbf{D}^{v,\text{CC2}}$ in analogy with eq. (4.2), we obtain generalized CC2-NTOs in which correlation effects have been included through the doubles part of the excitation vector. In figure 4.3(b) (green curve), we have calculated the lowest CC2 excitation energy of 11-cis-retinal in an XOS composed of CC2-NTOs only, and where the size of the XOS is increased progressively by including more CC2-NTOs based on their eigenvalues (the ones with the largest eigenvalues are included first). As we can see, those generalized CC2-NTOs can be used to reduce the dimension of the orbital space without introducing significant errors, even for the delocalized transition in 11-cis-retinal and without relying on LMOs. The CC2-NTOs thus provide a much more compact representation of the CC2 excitation process and the selection of the orbitals to be included in the XOS can be directly based on the eigenvalues of the density matrices in eq. (4.6). However, such a strategy will not result in any computational savings for the calculation of CC2 excitation energies, since a solution of the CC2 eigenvalue problem in the full space is required to obtain the CC2-NTOs.

In order to obtain computational savings also when CC2 excitation energies are

targeted, we consider the following approximations to eq. (4.6),

$$D_{ij}^{o,\text{CIS}(\text{D}')} = D_{ij}^{o,\text{CIS}} + \frac{1}{2} \sum_{ABk} \tilde{R}_{ik}^{AB} \tilde{R}_{jk}^{AB}, \quad (4.8a)$$

$$D_{ab}^{v,\text{CIS}(\text{D}')} = D_{ab}^{v,\text{CIS}} + \frac{1}{2} \sum_{IJc} \tilde{R}_{IJ}^{ac} \tilde{R}_{IJ}^{bc}, \quad (4.8b)$$

where capital indices run over a subset of CIS-NTOs with the largest eigenvalues n_p^{CIS} . In addition, the doubles excitation vector has been approximated in the spirit of the CIS(D) model,¹⁰⁸

$$\tilde{R}_{ij}^{AB} = \frac{\bar{g}_{AiBj}}{\epsilon_i - F_{AA} + \epsilon_j - F_{BB} + \omega^{\text{CIS}}}, \quad (4.9a)$$

$$\tilde{R}_{IJ}^{ab} = \frac{\bar{g}_{aIbJ}}{F_{II} - \epsilon_a + F_{JJ} - \epsilon_b + \omega^{\text{CIS}}}, \quad (4.9b)$$

where the two-electron integrals are now only transformed with the CIS excitation vector and we have used diagonal elements of the Fock matrix instead of orbital energies when the CIS-NTO basis is used instead of canonical orbitals. The doubles vector \tilde{R}_{μ_2} , can thus be generated directly from CIS information only.

The NTOs obtained by diagonalization of the matrices in eq. (4.8) are expected to be a good approximation to the generalized CC2-NTOs and we denote them as CIS(D')-NTOs. In appendix B.9, we have shown that in the limit of large systems the computation of the CIS(D')-NTOs scales as $\mathcal{O}(N^3)$ with the system size compared to the generation of CC2-NTOs which scales as $\mathcal{O}(N^5)$ and requires iterative procedures. From figure 4.3(b) (red curve) we see that for the lowest state of 11-cis-retinal, the CIS(D')-NTOs provide a very good approximation to the CC2-NTOs, which indicates that computational savings are also possible for transitions with a more delocalized character.

In order to evaluate the quality of the CIS(D')-NTOs we have performed a series of CC2 calculations of excitation energies in an XOS defined by considering a subset of CIS(D')-NTOs based on their eigenvalues, $n_p^{o,\text{CIS}(\text{D}')}$ and $n_p^{v,\text{CIS}(\text{D}')}$. In table 4.3, we present a statistical analysis of the results obtained with this new strategy entitled SNOFLEx (Simplified Natural transition Orbital Framework for Large-scale coupled-cluster Excitation energy calculations). Three types of calculations are reported (*loose*, *standard*, and *tight*) corresponding to the different thresholds used to select the CIS-NTOs included in eq. (4.8) and to select the CIS(D')-NTOs to include in the XOS. The SNOFLEx strategy is presented in more details in appendix B.9. Even though the molecules used in our investigation are of limited sizes and often correspond to delocalized transitions (similar to 11-cis-retinal) the results in table 4.3 and appendix B.9 are very encouraging and indicate that the SNOFLEx strategy can be used to obtain accurate CC excitation energies for all types of transitions at a reduced computational cost. For example, when using the *standard* threshold, excitation energies with a mean absolute error of 0.01 eV are obtained compared to conventional

Table 4.3: Statistical analysis of the errors and the speed-ups obtained with the SNOFLE_x strategy, compared to conventional CC2 calculations in an aug-cc-pVDZ' basis. The *loose*, *standard*, and *tight* thresholds have been used to determine the CIS(D')-NTOs and the size of the XOS. See appendix B.9 for further details.

| Measure | <i>loose</i> | <i>standard</i> | <i>tight</i> |
|---------------------|--------------|-----------------|--------------|
| Mean absolute error | 0.11 | 0.01 | 0.00 |
| Max. absolute error | 0.28 | 0.02 | 0.01 |
| Mean error | 0.11 | -0.00 | -0.00 |
| Standard deviation | 0.07 | 0.01 | 0.00 |
| Max. speed-up | 96.2 | 54.7 | 33.5 |
| Min. speed-up | 1.5 | 1.0 | 0.8 |
| Mean speed-up | 6.7 | 3.9 | 2.6 |

CC2 calculations. Those calculations also correspond to a minimum and maximum speed-up of 1.0 and 54.7, respectively. These large deviations in the speed-ups come from the fact that the computational savings are very dependent on the size of the systems considered and that more important savings are usually obtained for larger molecules.

The use of correlated NTOs instead of the mixed orbital space used in LoFEx leads to two major simplifications. First, it avoids the localization of orbitals, which can become problematic or expensive when diffuse basis sets are used, as it is generally required in excited state calculations. And second, the quality of the CIS(D')-NTOs and of their associated eigenvalues seem to be sufficient to select the relevant orbitals to include in the XOS and the optimization of the XOS is no longer needed. More importantly, the strategy used in SNOFLE_x leads to computational savings for both local and delocalized transitions and thus overcomes the main limitation of the LoFEx scheme.

4.2.5 Treatment of multiple states

In a standard CC calculation of excitation energies, the CC Jacobian eigenvalue problem is solved in a common basis for all transitions of interest which ensure orthogonality between the different states. In the LoFEx and SNOFLE_x schemes however, each excitation energy is obtained by solving a Jacobian eigenvalue problem in the corresponding restricted XOS. The different XOSs are independent of each other and can be overlapping or not. It thus becomes important to ensure that, (i) for a given transition, the optimized eigenvalue corresponds to the targeted transition (the one used to generate the NTOs), and (ii) the optimized excitation vectors obtained in different XOSs are orthogonal to each other. In the LoFEx and SNOFLE_x schemes,

these two conditions are ensured by (i) targeting the Jacobian eigenvector that has the largest overlap with the starting guess provided by the CIS excitation vector, and (ii) projecting out previously optimized eigenvectors from the XOS of the transition under consideration to ensure orthogonality between the optimized excitation vectors.

Such a strategy was (partly) introduced in Ref. 9 and enabled the determination of multiple excitation energies. However, it is clear that the schemes presented here are very dependent on the quality of the CIS solutions, and transitions that do not appear in the CIS spectrum will not be recovered by higher level calculations. Improving our methods for multiple states calculations will thus have to be considered in future developments. We note however, that this dependence on the starting guess, is a general problem also present (albeit to a lesser extent) in conventional CC algorithms.

4.3 Selected review of the state-of-the-art

In this section we summarize other local CC methods for electronic transitions, with a focus on methods closely related to the LoFEx and SNOFLE_x schemes. Some of those methods are extensions of the models introduced in chapter 3 for ground state calculations, and the details that are in common between the formulations for ground states and electronic transitions are therefore not repeated here.

4.3.1 Direct local CC methods

Let us first look at two different extensions of the direct local CC methods to the calculation of CC2 excitation energies. The first one is a multistate approach relying on PAOs for the virtual orbitals, while the second method is state-specific and uses PNOs to span the virtual space. The two methods will thus be denoted as PAO-CC2 and PNO-CC2, respectively.

The PAO-CC2 model was introduced in Ref. 109 as a multistate version of the local CC2 algorithm presented in Ref. 110 (see also the pioneering work reported in Refs. 111–113). The method relies on the possibility to solve the CC2 Jacobian eigenvalue problem in the singles space only (instead of singles and doubles), as introduced in Ref. 107 and detailed in appendix A. The CC2 Jacobian eigenvalue problem is thus formulated as,

$$\sum_{\nu_1} A_{\mu_1\nu_1}^{\text{eff}}(\omega)R_{\nu_1} = \omega R_{\nu_1} \quad (4.10)$$

where the effective Jacobian matrix \mathbf{A}^{eff} is given by,

$$A_{\mu_1\nu_1}^{\text{eff}}(\omega) = A_{\mu_1\nu_1} - \sum_{\gamma_2} \frac{A_{\mu_1\gamma_2}A_{\gamma_2\nu_1}}{\epsilon_{\gamma_2} - \omega} \quad (4.11)$$

and the doubles component of the excitation vector can be obtained directly from eq. (4.7) in a canonical basis. In order to use the locality of correlation effects, a local basis has to be used, as discussed in chapter 3, and the partitioning of the CC2 equations described above seems to be compromised. However, a Laplace transformation of the orbital energy denominator in eq. (4.11) can be used to circumvent this problem and preserve the partitioning of the CC2 equations in a general (*i.e.*, non-canonical) basis.^{109,114}

Using these mathematical tricks, it is then possible to solve the CC2 equations in the complete singles space and to perform local approximations only in the generation of the doubles quantities (which are time-dominating in conventional CC2 implementations). As in PAO methods for ground states, the local approximations are introduced through orbital domains. However, to take into account the potential non-locality of electronic transitions, the orbital domains need to be adapted to each transition of interest. A reduced set of important local occupied orbitals is thus defined based on the single excitations vectors (either from CIS in the first iteration or from CC2 in the course of the optimization). Pair domains are then constructed from the union of singles domains with a reduced number of PAOs selected in the same way as for ground state PAO-based methods (see chapter 3). Since no approximations are introduced in the singles part of the excitation vector, the CC2 Jacobian eigenvalue problem can be solved (in the complete singles space) for all transitions of interest at the same time, which provides more flexibility and less dependence on the starting guess.

Test calculations revealed that the PAO-CC2 approach results in errors well below 0.1 eV compared to conventional CC2 excitation energies. Unfortunately the authors did not report calculations on systems that cannot be treated with a conventional CC2 implementation and it is thus difficult to quantify the performance of the method.^{109,115,116}

We now turn our attention to the generalization of PNO-based methods to the calculation of excitation energies. The generation of PNOs as presented in chapter 3, *i.e.*, based on approximated MP2 doubles amplitudes is not appropriate for a description of electronic transitions. Excited states PNOs can however be generated in a similar way, *i.e.*, by considering the CIS(D) doubles excitation vector, as suggested in Refs. 117 and 118, which can be approximated by relying on an intermediate PAO or OSV basis,

$$R_{ij}^{\check{a}\check{b}} = \frac{\bar{g}_{\check{a}\check{b}ij}}{F_{ii} - F_{\check{a}\check{a}} + F_{jj} - F_{\check{b}\check{b}} + \omega^{\text{CIS}}} \quad \forall \check{a}, \check{b} \in [ij]_{\text{PAO/OSV}}, \quad (4.12)$$

where the two-electrons integrals are transformed with the CIS excitation vector. Once the CC2 ground state equations have been solved in the ground state PNO basis, the Jacobian eigenvalue problem can be solved by restricting the indices of doubles quantities to the excited state PNO basis. Since the PNOs are specific to a given transition, an optimization procedure is repeated for each transition of interest, and

the Jacobian matrix is deflated, *i.e.*, all previously determined states are used to shift the corresponding eigenvalues in the spectrum and avoid collapsing to already known transitions.¹¹⁸ The excited state PNO basis is also updated whenever the overlap between the starting guess for the singles vector and the current singles excitation vector is too small.

Such a PNO-based CC2 model has shown promising results compared to a conventional implementation, both in terms of accuracy and computational cost.¹¹⁸ We note that, the algorithm is not specific to CC2 and can be extended to higher coupled cluster models or alternative second-order approximations.¹¹⁹

4.3.2 The incremental scheme

The incremental scheme presented in chapter 3 for ground state energies has also been applied to other properties, including first-order properties,¹²⁰ and frequency-dependent dipole polarizabilities.¹²¹ In this section, we summarize the application of the incremental scheme to the calculation of CCSD excitation energies as presented in Ref. 122.

In the incremental scheme the canonical occupied HF orbitals are first transformed to a mixed orbital space similar to the one used in LoFEx, *i.e.*, CIS-NTOs are calculated and the dominant occupied NTO is kept unaltered, while the remaining occupied orbitals are localized using the Pipek-Mezey method.⁴⁹ The mixed orbital space used in LoFEx was in fact inspired by Ref. 122. However, we note that in the incremental scheme, the virtual space is spanned by CMOs.

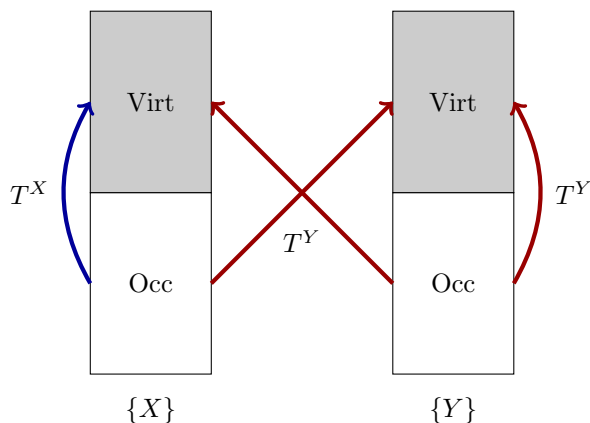
Once the mixed occupied orbital space has been generated, it is divided into single domains based on the distance between the orbitals' center of charge, such that each domain includes a predetermined number of occupied orbitals. The CC excitation energy corresponding to the current NTO is then expanded in a many-body series as,

$$\omega = \omega_{\mathbb{S}} + \sum_{\mathbb{D}} (\omega_{\mathbb{D}} - \omega_{\mathbb{S}}) + \dots \quad (4.13)$$

where \mathbb{S} denotes the single domain that includes the dominant occupied NTO, while \mathbb{D} denotes a pair domain built from the union of \mathbb{S} with another single domain. The excitation energy contributions $\omega_{\mathbb{X}}$ are then obtained by solving the CCSD eigenvalue problem in the restricted domain \mathbb{X} . We note that, since CMOs are used to span the virtual space, the complete set of virtual orbitals is included in each domain. For the calculation of several excitation energies, a root-homing strategy is employed to track the eigenvector with the largest overlap with the CIS starting guess, ensuring convergence to the correct state.

The incremental scheme with a two-body expansion has been tested on a set of small and medium-sized photoactive systems and compared to conventional CCSD results. Even though the complete set of virtual orbitals was included in each domain,

Figure 4.4: Schematic representation of the orbital space partitioning and excitation manifolds in multilevel coupled cluster theory. White block: occupied orbitals. Grey block: virtual orbitals. Blue arrow: excitations described by T^X . Red arrows: excitations described by T^Y .



the calculations presented in Ref. 122 resulted in some computational savings but with an average and maximum absolute deviations from the standard CCSD results of 0.08 and 0.3 eV, respectively. No improvements or extensions of this implementation have been reported so far.

4.3.3 Multilevel CC theory

In contrast with the direct local CC methods and the incremental scheme presented in the previous sections, the multilevel CC (MLCC) models have been designed specifically for the calculation of size-intensive properties such as excitation energies.

The basic idea of MLCC is to split the orbital space into subspaces determined based on their estimated importance to describe a given property. The cluster operator T is then partitioned into components that affect only some of the orbital subspaces and that can then be determined at different CC levels. For example, in the MLCC model entitled extended CC2 (ECC2),¹²³ the orbital space is divided into two parts ($\{X\}$ and $\{Y\}$, where $\{X\}$ is assumed to be more important than $\{Y\}$ for describing the targeted property) and the wave-function is written as,

$$|\text{ECC2}\rangle = \exp(T^X + T^Y) |\text{HF}\rangle, \quad (4.14)$$

where T^X performs excitations between orbitals included in $\{X\}$, while T^Y is allowed to perform excitations between orbitals included in $\{Y\}$ and between the two spaces $\{X\}$ and $\{Y\}$, as described in figure 4.4.

The MLCC amplitude equations are then defined by projecting the MLCC Schrödinger

equation against the different excitation manifolds,

$$\langle \mu^X | \exp(-T^X - T^Y) H \exp(T^X + T^Y) | \text{HF} \rangle = 0, \quad (4.15a)$$

$$\langle \mu^Y | \exp(-T^X - T^Y) H \exp(T^X + T^Y) | \text{HF} \rangle = 0, \quad (4.15b)$$

where the first equation determines the CC amplitudes in T^X , while the second equation determines T^Y . In the ECC2 model, both operators T^X and T^Y perform single and double excitations from the HF reference state, but in T^Y the doubles are approximated to be correct to first-order in the fluctuation potential, as in the CC2 model, while the doubles in T^X correspond to CCSD doubles.

Effectively, MLCC enables the description of different parts of a system at different CC levels, while maintaining couplings between all CC amplitudes. Such a strategy thus allows a high-level of description at a reduced computational cost. However, the choice of the MO basis and the partitioning of the orbital space is not obvious and usually relies on chemical intuition, which limits error control and the black-box character of standard CC theory is lost. Two main orbital space partitionings have been reported, (i) a selection based on orbital energies in the canonical basis (*i.e.*, frontier orbitals are chosen for $\{X\}$, while $\{Y\}$ correspond to the remaining orbitals) and (ii) a partitioning obtained from a Cholesky decomposition of the AO HF density matrix.¹²⁴ Several applications have been reported so far, including ECC2 and MLCC3 excitation energies,^{123,125} as well as core excitation energies.¹²⁶

4.4 Conclusion and perspective

The development of approximated CC models for the calculation of excitation energies and other frequency-dependent properties of large molecules is still in its infancy and a lot of work remains to be done. However, as discussed in this chapter, some progress has already been achieved and the combination of new computational models with more efficient computers already extends the calculation of CC excitation energies to larger molecules.

The LoFEx, SNOFLEx, and MLCC approaches have been designed specifically to take advantage of the size-intensivity of transition properties which enables a compact description of the transition effects and leads to important cost reductions. On the other hand, methods that are based on local CC approximations for ground states enable a more uniform description of size-intensive and size-extensive properties. This generality is however limiting the potential savings that can be obtained in the calculation of transition properties. In addition, we note that transition properties generally require larger orbital domains than ground state energies, leading to more expensive computational models.

Several other approximated CC methods have also been reported for the calculation of transition properties. We can for example mention the reduced virtual space^{127,128}

and the ONIOM^{129,130} strategies, which provide a pragmatic way to reduce the computational requirements of CC calculations.

In our perpetual quest for higher accuracy and lower computational cost, it will become important to address a number of challenges, such as the description of transitions dominated by more than one-electron replacements, and the treatment of the various kinds of frequency-dependent properties. More importantly, when targeting large molecules the density of electronic states becomes so high that several hundred states have to be computed to describe a significant part of the electronic spectrum. A conventional approach (diagonalization of the Jacobian matrix) is obviously not adapted in such cases and the state-specific algorithms often used in local approximations are even less appropriate. Alternative techniques which enable a description of electronic spectra without computing each transition individually are clearly needed. Such methods like damped response theory (also called complex polarization propagator (CPP) approach)^{131–133} or explicitly time-dependent approaches,¹³⁴ are already available, and a combination of those techniques with local approximations may be required for a proper description of electronic transitions of large molecules.

CHAPTER
FIVE

SUMMARY



5.1 English

This thesis describes the development of local approximations to coupled cluster (CC) theory for large molecules. Two different methods are presented, the divide–expand–consolidate scheme (DEC), for the calculation of ground state energies, and a local framework denoted LoFEx, for the calculation of electronic excitation energies and oscillator strengths. After an introduction to the relevant notions of electronic-structure theory, the principal aspects of DEC and LoFEx are summarized. For comparison, a selected review of the state-of-the-art is presented for each domain. This thesis should serve as an introduction to the work developed and presented in the scientific articles collected as appendices.

The DEC scheme has been applied successfully to the calculation of MP2, CCSD and CCSD(T) ground state energies. The intrinsic structure of DEC allows for a linear-scaling (with system size) and massively parallel implementation of CC theory. Applications to large molecules have been reported at the DEC-MP2 level but some limitations remain and prevent efficient and accurate large-scale applications of the DEC-CCSD and DEC-CCSD(T) models.

Regarding the calculation of electronic transition properties of large molecules, LoFEx has been introduced and applied to the CC2 and CCSD models. The black-box character of LoFEx has been demonstrated on medium-sized molecules and significant computational savings can be obtained depending on the character of the transition and on the size of the system. LoFEx has also been applied to large molecules with a computational cost competing with the most commonly used method (TDDFT), while maintaining CC accuracy. Finally, a new strategy has been proposed to overcome the main limitations of LoFEx and enable computational savings for all kinds of electronic transitions.

The development of CC theory for large molecules is still in its infancy, especially regarding the calculation of frequency-dependent molecular properties. Many challenges remain to be solved and some of the ideas presented in this thesis will hopefully open the door to more innovative and creative solutions.

5.2 Dansk

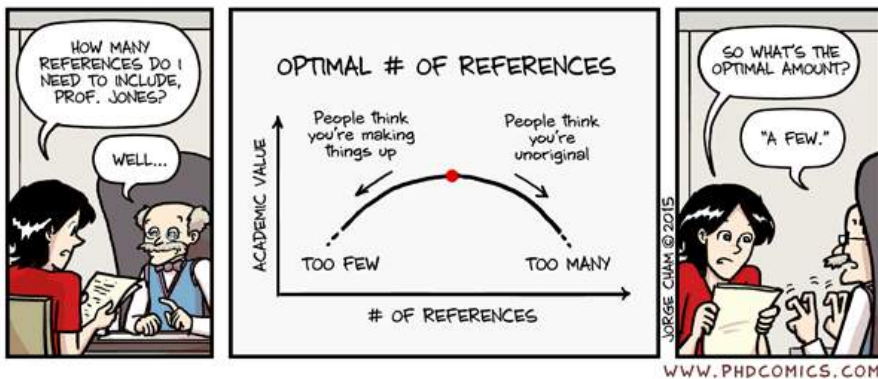
Denne afhandling beskriver udviklingen af lokale approksimationer til coupled cluster (CC) teori for store molekyler. To forskellige metoder er blevet præsenteret, i) divide-expand-consolidate (DEC), til beregning af grundtilstanden korrelation energier, og ii) LoFEx, et lokal framework til beregning af elektroniske eksitations energier og oscillator styrker. Efter en introduktion af de relevante begreber i elektron-struktur teori, er de vigtigste aspekter af DEC og LoFEx beskrevet. Til sammenligning, er en gennemgang af state-of-the-art for hvert domæne præsenteret. Denne afhandling skal tjene som en introduktion til arbejdet der er udviklet og præsenteret i de videnskabelige artikler samlet i appendix.

DEC metoden blevet anvendt med succes til beregning af MP2, CCSD og CCSD(T) grundtilstands energier. Strukturen af DEC giver mulighed for en linær-skalering (med systemet størrelse) og massivt parallel gennemførelse af CC teori. Anvendelse på store molekyler er blevet rapporteret ved DEC-MP2 modeller, men der er stadig nogle begrænsninger der forhindrer en effektiv og præcis anvendelser af DEC-CCSD og DEC-CCSD(T) modeller på stor skala.

Til beregning af elektroniske overgangsegenskaber af store molekyler, er LoFEx metoden blevet introduceret og udviklet for CC2 og CCSD modellerne. Black-box karakteren af LoFEx er blevet demonstreret på mellemstore molekyler og betydelige beregningsmæssige besparelser kan opnås afhængigt af karakteren på overgangen og størrelsen af systemet. LoFEx er også blevet anvendt på store molekyler, og det er vist at de beregningsmæssige omkostninger kan konkurrere med de mest almindeligt anvendte fremgangsmåder (TDDFT), under opretholdelse af CC nøjagtighed.

Udviklingen af CC teori for store molekyler er stadig i sin spæde begyndelse, især med henblik på beregning af frekvensafhængige molekylære egenskaber. Der er stadig mange udfordringer der skal løses, og forhåbentlig kan nogle af de ideer der præsenteres i denne afhandling åbne døren til mere innovative og kreative løsninger.

REFERENCES



- [1] K. Aidas, C. Angeli, K. L. Bak, V. Bakken, R. Bast, L. Boman, O. Christiansen, R. Cimiraglia, S. Coriani, P. Dahle, E. K. Dalskov, U. Ekström, T. Enevoldsen, J. J. Eriksen, P. Ettenhuber, B. Fernández, L. Ferrighi, H. Fliegl, L. Frediani, K. Hald, A. Halkier, C. Hättig, H. Heiberg, T. Helgaker, A. C. Hennum, H. Hettema, E. Hjertenaes, S. Høst, I.-M. Høyvik, M. F. Iozzi, B. Jansík, H. J. A. Jensen, D. Jonsson, P. Jørgensen, J. Kauczor, S. Kirpekar, T. Kjærgaard, W. Klopper, S. Knecht, R. Kobayashi, H. Koch, J. Kongsted, A. Krapp, K. Kristensen, A. Ligabue, O. B. Lutnaes, J. I. Melo, K. V. Mikkelsen, R. H. Myhre, C. Neiss, C. B. Nielsen, P. Norman, J. Olsen, J. M. H. Olsen, A. Osted, M. J. Packer, F. Pawłowski, T. B. Pedersen, P. F. Provasi, S. Reine, Z. Rinkevicius, T. a. Ruden, K. Ruud, V. V. Rybkin, P. Sałek, C. C. M. Samson, A. M. J. Sánchez de Merás, T. Saue, S. P. A. Sauer, B. Schimmelpfennig, K. Sneskov, A. H. Steindal, K. O. Sylvester-Hvid, P. R. Taylor, A. M. Teale, E. I. Tellgren, D. P. Tew, A. J. Thorvaldsen, L. Thøgersen, O. Vahtras, M. a. Watson, D. J. D. Wilson, M. Ziolkowski, and H. Ågren. *WIREs Comput. Mol. Sci.* **4**, 269 (2014).
- [2] *LSDalton, a linear-scaling molecular electronic structure program, Release Dalton2016 (2015), see <http://daltonprogram.org>.*
- [3] E. F. Pettersen, T. D. Goddard, C. C. Huang, G. S. Couch, D. M. Greenblatt, E. C. Meng, and T. E. Ferrin. *J. Comput. Phys.* **25**, 1605 (2004).
- [4] T. Kjærgaard, P. Baudin, D. Bykov, K. Kristensen, and P. Jørgensen. *Manuscript submitted to WIREs Comput. Mol. Sci.* 1–26 (2017).
- [5] P. Ettenhuber, P. Baudin, T. Kjærgaard, P. Jørgensen, and K. Kristensen. *J. Chem. Phys.* **144**, 164116 (2016).
- [6] P. Baudin, P. Ettenhuber, S. Reine, K. Kristensen, and T. Kjærgaard. *J. Chem. Phys.* **144**, 054102 (2016).
- [7] J. J. Eriksen, P. Baudin, P. Ettenhuber, K. Kristensen, T. Kjærgaard, and P. Jørgensen. *J. Chem. Theory Comput.* **11**, 2984 (2015).
- [8] T. Kjærgaard, P. Baudin, D. Bykov, J. J. Eriksen, P. Ettenhuber, K. Kristensen, J. Larkin, D. Liakh, F. Pawłowski, A. Vose, Y. M. Wang, and P. Jørgensen. *Comput. Phys. Commun.* **212**, 152 (2017).
- [9] P. Baudin, and K. Kristensen. *J. Chem. Phys.* **144**, 224106 (2016).
- [10] P. Baudin, D. Bykov, D. Liakh, P. Ettenhuber, and K. Kristensen. *Mol. Phys.* **MQM2016**, 1 (2017).
- [11] P. Baudin, T. Kjærgaard, and K. Kristensen. *Manuscript submitted to J. Chem. Phys.* 1–29 (2017).

- [12] P. Baudin, and K. Kristensen. *Manuscript in preparation* 1–33 (2017).
- [13] T. Helgaker, P. Jørgensen, and J. Olsen. *Molecular Electronic-Structure Theory*. First edition. John Wiley & Sons, Ltd, Chichester, UK (2000).
- [14] J. Čížek. *J. Chem. Phys.* **45**, 4256 (1966).
- [15] G. D. Purvis, and R. J. Bartlett. *J. Chem. Phys.* **76**, 1910 (1982).
- [16] H. Koch, O. Christiansen, R. Kobayashi, P. Jørgensen, and T. Helgaker. *Chem. Phys. Lett.* **228**, 233 (1994).
- [17] C. Møller, and M. S. Plesset. *Phys. Rev.* **46**, 618 (1934).
- [18] J. Olsen, O. Christiansen, H. Koch, and P. Jørgensen. *J. Chem. Phys.* **105**, 5082 (1996).
- [19] M. L. Leininger, W. D. Allen, H. F. Schaefer III, and C. D. Sherrill. *J. Chem. Phys.* **112**, 9213 (2000).
- [20] O. Christiansen, H. Koch, and P. Jørgensen. *Chem. Phys. Lett.* **243**, 409 (1995).
- [21] H. Koch, O. Christiansen, P. Jørgensen, A. M. J. Sánchez de Merás, and T. Helgaker. *J. Chem. Phys.* **106**, 1808 (1997).
- [22] J. F. Stanton, and J. Gauss. *J. Chem. Phys.* **103**, 1064 (1995).
- [23] S. R. Gwaltney, M. Nooijen, and R. J. Bartlett. *Chem. Phys. Lett.* **248**, 189 (1996).
- [24] J. Schirmer. *Phys. Rev. A* **26**, 2395 (1982).
- [25] E. S. Nielsen, P. Jørgensen, and J. Oddershede. *J. Chem. Phys.* **73**, 6238 (1980).
- [26] K. L. Bak, H. Koch, J. Oddershede, O. Christiansen, and S. P. A. Sauer. *J. Chem. Phys.* **112**, 4173 (2000).
- [27] O. Christiansen, H. Koch, and P. Jørgensen. *J. Chem. Phys.* **105**, 1451 (1996).
- [28] J. D. Watts, and R. J. Bartlett. *Chem. Phys. Lett.* **233**, 81 (1995).
- [29] J. D. Watts, and R. J. Bartlett. *Chem. Phys. Lett.* **258**, 581 (1996).
- [30] K. Kowalski, and P. Piecuch. *J. Chem. Phys.* **120**, 1715 (2004).
- [31] K. Raghavachari, G. W. Trucks, J. A. Pople, and M. Head-Gordon. *Chem. Phys. Lett.* **157**, 479 (1989).
- [32] J. J. Sakurai, and J. J. Napolitano. *Modern Quantum Mechanics*. Second edition. Addison-Wesley (2011).

- [33] L. González, D. Escudero, and L. Serrano-Andrés. *ChemPhysChem* **13**, 28 (2012).
- [34] K. Sneskov, and O. Christiansen. *WIREs Comput. Mol. Sci.* **2**, 566 (2012).
- [35] O. Christiansen, P. Jørgensen, and C. Hättig. *Int. J. Quantum Chem.* **68**, 1 (1998).
- [36] F. Pawłowski, J. Olsen, and P. Jørgensen. *J. Chem. Phys.* **142**, 114109 (2015).
- [37] H. Sams. *Phys. Rev. A* **7**, 2203 (1973).
- [38] F. Jensen. *Introduction to Computational Chemistry*. Second edition. John Wiley & Sons, Ltd, Chichester, UK (2007).
- [39] T. Helgaker, S. Coriani, P. Jørgensen, K. Kristensen, J. Olsen, and K. Ruud. *Chem. Rev.* **112**, 543 (2012).
- [40] O. Christiansen, A. Halkier, H. Koch, P. Jørgensen, and T. Helgaker. *J. Chem. Phys.* **108**, 2801 (1998).
- [41] J. F. Stanton, and R. J. Bartlett. *J. Chem. Phys.* **98**, 7029 (1993).
- [42] A. I. Krylov. *Annu. Rev. Phys. Chem.* **59**, 433 (2008).
- [43] H. Koch, R. Kobayashi, A. M. J. Sánchez de Merás, and P. Jørgensen. *J. Chem. Phys.* **100**, 4393 (1994).
- [44] M. Caricato, G. W. Trucks, and M. J. Frisch. *J. Chem. Phys.* **131**, 1 (2009).
- [45] E. Aprà, A. P. Rendell, R. J. Harrison, V. Tipparaju, W. a. DeJong, and S. S. Xantheas. *Proceedings of the Conference on High Performance Computing Networking, Storage Analysis - SC09* **66.1** (2009).
- [46] M. Katouda, and T. Nakajima. *J. Chem. Theory Comput.* **9**, 5373 (2013).
- [47] R. K. Nesbet. *Adv. Chem. Phys.* **IX**, 321 (1965).
- [48] S. Sæbø, and P. Pulay. *Annu. Rev. Phys. Chem.* **44**, 213 (1993).
- [49] J. Pipek, and P. G. Mezey. *J. Chem. Phys.* **90**, 4916 (1989).
- [50] S. F. Boys. *Rev. Mod. Phys.* **32**, 296 (1960).
- [51] C. Edmiston, and K. Ruedenberg. *Rev. Mod. Phys.* **35**, 457 (1963).
- [52] B. Jansík, S. Høst, K. Kristensen, and P. Jørgensen. *J. Chem. Phys.* **134**, 194104 (2011).
- [53] I.-M. Høyvik, B. Jansík, and P. Jørgensen. *J. Chem. Phys.* **137**, 224114 (2012).

- [54] I.-M. Høyvik, and P. Jørgensen. *Chem. Rev.* **116**, 3306 (2016).
- [55] I.-M. Høyvik, B. Jansík, and P. Jørgensen. *J. Chem. Theory Comput.* **8**, 3137 (2012).
- [56] P. Pulay. *Chem. Phys. Lett.* **100**, 151 (1983).
- [57] J. Yang, Y. Kurashige, F. R. Manby, and G. K.-L. Chan. *J. Chem. Phys.* **134**, 044123 (2011).
- [58] P.-O. Löwdin. *Phys. Rev.* **97**, 1474 (1955).
- [59] C. Edmiston. *J. Chem. Phys.* **45**, 1833 (1966).
- [60] G. Hetzer, P. Pulay, and H.-J. Werner. *Chem. Phys. Lett.* **290**, 143 (1998).
- [61] S. Reine, A. Krapp, M. F. Iozzi, V. Bakken, T. Helgaker, F. Pawłowski, and P. Sałek. *J. Chem. Phys.* **133**, 044102 (2010).
- [62] K. Kristensen, T. Kjærgaard, I.-M. Høyvik, P. Etenhuber, P. Jørgensen, B. Jansík, S. Reine, and J. Jakowski. *Mol. Phys.* **111**, 1196 (2013).
- [63] C. Riplinger, and F. Neese. *J. Chem. Phys.* **138**, 034106 (2013).
- [64] H.-J. Werner, G. Knizia, C. Krause, M. Schwilk, and M. Dornbach. *J. Chem. Theory Comput.* **11**, 484 (2015).
- [65] H.-J. Werner, and M. Schütz. *J. Chem. Phys.* **135**, 144116 (2011).
- [66] C. Riplinger, B. Sandhoefer, A. Hansen, and F. Neese. *J. Chem. Phys.* **139**, 134101 (2013).
- [67] M. Schütz, J. Yang, G. K.-L. Chan, F. R. Manby, and H.-J. Werner. *J. Chem. Phys.* **138**, 054109 (2013).
- [68] G. Schmitz, and C. Hättig. *J. Chem. Phys.* **145**, 234107 (2016).
- [69] J. W. Boughton, and P. Pulay. *J. Comput. Chem.* **14**, 736 (1993).
- [70] H.-J. Werner, F. R. Manby, and P. J. Knowles. *J. Chem. Phys.* **118**, 8149 (2003).
- [71] J. Yang, G. K.-L. Chan, F. R. Manby, M. Schütz, and H.-J. Werner. *J. Chem. Phys.* **136**, 144105 (2012).
- [72] Y. Kurashige, J. Yang, G. K.-L. Chan, and F. R. Manby. *J. Chem. Phys.* **136**, 124106 (2012).
- [73] F. Neese, F. Wennmohs, and A. Hansen. *J. Chem. Phys.* **130**, 114108 (2009).

- [74] P. Pinski, C. Riplinger, E. Valeev, and F. Neese. *J. Chem. Phys.* **143**, 34108 (2015).
- [75] G. Schmitz, B. Helmich, and C. Hättig. *Mol. Phys.* **111**, 2463 (2013).
- [76] C. Riplinger, P. Pinski, U. Becker, E. Valeev, and F. Neese. *J. Chem. Phys.* **144**, 024109 (2016).
- [77] J. L. Whitten. *J. Chem. Phys.* **58**, 4496 (1973).
- [78] M. Feyereisen, G. Fitzgerald, and A. Komornicki. *Chem. Phys. Lett.* **208**, 359 (1993).
- [79] N. H. F. Beebe, and J. Linderberg. *Int. J. Quantum Chem.* **12**, 683 (1977).
- [80] H. Koch, A. M. J. Sánchez de Merás, and T. B. Pedersen. *J. Chem. Phys.* **118**, 9481 (2003).
- [81] W. Li, Z. Ni, and S. Li. *Mol. Phys.* **114**, 1447 (2016).
- [82] Z. Rolik, L. Szegedy, I. Ladjánszki, B. Ladóczki, and M. Kállay. *J. Chem. Phys.* **139**, 094105 (2013).
- [83] P. R. Nagy, G. Samu, and M. Kállay. *J. Chem. Theory Comput.* **12**, 4897 (2016).
- [84] H. Stoll. *Chem. Phys. Lett.* **191**, 548 (1992).
- [85] J. Friedrich, M. Hanrath, and M. Dolg. *J. Chem. Phys.* **126**, 154110 (2007).
- [86] J. Friedrich, and M. Dolg. *J. Chem. Theory Comput.* **5**, 287 (2009).
- [87] K. Walczak, J. Friedrich, and M. Dolg. *Chem. Phys.* **376**, 36 (2010).
- [88] K. Kristensen, P. Jørgensen, B. Jansík, T. Kjærgaard, and S. Reine. *J. Chem. Phys.* **137**, 114102 (2012).
- [89] D. Bykov, K. Kristensen, and T. Kjærgaard. *J. Chem. Phys.* **145**, 024106 (2016).
- [90] Y. M. Wang, C. Hättig, S. Reine, E. Valeev, T. Kjærgaard, and K. Kristensen. *J. Chem. Phys.* **144**, 204112 (2016).
- [91] R. J. Bartlett, and G. D. Purvis. *Int. J. Quantum Chem.* **14**, 561 (1978).
- [92] R. J. Bartlett. *Annu. Rev. Phys. Chem.* **32**, 359 (1981).
- [93] H. Koch, H. J. A. Jensen, P. Jørgensen, and T. Helgaker. *J. Chem. Phys.* **93**, 3345 (1990).
- [94] T. Etienne. *J. Chem. Theory Comput.* **11**, 1692 (2015).

- [95] T. D. Crawford. In P. Cársky, J. Paldus, and J. Pittner (Eds.), *Recent Progress in Coupled Cluster Methods: Theory and Applications*, volume 53, chapter 2, 37–55. Springer Netherlands, Dordrecht (2010).
- [96] A. J. Cohen, P. Mori-Sanchez, and W. Yang. *Science* **321**, 792 (2008).
- [97] A. Dreuw, and M. Head-Gordon. *J. Am. Chem. Soc.* **126**, 4007 (2004).
- [98] J. J. Eriksen, S. P. A. Sauer, K. V. Mikkelsen, O. Christiansen, H. J. A. Jensen, and J. Kongsted. *Mol. Phys.* **111**, 1235 (2013).
- [99] A. V. Luzanov, A. A. Sukhorukov, and V. E. Umanskii. *Theor. Exp. Chem.* **10**, 354 (1976).
- [100] R. L. Martin. *J. Chem. Phys.* **118**, 4775 (2003).
- [101] T. Etienne. *J. Chem. Phys.* **142**, 244103 (2015).
- [102] F. Plasser, B. Thomitzni, S. A. Bäßler, J. Wenzel, D. R. Rehn, M. Wormit, and A. Dreuw. *J. Comput. Chem.* **36**, 1609 (2015).
- [103] F. Plasser. *J. Chem. Phys.* **144**, 194107 (2016).
- [104] C. M. Isborn, N. Luehr, I. S. Ufimtsev, and T. J. Martínez. *J. Chem. Theory Comput.* **7**, 1814 (2011).
- [105] J. J. Goings, M. Caricato, M. J. Frisch, and X. Li. *J. Chem. Phys.* **141**, 164116 (2014).
- [106] H. H. Falden, K. R. Falster-Hansen, K. L. Bak, S. Rettrup, and S. P. A. Sauer. *J. Phys. Chem. A* **113**, 11995 (2009).
- [107] C. Hättig, and F. Weigend. *J. Chem. Phys.* **113**, 5154 (2000).
- [108] M. Head-Gordon, R. J. Rico, M. Oumi, and T. J. Lee. *Chem. Phys. Lett.* **219**, 21 (1994).
- [109] D. Kats, and M. Schütz. *J. Chem. Phys.* **131**, 124117 (2009).
- [110] D. Kats, T. Korona, and M. Schütz. *J. Chem. Phys.* **125**, 104106 (2006).
- [111] D. Kats, T. Korona, and M. Schütz. *J. Chem. Phys.* **127**, 064107 (2007).
- [112] T. D. Crawford, and R. A. King. *Chem. Phys. Lett.* **366**, 611 (2002).
- [113] T. Korona, and H.-J. Werner. *J. Chem. Phys.* **118**, 3006 (2003).
- [114] J. Almlöf. *Chem. Phys. Lett.* **181**, 319 (1991).
- [115] D. Kats, and M. Schütz. *Zeitschrift für Phys. Chemie* **224**, 601 (2010).

- [116] K. Freundorfer, D. Kats, T. Korona, and M. Schütz. *J. Chem. Phys.* **133**, 244110 (2010).
- [117] B. Helmich, and C. Hättig. *J. Chem. Phys.* **135**, 214106 (2011).
- [118] B. Helmich, and C. Hättig. *J. Chem. Phys.* **139**, 084114 (2013).
- [119] B. Helmich, and C. Hättig. *Comput. Theor. Chem.* **1040-1041**, 35 (2014).
- [120] J. Friedrich, S. Coriani, T. Helgaker, and M. Dolg. *J. Chem. Phys.* **131**, 154102 (2009).
- [121] J. Friedrich, H. R. McAlexander, A. Kumar, and T. D. Crawford. *Phys. Chem. Chem. Phys.* **17**, 14284 (2015).
- [122] R. A. Mata, and H. Stoll. *J. Chem. Phys.* **134**, 034122 (2011).
- [123] R. H. Myhre, A. M. J. Sánchez de Merás, and H. Koch. *Mol. Phys.* **111**, 1109 (2013).
- [124] R. H. Myhre, A. M. J. Sánchez de Merás, and H. Koch. *J. Chem. Phys.* **141**, 224105 (2014).
- [125] R. H. Myhre, and H. Koch. *J. Chem. Phys.* **145**, 044111 (2016).
- [126] R. H. Myhre, S. Coriani, and H. Koch. *J. Chem. Theory Comput.* **12**, 2633 (2016).
- [127] R. Send, V. R. I. Kaila, and D. Sundholm. *J. Chem. Phys.* **134**, 1 (2011).
- [128] A. Kumar, and T. D. Crawford. *J. Phys. Chem. A* **Article**, ASAP (2017).
- [129] M. Caricato, T. Vreven, G. W. Trucks, and M. J. Frisch. *J. Chem. Phys.* **133**, 054104 (2010).
- [130] M. Caricato, T. Vreven, G. W. Trucks, and M. J. Frisch. *J. Chem. Theory Comput.* **7**, 180 (2011).
- [131] B. J. Orr, and J. F. Ward. *Mol. Phys.* **30**, 513 (1971).
- [132] P. Norman, D. M. Bishop, H. J. A. Jensen, and J. Oddershede. *J. Chem. Phys.* **123**, 194103 (2005).
- [133] K. Kristensen, J. Kauczor, T. Kjærgaard, and P. Jørgensen. *J. Chem. Phys.* **131**, 044112 (2009).
- [134] D. R. Nascimento, and A. E. DePrince. *J. Chem. Theory Comput.* **12**, 5834 (2016).
- [135] C. Hättig, and A. Köhn. *J. Chem. Phys.* **117**, 6939 (2002).

CCS AND CC2 WORKING EQUATIONS



A.1 Overview

In section 2.5 we arrived at a set of general equations for the calculation of excitation energies and transition strengths using CC linear response theory. In this appendix we go in more details about the form of the equations for the CCS and CC2 models and derive working equations that can be directly implemented in quantum chemistry programs. The original goal of this derivation was to recover the working equations presented in Refs. 107, 135 and to implement them in the LSDALTON program.^{1,2}

In the following derivation we focus primarily on the CC2 equations from which the CCS equations follow straightforwardly. A canonical basis of spin-free HF orbitals is used throughout the derivations and we assume the ground state amplitudes to be already optimized, *i.e.*, the following non-linear equations have been solved,

$$\Omega_i^a = \langle \tilde{a} | \tilde{H} + [\tilde{H}, T_2] | \text{HF} \rangle = 0 \quad (\text{A.1})$$

$$\Omega_{ij}^{ab} = \langle \tilde{ab} | \tilde{H} + [F, T_2] | \text{HF} \rangle = 0 \quad (\text{A.2})$$

where the double cluster operator is given by

$$T_2 = \frac{1}{2} \sum_{aibj} t_{ij}^{ab} E_{ai} E_{bj}. \quad (\text{A.3})$$

And the following biorthonormal basis is used,

$$\langle \tilde{ab} |_{ji} = \langle \text{HF} | E_{jb} E_{ia}, \quad (\text{A.4a})$$

$$| \tilde{ab} \rangle_{ji} = E_{ai} E_{bj} | \text{HF} \rangle, \quad (\text{A.4b})$$

$$\langle \tilde{ab} |_{ij} = \frac{1}{1 + \delta_{ai,bj}} \left(\frac{1}{3} \langle \tilde{ab} |_{ij} + \frac{1}{6} \langle \tilde{ab} |_{ji} \right), \quad (\text{A.4c})$$

$$\langle \tilde{ab} |_{ij} | \tilde{cd} \rangle_{kl} = \delta_{aibj,ckdl}. \quad (\text{A.4d})$$

Once the ground state amplitudes have been optimized the calculation of transition strengths (and excitation energies) requires the determination of the following quantities (see section 2.5).

- The zero-order (frequency-independent) Lagrange multipliers $\bar{\mathbf{t}}$,

$$\bar{\mathbf{t}}\mathbf{J} = -\boldsymbol{\eta}, \quad (\text{A.5})$$

- the right Jacobian excitation vectors \mathbf{R} ,

$$\mathbf{J}\mathbf{R} = \boldsymbol{\omega}\mathbf{R} \quad (\text{A.6})$$

- the left Jacobian excitation vectors \mathbf{L}

$$\mathbf{L}\mathbf{J} = \mathbf{L}\boldsymbol{\omega} \quad (\text{A.7})$$

- and the transition moment Lagrange multipliers $\bar{\mathbf{M}}$

$$\bar{\mathbf{M}}(\mathbf{J} + \omega \mathbf{1}) = -(\mathbf{R})^T \mathbf{F} \quad (\text{A.8})$$

where we have dropped the indices denoting the targeted (excited) state. Eqs. (A.5) and (A.6) must be solved before eq. (A.8) since the right-hand-side of eq. (A.8) depends on $\bar{\mathbf{t}}$ and \mathbf{R} .

A.1.1 The CC2 effective Jacobian

The CC2 Jacobian can be obtained by differentiation of the CC2 vector function with respect to the ground state amplitudes. To avoid δ factors in the Jacobian we rewrite the doubles cluster operator as,

$$T_2 = \frac{1}{2} \sum_{aibj} (1 + \delta_{ij} \delta_{ab}) \check{t}_{ij}^{ab} E_{ai} E_{ij} \quad (\text{A.9})$$

where

$$\check{t}_{ij}^{ab} = \frac{1}{1 + \delta_{ij} \delta_{ab}} t_{ij}^{ab} = \frac{1}{(1 + \delta_{ij} \delta_{ab})} \frac{\tilde{g}_{aibj}}{(\epsilon_i - \epsilon_a + \epsilon_j - \epsilon_b)} \quad (\text{A.10})$$

The CC2 Jacobian can then be defined as,

$$J_{\mu_i \nu_j} = \frac{\partial \Omega_{\mu_i}}{\partial \check{t}_{\nu_j}} \quad (\text{A.11})$$

$$J_{ai,ck} = \langle \tilde{a} | [\tilde{H}, E_{ck}] + [[\tilde{H}, E_{ck}], T_2] | \text{HF} \rangle \quad (\text{A.12})$$

$$J_{ai,ckdl} = \langle \tilde{a} | [\tilde{H}, E_{ck} E_{dl}] | \text{HF} \rangle \quad (\text{A.13})$$

$$J_{aibj,ck} = \langle \tilde{a} | [\tilde{H}, E_{ck}] | \text{HF} \rangle \quad (\text{A.14})$$

$$J_{aibj,ckdl} = \langle \tilde{a} | [F, E_{ck} E_{dl}] | \text{HF} \rangle = \delta_{aibj,ckdl} (\epsilon_a - \epsilon_i + \epsilon_b - \epsilon_j) \quad (\text{A.15})$$

Due to the diagonal form of the doubles-doubles block of the CC2 Jacobian, eqs. (A.5) to (A.8), can be formulated as effective singles equations in which the doubles quantities are computed on-the-fly. By anticipation, let us introduce the following effective CC2 Jacobian matrix,

$$J_{ai,bj}^{\text{eff}}(\omega) = \left[J_{ai,bj} - \sum_{ckdl} \frac{J_{ai,ckdl} J_{ckdl,bj}}{\epsilon_c - \epsilon_k + \epsilon_d - \epsilon_l - \omega} \right] \quad (\text{A.16})$$

$$= \left[J_{ai,bj} + \sum_{ckdl} \frac{J_{ai,ckdl} J_{ckdl,bj}}{\epsilon_k - \epsilon_c + \epsilon_l - \epsilon_d + \omega} \right] \quad (\text{A.17})$$

where the summation is not restricted and does not contain a factor half. We note that eqs. (A.5), (A.7) and (A.8) can be written in the following general form (see table A.1),

$$\mathbf{XJ} = \alpha \omega \mathbf{X} - \beta, \quad (\text{A.18})$$

Table A.1: General form of the left equations for CC2 transition strengths.

| $\mathbf{XJ} = \alpha\omega\mathbf{X} - \boldsymbol{\beta}$ | \mathbf{X} | α | $\boldsymbol{\beta}$ |
|---|--------------------|----------|----------------------------|
| $\bar{\mathbf{t}}\mathbf{J} = -\boldsymbol{\eta}$ | $\bar{\mathbf{t}}$ | 0 | $\boldsymbol{\eta}$ |
| $\mathbf{LJ} = \omega\mathbf{L}$ | \mathbf{L} | 1 | $\mathbf{0}$ |
| $\bar{\mathbf{M}}\mathbf{J} = -\omega\bar{\mathbf{M}} - (\mathbf{R})^T\mathbf{F}$ | $\bar{\mathbf{M}}$ | -1 | $(\mathbf{R})^T\mathbf{F}$ |

which can be reformulated as,

$$(X_1, X_2) \begin{pmatrix} J_{11}, & J_{12} \\ J_{21}, & \epsilon_2\mathbf{1} \end{pmatrix} = \alpha\omega(X_1, X_2) - (\beta_1, \beta_2) \quad (\text{A.19})$$

where ϵ_2 corresponds to a linear combination of orbital energies such as $\epsilon_a - \epsilon_i + \epsilon_b - \epsilon_j$. From eq. (A.18) we get the following system of equations,

$$\begin{cases} X_1 J_{11} + X_2 J_{21} = \alpha\omega X_1 - \beta_1 \\ X_1 J_{12} + X_2 \epsilon_2 = \alpha\omega X_2 - \beta_2 \end{cases} \quad (\text{A.20})$$

From the second line we get,

$$X_2(\epsilon_2 - \alpha\omega) = -\beta_2 - X_1 J_{12} \quad (\text{A.21})$$

The doubles can then be computed directly as,

$$X_2 = -\frac{\beta_2 + X_1 J_{12}}{\epsilon_2 - \alpha\omega} \quad (\text{A.22})$$

Using X_2 in the first line of eq. (A.20) we get,

$$X_1 J_{11} - \frac{\beta_2 + X_1 J_{12}}{\epsilon_2 - \alpha\omega} J_{21} = \alpha\omega X_1 - \beta_1, \quad (\text{A.23})$$

rearranging,

$$X_1 \left[J_{11} - \frac{J_{12} J_{21}}{\epsilon_2 - \alpha\omega} - \alpha\omega \right] = -\left[\beta_1 - \frac{\beta_2 J_{21}}{\epsilon_2 - \alpha\omega} \right], \quad (\text{A.24})$$

$$X_1 \left[J_{11}^{\text{eff}}(\alpha\omega) - \alpha\omega \right] = -\beta_1^{\text{eff}}, \quad (\text{A.25})$$

Using table A.1, we finally obtain the following effective singles equations,

$$\bar{\mathbf{t}}_1 \mathbf{J}_{11}^{\text{eff}}(0) = -\boldsymbol{\eta}_1^{\text{eff}}, \quad (\text{A.26})$$

$$\mathbf{L}_1 \mathbf{J}_{11}^{\text{eff}}(\omega) = \mathbf{L}_1 \omega, \quad (\text{A.27})$$

$$\bar{\mathbf{M}}_1 \left[\mathbf{J}_{11}^{\text{eff}}(-\omega) + \omega\mathbf{1} \right] = -\bar{\mathbf{m}}_1^{\text{eff}}, \quad (\text{A.28})$$

where,

$$\eta_{ai}^{\text{eff}} = \eta_{ai} + \sum_{ckdl} \frac{\eta_{kl}^{cd} J_{ckdl,ai}}{\epsilon_k - \epsilon_c + \epsilon_l - \epsilon_d} \quad (\text{A.29})$$

$$\bar{m}_{ai}^{\text{eff}} = \bar{m}_{ai} + \sum_{ckdl} \frac{\bar{m}_{kl}^{cd} J_{ckdl,ai}}{\epsilon_k - \epsilon_c + \epsilon_l - \epsilon_d - \omega} \quad (\text{A.30})$$

with $\bar{\mathbf{m}} = (\mathbf{R})^T \mathbf{F}$. A similar expression is easily obtained for the right eigenvalue problem,

$$\mathbf{J}_{11}^{\text{eff}}(\omega) \mathbf{R}_1 = \omega \mathbf{R}_1. \quad (\text{A.31})$$

In order to solve the above equations in a standard quantum chemistry program we need to obtain working equations for a trial vector \mathbf{b}_1 contracted with the effective CC2 Jacobian matrix from the right,

$$\sigma_{ai} = \sum_{bj} J_{ai,bj}^{\text{eff}}(\omega) b_{bj}, \quad (\text{A.32})$$

or from the left,

$$\bar{\sigma}_{ai} = \sum_{bj} b_{bj} J_{bj,ai}^{\text{eff}}(\omega). \quad (\text{A.33})$$

In addition we need explicit expressions for the effective right-hand-sides in eqs. (A.29) and (A.30). All those quantities are derived in details in the next sections. If the reader is only interested in the working equations and not in the extremely boring derivations that follows, we refer to appendix B.8. In the following sections the notation for two-electrons integrals is extended such that,

$$g_{pqrs} = (pq|rs) \quad (\text{A.34})$$

$$L_{pqrs} = 2(pq|rs) - (ps|rq). \quad (\text{A.35})$$

We also make extensive use of the notation and pre-derived quantities in appendices A.8 and A.9 and in boxes 13.1 and 13.2 in page 688 of Ref. 13. Finally, in appendix A.6 we also derive how all these quantities are used in the calculation of the transition moments and transition strengths *via* one-particle density matrices.

A.2 Right-hand-side for the ground state Lagrangian multipliers

The η matrix is defined as follows,

$$\eta_{\mu} = \frac{\partial E_{\text{CC2}}}{\partial \check{v}_{\mu}} \quad (\text{A.36})$$

where the CC2 correlation energy is introduced as,

$$E_{\text{CC2}} = \sum_{aibj} [t_i^a t_j^b + t_{ij}^{ab}] [2(ia|jb) - (ib|ja)] \quad (\text{A.37})$$

$$= \sum_{aibj} [t_i^a t_j^b + (1 + \delta_{ab} \delta_{ij}) \check{t}_{ij}^{ab}] [2(ia|jb) - (ib|ja)] \quad (\text{A.38})$$

which leads to the following expressions,

$$\eta_i^a = 2 \sum_{bj} t_j^b [2(ia|jb) - (ib|ja)] = 2\tilde{F}_{ia} \quad (\text{A.39})$$

$$\eta_{ij}^{ab} = 2[2(ia|jb) - (ib|ja)] = 2L_{iajb}. \quad (\text{A.40})$$

The right-hand-side has thus one contribution corresponding to η_i^a and a second contribution that requires the contraction of η_{ij}^{ab} with the doubles-singles block of the CC2 Jacobian. We introduce the following matrix,

$$\bar{\eta}_{ij}^{ab} = 2 \frac{2(ia|jb) - (ib|ja)}{\epsilon_i - \epsilon_a + \epsilon_j - \epsilon_b} \quad (\text{A.41})$$

and get the final working equation for the right-hand-side of the ground state Lagrangian multipliers as,

$$\eta_{ai}^{\text{eff}} = \eta_{ai} + \sum_{ckdl} \frac{\eta_{kl}^{cd} J_{ckdl,ai}}{\epsilon_k - \epsilon_c + \epsilon_l - \epsilon_d} \quad (\text{A.42})$$

$$= 2\tilde{F}_{ia} + \sum_{ckdl} \bar{\eta}_{kl}^{cd} J_{ckdl,ai} \quad (\text{A.43})$$

$$= 2\tilde{F}_{ia} + \sum_{ckdl} \bar{\eta}_{kl}^{cd} \langle \tilde{c}^d | [\tilde{H}, E_{ai}] | \text{HF} \rangle \quad (\text{A.44})$$

$$= 2\tilde{F}_{ia} + \sum_{ckdl} \bar{\eta}_{kl}^{cd} (ck|da) \delta_{li} - \sum_{bj} \bar{\eta}_{kl}^{cd} (ck|il) \delta_{ad} \quad (\text{A.45})$$

$$= 2\tilde{F}_{ia} + \sum_{ckd} \bar{\eta}_{ki}^{cd} (ck|da) - \sum_{ckl} \bar{\eta}_{kl}^{ca} (ck|il) \quad (\text{A.46})$$

A.3 Right linear transformation

In this section we give the working equation for the right linear-transformed vector,

$$\sigma_{ai} = \sum_{bj} J_{ai,bj}^{\text{eff}}(\omega) b_{bj} \quad (\text{A.47})$$

A.3.1 Part A

$$\sigma_{ai}^A = \sum_{bj} J_{ai,bj} b_{bj} \quad (\text{A.48})$$

$$= \sum_{bj} \langle \tilde{a}_i | [\tilde{H}, E_{bj}] + [[\tilde{H}, E_{bj}], T_2] | \text{HF} \rangle b_{bj} \quad (\text{A.49})$$

$$= \sum_{bj} \langle \tilde{a}_i | [\tilde{H}, E_{bj}] | \text{HF} \rangle b_{bj} + \sum_{bj} \langle \tilde{a}_i | [[\tilde{H}, E_{bj}], T_2] | \text{HF} \rangle b_{bj} \quad (\text{A.50})$$

$$= \sigma_{ai}^{A.1} + \sigma_{ai}^{A.2} \quad (\text{A.51})$$

$$\sigma_{ai}^{A.1} = \sum_{bj} \langle \tilde{a}_i | [\tilde{H}, E_{bj}] | \text{HF} \rangle b_{bj} \quad (\text{A.52})$$

$$= \sum_{bj} \tilde{F}_{ab} b_{bj} \delta_{ij} - \sum_{bj} \tilde{F}_{ji} b_{bj} \delta_{ab} + \sum_{bj} \tilde{L}_{aijb} b_{bj} \quad (\text{A.53})$$

$$= \sum_b \tilde{F}_{ab} b_{bi} - \sum_j \tilde{F}_{ji} b_{aj} + \sum_{bj} \tilde{L}_{aijb} b_{bj} \quad (\text{A.54})$$

$$= \sigma_{ai}^{0.1} + \sum_{ck} [2(kc|ai) - (ki|ac)] b_{ck} \quad (\text{A.55})$$

$$= \sigma_{ai}^{0.1} + \sigma_{ai}^J \quad (\text{A.56})$$

Using the commutator relation in Eq. (A.323),

$$\sigma_{ai}^{A.2} = \sum_{bj} \frac{1}{2} \sum_{ckdl} t_{kl}^{cd} \langle \tilde{a}_i | [[\tilde{H}, E_{bj}], E_{ck} E_{dl}] | \text{HF} \rangle b_{bj} \quad (\text{A.57})$$

$$\begin{aligned} &= \sum_{bj} \frac{1}{2} \sum_{ckdl} t_{kl}^{cd} \langle \tilde{a}_i | [[[\tilde{H}, E_{bj}], E_{ck}], E_{dl}] | \text{HF} \rangle b_{bj} \\ &\quad + \sum_{bj} \frac{1}{2} \sum_{ckdl} t_{kl}^{cd} \langle \tilde{a}_i | E_{dl} [[\tilde{H}, E_{bj}], E_{ck}] | \text{HF} \rangle b_{bj} \\ &\quad + \sum_{bj} \frac{1}{2} \sum_{ckdl} t_{kl}^{cd} \langle \tilde{a}_i | E_{ck} [[\tilde{H}, E_{bj}], E_{dl}] | \text{HF} \rangle b_{bj} \end{aligned} \quad (\text{A.58})$$

$$\begin{aligned} &= \sum_{bj} \frac{1}{2} \sum_{ckdl} t_{kl}^{cd} \langle \tilde{a}_i | [[[\tilde{H}, E_{bj}], E_{ck}], E_{dl}] | \text{HF} \rangle b_{bj} \\ &\quad + \sum_{bj} \frac{1}{2} \sum_{ck} t_{ki}^{ca} \langle \text{HF} | [[\tilde{H}, E_{bj}], E_{ck}] | \text{HF} \rangle b_{bj} \\ &\quad + \sum_{bj} \frac{1}{2} \sum_{dl} t_{il}^{ad} \langle \text{HF} | [[\tilde{H}, E_{bj}], E_{dl}] | \text{HF} \rangle b_{bj} \end{aligned} \quad (\text{A.59})$$

$$\begin{aligned}
\sigma_{ai}^{A.2} &= \frac{1}{2} \sum_{bj} \sum_{ckdl} t_{kl}^{cd} \langle \tilde{a}_i | [[\tilde{H}, E_{bj}], E_{ck}], E_{dl}] | \text{HF} \rangle b_{bj} \\
&\quad + \sum_{bj} \sum_{ck} t_{ki}^{ca} \langle \text{HF} | [[\tilde{H}, E_{bj}], E_{ck}] | \text{HF} \rangle b_{bj} \\
&= \sigma_{ai}^{A.2.1} + \sigma_{ai}^{A.2.2}
\end{aligned} \tag{A.60}$$

where we have used the symmetry of the amplitudes and renaming of dummy indices.

$$\sigma_{ai}^{A.2.1} = \frac{1}{2} \sum_{bj} \sum_{ckdl} t_{kl}^{cd} \langle \tilde{a}_i | [[\tilde{H}, E_{bj}], E_{ck}], E_{dl}] | \text{HF} \rangle b_{bj} \tag{A.61}$$

$$= -\frac{1}{2} \sum_{bj} \sum_{ckdl} t_{kl}^{cd} b_{bj} P_{jkl}^{bcd} \left(\tilde{L}_{kcjd} \delta_{ab} \delta_{il} \right) \tag{A.62}$$

$$\begin{aligned}
&= -\frac{1}{2} \sum_{bj} \sum_{ckdl} t_{kl}^{cd} b_{bj} \left(\tilde{L}_{kcjd} \delta_{ab} \delta_{il} + \tilde{L}_{ldjc} \delta_{ab} \delta_{ik} \right. \\
&\quad \left. + \tilde{L}_{jbkd} \delta_{ac} \delta_{il} + \tilde{L}_{ldkb} \delta_{ac} \delta_{ij} + \tilde{L}_{jbkc} \delta_{ad} \delta_{ik} + \tilde{L}_{kclb} \delta_{ad} \delta_{ij} \right)
\end{aligned} \tag{A.63}$$

$$\begin{aligned}
&= -\frac{1}{2} \sum_j \sum_{ckdl} t_{ki}^{cd} b_{aj} \tilde{L}_{kcjd} - \frac{1}{2} \sum_j \sum_{cld} t_{il}^{cd} b_{aj} \tilde{L}_{ldjc} \\
&\quad - \frac{1}{2} \sum_{bj} \sum_{kd} t_{ki}^{ad} b_{bj} \tilde{L}_{jbkd} - \frac{1}{2} \sum_b \sum_{kdl} t_{kl}^{ad} b_{bi} \tilde{L}_{ldkb} \\
&\quad - \frac{1}{2} \sum_{bj} \sum_{cl} t_{il}^{ca} b_{bj} \tilde{L}_{jblc} - \frac{1}{2} \sum_b \sum_{ckl} t_{kl}^{ca} b_{bi} \tilde{L}_{kclb}
\end{aligned} \tag{A.64}$$

$$= -\sum_j \sum_{ckd} t_{ki}^{cd} b_{aj} \tilde{L}_{kcjd} - \sum_{bj} \sum_{kd} t_{ki}^{ad} b_{bj} \tilde{L}_{jbkd} - \sum_b \sum_{kdl} t_{kl}^{ad} b_{bi} \tilde{L}_{ldkb} \tag{A.65}$$

$$\sigma_{ai}^{A.2.2} = \sum_{bj} \sum_{ck} t_{ki}^{ca} \langle \text{HF} | [[\tilde{H}, E_{bj}], E_{ck}] | \text{HF} \rangle b_{bj} \tag{A.66}$$

$$= 2 \sum_{bj} \sum_{ck} t_{ki}^{ca} \tilde{L}_{jbkc} b_{bj} \tag{A.67}$$

$$\sigma_{ai}^{A.2} = \sigma_{ai}^{A.2.1} + \sigma_{ai}^{A.2.2} \tag{A.68}$$

$$\begin{aligned}
&= 2 \sum_{bj} \sum_{ck} t_{ki}^{ca} \tilde{L}_{jbkc} b_{bj} - \sum_j \sum_{ckd} t_{ki}^{cd} b_{aj} \tilde{L}_{kcjd} \\
&\quad - \sum_{bj} \sum_{kd} t_{ki}^{ad} b_{bj} \tilde{L}_{jbkd} - \sum_b \sum_{kdl} t_{kl}^{ad} b_{bi} \tilde{L}_{ldkb}
\end{aligned} \tag{A.69}$$

$$= \sum_{bj} \sum_{ck} t_{ki}^{ca} \tilde{L}_{jbkc} b_{bj} - \sum_j \sum_{ckd} t_{ki}^{cd} b_{aj} \tilde{L}_{kcjd} - \sum_b \sum_{kdl} t_{kl}^{ad} b_{bi} \tilde{L}_{ldkb} \tag{A.70}$$

$$\sigma_{ai}^{A,2} = \sum_{ck} \hat{t}_{ki}^{ca} \bar{F}_{kc} - \sum_j \sum_{ckd} t_{ki}^{cd} b_{aj} \tilde{L}_{kcjd} - \sum_b \sum_{kdl} t_{kl}^{ad} b_{bi} \tilde{L}_{ldkb} \quad (\text{A.71})$$

$$= \sum_{ck} \hat{t}_{ki}^{ca} \bar{F}_{kc} - \sum_j b_{aj} \sum_{ckd} \hat{t}_{ki}^{cd} (kc|jd) - \sum_b b_{bi} \sum_{kdl} \hat{t}_{kl}^{ad} (ld|kb) \quad (\text{A.72})$$

$$= \sigma_{ai}^{I,2} + \sigma_{ai}^{0,2} \quad (\text{A.73})$$

where we have introduced,

$$\hat{t}_{ki}^{ca} = 2t_{ki}^{ca} - t_{ik}^{ca} \quad (\text{A.74})$$

$$\bar{F}_{kc} = \sum_{bj} \tilde{L}_{jbkc} b_{bj} = \sum_{bj} [2(jb|kc) - (jc|kb)] b_{bj} \quad (\text{A.75})$$

A.3.2 Part B

We now look at the other part of the linear-transformed vector and decompose it into small elements that will be combined at the end.

$$\sum_{ck} J_{aibj,ck} b_{ck} = \sum_{ck} \langle \tilde{a}_i^b | [\tilde{H}, E_{ck}] | \text{HF} \rangle b_{ck} \quad (\text{A.76})$$

$$= \sum_{ck} (ai|\tilde{b}c) b_{ck} \delta_{jk} - \sum_{ck} (ai|\tilde{k}j) b_{ck} \delta_{cb} \quad (\text{A.77})$$

$$= \sum_c (ai|\tilde{b}c) b_{cj} - \sum_k (ai|\tilde{k}j) b_{bk} \quad (\text{A.78})$$

$$\sum_{bj} J_{ckdl,bj} b_{bj} = \sum_{bj} \langle \tilde{c}_d^l | [\tilde{H}, E_{bj}] | \text{HF} \rangle b_{bj} \quad (\text{A.79})$$

$$= \sum_{bj} (ck|\tilde{d}b) b_{bj} \delta_{lj} - \sum_{bj} (ck|\tilde{j}l) b_{bj} \delta_{bd} \quad (\text{A.80})$$

$$= \sum_b (ck|\tilde{d}b) b_{bl} - \sum_j (ck|\tilde{j}l) b_{dj} \quad (\text{A.81})$$

Using the commutator relation in Eq. (A.319) we write,

$$J_{ai,ckdl} = \langle \tilde{a}_i^a | [\tilde{H}, E_{ck} E_{dl}] | \text{HF} \rangle \quad (\text{A.82})$$

$$\begin{aligned} &= \langle \tilde{a}_i^a | [[\tilde{H}, E_{ck}] E_{dl}] | \text{HF} \rangle \\ &\quad + \langle \tilde{a}_i^a | E_{dl} [\tilde{H}, E_{ck}] | \text{HF} \rangle \\ &\quad + \langle \tilde{a}_i^a | E_{ck} [\tilde{H}, E_{dl}] | \text{HF} \rangle \end{aligned} \quad (\text{A.83})$$

$$\begin{aligned} &= -P_{kl}^{cd} \left(\tilde{F}_{kd} \delta_{ac} \delta_{il} + \tilde{L}_{kild} \delta_{ac} - \tilde{L}_{acld} \delta_{ik} \right) \\ &\quad + \delta_{ai,dl} \langle \text{HF} | [\tilde{H}, E_{ck}] | \text{HF} \rangle \\ &\quad + \delta_{ai,ck} \langle \text{HF} | [\tilde{H}, E_{dl}] | \text{HF} \rangle \end{aligned} \quad (\text{A.84})$$

$$\begin{aligned} &= -\tilde{F}_{kd} \delta_{ac} \delta_{il} - \tilde{L}_{kild} \delta_{ac} + \tilde{L}_{acld} \delta_{ik} \\ &\quad - \tilde{F}_{lc} \delta_{ad} \delta_{ik} - \tilde{L}_{likc} \delta_{ad} + \tilde{L}_{adkc} \delta_{il} \\ &\quad + 2\delta_{ai,dl} \tilde{F}_{kc} + 2\delta_{ai,ck} \tilde{F}_{ld} \end{aligned} \quad (\text{A.85})$$

$$\begin{aligned}
& \sum_{ckdl} J_{ai,ckdl} \sum_{bj} J_{ckdl,bj} b_{bj} = \\
& = - \sum_{ckdl} \sum_b (ck|db) b_{bl} \tilde{F}_{kd} \delta_{ac} \delta_{il} - \sum_{ckdl} \sum_b (ck|db) b_{bl} \tilde{L}_{kild} \delta_{ac} \\
& + \sum_{ckdl} \sum_b (ck|db) b_{bl} \tilde{L}_{acld} \delta_{ik} - \sum_{ckdl} \sum_b (ck|db) b_{bl} \tilde{F}_{lc} \delta_{ad} \delta_{ik} \\
& - \sum_{ckdl} \sum_b (ck|db) b_{bl} \tilde{L}_{likc} \delta_{ad} + \sum_{ckdl} \sum_b (ck|db) b_{bl} \tilde{L}_{adkc} \delta_{il} \\
& + 2 \sum_{ckdl} \sum_b (ck|db) b_{bl} \delta_{ai,dl} \tilde{F}_{kc} + 2 \sum_{ckdl} \sum_b (ck|db) b_{bl} \delta_{ai,ck} \tilde{F}_{ld} \\
& + \sum_{ckdl} \sum_j (ck|jl) b_{dj} \tilde{F}_{kd} \delta_{ac} \delta_{il} + \sum_{ckdl} \sum_j (ck|jl) b_{dj} \tilde{L}_{kild} \delta_{ac} \\
& - \sum_{ckdl} \sum_j (ck|jl) b_{dj} \tilde{L}_{acld} \delta_{ik} + \sum_{ckdl} \sum_j (ck|jl) b_{dj} \tilde{F}_{lc} \delta_{ad} \delta_{ik} \\
& + \sum_{ckdl} \sum_j (ck|jl) b_{dj} \tilde{L}_{likc} \delta_{ad} - \sum_{ckdl} \sum_j (ck|jl) b_{dj} \tilde{L}_{adkc} \delta_{il} \\
& - 2 \sum_{ckdl} \sum_j (ck|jl) b_{dj} \delta_{ai,dl} \tilde{F}_{kc} - 2 \sum_{ckdl} \sum_j (ck|jl) b_{dj} \delta_{ai,ck} \tilde{F}_{ld} \quad (A.86)
\end{aligned}$$

$$\begin{aligned}
& = - \sum_{kd} \sum_b (ak|db) b_{bl} \tilde{F}_{kd} - \sum_{kdl} \sum_b (ak|db) b_{bl} \tilde{L}_{kild} \\
& + \sum_{cdl} \sum_b (ci|db) b_{bl} \tilde{L}_{acld} - \sum_{cl} \sum_b (ci|ab) b_{bl} \tilde{F}_{lc} \\
& - \sum_{ckl} \sum_b (ck|ab) b_{bl} \tilde{L}_{likc} + \sum_{ckd} \sum_b (ck|db) b_{bl} \tilde{L}_{adkc} \\
& + 2 \sum_{ck} \sum_b (ck|ab) b_{bl} \tilde{F}_{kc} + 2 \sum_{dl} \sum_b (ai|db) b_{bl} \tilde{F}_{ld} \\
& + \sum_{kd} \sum_j (ak|ji) b_{aj} \tilde{F}_{kd} + \sum_{kdl} \sum_j (ak|jl) b_{dj} \tilde{L}_{kild} \\
& - \sum_{cdl} \sum_j (ci|jl) b_{dj} \tilde{L}_{acld} + \sum_{cl} \sum_j (ci|jl) b_{aj} \tilde{F}_{lc} \\
& + \sum_{ckl} \sum_j (ck|jl) b_{aj} \tilde{L}_{likc} - \sum_{ckd} \sum_j (ck|ji) b_{dj} \tilde{L}_{adkc} \\
& - 2 \sum_{ck} \sum_j (ck|ji) b_{aj} \tilde{F}_{kc} - 2 \sum_{dl} \sum_j (ai|jl) b_{dj} \tilde{F}_{ld} \quad (A.87)
\end{aligned}$$

$$\begin{aligned}
&= - \sum_{kd} (ak|\tilde{d}\bar{i})\tilde{F}_{kd} - \sum_{kdl} (ak|\tilde{d}\bar{l})\tilde{L}_{kild} + \sum_{cdl} (ci|\tilde{d}\bar{l})\tilde{L}_{acld} - \sum_{cl} (ci|\tilde{a}\bar{l})\tilde{F}_{lc} \\
&\quad - \sum_{ckl} (ck|\tilde{a}\bar{l})\tilde{L}_{likc} + \sum_{ckd} (ck|\tilde{d}\bar{i})\tilde{L}_{adkc} + 2 \sum_{ck} (ck|\tilde{a}\bar{i})\tilde{F}_{kc} + 2 \sum_{dl} (ai|\tilde{d}\bar{l})\tilde{F}_{ld} \\
&\quad - \sum_{kd} (ak|\tilde{d}\bar{i})\tilde{F}_{kd} - \sum_{kdl} (ak|\tilde{d}\bar{l})\tilde{L}_{kild} + \sum_{cdl} (ci|\tilde{d}\bar{l})\tilde{L}_{acld} - \sum_{cl} (ci|\tilde{a}\bar{l})\tilde{F}_{lc} \\
&\quad - \sum_{ckl} (ck|\tilde{a}\bar{l})\tilde{L}_{likc} + \sum_{ckd} (ck|\tilde{d}\bar{i})\tilde{L}_{adkc} + 2 \sum_{ck} (ck|\tilde{a}\bar{i})\tilde{F}_{kc} + 2 \sum_{dl} (ai|\tilde{d}\bar{l})\tilde{F}_{ld} \quad (\text{A.88})
\end{aligned}$$

$$\begin{aligned}
&= 2 \sum_{ck} (ck|\tilde{a}\bar{i})\tilde{F}_{kc} + 2 \sum_{ck} (ai|\tilde{c}\bar{k})\tilde{F}_{kc} + 2 \sum_{ck} (ck|\tilde{a}\bar{i})\tilde{F}_{kc} + 2 \sum_{ck} (ai|\tilde{c}\bar{k})\tilde{F}_{kc} \\
&\quad - \sum_{ck} (ak|\tilde{c}\bar{i})\tilde{F}_{kc} - \sum_{ck} (ci|\tilde{a}\bar{k})\tilde{F}_{kc} - \sum_{ck} (ak|\tilde{c}\bar{i})\tilde{F}_{kc} - \sum_{ck} (ci|\tilde{a}\bar{k})\tilde{F}_{kc} \\
&\quad - \sum_{ckl} (al|\tilde{c}\bar{k})\tilde{L}_{likc} + \sum_{cdk} (di|\tilde{c}\bar{k})\tilde{L}_{adkc} - \sum_{ckl} (ck|\tilde{a}\bar{l})\tilde{L}_{likc} + \sum_{cdk} (ck|\tilde{d}\bar{i})\tilde{L}_{adkc} \\
&\quad - \sum_{ckl} (al|\tilde{c}\bar{k})\tilde{L}_{likc} + \sum_{cdk} (di|\tilde{c}\bar{k})\tilde{L}_{adkc} - \sum_{ckl} (ck|\tilde{a}\bar{l})\tilde{L}_{likc} + \sum_{cdk} (ck|\tilde{d}\bar{i})\tilde{L}_{adkc} \quad (\text{A.89})
\end{aligned}$$

$$\begin{aligned}
&= 2 \sum_{ck} (ai|\tilde{c}\bar{k})\tilde{F}_{kc} - \sum_{ck} (ak|\tilde{c}\bar{i})\tilde{F}_{kc} \\
&\quad + \sum_{cdk} \left[(di|\tilde{c}\bar{k}) + (ck|\tilde{d}\bar{i}) + (di|\tilde{c}\bar{k}) + (ck|\tilde{d}\bar{i}) \right] \left[2(ad|\tilde{k}c) - (ac|\tilde{k}d) \right] \\
&\quad - \sum_{ckl} \left[(al|\tilde{c}\bar{k}) + (ck|\tilde{a}\bar{l}) + (al|\tilde{c}\bar{k}) + (ck|\tilde{a}\bar{l}) \right] \left[2(li|\tilde{k}c) - (lc|\tilde{k}i) \right] \quad (\text{A.90})
\end{aligned}$$

$$\begin{aligned}
&= 2 \sum_{ck} (ai|\tilde{c}\bar{k})\tilde{F}_{kc} - \sum_{ck} (ak|\tilde{c}\bar{i})\tilde{F}_{kc} \\
&\quad + 2 \sum_{cdk} (di|\tilde{c}\bar{k})(ad|\tilde{k}c) - \sum_{cdk} (di|\tilde{c}\bar{k})(ac|\tilde{k}d) \\
&\quad - 2 \sum_{ckl} (al|\tilde{c}\bar{k})(li|\tilde{k}c) + \sum_{ckl} (al|\tilde{c}\bar{k})(lc|\tilde{k}i) \quad (\text{A.91})
\end{aligned}$$

$$\begin{aligned}
&= \sum_{ck} \left[2(ai|\tilde{c}\bar{k}) - (ak|\tilde{c}\bar{i}) \right] \tilde{F}_{kc} \\
&\quad + \sum_{cdk} \left[2(di|\tilde{c}\bar{k}) - (dk|\tilde{c}\bar{i}) \right] (ad|\tilde{k}c) \\
&\quad - \sum_{ckl} \left[2(al|\tilde{c}\bar{k}) - (ak|\tilde{c}\bar{l}) \right] (li|\tilde{k}c) \quad (\text{A.92})
\end{aligned}$$

where we have introduced the barred transformed integrals,

$$(pq|\bar{r}s) = P_{qs}^{pr} \sum_{\alpha\beta\gamma\delta} (\bar{X}_{\alpha p} Y_{\beta q} + X_{\alpha p} \bar{Y}_{\beta q}) X_{\gamma r} Y_{\delta s} (\alpha\beta|\gamma\delta) \quad (\text{A.93})$$

$$\bar{h}_{pq} = \sum_{\alpha\beta} (\bar{X}_{\alpha p} Y_{\beta q} + X_{\alpha p} \bar{Y}_{\beta q}) h_{\alpha\beta} \quad (\text{A.94})$$

$$\begin{aligned}\bar{X}_{\alpha i} &= 0 & \bar{X}_{\alpha a} &= -\sum_i C_{\alpha i} b_i^a \\ \bar{Y}_{\alpha i} &= \sum_a C_{\alpha a} b_i^a & \bar{Y}_{\alpha a} &= 0\end{aligned}\quad (\text{A.95})$$

with \mathbf{C} being the canonical MO coefficients. Finally, we get the last contributions to the linear-transformed vector,

$$\sigma_{ai}^B = \sum_{ckdl} \sum_{bj} \frac{J_{ai,ckdl} J_{ckdl,bj}}{\epsilon_k - \epsilon_c + \epsilon_l - \epsilon_d + \omega} b_{bj} \quad (\text{A.96})$$

$$= \sum_{ck} \hat{b}_{ik}^{ac} \tilde{F}_{kc} + \sum_{cdk} \hat{b}_{ik}^{dc} (ad|kc) - \sum_{ckl} \hat{b}_{lk}^{ac} (li|kc) \quad (\text{A.97})$$

$$= \sigma_{ai}^{I,1} + \sigma_{ai}^G + \sigma_{ai}^H \quad (\text{A.98})$$

where we have introduced the doubles quantity,

$$\hat{b}_{ij}^{ab} = 2b_{ij}^{ab} - b_{ji}^{ab} = \frac{2(ai|bj) - (aj|bi)}{\epsilon_i - \epsilon_a + \epsilon_j - \epsilon_b + \omega} \quad (\text{A.99})$$

A.3.3 Summary

$$\sigma_{ai} = \sigma_{ai}^{0,1} + \sigma_{ai}^J + \sigma_{ai}^{I,2} + \sigma_{ai}^{0,2} + \sigma_{ai}^{I,1} + \sigma_{ai}^G + \sigma_{ai}^H \quad (\text{A.100})$$

$$\sigma_{ai}^{0,1} = \sum_b \tilde{F}_{ab} b_{bi} - \sum_j \tilde{F}_{ji} b_{aj} \quad (\text{A.101})$$

$$\sigma_{ai}^J = \sum_{ck} [2(kc|\tilde{a}i) - (ki|\tilde{a}c)] b_{ck} \quad (\text{A.102})$$

$$\sigma_{ai}^{I,2} = \sum_{ck} \hat{t}_{ki}^{ca} \tilde{F}_{kc} \quad (\text{A.103})$$

$$\sigma_{ai}^{0,2} = -\sum_j b_{aj} \sum_{ckd} \hat{t}_{ki}^{cd} (kc|jd) - \sum_b b_{bi} \sum_{kdl} \hat{t}_{kl}^{ad} (ld|kb) \quad (\text{A.104})$$

$$\sigma_{ai}^{I,1} = \sum_{ck} \hat{b}_{ik}^{ac} \tilde{F}_{kc} \quad (\text{A.105})$$

$$\sigma_{ai}^G = \sum_{cdk} \hat{b}_{ik}^{dc} (ad|kc) \quad (\text{A.106})$$

$$\sigma_{ai}^H = -\sum_{ckl} \hat{b}_{lk}^{ac} (li|kc) \quad (\text{A.107})$$

After rearrangement we get,

$$\sigma_{ai} = \sigma_{ai}^0 + \sigma_{ai}^G + \sigma_{ai}^H + \sigma_{ai}^I + \sigma_{ai}^J \quad (\text{A.108})$$

$$\sigma_{ai}^0 = \sum_b \left[\tilde{F}_{ab} - \sum_{kdl} \hat{t}_{kl}^{ad} (ld|kb) \right] b_{bi} - \sum_j \left[\tilde{F}_{ji} + \sum_{ckd} \hat{t}_{ki}^{cd} (kc|jd) \right] b_{aj} \quad (\text{A.109})$$

$$\sigma_{ai}^0 = \sum_b E_{ab} b_{bi} - \sum_j E_{ji} b_{aj} \quad (\text{A.110})$$

$$\sigma_{ai}^G = \sum_{cdk} \hat{b}_{ik}^{dc} (a\tilde{d}|kc) \quad (\text{A.111})$$

$$\sigma_{ai}^H = - \sum_{ckl} \hat{t}_{lk}^{ac} (l\tilde{i}|kc) \quad (\text{A.112})$$

$$\sigma_{ai}^I = \sum_{ck} \left[\hat{t}_{ik}^{ac} \tilde{F}_{kc} + \hat{t}_{ik}^{ac} \bar{F}_{kc} \right] \quad (\text{A.113})$$

$$\sigma_{ai}^J = \sum_{ck} [2(kc|\tilde{a}i) - (k\tilde{i}|ac)] b_{ck} \quad (\text{A.114})$$

A.4 Left linear transformation

In this section we give the working equation for the left linear-transformed vector,

$$\bar{\sigma}_{ai} = \sum_{bj} b_{bj} J_{bj,ai}^{\text{eff}}(\omega) \quad (\text{A.115})$$

The equations can be derived in the same way as for the right linear-transformed vector and we thus give only the final equations here,

$$\bar{\sigma}_{ai} = \bar{\sigma}_{ai}^0 + \bar{\sigma}_{ai}^G + \bar{\sigma}_{ai}^H + \bar{\sigma}_{ai}^I + \bar{\sigma}_{ai}^J \quad (\text{A.116})$$

$$\bar{\sigma}_{ai}^0 = \sum_b \left[\tilde{F}_{ba} - \sum_{ckl} \hat{t}_{lk}^{bc} (kc|la) \right] b_i^b - \sum_j \left[\tilde{F}_{ij} + \sum_{cdk} \hat{t}_{jk}^{dc} (kc|id) \right] b_j^a \quad (\text{A.117})$$

$$\bar{\sigma}_{ai}^G = \sum_{cdk} \bar{b}_{ik}^{dc} (ck|\tilde{d}a) \quad (\text{A.118})$$

$$\bar{\sigma}_{ai}^H = - \sum_{ckl} \bar{b}_{lk}^{ac} (ck|\tilde{i}l) \quad (\text{A.119})$$

$$\bar{\sigma}_{ai}^I = \sum_{ck} [2(kc|\tilde{i}a) - (ka|\tilde{i}c)] C_k^c \quad (\text{A.120})$$

$$\bar{\sigma}_{ai}^J = \sum_{ck} [2(ck|\tilde{i}a) - (ca|\tilde{i}k)] b_k^c \quad (\text{A.121})$$

where,

$$\bar{b}_{ij}^{ab} = \frac{2(ia|\tilde{j}b) - (ib|\tilde{j}a) + P_{ij}^{ab} [2b_i^a \tilde{F}_{jb} - b_j^a \tilde{F}_{ib}]}{\epsilon_i - \epsilon_a + \epsilon_j - \epsilon_b + \omega} \quad (\text{A.122})$$

$$C_i^a = \sum_{bj} \hat{t}_{ij}^{ab} b_j^b \quad (\text{A.123})$$

and the following integrals have been introduced,

$$(pq|\check{r}s) = P_{qs}^{pr} \sum_{\alpha\beta\gamma\delta} (\check{X}_{\alpha p} Y_{\beta q} + X_{\alpha p} \check{Y}_{\beta q}) X_{\gamma r} Y_{\delta s} (\alpha\beta|\gamma\delta) \quad (\text{A.124})$$

$$\begin{aligned} \check{X}_{\alpha i} &= \sum_a X_{\alpha a} b_i^a & \check{X}_{\alpha a} &= 0 \\ \check{Y}_{\alpha i} &= 0 & \check{Y}_{\alpha a} &= - \sum_i Y_{\alpha i} b_i^a \end{aligned} \quad (\text{A.125})$$

A.5 Right-hand-side of the transition Lagrangian multipliers

Following the derivations in Ref. 135, let us express the \mathbf{F} matrix as,

$$F_{\mu\nu} = \frac{\partial \eta_\mu}{\partial t_\nu} + \sum_\gamma \bar{t}_\gamma B_{\gamma\mu\nu}, \quad (\text{A.126})$$

where,

$$B_{\mu\nu\gamma} = \frac{\partial J_{\mu\nu}}{\partial t_\gamma} \quad (\text{A.127})$$

We can now express the right-hand-side of the transition Lagrangian multipliers in eq. (A.30) as,

$$\bar{m}_{ai}^{\text{eff}} = \bar{m}_{ai}^{\text{A}} + \bar{m}_{ai}^{\text{B}} + \bar{m}_{ai}^{\text{C}} + \bar{m}_{ai}^{\text{D}} + \bar{m}_{ai}^{\text{E}} \quad (\text{A.128})$$

$$\bar{m}_{ai}^{\text{A}} = \sum_{bj} R_j^b \langle \text{HF} | [[H, E_{bj}], E_{ai}] | \text{HF} \rangle \quad (\text{A.129})$$

$$\bar{m}_{ai}^{\text{B}} = \sum_{bj, ck} \bar{t}_j^b B_{bj, ck, ai} R_k^c \quad (\text{A.130})$$

$$\bar{m}_{ai}^{\text{C}} = \sum_{bjck} \sum_{dl} \bar{t}_{jk}^{bc} B_{bjck, dl, ai} R_l^d \quad (\text{A.131})$$

$$\bar{m}_{ai}^{\text{D}} = \frac{1}{2} \sum_{bj} \sum_{ckdl} \bar{t}_j^b B_{bj, ckdl, ai} R_{kl}^{cd} \quad (\text{A.132})$$

$$\bar{m}_{ai}^{\text{E}} = \sum_{bjck} \frac{\bar{m}_{jk}^{bc} J_{bjck, ai}}{\epsilon_j - \epsilon_b + \epsilon_k - \epsilon_c - \omega} \quad (\text{A.133})$$

where the doubles right-hand-side vector is now given by,

$$\bar{m}_{ij}^{ab} = \sum_{ck, dl} \bar{t}_k^c B_{ck, dl, aibj} R_l^d \quad (\text{A.134})$$

A.5.1 Part A

$$\bar{m}_{ai}^{\text{A}} = \sum_{bj} R_j^b \langle \text{HF} | [[H, E_{bj}], E_{ai}] | \text{HF} \rangle \quad (\text{A.135})$$

$$= 2 \sum_{bj} R_j^b [2(jb|ia) - (ja|ib)] \quad (\text{A.136})$$

This term is denoted \bar{m}_{ai}^{X} in our notes and corresponds to eq. (44) in Ref. 135 where a factor 2 is missing.

A.5.2 Part B

$$B_{bj,ck,ai} = \frac{\partial}{\partial t_i^a} \langle \tilde{b}_j | [\tilde{H}, E_{ck}] + [[\tilde{H}, E_{ck}], T_2] | \text{HF} \rangle \quad (\text{A.137})$$

$$= \langle \tilde{b}_j | [[\tilde{H}, E_{ai}], E_{ck}] | \text{HF} \rangle + \langle \tilde{b}_j | [[[\tilde{H}, E_{ai}], E_{ck}], T_2] | \text{HF} \rangle \quad (\text{A.138})$$

$$= \langle \tilde{b}_j | [[\tilde{H}, E_{ai}], E_{ck}] | \text{HF} \rangle \quad (\text{A.139})$$

$$= -F_{ik}^{ac} [\tilde{F}_{ic} \delta_{ba} \delta_{jk} + \sum_l \tilde{L}_{ilkc} \delta_{ba} \delta_{jl} - \sum_d \tilde{L}_{dakc} \delta_{bd} \delta_{ji}] \quad (\text{A.140})$$

$$= -\tilde{F}_{ic} \delta_{ba} \delta_{jk} - \sum_l \tilde{L}_{ilkc} \delta_{ba} \delta_{jl} + \sum_d \tilde{L}_{dakc} \delta_{bd} \delta_{ji} \\ - \tilde{F}_{ka} \delta_{bc} \delta_{ji} - \sum_l \tilde{L}_{klia} \delta_{bc} \delta_{jl} + \sum_d \tilde{L}_{dcia} \delta_{bd} \delta_{jk} \quad (\text{A.141})$$

$$= -\tilde{F}_{ic} \delta_{ba} \delta_{jk} - \tilde{L}_{ijkc} \delta_{ba} + \tilde{L}_{bakc} \delta_{ji} \quad (\text{A.142})$$

$$- \tilde{F}_{ka} \delta_{bc} \delta_{ji} - \tilde{L}_{kjia} \delta_{bc} + \tilde{L}_{bcia} \delta_{jk} \quad (\text{A.143})$$

where the second term is zero because of rank-reduction and the fact that the Hamiltonian is a two-electron operator (see Ref. 13 for details).

$$\bar{m}_{ai}^B = \sum_{bj,ck} \bar{t}_j^b B_{bj,ck,ai} R_k^c \quad (\text{A.144})$$

$$= \sum_{bj,ck} \bar{t}_j^b \langle \tilde{b}_j | [[\tilde{H}, E_{ai}], E_{ck}] | \text{HF} \rangle R_k^c \quad (\text{A.145})$$

$$= - \sum_{bj,ck} \bar{t}_j^b R_k^c \tilde{F}_{ic} \delta_{ba} \delta_{jk} - \sum_{bj,ck} \bar{t}_j^b R_k^c \tilde{L}_{ijkc} \delta_{ba} + \sum_{bj,ck} \bar{t}_j^b R_k^c \tilde{L}_{bakc} \delta_{ji} \\ - \sum_{bj,ck} \bar{t}_j^b R_k^c \tilde{F}_{ka} \delta_{bc} \delta_{ji} - \sum_{bj,ck} \bar{t}_j^b R_k^c \tilde{L}_{kjia} \delta_{bc} + \sum_{bj,ck} \bar{t}_j^b R_k^c \tilde{L}_{bcia} \delta_{jk} \quad (\text{A.146})$$

$$= - \sum_{ck} \bar{t}_k^a R_k^c \tilde{F}_{ic} - \sum_{j,ck} \bar{t}_j^a R_k^c \tilde{L}_{ijkc} + \sum_{b,ck} \bar{t}_i^b R_k^c \tilde{L}_{bakc} \\ - \sum_{ck} \bar{t}_i^c R_k^c \tilde{F}_{ka} - \sum_{j,ck} \bar{t}_j^c R_k^c \tilde{L}_{kjia} + \sum_{b,ck} \bar{t}_k^b R_k^c \tilde{L}_{bcia} \quad (\text{A.147})$$

$$= - \sum_j \bar{t}_j^a \left[\sum_b R_j^b \tilde{F}_{ib} + \sum_{ck} R_k^c \tilde{L}_{ijkc} \right] \\ + \sum_b \bar{t}_i^b \left[- \sum_j R_j^b \tilde{F}_{ja} + \sum_{ck} R_k^c \tilde{L}_{bakc} \right] \\ - \sum_{j,ck} \bar{t}_j^c R_k^c \tilde{L}_{kjia} + \sum_{b,ck} \bar{t}_k^b R_k^c \tilde{L}_{bcia} \quad (\text{A.148})$$

$$\begin{aligned} \bar{m}_{ai}^B &= - \sum_j \bar{t}_j^a \bar{F}_{ij} + \sum_b \bar{t}_i^b \bar{F}_{ba} + 2 \sum_{jc} \bar{t}_j^c (\bar{c}\tilde{j}|ia) - \sum_{jc} \bar{t}_j^c (\bar{c}a|i\tilde{j}) \\ &\quad + 2 \sum_{bk} \bar{t}_k^b (\tilde{b}\bar{k}|ia) - \sum_{bk} \bar{t}_k^b (\tilde{b}a|i\bar{k}) \end{aligned} \quad (\text{A.149})$$

$$= \bar{m}_{ai}^{0,1} + 2 \sum_{bj} \bar{t}_j^b [(\bar{b}\tilde{j}|ia) + (\tilde{b}\bar{j}|ia)] - \sum_{bj} \bar{t}_j^b [(\bar{b}a|i\tilde{j}) + (\tilde{b}a|i\bar{j})] \quad (\text{A.150})$$

$$= \bar{m}_{ai}^{0,1} + \sum_{bj} \bar{t}_j^b [2(b\bar{j}|ia) - (ba|i\bar{j})] \quad (\text{A.151})$$

$$= \bar{m}_{ai}^{0,1} + \bar{m}_{ai}^J \quad (\text{A.152})$$

where all quantities have been defined implicitly and more details regarding the barred Fock matrices is given in Appendix A.8.

A.5.3 Part C

$$B_{bjck,dl,ai} = \frac{\partial}{\partial t_i^a} \langle \tilde{b}_c^{\tilde{c}} | [\tilde{H}, E_{dl}] | \text{HF} \rangle \quad (\text{A.153})$$

$$= \langle \tilde{b}_c^{\tilde{c}} | [[\tilde{H}, E_{ai}], E_{dl}] | \text{HF} \rangle \quad (\text{A.154})$$

$$\begin{aligned} &= -P_{il}^{ad} [(i\tilde{d}|ck)\delta_{ba}\delta_{jl} + (i\tilde{j}|cd)\delta_{ba}\delta_{kl}] \\ &\quad + (i\tilde{j}|lk)\delta_{ba}\delta_{cd} + (ba\tilde{c}|d)\delta_{ji}\delta_{kl} \end{aligned} \quad (\text{A.155})$$

$$\begin{aligned} &= - (i\tilde{d}|ck)\delta_{ba}\delta_{jl} - (i\tilde{j}|cd)\delta_{ba}\delta_{kl} \\ &\quad - (la\tilde{c}|k)\delta_{bd}\delta_{ji} - (l\tilde{j}|ca)\delta_{bd}\delta_{ki} \\ &\quad + (i\tilde{j}|lk)\delta_{ba}\delta_{cd} + (ba\tilde{c}|d)\delta_{ji}\delta_{kl} \end{aligned} \quad (\text{A.156})$$

$$\bar{m}_{ai}^C = \sum_{bjck} \sum_{dl} \bar{t}_{jk}^{\tilde{b}\tilde{c}} B_{bjck,dl,ai} R_l^d \quad (\text{A.157})$$

$$\begin{aligned} &= - \sum_{ck} \sum_{dl} \bar{t}_{lk}^{\tilde{a}\tilde{c}} R_l^d (i\tilde{d}|ck) - \sum_{jc} \sum_{dl} \bar{t}_{jl}^{\tilde{a}\tilde{c}} R_l^d (i\tilde{j}|cd) \\ &\quad - \sum_{ck} \sum_{dl} \bar{t}_{ik}^{\tilde{d}\tilde{c}} R_l^d (la\tilde{c}|k) - \sum_{jc} \sum_{dl} \bar{t}_{ji}^{\tilde{d}\tilde{c}} R_l^d (l\tilde{j}|ca) \\ &\quad + \sum_{jk} \sum_{dl} \bar{t}_{jk}^{\tilde{a}\tilde{d}} R_l^d (i\tilde{j}|lk) + \sum_{bc} \sum_{dl} \bar{t}_{il}^{\tilde{b}\tilde{c}} R_l^d (ba\tilde{c}|d) \end{aligned} \quad (\text{A.158})$$

$$\begin{aligned} &= - \sum_{ckl} \bar{t}_{lk}^{\tilde{a}\tilde{c}} (i\bar{l}|\tilde{c}\bar{k}) - \sum_{jcl} \bar{t}_{jl}^{\tilde{a}\tilde{c}} (i\tilde{j}|\tilde{c}\bar{l}) \\ &\quad + \sum_{ckd} \bar{t}_{ik}^{\tilde{d}\tilde{c}} (\bar{d}a|\tilde{c}\bar{k}) + \sum_{jcd} \bar{t}_{ji}^{\tilde{d}\tilde{c}} (\bar{d}\bar{j}|\tilde{c}a) \\ &\quad - \sum_{jkd} \bar{t}_{jk}^{\tilde{a}\tilde{d}} (i\tilde{j}|\bar{d}\bar{k}) + \sum_{bcl} \bar{t}_{il}^{\tilde{b}\tilde{c}} (\tilde{b}a|\tilde{c}\bar{l}) \end{aligned} \quad (\text{A.159})$$

$$\begin{aligned}\bar{m}_{ai}^C &= - \sum_{ckl} \bar{t}_{lk}^{ac} [(i\bar{l}|\tilde{c}\tilde{k}) + (i\bar{l}|\tilde{c}\bar{k}) + (i\bar{l}|\tilde{c}\tilde{k})] \\ &\quad + \sum_{ckd} \bar{t}_{ik}^{dc} [(\bar{d}a|\tilde{c}\tilde{k}) + (\bar{d}a|\tilde{c}\bar{k}) + (\bar{d}a|\tilde{c}\tilde{k})]\end{aligned}\tag{A.160}$$

$$= - \sum_{ckl} \bar{t}_{lk}^{ac} (i\bar{l}|ck) + \sum_{ckd} \bar{t}_{ik}^{dc} (da|\bar{c}k)\tag{A.161}$$

$$= - \sum_{ckl} \bar{t}_{lk}^{ac} (ck|\bar{i}l) + \sum_{ckd} \bar{t}_{ik}^{dc} (ck|\bar{d}a)\tag{A.162}$$

$$= \bar{m}_{ai}^{H,2} + \bar{m}_{ai}^{G,2}\tag{A.163}$$

A.5.4 Part D

$$B_{bj,ckdl,ai} = \frac{\partial}{\partial t_i^a} \langle \tilde{b}_j | [\tilde{H}, E_{ck} E_{dl}] | \text{HF} \rangle\tag{A.164}$$

$$= \langle \tilde{b}_j | [[\tilde{H}, E_{ai}], E_{ck} E_{dl}] | \text{HF} \rangle\tag{A.165}$$

Using the commutator in Eq. (A.323), we get,

$$\begin{aligned}B_{bj,ckdl,ai} &= \langle \tilde{b}_j | [[[\tilde{H}, E_{ai}], E_{ck}], E_{dl}] | \text{HF} \rangle \\ &\quad + \langle \text{HF} | [[\tilde{H}, E_{ai}], E_{ck}] | \text{HF} \rangle \delta_{bd} \delta_{jl} \\ &\quad + \langle \text{HF} | [[\tilde{H}, E_{ai}], E_{dl}] | \text{HF} \rangle \delta_{bc} \delta_{jk}\end{aligned}\tag{A.166}$$

$$= - P_{ikl}^{acd} \tilde{L}_{kcid} \delta_{ba} \delta_{jl} + 2L_{iakc} \delta_{bd} \delta_{jl} + 2L_{iald} \delta_{bc} \delta_{jk}\tag{A.167}$$

$$\begin{aligned}&= 2L_{iakc} \delta_{bd} \delta_{jl} + 2L_{iald} \delta_{bc} \delta_{jk} \\ &\quad - \tilde{L}_{kcid} \delta_{ba} \delta_{jl} - \tilde{L}_{ldic} \delta_{ba} \delta_{jk} \\ &\quad - \tilde{L}_{iakd} \delta_{bc} \delta_{jl} - \tilde{L}_{ldka} \delta_{bc} \delta_{ji} \\ &\quad - \tilde{L}_{ialc} \delta_{bd} \delta_{jk} - \tilde{L}_{kcla} \delta_{bd} \delta_{ji}\end{aligned}\tag{A.168}$$

$$\bar{m}_{ai}^D = \frac{1}{2} \sum_{bj} \sum_{ckdl} \bar{t}_j^b B_{bj,ckdl,ai} R_{kl}^{cd}\tag{A.169}$$

$$\begin{aligned}&= \sum_{ckdl} \bar{t}_l^d R_{kl}^{cd} L_{iakc} + \sum_{ckdl} \bar{t}_k^c R_{kl}^{cd} L_{iald} \\ &\quad - \frac{1}{2} \left(\sum_{ckdl} \bar{t}_l^a R_{kl}^{cd} \tilde{L}_{kcid} + \sum_{ckdl} \bar{t}_k^a R_{kl}^{cd} \tilde{L}_{ldic} + \sum_{ckdl} \bar{t}_l^c R_{kl}^{cd} \tilde{L}_{iakd} \right) \\ &\quad - \frac{1}{2} \left(\sum_{ckdl} \bar{t}_i^c R_{kl}^{cd} \tilde{L}_{ldka} + \sum_{ckdl} \bar{t}_k^d R_{kl}^{cd} \tilde{L}_{ialc} + \sum_{ckdl} \bar{t}_i^d R_{kl}^{cd} \tilde{L}_{kcla} \right)\end{aligned}\tag{A.170}$$

$$\begin{aligned} \bar{m}_{ai}^D &= \frac{1}{2} \sum_{ckdl} \bar{t}_l^d (2R_{kl}^{cd} - R_{kl}^{dc}) L_{iakc} + \frac{1}{2} \sum_{ckdl} \bar{t}_k^c (2R_{kl}^{cd} - R_{kl}^{dc}) L_{iald} \\ &\quad - \sum_{ckdl} \bar{t}_l^a R_{kl}^{cd} \tilde{L}_{kcid} - \sum_{ckdl} \bar{t}_i^c R_{kl}^{cd} \tilde{L}_{ldka} \end{aligned} \quad (\text{A.171})$$

$$= \sum_{ckdl} \bar{t}_l^d \hat{R}_{kl}^{cd} L_{iakc} - \sum_{ckdl} \bar{t}_l^a \hat{R}_{kl}^{cd} (kc|id) - \sum_{ckdl} \bar{t}_i^c \hat{R}_{kl}^{cd} (ld|ka) \quad (\text{A.172})$$

$$= \bar{m}_{ai}^I + \bar{m}_{ai}^{0,2} \quad (\text{A.173})$$

A.5.5 Part E

$$B_{ck,dl,aibj} = \frac{\partial}{\partial \tilde{t}_{ij}^{ab}} \langle \tilde{c}_k | [\tilde{H}, E_{dl}] + [[\tilde{H}, E_{dl}], T_2] | \text{HF} \rangle \quad (\text{A.174})$$

$$= \langle \tilde{c}_k | [[\tilde{H}, E_{dl}], E_{ai} E_{bj}] | \text{HF} \rangle \quad (\text{A.175})$$

We note that $B_{bj,ckdl,ai} = B_{bj,ai,ckdl}$ and write the doubles right-and-side as,

$$\bar{m}_{kl}^{cd} = \sum_{ai,bj} \bar{t}_j^b B_{bj,ai,ckdl} R_i^a \quad (\text{A.176})$$

$$\begin{aligned} &= 2 \sum_{ai} \bar{t}_l^d R_i^a L_{iakc} + 2 \sum_{ai} \bar{t}_k^c R_i^a L_{iald} \\ &\quad - \sum_{ai} \bar{t}_l^a R_i^a \tilde{L}_{kcid} - \sum_{ai} \bar{t}_k^a R_i^a \tilde{L}_{ldic} \\ &\quad - \sum_{ai} \bar{t}_l^c R_i^a \tilde{L}_{iakd} - \sum_{ai} \bar{t}_i^c R_i^a \tilde{L}_{ldka} \\ &\quad - \sum_{ai} \bar{t}_k^d R_i^a \tilde{L}_{ialc} - \sum_{ai} \bar{t}_i^d R_i^a \tilde{L}_{kcla} \end{aligned} \quad (\text{A.177})$$

$$\begin{aligned} &= 2\bar{t}_l^d \bar{F}_{kc} - \bar{t}_k^d \bar{F}_{lc} + 2\bar{t}_k^c \bar{F}_{ld} - \bar{t}_l^c \bar{F}_{kd} \\ &\quad - \sum_{ai} \bar{t}_l^a R_i^a L_{kcid} - \sum_{ai} \bar{t}_k^a R_i^a L_{ldic} \\ &\quad - \sum_{ai} \bar{t}_i^c R_i^a L_{ldka} - \sum_{ai} \bar{t}_i^d R_i^a L_{kcla} \end{aligned} \quad (\text{A.178})$$

$$\begin{aligned} &= P_{kl}^{cd} (2\bar{t}_k^c \bar{F}_{ld} - \bar{t}_l^c \bar{F}_{kd}) \\ &\quad - P_{kl}^{cd} \left(\sum_{ai} \bar{t}_k^a R_i^a L_{icld} + \sum_{ai} \bar{t}_i^c R_i^a L_{kald} \right) \end{aligned} \quad (\text{A.179})$$

$$= 2(\widetilde{kc|ld}) - (\widetilde{kd|lc}) + P_{kl}^{cd} (2\bar{t}_k^c \bar{F}_{ld} - \bar{t}_l^c \bar{F}_{kd}) \quad (\text{A.180})$$

where we have implicitly defined the integrals,

$$(\widetilde{kc|ld}) = -P_{kl}^{cd} \left(\sum_{ai} \bar{t}_k^a R_i^a (ic|ld) + \sum_{ai} \bar{t}_i^c R_i^a (ka|ld) \right) \quad (\text{A.181})$$

By anticipation we define the quantity,

$$F_{jk}^{bc} = \frac{\bar{m}_{jk}^{bc}}{\epsilon_j - \epsilon_b + \epsilon_k - \epsilon_c - \omega} \quad (\text{A.182})$$

and write the E part of the right-hand-side as,

$$\bar{m}_{ai}^E = \sum_{bjck} \frac{\bar{m}_{jk}^{bc} J_{bjck,ai}}{\epsilon_j - \epsilon_b + \epsilon_k - \epsilon_c - \omega} \quad (\text{A.183})$$

$$= \sum_{bjck} F_{jk}^{bc} J_{bjck,ai} \quad (\text{A.184})$$

$$\bar{m}_{ai}^E = \sum_{bjck} F_{jk}^{bc} \langle \tilde{b}^c | [\tilde{H}, E_{ai}] | \text{HF} \rangle \quad (\text{A.185})$$

$$= \sum_{bjck} F_{jk}^{bc} \left[(bj\bar{]}ca) \delta_{ki} - (bj\bar{]}ik) \delta_{ca} \right] \quad (\text{A.186})$$

$$= \sum_{bjc} F_{ji}^{bc} (bj\bar{]}ca) - \sum_{bjk} F_{jk}^{ba} (bj\bar{]}ik) \quad (\text{A.187})$$

$$= \bar{m}_{ai}^{G,1} + \bar{m}_{ai}^{H,1} \quad (\text{A.188})$$

A.5.6 Summary

$$\begin{aligned} \bar{m}_{ai}^{\text{eff}} &= \bar{m}_{ai}^{0,1} + \bar{m}_{ai}^J + \bar{m}_{ai}^{H,2} + \bar{m}_{ai}^{G,2} + \bar{m}_{ai}^I + \bar{m}_{ai}^{0,2} \\ &\quad + \bar{m}_{ai}^{G,1} + \bar{m}_{ai}^{H,1} + 2\bar{m}_{ai}^X \end{aligned} \quad (\text{A.189})$$

$$\bar{m}_{ai}^{0,1} = - \sum_j \bar{t}_j^a \bar{F}_{ij} + \sum_b \bar{t}_i^b \bar{F}_{ba} \quad (\text{A.190})$$

$$\bar{m}_{ai}^J = \sum_{bj} \bar{t}_j^b [2(bj\bar{]}ia) - (ba\bar{]}ij)] \quad (\text{A.191})$$

$$\bar{m}_{ai}^{H,2} + \bar{m}_{ai}^{G,2} = - \sum_{ckl} \bar{t}_{lk}^{ac} (ck\bar{]}il) + \sum_{ckd} \bar{t}_{ik}^{dc} (ck\bar{]}da) \quad (\text{A.192})$$

$$\begin{aligned} \bar{m}_{ai}^I &= \sum_{ckdl} \bar{t}_l^d \hat{R}_{kl}^{cd} L_{iakc} \\ &= \sum_{ck} [2(ia|kc) - (ic|ka)] \bar{C}_k^c \end{aligned} \quad (\text{A.193})$$

$$\bar{m}_{ai}^{0,2} = - \sum_j \bar{t}_j^a \sum_{bdl} \hat{R}_{jl}^{bd} (ld|ib) - \sum_b \bar{t}_i^b \sum_{jdl} \hat{R}_{jl}^{bd} (ld|ja) \quad (\text{A.194})$$

$$\bar{m}_{ai}^{G,1} + \bar{m}_{ai}^{H,1} = \sum_{bjc} F_{ji}^{bc} (bj\bar{]}ca) - \sum_{bjk} F_{jk}^{ba} (bj\bar{]}ik) \quad (\text{A.195})$$

$$\bar{m}_{ai}^X = \sum_{bj} R_j^b [2(jb|ia) - (ja|ib)] \quad (\text{A.196})$$

After rearrangement we obtain,

$$\bar{m}_{ai}^{\text{eff}} = \bar{m}_{ai}^0 + \bar{m}_{ai}^G + \bar{m}_{ai}^H + \bar{m}_{ai}^I + \bar{m}_{ai}^J + 2\bar{m}_{ai}^X \quad (\text{A.197})$$

$$\bar{m}_{ai}^0 = \sum_b \bar{t}_i^b \left[\bar{F}_{ba} - \sum_{jdl} \hat{R}_{jl}^{bd}(ld|ja) \right] - \sum_j \bar{t}_j^a \left[\bar{F}_{ij} + \sum_{bdl} \hat{R}_{jl}^{bd}(ld|ib) \right] \quad (\text{A.198})$$

$$= \sum_b \bar{t}_i^b \bar{E}_{ba} - \sum_j \bar{t}_j^a \bar{E}_{ij} \quad (\text{A.199})$$

$$\bar{m}_{ai}^G = \sum_{bjc} F_{ji}^{bc}(bj|ca) + \sum_{ckd} \bar{t}_{ik}^{dc}(ck|da) \quad (\text{A.200})$$

$$\bar{m}_{ai}^H = - \sum_{bjk} F_{jk}^{ba}(bj|ik) - \sum_{ckl} \bar{t}_{lk}^{ac}(ck|il) \quad (\text{A.201})$$

$$\bar{m}_{ai}^I = \sum_{ck} [2(ia|kc) - (ic|ka)] \bar{C}_k^c \quad (\text{A.202})$$

$$\bar{m}_{ai}^J = \sum_{bj} \bar{t}_j^b [2(bj|ia) - (ba|ij)] \quad (\text{A.203})$$

$$\bar{m}_{ai}^X = \sum_{bj} R_j^b [2(jb|ia) - (ja|ib)] \quad (\text{A.204})$$

A.6 Transition strengths

Transition strengths for a transition from the ground state to the n -th excited state for the two operators V_1 and V_2 can be calculated as (see section 2.5),

$$S_{0n}^{V_1, V_2} = \frac{1}{2} \left(T_{0n}^{V_1} T_{n0}^{V_2} + (T_{0n}^{V_2} T_{n0}^{V_1})^* \right) \quad (\text{A.205})$$

where the left and right transition moments are given by,

$$T_{n0}^V = \sum_{ai} L_i^a \xi_{ai}^V + \sum_{aibj} L_{ij}^{ab} \xi_{aibj}^V \quad (\text{A.206})$$

$$\begin{aligned} T_{0n}^V &= \sum_{ai} \eta_{ai}^V R_i^a + \sum_{aibj} \eta_{aibj}^V R_{ij}^{ab} \\ &+ \sum_{ai} \bar{M}_i^a \xi_{ai}^V + \sum_{aibj} \bar{M}_{ij}^{ab} \xi_{aibj}^V. \end{aligned} \quad (\text{A.207})$$

In the following we show how the expressions for the CC2 transition moments can be reformulated to involve one-particle density matrices.

A.6.1 Introducing the ξ one-particle CC2 density matrix

Let us consider a T1-transformed one electron operator as,

$$\tilde{V} = \sum_{pq} \tilde{V}_{pq} E_{pq} \quad (\text{A.208})$$

First we derive expressions for the ξ_1^V singles matrix,

$$\xi_{ai}^V = \langle \tilde{a}_i | \tilde{V} + [\tilde{V}, T_2] | \text{HF} \rangle \quad (\text{A.209})$$

$$= \sum_{pq} \tilde{V}_{pq} \delta_{ap} \delta_{iq} + \frac{1}{2} \sum_{bjck} t_{jk}^{bc} \langle \tilde{a}_i | [\tilde{V}, E_{bj} E_{ck}] | \text{HF} \rangle \quad (\text{A.210})$$

$$= \tilde{V}_{ai} + \xi_{ai}^{V,2} \quad (\text{A.211})$$

Using the commutator relation in Eq. (A.319) we write,

$$\xi_{ai}^{V,2} = \frac{1}{2} \sum_{bjck} t_{jk}^{bc} \langle \tilde{a}_i | [\tilde{V}, E_{bj} E_{ck}] | \text{HF} \rangle \quad (\text{A.212})$$

$$\begin{aligned} &= \frac{1}{2} \sum_{ckdl} t_{kl}^{cd} \langle \tilde{a}_i | [[\tilde{V}, E_{ck}], E_{dl}] | \text{HF} \rangle \\ &\quad + \frac{1}{2} \sum_{ckdl} t_{kl}^{cd} \delta_{ad} \delta_{il} \langle \text{HF} | [\tilde{V}, E_{ck}] | \text{HF} \rangle \\ &\quad + \frac{1}{2} \sum_{ckdl} t_{kl}^{cd} \delta_{ac} \delta_{ik} \langle \text{HF} | [\tilde{V}, E_{dl}] | \text{HF} \rangle \end{aligned} \quad (\text{A.213})$$

$$= \frac{1}{2} \sum_{ckdl} t_{kl}^{cd} \langle \tilde{a}_i | [[\tilde{V}, E_{ck}], E_{dl}] | \text{HF} \rangle + \sum_{ck} t_{ki}^{ca} \langle \text{HF} | [\tilde{V}, E_{ck}] | \text{HF} \rangle \quad (\text{A.214})$$

We now use the relations for one-electron operators against the HF state in Eqs. (A.342) and (A.343) to write,

$$\xi_{ai}^{V,2} = -\frac{1}{2} \sum_{ckdl} t_{kl}^{cd} \tilde{V}_{kd} \delta_{ac} \delta_{il} - \frac{1}{2} \sum_{ckdl} t_{kl}^{cd} \tilde{V}_{lc} \delta_{ad} \delta_{ik} + 2 \sum_{ck} t_{ki}^{ca} \tilde{V}_{kc} \quad (\text{A.215})$$

$$= -\frac{1}{2} \sum_{kd} t_{ki}^{ad} \tilde{V}_{kd} - \frac{1}{2} \sum_{cl} t_{il}^{ca} \tilde{V}_{lc} + 2 \sum_{ck} t_{ki}^{ca} \tilde{V}_{kc} \quad (\text{A.216})$$

$$= -\frac{1}{2} \sum_{ck} t_{ki}^{ac} \tilde{V}_{kc} - \frac{1}{2} \sum_{ck} t_{ik}^{ca} \tilde{V}_{kc} + 2 \sum_{ck} t_{ki}^{ca} \tilde{V}_{kc} \quad (\text{A.217})$$

$$= \sum_{ck} \tilde{t}_{ki}^{ca} \tilde{V}_{kc} = \sum_{ck} \tilde{t}_{ki}^{ca} V_{kc} \quad (\text{A.218})$$

By contracting the singles ξ_1^V matrix with a given singles vector $\mathbf{X}_1 = \mathbf{L}_1$ or $\bar{\mathbf{M}}_1$, we get,

$$\sum_{ai} X_i^a \xi_{ai}^V = \sum_{ai} X_i^a \tilde{V}_{ai} + \sum_{aick} X_i^a \tilde{t}_{ki}^{ca} \tilde{V}_{kc} \quad (\text{A.219})$$

$$= \sum_{ai} X_i^a \tilde{V}_{ai} + \sum_{aick} X_k^c \tilde{t}_{ik}^{ac} \tilde{V}_{ia} \quad (\text{A.220})$$

$$= \sum_{ai} \left[D_{ai}^\xi(\mathbf{X}) \tilde{V}_{ai} + D_{ia}^\xi(\mathbf{X}) V_{ia} \right] \quad (\text{A.221})$$

where we have implicitly introduced blocks of the one particle ξ density matrix. We now derive expressions for the ξ_2^V doubles matrix,

$$\xi_{aibj}^V = \langle \tilde{a}^b | [\tilde{V}, T_2] | \text{HF} \rangle = \frac{1}{2} \sum_{ckdl} t_{kl}^{cd} \langle \tilde{a}^b | [\tilde{V}, E_{ck} E_{dl}] | \text{HF} \rangle \quad (\text{A.222})$$

Using the commutator relation in Eq. (A.319) and the relations for one-electron operators against the HF state in Eqs. (A.342) and (A.343), we write,

$$\begin{aligned} \xi_{aibj}^V &= \frac{1}{2} \sum_{ckdl} t_{kl}^{cd} \langle \tilde{a}^b | [[\tilde{V}, E_{ck}], E_{dl}] | \text{HF} \rangle \\ &\quad + \sum_{ckdl} t_{kl}^{cd} \langle \tilde{a}^b | E_{dl} [\tilde{V}, E_{ck}] | \text{HF} \rangle \end{aligned} \quad (\text{A.223})$$

$$\begin{aligned} &= -\frac{1}{2} \sum_{ckdl} t_{kl}^{cd} \langle \tilde{a}^b | P_{kl}^{cd} \tilde{V}_{kd} E_{cl} | \text{HF} \rangle \\ &\quad + \sum_{ckdl} t_{kl}^{cd} \langle \tilde{a}^b | E_{dl} \sum_e \tilde{V}_{ec} E_{ek} | \text{HF} \rangle - \sum_{ckdl} t_{kl}^{cd} \langle \tilde{a}^b | E_{dl} \sum_m \tilde{V}_{km} E_{cm} | \text{HF} \rangle \end{aligned} \quad (\text{A.224})$$

$$= \sum_{ckdle} t_{kl}^{cd} \tilde{V}_{ec} \delta_{aibj, dlek} - \sum_{ckdlm} t_{kl}^{cd} \tilde{V}_{km} \delta_{aibj, dlcm} \quad (\text{A.225})$$

$$= \sum_c t_{ji}^{ca} \tilde{V}_{bc} - \sum_k t_{ki}^{ba} \tilde{V}_{kj} \quad (\text{A.226})$$

By contracting the doubles ξ_2^V matrix with a given doubles vector $\mathbf{X}_2 = \mathbf{L}_2$ or $\bar{\mathbf{M}}_2$, we get,

$$\sum_{aibj} X_{ij}^{ab} \xi_{aibj}^V = \sum_{aibj} X_{ij}^{ab} \sum_c t_{ji}^{ca} \tilde{V}_{bc} - \sum_{aibj} X_{ij}^{ab} \sum_k t_{ki}^{ba} \tilde{V}_{kj} \quad (\text{A.227})$$

$$= \sum_{ab} \tilde{V}_{ab} \sum_{ijc} X_{ij}^{ac} t_{ij}^{bc} - \sum_{ij} \tilde{V}_{ij} \sum_{abk} X_{jk}^{ab} t_{ik}^{ab} \quad (\text{A.228})$$

$$= \sum_{ab} \tilde{V}_{ab} D_{ab}^\xi(\mathbf{X}) + \sum_{ij} \tilde{V}_{ij} D_{ij}^\xi(\mathbf{X}) \quad (\text{A.229})$$

where we have implicitly introduced two other blocks of the one-particle ξ density matrix.

A.6.2 Introducing the η one-particle CC2 density matrix

We now derive expressions for the η_1^V singles matrix,

$$\begin{aligned} \eta_{ai}^V &= \langle \text{HF} | [\tilde{V}, E_{ai}] | \text{HF} \rangle + \sum_{ck} \bar{t}_k^c \langle \tilde{c} | [\tilde{V}, E_{ai}] | \text{HF} \rangle \\ &\quad + \sum_{ckdl} \bar{t}_{kl}^{cd} \langle \tilde{c}^d | [\tilde{V}, E_{ai}] | \text{HF} \rangle + \sum_{ckdl} \bar{t}_{kl}^{cd} \langle \tilde{c}^d | [[\tilde{V}, T_2], E_{ai}] | \text{HF} \rangle \end{aligned} \quad (\text{A.230})$$

$$= \eta_{ai}^{V:1} + \eta_{ai}^{V:2} + \eta_{ai}^{V:3} + \eta_{ai}^{V:4} \quad (\text{A.231})$$

$$\eta_{ai}^{V,1} = \langle \text{HF} | [\tilde{V}, E_{ai}] | \text{HF} \rangle = 2\tilde{V}_{ia} = 2V_{ia} \quad (\text{A.232})$$

$$\eta_{ai}^{V,2} = \sum_{ck} \bar{t}_k^c \langle \tilde{c}_k | [\tilde{V}, E_{ai}] | \text{HF} \rangle \quad (\text{A.233})$$

$$= \sum_{ck} \bar{t}_k^c \sum_b \tilde{V}_{ba} \langle \tilde{c}_k | E_{bi} | \text{HF} \rangle - \sum_{ck} \bar{t}_k^c \sum_j \tilde{V}_{ij} \langle \tilde{c}_k | E_{aj} | \text{HF} \rangle \quad (\text{A.234})$$

$$= \sum_c \bar{t}_i^c \tilde{V}_{ca} - \sum_k \bar{t}_k^a \tilde{V}_{ik} \quad (\text{A.235})$$

$$\eta_{ai}^{V,3} = \sum_{ckdl} \bar{t}_{kl}^{cd} \langle \tilde{cd}_{kl} | [\tilde{V}, E_{ai}] | \text{HF} \rangle = 0 \quad (\text{A.236})$$

Using the commutator relation in Eq. (A.330), we write,

$$\eta_{ai}^{V,4} = \frac{1}{2} \sum_{a'i'b'j'} t_{i'j'}^{a'b'} \sum_{ckdl} \bar{t}_{kl}^{cd} \langle \tilde{cd}_{kl} | [[\tilde{V}, E_{a'i'} E_{b'j'}], E_{ai}] | \text{HF} \rangle \quad (\text{A.237})$$

$$= \sum_{a'i'b'j'} t_{i'j'}^{a'b'} \sum_{ckdl} \bar{t}_{kl}^{cd} \langle \tilde{cd}_{kl} | E_{a'i'} [[V, E_{b'j'}], E_{ai}] | \text{HF} \rangle \quad (\text{A.238})$$

$$= - \sum_{a'i'b'j'} t_{i'j'}^{a'b'} \sum_{ckdl} \bar{t}_{kl}^{cd} P_{j'i}^{b'a} V_{j'a} \langle \tilde{cd}_{kl} | E_{a'i'} E_{b'i} | \text{HF} \rangle \quad (\text{A.239})$$

$$= - \sum_{a'i'b'j'} t_{i'j'}^{a'b'} \sum_{ckdl} \bar{t}_{kl}^{cd} (V_{j'a} \delta_{ckdl, a'i'b'i} + V_{ib'} \delta_{ckdl, a'i'aj'}) \quad (\text{A.240})$$

$$= - \sum_{ckdj'} t_{kj'}^{cd} \bar{t}_{ki}^{cd} V_{j'a} - \sum_{ckb'l} t_{kl}^{cb'} \bar{t}_{kl}^{ca} V_{ib'} \quad (\text{A.241})$$

$$= - \sum_l \left(\sum_{ckd} t_{kl}^{cd} \bar{t}_{ki}^{cd} \right) V_{la} - \sum_d \left(\sum_{ckl} t_{kl}^{cd} \bar{t}_{kl}^{ca} \right) V_{id} \quad (\text{A.242})$$

By contracting the singles η_1^V matrix with the right singles excitation vector \mathbf{R}_1 we get,

$$\begin{aligned} \sum_{ai} R_i^a \eta_{ai}^V &= 2 \sum_{ai} R_i^a V_{ia} + \sum_{ai} R_i^a \sum_c \bar{t}_i^c \tilde{V}_{ca} - \sum_{ai} R_i^a \sum_k \bar{t}_k^a \tilde{V}_{ik} \\ &\quad - \sum_{ai} \sum_l \left(\sum_{ckd} t_{kl}^{cd} \bar{t}_{ki}^{cd} \right) V_{la} R_i^a - \sum_{ai} \sum_d \left(\sum_{ckl} t_{kl}^{cd} \bar{t}_{kl}^{ca} \right) V_{id} R_i^a \end{aligned} \quad (\text{A.243})$$

$$= \sum_{ai} V_{ia} \left[2R_i^a - \sum_l \left(\sum_{ckd} t_{kl}^{cd} \bar{t}_{ki}^{cd} \right) R_l^a - \sum_d \left(\sum_{ckl} t_{kl}^{cd} \bar{t}_{kl}^{ca} \right) R_d^a \right] \quad (\text{A.244})$$

$$\begin{aligned} &+ \sum_{ab} \tilde{V}_{ab} \sum_i \bar{t}_i^a R_i^b - \sum_{ij} \tilde{V}_{ij} \sum_a \bar{t}_j^a R_i^a \\ &= \sum_{ai} V_{ia} D_{ia}^{\eta,1}(\mathbf{R}) + \sum_{ab} \tilde{V}_{ab} D_{ab}^{\eta,1}(\mathbf{R}) + \sum_{ij} \tilde{V}_{ij} D_{ij}^{\eta,1}(\mathbf{R}) \end{aligned} \quad (\text{A.245})$$

where we have implicitly introduced blocks of the one-particle η density matrix. Note that those blocks are not complete yet. We now derive expressions for the η_2^V doubles matrix,

$$\eta_{aibj}^V = \sum_{ck} \bar{t}_k^c \langle \tilde{c}_k | [\tilde{V}, E_{ai} E_{bj}] | \text{HF} \rangle + \sum_{ckdl} \bar{t}_{kl}^{cd} \langle \tilde{cd}_{kl} | [\tilde{V}, E_{ai} E_{bj}] | \text{HF} \rangle \quad (\text{A.246})$$

$$\begin{aligned} &= \sum_{ck} \bar{t}_k^c \langle \tilde{c}_k | [[\tilde{V}, E_{ai}], E_{bj}] | \text{HF} \rangle + \sum_{ck} \bar{t}_k^c \langle \tilde{c}_k | E_{bj} [\tilde{V}, E_{ai}] | \text{HF} \rangle \\ &+ \sum_{ck} \bar{t}_k^c \langle \tilde{c}_k | E_{ai} [\tilde{V}, E_{bj}] | \text{HF} \rangle + \sum_{ckdl} \bar{t}_{kl}^{cd} \langle \tilde{cd}_{kl} | [[\tilde{V}, E_{ai}], E_{bj}] | \text{HF} \rangle \\ &+ \sum_{ckdl} \bar{t}_{kl}^{cd} \langle \tilde{cd}_{kl} | E_{bj} [\tilde{V}, E_{ai}] | \text{HF} \rangle + \sum_{ckdl} \bar{t}_{kl}^{cd} \langle \tilde{cd}_{kl} | E_{ai} [\tilde{V}, E_{bj}] | \text{HF} \rangle \end{aligned} \quad (\text{A.247})$$

$$\begin{aligned} &= \sum_{ck} \bar{t}_k^c \langle \tilde{c}_k | [[\tilde{V}, E_{ai}], E_{bj}] | \text{HF} \rangle + \sum_{ck} \bar{t}_k^c \delta_{cb} \delta_{kj} \langle \text{HF} | [\tilde{V}, E_{ai}] | \text{HF} \rangle \\ &+ \sum_{ck} \bar{t}_k^c \delta_{ca} \delta_{ki} \langle \text{HF} | [\tilde{V}, E_{bj}] | \text{HF} \rangle \\ &+ \sum_{ckdl} \bar{t}_{kl}^{cd} \langle \tilde{cd}_{kl} | E_{bj} [\tilde{V}, E_{ai}] | \text{HF} \rangle + \sum_{ckdl} \bar{t}_{kl}^{cd} \langle \tilde{cd}_{kl} | E_{ai} [\tilde{V}, E_{bj}] | \text{HF} \rangle \end{aligned} \quad (\text{A.248})$$

$$= \sum_{ck} \bar{t}_k^c \langle \tilde{c}_k | [[\tilde{V}, E_{ai}], E_{bj}] | \text{HF} \rangle + P_{ij}^{ab} \left[2\bar{t}_j^b V_{ia} + \sum_{ckdl} \bar{t}_{kl}^{cd} \langle \tilde{cd}_{kl} | E_{bj} [\tilde{V}, E_{ai}] | \text{HF} \rangle \right] \quad (\text{A.249})$$

$$= P_{ij}^{ab} \left[- \sum_{ck} \bar{t}_k^c V_{ib} \delta_{ca} \delta_{kj} + 2\bar{t}_j^b V_{ia} + \sum_{ckdl} \bar{t}_{kl}^{cd} \langle \tilde{cd}_{kl} | E_{bj} [\tilde{V}, E_{ai}] | \text{HF} \rangle \right] \quad (\text{A.250})$$

$$= P_{ij}^{ab} \left[2\bar{t}_j^b V_{ia} - \bar{t}_j^a V_{ib} + \sum_{ckdl} \bar{t}_{kl}^{cd} \langle \tilde{cd}_{kl} | E_{bj} [\tilde{V}, E_{ai}] | \text{HF} \rangle \right] \quad (\text{A.251})$$

$$= P_{ij}^{ab} \left[2\bar{t}_j^b V_{ia} - \bar{t}_j^a V_{ib} + \sum_{ckdl} \bar{t}_{kl}^{cd} \sum_e \tilde{V}_{ea} \delta_{ckdl, bjei} - \sum_{ckdl} \bar{t}_{kl}^{cd} \sum_m \tilde{V}_{im} \delta_{ckdl, bjam} \right] \quad (\text{A.252})$$

$$= P_{ij}^{ab} \left[2\bar{t}_j^b V_{ia} - \bar{t}_j^a V_{ib} + \sum_d \bar{t}_{ji}^{bd} \tilde{V}_{da} - \sum_l \bar{t}_{jl}^{ba} \tilde{V}_{il} \right] \quad (\text{A.253})$$

By contracting the doubles η_2^V matrix with the right doubles excitation vector \mathbf{R}_2 we get,

$$\frac{1}{2} \sum_{aibj} R_{ij}^{ab} \eta_{aibj}^V = \sum_{aibj} R_{ij}^{ab} \left[2\bar{t}_j^b V_{ia} - \bar{t}_j^a V_{ib} + \sum_d \bar{t}_{ji}^{bd} \tilde{V}_{da} - \sum_l \bar{t}_{jl}^{ba} \tilde{V}_{il} \right] \quad (\text{A.254})$$

$$\begin{aligned} \frac{1}{2} \sum_{aibj} R_{ij}^{ab} \eta_{aibj}^V &= \sum_{ai} V_{ia} \sum_{bj} [2R_{ij}^{ab} - R_{ji}^{ab}] \bar{t}_{ij}^b \\ &+ \sum_{ab} \tilde{V}_{ab} \sum_{ijc} R_{ij}^{bc} \bar{t}_{ji}^{ca} - \sum_{ij} \tilde{V}_{ij} \sum_{abk} R_{ik}^{ab} \bar{t}_{kj}^{ba} \end{aligned} \quad (\text{A.255})$$

$$= \sum_{ai} V_{ia} D_{ia}^{\eta,2}(\mathbf{R}) + \sum_{ab} \tilde{V}_{ab} D_{ab}^{\eta,2}(\mathbf{R}) + \sum_{ij} \tilde{V}_{ij} D_{ij}^{\eta,2}(\mathbf{R}) \quad (\text{A.256})$$

where we have implicitly introduced blocks of the one-particle η density matrix. Note that those blocks are not complete yet.

A.6.3 Summary

The CC2 transition moments can now be expressed in terms of one-particle density matrices contracted with one-electron T1-transformed integrals,

$$T_{0n}^V = \sum_{pq} [D_{pq}^{\eta}(\mathbf{R}) + D_{pq}^{\xi}(\bar{\mathbf{M}})] \tilde{V}_{pq} \quad (\text{A.257})$$

$$T_{n0}^V = \sum_{pq} D_{pq}^{\xi}(\mathbf{L}) \tilde{V}_{pq} \quad (\text{A.258})$$

where the one-particle density matrices are given by,

$$D_{ij}^{\xi}(\mathbf{X}) = - \sum_{abk} X_{jk}^{ab} \bar{t}_{ik}^{ab} \quad (\text{A.259})$$

$$D_{ia}^{\xi}(\mathbf{X}) = \sum_{ck} X_{ck} \bar{t}_{ik}^{ac} \quad (\text{A.260})$$

$$D_{ai}^{\xi}(\mathbf{X}) = X_{ai} \quad (\text{A.261})$$

$$D_{ab}^{\xi}(\mathbf{X}) = \sum_{ijc} X_{ij}^{ac} \bar{t}_{ij}^{bc} \quad (\text{A.262})$$

$$D_{ij}^{\eta}(\mathbf{R}) = - \sum_a \bar{t}_{aj} R_{ai} - \sum_{abk} \bar{t}_{jk}^{ab} R_{ik} \quad (\text{A.263})$$

$$D_{ia}^{\eta}(\mathbf{R}) = 2R_{ia} + \sum_{ck} \bar{t}_{ck} \hat{R}_{ik}^{ac} - \sum_b \left(\sum_{kjc} \bar{t}_{kj}^{bc} \bar{t}_{kj}^{ac} \right) R_{bi} - \sum_j \left(\sum_{cbk} \bar{t}_{jk}^{cb} \bar{t}_{ik}^{cb} \right) R_{aj} \quad (\text{A.264})$$

$$D_{ai}^{\eta}(\mathbf{R}) = 0 \quad (\text{A.265})$$

$$D_{ab}^{\eta}(\mathbf{R}) = \sum_i \bar{t}_{ai} R_{bi} + \sum_{ijc} \bar{t}_{ij}^{ac} R_{ij}^{bc} \quad (\text{A.266})$$

A.7 CCS equations for transition strengths

The CCS equations are obtained directly from the CC2 equations derived in the previous sections by setting all doubles quantities equal to zero.

A.7.1 Ground state equations

Let us first consider the ground state equations.

$$\Omega_{ai} = \langle \tilde{a}_i^a | \tilde{H} | \text{HF} \rangle = 0 \quad (\text{A.267})$$

$$= \tilde{F}_{ai} = 0 \quad (\text{A.268})$$

which is solve trivially for $t_i^a = 0$. Note that this means no T_1 -transformation and $E_{\text{CCS}} = E_{\text{HF}}$.

A.7.2 CCS Jacobian

$$J_{ai,bj} = \frac{\partial \Omega_{ai}}{\partial t_j^b} = \langle \tilde{a}_i^a | [H, E_{bj}] | \text{HF} \rangle \quad (\text{A.269})$$

$$= (\epsilon_a - \epsilon_i) \delta_{ab} \delta_{ij} + L_{bjia} \quad (\text{A.270})$$

where we have assumed canonical orbitals. The equation for a right or left linear-transformed vector is trivially obtain by considering,

$$\sigma_{ai} = \sum_{bj} J_{ai,bj} b_{bj} \quad (\text{A.271})$$

and because the CCS Jacobian is symmetric, the right and left eigenvalue problem will lead to the same eigenvectors,

$$R_i^a = L_i^a. \quad (\text{A.272})$$

Note that, the CCS and CIS models are equivalent for ground state and excitation energies but differ for transition strengths.

A.7.3 The CCS ground state multipliers

Let us now consider the CCS equation for the ground state multipliers,

$$\sum_{bj} \bar{t}_j^b J_{bj,ai} = -\eta_i^a, \quad (\text{A.273})$$

where,

$$\eta_i^a = \langle \text{HF} | [H, E_{ai}] | \text{HF} \rangle \quad (\text{A.274})$$

which is equal to zero for a HF reference by virtue of the Brillouin theorem. Therefore, as for the ground state amplitudes, the ground state multipliers are trivially zero,

$$\bar{t}_i^a = 0 \quad (\text{A.275})$$

A.7.4 The CCS transition moment multipliers

The transition moment multipliers are obtain by solving,

$$\sum_{bj} \bar{M}_j^b (\omega \delta_{ab} \delta_{ij} + J_{bj,ai}) = - \sum_{bj} R_j^b F_{bj,ai}, \quad (\text{A.276})$$

where the \mathbf{F} matrix is given by,

$$F_{bj,ai} = \langle \text{HF} | [[H, E_{bj}], E_{ai}] | \text{HF} \rangle = 2L_{iajb} \quad (\text{A.277})$$

and all the other quantities are already known.

A.7.5 The CCS transition moments

We now give explicit expression of the CCS transition density matrices and transition moments by extrapolation of the corresponding CC2 equations. By setting all doubles quantities to zero as well as,

$$t_i^a = 0 \quad (\text{A.278})$$

$$\bar{t}_i^a = 0 \quad (\text{A.279})$$

$$R_i^a = L_i^a \quad (\text{A.280})$$

we obtain,

$$D_{ia}^\eta(\mathbf{R}) = 2R_i^a \quad (\text{A.281})$$

$$D_{ai}^\xi(\mathbf{X}) = X_i^a \quad (\text{A.282})$$

which leads to the following equation for the CCS transition moments,

$$T_{0f}^V = \sum_{pq} [D_{pq}^\eta(\mathbf{R}) + D_{pq}^\xi(\bar{\mathbf{M}})] \tilde{V}_{pq} \quad (\text{A.283})$$

$$= \sum_{ai} [2R_i^a + \bar{M}_i^a] V_{ai} \quad (\text{A.284})$$

where we have used that the dipole integrals are symmetric without the T_1 transformation, $V_{ai} = V_{ia}$.

$$T_{f0}^V = \sum_{pq} D_{pq}^\xi(\mathbf{L}) \tilde{V}_{pq} \quad (\text{A.285})$$

$$= \sum_{ai} R_i^a V_{ai} \quad (\text{A.286})$$

A.8 Expressions for Fock matrices

The standard inactive Fock matrix is defined as,

$$F_{pq} = h_{pq} + \sum_i [2(pq|ii) - (pi|i q)] \quad (\text{A.287})$$

$$= \sum_{\alpha\beta} C_{\alpha p} h_{\alpha\beta} C_{\beta q} + \sum_{\alpha\beta} C_{\alpha p} C_{\beta q} \sum_i [2(\alpha\beta|ii) - (\alpha i|i\beta)] \quad (\text{A.288})$$

$$= \sum_{\alpha\beta} C_{\alpha p} F_{\alpha\beta} C_{\beta q} \quad (\text{A.289})$$

which for Hartree-Fock canonical orbitals can be re-written as,

$$F_{ij} = \epsilon_i \delta_{ij} \quad (\text{A.290})$$

$$F_{ia} = 0 \quad (\text{A.291})$$

$$F_{ai} = 0 \quad (\text{A.292})$$

$$F_{ab} = \epsilon_a \delta_{ab} \quad (\text{A.293})$$

We now introduce the T1-transformed inactive Fock matrix,

$$\tilde{F}_{pq} = \tilde{h}_{pq} + \sum_i [2(pq|\tilde{i}i) - (p\tilde{i}|i q)] \quad (\text{A.294})$$

$$= \sum_{\alpha\beta} X_{\alpha p} h_{\alpha\beta} Y_{\beta q} + \sum_{\alpha\beta} X_{\alpha p} Y_{\beta q} \sum_i [2(\alpha\beta|\tilde{i}i) - (\alpha\tilde{i}|i\beta)] \quad (\text{A.295})$$

$$= \sum_{\alpha\beta} X_{\alpha p} h_{\alpha\beta} Y_{\beta q} + \sum_{\alpha\beta} X_{\alpha p} Y_{\beta q} \sum_i [2(\alpha\beta|ii) - (\alpha i|i\beta)] \\ + \sum_{\alpha\beta} X_{\alpha p} Y_{\beta q} \sum_{ai} t_i^a [2(\alpha\beta|ia) - (\alpha a|i\beta)] \quad (\text{A.296})$$

$$= \sum_{\alpha\beta} X_{\alpha p} F_{\alpha\beta} Y_{\beta q} + \sum_{\alpha\beta} X_{\alpha p} Y_{\beta q} \sum_{ai} t_i^a [2(\alpha\beta|ia) - (\alpha a|i\beta)] \quad (\text{A.297})$$

$$= \sum_{\alpha\beta} X_{\alpha p} F_{\alpha\beta} Y_{\beta q} + \sum_{ai} t_i^a [2(pq|\tilde{i}a) - (p\tilde{i}|a q)] \quad (\text{A.298})$$

which for Hartree-Fock canonical orbitals can be re-written as,

$$\tilde{F}_{ij} = \sum_{\alpha\beta} C_{\alpha i} F_{\alpha\beta} (C_{\beta j} + \sum_b C_{\beta b} t_j^b) + \sum_{ck} t_k^c [2(ij|\tilde{k}c) - (i\tilde{k}|cj)] \quad (\text{A.299})$$

$$= \epsilon_i \delta_{ij} + \sum_{ck} t_k^c [2(ij|\tilde{k}c) - (i\tilde{k}|cj)] \quad (\text{A.300})$$

$$\tilde{F}_{ia} = \sum_{ck} t_k^c [2(ia|kc) - (ic|ka)] \quad (\text{A.301})$$

$$\begin{aligned} \tilde{F}_{ai} &= \sum_{\alpha\beta} (C_{\alpha a} - \sum_j C_{\alpha j} t_j^a) F_{\alpha\beta} (C_{\beta i} + \sum_b C_{\beta b} t_i^b) \\ &\quad + \sum_{ck} t_k^c [2(ai|kc) - (ac|ki)] \end{aligned} \quad (\text{A.302})$$

$$= F_{ai} - \sum_j t_j^a F_{ji} + \sum_b F_{ab} t_i^b - \sum_{bj} t_j^a F_{jb} t_i^b \quad (\text{A.303})$$

$$+ \sum_{ck} t_k^c [2(ai|kc) - (ac|ki)] \quad (\text{A.304})$$

$$= (\epsilon_a - \epsilon_i) t_i^a + \sum_{ck} t_k^c [2(ai|kc) - (ac|ki)] \quad (\text{A.305})$$

$$\tilde{F}_{ab} = \sum_{\alpha\beta} (C_{\alpha a} - \sum_j C_{\alpha j} t_j^a) F_{\alpha\beta} C_{\beta b} + \sum_{ck} t_k^c [2(ab|kc) - (ac|kb)] \quad (\text{A.306})$$

$$= \epsilon_a \delta_{ab} + \sum_{ck} t_k^c [2(ab|kc) - (ac|kb)] \quad (\text{A.307})$$

We now introduce the inactive Fock matrix transformed with excitation amplitudes,

$$\bar{F}_{pq} = \bar{h}_{pq} + \sum_i [2(pq|ii) - (pi|iq)]. \quad (\text{A.308})$$

Using the definition of the barred integrals we get,

$$\bar{F}_{ij} = \sum_b R_j^b \left[h_{ib} + \sum_k [2(ib|kk) - (ik|kb)] \right] + \sum_{kc} R_k^c [2(ij|kc) - (ic|kj)] \quad (\text{A.309})$$

$$= \sum_b R_j^b \tilde{F}_{ib} + \sum_{kc} R_k^c [2(ij|kc) - (ic|kj)] \quad (\text{A.310})$$

$$\bar{F}_{ia} = \sum_{kc} R_k^c [2(ia|kc) - (ic|ka)] \quad (\text{A.311})$$

$$\begin{aligned} \bar{F}_{ai} &= \sum_b R_j^b \left[\tilde{h}_{ab} + \sum_k [2(ab|kk) - (ak|kb)] \right] \\ &\quad - \sum_j R_j^a \left[\tilde{h}_{ji} + \sum_k [2(ji|kk) - (jk|ki)] \right] \\ &\quad + \sum_{kc} R_k^c [2(ai|kc) - (ac|ki)] \end{aligned} \quad (\text{A.312})$$

$$= \sum_b R_j^b \tilde{F}_{ab} - \sum_j R_j^a \tilde{F}_{ji} + \sum_{kc} R_k^c [2(ai|kc) - (ac|ki)] \quad (\text{A.313})$$

$$\begin{aligned}\bar{F}_{ab} &= - \sum_j R_j^a \left[h_{jb} + \sum_k [2(jb|kk) - (jk|kb)] \right] \\ &\quad + \sum_{kc} R_k^c [2(ab|kc) - (ac|kb)]\end{aligned}\tag{A.314}$$

$$= - \sum_j R_j^a \tilde{F}_{jb} + \sum_{kc} R_k^c [2(ab|kc) - (ac|kb)]\tag{A.315}$$

A.9 Commutator relations

A.9.1 Relation 1

$$[\tilde{H}, E_{ck}E_{dl}] = [\tilde{H}, E_{ck}]E_{dl} + E_{ck}[\tilde{H}, E_{dl}]\tag{A.316}$$

$$[[\tilde{H}, E_{ck}], E_{dl}] = [\tilde{H}, E_{ck}]E_{dl} - E_{dl}[\tilde{H}, E_{ck}]\tag{A.317}$$

$$[\tilde{H}, E_{ck}]E_{dl} = [[\tilde{H}, E_{ck}], E_{dl}] + E_{dl}[\tilde{H}, E_{ck}]\tag{A.318}$$

$$[\tilde{H}, E_{ck}E_{dl}] = [[\tilde{H}, E_{ck}], E_{dl}] + E_{dl}[\tilde{H}, E_{ck}] + E_{ck}[\tilde{H}, E_{dl}]\tag{A.319}$$

A.9.2 Relation 2

$$[[\tilde{H}, E_{ai}], E_{ck}E_{dl}] = [[\tilde{H}, E_{ai}], E_{ck}]E_{dl} + E_{ck}[[\tilde{H}, E_{ai}], E_{dl}]\tag{A.320}$$

$$[[[\tilde{H}, E_{ai}], E_{ck}], E_{dl}] = [[\tilde{H}, E_{ai}], E_{ck}]E_{dl} - E_{dl}[[\tilde{H}, E_{ai}], E_{ck}]\tag{A.321}$$

$$[[\tilde{H}, E_{ai}], E_{ck}]E_{dl} = [[[\tilde{H}, E_{ai}], E_{ck}], E_{dl}] + E_{dl}[[\tilde{H}, E_{ai}], E_{ck}]\tag{A.322}$$

$$\begin{aligned}[[\tilde{H}, E_{ai}], E_{ck}E_{dl}] &= [[[\tilde{H}, E_{ai}], E_{ck}], E_{dl}] \\ &\quad + E_{dl}[[\tilde{H}, E_{ai}], E_{ck}] \\ &\quad + E_{ck}[[\tilde{H}, E_{ai}], E_{dl}]\end{aligned}\tag{A.323}$$

A.9.3 Relation 3

For a given one electron operator,

$$V = \sum_{pq} V_{pq} E_{pq}\tag{A.324}$$

$$[[V, E_{ai}E_{bj}], E_{ck}] = [[V, E_{ai}], E_{bj}], E_{ck}] + P_{ij}^{ab} ([E_{ai}[V, E_{bj}], E_{ai}])\tag{A.325}$$

$$[E_{ai}[V, E_{bj}], E_{ai}] = E_{ai}[[V, E_{bj}], E_{ck}] + [E_{ai}, E_{ck}][V, E_{bj}]\tag{A.326}$$

$$= E_{ai}[[V, E_{bj}], E_{ck}] + (E_{ak}\delta_{ci} - E_{ci}\delta_{ak})[V, E_{bj}]\tag{A.327}$$

$$= E_{ai}[[V, E_{bj}], E_{ck}] + E_{ak}[V, E_{bj}]\delta_{ci} - E_{ci}[V, E_{bj}]\delta_{ak}\tag{A.328}$$

$$= E_{ai}[[V, E_{bj}], E_{ck}]\tag{A.329}$$

Using the cluster commutation relation for one electron operators we get only,

$$[[V, E_{ai}E_{bj}], E_{ck}] = P_{ij}^{ab} E_{ai} [[V, E_{bj}], E_{ck}] \quad (\text{A.330})$$

A.9.4 Relation 4

For a given one electron operator,

$$V = \sum_{pq} V_{pq} E_{pq} \quad (\text{A.331})$$

we have the following non-zero commutators with single-excitation operators,

$$[V, E_{ai}] = \sum_{pq} V_{pq} [E_{pq}, E_{ai}] = \sum_{pq} V_{pq} E_{pi} \delta_{aq} - \sum_{pq} V_{pq} E_{aq} \delta_{pi} \quad (\text{A.332})$$

$$= \sum_p V_{pa} E_{pi} - \sum_q V_{iq} E_{aq} \quad (\text{A.333})$$

$$[[V, E_{ai}], E_{bj}] = \sum_{pq} V_{pq} [[E_{pq}, E_{ai}], E_{bj}] \quad (\text{A.334})$$

$$= \sum_{pq} V_{pq} [E_{pi}, E_{bj}] \delta_{aq} - \sum_{pq} V_{pq} [E_{aq}, E_{bj}] \delta_{pi} \quad (\text{A.335})$$

$$= \sum_p V_{pa} (E_{pj} \delta_{bi} - E_{bi} \delta_{pj}) - \sum_q V_{iq} (E_{aj} \delta_{bq} - E_{bq} \delta_{aj}) \quad (\text{A.336})$$

$$= - \sum_p V_{pa} E_{bi} \delta_{pj} - \sum_q V_{iq} E_{aj} \delta_{bq} \quad (\text{A.337})$$

$$= - V_{ja} E_{bi} - V_{ib} E_{aj} \quad (\text{A.338})$$

$$= - P_{ij}^{ab} V_{ib} E_{aj} \quad (\text{A.339})$$

When the commutators are projected against the HF ket state we obtain,

$$[V, E_{ai}] |\text{HF}\rangle = \sum_p V_{pa} E_{pi} |\text{HF}\rangle - \sum_q V_{iq} E_{aq} |\text{HF}\rangle \quad (\text{A.340})$$

$$= \sum_j V_{ja} E_{ji} |\text{HF}\rangle + \sum_b V_{ba} E_{bi} |\text{HF}\rangle - \sum_j V_{ij} E_{aj} |\text{HF}\rangle \quad (\text{A.341})$$

$$= 2V_{ia} |\text{HF}\rangle + \sum_b V_{ba} E_{bi} |\text{HF}\rangle - \sum_j V_{ij} E_{aj} |\text{HF}\rangle \quad (\text{A.342})$$

$$[[V, E_{ai}], E_{bj}] |\text{HF}\rangle = - P_{ij}^{ab} V_{ib} E_{aj} |\text{HF}\rangle \quad (\text{A.343})$$

SCIENTIFIC PAPERS



B.1 The Divide–Expand–Consolidate coupled cluster scheme

T. Kjærgaard, P. Baudin, D. Bykov, K. Kristensen, and P. Jørgensen.

Manuscript submitted to *WIREs Comput. Mol. Sci.* (2017).

This manuscript has been submitted as an invited advanced review article.

Major contribution: writing process, (some parts of chapter 3 were used as a first draft for this manuscript).

The Divide-Expand-Consolidate Coupled Cluster Scheme

Thomas Kjærgaard,^{1, a)} Pablo Baudin,¹ Dmytro Bykov,¹ Kasper Kristensen,¹ and Poul Jørgensen¹
*qLEAP Center for Theoretical Chemistry, Department of Chemistry, Aarhus University, Langelandsgade 140,
DK-8000 Aarhus C, Denmark*

(Dated: 18 January 2017)

The Divide-Expand-Consolidate (DEC) scheme is a linear-scaling and massively parallel framework for high accuracy coupled cluster (CC) calculations on large molecular systems. It is designed as a black-box method, which ensures error control in the correlation energy and molecular properties. DEC is combined with a massively parallel implementation to fully utilize modern manycore architectures providing a fast time to solution. The implementation ensures performance portability and will thus easily benefit from new hardware developments. The DEC scheme has been applied to several levels of CC theory and extended the range of application of those methods.

INTRODUCTION

Coupled-cluster (CC) theory¹ has proven very successful for the calculation of energies and molecular properties of small molecular systems dominated by a single configuration. However, conventional CC calculations exhibit a high computational scaling with system size. Even the lowest rung of the CC hierarchy, second-order Møller-Plesset perturbation theory (MP2), scales as $\mathcal{O}(N^5)$, while the highly successful CC singles and doubles with perturbed triples (CCSD(T)) model scales as $\mathcal{O}(N^7)$ where N is a measure of the system size. This scaling behavior prohibits CC calculations on large systems of interest in, e.g., biochemistry or materials science. For example, one of the largest conventional CCSD(T) calculations was performed on a cluster of 20 water molecules² (1020 basis functions), while, for the MP2 model, a calculation was reported on two graphene sheets ($C_{150}H_{30}$)^{3,4} (9840 basis functions).

The scaling problems of the conventional CC algorithms originate from the use of delocalized canonical Hartree-Fock (HF) molecular orbitals to describe electron correlation effects which are local by nature. Local electron correlation effects include short-range electron-electron interactions (the so-called Coulomb holes in the wave function) and dispersion forces, which decay as R^{-6} with the distance between induced dipoles. It is thus necessary to abandon the canonical basis and devise local correlation methods that enable an efficient description of correlation effects to bypass the scaling wall of conventional CC formulations. We present a brief review of local correlation methods in the next section.

CC calculations face another problem in addition to the computational scaling. Conventional CC algorithms are hard to parallelize and the vast majority of CC calculations today are carried out on laptop computers or local clusters with a few hundred cores. However, during the last decade, the speed of a single computer core has remained virtually unchanged, while the number of

cores on a typical local cluster has increased dramatically and will continue to do so. The importance of developing massively parallel algorithms has thus increased immensely over the last decade, and this development will accelerate over the next decade where new local clusters with millions of cores becomes available at universities and private research institutions. Various massively parallel conventional CC implementations based on distributed-memory tensor contraction frameworks have been presented at substantial implementation effort.⁵⁻⁹ In spite of these impressive implementations the underlying scaling of the CC models prohibits large scale CC calculations.

In order to enable CC calculations for large molecular systems, the CC algorithms must thus not only exploit the locality of electron correlation to bypass the scaling wall of conventional implementations but also exploit the technological advances of the manycore computer architectures. In other words, the next generation of CC methods must be both linear-scaling and massively parallel. For proper utilization of large manycore architectures the algorithms must be embarrassingly parallel in the sense that little or no effort is needed to separate the problem into a number of parallel tasks. The Divide-Expand-Consolidate (DEC) scheme,¹⁰⁻²³ which is the subject of this review, is a linear-scaling, massively parallel, and task-based local correlation method suited for highly accurate CC calculations on contemporary and future manycore architectures.

LOCAL CORRELATION METHODS

In this section we briefly review existing local correlation methods for calculating CC energies. A common feature of local correlation methods is that the correlated calculation is expressed in a local basis and that approximations are introduced in order to reduce the computational complexity compared to a conventional CC implementation without introducing unacceptable errors in the calculated energy. The key to success is to use a highly local orbital basis and to find a proper balance between cost and accuracy. We may divide local

^{a)} tkjaergaard@chem.au.dk

correlation approaches into two subcategories—the wave function-based approximations and the fragment-based approximations.

The main philosophy of the wave function-based approximations is to express the standard CC wave function Ψ_{CC} with a reduced set of parameters,

$$\Psi_{\text{CC}} \rightarrow \tilde{\Psi}_{\text{CC}}. \quad (1)$$

The approximations in $\tilde{\Psi}_{\text{CC}}$ typically involve that the virtual excitation domain for each pair of occupied localized molecular orbitals (LMOs) is restricted and that pair correlation contributions between well separated occupied LMOs are neglected or approximated in some way. Given a set of approximations the full molecular CC amplitude equations are solved for the approximate wave function $\tilde{\Psi}_{\text{CC}}$ to yield the CC amplitudes and correlation energy.

In contrast, for fragmentation-based approximations, the CC amplitude equations are not solved for the full molecular system in terms of a single calculation. Rather, the energy E is divided into fragment energy contributions E_f ,

$$E \rightarrow \sum_f E_f, \quad (2)$$

and a calculation on a large molecular system is partitioned into many small and (usually) independent fragment calculations. A set of reduced CC amplitude equations is solved for each fragment to obtain the fragment energy E_f , and the fragment energies are added up to yield the total energy.

The main drawback of the fragment-based approximations compared to the wave function-based approximations is that the fragments generally overlap, which leads to recalculations of many integrals and CC amplitudes. On the other hand, the fragment-based approaches are by design easy to parallelize and therefore better suited for modern manycore architectures than the wave function-based approaches. Furthermore, the storage requirements become independent of system size for fragment-based approaches, while they grow (at least linearly) with system size for the wave-function based approaches, which leads to limitations in the system sizes than can be treated. Clearly, there are pros and cons of each approach, and in the following subsections we discuss the most prominent examples of wave function-based and fragment-based approximations along with the local basis employed.

Wave function-based local CC approximations

The wave function-based local CC approximations originate from the work of Pulay and Sæbø where the CC calculation was expressed in terms of a set of occupied LMOs and a set of projected atomic orbitals (PAOs) for the virtual space.^{24–27} The method was later refined and

also extended to gradients.^{28–43} For each pair of occupied LMOs a local correlation domain containing a subset of PAOs is assigned. The PAOs constitute a nonorthogonal and redundant basis for the virtual orbital space, and the standard (canonical) CC algorithms must thus be modified to take this into account.

While the PAO basis allows for significant reductions in terms of the number of CC amplitudes to consider, the virtual parameter space may be further compressed using pair natural orbitals (PNOs),^{44–49} which are constructed from (an approximation to) the MP2 correlation density matrix for each electron pair. For example, the domain based local PNO (DLPNO) CCSD(T) method^{46,48} have been used successfully for many applications within computational chemistry.^{50–54} Local CC methods relying on orbital-specific virtuals (OSVs)^{55,56} have also been developed and are closely related to PNOs.

Fragmentation-based local CC approximations

The fragmentation-based approaches may be further subdivided into methods that partition both the HF and correlated parts of the CC calculation and methods that partition only the correlated calculation.

Fragment-based HF and correlation approaches

One example of such methods is the divide-and-conquer (DC) approach, which was originally developed for HF and density-functional-theory (DFT)^{57–59} and later extended to CC methods.^{60–62} In the DC formalism,⁵⁹ the one-electron density matrix is constructed from subsystem density matrices, thus avoiding the $\mathcal{O}(N^3)$ scaling solution of the Roothaan-Hall equations. The correlated treatment in DC approaches makes use of subsystem orbitals obtained in the DC variant of the HF method.

Another contribution to this category is the Fragment Molecular Orbital (FMO) approach,⁶³ in which a physical fragmentation of the molecular system is performed. The fragmentation is done such that bond electron pairs are preserved when electrons are assigned to fragments. The FMO approach effectively eliminates memory bottlenecks and have been applied to very large systems.^{64,65} The algorithm is embarrassingly parallel but the physical fragmentation puts a limit on the accuracy that may be achieved.⁶⁶ Similar physical fragmentation approaches with (capped) fragments have also been reported.^{67–75}

Fragment-based correlation approaches

As for the wave function-based approximations, the fragment-based correlation methods rely on a conventional HF calculation. Three main schemes have been developed in this category. In the incremental scheme,^{76–79}

the correlation energy is expressed as a many-body expansion. The molecular orbitals are thus divided into single fragments (one-body) and the accuracy is controlled by the size of the fragments as well as the order of the expansion (usually using a two-body or three-body expansion). In the Cluster-in-Molecule (CIM)^{80–91} approach, occupied LMOs are used to partition the calculation of the correlation energy into small and independent fragment calculations that each uses a subset of the total orbital space. We note that the original formulation of the CIM method⁸⁰ employed a partitioning approach in terms of single and pair orbital clusters, while this approach has been abandoned in favor of having only single clusters.⁸¹ Some of the pairs were later reintroduced for improved accuracy.⁸⁶ The original formulation of the CIM method⁸⁰ also employed localized virtual orbitals, which was later abandoned in favour of a set of local virtual orbitals constructed for each fragment from PAOs.⁸¹

Finally, the DEC scheme also belongs to this category and is closely related to the CIM approach. DEC differs from CIM, since the correlation energy is partitioned into atomic fragments and pair fragments, rather than single orbital clusters, and the DEC fragments are determined dynamically in order to ensure error control in the final correlation energy. The DEC scheme is reviewed in detail below.

Local orbital basis

A large variety of local occupied and local virtual orbitals have been used in the different local correlation methods. The wave function-based CC approximations and the fragmentation-based correlation approaches use local occupied orbitals that most often have been determined using Boys⁹² or Pipek-Mezey⁹³ localization functions. Recently, advanced orbital localization functions, such as the square of the fourth central moment localization function,⁹⁴ have been introduced where the localized orbitals are less system dependent than the Boys or Pipek-Mezey localized orbitals. The more advanced localization functions combined with a robust optimization strategy⁹⁵ makes it possible to determine localized virtual orbitals, even for systems that are traditionally considered to have delocalized electronic structure.^{96,97} The localized virtual orbitals constitute an orthogonal and non-redundant set, and are very convenient for a straightforward application of standard CC implementations in local correlation methods.

PAOs have played a central role in the development of local correlation methods. However, they constitute a nonorthogonal and redundant set of virtual orbitals which often complicates the algorithmic expressions. In wave function-based approximations, PAOs can be used as a basis for expanding PNOs⁴⁶ or OSVs,⁹⁸ which further complicates the CC algorithms but lead to a very compact representation of the CC amplitudes.⁹⁸ On the other hand, it has also been shown that localized virtual

orbitals obtained using advanced localization functions are more spatially local than PAOs.^{96,97} Clearly, the optimal choice of orbitals in local correlation methods is still a very active research field.

THE DIVIDE-EXPAND-CONSOLIDATE SCHEME

The DEC scheme is designed to be a linear-scaling, highly accurate, and massively parallel CC method applicable to very large molecular systems. It is implemented in the LSDalton program,⁹⁹ which is a part of the Dalton suite.¹⁰⁰

The three most important features of the DEC scheme compared to other local correlation methods are the following:

- The sizes of the fragments are determined *dynamically* in a black-box manner to ensure error control.
- The DEC scheme is combined with a massively parallel implementation, with three levels of parallelism.
- The virtual space is described using localized virtual orbitals.^{94,95,97,101,102}

The theoretical foundation for the DEC scheme and its implementation will be detailed in the following sections.

The Divide-Expand-Consolidate energy expression

In CC theory the total energy of a molecular system may be written as a sum of a HF and a correlation contribution

$$E_{CC} = E_{HF} + E_{corr}, \quad (3)$$

where the CC correlation energy for a closed-shell system is defined as

$$E_{corr} = \sum_{ij} \sum_{ab} (t_{ij}^{ab} + t_i^a t_j^b) (2g_{aibj} - g_{biaj}), \quad (4)$$

Here, g_{aibj} are the electron repulsion integrals (ERIs) using the Mulliken notation, t_i^a and t_{ij}^{ab} denote singles and doubles CC amplitudes, and indices i, j, \dots refer to occupied HF orbitals, while a, b, \dots refer to virtual HF orbitals.

In a DEC calculation we initially determine a set of localized occupied and virtual HF molecular orbitals (MOs) and assign these to the atomic site nearest to the MO's center of charge. The CC correlation energy E_{corr} may then be expressed as

$$E_{corr} = \sum_P^{N_{frag}} \left[E_P + \sum_{Q < P}^{N_{frag}} \Delta E_{PQ} \right] \quad (5)$$

where N_{frag} is the number of the atomic fragments and the atomic fragment energy E_P and the pair fragment interaction energy ΔE_{PQ} are defined according to,

$$E_P = \sum_{ij \in \underline{P}} \sum_{ab} (t_{ij}^{ab} + t_i^a t_j^b) (2g_{aibj} - g_{biaj}), \quad (6)$$

$$\begin{aligned} \Delta E_{PQ} = & \sum_{\substack{i \in \underline{P} \\ j \in \underline{Q}}} \sum_{ab} (t_{ij}^{ab} + t_i^a t_j^b) (2g_{aibj} - g_{biaj}) \\ & + \sum_{\substack{i \in \underline{Q} \\ j \in \underline{P}}} \sum_{ab} (t_{ij}^{ab} + t_i^a t_j^b) (2g_{aibj} - g_{biaj}), \end{aligned} \quad (7)$$

where the MOs are now assumed to be local and \underline{P} denotes the set of local occupied orbitals assigned to atomic site P .

The correlation energy in Eq. (5), (6), and (7) does not contain any approximations and using these equations yield the exact correlation energy. In DEC we have thus divided the calculation of the correlation energy into $N_{\text{frag}} + 1/2 \cdot N_{\text{frag}}(N_{\text{frag}} - 1)$ independent fragment calculations. The computational savings arise when screening techniques are used on each fragment calculation. The screening used to reduce the computational effort arises from the locality of the MOs. The integral g_{aibj} vanishes when the molecular orbital ϕ_a is spatially far from ϕ_i and the summation over the virtual orbitals in Eq. (6) and Eq. (7) may therefore be restricted. The set of virtual orbitals that are important for atomic site P is denoted $[\overline{P}]$.

The summation restrictions in the fragment energy calculations are determined in a black-box manner (see next subsection) and allow us to write atomic fragment and pair fragment interaction energies as

$$E_P = \sum_{ij \in \underline{P}} \sum_{ab \in [\overline{P}]} (t_{ij}^{ab} + t_i^a t_j^b) (2g_{aibj} - g_{biaj}), \quad (8)$$

$$\begin{aligned} \Delta E_{PQ} = & \sum_{\substack{i \in \underline{P} \\ j \in \underline{Q}}} \sum_{ab \in [\overline{P}] \cup [\overline{Q}]} (t_{ij}^{ab} + t_i^a t_j^b) (2g_{aibj} - g_{biaj}) \\ & + \sum_{\substack{i \in \underline{Q} \\ j \in \underline{P}}} \sum_{ab \in [\overline{P}] \cup [\overline{Q}]} (t_{ij}^{ab} + t_i^a t_j^b) (2g_{aibj} - g_{biaj}), \end{aligned} \quad (9)$$

The set of virtual orbitals used for the pair fragment interaction energies are chosen as the union of constituting atomic fragment spaces, justified through a locality analysis.^{11,12} Note that the definition of ΔE_{PQ} have changed since the original expression¹⁰ had an inherent error similar to the basis set superposition error (BSSE).¹¹

The CCSD(T) model is often described as the *gold standard* of quantum chemistry and it is therefore of utmost importance to enable CCSD(T) calculation with the DEC scheme. However, the conventional formulation

of the (T) correction to the CCSD correlation energy¹⁰³ cannot easily be partitioned into atomic fragment and pair fragment energy contributions. In Ref. 23 it was shown how the (T) correction could be expressed in an alternative form which only requires an additional o^3v^4 scaling step compared to a conventional CCSD(T) implementation but can be partitioned in analogy with the standard CC correlation energy (see Ref. 23 for further details),

$$E^{(T)} = \sum_P \left[E_P^{(T)} + \sum_{Q < P} \Delta E_{PQ}^{(T)} \right] \quad (10)$$

with

$$E_P^{(T)} = 2 \sum_{ij \in \underline{P}} \sum_{ab \in [\overline{P}]} (2t_{ij}^{ab} - t_{ji}^{ab}) T_{ij}^{ab} + 2 \sum_{i \in \underline{P}} \sum_{a \in \overline{P}} t_i^a T_i^a \quad (11)$$

$$\begin{aligned} \Delta E_{PQ}^{(T)} = & 2 \left(\sum_{\substack{i \in \underline{P} \\ j \in \underline{Q}}} + \sum_{\substack{i \in \underline{Q} \\ j \in \underline{P}}} \right) \sum_{ab \in [\overline{P}] \cup [\overline{Q}]} (2t_{ij}^{ab} - t_{ji}^{ab}) T_{ij}^{ab} \\ & + 2 \left(\sum_{\substack{a \in \overline{P} \\ i \in \underline{Q}}} + \sum_{\substack{a \in \overline{Q} \\ i \in \underline{P}}} \right) t_i^a T_i^a. \end{aligned} \quad (12)$$

The T_{ij}^{ab} and T_i^a intermediates are defined as:¹⁰⁴

$$\begin{aligned} T_{ij}^{ab} = & \sum_{cd \in [\overline{P}]} \sum_{k \in [\underline{P}]} (t_{ijk}^{acd} L_{bckd} - t_{kji}^{acd} g_{kdbc}) \\ & - \sum_{c \in [\overline{P}]} \sum_{kl \in [\underline{P}]} (t_{ikl}^{abc} L_{kjl c} - t_{lki}^{abc} g_{kjlc}) \end{aligned} \quad (13a)$$

$$T_i^a = \sum_{cd \in [\overline{P}]} \sum_{kl \in [\underline{P}]} (t_{ikl}^{acd} - t_{lki}^{acd}) L_{kcld}. \quad (13b)$$

where, by analogy with the virtual spaces, $[\underline{P}]$ denotes the set of occupied orbitals assigned to atomic sites in the vicinity of center P . The triples amplitudes t_{ijk}^{abc} are obtained from the CCSD doubles amplitudes (see Ref. 23 for further details) and $L_{aibj} = 2g_{aibj} - g_{biaj}$.

The energy partitioning presented in Eq. (8) and (9) is based on the assignment of local occupied orbitals to atomic sites and is denoted the occupied partitioning scheme. However, since in DEC we use both local occupied and local virtual orbitals we may also formulate a virtual and a Lagrangian partitioning scheme.¹³ The three partitioning schemes yield independent ways of evaluating the correlation energy and may therefore be used to estimate the error associated with a DEC calculation. Virtual orbitals are usually less local than occupied orbitals⁹⁷ and larger fragments occur in the virtual and Lagrangian partitioning scheme than in the occupied partitioning scheme which is therefore generally preferred. However, the virtual partitioning scheme is necessary in DEC calculations of molecular gradients.^{14,18}

The atomic fragment optimization

In the previous section we described how the correlation energy may be partitioned into atomic fragment and pair fragment interaction energies. In this section we describe how the occupied and virtual orbital spaces $[\underline{P}]$ and $[\overline{P}]$ can be optimized for atomic fragment P to give a fragment energy E_P with an error determined by the fragment optimization threshold (FOT).

The atomic fragment energy E_P in Eq. (8) may be determined from the energy orbital space (EOS), $P_{\text{EOS}} \equiv \underline{P} \cup [\overline{P}]$. However, due to the coupling between the CC amplitudes it is not possible to simply solve the CC amplitude equation in P_{EOS} . The coupling can be taken into account by solving the CC amplitude equations in an extended orbital space, which includes additional occupied buffer orbitals denoted the amplitude orbital space (AOS), $P_{\text{AOS}} \equiv [\underline{P}] \cup [\overline{P}]$. Note that the occupied orbitals in the EOS ($i \in \underline{P}$) are fixed by the orbital assignment and that the virtual orbital space is the same for the EOS and the AOS. Assuming $[\underline{P}]$ and $[\overline{P}]$ to be known, the calculation of the atomic fragment energy E_P can be performed as follows:

1. Solve the CC amplitude equations in P_{AOS} .
2. Extract the CC amplitudes from P_{AOS} to P_{EOS} .
3. Calculate the two-electron integrals in P_{EOS} .
4. Use the CC amplitudes and integrals in P_{EOS} to calculate the atomic fragment energy as in Eq. (8).

The strategy used in DEC to determine the spaces $[\underline{P}]$ and $[\overline{P}]$ that give atomic fragment energies to the FOT accuracy can be divided into two steps, a fragment expansion step followed by a fragment reduction step. In the fragment expansion we generate a priority list l_r^P that describe the importance of each local orbital for the fragment energy E_P . Due to the locality of correlation effects, the distance between the center of charge of a given orbital and the atomic site P has been used to generate the list l_r^P , but other lists, for example, based on the numerical overlap of the orbitals or the Fock matrix elements have also been tested and led to similar results.

The fragment expansion starts by selecting an initial space ($[\underline{P}]$ and $[\overline{P}]$) from the priority list and calculating the fragment energy according to the recipe outlined above. The orbital spaces may then be expanded based on the priority list and an improved fragment energy is calculated. This process is repeated until the difference between the last two fragment energies is below the FOT. The fragment expansion procedure is illustrated in the left part of Figure 1. Note that at each expansion step we have to make sure that a sufficient number of orbitals is added to avoid false convergence.

Pair fragment interaction energies ΔE_{PQ} , are calculated in the union of the atomic fragment spaces $PQ_{\text{AOS}} \equiv P_{\text{AOS}} \cup Q_{\text{AOS}}$. However, it is clear that the pair fragment orbital spaces may become much larger than

the atomic fragment spaces, and that many more pair fragments than atomic fragments have to be calculated. As a consequence, any reduction in the size of the AOS for the atomic fragments will lead to important computational savings for the pair fragments. For that reason, we have introduced a fragment reduction procedure for the expanded AOS where a binary search is carried out to remove orbitals without introducing errors larger than the FOT in the atomic fragment energy. The determination of the fragment orbital spaces is summarized in Figure 1 and is considered in greater details in Ref. 12. The error control of the atomic fragment optimization comes with an overhead, and an improved fragment optimization procedure is an ongoing research direction in optimizing the DEC scheme.

Finally, we note that for DEC-CCSD or DEC-CCSD(T) calculations, the fragment optimization procedure may be performed at a lower level of theory. In Ref. 23 the fragment optimization procedure was performed at the DEC-MP2 level of theory, instead of the targeted DEC-CCSD and DEC-CCSD(T) models.

The locality of electron correlation is system dependent and the aim of the fragment optimization procedure is to obtain a method that provides the same recovery of the correlation energy for all systems, independently of the complexity of the electronic structure. The fragment spaces tend to be bigger for systems characterized by a delocalized electronic-structure such as graphene than for systems containing only non-conjugated covalent bonds. In particular for systems with a delocalized electronic-structure it is important to use the most advanced orbital localization functions, such as the squared fourth moment localization function,⁹⁴ since these localization functions are capable of giving localized sets of orbitals that are very little system dependent.⁹⁷

The pseudo-canonical basis and the DEC amplitude equations

In the fragment energy calculations of the DEC scheme the CC amplitude equations must be solved in the AOS. This is done by transforming the set of local orbitals into a pseudo-canonical basis, which is defined by diagonalizing the local Fock matrix blocks F_{ij} ($ij \in [\underline{P}]$) and F_{ab} ($ab \in [\overline{P}]$). The pseudo-canonical basis is traditionally denoted using capital letters I, J .

The CC amplitude equations are better conditioned in the pseudo-canonical basis and the MP2 amplitudes¹⁶ and (T) intermediates²³ can be obtained in a non-iterative fashion using standard canonical CC algorithms. Once the amplitude equations have been solved in the AOS, the amplitudes must be transformed back to the local basis ($t_{IJ}^{AB} \rightarrow t_{ij}^{ab}$) in order to extract the EOS amplitudes and calculate the fragment energy. A similar operation is performed for the (T) intermediates (T_{ij}^{ab} and T_i^a in Eq. (13)).

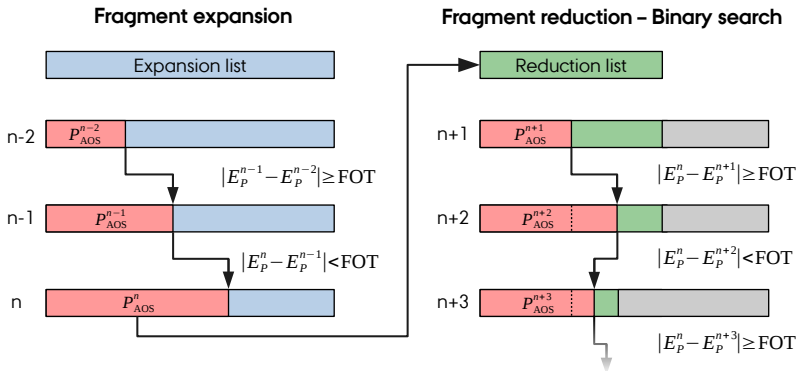


FIG. 1. Illustration of the fragment optimization procedure, E_P is the atomic fragment energy associated to atomic site P , P_{AOS} denotes the space in which the CC amplitude equations are solved and FOT is a user-defined threshold.

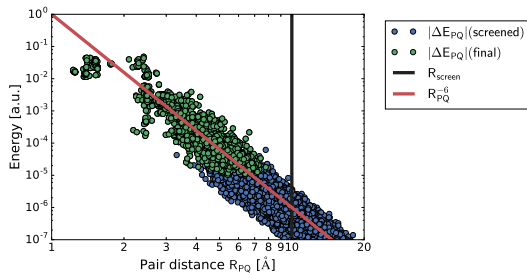


FIG. 2. Decay of the MP2 pair fragment interaction energies $|\Delta E_{PQ}|$ with the pair distance R_{PQ} for a reduced titin protein¹⁰⁵ (392 atoms) using a cc-pVDZ basis set (3772 basis functions). The expected R_{PQ}^{-6} pair decay is also plotted. The pair fragment interaction energies are separated into the calculated “final” pairs (in green) and the pairs screened away by the pair screening procedure (in blue).

The Pair Fragment calculations

The DEC scheme is only linear-scaling provided that the number of pair fragments scales linearly with the system size. Due to the decay of dispersion interactions, the pair fragment interaction energy ΔE_{PQ} decay as R_{PQ}^{-6} with the distance R_{PQ} between atomic sites P and Q . A real-space cut-off R_{screen} may therefore be used to screen away pairs with a distance greater than the distance screening threshold, e.g. $R_{PQ} > R_{\text{screen}}$, leading to a linear-scaling algorithm. This procedure was used in Ref. 10,13–16,106–108. Two issues arise with such a strategy: (i) the number of pair fragment interaction energies calculated becomes independent of the FOT and in order to converge to the standard CC correlation energy both the FOT and R_{screen} would have to be adjusted, (ii) the pair fragment interaction energies for a given pair distance

can spread over several orders of magnitude (see Figure 2), hence, a significant number of the pairs included with a distance screening threshold are less important than some of the pairs screened away. Those issues can be addressed by considering a pair screening strategy based on an estimation of the pair fragment interaction energies. To introduce such a strategy we rewrite the correlation energy in Eq. (5) in terms of a sum of effective atomic fragment energies ϵ_P

$$E_{\text{corr}} = \sum_P^{N_{\text{frag}}} \epsilon_P. \quad (14)$$

where the effective atomic fragment energy for atomic fragment P is a sum of the atomic fragment energy E_P and an average pair fragment interaction energy E_P^{av} that describes the interaction between the atomic site P and the other atomic sites

$$\epsilon_P = E_P + E_P^{av}. \quad (15)$$

where

$$E_P^{av} = \frac{1}{2} \sum_{Q \neq P} \Delta E_{PQ}. \quad (16)$$

In a previous section we described how an atomic fragment energy E_P may be determined to the FOT accuracy. In the rest of this section we describe how a pair fragment screening may be applied to ensure that the average pair fragment interaction energy is also determined to the FOT accuracy.

To obtain such a pair fragment screening we calculate pair energy estimates at the MP2 level, using minimal orbital spaces, chosen based on the priority list l_r^P , such that we obtain pair energy estimates $\Delta E_{PQ}^{\text{esti}}$ which recover 80-95% of the “exact” MP2 pair fragment interaction energies while being very cheap in terms of computational resources. A very conservative real-space cut-off

$R_{\text{screen}} = 30\text{\AA}$ ensures a linear-scaling number of pair energy estimates.

Once the pair energy estimates have been calculated, the screening strategy proceeds as follows,

1. Order all pair energy estimates associated with a given site P ,

$$|\Delta E_{P1}^{\text{esti}}| \leq |\Delta E_{P2}^{\text{esti}}| \cdots \leq |\Delta E_{PN_{\text{frag}}}^{\text{esti}}|, \quad (17)$$

where N_{frag} is the total number of atomic sites in the molecule.

2. Sum up the estimated contributions in the list starting with the smallest values until it adds up to the FOT,

$$\max_{I_P} \left(\frac{1}{2} \sum_{Q=1}^{I_P} |\Delta E_{PQ}^{\text{esti}}| \right) \leq \text{FOT} \quad (18)$$

3. All pairs $\Delta E_{PQ}^{\text{esti}}$ in the ordered list for which $Q \leq I_P$ are then screened away and not calculated, at the target CC level.

4. Repeat Step 1-3 for all atomic sites.

In Figure 2, we have plotted the decay of MP2 pair fragment interaction energies with the pair distance R_{PQ} for a reduced titin protein (FOT = 10^{-4} a.u.), see Ref. 105 for molecular structure. The plot shows which pairs are kept and which are screened away by the procedure outlined above. In the reduced titin example only about 15% of the pair fragment interaction energies have to be calculated.

The procedure presented in this section has been applied to supramolecular wires comprising up to 40 monomers of 1-aza-adamantane-trione (AAT) molecules (2440 atoms and 24440 basis functions)²⁰ in order to demonstrate the linear-scaling feature of the DEC scheme. This is shown in Figure 3.

Error Estimates

The atomic fragment optimization and the pair screening procedures described in the previous sections have been designed to ensure an error of the order of the FOT in both the atomic fragment energy E_P and the average pair fragment interaction energy E_P^{av} . In total the error of a DEC calculation thus contains a correlation error

$$\delta E_{\text{corr}} \approx 2N_{\text{frag}} \text{FOT} \quad (19)$$

The absolute error in the DEC correlation energy therefore increase linearly with the number of sites in the system, while the error in the individual atomic fragment energies is size-intensive. The electronic structure

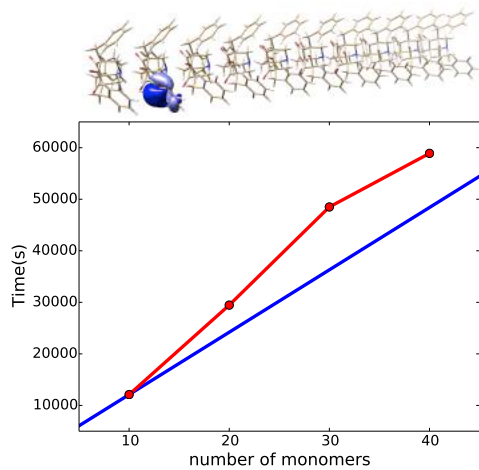


FIG. 3. Computational scaling with system size for AAT molecular wires of increasing lengths using 14952 Titan nodes.²⁰ The blue line displays the ideal linear-scaling behavior. A molecular wire containing 10 AAT monomers and one of the localized molecular orbitals are also shown.

is therefore described with a uniform accuracy for the total molecular system and size-intensive molecular properties, such as molecular gradients, may therefore be determined to the FOT precision. The recovery of the full correlation energy

$$\Delta_{\text{DEC}} = \frac{E^{\text{DEC}}}{E^{\text{corr}}}, \quad (20)$$

is also size-intensive, and for the array of calculations presented so far,^{15,17,19,20,22} Table I gives typical recoveries for several FOTs. In summary, the FOT determines the accuracy of both the individual atomic fragment energies and the total correlation energy. This is an important feature of the DEC scheme.

TABLE I. Typical recoveries for several FOTs.

| FOT | $\Delta_{\text{DEC}}(\%)$ |
|-----------|---------------------------|
| 10^{-3} | 98.2 |
| 10^{-4} | 99.8 |
| 10^{-5} | 99.985 |
| 10^{-6} | 99.998 |

The Divide-Expand-Consolidate parallelization

The DEC algorithm presented so far, scales linearly with the system size for large enough systems, i.e. when the orbital spaces are saturated for a given FOT and when the number of pair fragments that survive the

screening procedure grows linearly. However, the linear-scaling feature of DEC comes with a large prefactor and the crossover with conventional algorithm occurs for large systems. Nonetheless, the DEC scheme can be extended to a wider range of molecules by realizing that the atomic and pair fragment calculations are independent of each other and can therefore be performed in parallel. This significantly reduces the time-to-solution compared to a conventional calculation. This feature is common to all fragmentation approaches and makes the DEC algorithm well suited for supercomputers and future architectures with a large number of cores.

The DEC algorithm has been designed with three levels of parallelization:^{16,20} Coarse, medium, and fine-grained. The coarse-grained parallelization takes advantage of the independence of the fragment energy calculations, which can therefore be performed in parallel on different computing units. The medium and fine-grained level of parallelizations are not specific to DEC and are designed to parallelize the solution of the CC amplitude equations for each fragment. The fragment CC amplitude equations are standard CC amplitude equations and standard methods can be used for the parallelization of each model. In the following, we therefore focus on discussing the coarse-grained level of parallelization.

At the coarse-grained level, the available computing units are divided into a *global master*, driving the DEC calculation through a set of *local masters* that each is in command of a set of *local slaves* to execute the individual fragment calculations. The global master starts by constructing a job list where each job (an atomic or pair fragment interaction energy calculation) is ordered based on an estimation of the workload (the size of the fragment orbital space). The global master then communicates to each local master the information necessary to calculate a given fragment energy, starting with the largest fragments. Once every local master has been assigned a fragment calculation, the global master waits for the results from the local masters, and distributes the remaining fragment calculations on the joblist as the local masters become available. When all the jobs have been distributed, the global master waits for all the local masters to finish. Finally the global master calculates the correlation energy based on Eq. (5). The parallelization of the DEC scheme is illustrated in Figure 4.

Regarding the medium-grained parallelization, the number of local slaves allocated to each local master is determined on-the-fly, based on the workload of the current job. Due to the steep scaling with fragment sizes there is a huge difference in the computational cost of the smallest and largest fragments. The medium-grained parallelism ensures that more computational resources are used for the more expensive jobs and thereby offsets this difference to some extent. In practice each local master starts with a large number of local slaves and during the calculation each local master will be requested to perform smaller and smaller calculations (due to the ordered job list). Once the number of slaves is too large com-

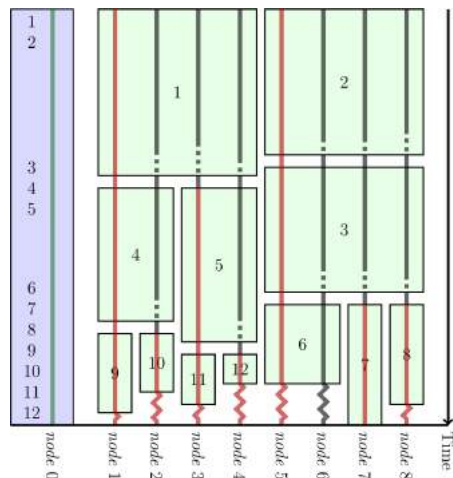


FIG. 4. Schematic representation of the coarse and medium-grained parallelization of the DEC scheme for a 12 fragment calculation on 9 nodes. Node 0 corresponds to the global master while each light green block correspond to a fragment calculation. The red and grey lines denote local master and slaves, respectively. Finally, the dashes inside the fragments correspond to idle time during the medium-grained parallelization, while the wiggles denote idle time during the coarse-grained parallelization.

pared to the workload the local master appoints a new local master from its set of slaves and divides the slaves among the two local masters. This dynamic scheduling is important in order to minimize the idling time of all the computing units (see Figure 4). Such a parallelism strategy allows the DEC algorithm to efficiently utilize several thousands computer nodes as demonstrated in Ref. 16 and 20. The strong scaling behavior with up to 18400 nodes has been demonstrated for 10 monomers of AATs,²⁰ see Figure 5.

In the atomic fragment optimization, the workload associated with a given fragment varies and cannot be known in advance. In that part of the calculation, we therefore assign a fixed number of nodes to all fragments. This can lead to significant idle time which is reduced by distributing the calculation of the many pair energy estimates to the nodes that are already done with the fragment optimization.

Using CC methodologies that require large amounts of I/O could result in a situation where all nodes read or write to the file system simultaneously and this pose a problem for parallel distributed file systems. Furthermore, the future of file systems are unknown, and optimal I/O behavior often hinders portability. Thus, in the DEC scheme integral direct algorithms and parallel distributed-memory storage have been exploited to avoid I/O altogether.

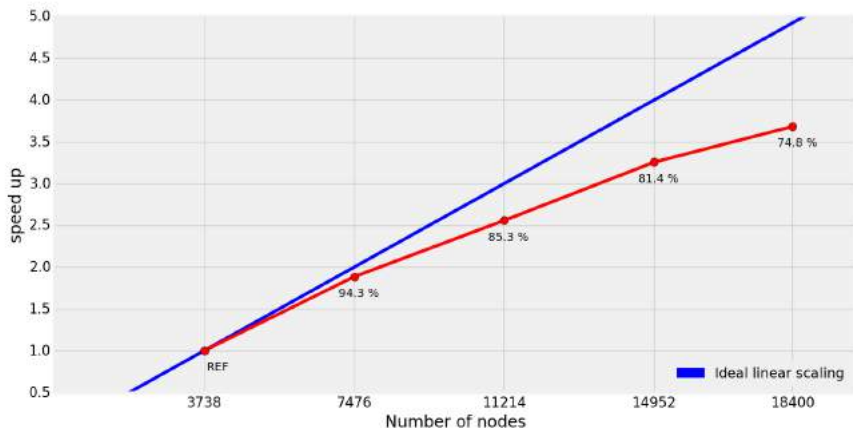


FIG. 5. Strong scaling plot for coarse-grained parallelization: AAT_{10} using 3738 to 18400 nodes with strong scaling efficiency numbers along the curve. The blue line displays ideal strong scaling behavior.

Overview of DEC developments

The DEC scheme was first introduced in Ref. 10 together with proof-of-concept calculations at the MP2 and CCSD levels. A locality analysis of the MP2 and CCSD amplitude equations was then presented¹¹ and refined¹² along with a practical implementation of the DEC algorithm. The virtual and Lagrangian DEC partitioning schemes were introduced in Ref. 13 to provide an internal consistency check of the calculated correlation energy. These partitioning schemes were also central for developing the DEC-MP2 molecular gradient.¹⁴ As a first real application, we performed DEC-MP2 calculations on a single insulin monomer (787 atoms, 7604 basis functions) and reported the correlation energy and the electrostatic potential of the molecule in a cc-pVDZ basis.¹⁵ The DEC-MP2 results were then used to benchmark DFT functionals for large molecular systems^{107,108} as described in Figure 6. The three-level parallelism strategy of DEC was detailed in Ref. 16 with calculations on two molecular systems containing 528 and 1056 atoms (4278 and 8556 basis functions) and using 47,120 and 94,240 cores. To reduce the computational requirements of the DEC-MP2 model we applied the resolution-of-the-identity (RI) approximation to the two-electron integrals,^{17,18} ported parts of the code to general purpose graphics processing units (GPGPUs),¹⁹ and applied the resulting code to supramolecular wires containing up to 40 monomers of AATs (2440 atoms and 24440 basis functions).²⁰ The DEC-RI-MP2 method has also been extended with explicitly correlated (F_{12}) techniques to provide faster convergence to the complete basis set limit,²¹ and it has been augmented with a Laplace transformation²² (DEC-LT-RIMP2), which offers signif-

icant speedup. Finally, the DEC-CCSD(T) model was recently introduced along with proof-of-concept calculations on medium-sized molecules.²³

DISCUSSION AND OUTLOOK

We have presented the DEC scheme as summarized in Figure 7, which is a linear-scaling and massively parallel framework for CC calculations that ensures error control in a black-box manner. These features enables DEC-CC calculations that are outside the scope of standard CC algorithms.^{15,16,19,20} Although DEC is a linear-scaling method, its prefactor is very high since the orbital spaces for the different fragments overlap, leading to recalculations of integrals and amplitudes. For calculations on a single compute node, the cross-over point in terms of computational effort between DEC and a conventional (canonical) calculation therefore occurs for rather large molecular systems, and if a canonical calculation is feasible it is likely faster than the DEC calculation.¹⁷ However, if many compute nodes are available, the massively parallel attributes of the DEC algorithm will lead to a shorter time-to-solution than a canonical calculation. In the future the floating point operations will likely continue to become cheaper and the number of cores on a compute node will continue to increase. In such an environment, parallelization is crucial and a large amount of recalculation is acceptable if it allows for a massively parallel computational strategy.

The large-scale DEC calculations performed so far have been carried out using the MP2 model,^{15,16,19,20} and at this stage the redundancy in a DEC-LT-RIMP2²² calculation is so limited that it is poised to become a mainstream method, applicable on all computational architec-

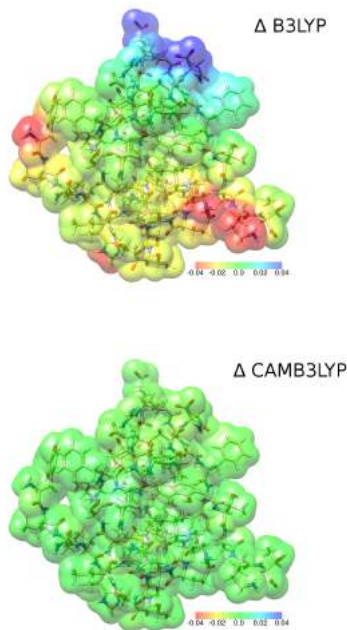


FIG. 6. Benchmarking DFT functionals against DEC-MP2 electrostatic potential. Top: difference between the MP2 and B3LYP electrostatic potential. Bottom: difference between the MP2 and CAMB3LYP electrostatic potential. It was demonstrated¹⁰⁷ that B3LYP incorrectly predict partial electron transfer from anionic to cationic sites due to a combination of self-interaction errors and an incorrect distance dependencies of the B3LYP functional. On the other hand, the range-separated CAMB3LYP functional performs much better because of the elimination of self-interaction errors at long distances.

tures. The DEC-LT-RIMP2 method is effectively limited by the preliminary HF calculation and orbital localization.

In principle, the DEC scheme provides the framework for a linear-scaling and massively parallel implementations of any CC model, but some technical challenges remain to be solved before DEC becomes a mainstream tool for the more accurate CC models. For example, while the error control of the DEC-CCSD(T) method has been demonstrated,²³ the current DEC-CCSD(T) algorithm can only be applied to large molecules for loose FOT values, due to the sizes of the fragments encountered. For large compact molecules and using basis sets of triple- ζ quality, the fragments often contain more than 1000 basis functions.¹⁹ Such dimensions are out of reach even for massively parallel CCSD(T) implementations and thus prevent high-accuracy DEC-CCSD(T) applications. However, the large pair fragments are often associated with a minor energy contributions and it may be

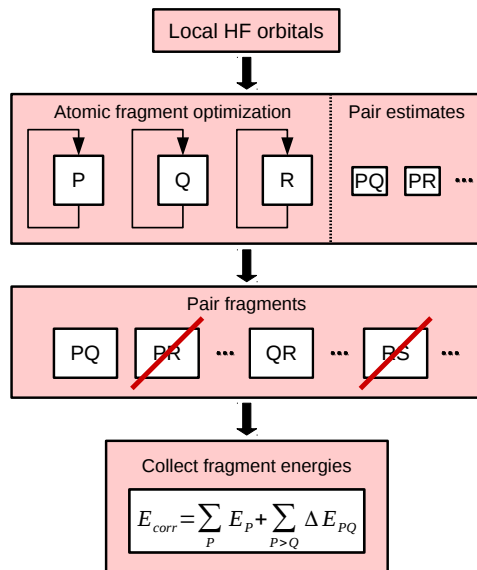


FIG. 7. Overview of a typical DEC calculation. The HF orbitals are localized and assigned to atomic sites. The atomic fragment optimization is then performed as described in Figure 1 along with the calculation of pair energy estimates used for the pair screening procedure. The pairs that have not been screened away are then calculated (usually the time-dominating part). Finally, the fragment energies are collected and added to obtain the total correlation energy.

possible to reduce the pair orbital spaces further without compromising the precision of the final correlation energy. Alternatively, it may also be possible to reduce the scaling of the high-level CC fragment calculations by considering tensor factorization techniques, PNOs, or other fragment specific orbitals. For example, the DEC scheme could be combined with PNO-based local CC methods to fully exploit the sparsity of correlation effects in each fragment calculation. Such a combination would allow for CC calculations on systems of unprecedented sizes where all bottlenecks of wave function-based approximations are removed through the DEC scheme.

Finally we note that the implementation of the DEC scheme ensures performance portability and the DEC scheme will thus automatically benefit from new hardware developments and automatically extend its application range as computational resources become more affordable.

ACKNOWLEDGMENTS

This research used resources of the Oak Ridge Leadership Computing Facility at Oak Ridge National Lab-

oratory, which is supported by the Office of Science of the Department of Energy under Contract DE-AC05-00OR22725.

The research leading to these results has received funding from the European Research Council under the European Unions Seventh Framework Programme (FP/2007-2013)/ERC Grant Agreement no. 291371.

We acknowledge PRACE for awarding us access to resource CURIE based in France at the Trs Grand Centre de Calcul (TGCC) operated by CEA near Paris.

D.B. acknowledges the Marie Curie Individual Fellowship funding for "DECOS", project number 657514.

REFERENCES

- 1 I. Shavitt and R. J. Bartlett, *Many-Body Methods in Chemistry and Physics. MBPT and Coupled-Cluster Theory* (Cambridge Uni. Press, Cambridge, 2009).
- 2 E. Apra, R. Harrison, W. deJong, A. Rendell, V. Tippa-raj, and S. Xantheas, SC09, submission for Gordon Bell prize (2009).
- 3 M. Katouda and T. Nakajima, *Journal of Chemical Theory and Computation* **9**, 5373 (2013).
- 4 M. Katouda, A. Naruse, Y. Hirano, and T. Nakajima, *Journal of Computational Chemistry* **37**, 2623 (2016).
- 5 E. Solomonik, D. Matthews, J. R. Hammond, J. F. Stanton, and J. Demmel, *Journal of Parallel and Distributed Computing* **74**, 3176 (2014), domain-Specific Languages and High-Level Frameworks for High-Performance Computing.
- 6 E. Solomonik, D. Matthews, J. Hammond, and J. Demmel, "Cyclops tensor framework: reducing communication and eliminating load imbalance in massively parallel contractions," Tech. Rep. UCB/EECS-2012-210 (EECS Department, University of California, Berkeley, 2012).
- 7 J. Nieplocha, R. J. Harrison, and R. J. Littlefield, *The Journal of Supercomputing* **10**, 169 (1996).
- 8 V. Lotrich, N. Flocke, M. Ponton, B. A. Sanders, E. Deumens, R. J. Bartlett, and A. Perera, in *Proceedings of the 23rd International Conference on Supercomputing*, ICS '09 (ACM, New York, NY, USA, 2009) pp. 523-524.
- 9 C. Peng, J. A. Calvin, F. Pavoevi, J. Zhang, and E. F. Valeev, *The Journal of Physical Chemistry A* **120**, 10231 (2016).
- 10 M. Ziolkowski, B. Jansik, T. Kjergaard, and P. Jørgensen, *J. Chem. Phys.* **133**, 014107 (2010).
- 11 K. Kristensen, M. Ziolkowski, B. Jansik, T. Kjergaard, and P. Jørgensen, *J. Chem. Theory Comput.* **7**, 1677 (2011).
- 12 P. Ettenhuber, P. Baudin, T. Kjergaard, P. Jørgensen, and K. Kristensen, *The Journal of Chemical Physics* **144**, 164116 (2016), <http://dx.doi.org/10.1063/1.4947019>.
- 13 I.-M. Høyvik, K. Kristensen, B. Jansik, and P. Jørgensen, *The Journal of Chemical Physics* **136**, 014105 (2012).
- 14 K. Kristensen, P. Jørgensen, B. Jansik, T. Kjergaard, and S. Reine, *J. Chem. Phys.* **137**, 114102 (2012).
- 15 K. Kristensen, I.-M. Høyvik, B. Jansik, P. Jørgensen, T. Kjergaard, S. Reine, and J. Jakowski, *Phys. Chem. Chem. Phys.* **14**, 15706 (2012).
- 16 K. Kristensen, T. Kjergaard, I.-M. Høyvik, P. Ettenhuber, P. Jørgensen, B. Jansik, S. Reine, and J. Jakowski, *Molecular Physics* **111**, 1196 (2013).
- 17 P. Baudin, P. Ettenhuber, S. Reine, K. Kristensen, and T. Kjergaard, *The Journal of Chemical Physics* **144**, 054102 (2016), <http://dx.doi.org/10.1063/1.4940732>.
- 18 D. Bykov, K. Kristensen, and T. Kjergaard, *The Journal of Chemical Physics* **145**, 024106 (2016), <http://dx.doi.org/10.1063/1.4956454>.
- 19 D. Bykov and T. Kjergaard, *Journal of Computational Chemistry* **38**, 228 (2017).
- 20 T. Kjergaard, P. Baudin, D. Bykov, J. J. Eriksen, P. Ettenhuber, K. Kristensen, J. Larkin, D. Liakh, F. Pawlowski, A. Vose, Y. M. Wang, and P. Jørgensen, *Computer Physics Communications* **212**, 152 (2017).
- 21 Y. M. Wang, C. Hättig, S. Reine, E. Valeev, T. Kjergaard, and K. Kristensen, *The Journal of Chemical Physics* **144**, 204112 (2016), <http://dx.doi.org/10.1063/1.4951696>.
- 22 T. Kjergaard, *The Journal of Chemical Physics* (2016).
- 23 J. J. Eriksen, P. Baudin, P. Ettenhuber, K. Kristensen, T. Kjergaard, and P. Jørgensen, *Journal of Chemical Theory and Computation* **11**, 2984 (2015).
- 24 P. Pulay, *Chem. Phys. Letters* **100**, 151 (1983).
- 25 E. Kapuy, Z. Csépes, and C. Kozmutza, *International Journal of Quantum Chemistry* **23**, 981 (1983).
- 26 S. Saebo and P. Pulay, *Ann. Rev. Phys. Chem.* **44**, 213 (1993).
- 27 P. Pulay and S. Saebo, *Theoretica chimica acta* **69**, 357 (1986).
- 28 G. Hetzer, P. Pulay, and H.-J. Werner, *Chemical Physics Letters* **290**, 143 (1998).
- 29 M. Schütz, G. Hetzer, and H.-J. Werner, *Journal of Chemical Physics* **111**, 5691 (1999).
- 30 C. Hampel and H.-J. Werner, *J. Chem. Phys.* **104**, 6286 (1996).
- 31 A. E. Azhary, G. Rauhut, P. Pulay, and H.-J. Werner, *J. Chem. Phys.* **108**, 5185 (1998).
- 32 M. Schütz, *J. Chem. Phys.* **113**, 9986 (2000).
- 33 M. Schütz and H.-J. Werner, *J. Chem. Phys.* **114**, 661 (2001).
- 34 H.-J. Werner, F. R. Manby, and P. J. Knowles, *The Journal of Chemical Physics* **118**, 8149 (2003).
- 35 M. Schütz, H.-J. Werner, R. Lindh, and F. Manby, *Journal of Chemical Physics* **121**, 737 (2004).
- 36 H.-J. Werner and F. Manby, *Journal of Chemical Physics* **124** (2006), [10.1063/1.2150817](http://dx.doi.org/10.1063/1.2150817).
- 37 D. Kats, D. Usvyat, and M. Schutz, *Phys. Chem. Chem. Phys.* **10**, 3430 (2008).
- 38 F. Neese, A. Hansen, and D. G. Liakos, *J. Chem. Phys.* **131**, 064103 (2009).
- 39 S. Kossmann and F. Neese, *Journal of Chemical Theory and Computation* **6**, 2325 (2010).
- 40 H.-J. Werner and M. Schütz, *J. Chem. Phys.* **135**, 144116 (2011).
- 41 R. B. Murphy, M. D. Beachy, R. A. Friesner, and M. N. Ringnalda, *The Journal of Chemical Physics* **103**, 1481 (1995).
- 42 P. Maslen and M. Head-Gordon, *Chemical Physics Letters* **283**, 102 (1998).
- 43 J. E. Subotnik, A. Sodt, and M. Head-Gordon, *J. Chem. Phys.* **125**, 074116 (2006).
- 44 C. Edmiston and M. Krauss, *The Journal of Chemical Physics* **42**, 1119 (1965).
- 45 F. Neese, F. Wennmohs, and A. Hansen, *The Journal of Chemical Physics* **130**, 114108 (2009), <http://dx.doi.org/10.1063/1.3086717>.
- 46 C. Riplinger and F. Neese, *The Journal of Chemical Physics* **138**, 034106 (2013), <http://dx.doi.org/10.1063/1.4773581>.
- 47 P. Pinski, C. Riplinger, E. F. Valeev, and F. Neese, *The Journal of Chemical Physics* **143**, 034108 (2015), <http://dx.doi.org/10.1063/1.4926879>.
- 48 C. Riplinger, P. Pinski, U. Becker, E. F. Valeev, and F. Neese, *The Journal of Chemical Physics* **144**, 024109 (2016), <http://dx.doi.org/10.1063/1.4939030>.
- 49 G. Schmitz, B. Helmich, and C. Hättig, *Molecular Physics* **111**, 2463 (2013).
- 50 Y. Minenkov, E. Chermak, and L. Cavallo, *Journal of Chemical Theory and Computation* **11**, 4664 (2015).
- 51 D. G. Liakos and F. Neese, *Journal of Chemical Theory and Computation* **11**, 4054 (2015).
- 52 M. Sparta, D. Bykov, and F. Neese, *Moess. Eff. Ref. Data J.* **37**, 69 (2014).
- 53 M. Sparta, C. Riplinger, and F. Neese, *Journal of Chemical Theory and Computation* **10**, 1099 (2014).

- ⁵⁴M. Sparta and F. Neese, *Chem. Soc. Rev.* **43**, 5032 (2014).
- ⁵⁵J. Yang, Y. Kurashige, F. R. Manby, and G. K. L. Chan, *J. Chem. Phys.* **134**, 044123 (2011).
- ⁵⁶J. Yang, G. K. L. Chan, F. R. Manby, M. Schütz, and H.-J. Werner, *J. Chem. Phys.* **136**, 114105 (2012).
- ⁵⁷W. Yang, *Phys. Rev. Lett.* **66**, 1438 (1991).
- ⁵⁸W. Yang, *Phys. Rev. A* **44**, 7823 (1991).
- ⁵⁹W. Yang and T. Lee, *The Journal of Chemical Physics* **103**, 5674 (1995).
- ⁶⁰M. Kobayashi, Y. Imamura, and H. Nakai, *J. Chem. Phys.* **127**, 074103 (2007).
- ⁶¹M. Kobayashi and H. Nakai, *The Journal of Chemical Physics* **129**, 044103 (2008), <http://dx.doi.org/10.1063/1.2956490>.
- ⁶²M. Kobayashi and H. Nakai, *The Journal of Chemical Physics* **131**, 114108 (2009), <http://dx.doi.org/10.1063/1.3211119>.
- ⁶³K. Kitaura, E. Ikeo, T. Asada, T. Nakano, and M. Uebayasi, *Chemical Physics Letters* **313**, 701 (1999).
- ⁶⁴Y. Mochizuki, K. Yamashita, T. Murase, T. Nakano, K. Fukuzawa, K. Takematsu, H. Watanabe, and S. Tanaka, *Chemical Physics Letters* **457**, 396 (2008).
- ⁶⁵S. Tanaka, Y. Mochizuki, Y. Komeiji, Y. Okiyama, and K. Fukuzawa, *Phys. Chem. Chem. Phys.* **16**, 10310 (2014).
- ⁶⁶D. Cremer, *Wiley Interdisciplinary Reviews: Computational Molecular Science* **1**, 509 (2011).
- ⁶⁷D. W. Zhang and J. Z. H. Zhang, *The Journal of Chemical Physics* **119**, 3599 (2003).
- ⁶⁸N. Flocke and R. J. Bartlett, *J. Chem. Phys.* **121**, 10935 (2004).
- ⁶⁹V. Deev and M. A. Collins, *J. Chem. Phys.* **122**, 154102 (2005).
- ⁷⁰W. Li, T. Fang, and S. Li, *The Journal of Chemical Physics* **124**, 154102 (2006), <http://dx.doi.org/10.1063/1.2186997>.
- ⁷¹R. P. A. Bettens and A. M. Lee, *The Journal of Physical Chemistry A* **110**, 8777 (2006).
- ⁷²X. He and J. Z. H. Zhang, *The Journal of Chemical Physics* **124**, 184703 (2006), <http://dx.doi.org/10.1063/1.2194535>.
- ⁷³W. Li, S. Li, and Y. Jiang, *The Journal of Physical Chemistry A* **111**, 2193 (2007).
- ⁷⁴A. P. Rahalkar, M. Katouda, S. R. Gadre, and S. Nagase, *J. Comput. Chem.* **31**, 2405 (2010).
- ⁷⁵H.-A. Le, H.-J. Tan, J. F. Ouyang, and R. P. A. Bettens, *Journal of Chemical Theory and Computation* **8**, 469 (2012).
- ⁷⁶H. Stoll, *Phys. Rev. B* **46**, 6700 (1992).
- ⁷⁷J. Friedrich, M. Hanrath, and M. Dolg, *J. Chem. Phys.* **126**, 154110 (2007).
- ⁷⁸J. Friedrich and M. Dolg, *J. Chem. Theory Comput.* **5**, 287 (2009).
- ⁷⁹T. Anacker, D. P. Tew, and J. Friedrich, *Journal of Chemical Theory and Computation* **12**, 65 (2016).
- ⁸⁰S. Li, J. Ma, and Y. Jiang, *Journal of Computational Chemistry* **23**, 237 (2002).
- ⁸¹S. Li, J. Shen, W. Li, and Y. Jiang, *The Journal of Chemical Physics* **125**, 074109 (2006), <http://dx.doi.org/10.1063/1.2244566>.
- ⁸²W. Li, P. Piecuch, J. R. Gour, and S. Li, *The Journal of Chemical Physics* **131**, 114109 (2009), <http://dx.doi.org/10.1063/1.3218842>.
- ⁸³W. Li and P. Piecuch, *The Journal of Physical Chemistry A* **114**, 6721 (2010).
- ⁸⁴W. Li and P. Piecuch, *The Journal of Physical Chemistry A* **114**, 8644 (2010).
- ⁸⁵Z. Rolik and M. Kállay, *The Journal of Chemical Physics* **135**, 104111 (2011), <http://dx.doi.org/10.1063/1.3632085>.
- ⁸⁶W. Li, Y. Guo, and S. Li, *Phys. Chem. Chem. Phys.* **14**, 7854 (2012).
- ⁸⁷Z. Rolik, L. Szegegy, I. Ladjánszki, B. Ladóczy, and M. Kállay, *The Journal of Chemical Physics* **139**, 094105 (2013), <http://dx.doi.org/10.1063/1.4819401>.
- ⁸⁸Y. Guo, W. Li, and S. Li, *The Journal of Physical Chemistry A* **118**, 8996 (2014).
- ⁸⁹A. D. Findlater, F. Zahariev, and M. S. Gordon, *The Journal of Physical Chemistry A* **119**, 3587 (2015).
- ⁹⁰W. Li, Z. Ni, and S. Li, *Molecular Physics* **114**, 1447 (2016).
- ⁹¹P. R. Nagy, G. Samu, and M. Kállay, *Journal of Chemical Theory and Computation* **12**, 4897 (2016).
- ⁹²S. F. Boys, *Rev. Mod. Phys.* **32**, 296 (1960).
- ⁹³J. Pipek and P. G. Mezey, *J. Chem. Phys.* **90**, 4916 (1989).
- ⁹⁴I.-M. Høyvik, B. Jansik, and P. Jørgensen, *The Journal of Chemical Physics* **137**, 224114 (2012).
- ⁹⁵I.-M. Høyvik, B. Jansik, and P. Jørgensen, *Journal of Chemical Theory and Computation* **8**, 3137 (2012).
- ⁹⁶I.-M. Høyvik, K. Kristensen, T. Kjærgaard, and P. Jørgensen, *Theoretical Chemistry Accounts* **133**, 1417 (2013), [10.1007/s00214-013-1417-x](https://doi.org/10.1007/s00214-013-1417-x).
- ⁹⁷I.-M. Høyvik and P. Jørgensen, *Chemical Reviews* **116**, 3306 (2016).
- ⁹⁸C. Krause and H.-J. Werner, *Phys. Chem. Chem. Phys.* **14**, 7591 (2012).
- ⁹⁹LSDalton, a linear scaling molecular electronic structure program, Release Dalton2016 (2016), see <http://daltonprogram.org>.
- ¹⁰⁰K. Aidas, C. Angeli, K. L. Bak, V. Bakken, R. Bast, L. Boman, O. Christiansen, R. Cimraglia, S. Coriani, P. Dahle, E. K. Dalskov, U. Ekström, T. Enevoldsen, J. J. Eriksen, P. Ettenhuber, B. Fernández, L. Ferrighi, H. Fliegl, L. Frediani, K. Hald, A. Halkier, C. Hättig, H. Heiberg, T. Helgaker, A. C. Hennum, H. Hettema, E. Hjertenæs, S. Høst, I.-M. Høyvik, M. F. Iozzi, B. Jansik, H. J. A. Jensen, D. Jonsson, P. Jørgensen, J. Kauczor, S. Kirpekar, T. Kjærgaard, W. Klopper, S. Knecht, R. Kobayashi, H. Koch, J. Kongsted, A. Krapp, K. Kristensen, A. Ligabue, O. B. Lutnæs, J. I. Melo, K. V. Mikkelsen, R. H. Myhre, C. Neiss, C. B. Nielsen, P. Norman, J. Olsen, J. M. H. Olsen, A. Osted, M. J. Packer, F. Pawłowski, T. B. Pedersen, P. F. Provasi, S. Reine, Z. Rinkevicius, T. A. Ruden, K. Ruud, V. Rybkin, P. Salek, C. C. M. Samson, A. S. de Merás, T. Saue, S. P. A. Sauer, B. Schimmelpennig, K. Snegov, A. H. Steindal, K. O. Sylvester-Hvid, P. R. Taylor, A. M. Teale, E. I. Tellgren, D. P. Tew, A. J. Thorvaldsen, L. Thøgersen, O. Vahtras, M. A. Watson, D. J. D. Wilson, M. Ziolkowski, and H. Ågren, *WIREs Comput. Mol. Sci.* **4**, 269 (2013).
- ¹⁰¹M. Ziolkowski, B. Jansík, P. Jørgensen, and J. Olsen, *The Journal of Chemical Physics* **131**, 124112 (2009).
- ¹⁰²B. Jansík, S. Høst, K. Kristensen, and P. Jørgensen, *The Journal of Chemical Physics* **134**, 194104 (2011).
- ¹⁰³K. Raghavachari, G. W. Trucks, J. A. Pople, and M. Head-Gordon, *Chem. Phys. Letters* **157**, 479 (1989).
- ¹⁰⁴T. Helgaker, P. Jørgensen, and J. Olsen, *Molecular Electronic Structure Theory, First Edition* (Wiley, Chichester, England, 2000).
- ¹⁰⁵S. Reine, A. Krapp, M. F. Iozzi, V. Bakken, T. Helgaker, F. Pawłowski, and P. Salek, *J. Chem. Phys.* **133**, 044102 (2010).
- ¹⁰⁶K. Kristensen, M. Ziolkowski, B. Jansík, T. Kjærgaard, and P. Jørgensen, *Journal of Chemical Theory and Computation* **7**, 1677 (2011).
- ¹⁰⁷S. Jakobsen, K. Kristensen, and F. Jensen, *Journal of Chemical Theory and Computation* **9**, 3978 (2013).
- ¹⁰⁸J. M. H. Olsen, N. H. List, K. Kristensen, and J. Kongsted, *Journal of Chemical Theory and Computation* **11**, 1832 (2015).

B.2 Orbital spaces in the Divide–Expand–Consolidate coupled cluster method

P. Ettenhuber, [P. Baudin](#), T. Kjærgaard, P. Jørgensen, and K. Kristensen

J. Chem. Phys. **144**, 164116 (2016).

Major contributions: production of the data contained in the *numerical illustrations* section, and code implementation (atomic fragment optimization).

Proportional contribution: writing process.

Orbital spaces in the divide-expand-consolidate coupled cluster method

Patrick Ettenhuber,^{a)} Pablo Baudin, Thomas Kjærgaard, Poul Jørgensen,
and Kasper Kristensen

*qLEAP Center for Theoretical Chemistry, Department of Chemistry, Aarhus University,
Langelandsgade 140, DK-8000 Aarhus C, Denmark*

(Received 5 February 2016; accepted 5 April 2016; published online 28 April 2016)

The theoretical foundation for solving coupled cluster singles and doubles (CCSD) amplitude equations to a desired precision in terms of independent fragment calculations using restricted local orbital spaces is reinvestigated with focus on the individual error sources. Four different error sources are identified theoretically and numerically and it is demonstrated that, for practical purposes, local orbital spaces for CCSD calculations can be identified from calculations at the MP2 level. The development establishes a solid theoretical foundation for local CCSD calculations for the independent fragments, and thus for divide-expand-consolidate coupled cluster calculations for large molecular systems with rigorous error control. Based on this theoretical foundation, we have developed an algorithm for determining the orbital spaces needed for obtaining the single fragment energies to a requested precision and numerically demonstrated the robustness and precision of this algorithm. *Published by AIP Publishing.* [<http://dx.doi.org/10.1063/1.4947019>]

I. INTRODUCTION

Highly accurate calculations of molecular energies and properties have been feasible for many years using coupled cluster (CC) theory. While it is possible to achieve accuracies challenging experiment,¹ the CC hierarchy of methods in a conventional formulation is restricted to small molecules due to an inherent high-polynomial scaling. With the increasing experimental possibilities and general interest in life and material sciences to address more and more complex chemical systems, the need for highly accurate electronic structure calculations for large molecules is growing rapidly. Since the steep scaling of the CC methods is a direct consequence of the nonlocal nature of the routinely used canonical Hartree-Fock (HF) orbitals, it was realized early that local orbitals would allow for an accurate linear-scaling description of the electronic correlation effects in large molecules and several local CC methods have been developed since.

Local correlation methods were pioneered by Pulay and Saebo,^{2,3} and an early prominent contribution is the local coupled cluster (LCC) method of Werner and coworkers.^{4,5} Many other local CC methods have been proposed, e.g., the atomic orbital (AO)-based CC,^{6,7} the natural linear scaling approach,⁸ the cluster-in-a-molecule approach,⁹⁻¹¹ the divide-and-conquer approach,^{12,13} the fragment molecular orbital (MO) approach,^{14,15} and the incremental scheme.^{16,17} Linear scaling has also been achieved in second order Møller-Plesset perturbation theory (MP2) calculations using a Laplace-transformation of the energy denominator¹⁸ with an effective integral screening.^{19,20} In recent years the highly successful pair natural orbitals²¹⁻²³ and orbital specific virtual orbitals²⁴ have been used in order to achieve linear scaling

for CC methods. In local CC methods, *ad hoc* approximations have often been introduced, for example, by assigning fixed virtual correlating orbital spaces to local occupied orbitals, or by a physical fragmentation of the molecule. The precision of a local correlated calculation compared to a standard calculation is in general made unclear by these approximations.

In the standard CC methods, the precision of a calculation is determined by the residual norm threshold for the cluster amplitude equations. The precision is thus defined prior to a calculation. This *a priori* knowledge of the precision is an important feature and one of the reasons for the success of CC calculations on small molecular systems. In the recently introduced divide-expand-consolidate (DEC) local CC method,²⁵⁻³² the precision is similarly defined prior to a calculation. In the DEC method, a calculation on a full molecular system is divided into a sequence of single fragment and pair fragment calculations referencing small parts of the orbital space of the full molecular system and the precision is defined by the fragment optimization threshold (FOT) that is imposed on the single fragment energy calculations. The FOT is used to identify the orbital spaces where the cluster amplitude equations have to be solved to give the single fragment energies to the FOT precision. Using unions of single fragment orbital spaces in the pair fragment calculations, the precision of the total energy is ultimately determined by the FOT value as demonstrated numerically in Refs. 25-27, 31, and 32. In this paper, we describe how these orbital spaces for the single fragment calculations may be determined for the MP2 and CC with singles and doubles excitations (CCSD) models. The screening of pair fragments that is necessary to obtain a linear-scaling algorithm for determining the total correlation energy with rigorous error control will be described in a forthcoming publication.

A DEC calculation may be described both in terms of an occupied and a virtual partitioning of the CC correlation

^{a)}Electronic mail: pettenhuber@gmail.com

energy,²⁷ which provide two alternative ways of partitioning the correlation energy for the full molecular system into fragment calculations using subsets of the complete molecular orbital space. These two partitioning schemes therefore provide an internal consistency check of the precision²⁹ and both schemes have been required for calculating molecular gradients.²⁸ We have previously carried out a locality analysis for the occupied partitioning scheme, which demonstrates how orbital spaces may be selected for evaluating the single fragment energies.²⁶ In this paper, we improve and generalize this locality analysis to include the virtual partitioning scheme. We analyze the general coupling mechanisms in the MP2 and CCSD amplitude equations theoretically as well as numerically, and we investigate the resulting errors when the amplitude equations are solved in a restricted local orbital space. For MP2, the only coupling mechanism is caused by short-ranged Fock matrix terms in the MP2 amplitude equations, while for the CCSD model, orbital space extensions may also occur via a mechanism involving long-range interactions originating from two-electron integrals in the CCSD amplitude equations. We demonstrate that both the MP2 and CCSD equations may be solved in local restricted orbital spaces with rigorous error control in the single fragment energy.

In Section II we summarize the DEC algorithm. In Section III we analyze the locality of the MP2 and CCSD amplitude equations and identify the coupling mechanisms in the amplitude equations. In Section IV we use this information to develop a practical black-box algorithm that may be used to determine the single fragment energies to the FOT precision. In Section V we analyze the efficiency of the single fragment optimization algorithm numerically and in Section VI we give some concluding remarks.

II. THE DEC ALGORITHM SUMMARIZED

In this section we briefly summarize the DEC-CC method with emphasis on giving the background that is required for determining the local orbital spaces needed to solve cluster amplitude equations and obtain the single fragment energies to the predefined FOT tolerance.

The CC correlation energy for a closed-shell molecular system may be expressed as

$$E_{corr} = \sum_{iajb} (t_{ij}^{ab} + t_i^a t_j^b) (2g_{iajb} - g_{ibja}) = \sum_{iajb} \tau_{ij}^{ab} L_{iajb}, \quad (1)$$

where t_i^a and t_{ij}^{ab} are the singles and doubles cluster amplitudes, respectively, g_{iajb} are two-electron integrals in the Mulliken notation, and we have introduced $\tau_{ij}^{ab} = t_{ij}^{ab} + t_i^a t_j^b$ and $L_{iajb} = 2g_{iajb} - g_{ibja}$. Indices i, j (a, b) refer to occupied (unoccupied) HF molecular orbitals (MOs) $\{\phi\}$ and indices p, q, r, s, t denote MO indices of unspecified occupation. For simplicity we assume real MOs throughout the paper.

For a set of local HF orbitals, each orbital may be assigned to a site (e.g., an orbital, a collection of neighboring orbitals, an atom, or a collection thereof) P, Q, \dots . Each site P thus gets

assigned a set of occupied \underline{P} and unoccupied \overline{P} orbital indices. For local orbitals a charge distribution $\omega_{pq} = \phi_p \phi_q$ is nonzero only if the MOs ϕ_p and ϕ_q are close in space. An integral g_{iajb} is thus non-negligible only if the charge distributions ω_{ia} and ω_{jb} are non-negligible, i.e., orbitals ϕ_i and ϕ_a are assigned to sites that are close to each other and similarly for orbitals ϕ_j and ϕ_b . If ϕ_i and ϕ_j (ϕ_a and ϕ_b) are both assigned to site P , we will write $i, j \in \underline{P}$ ($a, b \in \overline{P}$), and g_{iajb} is non-negligible and contributes to the energy only if $a, b \in [\overline{P}]$ ($i, j \in [\underline{P}]$), where the bracket denotes the set of orbitals spatially close to site P , including P itself. For compactness we will collectively refer to the local occupied $[\underline{P}]$ and virtual $[\overline{P}]$ orbital spaces as $[P]$.

Replacing the summations in Eq. (1) by summations over sites and pairs of sites and using that some of the two-electron integrals may be neglected (to a given precision), we may write the correlation energy as^{25,27}

$$E_{corr}^x = \sum_P [E_P^x + \sum_{Q < P} E_{PQ}^x], \quad (2)$$

where x refers to either the occupied ($x = o$) or the virtual ($x = v$) partitioning scheme. The occupied single fragment energy E_P^o for site P and occupied pair interaction energy E_{PQ}^o between sites P and Q may be expressed as

$$E_P^o = \sum_{i,j \in \underline{P}} \sum_{a,b \in [\overline{P}]} \tau_{ij}^{ab} L_{iajb} \quad (3)$$

and

$$E_{PQ}^o = \sum_{\substack{i \in \underline{P} \\ j \in \underline{Q}}} + \sum_{\substack{j \in \underline{P} \\ i \in \underline{Q}}} \sum_{a,b \in [\overline{P}] \cup [\overline{Q}]} \tau_{ij}^{ab} L_{iajb}. \quad (4)$$

The virtual single fragment energy E_P^v and pair interaction energy E_{PQ}^v may similarly be calculated according to

$$E_P^v = \sum_{a,b \in \overline{P}} \sum_{i,j \in [\underline{P}]} \tau_{ij}^{ab} L_{iajb} \quad (5)$$

and

$$E_{PQ}^v = \sum_{\substack{a \in \overline{P} \\ b \in \overline{Q}}} + \sum_{\substack{b \in \overline{P} \\ a \in \overline{Q}}} \sum_{i,j \in [\underline{P}] \cup [\underline{Q}]} \tau_{ij}^{ab} L_{iajb}. \quad (6)$$

If all orbitals are included in $[\underline{P}]$ and $[\overline{P}]$ for all sites P then Eqs. (1) and (2) are identical for both the occupied and the virtual partitioning schemes.

The evaluation of the occupied single fragment energy E_P^o requires the amplitudes of the occupied energy orbital space (EOS) in Eq. (3). To indicate that a four-index quantity, X_{ij}^{ab} , is restricted to the occupied EOS, we write

$$X_{ij}^{ab} \in \mathcal{P}_{\text{EOS}}^o, \quad (7)$$

where $\mathcal{P}_{\text{EOS}}^o$ refers to a collection of four orbital indices with $i, j \in \underline{P}$ and $a, b \in [\overline{P}]$. We will use the following compact notation for $\mathcal{P}_{\text{EOS}}^o$:

$$\mathcal{P}_{\text{EOS}}^o \equiv \underline{P} \times \underline{P} \times [\overline{P}] \times [\overline{P}] = \underline{P}^2 \times [\overline{P}]^2. \quad (8)$$

Similarly, E_P^v requires the amplitudes of the virtual EOS from Eq. (5), which can be written as

$$\mathcal{P}_{\text{EOS}}^v \equiv [\underline{P}]^2 \times \overline{P}^2. \quad (9)$$

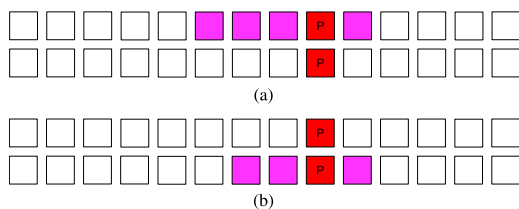


FIG. 1. Schematic illustration where the upper and lower rows of squares symbolize the sets of virtual and occupied orbitals assigned to a center, respectively. The orbitals assigned to site P are shown as red squares. The space outside P where the integrals L_{iajb} entering the fragment energy E_P^x are non-negligible is shown in magenta for the occupied (a) and virtual (b) partitioning schemes. (a) Schematic drawing of $\mathcal{P}_{\text{EOS}}^o$. (b) Schematic drawing of $\mathcal{P}_{\text{EOS}}^v$.

$\mathcal{P}_{\text{EOS}}^o$ and $\mathcal{P}_{\text{EOS}}^v$ are depicted schematically in Fig. 1. We henceforth use the generic $\mathcal{P}_{\text{EOS}}^x$, E_P^x , and E_{PQ}^x to refer to one of the partitioning schemes. In order to obtain the single fragment and pair interaction energies to the predefined precision, the amplitudes of $\mathcal{P}_{\text{EOS}}^x$ have to be known, and the accurate determination of these is the focus of the following discussion.

When evaluating fragment energies E_P^x in local orbital spaces, two primary error types arise. To illustrate these two error types, we consider the evaluation of a fragment energy E_P^o of the occupied partitioning scheme. The two error types may be summarized as follows:

1. the summation restriction $ab \in [\bar{P}]$ in Eq. (3) in the evaluation of E_P^o ;
2. the amplitudes used for evaluating E_P^o are obtained by solving the amplitude equations in a restricted orbital space.

Note that in the limit where the amplitudes are obtained from a calculation that includes the total orbital space, only error type 1 is present. To schematically illustrate how the two error types affect the size of the orbital space, we have plotted the errors in E_P^o in Fig. 2 for a typical system. The errors in

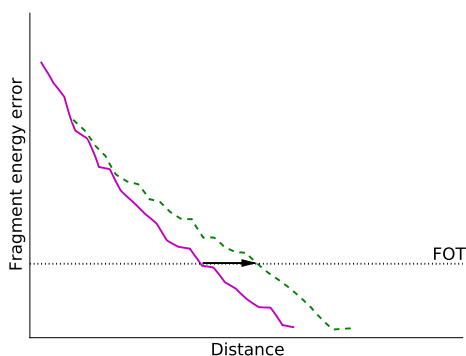


FIG. 2. Schematic illustration of the different error types that are present when fragment energies E_P^o are evaluated. Each point represents the fragment energy error when orbitals within a certain distance cutoff from site P are included. Magenta, solid line: error type 1; green, dashed line: error types 1 and 2; black arrow: error type 2. See text for details.

E_P^o are then given for two cases where the orbital space is truncated at a given distance from site P . For the solid magenta line, amplitudes have been obtained from a calculation that includes the total molecular orbital space and the summation (Eq. (3)) has been truncated. The magenta line therefore only displays the decay of errors of type 1. For the green dashed line, amplitudes are used where the amplitude equations have been solved in an orbital space that has been truncated at the same distance from P as used for the EOS. Thus, the dashed line contains errors of both types 1 and 2. The difference between the dashed and solid lines therefore represents errors of type 2. In order to evaluate E_P^o to the requested FOT precision in a practical calculation, it is therefore necessary to include the coupling space, denoted by the arrow, in addition to the EOS. The mechanisms which define the coupling space in MP2 and CCSD calculations are identified in Section III.

III. THEORETICAL ANALYSIS: ORBITAL SPACES IN DEC-CC FRAGMENT ENERGY CALCULATIONS

In this section we carry out a theoretical locality analysis to identify the mechanisms that are responsible for introducing the coupling between the amplitudes of the EOS and the amplitudes of the neighboring orbital spaces. After these mechanisms have been established, we discuss how the coupling may be included in a fragment energy calculation to obtain EOS amplitudes giving the single fragment energy to a predefined precision. In Sections III A and III B we describe the MP2 and CCSD models, respectively, while Section III C contains numerical support for the theoretical analysis. Note that the following discussion is a theoretical analysis, while the practical implementation is described in Section IV.

A. Space extensions in MP2 fragment calculations

The MP2 amplitude equations constitute a set of linear equations with a positive definite coefficient matrix

$$\sum_c t_{ij}^{cb} F_{ac} + \sum_c t_{ij}^{ac} F_{bc} - \sum_k t_{kj}^{ab} F_{ki} - \sum_k t_{ik}^{ab} F_{kj} = -g_{aibj}. \quad (10)$$

If a canonical HF basis is used, the Fock matrix is diagonal and Eq. (10) is solved in one iteration. If a basis of local orbitals is used, the Fock matrix is diagonally dominant³³ and Eq. (10) may be solved in a few iterations using standard iterative algorithms, such as the conjugate gradient or the conjugate residual methods.^{34,35} In this section, we will use the conjugate residual method as an analysis tool for solving the MP2 amplitude equations in a restricted orbital space. For the locality analysis we assume that Eq. (10) is expressed in terms of a set of local HF orbitals and that the Fock matrix and the two-electron integrals are local. These assumptions are backed up numerically in Appendix A for a set of molecules.

1. Iterative solution of the MP2 amplitude equations

When solving Eq. (10) using the conjugate residual algorithm, the amplitudes of iteration $(n + 1)$ are determined from the amplitudes of iteration n ,

$$t_{ij,n+1}^{ab} = t_{ij,n}^{ab} + \alpha R_{ij,n}^{ab}, \quad (11)$$

where the residual $R_{ij,n}^{ab}$ of iteration n

$$R_{ij,n}^{ab} = -g_{aibj} - \sum_c t_{ij,n}^{cb} F_{ac} - \sum_c t_{ij,n}^{ac} F_{bc} + \sum_k t_{kj,n}^{ab} F_{ki} + \sum_k t_{ik,n}^{ab} F_{kj} \quad (12)$$

is used as a search direction. In the conjugate residual method, a line search is performed along the residual direction by optimizing the α parameter. The line search affects the convergence rate of the algorithm, but it does not influence how new orbital spaces are introduced in the iterative algorithm. For simplicity, we therefore set $\alpha = 1$ in the rest of this analysis.

In iteration n , the single fragment energy for fragment P is

$$E_{P,n}^x = \sum_{\mathcal{P}_{\text{EOS}}^x} t_{ij,n}^{ab} L_{iajb}, \quad (13)$$

where the summation over $\mathcal{P}_{\text{EOS}}^x$ indicates a summation with $t_{ij}^{ab}, L_{iajb} \in \mathcal{P}_{\text{EOS}}^x$ as defined by Eqs. (8) and (9), i.e., for the occupied partitioning scheme ($x = o$), the indices will be restricted as $i, j \in \underline{P}$ and $a, b \in [\overline{P}]$, while, for the virtual partitioning scheme ($x = v$), $i, j \in [\underline{P}]$ and $a, b \in \overline{P}$. Using Eqs. (11) and (13) the energy change in iteration n , $\Delta E_{P,n}^x$, is given by

$$\begin{aligned} \Delta E_{P,n}^x &= E_{P,n}^x - E_{P,n-1}^x \\ &= \sum_{\mathcal{P}_{\text{EOS}}^x} R_{ij,n-1}^{ab} L_{iajb}, \end{aligned} \quad (14)$$

where $E_{P,0}^x \equiv 0$. The converged single fragment energy may then be written as

$$E_P^x = \sum_{n=1}^{n_{it}} \Delta E_{P,n}^x, \quad (15)$$

where we have used Eqs. (13) and (14) and where $E_P^x = E_{P,n_{it}}^x$ and n_{it} is the total number of iterations in the iterative scheme. The residual $R_n \in \mathcal{P}_{\text{EOS}}^x$ approaches zero with increasing n and $\Delta E_{P,n}^x$ therefore becomes negligible. In Sec. III A 2, we will apply the iterative procedure defined by Eqs. (11) and (12) and analyse the propagation of the orbital space throughout the iterative procedure to identify the target orbital space required for determining E_P^x to the predefined precision.

2. Propagation of orbital spaces during the iterative procedure

The EOS amplitudes are defined in the $\mathcal{P}_{\text{EOS}}^o$ and $\mathcal{P}_{\text{EOS}}^v$ spaces for the occupied and virtual partitioning schemes, respectively, see Fig. 1. However, it is convenient to extend these spaces slightly to put the locality analysis for the occupied and virtual partitioning schemes on an equal footing. We therefore introduce the target space, \mathcal{P}_1 ,

$$\mathcal{P}_1 = [\underline{P}]^2 \times [\overline{P}]^2, \quad (16)$$

which includes the EOS for both the occupied and virtual partitioning schemes, $(\mathcal{P}_{\text{EOS}}^o \cup \mathcal{P}_{\text{EOS}}^v) \subset \mathcal{P}_1$.

In the first iteration of the iterative procedure described in Eqs. (11) and (12), all amplitudes are set to zero,

$$t_{ij,1}^{ab} = 0, \quad (17)$$

and therefore $E_{P,1}^x = \Delta E_{P,1}^x = 0$. The single fragment energy is defined by the EOS amplitudes, and we therefore restrict the residual of the first iteration to the target space \mathcal{P}_1 . Using Eq. (12), we thus obtain

$$R_{ij,1}^{ab} = -g_{aibj} \in \mathcal{P}_1. \quad (18)$$

Using Eqs. (11) and (17), the amplitudes of the second iteration become

$$t_{ij,2}^{ab} = R_{ij,1}^{ab} \in \mathcal{P}_1. \quad (19)$$

The energy difference between the first and second iterations is thus

$$\Delta E_{P,2}^x = \sum_{\mathcal{P}_{\text{EOS}}^x} R_{ij,1}^{ab} L_{iajb}, \quad (20)$$

where we have used Eq. (14). The EOS amplitudes in Eq. (19) relax through the iterations and we now identify the coupling mechanism leading to this relaxation.

In the second iteration, the amplitudes in \mathcal{P}_1 couple directly to sites in the proximity of $[P]$ through summations with non-negligible Fock matrix elements in the residual of Eq. (12). The total (extended) coupling environment of the EOS amplitudes in iteration 2 is denoted $[P]_2$ ($[P] \subset [P]_2$). For example, the following terms of Eq. (12) for the second iteration illustrate space extensions of the occupied and virtual spaces, respectively,

$$\sum_{k \in [\underline{P}]} t_{ik,2}^{ab} F_{kj} \quad t_{ik,2}^{ab} \in \mathcal{P}_1, \quad j \in [\underline{P}]_2, \quad (21a)$$

$$\sum_{c \in [\overline{P}]} t_{ij,2}^{cb} F_{ac} \quad t_{ij,2}^{cb} \in \mathcal{P}_1, \quad a \in [\overline{P}]_2, \quad (21b)$$

where we have used Eq. (19) to restrict the summations in k and c . The residual of the second iteration is therefore extended to the space

$$\mathcal{P}_2 = [\underline{P}]_2^2 \times [\overline{P}]_2^2, \quad (22)$$

which is illustrated by Fig. 3 and may be written as

$$\begin{aligned} R_{ij,2}^{ab} &= -g_{aibj} - \sum_c t_{ij,2}^{cb} F_{ac} - \sum_c t_{ij,2}^{ac} F_{bc} + \sum_k t_{kj,2}^{ab} F_{ki} \\ &+ \sum_k t_{ik,2}^{ab} F_{kj}; \quad R_{ij,2}^{ab} \in \mathcal{P}_2, t_{ij,2}^{ab} \in \mathcal{P}_1. \end{aligned} \quad (23)$$

For the following analysis, it is convenient to generalize the notation of Eqs. (16) and (22) and introduce the space \mathcal{P}_n ,

$$\mathcal{P}_n = [\underline{P}]_n^2 \times [\overline{P}]_n^2, \quad (24)$$

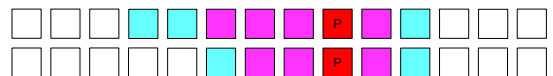


FIG. 3. Iteration 2: The \mathcal{P}_1 space is symbolized by the squares in red and magenta. The residual is generated in the \mathcal{P}_2 space (all colored boxes) where the cyan squares symbolize the space extension $\mathcal{P}_2 \setminus \mathcal{P}_1$ in iteration 2. This space interacts directly with the orbitals of the target space \mathcal{P}_1 .

where $[P]_n$ ($[\bar{P}]_n$) is the set of occupied (virtual) orbitals which have non-negligible Fock matrix elements with at least one of the orbitals in $[P]_{n-1}$ ($[\bar{P}]_{n-1}$) and where $[P]_1 \equiv [P]$ ($[\bar{P}]_1 \equiv [\bar{P}]$). We also note that $\mathcal{P}_{n-1} \subset \mathcal{P}_n$ and we will denote the space components of \mathcal{P}_n which are not contained in \mathcal{P}_{n-1} as $\mathcal{P}_n \setminus \mathcal{P}_{n-1}$.

The amplitudes of the third iteration $t_{ij,3}^{ab}$ will be generated in \mathcal{P}_2 according to Eqs. (11) and (21) giving the residual $R_{ij,3}^{ab} \in \mathcal{P}_3$, such that more, yet untouched components, of the environment of P enters the residual through the coupling mechanism described in Eq. (21). The new space components will not be coupled to \mathcal{P}_1 directly as the Fock matrix elements between these spaces are negligible, see Fig. 4. The amplitudes of the $\mathcal{P}_3 \setminus \mathcal{P}_2$ space thus interact directly with the amplitudes of the $\mathcal{P}_2 \setminus \mathcal{P}_1$ space which in turn couples with the amplitudes in the \mathcal{P}_1 space. Hence, the relaxation effects of the $\mathcal{P}_3 \setminus \mathcal{P}_2$ space on the EOS amplitudes will be small and indirect, and these effects will therefore be referred to as secondary coupling effects.

For the fourth and following iterations, these mechanisms are preserved, i.e., additional couplings are introduced in the already considered space and new spaces are introduced which indirectly couple to the \mathcal{P}_1 space through other spaces. The effects on the EOS amplitudes from the newly introduced spaces thus become more indirect and smaller for each successive iteration.

The above developments may be summarized as follows. To evaluate the fragment energies, we need the amplitudes of the $\mathcal{P}_{\text{EOS}}^x \subset \mathcal{P}_1$ space that were introduced in iteration 1. In the second iteration, direct coupling to the outside space $\mathcal{P}_2 \setminus \mathcal{P}_{\text{EOS}}^x$ is introduced which affects the EOS amplitudes significantly. The relaxation of the EOS amplitudes through the additional components in the $\mathcal{P}_2 \setminus \mathcal{P}_{\text{EOS}}^x$ space is therefore important for the evaluation of the single fragment energy. The effects of the additional spaces introduced in the following iterations affect the EOS amplitudes only indirectly. The requested precision will consequently define how much of the environment of P has to be considered. Thus, we may introduce an effective coupling space \mathcal{P}_{EFF} where the MP2 equations are solved to give the EOS amplitudes to the requested (FOT) precision. This effective space may be defined as

$$\mathcal{P}_{\text{EFF}} \equiv [P]_{\text{EFF}}^2 \times [\bar{P}]_{\text{EFF}}^2. \quad (25)$$

When calculating the single fragment energy, we may correspondingly replace $[P]$ and $[\bar{P}]$ in Eqs. (3) and (5) by $[P]_{\text{EFF}}$ and $[\bar{P}]_{\text{EFF}}$, giving the occupied and virtual effective EOS

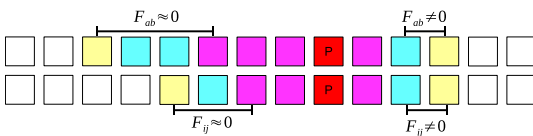


FIG. 4. Iteration 3: The residual is generated in the \mathcal{P}_3 space (all colored boxes) where the orbitals of sites with light yellow squares ($\mathcal{P}_3 \setminus \mathcal{P}_2$) symbolize the orbitals which interact directly with the orbitals of the $\mathcal{P}_2 \setminus \mathcal{P}_1$ space (cyan) through non-negligible Fock matrix elements, but not directly with the orbitals of the \mathcal{P}_1 space (red and magenta).

$$\mathcal{P}_{\text{EOS}}^{\text{a, EFF}} \equiv \underline{P}^2 \times [\bar{P}]_{\text{EFF}}^2, \quad (26)$$

$$\mathcal{P}_{\text{EOS}}^{\text{v, EFF}} \equiv [P]_{\text{EFF}}^2 \times \bar{P}^2, \quad (27)$$

which will be generically referred to as $\mathcal{P}_{\text{EOS}}^{\text{x, EFF}}$, while $[P]_{\text{EFF}}$ and $[\bar{P}]_{\text{EFF}}$ will be collectively referred to as $[P]_{\text{EFF}}$. The extent $[P]_{\text{EFF}}$ therefore defines both \mathcal{P}_{EFF} (where the amplitude equations are solved) and $\mathcal{P}_{\text{EOS}}^{\text{x, EFF}}$ (where the single fragment energy is evaluated).

B. Space extension in CCSD fragment calculations

The CCSD amplitude equations may be viewed as a nonlinear extension of the MP2 amplitude equations where the additional terms are of higher order in a Møller-Plesset perturbation analysis.¹ Thus, the energetically largest contributions leading to a space extension have been considered in Section III A 2. The focus of this section is to analyze the space extensions that may be introduced in the residual of Eq. (11) by the additional terms of the CCSD amplitude equations. The CCSD singles residual in the T_1 -transformed formulation may be expressed as¹

$$\text{CCSD } R^S = \Omega^{A1} + \Omega^{B1} + \Omega^{C1} + \Omega^{D1}, \quad (28)$$

and the CCSD doubles residual reads

$$\text{CCSD } R^D = \Omega^{A2} + \Omega^{B2} + \Omega^{C2} + \Omega^{D2} + \Omega^{E2}, \quad (29)$$

where the individual terms are given in Table I. The T_1 -transformed integrals (denoted by a tilde in Table I) are given by¹

$$\tilde{g}_{qrst} = \sum_{\mu\nu\rho\sigma} \Lambda_{\mu q}^p \Lambda_{\nu r}^h \Lambda_{\rho s}^p \Lambda_{\sigma t}^h g_{\mu\nu\rho\sigma}, \quad (30)$$

TABLE I. The CCSD residual equations as given in Ref. 1. Tildes denote T_1 -transformed integrals, see Eqs. (30)-(33).

Doubles terms:

$$\Omega_{aibj}^{A2} = \tilde{g}_{aibj} + \sum_{cd} t_{ij}^{cd} \tilde{g}_{acbd}$$

$$\Omega_{aibj}^{B2} = \sum_{kl} t_{kl}^{ab} (\tilde{g}_{klij} + \sum_{cd} t_{ij}^{cd} \tilde{g}_{kclad})$$

$$\Omega_{aibj}^{C2} = P_{ij}^{ab} (1 + \frac{1}{2} P_{ij}) [-\sum_{ck} t_{ki}^{bc} (\tilde{g}_{kjac} - \frac{1}{2} \sum_{dl} t_{ij}^{ad} \tilde{g}_{kdcl})]$$

$$\Omega_{aibj}^{D2} = \frac{1}{2} P_{ij}^{ab} [\sum_{ck} u_{jk}^{bc} (\tilde{L}_{aikc} + \frac{1}{2} \sum_{dl} u_{il}^{ad} \tilde{L}_{ldkc})]$$

$$\Omega_{aibj}^{E2} = P_{ij}^{ab} [\sum_{c} t_{ij}^{ac} (\tilde{F}_{bc} - \sum_{dkl} u_{kl}^{bd} \tilde{g}_{ldkc}) - \sum_{k} t_{ik}^{ab} (\tilde{F}_{kj} + \sum_{cdl} u_{ij}^{cd} \tilde{g}_{kdcl})]$$

Singles terms:

$$\Omega_{ai}^{A1} = \sum_{cdk} u_{ki}^{cd} \tilde{g}_{adkc}$$

$$\Omega_{ai}^{B1} = -\sum_{ckl} u_{kj}^{ac} \tilde{g}_{klic}$$

$$\Omega_{ai}^{C1} = \sum_{ck} u_{ik}^{ac} \tilde{F}_{kc}$$

$$\Omega_{ai}^{D1} = \tilde{F}_{ai}$$

Definitions:

$$P_{ij} X_{ij}^{ab} = X_{ji}^{ab}$$

$$P_{ij}^{ab} X_{ij}^{ab} = X_{ij}^{ab} + X_{ji}^{ba}$$

$$u_{ij}^{ab} = (2 - P_{ij}) t_{ij}^{ab}$$

$$\tilde{L}_{aibj} = (2 - P_{ij}) \tilde{g}_{aibj}$$

$$\tilde{F}_{pq} = \tilde{h}_{pq} + \sum_i (2\tilde{g}_{pqii} - \tilde{g}_{piiq}) = \tilde{h}_{pq} + \sum_{\rho\sigma} \tilde{D}_{\rho\sigma} (2\tilde{g}_{pq\rho\sigma} - \tilde{g}_{\rho\rho\sigma q})$$

$$\tilde{D}_{\rho\sigma} = \sum_i \Lambda_{\rho i}^p \Lambda_{\sigma i}^s$$

where $\mu, \nu, \rho,$ and σ are atomic orbital (AO) indices, and the particle Λ^p and hole Λ^h transformation matrices are defined via the MO coefficient matrix \mathbf{C} as

$$\Lambda^p = \mathbf{C}(\mathbf{1} - \mathbf{t}_1^T), \quad (31)$$

$$\Lambda^h = \mathbf{C}(\mathbf{1} + \mathbf{t}_1), \quad (32)$$

and the \mathbf{t}_1 matrix is

$$[\mathbf{t}_1]_{pq} = \begin{cases} t_q^p & \text{if } p \text{ virtual and } q \text{ occupied} \\ 0 & \text{otherwise} \end{cases}. \quad (33)$$

When the singles amplitudes are neglected, $\text{CCSD}R^D$ becomes the nonlinear CCD residual $\text{CCD}R$ (removing the tildes in the doubles terms in Table I). The starting point for analyzing orbital space extensions for CCSD single fragment energy calculations will be an analysis of the CCD residual in Section III B 1, while we consider the effect of the CCSD singles amplitudes in Section III B 2.

For the MP2 analysis in Section III A 2, we have encountered the space extension mechanism caused by non-negligible Fock matrix elements. For the CCD and CCSD analysis, additional space extension mechanisms can be identified. We will consider the following four mechanisms which collectively represent error type 2 of Section II:

1. Propagation due to non-negligible Fock matrix elements (identified in Section III A 2).
2. Propagation due to non-negligible charge distributions in two-electron integrals.
3. Propagation due to long-range interactions between charge distributions (dipole–dipole effects).
4. Propagation due to the Fock matrix constructed from a T_1 -transformed density (charge-polarization effects).

Mechanisms 1, 2, and 3 are present for CCD and will be discussed in Section III B 1, while mechanism 4 is present only for CCSD and will be discussed in Section III B 2.

1. Space extension mechanisms in the CCD model

To analyse the space extension process in a CCD context, we use the framework established for MP2 in Section III A with the only modification that, when solving the nonlinear CCD equations using the conjugate residual method, the residual $R_{ij,n}^{ab}$ defined in Eq. (12) is replaced by the residual $\text{CCD}R_{ij,n}^{ab}$.

The MP2 amplitude equations (Eq. (12)) correspond to g_{abj} in Ω^{A2} and the Fock matrix terms of Ω^{E2} in the CCD amplitude equations. The CCD equations thus contain additional terms where two-electron integrals are contracted linearly or quadratically with cluster amplitudes. The quadratic terms do not contribute to the space extension of the residual since all indices entering these contributions are fixed by the amplitudes of the previous iteration. For example, in the second part of the Ω_n^{B2} term, $\sum_{kl} \sum_{cd} t_{kl,n}^{ab} t_{ij,n}^{cd} g_{kcl}$, the integral indices are fixed to the space of the cluster amplitudes of iteration n and therefore no space extension is introduced by this component of the residual.

As an example for the space propagation according to mechanism 2, we consider the second term of $\Omega_{abj,n}^{A2}$, i.e.,

$$\Omega_{abj,n}^{A2.2} = \sum_{cd} t_{ij,n}^{cd} g_{acbd}. \quad (34)$$

At iteration n the amplitudes are defined in \mathcal{P}_{n-1} , and the dummy indices c and d are therefore restricted to this space. Hence, the free indices a, b of the integrals g_{acbd} are restricted by the locality of the charge distributions ω_{ac} and ω_{bd} .

All terms of CCD doubles residual may be grouped into the categories following mechanism 1 or 2 except for one of the terms in Ω_n^{D2} , denoted as $\Omega_n^{D2.1}$, which follows mechanism 3,

$$\Omega_{abj,n}^{D2.1} = \sum_{ck} t_{jk,n}^{bc} g_{aikc}. \quad (35)$$

Any additional space components $\mathcal{P}_n \setminus \mathcal{P}_{n-1}$ of iteration n contribute via this term to the single fragment energy as dipole–dipole interactions with an inverse sixth power decay with the distance between center P and the charge distribution ω_{kc} . This may be understood from the perspective of a residual component in the EOS, $\Omega_{abj,n}^{D2.1} \in \mathcal{P}_{\text{EOS}}^x$, which enters the single fragment energy in Eq. (14). The contribution of the new space components $\mathcal{P}_n \setminus \mathcal{P}_{n-1}$ where the charge distribution ω_{kc} may be located decays with its distance from $\mathcal{P}_{\text{EOS}}^x$ in an inverse sixth order manner because ω_{kc} occurs in Eq. (35) in both the two-electron integral and the amplitudes, both of which decay with the inverse third power²⁷ of the distance between ω_{kc} and P . Furthermore, the contribution from this direct long-range modification is expected to be small since it only slightly modifies one of many residual contributions $\Omega_{abj,n}^{D2.1} + \dots \in \mathcal{P}_{\text{EOS}}^x$ entering Eq. (14). Based on this discussion, we expect that mechanism 3 has a small effect on the single fragment energy which becomes important only when very high precision is requested, which will be substantiated numerically in Section III C and Appendix A.

2. Space extension mechanisms in the CCSD model with focus on the effect of singles

In Section III B 1, we have described the progression of the space extension for the cluster amplitudes in a CCD calculation. In this section we examine the space progression for CCSD with focus on the singles amplitudes. As for the doubles amplitudes, the singles EOS amplitudes are defined by Eqs. (3) and (5). We note from Table I that the indices i and a of the singles amplitude equations are coupled only by mechanisms 1 and 2, and their distance decay will thus be similar to the Fock matrix and two-electron integral decays (see Appendix A). Furthermore, since the singles amplitudes enter quadratically in Eqs. (3) and (5), their direct effect on the single fragment energy is expected to be significantly smaller than the effect of the doubles amplitudes. However we need to evaluate the coupling effects introduced by the singles into the CCSD residual. For this reason, we first consider how the T_1 -transformation introduces coupling effects through the two-electron integrals. After this, special attention is given to the T_1 -transformed Fock matrix.

As an illustrative example of the effect of the T_1 -transformation on the two-electron integrals, we consider the integral contribution \tilde{g}_{aibj} from Table I for the occupied EOS, i.e., $\tilde{g}_{aibj} \in \mathcal{P}_{\text{EOS}}^o$ in an analogous argument as for the $\Omega^{D2.1}$ term. Using Eq. (30) \tilde{g}_{aibj} may be written as

$$\tilde{g}_{aibj} = g_{aibj} + \sum_k t_k^a g_{kibj} + \dots + O(t_1^2), \quad (36)$$

where one example of a linear term is given and the dots indicate further linear contributions. Terms, which are quadratic and higher order in the singles amplitudes, are very small and may be neglected for the purpose of this analysis. Since we consider $\tilde{g}_{aibj} \in \mathcal{P}_{\text{EOS}}^o$, the linear term in Eq. (36) will only couple to the space outside $\mathcal{P}_{\text{EOS}}^o$ through non-negligible charge distributions ω_{ki} , where the k index expands through mechanism 2 and its effect on the single fragment energy quickly becomes negligible beyond \mathcal{P}_2 . This analysis thus suggests that the space extensions associated with the T_1 -transformed two-electron integrals are captured by the same mechanisms that describe the CCD space extension.

The Ω_n^{E2} , Ω_n^{C1} , and Ω_n^{D1} terms have Fock matrix contributions constructed from a T_1 -transformed density matrix which, using Eqs. (31) and (32), can be written as

$$\tilde{F}_{\rho\sigma} = h_{\rho\sigma} + \sum_{\mu\nu} \tilde{D}_{\mu\nu} (2g_{\rho\sigma\mu\nu} - g_{\rho\nu\mu\sigma}), \quad (37)$$

$$\tilde{D}_{\mu\nu} = D_{\mu\nu} + \sum_{ia} C_{\mu i} t_i^a C_{\nu a}, \quad (38)$$

where $D_{\mu\nu}$ is the HF density matrix for the full system. The singles polarized part of the density matrix in Eq. (38) introduces long-range charge-polarization effects into the AO Fock matrix in Eq. (37). In a practical DEC calculation, only the singles polarization effects within the $[P]_{\text{EFF}}$ space are captured. This error type was denoted mechanism 4 in the beginning of Section III B and it is only important for high precision calculations. One possible strategy for including long-range charge-polarization effects is to do as follows:

- Carry out all single fragment calculations and store the (short-ranged) singles amplitudes t_i^a with $i \in \underline{P}$ and $a \in [\bar{P}]_{\text{EFF}}$ for each fragment P .
- Collect all these contributions in a matrix t_1^{full} with full molecular dimensions.
- Construct an approximate T_1 transformed density matrix using t_1^{full} in Eq. (38) (full molecule).
- Construct an approximate T_1 transformed Fock matrix $\tilde{F}_{\mu\nu}$ according to Eq. (37) (full molecule).
- A second round of single (and pair) fragment calculations is carried out where the constructed Fock matrix $\tilde{F}_{\mu\nu}$ is used (using a different subset of AO indices $\{\mu, \nu\}$ for each fragment as described in Appendix B). In each fragment calculation $\tilde{F}_{\mu\nu}$ is kept fixed throughout the local CC iterations.

We illustrate the effect of using a long-range corrected T_1 transformed Fock matrix numerically in Section III C.

3. Summary for the space extension in a fragment CCSD calculation

In summary, the theoretical analysis of the present section demonstrates that, for both the MP2 and CCSD models, calculations may be carried out where the amplitude equations are solved in a subspace of the total orbital space. For the MP2 model, coupling is introduced through non-negligible Fock matrix elements (mechanism 1). For the CCD and CCSD models, which include terms of higher order in the fluctuation potential, additional coupling mechanisms have been identified. Coupling through non-negligible charge distributions in the two-electron integrals (mechanism 2) concerns all terms in the CCSD amplitude equations except the $\Omega^{D2.1}$ term in Eq. (35) (mechanism 3). Since the distance decay of coupling mechanism 2 is usually faster than the distance decay of the Fock matrix (see Appendix A), mechanism 2 is in general taken into account when mechanism 1 is considered. The coupling effects via long-range dipole–dipole interactions (mechanism 3) and the long-range polarization of the Fock matrix (mechanisms 4) are expected to contribute to the coupling error only to a small extent. We may therefore, in general, redefine the square bracket notation $[P]_{\text{EFF}}$ as the orbital space that interacts with P through any of the mechanisms 1-4, and conclude that the amplitude equations may be solved in the associated subspace \mathcal{P}_{EFF} of Eq. (25). The occupied ($x = o$) or virtual ($x = v$) fragment energies E_P^x are then evaluated in $\mathcal{P}_{\text{EOS}}^{x,\text{EFF}}$ of Eq. (26) or (27) to within the predefined precision. Furthermore, we can conclude that it may suffice to determine the fragment space $[P]_{\text{EFF}}$ for a CCSD calculation using the MP2 model, unless high precision is requested. Numerical results will be given in Section III C to substantiate this point. We also note that the perturbative triples correction to the CCSD energy, CCSD(T), may be evaluated using the same fragment spaces as for the DEC-CCSD calculation.³¹

Here, we have carried out the analysis of the fragment sizes for the fragments referencing a single site in Eqs. (3) and (5). We note that for the fragments referencing pairs of sites in Eqs. (4) and (6), an analogous analysis results in the same extensions due to the identical mechanisms in the MP2 and CCSD equations. The pair fragment spaces can thus be obtained as unions of single fragment spaces.

C. Numerical support for the theoretical developments

In this section we investigate the assumptions and conclusions from Sections III A and III B for three representative molecules with different chemical properties, (i) palmitic acid (semi-linear molecule), (ii) a glycine α -helix (bulky molecule), and (iii) Hexadeca-1,3,5,7,9,11,13,15-octaene (conjugated system), see Table II. The structures of these molecules are given as supplementary material.³⁹ All calculations in this section were performed with Dunning's cc-pVDZ basis set³⁶ using the frozen core approximation in order to have molecules with a reasonable spatial extent where it is still possible to carry out the reference calculations for the full system. The orbitals have been localized using the second power of the second moment orbitals.^{37,38}

TABLE II. Test set of molecules for the single fragment optimization algorithm. See supplementary material³⁹ for the atomic coordinates.

| System label | Chemical compound | Basis set |
|--------------|-------------------------------------|-----------|
| (i) | Palmitic acid | cc-pVDZ |
| (ii) | gly ₄ α -helix | cc-pVDZ |
| (iii) | Hexadeca-1,3,5,7,9,11,13,15-octaene | cc-pVDZ |
| (iv) | Lauric acid | cc-pVTZ |
| (v) | gly ₃ α -helix | cc-pVTZ |
| (vi) | Dodeca-1,3,5,7,9,11-hexene | cc-pVTZ |

The prerequisite for the theoretical fragment analysis of Section III was the distance decay of the two-electron integrals and the Fock matrix elements from a specific center P in the molecule. This prerequisite is confirmed in Appendix A for the set of test molecules and the single fragment energies E_P^x may therefore be determined to a predefined tolerance by solving the amplitude equations in a restricted orbital space \mathcal{P}_{EFF} .

In the following we will exemplify the sizes of coupling spaces that are necessary in actual calculations to determine the fragment energy E_P^x for a set of selected atomic sites P . Specifically we choose as site P the protonated oxygen of system (i), the α -carbon of the N-terminal glycine of system (ii), and one of the terminal carbons of system (iii). All sites were chosen at the rim of the molecules to better expose the distance decay behaviors of the fragment energy errors.

In Fig. 2 we have schematically illustrated how the coupling space can be identified. Below, we describe a practical realization of Fig. 2. To obtain the magenta line of Fig. 2, the absolute errors in E_P^x , $|\Delta E_P^x|$ are plotted for calculations where the amplitude equations have been solved in the full orbital space $\mathcal{P}_{\text{full}}$ (all orbitals of the molecular system are included) and $[P]_{\text{EFF}}$ in $\mathcal{P}_{\text{EOS}}^{x,\text{EFF}}$ is truncated at a given distance R_P from center P (denoted Approach A). For the green line in Fig. 2, a practical realization is obtained by plotting errors in E_P^x , where $[P]_{\text{EFF}}$ is truncated at a given distance R_P in both the space where the amplitude equations are solved \mathcal{P}_{EFF} and in the EOS $\mathcal{P}_{\text{EOS}}^{x,\text{EFF}}$ (denoted Approach B). The practical errors in E_P^x for both the occupied ($x = o$) and virtual ($x = v$) partitioning schemes are given in Fig. 5 for the three selected fragments in the upper and lower rows, respectively.

For approach A (magenta curves), the error in the single fragment energy converges rapidly and with a very similar rate with the distance R_P for both models (MP2^A or CCSD^A) and both partitioning schemes. For approach B (green curves), larger spaces are needed for both MP2^B (circles) and CCSD^B (triangles) models. The MP2^B fragment energy errors are always positive and converge smoothly to the correct result, whereas the CCSD^B fragment energy errors have a somewhat more erratic behavior as well as occasional artificially low errors due to changes in the sign of the CCSD^B fragment energy errors when increasing the fragment orbital space. The sign of the fragment energy errors for MP2^B may be understood from the MP2 correlation energy expression in

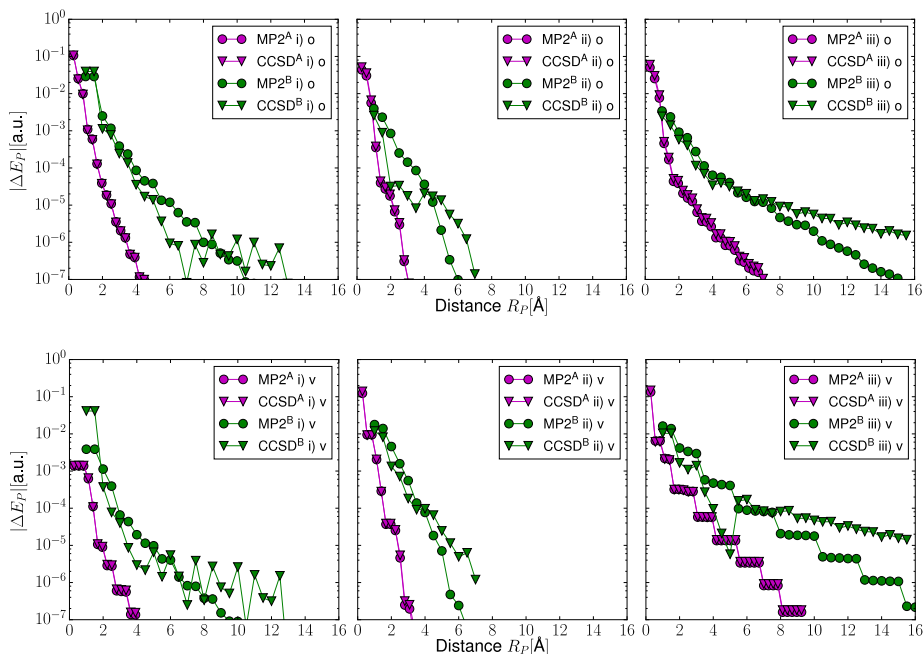


FIG. 5. Decay of the MP2 and CCSD fragment energy errors, upon increasing the orbital space for the three test systems (i), (ii), and (iii) and both the occupied (o) and virtual (v) partitioning schemes, given in the upper and lower rows, respectively. The amplitude equations have been solved in the full space (only error type 1, magenta, superscript A) and in a restricted orbital space (error type 1+2, green, superscript B).

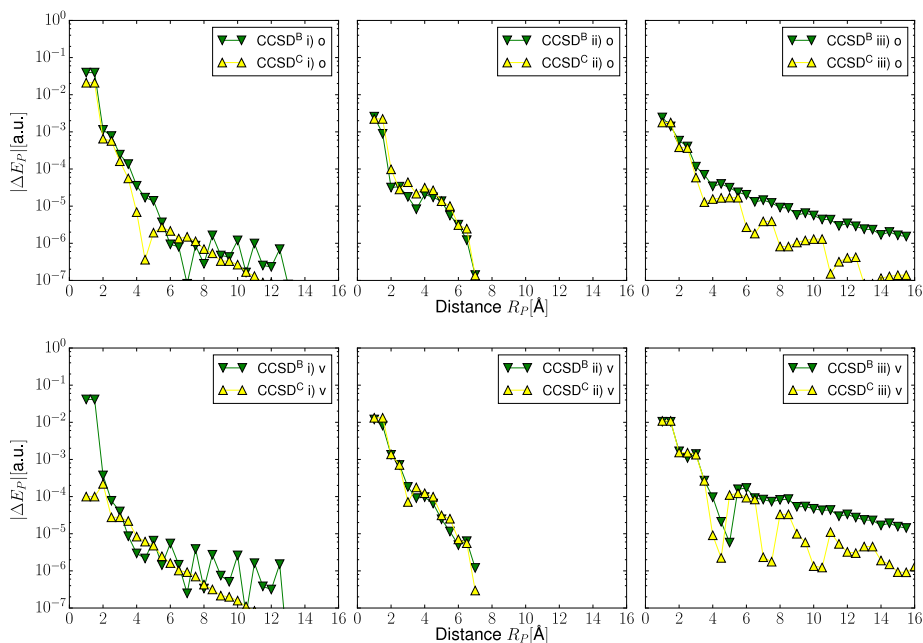


FIG. 6. Effect of the singles polarization in the Fock matrix (mechanism 4) for the three test systems (i), (ii), and (iii) for both the occupied (o) and virtual (v) partitionings, given in the upper and lower rows, respectively. The green curves (CCSD^B) include the error introduced by mechanism 4, which has been removed for the yellow curves (CCSD^C) by using the exact singles polarized Fock matrix.

the canonical basis, which effectively contains a summation over squared two-electron integrals divided by *negative* orbital energy differences. Hence, any truncation of this expression would lead to an energy that is less negative than the true canonical MP2 energy. Although the fragment energies are evaluated in the local basis, this feature carries over to the MP2 fragment energies, i.e., any truncation leads to MP2^B fragment energies that are not negative enough. No such simple expression exists for the standard CCSD energy, which requires the solution of the non-linear CCSD amplitude equations, and the sign of the CCSD^B fragment errors can therefore alternate as the fragment is expanded due to changes in the coupling environment in the CCSD fragment amplitude equations.

The horizontal difference between the green and magenta curves in Fig. 5 displays the size of the coupling space needed for a given precision. We note that the size of the coupling space depends on the model, the molecule, and the partitioning scheme. For $|\Delta E_p^x|$ values larger than 10^{-4} a.u., the coupling spaces are of similar size for the three test fragments. For smaller $|\Delta E_p^x|$ values, the conjugated system (iii) requires larger coupling spaces than systems (i) and (ii), in particular for the virtual partitioning scheme.

In order to study the effect of the polarization of the Fock matrix by the singles amplitudes (mechanism 4, in Section III B 2), we introduce the CCSD^C model where we eliminate errors from coupling mechanism 4 by using a singles polarized Fock matrix \tilde{F} (see Table I) constructed from the converged singles amplitudes (no approximations in Eq. (38)).

In Fig. 6, we report calculations for the three test fragments for the models CCSD^B and CCSD^C. From Fig. 6 it is evident that eliminating mechanism 4 in general decreases the CCSD fragment energy error. In particular, for the conjugated system, correcting for coupling mechanism 4 leads to reduced fragment sizes in the high-precision regime.

In summary, the calculations of the current section support the general conclusion of Sections III A and III B. Fragment energies to a given precision can be obtained by solving the CC amplitude equations in a restricted space when local orbitals are used, and unless high precision is requested, the fragment orbital spaces obtained at the MP2 level may be sufficient for CCSD calculations. For high-precision calculations, it was shown that it may be beneficial to account for the singles polarization of the Fock matrix in order to obtain smaller fragments. However, the investigation also shows that the coupling spaces depend on the model, the partitioning scheme, and the molecule and, in particular, that larger spaces may be necessary for the virtual partitioning scheme. In Section IV we develop a black box algorithm for determining the local fragment orbital spaces.

IV. PRACTICAL IMPLEMENTATION: DETERMINING SINGLE FRAGMENT ORBITAL SPACES

In the theoretical locality analysis of Section III, we have identified the various coupling mechanisms that arise when MP2 and CCSD amplitude equations are solved in a

restricted orbital space. In this section we describe a practical implementation for the determination of single fragment orbital spaces such that the single fragment energy error is of the requested (FOT) precision.

The single fragment optimization algorithm for the single fragment energy E_p^x includes two main steps: the single fragment expansion procedure where $[P]_{\text{EFF}}$ is increased until the energy difference between the last two expansion steps is lower than the FOT, and the reduction procedure where $[P]_{\text{EFF}}$ is fine tuned (reduced) without compromising the precision of the single fragment energy.

For the discussion of the single fragment optimization procedure, it is convenient to introduce the reference single fragment energies $E_p^{x,f}$, evaluated from $\mathcal{P}_{\text{EOS}}^{x,\text{full}}$ (all orbitals included in Eqs. (26) and (27))

$$E_p^{o,f} = \sum_{i,j \in \underline{P}} \sum_{ab} \tau_{ij}^{ab,f} L_{iajb}, \quad (39)$$

$$E_p^{v,f} = \sum_{ij} \sum_{a,b \in \bar{P}} \tau_{ij}^{ab,f} L_{iajb}, \quad (40)$$

where the amplitudes $\tau_{ij}^{ab,f}$ are obtained from $\mathcal{P}_{\text{full}}$.

A. Expansion of the orbital space

In the first step of the single fragment expansion algorithm, the local orbitals are ordered according to a measure that estimates their contribution to the single fragment energy E_p^x . Based on the analysis in Section III, a simple yet reasonable measure is the distance between the orbital's center of charge and the center P of the single fragment. In each expansion step a predefined number of orbitals (*vide infra*) is added to the single fragment orbital space $[P]_{\text{EFF}}$. The single fragment expansion is illustrated in Fig. 7 (left). In each expansion step, the energy is evaluated at the requested level of theory using Eqs. (3) and (5), and the energy difference between two subsequent steps i and $i+1$ is calculated,

$$\delta_e E_p^x(i) = |E_p^x(i) - E_p^x(i+1)|. \quad (41)$$

The expansion procedure continues until $\delta_e E_p^x(n-1) < \text{FOT}$, and the energy contribution from orbitals not included in $[P]_{\text{EFF}}$ of step n is therefore assumed to be below the requested precision. In the following, we consider the space

of expansion step n , $[P]_{\text{EFF}}^n$, as the reference space $[P]_{\text{REF}}$ and its associated energy, $E_p^x(n)$, as the reference energy E_p^{REF} for the single fragment reduction procedure. Thus, for the requested (FOT) precision, we assume $|E_p^{\text{REF}} - E_p^{x,f}| \ll \text{FOT}$, which is a reasonable assumption due to the rapid decay of the single fragment energy with respect to the inclusion of additional orbitals provided enough orbitals are included in each step, see, e.g., Fig. 5. In order for $|E_p^{\text{REF}} - E_p^{x,f}| \ll \text{FOT}$ to hold, the number of orbitals added in each expansion step needs to be large enough to avoid false convergence, but also small enough to avoid that the expanded orbital space $[P]_{\text{REF}}$ becomes unacceptably large. In practice we include $5 \cdot n_{\text{orb}}/n_{\text{atoms}}$ orbitals in each expansion step, where n_{atoms} is the number of atoms and n_{orb} is the number of orbitals in the molecule. Extensive testing has shown that this choice is a reasonable compromise between accuracy and computational cost.

B. Reduction of the orbital space

The reduction step defines the final single fragment orbital spaces and thus the pair fragment orbital spaces which are obtained as unions of single fragment spaces. Since the pair fragment calculations dominate the total DEC calculation, it is crucial to reduce the single fragment sizes as much as possible within the chosen FOT precision to reduce the cost of the total calculation. To achieve this, a binary search algorithm is used in connection with a priority list of orbitals where the energy of the expanded single fragment, E_p^{REF} , serves as a reference. For the calculations presented in Section V, we have chosen the same distance ordered list as in the expansion procedure. This is an obvious choice but other lists that produce similar results have also been tested (e.g., a list based on orbital contributions to the single fragment energy, or the absolute size of Fock matrix elements). The priority list is used to remove the least important orbitals of the $[P]_{\text{REF}}$ orbital space in the reduction procedure, see Fig. 7 (right). After each step j in the binary search algorithm, the energy is evaluated and compared to the energy of the reference single fragment,

$$\delta_r E_p^x(n+j) = |E_p^x(n+j) - E_p^{\text{REF}}|. \quad (42)$$

The step is accepted if

$$\delta_r E_p^x(n+j) < \text{FOT}, \quad (43)$$

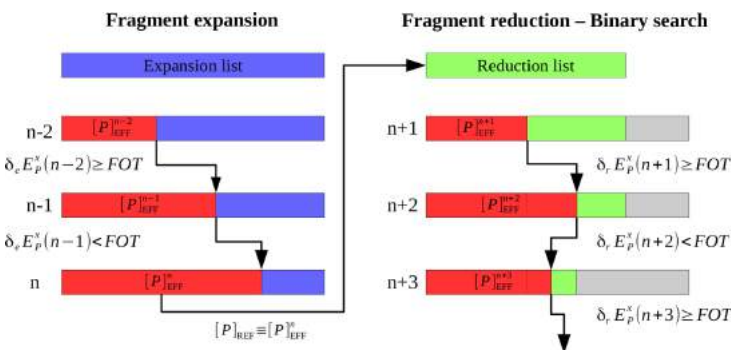


FIG. 7. The general single fragment optimization algorithm consists of two steps. In the single fragment expansion procedure (left), a reference orbital space is determined based on Eq. (41). In the reduction procedure (right), this reference orbital space is fine-tuned using a binary search algorithm where the step direction is based on Eq. (42). Red: Orbitals included in the current single fragment. Blue: Expansion priority list of orbitals. Green: Reduction priority list of orbitals. Grey: Discarded orbitals.

and in this case the next step is chosen to further decrease the single fragment size. On the other hand, if $\delta E_p^x \geq \text{FOT}$, the next step is chosen to increase the single fragment size, see Fig. 7. This process is repeated until the orbital space $[P]_{\text{EFF}}$ does not change significantly, e.g., if the difference in the number of orbitals between two subsequent steps is less than 5% of the number of orbitals in $[P]_{\text{REF}}$. The final single fragment orbital space is the one that corresponds to the last accepted step of the reduction procedure.

C. Summary and cost reduction considerations

The single fragment optimization algorithm in Fig. 7 is by no means unique but it is a model- and molecule-independent and easily programmable black-box approach, which ensures that each single fragment energy has a precision corresponding to the input FOT and thus ultimately defines the precision of

the total calculation. We also note, that the single fragment optimization may be performed for $x = o$, $x = v$, or both simultaneously.

In order to reduce the cost of the single fragment optimization, it can be performed at a lower level of theory than that of the target model. For example, for a DEC-CCSD calculation, it may be possible to determine the single fragment orbital spaces by applying the procedure in Fig. 7 to the MP2 model. As will be described in Section V, this is a feasible approach for a typical FOT (e.g., $\text{FOT} = 10^{-4}$ a.u.), while for high-precision work, a reliable DEC-CCSD energy requires that the CCSD model is also used for the single fragment optimization algorithm in Fig. 7, in particular if the virtual partitioning scheme is used. In this case, the convergence of the single fragment optimization procedure is evaluated based on both the CCSD and the MP2 single fragment energies (MP2/CCSD) in order to avoid false convergence that might

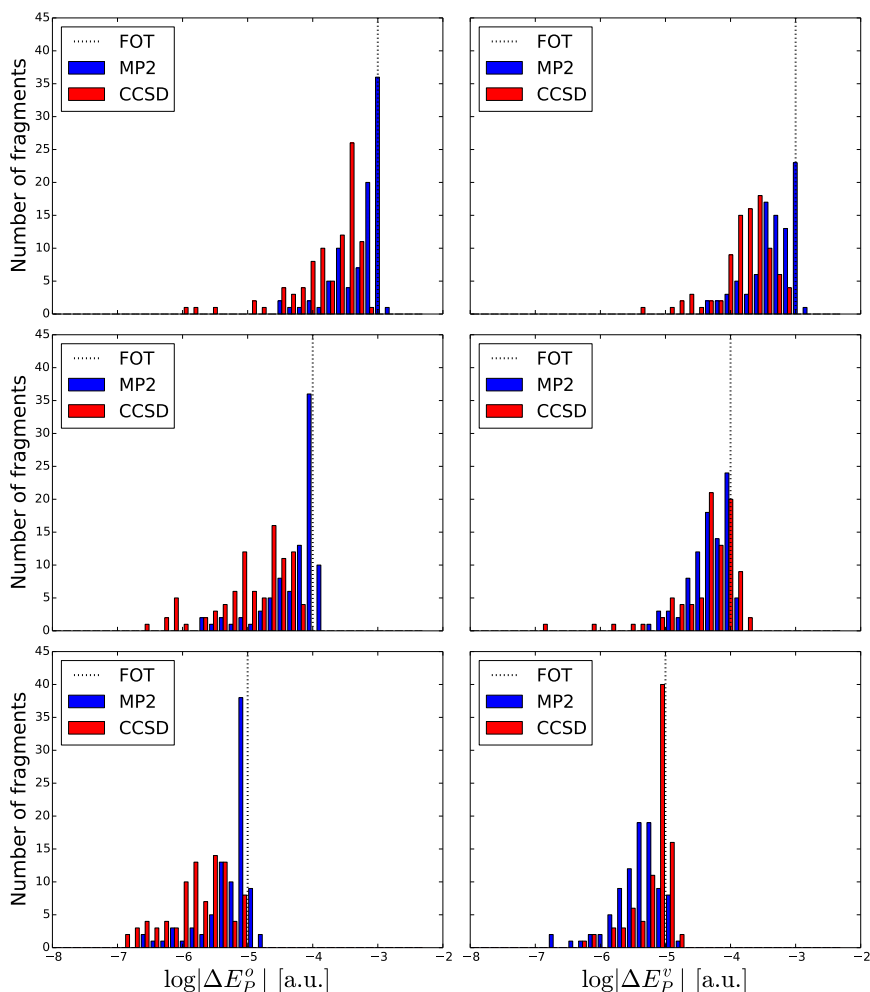


FIG. 8. Distribution of the absolute single fragment energy errors $|\Delta E_p^x|$ with respect to calculations in the full orbital spaces for both occupied ($x = o$, left column) and virtual ($x = v$, right column) partitioning schemes. The DEC single fragment orbital spaces have been optimized at the MP2 and MP2/CCSD levels of theory to obtain the MP2 and CCSD single fragment energy errors, respectively. Top panel: $\text{FOT} = 10^{-3}$ a.u.; middle panel: $\text{FOT} = 10^{-4}$ a.u.; bottom panel: $\text{FOT} = 10^{-5}$ a.u.

occur because the sign of the CCSD errors might alternate during the expansion/reduction procedure (MP2 errors are in general positive). It is also possible to further reduce the cost by invoking, e.g., the resolution-of-the-identity (RI) in the single fragment optimization algorithm.³²

Finally, we note that in each fragment calculation, the AO space is truncated by fitting the MOs as described in Appendix B. This reduces the number of AO integrals that need to be evaluated.

V. NUMERICAL ILLUSTRATIONS

The algorithm devised in Fig. 7 is a black-box method that operates based on the locality considerations of Section III. In this section we numerically demonstrate that this algorithm leads to single fragment energies with the requested precision.

We have performed a series of calculations on six different systems using Dunning's correlation consistent cc-pVDZ and cc-pVTZ basis sets³⁶ (see Table II and supplementary material³⁹ for the atomic coordinates), and for the orbital localization, we have used the second power of the second moment localized orbitals.^{37,38} For all calculations, the single fragment optimization in Fig. 7 was carried out for both partitioning schemes simultaneously. The calculations used the frozen core approximation and were carried out using a local version of the program.^{40,41} For the CCSD calculations, we have not used the long-range corrected Fock matrix.

In Fig. 8, we have plotted the distributions of the numerical values of the single fragment energy errors $|\Delta E_p^x| = |E_p^x - E_p^{x,f}|$, where $E_p^{x,f}$ is given by Eqs. (39) and (40) and requires calculations on the full molecular systems. This investigation is therefore limited to molecules for which the

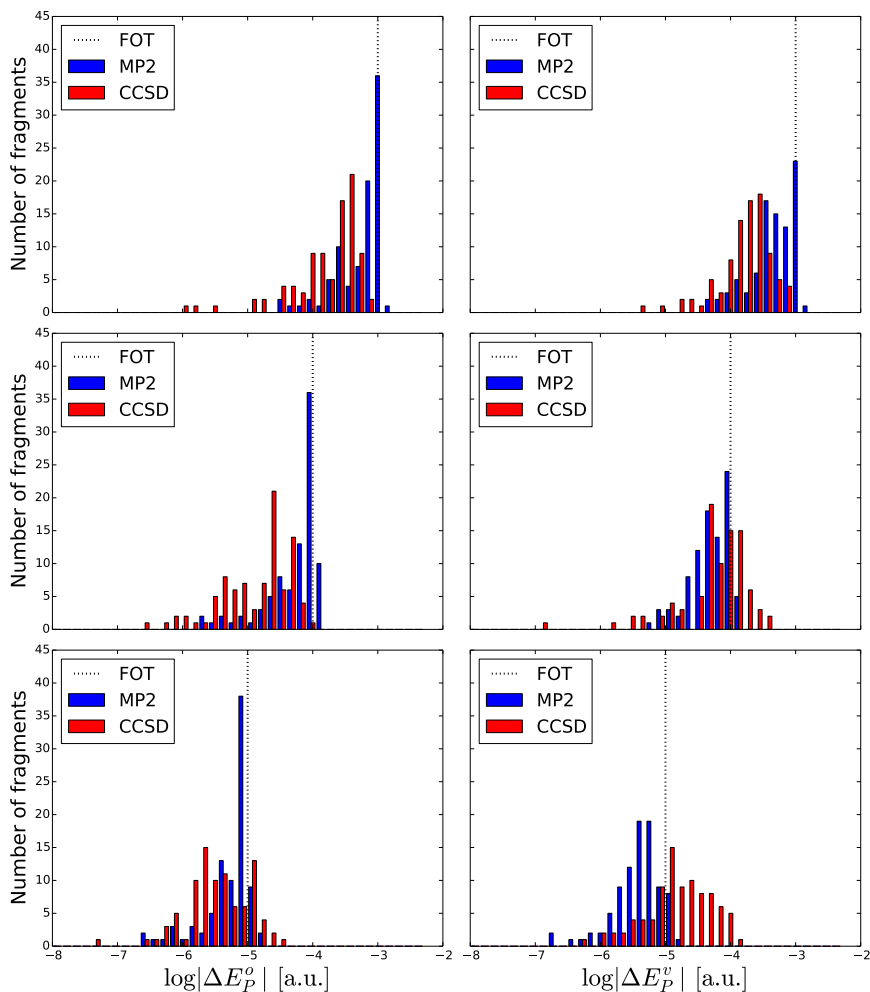


FIG. 9. Distribution of the absolute single fragment energy errors $|\Delta E_p^x|$ with respect to calculations in the full orbital spaces for both occupied ($x = o$, left column) and virtual ($x = v$, right column) partitioning schemes. The DEC single fragment orbital spaces have been optimized at the MP2 level of theory to obtain the MP2 and CCSD single fragment energy errors. Top panel: FOT = 10^{-3} a.u.; middle panel: FOT = 10^{-4} a.u.; bottom panel: FOT = 10^{-5} a.u.

full calculation is feasible at the MP2 and CCSD levels of theory. The orbital spaces ($[P]_{\text{EFF}}$) for the calculations presented in Fig. 8 were optimized at the MP2 level of theory for the MP2 single fragment energy errors, and at the combined MP2/CCSD level of theory for the CCSD single fragment energy errors using the algorithm in Fig. 7 and for decreasing values of the FOT (top panels 10^{-3} a.u., middle panels 10^{-4} a.u., lower panels 10^{-5} a.u.). In general, the single fragment optimization procedure leads to errors that are of the requested precision, but errors slightly larger than the FOT may occur, because the single fragment reduction procedure in Fig. 7 relies on the assumption $|E_p^{\text{REF}} - E_p^{x,f}| \ll \text{FOT}$, see Section IV A. However, in general Fig. 8 shows that when the FOT is specified, the expansion–reduction procedure in Fig. 7 gives single fragment energies that are of the size of the FOT (or smaller).

In Fig. 9, we have plotted the distributions of the numerical values of the single fragment energy errors $|\Delta E_p^x| = |E_p^x - E_p^{x,f}|$ when the orbital spaces $[P]_{\text{EFF}}$ have been optimized at the MP2 level of theory to obtain both the MP2 and CCSD single fragment energy errors using the algorithm in Fig. 7 and for decreasing values of the FOT. The MP2 single fragment energy errors are of course the same as in Fig. 8. However, the CCSD single fragment energy errors are not as well-behaved as in Fig. 8. For example, for the virtual partitioning scheme, the CCSD errors are in general below the requested precision for $\text{FOT} = 10^{-3}$ a.u., while single fragment energy errors of $5 \cdot 10^{-4}$ ($1 \cdot 10^{-4}$) a.u. occur for a FOT of 10^{-4} (10^{-5}) a.u. For the occupied partitioning scheme, the single fragment energy errors are surprisingly well-behaved and the CCSD single fragment energy errors are in general of the size of the FOT. From a pragmatic point of view, an important implication is that for the FOTs of practical interest considered here, the local orbital spaces determined at the MP2 level of theory can also be used for CCSD calculations, if only the occupied partitioning is used. This leads to significant savings compared to carrying out the single fragment optimization at the CCSD level of theory, particularly for the largest single fragment calculation (the n th step in Fig. 7). It is, however, important to emphasize that a DEC-CCSD calculation with rigorous error control requires that the single fragment optimization is carried out at the combined MP2/CCSD level of theory. This becomes especially important when both partitioning schemes are needed in order to calculate molecular gradients.²⁸

As a last point of this section, we would like to emphasize the importance of the second part of the single fragment optimization algorithm in Fig. 7, the single fragment reduction procedure. A comparison of the size of the orbital space before and after the single fragment reduction shows a reduction of the occupied space by 28% on average, while the virtual space is typically reduced by 35% to 40%. In terms of a V^4O^2 scaling CCSD algorithm, that corresponds to a mean cost reduction of each fragment calculation by more than one order of magnitude. Such savings are crucial to reduce the computational cost for the pair fragments (unions of single fragment spaces) which dominate the calculation.

In conclusion, the numerical data provided in this section support the theoretical analysis in Section III and show that

the algorithm in Fig. 7 is a useful practical implementation for determining local orbital spaces.

VI. CONCLUSION

In this article we have carried out a theoretical locality analysis and a subsequent practical implementation to demonstrate how the nonlinear set of CCSD amplitude equations for DEC fragment calculations may be solved to within a desired precision using a restricted set of local HF orbitals. A practical algorithm for determining the local orbital spaces needed to obtain the single fragment (and hence pair fragment) energies to within the requested precision has been implemented based on the principles identified in the theoretical analysis. The practical algorithm is focused on determining the smallest possible single fragment spaces (within the desired precision) in order to reduce the cost for the time-dominating pair fragment calculations as much as possible. We have finally demonstrated the numerical effectiveness and robustness of the single fragment optimization algorithm. In short, a solid theoretical foundation for local CCSD calculations and the identification of local orbital spaces has been established.

With the theoretical analysis, we have identified two error sources that are present when the single fragment energy is evaluated in a restricted orbital space, i.e., (a) the direct energy contribution of omitted orbitals and (b) the relaxation effects of omitted space components when solving the amplitude equations. When solving the CCSD amplitude equations in a restricted orbital space, four distinct relaxation mechanisms have been identified, i.e., a relaxation through (1) non-vanishing Fock matrix elements, (2) non-vanishing charge distributions in the two-electron integrals, (3) long-range (dipole–dipole) contributions in the two-electron integrals, and (4) long-range (charge-polarization) contributions from the T_1 -transformed Fock matrix. Mechanism (1) was found to be the dominant mechanism, and only when higher precision is requested ($\text{FOT} < 10^{-4}$ a.u.) mechanisms (2)–(4) become important. It was demonstrated that the effects of mechanisms (2) and (3) had a similar spatial extent as mechanism (1), while the effects of mechanism (4) could be partially remedied by constructing an approximate long-range T_1 transformed density matrix with singles amplitude contributions from all single fragments. For the occupied partitioning scheme, the single fragment orbital spaces may be determined at the MP2 level for a DEC-CCSD calculation, while, for the virtual partitioning scheme, it is in general necessary to determine the single fragment orbital spaces at the CCSD level to ensure robustness of the results. In general, the theoretical and numerical results thus demonstrate that the local orbital spaces are model- and molecule-dependent, underlining the importance of using a black-box algorithm for determining the local orbital spaces.

ACKNOWLEDGMENTS

The research leading to these results has received funding from the European Research Council under the

European Union's Seventh Framework Programme (FP/2007-2013)/ERC Grant Agreement No. 291371.

This research used resources of the Oak Ridge Leadership Computing Facility at Oak Ridge National Laboratory, which is supported by the Office of Science of the Department of Energy under Contract No. DE-AC05-00OR22725.

We also acknowledge the PRACE Research Infrastructure resource Curie at the Très Grand Centre de Calcul (TGCC) operated by CEA near Paris, France.

APPENDIX A: CHECKING THE INITIAL CONDITIONS OF THE FRAGMENT ANALYSIS

The prerequisites for the theoretical fragment analysis in Section III were that the two-electron integrals and the Fock matrix decay with the distance seen from a specific center P in the molecule. In this appendix, we numerically verify this assumption. In Fig. 10, we display the decay of the Fock matrix and the two-electron integrals from the perspective of the centers used in Section III C. For simplifying the plots, only the maximum value within intervals of 1.3 Å is given.

From Fig. 10, it is evident that the initial assumptions of Section III hold for all three chosen fragments, although there are minimal differences for the systems. Note that for all three systems, the virtual–virtual block (blue circles) of

the Fock matrix (mechanism 1) has the largest contributions at a given distance. The observed difference between the charge distribution decay (red pluses, mechanism 2) and the long-range dipole–dipole decay (cyan triangles, mechanism 3) of the two-electron integrals for the three fragments under investigation is minimal.

In Fig. 11 we compare the (charge distribution) decay of the singles (blue circles) and doubles (green x) amplitudes for the three fragments under investigation. As expected, the doubles amplitude decays roughly follow the decay behaviours of the corresponding two-electron integrals (mechanism 2) in Fig. 10 and thus the decay is slowest for system (iii).

APPENDIX B: DEFINING LOCALITY OF MOLECULAR ORBITALS AND SINGLE FRAGMENT EXTENTS

In a DEC calculation, a localized HF MO ϕ_r^P is assigned to the atomic site P where its Löwdin atomic charge Q_r^{atom} is largest. In case two atoms have similar Löwdin atomic charges, it is not important which atom a local orbital is assigned to, since the fragment optimization procedure ensures that the local orbital spaces are adapted to the specific orbital assignment, such that the atomic fragment energy is determined to the requested precision. Even though the bulk of ϕ_r^P is confined to a small volume of space, ϕ_r^P has small

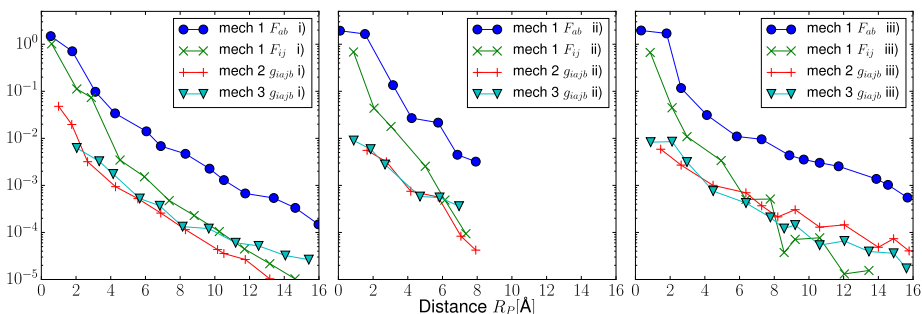


FIG. 10. The decay of the occupied–occupied Fock matrix elements F_{ij} with $i \in P, j \in [P]$ (mechanism 1, green x) and the virtual–virtual Fock matrix elements F_{ab} with $a \in P, b \in [P]$ (mechanism 1, blue circles) with the distance from the chosen sites P for systems (i), (ii), and (iii) is compared to the charge distribution decay in the two-electron integrals g_{aibj} with $i, j, b \in P, a \in [P]$ (mechanism 2, red pluses) and the long-range dipole–dipole decay in g_{aibj} with $i, a \in P, j, a \in [P]$ (mechanism 4, cyan triangles).

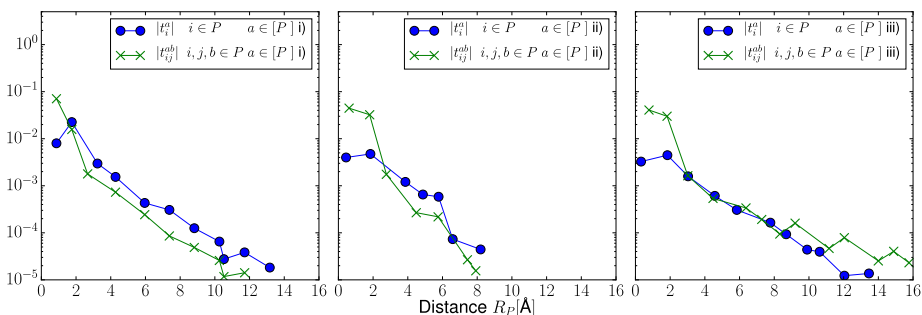


FIG. 11. The decay behaviours of the singles (blue circles) and doubles (green x) amplitudes with the distance to the chosen sites P of systems (i), (ii), and (iii).

expansion coefficients on AOs located some distance away from P . In this appendix we describe how this tail region may be treated without considering explicitly the AOs at which the small expansion coefficients are situated. This development is used to reduce the number of AOs and thereby the number of AO integrals which have to be evaluated. The procedure described here is very similar to the one described in Section 6.1 of Ref. 26. However, there are subtle differences, and for completeness the current implementation of the procedure is summarized here.

The HF orbital ϕ_r^P ,

$$\phi_r^P = \sum_{\mu} \chi_{\mu} c_{\mu r}^P, \quad (\text{B1})$$

may be approximated in the following way:

$$\tilde{\phi}_r^P = \sum_{\tilde{\mu}} \chi_{\tilde{\mu}} \tilde{c}_{\tilde{\mu} r}^P, \quad (\text{B2})$$

where the $\tilde{\mu}$ -summation is restricted to AOs which in some sense are neighboring the atomic site P (to be detailed below). The expansion coefficients of $\tilde{\phi}_r^P$ may be determined from a least squares fit, i.e., by minimizing the function $f(\tilde{c}^P)$,

$$f(\tilde{c}^P) = \|\tilde{\phi}_r^P - \phi_r^P\| = \langle \tilde{\phi}_r^P - \phi_r^P | \tilde{\phi}_r^P - \phi_r^P \rangle, \quad (\text{B3})$$

with respect to the \tilde{c} coefficients. This gives the expansion coefficients

$$\tilde{c}_{\tilde{\mu} r}^P = \sum_{\tilde{\nu}\eta} (\tilde{\mathbf{S}})_{\tilde{\mu}\tilde{\nu}}^{-1} S_{\tilde{\nu}\eta} c_{\eta r}^P, \quad (\text{B4})$$

where the dimensions of the overlap matrices are defined by the restrictions that are imposed on the AO indices, i.e.,

$$\tilde{\mathbf{S}}_{\tilde{\mu}\tilde{\nu}} = \langle \chi_{\tilde{\mu}} | \chi_{\tilde{\nu}} \rangle, \quad (\text{B5})$$

$$S_{\tilde{\nu}\eta} = \langle \chi_{\tilde{\nu}} | \chi_{\eta} \rangle. \quad (\text{B6})$$

For each MO ϕ_r^P , a prioritized list of AOs may be generated by quantifying the importance of each AO χ_{μ} according to its Löwdin charge Q_{μ}^r , noting that the sum over all Löwdin charges for MO ϕ_r^P equals one. We include AOs from this list until one minus the sum of Löwdin charges is smaller than a given threshold δ ,

$$1 - \sum_{\tilde{\mu}} Q_{\tilde{\mu}}^r < \delta, \quad (\text{B7})$$

where δ is a small prefixed number. This procedure defines a set of AOs for each MO ϕ_r^P , which we denote the orbital extent $\{\phi_r^P\}$. The union of orbital extents for all MOs in the effective orbital space $[P]_{\text{EFF}}$ is denoted the *atomic fragment extent* $\{P\}$. The $\{P\}$ space defines the set of AOs used to describe the MOs in single fragment P , i.e., it defines the restriction on the $\tilde{\mu}$ -summation in Eq. (B2). Thus, all MOs in the fragment are fitted using the same set of AOs to ensure a uniform description. We note that a screening of atomic centers in accordance with Eq. (B7) was used by Boughton and Pulay⁴² for the occupied HF orbitals as a completeness criteria for the assignment of local excitation spaces.

In practice we use $\delta = 0.05$ to define the orbital extents. This might appear to be a very crude value; however, the effect of approximating the MOs is minor because they are fitted using the *union* of all orbital extents. In particular, for the MOs

close to site P (large single fragment energy contributions), the fitting procedure has virtually no effect, while it slightly modifies the MOs far from P (small single fragment energy contributions). The fitting procedure therefore has a very minor effect on the single fragment energy. Furthermore, each step of the fragment expansion in Fig. 7 not only includes new energy contributions and new coupling effects by including more MOs, but it also improves the description of the MOs already included in the previous fragment ($\{P\}$ is enlarged). The effect of the approximation in Eq. (B2) is thus automatically taken into account by the fragment optimization procedure.

¹T. Helgaker, P. Jørgensen, and J. Olsen, *Molecular Electronic Structure Theory*, 1st ed. (Wiley, Chichester, England, 2000).

²P. Pulay, *Chem. Phys. Lett.* **100**, 151 (1983).

³S. Saebø and P. Pulay, *Annu. Rev. Phys. Chem.* **44**, 213 (1993).

⁴C. Hampel and H.-J. Werner, *J. Chem. Phys.* **104**, 6286 (1996).

⁵M. Schütz, G. Hetzer, and H.-J. Werner, *J. Chem. Phys.* **111**, 5691 (1999).

⁶P. Y. Ayala and G. E. Scuseria, *J. Chem. Phys.* **110**, 3660 (1999).

⁷V. Weijo, P. Manninen, P. Jørgensen, O. Christiansen, and J. Olsen, *J. Chem. Phys.* **127**, 074106 (2007).

⁸N. Flocke and R. J. Bartlett, *J. Chem. Phys.* **121**, 10935 (2004).

⁹S. Li, J. Ma, and Y. Jiang, *J. Comput. Chem.* **23**, 237 (2002).

¹⁰Z. Rolik and M. Kállay, *J. Chem. Phys.* **135**, 104111 (2011).

¹¹W. Li, Y. Guo, and S. Li, *Phys. Chem. Chem. Phys.* **14**, 7854 (2012).

¹²W. Li and S. Li, *J. Chem. Phys.* **121**, 6649 (2004).

¹³M. Kobayashi and H. Nakai, *J. Chem. Phys.* **129**, 044103 (2008).

¹⁴D. G. Fedorov and K. Kitaura, *J. Chem. Phys.* **123**, 134103 (2005).

¹⁵D. G. Fedorov, T. Nagata, and K. Kitaura, *Phys. Chem. Chem. Phys.* **14**, 7562 (2012).

¹⁶H. Stoll, *Chem. Phys. Lett.* **191**, 548 (1992).

¹⁷J. Friedrich, M. Hanrath, and M. Dolg, *J. Chem. Phys.* **126**, 154110 (2007).

¹⁸M. Häser and J. Almlöf, *J. Chem. Phys.* **96**, 489 (1992).

¹⁹B. Doser, D. S. Lambrecht, and C. Ochsenfeld, *Phys. Chem. Chem. Phys.* **10**, 3335 (2008).

²⁰S. Schweizer, B. Doser, and C. Ochsenfeld, *J. Chem. Phys.* **128**, 154101 (2008).

²¹F. Neese, F. Wennmohs, and A. Hansen, *J. Chem. Phys.* **130**, 114108 (2009).

²²F. Neese, A. Hansen, and D. G. Liakos, *J. Chem. Phys.* **131**, 064103 (2009).

²³C. Riplinger and F. Neese, *J. Chem. Phys.* **138**, 034106 (2013).

²⁴J. Yang, G. K. L. Chan, F. R. Manby, M. Schütz, and H.-J. Werner, *J. Chem. Phys.* **136**, 114105 (2012).

²⁵M. Ziolkowski, B. Jansík, T. Kjærgaard, and P. Jørgensen, *J. Chem. Phys.* **133**, 014107 (2010).

²⁶K. Kristensen, M. Ziolkowski, B. Jansík, T. Kjærgaard, and P. Jørgensen, *J. Chem. Theory Comput.* **7**, 1677 (2011).

²⁷I.-M. Høyvik, K. Kristensen, B. Jansík, and P. Jørgensen, *J. Chem. Phys.* **136**, 014105 (2012).

²⁸K. Kristensen, P. Jørgensen, B. Jansík, T. Kjærgaard, and S. Reine, *J. Chem. Phys.* **137**, 114102 (2012).

²⁹K. Kristensen, I.-M. Høyvik, B. Jansík, P. Jørgensen, T. Kjærgaard, S. Reine, and J. Jakowski, *Phys. Chem. Chem. Phys.* **14**, 15706 (2012).

³⁰K. Kristensen, T. Kjærgaard, I.-M. Høyvik, P. Ettenhuber, P. Jørgensen, B. Jansík, S. Reine, and J. Jakowski, *Mol. Phys.* **111**, 1196 (2013).

³¹J. J. Eriksen, P. Baudin, P. Ettenhuber, K. Kristensen, T. Kjærgaard, and P. Jørgensen, *J. Chem. Theory Comput.* **11**, 2984 (2015).

³²P. Baudin, P. Ettenhuber, S. Reine, K. Kristensen, and T. Kjærgaard, *J. Chem. Phys.* **144**, 054102 (2016).

³³I.-M. Høyvik, K. Kristensen, T. Kjærgaard, and P. Jørgensen, *Theor. Chem. Acc.* **133**(1), 1417 (2013).

³⁴M. Ziolkowski, V. Weijo, P. Jørgensen, and J. Olsen, *J. Chem. Phys.* **128**, 204105 (2008).

³⁵P. Ettenhuber and P. Jørgensen, *J. Chem. Theory Comput.* **11**, 1518 (2015).

³⁶T. H. Dunning, Jr., *J. Chem. Phys.* **90**, 1007 (1989).

³⁷M. Ziolkowski, B. Jansík, P. Jørgensen, and J. Olsen, *J. Chem. Phys.* **131**, 124112 (2009).

³⁸I.-M. Høyvik, B. Jansík, and P. Jørgensen, *J. Chem. Theory Comput.* **8**, 3137 (2012).

³⁹See supplementary material at <http://dx.doi.org/10.1063/1.4947019> for molecular geometries and the correlation energy of the systems presented in the result section.

⁴⁰LSDALTON, a linear scaling molecular electronic structure program, Release Dalton2016, see <http://daltonprogram.org> (2016).

⁴¹K. Aidas, C. Angeli, K. L. Bak, V. Bakken, R. Bast, L. Boman, O. Christiansen, R. Cimraglia, S. Coriani, P. Dahle, E. K. Dalskov, U. Ekström, T. Enevoldsen, J. J. Eriksen, P. Ettenhuber, B. Fernández, L. Ferrighi, H. Fliegl, L. Frediani, K. Hald, A. Halkier, C. Hättig, H. Heiberg, T. Helgaker, A. C. Hennum, H. Hettema, E. Hjertenæs, S. Høst, I.-M. Høyvik, M. F. Izzi, B. Jansík, H. J. A. Jensen, D. Jonsson, P. Jørgensen, J. Kauczor, S. Kirpekar, T.

Kjærgaard, W. Klopper, S. Knecht, R. Kobayashi, H. Koch, J. Kongsted, A. Krapp, K. Kristensen, A. Ligabue, O. B. Lutnæs, J. I. Melo, K. V. Mikkelsen, R. H. Myhre, C. Neiss, C. B. Nielsen, P. Norman, J. Olsen, J. M. H. Olsen, A. Osted, M. J. Packer, F. Pawłowski, T. B. Pedersen, P. F. Provasi, S. Reine, Z. Rinkevicius, T. A. Ruden, K. Ruud, V. V. Rybkin, P. Salek, C. C. M. Samson, A. S. de Merás, T. Saue, S. P. A. Sauer, B. Schimmelpfennig, K. Sneskov, A. H. Steindal, K. O. Sylvester-Hvid, P. R. Taylor, A. M. Teale, E. I. Tellgren, D. P. Tew, A. J. Thorvaldsen, L. Thøgersen, O. Vahtras, M. A. Watson, D. J. D. Wilson, M. Ziolkowski, and H. Ågren, *Wiley Interdiscip. Rev.: Comput. Mol. Sci.* **4**, 269 (2013).

⁴²J. W. Boughton and P. Pulay, *J. Comput. Chem.* **14**, 736 (1993).

B.3 Efficient linear-scaling second-order Møller–Plesset perturbation theory: The Divide–Expand–Consolidate RI-MP2 model

P. Baudin, P. Ettenhuber, S. Reine, K. Kristensen, and T. Kjærgaard

J. Chem. Phys. **144**, 054102 (2016).

Major contribution: writing process.

Proportional contribution: production of some of the data contained in the *numerical results* section.

Minor contribution: code implementation (atomic fragment optimization).



Efficient linear-scaling second-order Møller-Plesset perturbation theory: The divide–expand–consolidate RI-MP2 model

Pablo Baudin,^{1,a)} Patrick Ettenhuber,¹ Simen Reine,² Kasper Kristensen,¹ and Thomas Kjærgaard^{1,b)}

¹*qLEAP Center for Theoretical Chemistry, Department of Chemistry, Aarhus University, Langelandsgade 140, DK-8000 Aarhus C, Denmark*

²*Centre for Theoretical and Computational Chemistry, Department of Chemistry, University of Oslo, P.O. Box 1033, N-1315 Blindern, Norway*

(Received 15 October 2015; accepted 13 January 2016; published online 1 February 2016)

The Resolution of the Identity second-order Møller-Plesset perturbation theory (RI-MP2) method is implemented within the linear-scaling Divide-Expand-Consolidate (DEC) framework. In a DEC calculation, the full molecular correlated calculation is replaced by a set of independent fragment calculations each using a subset of the total orbital space. The number of independent fragment calculations scales linearly with the system size, rendering the method linear-scaling and massively parallel. The DEC-RI-MP2 method can be viewed as an approximation to the DEC-MP2 method where the RI approximation is utilized in each fragment calculation. The individual fragment calculations scale with the fifth power of the fragment size for both methods. However, the DEC-RI-MP2 method has a reduced prefactor compared to DEC-MP2 and is well-suited for implementation on massively parallel supercomputers, as demonstrated by test calculations on a set of medium-sized molecules. The DEC error control ensures that the standard RI-MP2 energy can be obtained to the predefined precision. The errors associated with the RI and DEC approximations are compared, and it is shown that the DEC-RI-MP2 method can be applied to systems far beyond the ones that can be treated with a conventional RI-MP2 implementation. © 2016 AIP Publishing LLC. [<http://dx.doi.org/10.1063/1.4940732>]

I. INTRODUCTION

The resolution-of-the-identity (RI) approximation^{1–5} has emerged as an important tool to reduce the computational cost of second-order Møller-Plesset perturbation theory⁶ (MP2) and related methods. The RI approximation was first applied to MP2 by Feyereisen *et al.*,⁷ and subsequently implemented by different groups.^{8–18} For reviews, the reader is referred to Refs. 19 and 20. In RI-MP2, also denoted density-fitting MP2 (DF-MP2), the four-center electron repulsion integrals (ERIs) are decomposed into a sum involving only two-center and three-center ERIs. The RI technique reduces the computational cost as well as the required memory considerably by removing the linear dependencies of the original atomic orbital (AO) product basis while maintaining reliable accuracies for practical chemical applications. The development of optimized auxiliary basis sets^{21–25} has reduced the error introduced by the RI approximation, and the error is often judged to be so small that RI-MP2 is the recommended method for calculating energies of MP2 quality. It should also be noted that MP2 with Cholesky decomposition of the ERIs is in many ways similar to RI-MP2.^{26–28}

For large molecular systems, conventional RI-MP2 implementations encounter a scaling wall, both memory- and time-wise. The correlation effects described by the RI-MP2

method are local, and the steep scaling of the method with the system size — $O(N^5)$ where N is a measure of the system size — is therefore unphysical. In the last decades, many groups have been developing alternative implementations of RI-MP2 in order to reduce the fifth order scaling using the locality of correlation effects (see Ref. 20 for a review of new developments within MP2 theory). One approach consists in compressing the number of wave function parameters required to describe the correlation energy by using projected atomic orbitals (PAOs) and pair natural orbitals (PNOs)^{12,29} or orbital specific virtual orbitals (OSVs).³⁰ Ochsenfeld and co-workers have developed an AO-MP2 algorithm, where the orbital energy denominator is eliminated from the conventional molecular orbital (MO)-based MP2 energy expression by means of a Laplace transformation^{31,32} to obtain a formulation in terms of AO integrals. Since AOs are local by construction, efficient integral screening may be performed.^{33–35} Pioneer work in that direction was done by Ayala and Scuseria.³⁶ Another commonly used approach for carrying out approximations in a MP2 calculation relies on a physical fragmentation of the molecular system and performing standard canonical calculations for each of the fragments before collecting the information for the full system. This category of methods includes the divide and conquer (DC),³⁷ the Fragment Molecular Orbital (FMO) methods,^{38–41} the Molecular Tailoring Approach (MTA),⁴² and the systematic molecular fragmentation approach.⁴³

Yet another category of methods for obtaining linear-scaling MP2 energies relies on a partitioning of the orbital

^{a)}Electronic mail: pablo.baudin@chem.au.dk

^{b)}Electronic mail: tkjaergaard@chem.au.dk

space rather than on a physical fragmentation of the molecule. This category contains the cluster in a molecule (CIM) method,^{44,45} the incremental scheme,⁴⁶ and our recently proposed local correlation method, the Divide-Expand-Consolidate (DEC) scheme.^{47–52} In a DEC calculation, the correlation energy is expressed in terms of local molecular orbitals,^{53–64} and the full molecular calculation is replaced by a set of independent fragment calculations. The number of fragments scales linearly with the system size, rendering the method linear-scaling and massively parallel. The linear-scaling and parallel performance of the DEC-MP2 model has been demonstrated recently.⁶⁵

In this paper, the DEC scheme is applied in connection with the RI-MP2 method. The overall linear-scaling properties of the DEC-MP2 scheme are not affected when the RI approximation is applied in the fragment calculations. However, the DEC-RI-MP2 method has a reduced computational cost as well as reduced memory requirements compared to the DEC-MP2 method. The resulting DEC-RI-MP2 method thus provides an efficient linear-scaling and massively parallel algorithm for the calculation of MP2 energies with rigorous error control.

In a DEC-MP2 calculation, the error introduced compared to a canonical MP2 calculation is controlled by the fragment optimization threshold (FOT).^{47,48} The canonical MP2 result is thus systematically approached when the FOT is tightened. Compared to the canonical MP2 energy, the DEC-RI-MP2 model contains an intrinsic DEC error governed by the FOT as well as an error associated with the RI approximation. In this work, we compare these two errors to analyze the performance of the DEC-RI-MP2 model. We also show that the DEC-RI-MP2 algorithm can be applied to systems that are much larger than the ones that can be treated using a standard RI-MP2 implementation.

The paper is organized as follows. In Section II, we present the basic equations of the DEC model and introduce the RI approximation. In Section III, we present numerical results and perform a detailed error and performance analysis for the DEC-RI-MP2 model. The parallel performance is discussed in Section IV, while Section V contains some conclusive remarks.

II. THEORY

A. The divide-expand-consolidate energy expression

The MP2 correlation energy $E_{\text{corr}}^{\text{MP2}}$ for a closed shell molecule may be expressed as⁶⁶

$$E_{\text{corr}}^{\text{MP2}} = \sum_{ijab} t_{ij}^{ab} (2g_{aibj} - g_{biaj}), \quad (1)$$

where t_{ij}^{ab} are the MP2 doubles amplitudes. In this article, the indices i, j (a, b) refer to occupied (virtual) *localized* real HF orbitals, and g_{aibj} is a 4-center ERI in the local molecular orbital (MO) basis using the Mulliken notation. Assigning each orbital to an atomic site (given by the nuclear positions P, Q, \dots), the summation over two occupied orbitals in Eq. (1) may be replaced by a summation over atomic sites and pair

sites,

$$E_{\text{corr}}^{\text{MP2}} = \sum_P E_P + \sum_{P>Q} \Delta E_{PQ}. \quad (2)$$

The atomic fragment energy E_P and the pair interaction energy ΔE_{PQ} are defined according to

$$E_P = \sum_{ij \in \underline{P}} \sum_{ab} t_{ij}^{ab} (2g_{aibj} - g_{biaj}), \quad (3)$$

$$\Delta E_{PQ} = \sum_{\substack{i \in \underline{P} \\ j \in \underline{Q}}} \sum_{ab} t_{ij}^{ab} (2g_{aibj} - g_{biaj}) + \sum_{\substack{i \in \underline{Q} \\ j \in \underline{P}}} \sum_{ab} t_{ij}^{ab} (2g_{aibj} - g_{biaj}), \quad (4)$$

where \underline{P} denotes the set of occupied orbitals assigned to atomic site P .

Using a local HF orbital basis, the free summations over virtual orbitals ab in the atomic fragment energy E_P may be restricted. This is justified by the fact that the integrals g_{aibj} (with $ij \in \underline{P}$) vanish for virtual orbitals spatially far from the atomic site P . We introduce the notation $[\bar{P}]$ for the set of virtual orbitals spatially close to atomic site P in the sense that the integrals g_{aibj} are non-vanishing (to the desired precision), and the virtual summations in Eq. (3) may thus be restricted to the $[\bar{P}]$ space. A similar replacement leading to the union of orbital spaces is introduced for the pair interaction energy ΔE_{PQ} ,⁴⁸ and Eqs. (3) and (4) may thus be written as

$$E_P = \sum_{ij \in \underline{P}} \sum_{ab \in [\bar{P}]} t_{ij}^{ab} (2g_{aibj} - g_{biaj}), \quad (5)$$

$$\begin{aligned} \Delta E_{PQ} = & \sum_{ab \in [\bar{P}] \cup [\bar{Q}]} \sum_{\substack{i \in \underline{P} \\ j \in \underline{Q}}} t_{ij}^{ab} (2g_{aibj} - g_{biaj}) \\ & + \sum_{\substack{i \in \underline{Q} \\ j \in \underline{P}}} t_{ij}^{ab} (2g_{aibj} - g_{biaj}). \end{aligned} \quad (6)$$

The details on how each local molecular orbital is assigned to atomic sites and how the $[\bar{P}]$ space is obtained is not the subject of this paper, and the reader is referred to Ref. 48. Here we just note that the $[\bar{P}]$ space is determined in a black box manner such that the error of E_P is smaller than the FOT, which is the central threshold that defines the precision of a DEC calculation. Naturally, in the limit where the space $[\bar{P}]$ includes all virtual orbitals for all atomic sites P , the conventional MP2 correlation energy is recovered. The approximations introduced in Eqs. (5) and (6) are summarized in Section II C along with other approximations of the DEC-RI-MP2 scheme.

The set of orbitals used to evaluate the fragment energy is denoted the *energy orbital space* (EOS), i.e., for atomic fragment P in Eq. (5) this corresponds to $\underline{P} \cup [\bar{P}]$. In order to describe coupling effects between the amplitudes in the EOS and the amplitudes outside the EOS, the MP2 equations (Eq. (7)) have to be solved in an extended space, and $[\underline{P}] \cup [\bar{P}]$ denoted the *amplitude orbital space* (AOS), where $[\underline{P}]$ includes \underline{P} as well as additional occupied orbitals involved in the coupling mechanism. As for the $[\bar{P}]$ space, the practical determination of $[\underline{P}]$ is described in Ref. 48.

Equation (5) requires amplitudes and integrals in the local basis. However, in practice, the solution of the amplitude

equation in the AOS is simplified by transforming the subset of localized HF orbitals to a pseudocanonical basis,⁶⁷ which is defined by diagonalizing the local Fock matrix blocks F_{ij} ($ij \in [P]$) and F_{ab} ($ab \in [\bar{P}]$). The amplitudes are then constructed directly in a pseudocanonical basis according to

$$t_{IJ}^{AB} = -g_{AIBJ}(\epsilon_A + \epsilon_B - \epsilon_I - \epsilon_J)^{-1}, \quad (7)$$

where I, J (A, B) are occupied (virtual) MO indices in the pseudocanonical basis, and $\epsilon_I, \epsilon_J, \epsilon_A,$ and ϵ_B are the diagonal Fock matrix elements in the pseudocanonical basis. The amplitudes are later transformed to the local basis where the energy is evaluated using Eq. (5). This transformation is necessary since the occupied summation restriction in Eq. (5) is only defined in the local basis.

The DEC algorithm described above scales quadratically with system size due to the number of pair calculations in Eq. (2). However, the pair energies describe dispersion interactions decaying with the inverse pair distance to the sixth power. Distant pairs with small energy contributions may therefore be neglected without affecting the precision of the total correlation energy, which already contains an error of size FOT for each atomic fragment. In the simplest approach, a distance-based cutoff can be used to determine which pairs to include.⁴⁸ A more elaborate scheme based on approximate pair energy contributions will be described in a forthcoming paper.

The DEC-MP2 algorithm may be summarized as follows:

1. Determine localized occupied and virtual HF molecular orbitals.
2. For each atomic fragment P , determine the optimized orbital spaces $[\bar{P}]$ and $[P]$ (the AOS) as detailed in Ref. 48. This step also provides all atomic fragment energies E_P . Each fragment calculation is carried out using the following procedure:
 - (a) Transform the local HF orbitals of the AOS into a pseudocanonical basis in order to generate the doubles amplitudes using Eq. (7).
 - (b) Transform the integrals and amplitudes back to the local HF basis and extract their EOS contributions.
 - (c) Evaluate the fragment energy using Eq. (5).
3. Pair screening: Use pair energy estimates to screen away pairs with negligible contributions (detailed in a

forthcoming paper) to get a list of the important pair fragments.

4. For each important pair fragment PQ , calculate ΔE_{PQ} according to steps 2(a)-2(c) above, where Eq. (6) is used in step 2(c).
5. Add up the fragment energies to obtain the total DEC-MP2 energy using Eq. (2).

B. The resolution of the identity within a DEC framework

The resolution of the identity can be expressed in its standard V approximation⁵ using the symmetric decomposition,⁶⁸

$$g_{ai bj} \approx \sum_{\alpha\beta} (ai|\alpha)(\alpha|\beta)^{-1}(\beta|bj),$$

$$g_{ai bj} \approx \sum_{\alpha\beta\gamma} (ai|\alpha)(\alpha|\gamma)^{-1/2}(\gamma|\beta)^{-1/2}(\beta|bj) = \sum_{\gamma} C_{ai}^{\gamma} C_{bj}^{\gamma}, \quad (8)$$

where $(ai|\alpha)$ is a 3-center ERI, $(\alpha|\beta)$ is a 2-center ERI, and $C_{ai}^{\gamma} = \sum_{\alpha} (ai|\alpha)(\alpha|\gamma)^{-1/2}$. We let $\{\alpha, \beta, \gamma\}$ refer to auxiliary AO indices, while $\{\mu, \nu\}$ are used for standard AO indices. We can directly apply the DEC-MP2 algorithm summarized in Section II A to the DEC-RI-MP2 model by calculating 2-electron integrals using Eq. (8).

Algorithm 1 shows in detail how the EOS amplitudes and EOS integrals entering Eqs. (5) and (6) are determined in the DEC-RI-MP2 method. Here, the i, j, a, b indices refer to localized HF orbitals in the EOS, while the I, J, A, B indices label pseudocanonical orbitals in the AOS. We use $C_{\mu I}$ ($C_{\mu A}$) to denote elements of the transformation matrix from the AOs to the occupied (virtual) pseudocanonical orbitals, while U_{Ii} (U_{Aa}) represents a transformation from the occupied (virtual) pseudocanonical orbitals to the occupied (virtual) local orbitals. The cost of the fragment calculation is determined by the number of occupied MOs in the EOS (O_{EOS}), occupied MOs in the AOS (O_{AOS}), virtual MOs in the AOS (V_{AOS}), standard AOs ($N_{AO, AOS}$), and auxiliary AOs ($N_{aux, AOS}$). Note that these dimensions all refer to a fragment (EOS or AOS subscript), not the full molecular system. The determination of $N_{AO, AOS}$ and $N_{aux, AOS}$ is discussed below. The scaling of each step is shown in Algorithm 1.

ALGORITHM 1. DEC-RI-MP2 algorithm for calculating EOS amplitudes t_{ij}^{ab} and EOS integrals $g_{ai bj}$. The scaling with the fragment size of the time-dominating step is given in parentheses for each term. Bold: Done by local master using OpenMP parallelization. Normal font: MPI-parallelized across n nodes, where each MPI process utilizes OpenMP parallelization. The notation is described in the text.

| | |
|---|--|
| 1 Calculate $(\alpha \mu\nu)$ | $(N_{aux, AOS} N_{AO, AOS}^2)$ |
| 2 Calculate $(\alpha \beta)$ | $(N_{aux, AOS}^2)$ |
| 3 Construct $(\alpha \beta)^{-\frac{1}{2}}$ | $(N_{aux, AOS}^3)$ |
| 4 $(\beta AI) = \sum_{\mu} C_{\mu A} [\sum_{\nu} C_{\nu I} (\beta \mu\nu)]$ | $(N_{aux, AOS} N_{AO, AOS}^2 O_{AOS})$ |
| 5 $C_{AI}^{\alpha} = \sum_{\beta} (\alpha \beta)^{-\frac{1}{2}} (\beta AI)$ | $(N_{aux, AOS}^2 V_{AOS} O_{AOS})$ |
| 6 $t_{IJ}^{AB} = \sum_{\alpha} \frac{C_{AI}^{\alpha} C_{BJ}^{\alpha}}{\epsilon_I + \epsilon_J - \epsilon_A - \epsilon_B}$ | $(N_{aux, AOS} V_{AOS}^2 O_{AOS}^2)$ |
| 7 $t_{ij}^{ab} = \sum_A U_{aA} \sum_B U_{bB} [\sum_I U_{iI} (\sum_J U_{jJ} t_{IJ}^{AB})]$ | $(O_{EOS} V_{AOS}^2 O_{AOS}^2)$ |
| 8 $C_{ai}^{\alpha} = \sum_A U_{aA} (\sum_I U_{iI} C_{AI}^{\alpha})$ | $(N_{aux, AOS} V_{AOS} O_{AOS})$ |
| 9 $g_{ai bj} = \sum_{\alpha} C_{ai}^{\alpha} C_{bj}^{\alpha}$ | $(N_{aux, AOS} V_{AOS}^2)$ |

The memory requirements of the standard RI-MP2 method are very small, since the method does not require the storage of the full doubles amplitudes, but only requires the fitting coefficients ($N_{\text{aux}}^2 VO$) for the full molecular system. However, the DEC-RI-MP2 method additionally requires a transformation from the pseudocanonical basis to the local basis. In practice, pseudocanonical amplitudes t_{ij}^{AB} are generated and immediately transformed to the local EOS (first transformation in step 7 in Algorithm 1), $t_{ij}^{AB} \rightarrow t_{ij}^{AB}$, and the t_{ij}^{AB} amplitudes are stored before they are fully transformed to the local basis ($t_{ij}^{AB} \rightarrow t_{ij}^{ab}$). The memory requirements are therefore $V_{\text{AOS}}^2 O_{\text{AOS}} O_{\text{EOS}}$ in addition to the $N_{\text{aux,AOS}}^2 V_{\text{AOS}} O_{\text{AOS}}$ requirements for the fitting coefficients. Thus, although the memory requirements of the DEC-RI-MP2 scheme are slightly more involved than for the conventional RI-MP2 method, the storage of doubles amplitudes with four AOS indices (t_{ij}^{AB}) is avoided in the DEC-RI-MP2 scheme, which also does not use any I/O. We also note that, since the doubles amplitudes are stored in the local basis (t_{ij}^{ab}), it is also possible to construct the MP2 density, molecular gradient, electrostatic potential, etc., within the DEC framework.^{49,51,69} Once the EOS amplitudes and EOS integrals have been determined, the actual evaluation of the fragment energy (Eq. (5) or (6)) is a minor task, which is not shown in Algorithm 1.

The parallelization of the DEC-RI-MP2 scheme is discussed in detail in Section IV. For now, we just note that each fragment calculation is parallelized over n compute nodes, where one of the nodes is assigned to be the local master. In Algorithm 1, the steps that are performed only by the local master are shown in bold, while the steps which are parallelized across the n nodes using the message passing interface (MPI) are shown in regular font.

The number of occupied (O_{AOS}) and virtual (V_{AOS}) orbitals assigned to a fragment is defined by the fragment optimization procedure.⁴⁸ To determine the number of AOs in a fragment, $N_{\text{AO,AOS}}$, we need to consider the expansion of a localized MO assigned to atomic site P , ϕ_r^P , in terms of atomic orbitals χ_μ and MO coefficients $c_{\mu r}^P$,

$$\phi_r^P = \sum_{\mu} \chi_{\mu} c_{\mu r}^P, \quad (9)$$

where r is a general MO label which may refer to either an occupied or a virtual orbital. Even though the bulk of the localized MO ϕ_r^P is confined to a small volume of space, the localized MO has small tail coefficients far from P . To reduce the number of 4-center AO integrals to be determined, we therefore introduce an approximate MO $\tilde{\phi}_r^P$,

$$\tilde{\phi}_r^P = \sum_{\mu \in \{P\}} \chi_{\mu} \tilde{c}_{\mu r}^P, \quad (10)$$

where $\{P\}$ is the so-called atomic extent (AE) which is a subset of atomic orbitals close to atomic site P , and the $\tilde{c}_{\mu r}^P$ coefficients are determined such that $\tilde{\phi}_r^P$ resembles ϕ_r^P as much as possible in a least squares sense. The practical determination of $\{P\}$ and $\tilde{c}_{\mu r}^P$ is detailed in Ref. 48. The number of AOs ($N_{\text{AO,AOS}}$) thus corresponds to the number of atomic basis functions included in $\{P\}$.

Concerning the set of auxiliary AOs used in the RI approximation, we investigate two choices:

- A:** Include the full auxiliary AO basis set in all fragment calculations.
- B:** Include auxiliary AO basis functions on atoms of the atomic extent (e.g., for atomic fragment P , include auxiliary AOs on atoms in the $\{P\}$ space, see Eq. (10)).

Option **A** is only interesting for analysis purposes, since it would destroy the linear-scaling of the DEC-RI-MP2 algorithm ($N_{\text{aux,AOS}}$ in Algorithm 1 would be the full molecular system). Option **B** is the practical choice and is appealing due to its simplicity and since it ensures a linear-scaling DEC-RI-MP2 algorithm. Naturally, both options will lead to the full RI-MP2 result in the limit where the FOT approaches zero. The approximation associated with option **B** is expected to be small, since, for an atomic fragment P , only ERIs g_{aibj} ($i, j \in P$), where the local virtual orbitals a and b are far from P , will be poorly described using the RI approximation, and such integrals have very small energy contributions. In essence, option **B** corresponds to a local domain fitting procedure, and local domain fitting has previously been used successfully for MP2.^{12,70,71} Options **A** and **B** are compared in Section III C.

C. DEC-RI-MP2 approximations

In order to investigate the efficiency of the DEC-RI-MP2 model, it is convenient to summarize the approximations introduced so far:

- Approx AOS:** The amplitude equations are solved in the restricted AOS, and the virtual orbital summations are restricted in Eqs. (5) and (6).
- Approx AE:** The orbitals in the AOS are spanned by the restricted set of AOs in the atomic extent.
- Approx PAIR:** Distant pair interaction energies are neglected.

These approximations are present for all wave function models within the DEC framework, while the following two approximations arise from the introduction of the resolution of the identity:

- Approx AAE:** The auxiliary AOs are restricted to the atomic extent (option **B**).
- Approx RI:** The RI approximation.

Approx AE, **Approx AOS**, **Approx PAIR**, and **Approx AAE** are DEC specific, while **Approx RI** represents the intrinsic RI error. When the FOT is tightened, the errors associated with **Approx AE**, **Approx AOS**, **Approx PAIR**, and **Approx AAE** all decrease. However, the RI error persists. Thus, as the FOT approaches zero, the DEC-RI-MP2 energy approaches the RI-MP2 energy, not the canonical MP2 energy. In Section III B, we investigate the convergence of the DEC-RI-MP2 with the FOT and compare the DEC specific errors to the intrinsic RI error.

III. NUMERICAL RESULTS

A. Computational details and molecular systems

In order to investigate the performance of the DEC-RI-MP2 algorithm both in terms of errors in the total correlation energy and in terms of timings, we have selected a set of medium to large molecules (see supplementary material for the molecular geometries⁷²). All calculations have been performed using Dunning's correlation consistent cc-pVTZ basis set⁷³ and the cc-pVTZ-RI auxiliary basis set.^{23,74,75} The considered molecular systems are as follows:

- Coronene (C₂₄H₁₂): 78 occupied orbitals, 810 virtual orbitals, 888 atomic basis functions, 2304 auxiliary basis functions.
- Tetrahexacontanoic acid (C₆₄O₂H₁₂₈): 264 occupied orbitals, 3508 virtual orbitals, 3773 atomic basis functions, 9186 auxiliary basis functions.
- Heptapeptide (Asn-Phe-Gly-Ala-Ile-Leu-Ser): 208 occupied orbitals, 2240 virtual orbitals, 2448 atomic basis functions, 6155 auxiliary basis functions.
- Valinomycin (C₅₄H₉₀N₆O₁₈): 300 occupied orbitals, 3300 virtual orbitals, 3600 atomic basis functions, 9018 auxiliary basis functions.

These molecules have rather different chemical structures, including a delocalized aromatic electronic structure (coronene), a highly one-dimensional molecule (tetrahexacontanoic acid), and a more compact structure (valinomycin). Furthermore, all considered molecules are rather large, since the DEC-RI-MP2 scheme is only useful for large molecular systems, as we discuss will in detail in Section III D.

All calculations have been performed using a local version of the LSD program, and the methods used in this paper are part of the kernel of the D 2016 suite.^{76,77}

B. The DEC correlation energy

In this section, we want to study the effect of the different approximations (RI and DEC) on the canonical MP2 correlation energy. We therefore introduce the following notations to quantify energy errors:

$$\delta\text{RI} = |E_{\text{corr}}^{\text{DEC-RI-MP2}} - E_{\text{corr}}^{\text{DEC-MP2}}|, \quad (11)$$

$$\delta\text{DEC} = |E_{\text{corr}}^{\text{DEC-RI-MP2}} - E_{\text{corr}}^{\text{RI-MP2}}|, \quad (12)$$

$$\delta\text{DEC-RI} = |E_{\text{corr}}^{\text{DEC-RI-MP2}} - E_{\text{corr}}^{\text{MP2}}|, \quad (13)$$

TABLE I. Total errors (δDEC , δRI , and $\delta\text{DEC-RI}$, a.u.) and recovery (ΔDEC , %) in the total correlation energy of the coronene molecule for different values of the FOT (a.u.). Speed up of DEC-RI-MP2 with respect to canonical RI-MP2 is also reported.

| FOT | δDEC | δRI | $\delta\text{DEC-RI}$ | ΔDEC | Speed up |
|---------------------|-----------------------|-----------------------|-----------------------|--------------------|----------|
| $1.0 \cdot 10^{-3}$ | $7.576 \cdot 10^{-2}$ | $5.255 \cdot 10^{-4}$ | $7.632 \cdot 10^{-2}$ | 98.153 | 0.127 |
| $1.0 \cdot 10^{-4}$ | $6.475 \cdot 10^{-3}$ | $5.598 \cdot 10^{-4}$ | $7.032 \cdot 10^{-3}$ | 99.842 | 0.045 |
| $1.0 \cdot 10^{-5}$ | $4.430 \cdot 10^{-4}$ | $5.703 \cdot 10^{-4}$ | $1.000 \cdot 10^{-3}$ | 99.989 | 0.029 |
| $1.0 \cdot 10^{-6}$ | $2.447 \cdot 10^{-5}$ | $5.555 \cdot 10^{-4}$ | $5.816 \cdot 10^{-4}$ | 99.999 | 0.023 |
| $1.0 \cdot 10^{-7}$ | $8.749 \cdot 10^{-7}$ | $5.555 \cdot 10^{-4}$ | $5.580 \cdot 10^{-4}$ | 100.00 | 0.022 |

where δRI denote the error associated with the RI approximation, δDEC the error associated with the DEC scheme, and $\delta\text{DEC-RI}$ the error associated with both RI and DEC. We also introduce the DEC recovery of the canonical RI-MP2 correlation energy,

$$\Delta\text{DEC} = \frac{E_{\text{corr}}^{\text{DEC-RI-MP2}}}{E_{\text{corr}}^{\text{RI-MP2}}}. \quad (14)$$

The error associated with both RI and DEC ($\delta\text{DEC-RI}$) are only reported for the coronene system as the other systems were too large to perform a canonical MP2 calculation of triple zeta quality. Furthermore, the RI errors (δRI) are not reported for the heptapeptide and the valinomycin systems (the DEC-MP2 calculations can in principle be performed, but for these systems they are very expensive for tight FOT values).

In Tables I–IV, we examine the convergence of the total correlation energy as the FOT is tightened. As for the DEC-MP2 scheme, the error δDEC in the total energy decreases by roughly an order of magnitude when decreasing the FOT by an order of magnitude, demonstrating that the combined DEC error associated with **Approx AE**, **Approx AOS**, **Approx PAIR**, and **Approx AAE** systematically decreases with the FOT. Thus, although in principle there are several approximations in DEC, they are all controlled by one threshold.

From Table I, we note that the RI error (δRI) of the DEC-RI-MP2 calculation converges to the error associated with the RI approximation for the canonical calculations on coronene ($5.55 \cdot 10^{-4}$ a.u.) when tightening the FOT. The same observation can be made for the carbon chain in Table II even though the exact number could not be calculated. It is important to realize that at approximately FOT = 10^{-5} a.u., the DEC-RI-MP2 calculation is dominated by the RI error (**Approx RI**) and further tightening of the FOT is futile. We also note that the DEC-RI-MP2 model provides results of similar accuracy for the different systems under consideration in Tables I–IV, i.e., independently of the spatial structure (1, 2, or 3-dimensional) and the chemical structure (conjugated or not conjugated system).

C. Selection of the auxiliary basis functions (Approx AAE)

Having demonstrated the general convergence of the DEC-RI-MP2 energy with the FOT, we now examine **Approx AAE** in more detail. In Table V, we compare option **A** (include

TABLE II. Total errors (δ DEC and δ RI, a.u.) and recovery (Δ DEC, %) in the total correlation energy of the tetrahexacontanoic acid for different values of the FOT (a.u.). Speed up of DEC-RI-MP2 with respect to canonical RI-MP2 is also reported.

| FOT | δ DEC | δ RI | Δ DEC | Speed up |
|---------------------|-----------------------|-----------------------|--------------|----------|
| $1.0 \cdot 10^{-3}$ | $1.285 \cdot 10^{-1}$ | $1.823 \cdot 10^{-3}$ | 98.986 | 25.8 |
| $5.0 \cdot 10^{-4}$ | $6.492 \cdot 10^{-2}$ | $2.416 \cdot 10^{-3}$ | 99.488 | 24.8 |
| $1.0 \cdot 10^{-4}$ | $1.414 \cdot 10^{-2}$ | $2.066 \cdot 10^{-3}$ | 99.888 | 17.2 |
| $5.0 \cdot 10^{-5}$ | $8.393 \cdot 10^{-3}$ | $1.918 \cdot 10^{-3}$ | 99.934 | 14.6 |
| $1.0 \cdot 10^{-5}$ | $1.821 \cdot 10^{-3}$ | $2.050 \cdot 10^{-3}$ | 99.986 | 6.7 |
| $5.0 \cdot 10^{-6}$ | $8.520 \cdot 10^{-4}$ | $2.051 \cdot 10^{-3}$ | 99.993 | 3.7 |

all auxiliary functions) and option **B** (include auxiliary functions associated with atomic centers in the atomic extent $\{P\}$) for tetrahexacontanoic acid. The difference between options **A** and **B** (δ_{B-A} in Table V) should be compared with the DEC error for this molecule in Table II. It is clear that the error related to option **B** is minuscule compared to the error associated with the DEC partitioning scheme, and option **B** is therefore well-justified. Note that option **B** is the practical implementation used for all other DEC-RI-MP2 calculations reported in this paper.

The numbers in Table V indicate that it is in fact possible to further reduce the size of the auxiliary space. For the $FOT = 10^{-5}$ a.u. calculation, the largest and smallest fitting domains contained 3197 and 1147 auxiliary functions, respectively. These fitting domains are quite large compared to what has typically been used in the literature,^{12,14,70,71,78,79} and the δ_{B-A} numbers in Table V strongly support the conclusion that smaller auxiliary domains can be used without affecting the precision. In the present implementation, we have used option **B** due to the simplicity of the approach, but we are currently investigating alternative choices leading to smaller auxiliary domains. Possible options include the use of Natural Auxiliary Functions (NAFs),⁸⁰ or 3 center integral screening techniques such as the SQV ϵ ⁸¹ or Löwdin charges.¹²

D. Performance analysis

The overall goal of DEC is to provide a framework to calculate energies and properties at the CC level of theory for molecular systems where a conventional implementation hits a scaling wall. Furthermore, the DEC scheme is designed to utilize the thousands of computing cores available on modern supercomputers. One of the consequences of the massively parallel character of DEC is a large amount of recalculations, which makes it vastly inefficient for small molecular systems

TABLE III. Total errors (δ DEC, a.u.) and recovery (Δ DEC, %) in the total correlation energy of the heptaepptide for different values of the FOT (a.u.).

| FOT | δ DEC | Δ DEC |
|---------------------|-----------------------|--------------|
| $1.0 \cdot 10^{-3}$ | $1.162 \cdot 10^{-1}$ | 98.944 |
| $1.0 \cdot 10^{-4}$ | $1.455 \cdot 10^{-2}$ | 99.868 |
| $1.0 \cdot 10^{-5}$ | $1.575 \cdot 10^{-3}$ | 99.986 |
| $1.0 \cdot 10^{-6}$ | $1.606 \cdot 10^{-4}$ | 99.999 |

TABLE IV. Total errors (δ DEC, a.u.) and recovery (Δ DEC, %) in the total correlation energy of the valinomycin molecule for different values of the FOT (a.u.).

| FOT | δ DEC | Δ DEC |
|---------------------|-----------------------|--------------|
| $1.0 \cdot 10^{-3}$ | $2.349 \cdot 10^{-1}$ | 98.512 |
| $5.0 \cdot 10^{-4}$ | $1.205 \cdot 10^{-1}$ | 99.237 |
| $1.0 \cdot 10^{-4}$ | $3.064 \cdot 10^{-2}$ | 99.806 |
| $5.0 \cdot 10^{-5}$ | $1.774 \cdot 10^{-2}$ | 99.888 |

compared to a conventional implementation. In this section we analyze the general performance of the DEC-RI-MP2 algorithm and try to give simple rule of thumb for the general user to choose between DEC or conventional implementations to treat a given problem. We have therefore reported speed ups of the DEC-RI-MP2 simulations with respect to the canonical RI-MP2 calculations for both coronene and the tetrahexacontanoic acid (see Tables I and II).

The calculations on coronene were performed on the Eos cluster at Oak Ridge National Laboratory (ORNL).⁸² The speed ups given in Table I show that the coronene molecule is clearly too small to demonstrate the usefulness of the DEC algorithm, i.e., the crossover between a conventional implementation and the DEC scheme occurs for a system that is larger than coronene. Indeed, in the case of a small molecular system and a tight FOT value, the DEC algorithm is basically repeating a conventional calculation using (almost) the full orbital space for each fragment, and consequently no speed ups are observed in Table I. For coronene, there are 300 fragments if all pair fragments are included. In the limit where the FOT approaches zero, a DEC calculation would therefore be 300 times slower than a canonical RI-MP2 calculation. However, because the fragment calculations are completely independent, it is always possible to bring down the time to solution of a DEC calculation by using many nodes.

For the tetrahexacontanoic acid (Table II), the calculations were performed using our local cluster.⁸³ While using DEC on the coronene system is clearly unfavorable, the situation is very different for the highly linear tetrahexacontanoic acid. It is seen that even without using the massively parallel feature of DEC (all independent calculations are done one after another), the DEC-RI-MP2 simulation provides shorter time to solution than the standard method for all FOTs in Table II. We also note that at approximately $FOT = 10^{-5}$ a.u., the DEC-RI-MP2 calculation starts to be dominated by the RI error, and the DEC-RI-MP2 calculation is still 6.7 times faster than the conventional RI-MP2 calculation.

TABLE V. Comparison of options **A** and **B** concerning the choice of auxiliary basis functions for tetrahexacontanoic acid using a cc-pVTZ(cc-pVTZ-RI) basis.

| FOT | δ_{B-A} ^a |
|---------------------|-----------------------------|
| $1.0 \cdot 10^{-3}$ | $4.1 \cdot 10^{-6}$ |
| $1.0 \cdot 10^{-4}$ | $6.1 \cdot 10^{-7}$ |
| $1.0 \cdot 10^{-5}$ | $5.3 \cdot 10^{-8}$ |

^aDifference in total correlation energy between options **A** and **B**.

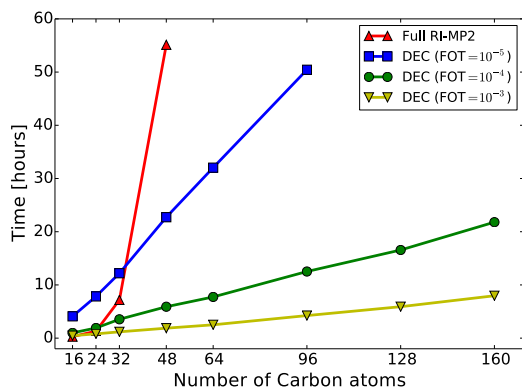


FIG. 1. Comparison of the linear-scaling DEC-RI-MP2 method and the N^5 scaling standard canonical RI-MP2 method for a set of alkane chains of increasing length. The cc-pVTZ(cc-pVTZ-RI) basis was employed.⁸³

In order to further illustrate the crossover between conventional and DEC implementations as well as to demonstrate the linear-scaling behavior of the DEC-RI-MP2 code, we have performed DEC-RI-MP2/cc-pVTZ(cc-pVTZ-RI) calculations on alkane chains of increasing sizes, from $C_{16}H_{34}$ (956 basis functions) to $C_{160}H_{322}$ (9308 basis functions). The results are given in Figure 1 for calculations performed using our local cluster.⁸³ It is seen that the DEC-RI-MP2 method indeed is scaling linearly with the system size (N), while the standard RI-MP2 method scales as N^5 . Obviously, tightening the FOT increases the prefactor, but it does not change the overall linear-scaling behavior of the method. Of course, the linear-scaling behavior emerges quite early for these highly linear systems, while 3-dimensional systems would enter the linear-scaling regime for larger system sizes.

The timings reported in Tables I and II and Figure 1 should guide the general user to choose between the conventional and DEC methods for RI-MP2 calculations. For highly linear systems, the DEC algorithm in general outperforms the conventional implementation. For more complicated structures, the conventional algorithm is to be preferred if it is at all feasible. However, when the canonical implementation hits the scaling wall, the DEC scheme is still feasible and becomes the method of choice. In particular, if many compute nodes are available, the DEC algorithm always provides a very short time to solution.

IV. PARALLELIZATION OF THE DEC SCHEME

In this section, we summarize the DEC parallelization strategy⁶⁵ and provide numerical results to investigate the parallel performance of the DEC-RI-MP2 scheme. As a test system, we use a cluster of 200 water molecules, $(H_2O)_{200}$, and the standard AO and auxiliary basis sets, cc-pVTZ and cc-pVTZ-RI, respectively. The calculations have been performed using a FOT = 10^{-4} a.u. and the Titan supercomputing system at ORNL.⁸⁴ In DEC, the different fragment calculations may be run in parallel because they are independent of each other.

We refer to this as *coarse grained parallelization*, while the parallelization of the individual fragment calculations is referred to as *medium grained parallelization* (Algorithm 1). The coarse grained parallelization is common to all wave function models (RI-MP2, MP2, CCSD, CCSD(T), ...), while the medium grained parallelization is dependent on the model of choice. At the coarse grained level of parallelization, one MPI process called the global master dynamically distributes the fragment jobs to the local masters according to a list where the computational demands of each fragment is prioritized (largest fragments are calculated first). At the medium grained level, each local master has a set of associated local slaves, which all together define a fragment slot. Each slot carries out the fragment calculation and sends back the fragment energy to the global master who adds up the fragment energy contributions. Since the fragment calculations are of very different size, we have chosen an approach where the slots divide dynamically to ensure a good medium grained parallelization. The medium grained parallelization is investigated in Section IV A, while the coarse grained parallel performance is discussed in Section IV B.

A. Medium grained parallelization

The *medium grained parallelization* of the DEC-RI-MP2 method is very similar to the parallelization of the standard canonical RI-MP2 calculation and as such several options are possible. Katouda and Nakajima¹⁰ performed the MPI work distribution based on the set of virtual orbitals, while in a previous paper,⁹ the MPI parallelization was based on the set of occupied orbitals. Hättig *et al.*⁸⁵ concluded that the time-determining steps of RI-MP2 was most efficiently parallelized over the pairs of occupied orbital indices, because a parallelization over auxiliary basis functions would require the communication of 4-index MO integrals and thus require transfer rates which can only be reached with high performance networks. However, in connection with the DEC-RI-MP2 code, the 4-index MO integrals and amplitudes that must be communicated are the ones residing in the small EOS space. The *medium grained parallelization* of the DEC-RI-MP2 model was therefore chosen to be based on a parallelization over auxiliary basis functions. Each node in the slot is thus simply assigned a subset of the auxiliary basis functions in each of the MPI-parallelized steps of Algorithm 1.

The individual fragment calculations can have significantly different sizes depending on the chemical environment. For example, the smallest pair fragment in the water cluster calculation (FOT = 10^{-4} a.u.), contained 17 occupied MOs, 222 virtual MOs, and 416 AOs, while the biggest fragment contained 73 occupied MOs, 902 virtual MOs, and 1928 AOs. The computational cost of the individual fragment calculations is the standard $O(N_{\text{frag}}^5)$ scaling, where N_{frag} is a measure of the fragment size (see Algorithm 1). These differences in fragment sizes thus lead to huge differences in terms of computational requirements.

To minimize the time-to-solution for the total calculation, it is important to know how many nodes can be used efficiently for a given fragment at the medium grained level of parallelization. In order to investigate the medium grained

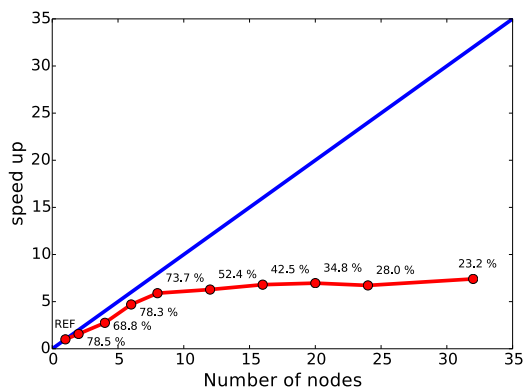


FIG. 2. Medium grained scaling: Speed up for a pair fragment consisting of 38 occupied orbitals, 350 virtual orbitals, 690 basis functions, and 1923 auxiliary basis functions in a DEC-RI-MP2/cc-pVTZ(cc-pVTZ-RI) energy calculation on a $(\text{H}_2\text{O})_{200}$ cluster using $\text{FOT} = 10^{-4}$ a.u. (The blue line represents ideal scaling and the relative speed up (in %) compared to ideal behavior are given for each point.)

parallel performance, we present relative timings for two fragments of very different sizes. In Figure 2, the relative timings are given for a small pair fragment (with 38 occupied orbitals, 350 virtual orbitals, 690 basis functions, and 1923 auxiliary basis functions) of the $(\text{H}_2\text{O})_{200}$ calculation, while Figure 3 shows the relative timings for a large pair fragment with 69 occupied orbitals, 723 virtual orbitals, 1397 basis functions, and 3999 auxiliary basis functions.

For the small fragment, the performance is quickly saturated and for six nodes, we obtain 78.3% of the idealized speed up. For the large fragment, the parallel performance is superlinear with the number of nodes. The reason for this superlinear behaviour is that the fitting coefficients C_{bj}^{γ} have been distributed among the nodes, and this reduces the datasize and improves cache memory performance. The

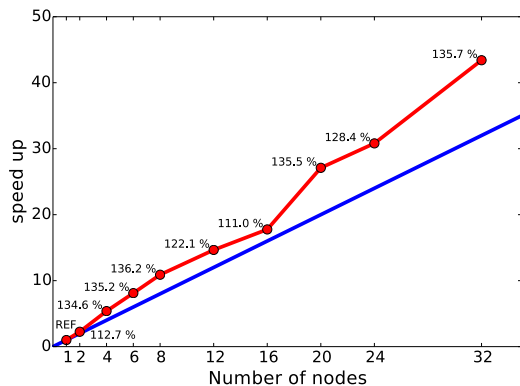


FIG. 3. Medium grained scaling: Speed up for a pair fragment consisting of 69 occupied orbitals, 723 virtual orbitals, 1397 basis functions, and 3999 auxiliary basis functions in a DEC-RI-MP2/cc-pVTZ(cc-pVTZ-RI) calculation on a $(\text{H}_2\text{O})_{200}$ cluster using $\text{FOT} = 10^{-4}$ a.u. (The blue line represents ideal scaling and the relative times (in %) compared to ideal behavior are given for each point.)

smaller memory requirements on the individual node also allow for more efficient AO to MO transformations.

The fragment size, which can be quantified in terms of $N_{\text{aux,AOS}}$, O_{AOS} , and V_{AOS} , thus determines the efficiency of the parallelization in Algorithm 1. The most expensive computational step (step 6 of the Algorithm 1) of a fragment calculation scales as $N_{\text{aux,AOS}}V_{\text{AOS}}^2O_{\text{AOS}}^2$, while, in the most expensive communication step, the 3 center ERIs ($\alpha|AI$) of size $N_{\text{aux,AOS}}V_{\text{AOS}}O_{\text{AOS}}$ are communicated among n nodes. We therefore require that the ratio between the computationally most expensive step and the most expensive communication step is large. Thus, roughly speaking, the larger $N_{\text{aux,AOS}}V_{\text{AOS}}^2O_{\text{AOS}}^2/(N_{\text{aux,AOS}}V_{\text{AOS}}O_{\text{AOS}}) = O_{\text{AOS}}V_{\text{AOS}}$ is, the more nodes can efficiently be used in Algorithm 1. In practice, we use the following condition to determine whether a slot containing n nodes should divide or not:

$$\text{Divide slot if: } n > O_{\text{AOS}}V_{\text{AOS}}/X. \quad (15)$$

The large number of fragments that must be calculated in a DEC calculation allows us to use a conservative number of nodes for each fragment, and empirical investigations have established that $X = 8000$ is a reasonable value. For example, if a slot of 4 nodes receives a fragment job where Eq. (15) is satisfied, the slot would divide into two new slots each containing two nodes. One of these slots would calculate the fragment job in question, while the other slot would receive another small fragment job from the global master.

B. Loss and coarse grained scaling

Concerning the parallel performance of the DEC-RI-MP2 scheme as a whole, we distinguish between local and global loss of efficiency.⁶⁵ The local loss occurs in the individual fragment calculation at the medium grained level of parallelization and was analyzed in Section IV A. Local loss is present due to nonideal load balancing, communication, and the non-parallelized steps in Algorithm 1. Global loss refers to the coarse grained parallelization level and occurs when all jobs have been distributed by the global master and some of the nodes wait for the remaining jobs to finish. It may in principle also occur if many local masters are trying to send/receive fragment job information to/from the global master at the same time, but we have not observed this to be a practical problem. In Figure 4, we investigate the coarse grained parallel performance for a calculation on the $(\text{H}_2\text{O})_{200}$ cluster using between 400 and 1600 nodes. The calculation using 400 nodes is taken as reference and corresponds to a time-to-solution of 8 h and 14 min. The coarse grained scaling behavior for the DEC-RI-MP2 code is close to ideal in the considered range, although it slowly starts to deteriorate for 1600 nodes for reasons detailed below.

Equation (15) was used to define the fragment slot sizes for the calculations in Figure 4, and some local loss is therefore expected. Global loss is present for any DEC calculation using more than one fragment slot. The local and global losses for the calculations in Figure 4 are compared in Table VI. The global loss is increasing with the number of nodes, reflecting the decrease in relative speed up in Figure 4, where the calculation with 400 nodes was used as reference. This

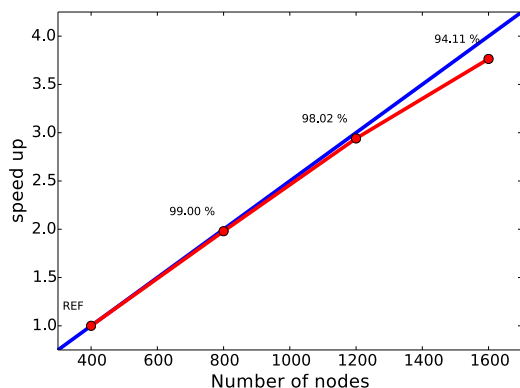


FIG. 4. Coarse grained scaling: Speed up for DEC-RI-MP2/cc-pVTZ(cc-pVTZ-RI) calculations on $(\text{H}_2\text{O})_{200}$ cluster using $\text{FOT} = 10^{-4}$ a.u. compared to the reference calculation using 400 nodes. The blue line represents ideal scaling and the relative times (in %) compared to ideal behavior are given for each point (relative to reference calculation).

TABLE VI. Local and global loss for DEC-RI-MP2/cc-pVTZ(cc-pVTZ-RI) calculations on $(\text{H}_2\text{O})_{200}$ cluster using $\text{FOT} = 10^{-4}$ a.u.

| Number of nodes: | 400 | 800 | 1200 | 1600 |
|------------------|------|------|------|------|
| Local loss (%) | 11.9 | 11.3 | 10.3 | 9.66 |
| Global loss (%) | 2.14 | 4.13 | 6.91 | 10.5 |

increase in global loss happens because, as the number of nodes is increased, more nodes are waiting for the last few fragment jobs to finish at the end of the calculation. The local loss from Table VI is roughly constant with the number of nodes ($\approx 10\%$), which means that the dividing procedure relying on Eq. (15) is working properly.

The current DEC-RI-MP2 parallelization scheme can be further improved, and work is being done in that direction. At present, Eq. (15) has been defined in order to use as many nodes as possible for a given fragment calculation without having a non-beneficial scaling behaviour (see Fig. 2) and keeping the local loss as low as possible. However, if a huge number of nodes is available, it may be beneficial to use more nodes for each fragment, which would reduce the global loss at the expense of increasing the local loss. An optimal balance between local and global losses to minimize the total loss would require a more advanced criterion for determining the slot sizes than the one in Eq. (15), or, at least X in Eq. (15) should be chosen in a more sophisticated manner than simply using a fixed predefined value. Nevertheless, the current status of the code allows us to efficiently exploit large supercomputer architectures and perform large DEC-RI-MP2 calculations with a short time-to-solution and low computational loss.

V. SUMMARY AND OUTLOOK

We have presented the linear-scaling and massively parallel DEC-RI-MP2 method, which shows substantial speed up compared to the DEC-MP2 algorithm. The method can be applied to systems that are much larger than the ones that

can be treated with the RI-MP2 method with small and controllable errors. The massively parallel character of the algorithm makes it particularly well suited for very large computer architectures for which several thousand nodes can be used efficiently, resulting in a very short time-to-solution. The DEC error control ensures that the standard RI-MP2 energy can be obtained to the desired precision.

The results indicate that the size of the auxiliary basis set can be further reduced, and work in this direction is ongoing. We also currently investigate the possibility of introducing a Laplace transformation of the orbital energy denominators^{16,17,31,32,86} to further reduce the computational cost of the DEC-RI-MP2 method. Current and future computer architectures utilize graphical processing units (GPUs), and the DEC-RI-MP2 scheme is ideally suited to exploit such hardware as has already been done for standard RI-MP2.^{15,87}

It is clear from the last two points that the DEC-RI-MP2 performance may be further improved — both concerning the algorithm itself and adaptation to modern computer hardware. It is therefore our intention to further develop DEC-RI-MP2 algorithm such that it will be able to offer a tractable alternative to density functional theory (DFT) calculations of molecular energies. Finally, we note that molecular gradient has already been implemented for the DEC-MP2 model.⁵¹ These developments are currently being adapted to the DEC-RI-MP2 model with the goal of extending the DEC-RI-MP2 model to be able to calculate molecular properties.

ACKNOWLEDGMENTS

This research used resources of the Oak Ridge Leadership Computing Facility at Oak Ridge National Laboratory, which is supported by the Office of Science of the Department of Energy under Contract No. DE-AC05-00OR22725.

The research leading to these results has received funding from the European Research Council under the European Union's Seventh Framework Programme (No. FP/2007-2013)/ERC Grant Agreement No. 291371. This work was further supported by the Research Council of Norway (RCN) through CoE Grant No. 179568/V30.

We acknowledge the PRACE Research Infrastructure resource Curie at the Très Grand Centre de Calcul (TGCC) operated by CEA near Paris, France.

¹J. L. Whitten, *J. Chem. Phys.* **58**, 4496 (1973).

²B. I. Dunlap, J. W. D. Connolly, and J. R. Sabin, *J. Chem. Phys.* **71**, 3396 (1979).

³B. I. Dunlap, J. W. D. Connolly, and J. R. Sabin, *J. Chem. Phys.* **71**, 4993 (1979).

⁴C. Van Alsenoy, *J. Comput. Chem.* **9**, 620 (1988).

⁵O. Vahtras, J. Almlöf, and M. W. Feyereisen, *Chem. Phys. Lett.* **213**, 514 (1993).

⁶C. Möller and M. S. Plesset, *Phys. Rev.* **46**, 618 (1934).

⁷M. Feyereisen, G. Fitzgerald, and A. Komornicki, *Chem. Phys. Lett.* **208**, 359 (1993).

⁸D. E. Bernholdt and R. J. Harrison, *Chem. Phys. Lett.* **250**, 477 (1996).

⁹M. Katouda and S. Nagase, *Int. J. Quantum Chem.* **109**, 2121 (2009).

¹⁰M. Katouda and T. Nakajima, *J. Chem. Theory Comput.* **9**, 5373 (2013).

¹¹L. Maschio, D. Usvyat, F. R. Manby, S. Casassa, C. Pisani, and M. Schütz, *Phys. Rev. B* **76**, 075101 (2007).

¹²H.-J. Werner, F. R. Manby, and P. J. Knowles, *J. Chem. Phys.* **118**, 8149 (2003).

¹³F. R. Manby, *J. Chem. Phys.* **119**, 4607 (2003).

- ¹⁴H.-J. Werner and F. R. Manby, *J. Chem. Phys.* **124**, 054114 (2006).
- ¹⁵L. Vogt, R. Olivares-Amaya, S. Kermes, Y. Shao, C. Amador-Bedolla, and A. Aspuru-Guzik, *J. Phys. Chem. A* **112**, 2049 (2008).
- ¹⁶A. F. Izmaylov and G. E. Scuseria, *Phys. Chem. Chem. Phys.* **10**, 3421 (2008).
- ¹⁷T. Nakajima and K. Hirao, *Chem. Phys. Lett.* **427**, 225 (2006).
- ¹⁸L. Maschio, *J. Chem. Theory Comput.* **7**, 2818 (2011).
- ¹⁹R. A. Kendall and H. A. Früchtl, *Theor. Chem. Acc.* **97**, 158 (1997).
- ²⁰D. Cremer, *WIREs Comput. Mol. Sci.* **1**, 509 (2011).
- ²¹D. E. Bernholdt and R. J. Harrison, *J. Chem. Phys.* **109**, 1593 (1998).
- ²²F. Weigend, M. Häser, H. Patzelt, and R. Ahlrichs, *Chem. Phys. Lett.* **294**, 143 (1998).
- ²³F. Weigend, A. Köhn, and C. Hättig, *J. Chem. Phys.* **116**, 3175 (2002).
- ²⁴C. Hättig, *Phys. Chem. Chem. Phys.* **7**, 59 (2005).
- ²⁵A. Hellweg and D. Rappoport, *Phys. Chem. Chem. Phys.* **17**, 1010 (2015).
- ²⁶F. Aquilante, R. Lindh, and T. Bondo Pedersen, *J. Chem. Phys.* **127**, 114107 (2007).
- ²⁷F. Aquilante, L. Gagliardi, T. Bondo Pedersen, and R. Lindh, *J. Chem. Phys.* **130**, 154107 (2009).
- ²⁸H. Koch, A. Sánchez De Merás, and T. Bondo Pedersen, *J. Chem. Phys.* **118**, 9481 (2003).
- ²⁹P. Pinski, C. Riplinger, E. F. Valeev, and F. Neese, *J. Chem. Phys.* **143**, 034108 (2015).
- ³⁰Y. Kurashige, J. Yang, G. K.-L. Chan, and F. R. Manby, *J. Chem. Phys.* **136**, 124106 (2012).
- ³¹J. Almlöf, *Chem. Phys. Lett.* **181**, 319 (1991).
- ³²M. Häser, *Theor. Chim. Acta* **87**, 147 (1993).
- ³³B. Doser, D. S. Lambrecht, J. Kussmann, and C. Ochsenfeld, *J. Chem. Phys.* **130**, 064107 (2009).
- ³⁴S. A. Maurer, D. S. Lambrecht, J. Kussmann, and C. Ochsenfeld, *J. Chem. Phys.* **138**, 014101 (2013).
- ³⁵B. Doser, J. Zienau, L. Clin, D. S. Lambrecht, and C. Ochsenfeld, *Z. Phys. Chem.* **224**, 397 (2010).
- ³⁶P. Y. Ayala and G. E. Scuseria, *J. Chem. Phys.* **110**, 3660 (1999).
- ³⁷M. Kobayashi, Y. Imamura, and H. Nakai, *J. Chem. Phys.* **127**, 074103 (2007).
- ³⁸Y. Mochizuki, K. Yamashita, T. Murase, T. Nakano, K. Fukuzawa, K. Takematsu, H. Watanabe, and S. Tanaka, *Chem. Phys. Lett.* **457**, 396 (2008).
- ³⁹T. Ishikawa and K. Kuwata, *Chem. Phys. Lett.* **474**, 195 (2009).
- ⁴⁰T. Ishikawa and K. Kuwata, *J. Phys. Chem. Lett.* **3**, 375 (2012).
- ⁴¹M. Katouda, *Theor. Chem. Acc.* **130**, 449 (2011).
- ⁴²A. P. Rahalkar, M. Katouda, S. R. Gadre, and S. Nagase, *J. Comput. Chem.* **31**, 2405 (2010).
- ⁴³V. Deev and M. A. Collins, *J. Chem. Phys.* **122**, 154102 (2005).
- ⁴⁴Y. Guo, W. Li, and S. Li, *J. Phys. Chem. A* **118**, 8996 (2014).
- ⁴⁵Y. Guo, W. Li, D. Yuan, and S. Li, *Sci. China: Chem.* **57**, 1393 (2014).
- ⁴⁶J. Friedrich and M. Dolg, *J. Chem. Theory Comput.* **5**, 287 (2009).
- ⁴⁷M. Ziolkowski, B. Jansík, T. Kjærgaard, and P. Jørgensen, *J. Chem. Phys.* **133**, 014107 (2010).
- ⁴⁸K. Kristensen, M. Ziolkowski, B. Jansík, T. Kjærgaard, and P. Jørgensen, *J. Chem. Theory Comput.* **7**, 1677 (2011).
- ⁴⁹K. Kristensen, I.-M. Høyvik, B. Jansík, P. Jørgensen, T. Kjærgaard, S. Reine, and J. Jakowski, *Phys. Chem. Chem. Phys.* **14**, 15706 (2012).
- ⁵⁰I.-M. Høyvik, K. Kristensen, B. Jansík, and P. Jørgensen, *J. Chem. Phys.* **136**, 014105 (2012).
- ⁵¹K. Kristensen, P. Jørgensen, B. Jansík, T. Kjærgaard, and S. Reine, *J. Chem. Phys.* **137**, 114102 (2012).
- ⁵²J. J. Eriksen, P. Baudin, P. Ettenhuber, K. Kristensen, T. Kjærgaard, and P. Jørgensen, *J. Chem. Theory Comput.* **11**, 2984 (2015).
- ⁵³M. Ziolkowski, B. Jansík, P. Jørgensen, and J. Olsen, *J. Chem. Phys.* **131**, 124112 (2009).
- ⁵⁴B. Jansík, S. Høst, K. Kristensen, and P. Jørgensen, *J. Chem. Phys.* **134**, 194104 (2011).
- ⁵⁵I.-M. Høyvik, B. Jansík, and P. Jørgensen, *J. Chem. Phys.* **137**, 224114 (2012).
- ⁵⁶I.-M. Høyvik, B. Jansík, and P. Jørgensen, *J. Chem. Theory Comput.* **8**, 3137 (2012).
- ⁵⁷I.-M. Høyvik, B. Jansík, and P. Jørgensen, *J. Comput. Chem.* **34**, 1456 (2013).
- ⁵⁸I.-M. Høyvik, K. Kristensen, T. Kjærgaard, and P. Jørgensen, *Theor. Chem. Acc.* **133**, 1417 (2013).
- ⁵⁹S. F. Boys, *Rev. Mod. Phys.* **32**, 296 (1960).
- ⁶⁰J. M. Foster and S. F. Boys, *Rev. Mod. Phys.* **32**, 300 (1960).
- ⁶¹C. Edmiston and K. Ruedenberg, *Rev. Mod. Phys.* **35**, 457 (1963).
- ⁶²C. Edmiston and K. Ruedenberg, *J. Chem. Phys.* **43**, S97 (1965).
- ⁶³J. Pipek and P. G. Mezey, *J. Chem. Phys.* **90**, 4916 (1989).
- ⁶⁴C. Zhang and S. Li, *J. Chem. Phys.* **141**, 244106 (2014).
- ⁶⁵K. Kristensen, T. Kjærgaard, I.-M. Høyvik, P. Ettenhuber, P. Jørgensen, B. Jansík, S. Reine, and J. Jakowski, *Mol. Phys.* **111**, 1196 (2013).
- ⁶⁶T. Helgaker, P. Jørgensen, and J. Olsen, *Molecular Electronic Structure Theory*, 1st ed. (Wiley, Chichester, England, 2000).
- ⁶⁷The term “fragment canonical basis” was previously used to denote this basis.
- ⁶⁸F. Weigend and M. Häser, *Theor. Chem. Acc.* **97**, 331 (1997).
- ⁶⁹S. Jakobsen, K. Kristensen, and F. Jensen, *J. Chem. Theory Comput.* **9**, 3978 (2013).
- ⁷⁰M. Schütz, H.-J. Werner, R. Lindh, and F. R. Manby, *J. Chem. Phys.* **121**, 737 (2004).
- ⁷¹D. Usvyat, L. Maschio, F. R. Manby, S. Casassa, M. Schütz, and C. Pisani, *Phys. Rev. B* **76**, 075102 (2007).
- ⁷²See supplementary material at <http://dx.doi.org/10.1063/1.4940732> for molecular geometries and the correlation energy of the systems presented in the result section.
- ⁷³A. K. Wilson, D. E. Woon, K. A. Peterson, and T. H. Dunning, *J. Chem. Phys.* **110**, 7667 (1999).
- ⁷⁴D. Feller, *J. Comput. Chem.* **17**, 1571 (1996).
- ⁷⁵K. L. Schuchardt, B. T. Didier, T. Elsethagen, L. Sun, V. Gurumoorthi, J. Chase, J. Li, and T. L. Windus, *J. Chem. Inf. Model.* **47**, 1045 (2007).
- ⁷⁶K. Aidas, C. Angeli, K. L. Bak, V. Bakken, R. Bast, L. Boman, O. Christiansen, R. Cimbriglia, S. Coriani, P. Dahle, E. K. Dalskov, U. Ekström, T. Enevoldsen, J. J. Eriksen, P. Ettenhuber, B. Fernández, L. Ferrighi, H. Flieg, L. Frediani, K. Hald, A. Halkier, C. Hättig, H. Heiberg, T. Helgaker, A. C. Hennum, H. Hettema, E. Hjertenes, S. Høst, I.-M. Høyvik, M. F. Izzi, B. Jansík, H. J. A. Jensen, D. Jonsson, P. Jørgensen, J. Kauczor, S. Kirpekar, T. Kjærgaard, W. Klopper, S. Knecht, R. Kobayashi, H. Koch, J. Kongsted, A. Krapp, K. Kristensen, A. Ligabue, O. B. Lutnæs, J. I. Melo, K. V. Mikkelsen, R. H. Myhre, C. Neiss, C. B. Nielsen, P. Norman, J. Olsen, J. M. H. Olsen, A. Osted, M. J. Packer, F. Pawłowski, T. B. Pedersen, P. F. Provasi, S. Reine, Z. Rinkevicius, T. A. Ruden, K. Ruud, V. Rybkin, P. Salek, C. C. M. Samson, A. S. de Merás, T. Saue, S. P. A. Sauer, B. Schimmelpenninck, G. Sneskov, A. H. Steindal, K. O. Sylvester-Hvid, P. R. Taylor, A. M. Teale, E. I. Tellgren, D. P. Tew, A. J. Thorvaldsen, L. Thøgersen, O. Vahtras, M. A. Watson, D. J. D. Wilson, M. Ziolkowski, and H. Ågren, *WIREs Comput. Mol. Sci.* **4**, 269 (2013).
- ⁷⁷LSD , a linear-scaling molecular electronic structure program, Release Dalton2016, 2015, <http://daltonprogram.org>.
- ⁷⁸D. Kats, T. Korona, and M. Schütz, *J. Chem. Phys.* **125**, 104106 (2006).
- ⁷⁹E. Goll, T. Leininger, F. R. Manby, A. Mitrushchenkov, H.-J. Werner, and H. Stoll, *Phys. Chem. Chem. Phys.* **10**, 3353 (2008).
- ⁸⁰M. Kállay, *J. Chem. Phys.* **141**, 244113 (2014).
- ⁸¹D. S. Hollman, H. F. Schaefer, and E. F. Valeev, *J. Chem. Phys.* **142**, 154106 (2015).
- ⁸²The calculations on Eos were performed using 20 XC30 compute-nodes, each with two sockets of 8 physical cores (Intel® Xeon® Processor E5-2670-2.60 GHz). Eos uses Cray’s Aries interconnect, and each node has 64 GB of memory available.
- ⁸³The calculations on Grendel cluster at the center for scientific computing aarhus (CCSCA) were performed using 21 SUN X2200 compute-nodes, each with 2 quadcore 2.3 GHz AMD Opteron CPU and 16GB of memory. The nodes are interconnected using a Gigabit Ethernet (GigE) network.
- ⁸⁴The calculations on Titan were performed using up to 1600 compute nodes of the Titan supercomputing system at ORNL. Each node consists of a 16-core 2.2 GHz AMD Opteron CPU and 32 GB of memory. Two nodes share a Gemini high-speed interconnect router.
- ⁸⁵C. Hättig, A. Hellweg, and A. Köhn, *Phys. Chem. Chem. Phys.* **8**, 1159 (2006).
- ⁸⁶D. Kats, D. Usvyat, and M. Schütz, *Phys. Chem. Chem. Phys.* **10**, 3430 (2008).
- ⁸⁷S. A. Maurer, J. Kussmann, and C. Ochsenfeld, *J. Chem. Phys.* **141**, 051106 (2014).

B.4 Linear-scaling coupled cluster with perturbative triple excitations: The Divide–Expand–Consolidate CCSD(T) model

J. J. Eriksen, P. Baudin, P. Etnhuber, K. Kristensen, T. Kjærgaard, and P. Jørgensen

J. Chem. Theory Comput. **11**, 2984 (2015).

Major contributions: production of the data contained in the *numerical results* section and writing process.

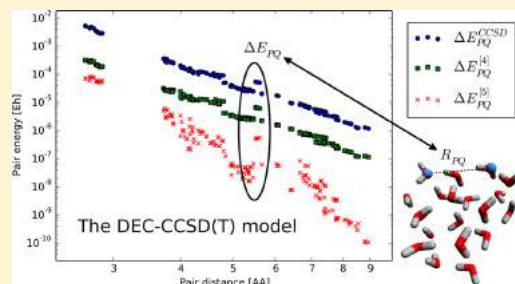
Minor contribution: code implementation (atomic fragment optimization, and molecular orbital based CCSD routines).

Linear-Scaling Coupled Cluster with Perturbative Triple Excitations: The Divide–Expand–Consolidate CCSD(T) Model

Janus J. Eriksen,* Pablo Baudin,* Patrick Ettenhuber, Kasper Kristensen, Thomas Kjærgaard, and Poul Jørgensen

qLEAP Center for Theoretical Chemistry, Department of Chemistry, Aarhus University, Langelandsgade 140, DK-8000 Aarhus C, Denmark

ABSTRACT: We propose a reformulation of the traditional (T) triples correction to the coupled cluster singles and doubles (CCSD) energy in terms of local Hartree–Fock (HF) orbitals such that its structural form aligns with our recently developed linear-scaling divide–expand–consolidate (DEC) coupled cluster family of local correlation methods. In a DEC-CCSD(T) calculation, a basis of local occupied and virtual HF orbitals is used to partition the correlated calculation on the full system into a number of independent atomic fragment and pair fragment calculations, each performed within a truncated set of the complete orbital space. In return, this leads to a massively parallel algorithm for the evaluation of the DEC-CCSD(T) correlation energy, which formally scales linearly with the size of the full system and has a tunable precision with respect to a conventional CCSD(T) calculation via a single energy-based input threshold. The theoretical developments are supported by proof of concept DEC-CCSD(T) calculations on a series of medium-sized molecular systems.



1. INTRODUCTION

In the quest for chemical accuracy in *ab initio* electronic structure calculations, the coupled cluster (CC) singles and doubles model¹ (CCSD) augmented by a perturbative treatment of triple excitations² (CCSD(T)) has proven itself the gold standard. However, despite the notable success of the CCSD(T) model in benchmarking electronic energies and other molecular properties for small molecular systems, its seventh-power scaling with system size remains a severe impediment of the model, generally preventing it from large-scale applications and hence from becoming beneficial beyond the niche of modest-sized molecular systems. In standard implementations, the scaling wall of the CCSD(T) model arises because the energy correction is expressed in a basis of highly nonlocal canonical Hartree–Fock (HF) molecular orbitals (MOs), making a local description of electron correlation effects unattainable.

Throughout the years, elaborate attempts have been made at pushing the limits for the CCSD(T) model by devising massively parallel implementations of the standard canonical formulation.^{3–11} However, it is evident that such attempts cannot significantly extend the application range of the model as the inherent scaling wall of the model is not overcome. If large molecular systems are to be addressed by the CCSD(T) model, the underlying algorithm is bound to be reformulated such that its implementation becomes not only massively parallel but also linearly scaling. Furthermore, if this alternative algorithm in itself is to be successful as a tool within high-

accuracy *ab initio* quantum chemistry, it is imperative that it possesses a strict error control through the use of a single parameter that directly identifies the precision of the calculation as compared to a standard calculation.

To accommodate the preceding requirements, a plethora of local correlation CCSD(T) methods have been introduced, many of which reduce the computational scaling to one that depends linearly on system size. The first successful of these was the local CCSD(T) method developed by Schütz and Werner,¹² and since then the CCSD(T) model has been implemented within various local correlation schemes such as the incremental scheme,¹³ the divide-and-conquer scheme,¹⁴ the cluster-in-molecule scheme,^{15,16} and most recently in terms of orbital-specific virtual orbitals¹⁷ as well as pair and triples natural orbitals.¹⁸ Common for all of these methods is the introduction of a set of parameters which regulate the overall accuracy of the calculation as compared to a conventional calculation. However, none of the methods have been designed to determine optimal local orbital spaces in an automated fashion based on a single energy criterion provided by the end user. In the present work, we propose a novel implementation of the CCSD(T) model, which has an error in the final energy that is indeed adjusted by the turn of a single knob, while at the same time being both linearly scaling and massively parallel. These advances are made possible through a reformulation of

Received: January 30, 2015

Published: May 27, 2015

the (T) correction to the CCSD energy such that its expression in terms of localized orbitals aligns with our recently developed divide-expand-consolidate (DEC) coupled cluster framework.^{19–23}

In a DEC-CC calculation, the inherent locality of the electron correlation problem is efficiently exploited in order to express the correlated wave function calculation on the full molecular system in terms of numerous small and independent fragment calculations that each uses a subset of the total orbital space. Importantly, the local orbital spaces used in the individual fragment calculations are determined in a black-box manner during the calculation to ensure that the calculated final energy is determined to within a predefined precision compared to a conventional calculation. An important prerequisite for the proposed DEC-CCSD(T) model—as for any DEC-CC model—is our recently developed strategy for generating a set of local orthogonal orbitals for both the occupied and virtual orbital spaces,²⁴ which allows us to describe local electron correlation effects without invoking, e.g., a set of linearly dependent nonorthogonal projected atomic orbitals.

The alternative formulation of the (T) triples energy correction used herein, which forms the basis for the DEC-CCSD(T) method, has a computational cost that is twice that of the standard expression. However, in contrast to the one conventionally used in standard implementations, which is restricted to the canonical HF basis, our alternative formulation may be expressed in any basis of optimized HF orbitals. As a consequence, the (T) correction can be expressed in a basis of localized orbitals, making it possible to take advantage of the locality of the triples amplitudes and, in return, obtain a reduced overall computational scaling of the energy correction.

In section 2, the conventional and alternative formulations of the (T) correction are compared to one another in terms of computational cost and the ability to be expressed in various bases of optimized HF orbitals. In section 3, we show how the coupling of the alternative expression for the (T) correction to the DEC scheme is made for a set of local HF orbitals, while numerical proof of concept DEC-CCSD(T) results are presented in section 4. Finally, section 5 gives some conclusive remarks.

2. CCSD(T) CORRELATION ENERGY

In a basis of spatial (spin-free) HF orbitals, the total CCSD energy for a closed-shell system is given as

$$E_{\text{CCSD}} = E^{\text{HF}} + E^{\text{CCSD}} \quad (2.0.1)$$

In eq 2.0.1, E^{HF} is the HF energy and E^{CCSD} the CCSD correlation energy, which reads²⁵

$$E^{\text{CCSD}} = \sum_{ab} \sum_{ij} (t_{ij}^{ab} + t_j^a t_i^b) L_{iajb} \quad (2.0.2)$$

where $\{t_i^a\}$ and $\{t_{ij}^{ab}\}$ are the CCSD singles and doubles amplitudes, respectively, and $L_{iajb} = 2g_{iajb} - g_{ibja}$ is an antisymmetrized two-electron integral written in Mulliken notation. In the following, the indices $\{i,j,k,l,m\}$ and $\{a,b,c,d,e\}$ will denote occupied and virtual HF orbitals, respectively.

The CCSD(T) energy is defined as²

$$E_{\text{CCSD(T)}} = E^{\text{HF}} + E^{\text{CCSD}} + E^{(\text{T})} \quad (2.0.3)$$

where $E^{(\text{T})}$ is the so-called (T) perturbative correction to the CCSD energy for the effect of triple excitations. The structure of $E^{(\text{T})}$ is defined by two energy contributions rationalized from many-body perturbation theory²⁶ (MBPT): $E^{[4]}$, a fourth-order term involving CCSD doubles amplitudes, and $E^{[5]}$, a fifth-order term involving CCSD singles amplitudes

$$E^{(\text{T})} = E^{[4]} + E^{[5]} \quad (2.0.4)$$

In a basis of canonical HF spatial orbitals, the expressions for the fourth- and fifth-order contributions may be derived from MBPT as²⁷

$$E^{[4]} = \sum_{abc} \sum_{ijk} \tau_{ijk}^{abc} t_{ijk}^{abc} \epsilon_{ijk}^{abc} \quad (2.0.5a)$$

$$E^{[5]} = \sum_{abc} \sum_{ijk} z_{ijk}^{abc} t_{ijk}^{abc} \epsilon_{ijk}^{abc} \quad (2.0.5b)$$

In eqs 2.0.5, the triples amplitudes $\{t_{ijk}^{abc}\}$ are given as

$$t_{ijk}^{abc} = -P_{ijk}^{abc} \frac{\sum_d t_{ij}^{ad} g_{ckbd} - \sum_l t_{il}^{ab} g_{cklj}}{\epsilon_{ijk}^{abc}} \quad (2.0.6)$$

where ϵ_{ijk}^{abc} denotes the orbital energy difference between the virtual and occupied orbitals of the excitation

$$\epsilon_{ijk}^{abc} = \epsilon_a + \epsilon_b + \epsilon_c - (\epsilon_i + \epsilon_j + \epsilon_k) \quad (2.0.7)$$

and P_{ijk}^{abc} is a symmetrization operator

$$P_{ijk}^{abc} x_{ijk}^{abc} = x_{ijk}^{abc} + x_{ikj}^{acb} + x_{jik}^{bac} + x_{kji}^{bca} + x_{kij}^{cab} + x_{kji}^{cba} \quad (2.0.8)$$

The z_{ijk}^{abc} coefficients in eq 2.0.5b are given as

$$z_{ijk}^{abc} = \frac{-(t_i^a g_{jbc} + t_j^b g_{iac} + t_k^c g_{iab})}{\epsilon_{ijk}^{abc}} \quad (2.0.9)$$

and the tilde notation on an arbitrary six-index quantity \tilde{x}_{ijk}^{abc} in eq 2.0.5 is defined as

$$\tilde{x}_{ijk}^{abc} = 2 \left(\frac{2}{3} x_{ijk}^{abc} - x_{ijk}^{acb} + \frac{1}{3} x_{ijk}^{bca} \right) \quad (2.0.10)$$

The expressions for the fourth- and fifth-order contributions in eqs 2.0.5 both contain orbital energy differences, and the evaluation of the (T) energy correction by this conventional formulation will thus be practically restricted to a basis of canonical HF orbitals. If, on the other hand, we were to express the correction in a more general, optimized HF basis (e.g., in terms of localized HF orbitals), the equation for the triples amplitudes in eq 2.0.6 would read

$$\begin{aligned} & \sum_c (t_{ijk}^{abc} F_{ac} + t_{ijk}^{acc} F_{bc} + t_{ijk}^{abc} F_{cc}) - \sum_m (t_{mjk}^{abc} F_{mi} + t_{imk}^{abc} F_{mj} + t_{ijm}^{abc} F_{mk}) \\ & = -P_{ijk}^{abc} \left(\sum_d t_{ij}^{ad} g_{ckbd} - \sum_l t_{il}^{ab} g_{cklj} \right) \end{aligned} \quad (2.0.11)$$

Since eq 2.0.11 is expressed in terms of off-diagonal elements of the Fock matrix, which become nonzero in the local HF basis,²⁸ the total (T) correction would have to be evaluated by means of an expensive iterative scheme, thereby drastically limiting the application range of the CCSD(T) model.

Alternatively, the two correction terms in eq 2.0.4 may be derived from Lagrangian-based CC perturbation theory for a HF reference state^{25,29} and expressed as

$$E^{[4]} = 2 \sum_{ab} \sum_{ij} (2t_{ij}^{ab} - t_{ji}^{ab}) T_{ij}^{ab} \quad (2.0.12a)$$

$$E^{[5]} = 2 \sum_a \sum_i t_i^a T_i^a \quad (2.0.12b)$$

In eqs 2.0.12, the fourth- and fifth-order contributions to the (T) correction are formulated in terms of the T_{ij}^{ab} and T_i^a intermediates, respectively

$$T_{ij}^{ab} = \sum_{cd} \sum_k (t_{ijk}^{acd} L_{bkcd} - t_{kji}^{acd} g_{kdbc}) - \sum_c \sum_{kl} (t_{ikl}^{abc} L_{kjlc} - t_{lki}^{abc} g_{kjlc}) \quad (2.0.13a)$$

$$T_i^a = \sum_{cd} \sum_{kl} (t_{ikl}^{acd} - t_{lki}^{acd}) L_{kcl} \quad (2.0.13b)$$

Comparing the evaluation of $E^{(T)}$ from eqs 2.0.5 and 2.0.12/2.0.13, we note that both expressions contain the triples amplitudes of eq 2.0.6, the generation of which scale as o^3v^4 (where o and v denote the number of occupied and virtual orbitals, respectively). The evaluation of the T_{ij}^{ab} intermediates in eq 2.0.13a contains an additional o^3v^4 scaling term, while the conventional expression in eq 2.0.5a contains no such term since each triples amplitude is immediately contracted with either itself or a z coefficient in an o^3v^3 step. As mentioned earlier, the contractions in eqs 2.0.5 are limited to the canonical HF basis. Thus, as the local nature of the triples amplitudes cannot be explored within this highly nonlocal basis, and the use of any other basis but that formed by the canonical HF orbitals will increase the computational cost, locality considerations cannot be used to reduce the overall computational scaling of the (T) energy correction whenever the formulations in eqs 2.0.5 are used. On the other hand, the alternative expressions in eqs 2.0.12 are valid within any basis of optimized HF orbitals, be that a canonical or a local basis. Since the intermediates in eqs 2.0.13 are constructed from triples amplitudes and MO integrals only, it is possible to take advantage of the locality of these two quantities when evaluating $\{T_{ij}^{ab}, T_i^a\}$ and, in return, $E^{(T)}$ in a local basis. As will be shown in section 3.2, eqs 2.0.12 and 2.0.13 thus provide a pathway toward a reduction of the overall computational scaling of the (T) energy correction.

In the present work, we will use the DEC-CC framework for determining the T_i^a and T_{ij}^{ab} intermediates in a basis of local HF orbitals. In practice, the intermediates in a DEC-CCSD(T) calculation will be determined from individual CCSD(T) calculations within local atomic fragment and pair fragment orbital spaces in analogy with the evaluation of CCSD singles and doubles amplitudes in the DEC-CCSD model.^{19,20} As we will demonstrate in sections 3 and 4, the alternative expressions for the (T) energy correction in eqs 2.0.12 facilitate a reduction in computational scaling of the $E^{\text{CCSD(T)}}$ energy to a linear dependence on system size, while retaining control of the error introduced as compared to a conventional CCSD(T) calculation.

3. DEC PARTITIONING OF THE CCSD AND CCSD(T) CORRELATION ENERGIES

To understand the similarities and differences between the DEC evaluation of the CCSD energy and the (T) energy correction, the foundation for both DEC formulations will be discussed next. In section 3.1, we give formally exact

expressions for both E^{CCSD} and $E^{(T)}$ in terms of DEC atomic fragment and pair interaction energies, while section 3.2 is devoted to the actual approximate evaluation of these.

3.1. Formulation in Terms of Atomic Fragment and Pair Interaction Energies. In the DEC-CC framework,^{19–23} we assign local HF orbitals to atomic sites P, Q, R, S, \dots and each atomic site P thus gets assigned a set of local occupied, \mathcal{P} , and virtual, $\bar{\mathcal{P}}$, HF orbitals. Reformulating the CCSD correlation energy in terms of summations over atomic sites and pair sites, eq 2.0.2 reads¹⁹

$$E^{\text{CCSD}} = \sum_P [E_P^{\text{CCSD}} + \sum_{Q < P} \Delta E_{PQ}^{\text{CCSD}}] \quad (3.1.1)$$

where the atomic fragment energy, E_P^{CCSD} , and the pair interaction energy, $\Delta E_{PQ}^{\text{CCSD}}$, are given as

$$E_P^{\text{CCSD}} = \sum_{ab} \sum_{ij \in \mathcal{P}} (t_{ij}^{ab} + t_i^a t_j^b) L_{iajb} \quad (3.1.2a)$$

$$\Delta E_{PQ}^{\text{CCSD}} = \sum_{ab} (\sum_{i \in \mathcal{P}} \sum_{j \in \mathcal{Q}} + \sum_{i \in \mathcal{Q}} \sum_{j \in \mathcal{P}}) (t_{ij}^{ab} + t_i^a t_j^b) L_{iajb} \quad (3.1.2b)$$

In eqs 3.1.1 and 3.1.2, the CCSD correlation energy is written in such a way that the summations over the two occupied orbitals, $\{ij\}$, in eq 2.0.2 are replaced by summations over atomic sites P and pair sites P, Q as well as summations over orbitals $\{ij\}$ assigned to the respective atomic sites.

Since the expression for the (T) correction in eqs 2.0.12 contains similar summations over occupied and virtual orbitals, we may likewise substitute these by summations over atomic sites P and pair sites P, Q as in eq 3.1.1

$$E^{(T)} = \sum_P [E_P^{(T)} + \sum_{Q < P} \Delta E_{PQ}^{(T)}] \quad (3.1.3)$$

where the triples atomic fragment energy, $E_P^{(T)}$, and triples pair interaction energy, $\Delta E_{PQ}^{(T)}$, are given as

$$E_P^{(T)} = E_P^{[4]} + E_P^{[5]} \quad (3.1.4a)$$

$$\Delta E_{PQ}^{(T)} = \Delta E_{PQ}^{[4]} + \Delta E_{PQ}^{[5]} \quad (3.1.4b)$$

The CCSD(T) fourth-order terms become

$$E_P^{[4]} = 2 \sum_{ab} \sum_{ij \in \mathcal{P}} (2t_{ij}^{ab} - t_{ji}^{ab}) T_{ij}^{ab} \quad (3.1.5a)$$

$$\Delta E_{PQ}^{[4]} = 2 \sum_{ab} (\sum_{i \in \mathcal{P}} \sum_{j \in \mathcal{Q}} + \sum_{i \in \mathcal{Q}} \sum_{j \in \mathcal{P}}) (2t_{ij}^{ab} - t_{ji}^{ab}) T_{ij}^{ab} \quad (3.1.5b)$$

while the fifth-order terms become

$$E_P^{[5]} = 2 \sum_{a \in \bar{\mathcal{P}}} \sum_{i \in \mathcal{P}} t_i^a T_i^a \quad (3.1.6a)$$

$$\Delta E_{PQ}^{[5]} = 2 (\sum_{a \in \bar{\mathcal{P}}} \sum_{i \in \mathcal{Q}} + \sum_{a \in \bar{\mathcal{Q}}} \sum_{i \in \mathcal{P}}) t_i^a T_i^a \quad (3.1.6b)$$

with the T_{ij}^{ab} and T_i^a intermediates given in eqs 2.0.13.

We note how the fourth-order term in eqs 3.1.5 is partitioned in the same way as E^{CCSD} in eq 3.1.2; that is, the summations over occupied orbitals are replaced by summations over the atomic sites and pair sites to which the local HF orbitals have been assigned. For the fifth-order term in eqs 3.1.6, however, we have chosen a partitioning in which both single excitation indices refer to the same atomic site for the atomic fragments,

while for the pair interaction energies, the indices are assigned to different atomic sites.

3.2. Evaluation of Atomic Fragment and Pair Interaction Energies. By replacing the summations over orbitals in E^{CCSD} and $E^{(\text{T})}$ by summations over atomic sites and pair sites as well as orbitals assigned to these sites in eqs 3.1.1 and 3.1.3, no approximations are introduced and no reductions will be obtained with respect to computational requirements. On the other hand, if restrictions can be made in the summations over the space of virtual orbitals in the atomic fragment and pair interaction calculations without compromising the overall accuracy of the calculation, then E^{CCSD} and $E^{(\text{T})}$ may be calculated using an algorithm that scales quadratically with system size. Furthermore, as we will see, many pair contributions may be neglected without compromising the precision of the calculated correlation energy, ultimately leading to a linear-scaling algorithm for the evaluation of the DEC-CCSD(T) energy.

We initially consider E^{CCSD} in eqs 3.1.2 and assume it is expressed in a basis of local HF orbitals. The atomic fragment energy, E_p^{CCSD} , in eq 3.1.2a contains the integrals L_{ijb} where both occupied indices $\{ij\}$ refer to local orbitals assigned to atomic site P . These integrals will be nonvanishing only if the virtual indices $\{a,b\} \in [\bar{P}]$, where the space $[\bar{P}]$ denotes the virtual HF orbital space that is spatially local to P (including \bar{P}); see Figure 1. For the pair interaction energy in eq 3.1.2b, the summations over the virtual orbital space may be restricted in a similar manner using unions of the atomic fragment orbital spaces for the constituent atomic sites, resulting in the

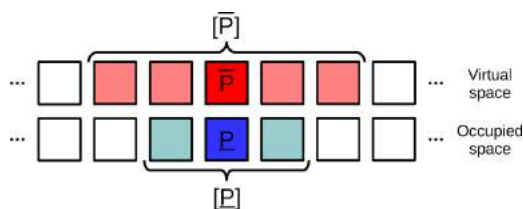


Figure 1. Different orbital spaces for a given atomic fragment P . Each box denotes a set of occupied or virtual orbitals assigned to an atomic site. The CCSD amplitude equations are solved in the $[\underline{P}] \cup [\bar{P}]$ space, and the CCSD atomic fragment energy is evaluated in the $\underline{P} \cup \bar{P}$ space.

following²⁰ DEC-CCSD atomic fragment and pair interaction energies

$$E_p^{\text{CCSD}} = \sum_{ab \in [\bar{P}]} \sum_{ij \in \underline{P}} (t_{ij}^{ab} + t_{ij}^{a,b}) L_{ijb} \quad (3.2.1a)$$

$$\Delta E_{pQ}^{\text{CCSD}} = \sum_{ab \in [\bar{P}] \cup [\bar{Q}]} \left(\sum_{i \in \underline{P}} \sum_{j \in \underline{Q}} + \sum_{i \in \underline{Q}} \sum_{j \in \underline{P}} \right) (t_{ij}^{ab} + t_{ij}^{a,b}) L_{ijb} \quad (3.2.1b)$$

In order to accurately determine the CCSD amplitudes in eq 3.2.1a, it is imperative that certain coupling effects to amplitudes outside the $\underline{P} \cup \bar{P}$ space are described. As elaborated upon in ref 20, most of these coupling effects arise from nonvanishing charge distributions in two-electron integrals in addition to the distance decay of the Fock matrix. As a result of these additional effects, the amplitudes of eq 3.2.1a have to be allowed to couple to, e.g., amplitudes t_{kl}^{ab} for which $\{k,l\} \in [\underline{P}]$, where $[\underline{P}]$ denotes the set of occupied orbitals that are spatially local to the atomic site P (including

\underline{P}); see Figure 1. In practice, the DEC-CCSD atomic fragment energy, E_p^{CCSD} , is thus determined by (i) solving the CCSD amplitude equations in the truncated $[\underline{P}] \cup [\bar{P}]$ space and (ii) extracting the amplitudes of the $\underline{P} \cup \bar{P}$ space that are needed for evaluating E_p^{CCSD} using eq 3.2.1a. Similarly, pair fragment energies are determined using unions of spaces in accordance with eq 3.2.1b. The $[\underline{P}]$ and $[\bar{P}]$ spaces are determined dynamically in a black-box manner during the calculation to ensure that the resulting error in the atomic fragment energy, E_p^{CCSD} , is below the so-called fragment optimization threshold (FOT). This procedure will thus account for the coupling effects mentioned earlier. The practical implementation of the fragment optimization procedure is described in ref 20.

Turning our attention to the (T) correction, the orbital spaces entering the expressions for the fourth-order DEC-CCSD(T) atomic fragment and pair interaction energies in eqs 3.1.5 may be truncated in a similar fashion

$$E_p^{[4]} = 2 \sum_{ab \in [\bar{P}]} \sum_{ij \in \underline{P}} (2t_{ij}^{ab} - t_{ij}^{ab}) T_{ij}^{ab} \quad (3.2.2a)$$

$$\Delta E_{pQ}^{[4]} = 2 \sum_{ab \in [\bar{P}] \cup [\bar{Q}]} \left(\sum_{i \in \underline{P}} \sum_{j \in \underline{Q}} + \sum_{i \in \underline{Q}} \sum_{j \in \underline{P}} \right) (2t_{ij}^{ab} - t_{ij}^{ab}) T_{ij}^{ab} \quad (3.2.2b)$$

while the expressions for the fifth-order energies in eqs 3.1.6 remain unchanged. In practice, the actual spaces required for the accurate evaluation of the (T) correction will be constrained to the truncated $[\underline{P}] \cup [\bar{P}]$ spaces used in the preceding calculation of the CCSD correlation energy due to two primary reasons. First, as the fourth- and fifth-order contributions to the (T) correction are constructed from CCSD singles and/or doubles amplitudes, these will only be satisfactorily described within truncated fragment spaces suitable for the CCSD model. Second, the total (T) correction is known from the literature to be roughly an order of magnitude smaller than the CCSD correlation energy,²⁵ and the errors introduced from reusing the CCSD fragment spaces are thus expected to be minor compared to the intrinsic FOT error. As a result, we will refrain from attempting to improve upon the underlying $[\underline{P}] \cup [\bar{P}]$ spaces obtained for the CCSD model when evaluating the (T) correction. Furthermore, we will also use union spaces in the calculation of (T) pair interaction energies. Both of these assumptions will be numerically justified from the DEC-CCSD(T) results in section 4.

In ref 21, it was illustrated how the dominating contributions to the CCSD pair interaction energies in eq 3.2.1b, that is, those that arise from the CCSD doubles amplitudes, decay asymptotically as r_{pQ}^{-6} (where r_{pQ} is the interatomic distance between atomic sites P and Q), thereby exhibiting a decay rate in accordance with that of regular dispersion energies. In short, the origin of this decay rate may be traced back to the fact that both the CCSD doubles amplitudes and the integrals entering eq 3.2.1b decay as r_{pQ}^{-3} , whenever $i \in \underline{P}$ and $j \in \underline{Q}$. For this reason, we may neglect pair interaction energies beyond a certain interatomic distance, again without compromising the precision of the total correlation energy. Neglecting contributions to E^{CCSD} from distant pairs thus reduces the total scaling into one that formally depends only linearly on the size of the system.

For the fourth- and fifth-order (T) pair interaction energies in eqs 3.2.2b and 3.1.6b, respectively, we initially note how the fifth-order contributions will typically be an order of magnitude smaller than the corresponding fourth-order contributions.²⁵

For this reason, the actual (T) correction for a pair at a large interatomic separation will be determined almost exclusively by the dominant fourth-order contributions, and when analyzing the distance decay of the (T) pair interaction energies, we may limit our analysis to these. In order to conduct a similar analysis for the (T) pair interaction energies as the one done for the CCSD counterparts, it is instructive to turn to an alternative formulation of the fourth-order contribution. From coupled cluster perturbation theory,^{25,29} this contribution may be written in terms of the Møller–Plesset fluctuation potential, $\hat{\Phi}$, as

$$E^{[4]} = \langle \text{HF} | [\hat{\Phi}, T_2^{[3]}] | \text{HF} \rangle \quad (3.2.3)$$

where $\tilde{T}_2^{[3]} = \sum_{\mu_2} \tilde{t}_{\mu_2}^{[3]} \hat{t}_{\mu_2}$ is a double excitation operator built from the following third-order doubles amplitudes

$$\tilde{t}_{\mu_2}^{[3]} = -\epsilon_{\mu_2}^{-1} \langle \mu_2 | [\hat{\Phi}, T_3] | \text{HF} \rangle \quad (3.2.4)$$

In eq 3.2.4, ϵ_{μ_2} is the orbital energy difference between the virtual and occupied orbitals of double excitation μ_2 (cf. eq 2.0.7), while T_3 is a triple excitation operator built from the amplitudes in eq 2.0.6.

Writing out the fourth-order contribution to the (T) correction in eq 3.2.3, we arrive at the following expression

$$E^{[4]} = \sum_{ab} \sum_{ij} \tilde{t}_{ij}^{ab,[3]} L_{iajb} \quad (3.2.5)$$

Comparing eq 3.2.5 to the corresponding expression for the doubles contribution to the CCSD energy in eq 2.0.2, we note how these greatly resemble one another. Since the third-order doubles amplitudes in eq 3.2.4 represent the lowest-order relaxation contribution from triple excitations to the doubles amplitudes in the coupled cluster singles, doubles, and triples model³⁰ (CCSDT), which decay with the interatomic distance between atomic sites P and Q in the same way as the CCSD doubles amplitudes, i.e., as r_{PQ}^{-3} , the fourth-order contribution to the (T) correction, and thus the total (T) correction, will decay as r_{PQ}^{-6} . For this reason, we may neglect contributions to $E^{(T)}$ from distant pairs following the same line of arguments that led to a reduction in the computational scaling of the CCSD energy and, in return, obtain an algorithm for the evaluation of the CCSD(T) energy that scales only linearly with the size of the system.

In outlining the final DEC-CCSD(T) algorithm, we note that two levels of approximations have been introduced for the fourth-order contributions in eqs 3.2.2 compared to the exact expressions in eq 2.0.12a, while only one of these have been introduced for the fifth-order contributions in eqs 3.1.6 compared to eq 2.0.12b. For the fourth-order contributions, the summations over the virtual space have been truncated (approximation i), and the CCSD amplitudes t_{ij}^{ab} as well as the T_{ij}^{ab} intermediates have been determined within a truncated set of localized HF orbitals (approximation ii). For example, the $[P]$ and $[\bar{P}]$ spaces have been used for atomic fragment P (see Figure 1). For the fifth-order contributions, only approximation ii has been invoked; i.e., truncated spaces have been used in the determination of the CCSD singles amplitudes t_i^a and the T_i^a intermediates.

The DEC-CCSD(T) algorithm can now be summarized as follows:

- (i) Determine localized occupied and virtual HF MOs.

- (ii) For each atomic site P , determine the optimized orbital spaces $[P]$ and $[\bar{P}]$ as detailed in ref 20.

- (iii) Solve the CCSD amplitude equations in the $[P] \cup [\bar{P}]$ space and evaluate the CCSD atomic fragment energy, E_P^{CCSD} , using eq 3.2.1a.

- (iv) Transform the local HF orbitals of the $[P] \cup [\bar{P}]$ space into a pseudocanonical basis in order to generate triples amplitudes on the fly using eq 2.0.6 (thus avoiding their storage) and evaluate the T_{ij}^{ab} and T_i^a intermediates (eqs 2.0.13) in this basis.

- (v) Transform T_{ij}^{ab} and T_i^a back into the local basis and evaluate $E_P^{(T)}$ in this basis using eqs 3.2.2a and 3.1.6a, recalling that the contractions between cluster amplitudes and intermediates are limited to the restricted sets of local orbitals $ij \in P$ and $a, b \in \bar{P}$.

- (vi) Repeat steps iii–v for the pair fragments PQ using unions of atomic fragment orbital spaces; see eqs 3.2.1b, 3.2.2b, and 3.1.6b; pair fragments with large interatomic distances (small energy contributions) may be neglected.

- (vii) Add up the CCSD and (T) atomic fragment and pair interaction energies to get the total DEC-CCSD(T) energy using eqs 3.1.1 and 3.1.3.

Finally, we stress how the intermediate transformations to and from a pseudocanonical fragment basis are collectively nothing but a computationally efficient way of evaluating the (T) correction in the local HF basis. By solving the equations for the T_{ij}^{ab} and T_i^a intermediates in a diagonal rather than a local basis, we are capable of generating individual triples amplitudes on demand, thereby circumventing the physical storage of the complete six-dimensional tensor of triples amplitudes. The actual summations over the occupied space in eqs 3.2.2 and 3.1.6, however, must be restricted to only those local orbitals that belong to the P and Q spaces, which is why we subsequently need to back-transform T_{ij}^{ab} and T_i^a to the original local basis.

4. NUMERICAL RESULTS

In the present section, we demonstrate how the DEC-CCSD(T) model—via a single input parameter (the FOT)—allows for error control and systematic convergence toward results obtained with the CCSD(T) model in its conventional canonical formulation. Proof of concept investigations are performed on a set of medium-sized molecules for which the conventional CCSD(T) model can be applied for a direct comparison. We will consider a test set consisting of the following molecules/systems:

- (i) two water clusters—one with 12 water molecules (system 1a) and one with 20 (system 1b)
- (ii) two linear, saturated fatty acids— $C_{12}H_{24}O_2$ (system 2a) and $C_{16}H_{32}O_2$ (system 2b)
- (iii) two α -helix structures—one with three glycine residues (system 3a) and one with four (system 3b)
- (iv) two conjugated hydrocarbons— $C_{12}H_{14}$ (system 4a) and $C_{16}H_{18}$ (system 4b)

All calculations are performed using the Dunning correlation-consistent cc-pVDZ and cc-pVTZ basis sets³¹ with the frozen-core approximation invoked.

While systems 1a, 2a, 3a, and 4a are small enough for conventional CCSD(T)/cc-pVTZ calculations to be performed, the calculations on the larger systems 1b, 2b, 3b, and 4b have only been carried out within the smaller cc-pVDZ basis set. All calculations—conventional as well as DEC calculations

Table 1. Conventional Canonical Correlation Energies (a.u.) Calculated within the cc-pVTZ Basis Set for Systems 1a, 2a, 3a, and 4a and the cc-pVDZ Basis Set for Systems 1b, 2b, 3b, and 4b

| model | MP2 | CCSD | [4] | [5] | (T) | CCSD(T) |
|-----------|----------|----------|----------|---------|----------|----------|
| System 1a | -3.22086 | -3.27285 | -0.10832 | 0.00313 | -0.10519 | -3.37803 |
| System 2a | -2.54756 | -2.66321 | -0.11362 | 0.00348 | -0.11014 | -2.77350 |
| System 3a | -2.53798 | -2.57194 | -0.12294 | 0.00618 | -0.11676 | -2.68870 |
| System 4a | -1.91519 | -1.99236 | -0.10457 | 0.00228 | -0.10230 | -2.09466 |
| System 1b | -4.19401 | -4.34508 | -0.08606 | 0.00381 | -0.08225 | -4.42733 |
| System 2b | -2.64643 | -2.85048 | -0.09245 | 0.00302 | -0.08943 | -2.93991 |
| System 3b | -2.64774 | -2.73911 | -0.10103 | 0.00709 | -0.09394 | -2.83305 |
| System 4b | -2.09819 | -2.23745 | -0.09706 | 0.00228 | -0.09478 | -2.33223 |

for the MP2, CCSD, and CCSD(T) models—have been performed using a local version of the `lsdalton` program^{32,33} (the DEC-CCSD(T) model in a pilot implementation), and for all of the presented proof of concept DEC calculations, regardless of the CC model, we have used atomic fragment orbital spaces optimized at the MP2 level of theory.²⁰

In section 4.1, we compare DEC-CC and conventional CC correlation energies for all of the eight test systems, while the decaying behavior of the DEC-CCSD(T) triples pair interaction energies with respect to interatomic distance is investigated in section 4.2.

4.1. DEC-CCSD(T) Correlation Energy. In this section, we compare DEC-CCSD(T) correlation energies calculated using FOT values of 10^{-3} , 10^{-4} , and 10^{-5} a.u. to conventional CCSD(T) results. In the following analyses, the total CCSD(T) correlation energy will be decomposed into the CCSD correlation energy and the (T) correction, which is further partitioned into the fourth- and fifth-order contributions of eq 2.0.4. The results for the CCSD correlation energy and the (T) correction will be reported alongside DEC-MP2 and conventional MP2 correlation energies for comparison. Table 1 gives conventional CC correlation energies for the systems of the test set. In Table 2, we investigate the performance of the DEC-MP2, DEC-CCSD, and DEC-CCSD(T) models by reporting the total error in the DEC-CC correlation energy, i.e., the difference between the DEC-CC correlation energy ($E^{\text{DEC-CC}}$) and the conventional CC correlation energy for the full molecule (E^{CC}),

$$\delta\text{CC} = E^{\text{DEC-CC}} - E^{\text{CC}} \quad (4.1.1)$$

as well as the DEC recovery of the full correlation energy,

$$\Delta\text{CC} = \frac{E^{\text{DEC-CC}}}{E^{\text{CC}}} \quad (4.1.2)$$

From the results in Table 2, we observe a reduction of the total error in the correlation energy (δCC) by roughly an order of magnitude whenever the FOT is reduced by an equal amount. This behavior is observed across all of the models and even holds for the (T) energy correction alone. For all of the test systems, the DEC recovery (ΔCC) for a given FOT is independent of the nature of the system in question (homo- or heterogeneous, saturated or unsaturated, one- or three-dimensional overall structure, dominated by covalent or hydrogen bonds, etc.). At a FOT of 10^{-4} a.u., for example, the DEC-CCSD(T) model succeeds in recovering between 99.83% and 99.96% of the conventional CCSD(T) result. Furthermore, we observe the same pattern for the relative errors in moving from a double- ζ to a triple- ζ basis set.

Upon inspecting the individual entries of Table 2, we notice how the CCSD and (T) total errors in the correlation energy

are of similar magnitude, indicating that neither of the two dominates the total CCSD(T) error. Phrased differently, no unnecessary efforts have been made at determining any of the two contributions to the total CCSD(T) correlation energy at a higher level of precision than the other. This is found to be true for both loose and tight FOT values. The smaller recoveries for the (T) correction, i.e., larger relative errors, in particular at lower FOT values, naturally arise due to the fact that the (T) correction is more than an order of magnitude smaller than the CCSD correlation energy. The total CCSD errors, however, appear at times to be artificially low; compare, e.g., the MP2 and CCSD errors for systems 1a and 2a at a FOT of 10^{-4} a.u. These low CCSD errors are due to cancellations of errors between the individual CCSD atomic fragment and pair fragment errors, which can have different signs. For the MP2 model and the (T) correction, the dominant fragment errors are positive, and such error cancellations are therefore much less prominent. Finally, we focus on the fourth- and fifth-order contributions to the (T) correction. As mentioned in section 3, the fourth-order contribution to the (T) energy correction is typically an order of magnitude larger in size than the fifth-order contribution, and from Table 2, we notice how this relationship holds for the total DEC errors as well. For this reason, both the total and relative DEC errors for the (T) correction will be entirely dominated by those for the fourth-order contribution. For the fifth-order contribution, we generally observe smaller total errors, but larger relative errors, than for the fourth-order contribution, due to the fact that the reference fifth-order contributions in Table 1 themselves are smaller. However, upon tightening the FOT, the relative fifth-order errors begin to close in on the same level of accuracy as observed for all of the other relative quantities in Table 2.

4.2. CCSD(T) Triples Pair Interaction Energies. As previously discussed for the MP2 and CCSD models,^{20,21} the decay of the pair interaction energies in eq 3.2.1b with interatomic distance is an integral part of the DEC method as it allows for a screening of negligible contributions from distant pairs. As mentioned in section 3.2, this screening reduces the scaling of the method from one that depends quadratically on system size to one that depends only linearly. In this section, we provide numerical results that support the theoretical investigations of section 3.2 on the rapid decay of the CCSD(T) triples pair interaction energies in eqs 3.2.2b and 3.1.6b with interatomic pair distance. In Figure 2, we plot the CCSD as well as the fourth- and fifth-order (T) pair interaction energies as a function of interatomic pair distance for system 1b. The results in Figure 2 have been obtained by carrying out a CCSD(T) calculation on the full water cluster and subsequently extracting the pair interaction energies using eqs 3.1.5b and 3.1.6b (and eq 3.1.2b for the CCSD pair energies).

Table 2. DEC-CC (MP2, CCSD, and CCSD(T)) Total Errors (δ CC, a.u.) and Recoveries (Δ CC, %) with Respect to the Conventional Correlation Energies in Table 1 for Different Values of the FOT (a.u.)

| FOT | 10^{-3} | 10^{-4} | 10^{-5} | 10^{-3} | 10^{-4} | 10^{-5} | |
|------------------|------------------------|------------------------|------------------------|------------------------|------------------------|------------------------|--|
| | | System 1a | | | System 1b | | |
| δ MP2 | 1.75×10^{-2} | 3.11×10^{-3} | 2.10×10^{-4} | 4.37×10^{-2} | 5.72×10^{-3} | 5.58×10^{-4} | |
| δ CCSD | 9.98×10^{-3} | -5.47×10^{-4} | -4.58×10^{-4} | 3.57×10^{-2} | 4.84×10^{-3} | 2.87×10^{-4} | |
| δ CCSD(T) | 1.70×10^{-2} | 2.42×10^{-3} | -8.99×10^{-5} | 4.70×10^{-2} | 7.11×10^{-3} | 6.61×10^{-4} | |
| δ (T) | 7.06×10^{-3} | 2.97×10^{-3} | 3.68×10^{-4} | 1.13×10^{-2} | 2.27×10^{-3} | 3.74×10^{-4} | |
| δ [4] | 7.49×10^{-3} | 3.12×10^{-3} | 4.05×10^{-4} | 1.20×10^{-2} | 2.39×10^{-3} | 4.00×10^{-4} | |
| δ [5] | -4.23×10^{-4} | -1.54×10^{-4} | -3.71×10^{-5} | -7.04×10^{-4} | -1.18×10^{-4} | -2.55×10^{-5} | |
| Δ MP2 | 99.46 | 99.90 | 99.99 | 98.96 | 99.86 | 99.99 | |
| Δ CCSD | 99.70 | 100.02 | 100.01 | 99.18 | 99.89 | 99.99 | |
| Δ CCSD(T) | 99.50 | 99.93 | 100.00 | 98.94 | 99.84 | 99.99 | |
| Δ (T) | 93.29 | 97.18 | 99.65 | 86.29 | 97.24 | 99.54 | |
| Δ [4] | 93.09 | 97.12 | 99.63 | 86.08 | 97.23 | 99.54 | |
| Δ [5] | 86.51 | 95.10 | 98.82 | 81.53 | 96.91 | 99.33 | |
| | | System 2a | | | System 2b | | |
| δ MP2 | 4.68×10^{-2} | 4.54×10^{-3} | 5.50×10^{-4} | 4.63×10^{-2} | 6.05×10^{-3} | 6.69×10^{-4} | |
| δ CCSD | 2.77×10^{-2} | 6.93×10^{-4} | -1.37×10^{-5} | 1.76×10^{-2} | 3.40×10^{-3} | 3.79×10^{-4} | |
| δ CCSD(T) | 3.78×10^{-2} | 2.59×10^{-3} | 3.49×10^{-4} | 2.90×10^{-2} | 5.11×10^{-3} | 6.29×10^{-4} | |
| δ (T) | 1.01×10^{-2} | 1.89×10^{-3} | 3.63×10^{-4} | 1.15×10^{-2} | 1.71×10^{-3} | 2.49×10^{-4} | |
| δ [4] | 1.04×10^{-2} | 1.96×10^{-3} | 3.66×10^{-4} | 1.20×10^{-2} | 1.77×10^{-3} | 2.55×10^{-4} | |
| δ [5] | -3.17×10^{-4} | -6.63×10^{-5} | -2.87×10^{-6} | -4.74×10^{-4} | -6.03×10^{-5} | -5.14×10^{-6} | |
| Δ MP2 | 98.16 | 99.82 | 99.98 | 98.25 | 99.77 | 99.97 | |
| Δ CCSD | 98.96 | 99.97 | 100.00 | 99.38 | 99.88 | 99.99 | |
| Δ CCSD(T) | 98.64 | 99.91 | 99.99 | 99.01 | 99.83 | 99.98 | |
| Δ (T) | 90.81 | 98.28 | 99.67 | 87.15 | 98.09 | 99.72 | |
| Δ [4] | 90.81 | 98.27 | 99.68 | 87.06 | 98.09 | 99.72 | |
| Δ [5] | 90.89 | 98.10 | 99.92 | 84.33 | 98.01 | 99.83 | |
| | | System 3a | | | System 3b | | |
| δ MP2 | 2.29×10^{-2} | 3.64×10^{-3} | 2.11×10^{-4} | 3.61×10^{-2} | 5.36×10^{-3} | 3.99×10^{-4} | |
| δ CCSD | 2.42×10^{-4} | -9.54×10^{-4} | -8.81×10^{-4} | 9.33×10^{-3} | 1.16×10^{-3} | -6.03×10^{-4} | |
| δ CCSD(T) | 1.02×10^{-2} | 1.10×10^{-3} | -5.35×10^{-4} | 2.06×10^{-2} | 3.06×10^{-3} | -2.81×10^{-4} | |
| δ (T) | 9.92×10^{-3} | 2.05×10^{-3} | 3.46×10^{-4} | 1.13×10^{-2} | 1.89×10^{-3} | 3.22×10^{-4} | |
| δ [4] | 1.09×10^{-2} | 2.26×10^{-3} | 4.15×10^{-4} | 1.26×10^{-2} | 2.20×10^{-3} | 3.90×10^{-4} | |
| δ [5] | -9.87×10^{-4} | -2.08×10^{-4} | -6.98×10^{-5} | -1.26×10^{-3} | -3.12×10^{-4} | -6.76×10^{-5} | |
| Δ MP2 | 99.10 | 99.86 | 99.99 | 98.64 | 99.80 | 99.98 | |
| Δ CCSD | 99.99 | 100.04 | 100.03 | 99.66 | 99.96 | 100.02 | |
| Δ CCSD(T) | 99.62 | 99.96 | 100.02 | 99.27 | 99.89 | 100.01 | |
| Δ (T) | 91.50 | 98.24 | 99.70 | 87.96 | 97.99 | 99.66 | |
| Δ [4] | 91.13 | 98.16 | 99.66 | 87.56 | 97.82 | 99.61 | |
| Δ [5] | 84.03 | 96.64 | 98.87 | 82.24 | 95.59 | 99.05 | |
| | | System 4a | | | System 4b | | |
| δ MP2 | 4.64×10^{-2} | 4.17×10^{-3} | 5.32×10^{-4} | 5.77×10^{-2} | 6.65×10^{-3} | 9.21×10^{-4} | |
| δ CCSD | 1.43×10^{-2} | -1.80×10^{-3} | 2.02×10^{-5} | 2.56×10^{-2} | 6.17×10^{-4} | -1.32×10^{-4} | |
| δ CCSD(T) | 2.96×10^{-2} | 1.17×10^{-3} | 4.84×10^{-4} | 4.03×10^{-2} | 3.63×10^{-3} | 5.26×10^{-4} | |
| δ (T) | 1.53×10^{-2} | 2.97×10^{-3} | 4.64×10^{-4} | 1.47×10^{-2} | 3.01×10^{-3} | 6.58×10^{-4} | |
| δ [4] | 1.54×10^{-2} | 3.04×10^{-3} | 4.82×10^{-4} | 1.51×10^{-2} | 3.12×10^{-3} | 6.89×10^{-4} | |
| δ [5] | -1.69×10^{-4} | -6.51×10^{-5} | -1.86×10^{-5} | -4.11×10^{-4} | -1.10×10^{-4} | -3.06×10^{-5} | |
| Δ MP2 | 97.58 | 99.78 | 99.97 | 97.25 | 99.68 | 99.96 | |
| Δ CCSD | 99.28 | 100.09 | 100.00 | 98.86 | 99.97 | 100.01 | |
| Δ CCSD(T) | 98.59 | 99.94 | 99.98 | 98.27 | 99.84 | 99.98 | |
| Δ (T) | 85.08 | 97.10 | 99.55 | 84.49 | 96.82 | 99.31 | |
| Δ [4] | 85.24 | 97.10 | 99.54 | 84.43 | 96.79 | 99.29 | |
| Δ [5] | 92.58 | 97.14 | 99.18 | 81.96 | 95.20 | 98.66 | |

In Figure 2, we observe how the CCSD as well as the fourth- and fifth-order (T) contributions all decay rapidly with

interatomic pair distance for system 1b. As expected, the fourth-order contributions are roughly an order of magnitude

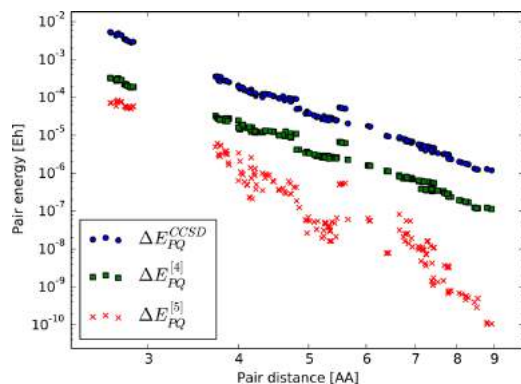


Figure 2. CCSD (ΔE_{PQ}^{CCSD} , blue circles) as well as fourth- and fifth-order (T) ($\Delta E_{PQ}^{[4]}$ / $\Delta E_{PQ}^{[5]}$, green squares and red crosses, respectively) contributions to the CCSD(T) pair interaction energy as a function of the interatomic pair distance for system 1b.

lower than the CCSD energies, while the fifth-order contributions are roughly 2 orders of magnitude lower in energy. In line with the discussion in section 3.2, the dominant fourth-order contributions to the (T) correction decay at the same formal rate as the total CCSD energy and the fourth-order contributions are hence found to remain below the corresponding CCSD energies for all pair interaction energies in Figure 2. By carrying out similar analyses for systems 2b, 3b, and 4b in Figure 3, this is found to be a general trend, although more dense plots are inevitably obtained for these systems due to their characteristics (i.e., heterogeneity). Thus, Figures 2 and 3 collectively show how the pairs which may be screened away in a DEC-CCSD calculation—because their energy contributions are negligible in comparison with the intrinsic DEC error—may also be omitted from a DEC-CCSD(T) calculation without compromising the overall accuracy of the calculation. In fact, since the (T) contribution to the total pair interaction energy is much smaller on average than the corresponding CCSD contribution, one could even consider more elaborate schemes where individual pairs are preordered according to their estimated energy contribution (or interatomic distance) and partitioned into three different levels; at the first level (the smallest energy contributions), the pair interaction energies are neglected altogether, while, at the two following levels, they are evaluated at the CCSD and CCSD(T) levels of theory,

respectively. The practical details of such schemes will be described elsewhere.

5. SUMMARY AND CONCLUSION

We have proposed a reformulation of the (T) triples correction to the CCSD energy in terms of local HF orbitals such that its structural form aligns with our recently developed linear-scaling DEC-CC framework. As a result of the coupling to the DEC scheme, the precision of the total DEC-CCSD(T) correlation energy with respect to that obtained from a conventional calculation may be tuned via a single energy-based input parameter. In the DEC-CCSD(T) model, a number of triples intermediates are initially determined from individual CCSD(T) calculations within local atomic fragment and pair fragment orbital spaces, and the (T) energy correction next evaluated in terms of atomic fragment and pair interaction energies from a formula that structurally resembles that for the DEC-CCSD correlation energy.

The reformulated expression for the (T) triples energy correction, which forms the basis for the DEC-CCSD(T) model, is found to exhibit a formal computational cost that is twice that of the standard expression. However, in contrast to the formulation of the correction used in standard implementations, which is restricted to the nonlocal canonical HF basis, the alternative expression of the present work may be evaluated in any basis of optimized HF orbitals. As a consequence, the (T) correction can be evaluated in a basis of localized orbitals, making it possible to take advantage of the locality of the triples amplitudes and obtain a reduced overall computational scaling.

We have discussed how coupled cluster triples effects—in a basis of localized HF orbitals—may be accurately treated within small subsets of the total orbital space for the full molecular system. In summary, we have found that the same fragment orbital spaces may be used in the calculation of the CCSD correlation energy and the (T) correction, which we have substantiated through the numerical results of a series of proof of concept calculations. From the dominant distance decay of the (T) pair interaction energies, which fall off at the same formal rate as the underlying CCSD counterparts, we have furthermore found that these may be neglected beyond a certain interatomic distance (as for the DEC-CCSD model). This ultimately leads to a linear-scaling algorithm for the evaluation of the (T) correction and, in return, the total CCSD(T) correlation energy. Additionally, since the CCSD(T) atomic fragment and pair interaction energies may be evaluated

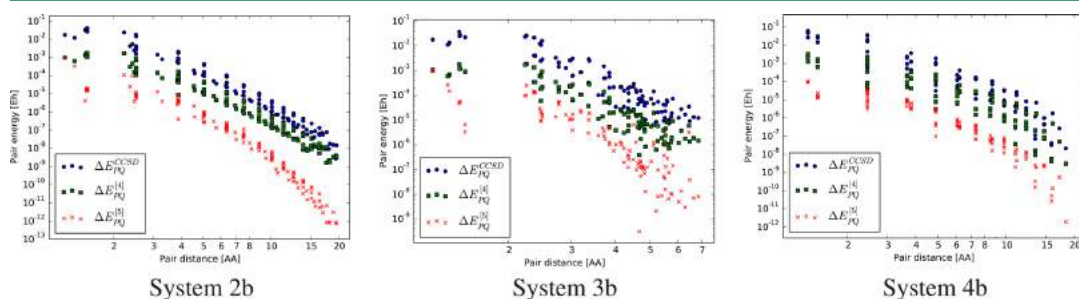


Figure 3. CCSD (ΔE_{PQ}^{CCSD} , blue circles) as well as fourth- and fifth-order (T) ($\Delta E_{PQ}^{[4]}$ / $\Delta E_{PQ}^{[5]}$, green squares and red crosses, respectively) contributions to the CCSD(T) pair interaction energy as a function of the interatomic pair distance for systems 2b, 3b, and 4b.

independently, the algorithm for the DEC-CCSD(T) model becomes massively parallel.

As a final outlook, we note how the general structure of the (T) energy correction within the DEC scheme will also be applicable to the energy corrections of alternative noniterative CC triples models, such as, e.g., the asymmetric CCSD(T) model (the ACCSD(T) model)^{34–36} and the so-called [T] variants of the CCSD(T) model (the CCSD[T] model³⁷) and the ACCSD(T) model (the ACCSD[T] model³⁸). Additionally, the perturbative energy corrections of the recently proposed CCSD(T-*n*) models^{38–40} may also be formulated such that they align with the structure of the (T) energy correction within the DEC scheme. Although all of these alternative models come at a higher computational cost than the CCSD(T) model, applying the DEC strategy will warrant that the models may also be evaluated using formally linear-scaling algorithms.

AUTHOR INFORMATION

Corresponding Authors

*(J.J.E.) E-mail: janusje@chem.au.dk.

*(P.B.) E-mail: pbaudin@chem.au.dk.

Funding

We acknowledge funding from the European Research Council (ERC) under the European Union's Seventh Framework Programme (FP/2007-2013)/ERC Grant Agreement no. 291371 and The Danish Council for Independent Research—Natural Sciences. The research leading to the results of the present work used resources of the Oak Ridge Leadership Computing Facility at Oak Ridge National Laboratory, TN, USA, which is supported by the Office of Science of the Department of Energy under Contract DE-AC05-00OR22725, as well as the PRACE Research Infrastructure resource Curie at the Très Grand Centre de Calcul (TGCC) operated by CEA near Paris, France.

Notes

The authors declare no competing financial interest.

ACKNOWLEDGMENTS

Insightful comments made by the anonymous reviewers are acknowledged.

REFERENCES

- (1) Purvis, G. D.; Bartlett, R. J. *J. Chem. Phys.* **1982**, *76*, 1910.
- (2) Raghavachari, K.; Trucks, G. W.; Pople, M.; Head-Gordon, J. A. *Chem. Phys. Lett.* **1989**, *157*, 479.
- (3) Werner, H.-J.; Knowles, P. J.; Knizia, G.; Manby, F.; Schütz, M. *WIREs Comput. Mol. Sci.* **2012**, *2*, 242.
- (4) (a) Lotrich, V.; Flocke, N.; Ponton, M.; Yau, A. D.; Perera, A.; Deumens, E.; Bartlett, R. J. *J. Chem. Phys.* **2008**, *128*, 15; (b) Deumens, E.; Lotrich, V.; Perera, A.; Ponton, M. J.; Sanders, B. A.; Bartlett, R. J. *WIREs Comput. Mol. Sci.* **2012**, *1*, 895.
- (5) Prochnow, E.; Harding, M. E.; Gauss, J. *J. Chem. Theory Comput.* **2010**, *6*, 2339.
- (6) (a) Janowski, T.; Ford, A. R.; Pulay, P. *J. Chem. Theory Comput.* **2007**, *3*, 1368; (b) Janowski, T.; Pulay, P. *J. Chem. Theory Comput.* **2008**, *4*, 1585.
- (7) (a) Bentz, J. L.; Olson, R. M.; Gordon, M. S.; Schmidt, M. W.; Kendall, R. A. *Comput. Phys. Commun.* **2007**, *176*, 589; (b) Olson, R. M.; Bentz, J. L.; Kendall, R. A.; Schmidt, M. W.; Gordon, M. S. *J. Chem. Theory Comput.* **2007**, *3*, 1312.
- (8) Rendell, A. P.; Lee, T. J.; Komornicki, A.; Wilson, S. *Theor. Chim. Acta* **1992**, *84*, 271.
- (9) Hirata, S. *J. Phys. Chem. A* **2003**, *107*, 9887.

- (10) (a) Kobayashi, R.; Rendell, A. P. *Chem. Phys. Lett.* **1997**, *265*, 1; (b) Valiev, M.; Bylaska, E. J.; Govind, N.; Kowalski, K.; Straatsma, T. P.; van Dam, H. J. J.; Wang, D.; Nieplocha, J.; Aprá, E.; Windus, T. L.; de Jong, W. A. *Comput. Phys. Commun.* **2010**, *181*, 1477.
- (11) (a) Aprá, E.; Harrison, R. J.; de Jong, W. A.; Rendell, A. P.; Tipparaju, V.; Xantheas, S. S. *Proceedings of the Conference on High Performance Computing Networking, Storage, and Analysis*, SC 2009; ACM/IEEE: New York, 2009. (b) Aprá, E.; Harrison, R. J.; Shelton, W. A.; Tipparaju, V.; Vázquez-Mayagoitia, A. *J. Phys.: Conf. Ser.* **2009**, *180*, 012027.
- (12) (a) Schütz, M.; Werner, H.-J. *Chem. Phys. Lett.* **2000**, *318*, 370; (b) Schütz, M. *J. Chem. Phys.* **2000**, *113*, 9986; (c) Werner, H.-J.; Schütz, M. *J. Chem. Phys.* **2011**, *135*, 144116.
- (13) Friedrich, J.; Dolg, M. *J. Chem. Theory Comput.* **2009**, *5*, 287.
- (14) Kobayashi, M.; Nakai, H. *J. Chem. Phys.* **2009**, *131*, 114108.
- (15) Li, W.; Piecuch, P.; Gour, J. R.; Li, S. *J. Chem. Phys.* **2009**, *131*, 114109.
- (16) (a) Rolik, Z.; Kállay, M. *J. Chem. Phys.* **2011**, *135*, No. 104111; (b) Rolik, Z.; Szegedy, L.; Ladjanski, I.; Ladóczki, B.; Kállay, M. *J. Chem. Phys.* **2013**, *139*, 094105.
- (17) Schütz, M.; Yang, J.; Chan, G. K.-L.; Manby, F. R.; Werner, H.-J. *J. Chem. Phys.* **2013**, *138*, 054109.
- (18) Riplinger, C.; Sandhoefer, B.; Hansen, A.; Neese, F. *J. Chem. Phys.* **2013**, *139*, 134101.
- (19) Ziolkowski, M.; Jansík, B.; Kjærgaard, T.; Jørgensen, P. *J. Chem. Phys.* **2010**, *133*, 014107.
- (20) Kristensen, K.; Ziolkowski, M.; Jansík, B.; Kjærgaard, T.; Jørgensen, P. *J. Chem. Theory Comput.* **2011**, *7*, 1677.
- (21) Høyvik, I.-M.; Kristensen, K.; Jansík, B.; Jørgensen, P. *J. Chem. Phys.* **2012**, *136*, 014105.
- (22) Kristensen, K.; Jørgensen, P.; Jansík, B.; Kjærgaard, T.; Reine, S. *J. Chem. Phys.* **2012**, *137*, 114102.
- (23) Kristensen, K.; Kjærgaard, T.; Høyvik, I.-M.; Ettenhuber, P.; Jørgensen, P.; Jansík, B.; Reine, S.; Jakowski, J. *Mol. Phys.* **2013**, *111*, 1196.
- (24) (a) Jansík, B.; Høst, S.; Kristensen, K.; Jørgensen, P. *J. Chem. Phys.* **2011**, *134*, 194104; (b) Høyvik, I.-M.; Jansík, B.; Jørgensen, P. *J. Chem. Phys.* **2012**, *8*, 3137.
- (25) Helgaker, T.; Jørgensen, P.; Olsen, J. *Molecular Electronic Structure Theory*, 1st ed.; John Wiley & Sons: West Sussex, England, 2000.
- (26) Shavitt, I.; Bartlett, R. J. *Many-Body Methods in Chemistry and Physics: Many-Body Perturbation Theory and Coupled-Cluster Theory*. Cambridge University Press: Cambridge, U.K., 2009.
- (27) Piecuch, P.; Kucharski, S. A.; Kowalski, K.; Musiał, M. *Comput. Phys. Commun.* **2002**, *149*, 71.
- (28) Watts, J. D.; Gauss, J.; Bartlett, R. J. *J. Chem. Phys.* **1993**, *98*, 8718.
- (29) Koch, H.; Christiansen, O.; Jørgensen, P.; Sanchez de Merás, A.; Helgaker, T. *J. Chem. Phys.* **1997**, *106*, 1808.
- (30) (a) Noga, J.; Bartlett, R. J. *J. Chem. Phys.* **1987**, *86*, 7041; (b) Scuseria, G. E.; Schaefer, H. F. *Chem. Phys. Lett.* **1988**, *152*, 382.
- (31) Dunning, T. H., Jr. *J. Chem. Phys.* **1989**, *90*, 1007.
- (32) LSDALTON, a linear-scaling molecular electronic structure program, Release Dalton 2015 (2015); see <http://daltonprogram.org>.
- (33) Aidas, K.; Angeli, C.; Bak, K. L.; Bakken, V.; Bast, R.; Boman, L.; Christiansen, O.; Cimiraglia, R.; Coriani, S.; Dahle, P.; Dalgaard, E. K.; Ekström, U.; Enevoldsen, T.; Eriksen, J. J.; Ettenhuber, P.; Fernández, B.; Ferrighi, L.; Fliegl, H.; Frediani, L.; Hald, K.; Halkier, A.; Hättig, C.; Heiberg, H.; Helgaker, T.; Hennum, A. C.; Hetttema, H.; Hjertenæs, E.; Høst, S.; Høyvik, I.-M.; Iozzi, M. F.; Jansík, B.; Jensen, H. J. A.; Jonsson, D.; Jørgensen, P.; Kauczor, J.; Kirpekar, S.; Kjærgaard, T.; Klopper, W.; Knecht, S.; Kobayashi, R.; Koch, H.; Kongsted, J.; Krapp, A.; Kristensen, K.; Ligabue, A.; Lutnæs, O. B.; Melo, J. L.; Mikkelsen, K. V.; Myhre, R. H.; Neiss, C.; Nielsen, C. B.; Norman, P.; Olsen, J.; Olsen, J. M. H.; Osted, A.; Packer, M. J.; Pawłowski, F.; Pedersen, T. B.; Provasi, P. F.; Reine, S.; Rinkevicius, Z.; Ruden, T. A.; Ruud, K.; Rybkin, V. V.; Salek, P.; Samson, C. C. M.; de Merás, A. S.; Saue, T.; Sauer, S. P. A.; Schimmelpfennig, B.;

Sneskov, K.; Steindal, A. H.; Sylvester-Hvid, K. O.; Taylor, P. R.; Teale, A. M.; Tellgren, E. I.; Tew, D. P.; Thorvaldsen, A. J.; Thøgersen, L.; Vahtras, O.; Watson, M. A.; Wilson, D. J. D.; Ziolkowski, M.; Ågren, H. *WIREs Comput. Mol. Sci.* **2014**, *4*, 269.

(34) (a) Kucharski, S. A.; Bartlett, R. J. *J. Chem. Phys.* **1998**, *108*, 5243; (b) Kucharski, S. A.; Bartlett, R. J. *J. Chem. Phys.* **1998**, *108*, 9221.

(35) Crawford, T. D.; Stanton, J. F. *Int. J. Quantum Chem.* **1998**, *70*, 601.

(36) (a) Taube, A. G.; Bartlett, R. J. *J. Chem. Phys.* **2008**, *128*, 044110; (b) Taube, A. G.; Bartlett, R. J. *J. Chem. Phys.* **2008**, *128*, 044111.

(37) Urban, M.; Noga, J.; Cole, S. J.; Bartlett, R. J. *J. Chem. Phys.* **1985**, *83*, 4041.

(38) Eriksen, J. J.; Jørgensen, P.; Gauss, J. *J. Chem. Phys.* **2015**, *142*, 014102.

(39) Eriksen, J. J.; Kristensen, K.; Kjærgaard, T.; Jørgensen, P.; Gauss, J. *J. Chem. Phys.* **2014**, *140*, 064108.

(40) Eriksen, J. J.; Jørgensen, P.; Olsen, J.; Gauss, J. *J. Chem. Phys.* **2014**, *140*, 174114.

B.5 Massively parallel and linear-scaling algorithm for second-order Møller–Plesset perturbation theory applied to the study of supramolecular wires

T. Kjærgaard, [P. Baudin](#), D. Bykov, J. J. Eriksen, P. Ettenhuber, K. Kristensen, J. Larkin, D. Liakh, F. Pawłowski, A. Vose, Y. M. Wang, and P. Jørgensen.

Comput. Phys. Commun. **212**, 152 (2017).

Proportional contribution: writing process.

Minor contribution: code implementation (atomic fragment optimization).



Massively parallel and linear-scaling algorithm for second-order Møller–Plesset perturbation theory applied to the study of supramolecular wires



Thomas Kjærgaard^{a,*}, Pablo Baudin^a, Dmytro Bykov^a, Janus Juul Eriksen^a, Patrick Ettenhuber^a, Kasper Kristensen^a, Jeff Larkin^d, Dmitry Liakh^b, Filip Pawłowski^a, Aaron Vose^c, Yang Min Wang^a, Poul Jørgensen^a

^a *qLEAP Center for Theoretical Chemistry, Department of Chemistry, Aarhus University, Langelandsgade 140, DK-8000 Aarhus C, Denmark*

^b *Scientific Computing Group, National Center for Computational Sciences, Oak Ridge National Laboratory, Oak Ridge, TN, 37831, USA*

^c *Cray Inc., USA*

^d *NVIDIA Inc., USA*

ARTICLE INFO

Article history:

Received 8 August 2016

Received in revised form 31 October 2016

Accepted 4 November 2016

Available online 16 November 2016

Keywords:

Linear Scaling Quantum Chemistry
Massively Parallel Quantum Chemistry
Implementation
Supramolecular wires
Method development

ABSTRACT

We present a scalable cross-platform hybrid MPI/OpenMP/OpenACC implementation of the Divide–Expand–Consolidate (DEC) formalism with portable performance on heterogeneous HPC architectures. The Divide–Expand–Consolidate formalism is designed to reduce the steep computational scaling of conventional many-body methods employed in electronic structure theory to linear scaling, while providing a simple mechanism for controlling the error introduced by this approximation. Our massively parallel implementation of this general scheme has three levels of parallelism, being a hybrid of the loosely coupled task-based parallelization approach and the conventional MPI +X programming model, where X is either OpenMP or OpenACC. We demonstrate strong and weak scalability of this implementation on heterogeneous HPC systems, namely on the GPU-based Cray XK7 Titan supercomputer at the Oak Ridge National Laboratory. Using the “resolution of the identity second-order Møller–Plesset perturbation theory” (RI-MP2) as the physical model for simulating correlated electron motion, the linear-scaling DEC implementation is applied to 1-aza-adamantane-trione (AAT) supramolecular wires containing up to 40 monomers (2440 atoms, 6800 correlated electrons, 24 440 basis functions and 91 280 auxiliary functions). This represents the largest molecular system treated at the MP2 level of theory, demonstrating an efficient removal of the scaling wall pertinent to conventional quantum many-body methods.

© 2016 Elsevier B.V. All rights reserved.

1. Introduction

In recent decades, quantum-mechanical electronic structure calculations have become an integral part of many disciplines of molecular sciences, e.g., chemistry, physics, material science, atomically precise manufacturing, molecular biology, and pharmacology. Electronic structure calculations have thus become an invaluable tool for the interpretation and rationalization of experimental results. Additionally, electronic structure calculations have also been proven important due to their *predictive power*, for example, in the design of new molecular structures and materials with desired properties. The reliability of such predictions increases with an increasing accuracy of the electronic structure calculations. Consequently, the development of high-accuracy electronic structure models has therefore become a task of high priority.

In electronic structure calculations, the electronic Schrödinger equation is solved approximately because of its unfavorable computational scaling. For smaller molecular systems, the coupled-cluster (CC) model is the state-of-the-art wave-function method, and a hierarchy of approximate CC models – MP2 [1] (second-order Møller–Plesset perturbation theory), CCSD [2] (coupled cluster with singles and doubles), and CCSD(T) [3] (coupled cluster with singles, doubles, and perturbative triples) – has been established, where the exact solution to the Schrödinger equation is approached in a *systematic* manner, and the accuracy of the calculations hence systematically controlled. Using the CC hierarchy of approximate models, energy levels, structures, and many molecular properties of small molecules can be computed to an accuracy challenging experimental results [4].

The standard formulation of the CC model hierarchy exhibits a steep polynomial computational scaling with the system size (number of simulated particles), which for many years has hindered the CC hierarchy from being applied to studying large

* Corresponding author.

E-mail address: tkjaergaard@chem.au.dk (T. Kjærgaard).

molecular systems. For this reason, electronic structure calculations of large molecular systems have for many years been carried out using density functional theory (DFT) methods. In DFT, it is proven that a universal density functional exists, however no clue is given to a *systematic* way for determining this functional. DFT is therefore a *semi-empirical* theory where a physical intuition and performance statistics have been guiding the development of new functionals, all with “improved performance”. Although successful and computationally efficient, the DFT approach may always be questioned for its reliability. In the long run it is “a must” for molecular sciences to have the capability of obtaining rigorous high-accuracy solutions to the electronic Schrödinger equation. At the same time, the corresponding high-accuracy many-body methods should still stay computationally affordable. Ideally a linear scaling of the computational cost with the system size is desired. Below we demonstrate how this goal can be achieved using the Divide–Expand–Consolidate formalism [5–7]. An important point is that the linear-scaling regime is activated only after some critical system size, thus requiring large-scale computational resources in order to get there. Consequently, a scalable parallel implementation of the DEC formalism is absolutely necessary in order to efficiently simulate large molecular systems. Taking into account the probable architecture of future large-scale HPC platforms, which is likely to be heterogeneous, the goal of this paper is to describe our massively parallel, accelerator-enabled implementation of the DEC formalism and to demonstrate its scalability on an existing large-scale heterogeneous HPC system, namely the GPU-based Cray XK7 Titan supercomputer located at the Oak Ridge National Laboratory.

The specific physical model we focus on in this paper is the lowest member of the CC hierarchy, the MP2 model. The computational cost of a conventional MP2 formulation scales as kN^5 , where N is the number of one-electron basis functions in the calculation and k is a prefactor. The complexity of a conventional MP2 formulation may be reduced using two different strategies: (i) reducing the prefactor k , and (ii) reducing the N^5 scaling to a lower power, ideally to a linear dependence on N . Both of these strategies require that approximations are introduced in the conventional MP2 model.

The prefactor k may be reduced using the RI approximation [8–12], which is a standard approximation used for reduction of the complexity of the conventional MP2 formulation that has led to the RI-MP2 method [13–22]. In the RI approximation, a resolution of the identity is introduced to replace the evaluation of four-center two-electron repulsion integrals (ERIs) by evaluation of two- and three-center integrals. The error of the RI approximation is fully controllable via the size and design of the auxiliary basis in which the resolution of the identity is expanded. In the limit of a complete (infinite) auxiliary basis, the conventional MP2 energy is thus recovered. As an alternative to the RI approximation, a Cholesky decomposition [23–25] of the ERIs may be performed. Massively parallel implementations have been reported for the RI-MP2 method [14,16]. However, these implementations do not provide a linear scaling of the computational cost and the corresponding calculations will inevitably hit the scaling wall when the size of the system is increased. Thus, a massively parallel implementation of the brute-force RI-MP2 approach only moderately extends its application range.

In practice it turns out that the N^5 scaling of the conventional MP2 algorithm may be reduced by exploiting the local nature of the electron correlation. The corresponding local correlation methods [26,27] are formulated either in the atomic orbital (AO) basis [28–30] or in a basis of *localized* molecular orbitals (MOs) [31–44]. Our recently introduced Divide–Expand–Consolidate (DEC) strategy [5–7] is a local MO-based correlation approach, in which a calculation of a large molecule is partitioned into a large number of smaller atomic fragment and pair fragment calculations.

It should be emphasized that a DEC calculation does not involve any physical fragmentation of the molecule, but merely a partitioning of the local orbital space. In principle, the number of pair fragments scales quadratically with the system size; however, due to the R^{-6} decay of the dispersion energies with the inter-fragment distance, R , distant pairs may be neglected without compromising the accuracy of the calculation [5,6], ultimately leading to a linear-scaling algorithm. As the calculations of individual fragments are independent of one another, DEC is also a massively parallel algorithm [45] by construction. The fragments and their sizes are *dynamically* determined in a black-box manner, such that the error due to partitioning of a molecule into fragments is fully controlled via a single parameter, the *fragment optimization threshold* (FOT). The precision of the DEC calculation may therefore be systematically increased by decreasing the FOT. In the limiting case of the FOT approaching zero, the conventional MP2 result is recovered. Combining our DEC strategy with the RI-MP2 model defines the DEC-RI-MP2 algorithm [46].

Other local MO-based MP2 correlation methods include the local coupled-cluster method of Werner and co-workers [32,47,48] and the domain-based local pair-natural-orbital coupled-cluster (DLPNO-CC) method of Neese and co-workers [36,44]. In these approaches a full molecular CC equation is solved where the excitation space for each pair of occupied orbitals is assigned a restricted local virtual orbital space, which is defined in terms of *fixed* (i.e., *not* dynamical) thresholds. The default values for these fixed thresholds have been determined empirically, and the precision of the correlation energy compared to a conventional calculation is therefore in general unknown. In addition to DEC, there exist other local correlation methods relying on a partitioning of the orbital space rather than on a physical fragmentation of the molecule, e.g., the cluster-in-molecule method [49,43] and the incremental scheme [50,35]. However, only DEC uses a *dynamical* adaptation of orbital fragment spaces to a predefined energy error. On the contrary, the Divide-and-Conquer MP2 [51,52] and the Fragment Molecular Orbital MP2 (FMO-MP2) [53,54] are two examples of a myriad of molecular fragmentation approaches [55–60]. In these methods, a physical fragmentation of a molecular system into fragments is performed based on a “chemical intuition”, making it impossible to estimate the error introduced compared to a conventional MP2 calculation [22].

The other group of local correlation approaches, for example the AO-based MP2 formulations, usually employ a Laplace transformation [61,62], where the orbital energy denominator is eliminated from the conventional MO-based MP2 energy expression to obtain a formulation in terms of AO integrals [28,63–65]. Since AOs are local by construction, efficient integral screening may be performed, where an R^{-4} decay may be exploited when ERIs are evaluated. However, as the integral decay (R^{-4}) is slower than the dispersion energy decay (R^{-6}), the locality of electronic dispersion effects is not fully exploited in the Laplace AO-based MP2 methods.

In this article we report a massively parallel linear-scaling DEC-RI-MP2 implementation enhanced with the accelerator support, where our DEC strategy is used to reduce the steep N^5 scaling of the MP2 method to linear scaling (N) and the RI approximation is used for reducing the prefactor k for individual fragment calculations. The DEC-RI-MP2 calculations are carried out for the stacked 1-aza-adamantane-trione supramolecular wires containing up to 40 monomers. The largest calculation comprises 2440 atoms, 6800 correlated electrons, 24 440 basis functions and 91 280 auxiliary functions. It ran on 14 952 out of 18 688 nodes of the Titan supercomputer, a GPU-based Cray XK7 HPC platform which is currently positioned # 3 in the TOP500 list. The presented calculation is 2.5 times larger than the largest conventional RI-MP2 calculation [16]. We also demonstrate the weak and strong parallel scalability of our DEC algorithm.

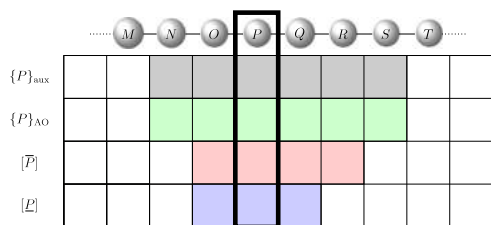


Fig. 1. Illustration of an atomic fragment P . The string of spheres is a schematic representation of a molecule with each sphere representing an atom. The local orbital spaces of occupied MOs $[P]$ (blue), unoccupied MOs $[\bar{P}]$ (red), standard AOs $\{P\}_{AO}$ (green), and auxiliary AOs $\{P\}_{aux}$ (gray) are indicated. The blue and red square encapsulated by the bold black box represents the spaces $[P]$ and $[\bar{P}]$. (For interpretation of the references to color in this figure legend, the reader is referred to the web version of this article.)

2. Theory

In the DEC-RI-MP2 scheme, localized occupied and unoccupied Hartree–Fock (HF) orbitals [66–82] are used to efficiently describe the short-ranged electron correlation effects, partitioning the calculation into many small and independent fragment calculations and ultimately obtaining a linear-scaling algorithm (for a recent review on the characterization and generation of local occupied and virtual HF orbitals see Ref. [83]).

In this section, we summarize the DEC-RI-MP2 algorithm and refer the reader to Ref. [46] for additional details. The first step in the DEC scheme is to assign each localized MO to an atomic site (P, Q, \dots). Each site P thus gets assigned a set of occupied, $[P]$, and unoccupied, $[\bar{P}]$, localized orbitals.

The RI-MP2 energy is the sum of the HF contribution, E_{HF} , which represents the mean-field electronic interactions, and the correlation contribution, E_{corr} , which represents the dynamical correlation among the electrons. In conventional implementations, the determination of the correlation energy is the time-dominating part, and we therefore focus on E_{corr} here and refer the reader to Refs. [84–94] for linear-scaling HF algorithms. In a DEC-RI-MP2 calculation, the correlation energy is partitioned into independent fragment calculations according to

$$E_{corr} = \sum_P E_P + \sum_{P>Q} \Delta E_{PQ}, \quad (1)$$

where the atomic fragment energy E_P and the pair fragment energy ΔE_{PQ} are given by,

$$E_P = \sum_{ij \in [P]} \sum_{ab \in [\bar{P}]} t_{aijb} (2g_{aijb} - g_{ajbi}), \quad (2)$$

$$\begin{aligned} \Delta E_{PQ} = & \sum_{\substack{i \in [P] \\ j \in [Q]}} \sum_{ab \in [\bar{P}] \cup [\bar{Q}]} t_{aijb} (2g_{aijb} - g_{ajbi}) \\ & + \sum_{\substack{i \in [Q] \\ j \in [P]}} \sum_{ab \in [\bar{P}] \cup [\bar{Q}]} t_{aijb} (2g_{aijb} - g_{ajbi}). \end{aligned} \quad (3)$$

Here, g_{aijb} and t_{aijb} are ERIs and RI-MP2 wave function amplitudes, respectively, expressed in the local orbital basis. The amplitudes and ERIs for the atomic fragment P are determined using a set of occupied MOs $[P]$, unoccupied MOs $[\bar{P}]$, standard AOs $\{P\}_{AO}$, and auxiliary AOs $\{P\}_{aux}$ spatially close to P , see Fig. 1 for a schematic illustration and Table 1 for an overview of the notation. The MOs are expanded in the $\{P\}_{AO}$ space, and the $\{P\}_{aux}$ space is used for the RI approximation of the ERIs.

Table 1

Notation for indices and dimensions of different local orbital spaces for an atomic fragment P .

| Explanation | Notation | Dim. |
|--------------------------------|--------------------------|-----------|
| Occupied MO, assigned to P | $i, j \in [P]$ | \bar{O} |
| Unoccupied MO, assigned to P | $a, b \in [\bar{P}]$ | \bar{V} |
| Occupied MO local space | $i, j \in [P]$ | O |
| Unoccupied MO local space | $a, b \in [\bar{P}]$ | V |
| Occupied pseudo-canonical | $I, J \in [\bar{P}]$ | O |
| Unoccupied pseudo-canonical | $A, B \in [\bar{P}]$ | V |
| Standard AO local space | $\mu \in \{P\}$ | N |
| Auxiliary AO local space | $\alpha \in \{P\}_{aux}$ | N_{aux} |

If one removes the restrictions in the summations over unoccupied orbitals in Eqs. (2) and (3), the standard RI-MP2 correlation energy is obtained, preventing any reduction in computational cost. However, using the locality of the orbitals (and hence of the ERIs and amplitudes), the orbital spaces $[\bar{P}]$ can be restricted to a small subset of the complete orbital space without affecting significantly the precision of the calculation while resulting in large computational savings. In practice, these local spaces are determined in a black box manner using a single parameter, the FOT [6]. The resulting fragment energy E_P is thus controlled by the FOT and ensured to reach a user-defined accuracy. The value of the FOT therefore determines the overall accuracy and the computational cost of a DEC-RI-MP2 calculation. While the number of atomic fragments scales linearly with system size, the number of pair fragments scales quadratically with the system size; however, due to the rapid decay of dispersion energies (inverse pair distance to the sixth power [95]), distant pairs may be neglected without compromising the precision of the calculation [6], ultimately leading to a linear-scaling algorithm.

In summary, a DEC-RI-MP2 energy calculation proceeds as follows:

1. First, the HF information is read (Fock matrix and localized MOs).
2. The orbital spaces $[\bar{P}]$ are optimized to provide atomic fragment energies, E_P , to the FOT precision.
3. A reduced set of pair fragments is selected based on estimations of their energy contribution (pair estimate calculations).
4. The pair fragment energies are computed for the selected pairs using Eq. (3) (this is the most expensive step).
5. Finally, the total correlation energy is calculated using Eq. (1).

There are three parallelization levels in the DEC scheme [45]: (1) coarse-grained parallelization, where independent fragment calculations (tasks) are distributed among groups of MPI processes, (2) medium-grained parallelization, where each fragment calculation is parallelized across a number of nodes constituting an MPI process group, and (3) fine-grained parallelization (OpenMP/OpenACC parallelization across the CPU/GPU cores on each node).

At the coarse-grained parallelization level, the independent tasks (individual and pair-fragment calculations) are sorted according to their size. The largest tasks are scheduled first, being distributed among MPI process groups. As the tasks become smaller in size, the original groups of MPI processes may split into smaller groups such that the size of each MPI process group is appropriate for the size of the tasks it is executing. The task based workflow together with the dynamic execution unit granularity adjustment ensures load balancing at the coarse-grained parallelization level and efficiency at the medium-grained parallelization level.

Regarding the medium-grained parallelism, each (atomic or pair) fragment can be seen as a standard RI-MP2 calculation in

a reduced orbital space and can be efficiently parallelized over a number of nodes. The evaluation of Eqs. (2) and (3) requires the determination of the local amplitudes t_{aij} . In order to obtain a non-iterative algorithm these amplitudes are first determined in a so-called pseudo-canonical basis t_{AIBJ} , which is generated by diagonalizing the local Fock matrices (F_{ij} with $ij \in [P]$ and F_{ab} with $ab \in [\bar{P}]$). Denoting the occupied/unoccupied diagonal elements of the Fock matrix in the pseudo-canonical basis as $(\epsilon_i, \epsilon_j)/(\epsilon_A, \epsilon_B)$, t_{AIBJ} is evaluated in the following step, which is the most expensive and scales as $N_{\text{aux}}V^2O^2$ (see Table 1),

$$t_{AIBJ} = \frac{g_{AIBJ}}{\epsilon_i + \epsilon_j - \epsilon_A - \epsilon_B} = \frac{\sum_{\alpha} C_{Ai}^{\alpha} C_{Bj}^{\alpha}}{\epsilon_i + \epsilon_j - \epsilon_A - \epsilon_B}, \quad (4)$$

where the RI approximation has been used to express the ERIs in terms of fitting coefficients C_{Ai}^{α} . The pseudo-canonical amplitudes and ERIs are subsequently transformed back to the local basis ($t_{AIBJ} \rightarrow t_{aij}$) for the evaluation of the fragment energy using Eqs. (2) or (3). Most of the computations required to obtain the fragment energies (e.g., Eq. (4)) can be performed by threaded/accelerated optimized libraries (BLAS) or compiler directive parallelized kernels (OpenMP on the CPU or OpenACC on the GPU). This corresponds to the fine-grained level of parallelization. The construction of the ERIs and the amplitudes, as well as the subsequent transformation from the pseudo-canonical to the local basis are thus performed on the GPU, while the fitting coefficients are currently constructed using a CPU only code.

In Fig. 2, the coarse-grained parallelism of DEC is exemplified for a calculation containing 12 fragments and using 9 nodes. Node 0 is the global master node (blue), and the remaining nodes are divided into slots each containing 4 nodes, where one of the nodes is chosen as the local master (red) and the remaining nodes are referred to as local slaves (gray). A local master and its local slaves are collectively referred to as a slot. The fragment calculations are ordered according to their size, and the global master distributes the fragment jobs to the local masters. Each local master then carries out its job in collaboration with its local slaves. When a slot has finished a job, the local master sends the fragment energy back to the global master, which then instructs the local master to carry out a new fragment calculation. The size of the fragments differ significantly for the various fragments and ultimately determines the efficiency of the medium-grained parallelization. We have therefore devised a scheme where the slots divide dynamically if the ratio between the most expensive computational step ($N_{\text{aux}}V^2O^2$) and the most expensive communication step ($N_{\text{aux}}VO$) is “too small”. Thus, roughly speaking, the larger OV is, the more nodes can efficiently be used at the medium-grained level. In practice we use the following condition to determine whether a slot containing n_{nodes} should divide or not,

$$\text{Divide slot if: } n_{\text{nodes}} > OV/X. \quad (5)$$

Empirical investigations have established that $X = 8000$ is a reasonable value. This ensures that a large fragment (e.g., $V = 2446$, $O = 181$) will be done using at least 27 nodes, while a small fragment (e.g., $V = 273$, $O = 18$) is done using a single node.

Although the ordering of fragments according to size and the splitting of slots according to Eq. (5) is an attempt to minimize the idle time, some loss is to be expected, and we distinguish between local (dotted lines) and global (wiggly lines) loss of efficiency in Fig. 2. The local loss is associated with the medium-grained parallelization and is present due to non-ideal load balancing among the local working nodes (local master and local slaves), while the global loss occurs when all jobs have been distributed by the global master and some of the nodes wait for the remaining jobs to finish.

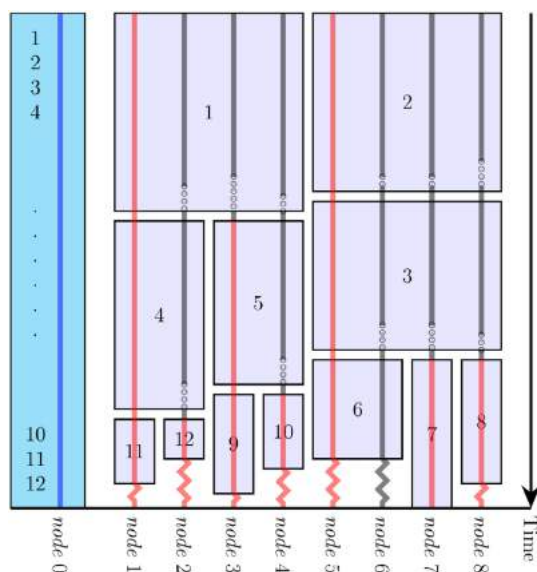


Fig. 2. Coarse-grained parallelization of the DEC scheme exemplified by a calculation with 12 fragments using 9 nodes. The fragment jobs are ordered according to size in descending order on the global master (blue). The local masters (red) receive job instructions, carry out job in collaboration with the local slaves (gray) in the slot, and send the fragment energy to the global master. The slots divide dynamically to ensure good medium-grained parallelization, see text. (For interpretation of the references to color in this figure legend, the reader is referred to the web version of this article.)

3. Molecular systems used to measure performance

As an example application for the DEC-RI-MP2 method, we consider a new class of molecules, the 1-aza-adamantanetriones (AATs) [96,97]. AATs spontaneously self-assemble into ordered nano-structures, and their electronic and physical properties can be experimentally tuned. Therefore, AATs are promising model materials, and in their supramolecular wire form they have potential applications in the fields of molecular electronics and optoelectronics. The intrinsic forces involved in the nanoscale self-assembly of these supramolecular structures are dominated by dispersion forces and π - π stacking interactions, that can only be accurately described using correlated methods. We will apply the DEC-RI-MP2 model to calculate interaction energies of AATs using the correlation-consistent cc-pVDZ basis set and the auxiliary cc-pVDZ-RI basis set [98]. We will present scientific results and error analysis of the DEC-RI-MP2 calculations for up to 10 monomers here and in the performance section we will demonstrate the computational efficiency of DEC-RI-MP2 by carrying out calculations for up to 40 stacked AATs, which is far beyond what can be done using a conventional implementation.

The AAT_n structure for a general n -mer was obtained by duplicating and translating the optimized AAT_2 structure ($n/2 - 1$) times, such that the distance between the two central nitrogen atoms in two adjacent AAT units was the same as in the optimized dimer (5.12 Å), see Fig. 3. The interaction energy for AAT_n (ΔE_{AAT_n}) was then calculated as the difference in energy between the AAT_n system and the two noninteracting AAT_{n-1} and AAT_1 systems,

$$\Delta E_{AAT_n} = E_{AAT_n} - E_{AAT_{n-1}} - E_{AAT_1}. \quad (6)$$

The $E_{AAT_{n-1}}$ and E_{AAT_1} monomer calculations were corrected for basis set superposition errors using the counterpoise correction

Table 2

Interaction energies ΔE_{AAT_n} for $n = 2, 4, 6, 8, 10$ calculated using the HF, conventional RI-MP2 (conv), and DEC-RI-MP2 models (using the cc-pVDZ basis). We also give the absolute errors of the DEC interaction energy and the DEC total energy compared to the conventional reference numbers with the recoveries of the correlation contribution ($E_{DEC}^{corr}/E_{conv}^{corr}$) given in parenthesis. All results are given in eV.

| n | HF | Conv | DEC | Interaction error | Total error |
|-----|-------|--------|--------|-------------------|----------------|
| 2 | 0.729 | -0.718 | -0.710 | 0.008 (99.43%) | 0.090 (99.97%) |
| 4 | 0.721 | -0.746 | -0.710 | 0.036 (97.52%) | 0.246 (99.95%) |
| 6 | 0.716 | -0.748 | -0.724 | 0.023 (98.41%) | 0.382 (99.95%) |
| 8 | 0.716 | -0.748 | -0.727 | 0.023 (98.43%) | 0.528 (99.95%) |
| 10 | 0.716 | | -0.724 | | |

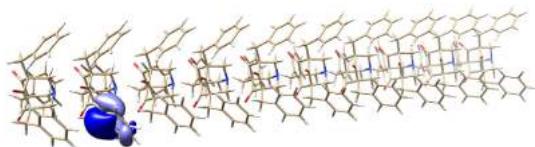


Fig. 3. Illustration of AAT₁₀ with one of the localized molecular orbitals shown in blue. (For interpretation of the references to color in this figure legend, the reader is referred to the web version of this article.)

[99]. The resulting interacting energies are given in Table 2 for HF, conventional RI-MP2, and DEC-RI-MP2 where we have used a FOT of 10^{-5} a.u. = 0.272 meV for the DEC calculations. The DEC errors compared to the conventional RI-MP2 calculations are also presented.

The HF model does not describe dispersion forces and it therefore wrongly predicts the interaction energies to be positive, i.e., the AAT units repel each other at the HF level of theory. On the contrary, the conventional RI-MP2 interaction energies are negative (attractive) and thus describe the correct physics due to the RI-MP2 correlation contribution, which represents dispersion effects. An inspection of the DEC errors in Table 2 shows that the DEC error of the total energy E_{AAT_n} increases linearly with system size, as expected, while the recovery of the conventional correlation energy is roughly constant at 99.95%. More importantly, the interaction energy error does not change significantly with system size. In fact, for the largest systems, the interaction energy error is more than an order of magnitude smaller than the total error—e.g., for AAT₈, the total error is 0.528 eV, while the error in the interaction energy is only 0.023 eV. In short, the DEC-RI-MP2 scheme is capable of accurately reproducing the conventional results.

4. System and environment where performance was measured

The experimental platform is the Titan supercomputer, a Cray XK7 system deployed by the US Department of Energy at the Oak Ridge National Laboratory, which currently occupies the third position on the Top500 list. The machine comprises 18 688 nodes, each consisting of a 16-core AMD Opteron 6274 processor with 32 GB of main memory and an NVIDIA Tesla K20x GPU accelerator (Kepler architecture) with 6 GB of GDDR5 memory. Titan's nodes are connected according to a 3D torus topology with the Cray Gemini network interfaces. The application-level communication layer is provided by the Cray MPI library implementing most of the MPI 3.0 features, a derivative of MPICH-2 from Argonne National Laboratory. The OpenMP v.3.0 and OpenACC v.2.0 runtimes implemented in Cray Compiler Environment v.8.4.2 are used for CPU multi-threading and GPU acceleration, respectively. The Cray OpenACC implementation available on Titan is specifically optimized for Nvidia Kepler GPU architecture. Finally, the Cray Lib-Sci v.13.2.0 scientific library provides optimized versions of linear algebra operations, namely the dgemm and dsyev routines (double precision arithmetic was used throughout the calculations).

We have measured the number of floating point operations (FLOPs¹) performed on the CPU using the PAPI library [100]. The FLOPs performed on the GPU were not directly measured, instead they were estimated using a CPU compiled version of the GPU kernels and analyzed using PAPI. During the performance calculations an estimated GPU FLOP count was added to the accumulated GPU FLOPs each time a GPU kernel was invoked. The CPU-only and hybrid CPU/GPU versions will perform the same number of FLOPs. To validate the estimated GPU FLOP count we used AAT₄ as a test system and found that the CPU PAPI-counted and GPU estimated FLOPs of the hybrid CPU/GPU code corresponded to 99.5% of the FLOPs measured by PAPI for the CPU-only code.

Efficient and lightweight checkpointing was added for the completed fragments, in the sense that the global master simply writes a file with the fragment energy and identity of the completed fragments. This limits I/O but means that each interrupted fragment calculation has to be restarted from scratch. During the performance calculations, Titan suffered from a higher than normal rate of node failures, and checkpointing was crucial for successful completion of the calculations. As the massively parallel architectures have an ever increasing number of nodes and thus risk of node failures, MPI fault tolerance is increasingly important. DEC is set up to exploit future MPI fault tolerance mechanisms, once this is part of the MPI standard, by reassigning the affected fragment to the available nodes. The checkpointing also allows for the fragment optimization and pair estimate calculations to be run using one set of nodes, while a larger set of nodes can be used for the computationally more demanding pair fragment calculations.

All results reported in Section 5 used the same value of the main DEC threshold (FOT = 10^{-5} a.u.) as in Section 3, and the calculated correlation energies are therefore highly accurate (expected 99.95% recovery of the conventional RI-MP2 correlation energy). The weak scaling analysis in Section 5 was performed for the full application including I/O (step 1–5 in Section 2) while the strong scaling analysis was performed for the time-dominating part only, the pair fragment calculations (step 4 in Section 2). We further emphasize that the construction of the localized HF orbitals is not part of the DEC application.

The DEC code is part of the LSDALTON program [101] and the source code is distributed free of charge as a part of the DALTON2016 suite [102]. The LSDALTON program have been used to construct the localized HF orbitals.

5. Performance results

In Table 3 and Fig. 4 we show strong scalability results for AAT₁₀ starting with 3738 nodes. Efficiencies from 74.8% to 94.3% are observed. The efficiency is quite remarkable considering the complexity of the problem. The AAT₁₀ calculation consists of 16 023 pair fragments and we used an initial slot size of 32 nodes resulting in (14 952/32) 467 slots (see Fig. 2 for an illustrative example of 12 fragments, 9 nodes, and 2 initial slots with a slot size of 4 nodes).

¹ FLOPs will denote FLOP in plural, while we will use FLOPs/s to denote FLOPs per second. Also, we use 1 EFLOPs = 10^{18} FLOPs.

Table 3

Strong scalability results on Titan for AAT_{10} using 3738–18 400 nodes. TTS denotes the Time-To-Solution and the last column denotes how many times a calculation was restarted due to hardware failures.

| # nodes | TTS (s) | Efficiency | Restarted |
|---------|---------|------------|-----------|
| 3738 | 39400 | | 1 |
| 7476 | 20900 | 94.3 | 0 |
| 11214 | 15400 | 85.3 | 0 |
| 14952 | 12100 | 81.5 | 1 |
| 18400 | 10700 | 74.8 | 2 |

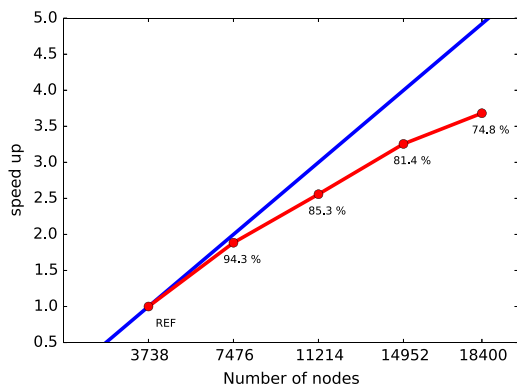


Fig. 4. Strong scaling plot for coarse-grained parallelization: AAT_{10} using 3738 to 18 400 nodes (same as Table 3) with strong scaling efficiency numbers along the curve. The blue line displays ideal strong scaling behavior. (For interpretation of the references to color in this figure legend, the reader is referred to the web version of this article.)

Due to the inhomogeneous fragment sizes (ranging from 1106 to 9366 auxiliary functions) and the fifth-order scaling with fragment size, the time for the individual fragment calculations ranges from 6 s using a single node to 1 h and 37 min using 32 nodes.

The efficiency is particularly impressive considering that the 14 952 node calculation had to be restarted once and the 18 400 node calculation twice due to hardware failures and each restart results in an increased global loss (see Fig. 2). Due to the short TTS for the large node jobs, hardware crashes become increasingly detrimental for the large node jobs.

Load balancing and job distribution are crucial for efficient strong scaling. For instance, in the case of the 18 400 node job, the 1 h and 37 min fragment calculation constitutes 54% of the total wall time. If a larger number of nodes is used the strong scaling performance will eventually be limited by the time for this fragment. The time for the largest fragments can in this case be reduced by using more than 32 nodes in each slot (see Fig. 5). The larger slot sizes improve the strong scaling by reducing the global loss, but the price is a decrease in the medium-grained parallelization efficiency (see Fig. 5), and hence an increase in the local loss (see Fig. 2). A larger slot size will also improve the checkpointing as only information for the completed fragment calculations are saved (see Section 4).

Fig. 6 shows the time-to-solution (TTS) for the different systems $\{AAT_{10}, AAT_{20}, AAT_{30}, AAT_{40}\}$ of increasing size using 14 952 Titan nodes. For these systems, the size of the individual fragments is constant with respect to the total system size due to the local nature of electron correlation, and the computational cost is therefore mainly determined by the number of fragments. The proper treatment of dispersion effects (Section 2) means that the linear-scaling regime is approached asymptotically. In particular, the number of pair fragments considered for AAT_{20} (33 992) is slightly larger than twice the number of pair fragments in AAT_{10} (16 023), while the number of pair fragments considered for AAT_{40} (69 390)

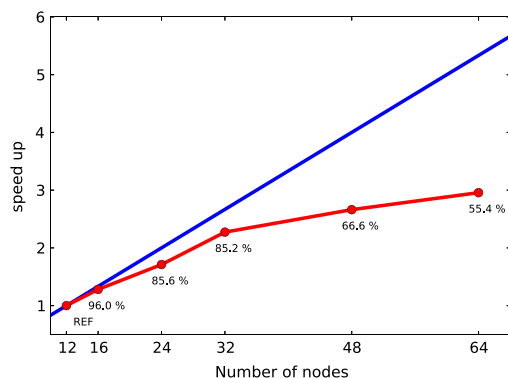


Fig. 5. Strong scaling plot for the medium-grained parallelization: The largest pair fragment in AAT_{10} using 12 to 64 Titan nodes. The numbers are efficiencies.

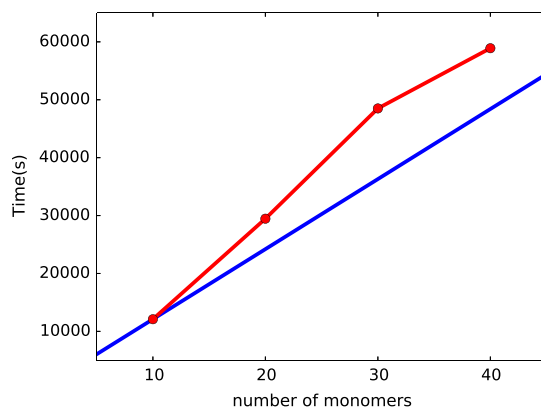


Fig. 6. Computational scaling with system size for AATs of increasing lengths using 14 952 Titan nodes. The blue line displays the ideal linear scaling behavior. (For interpretation of the references to color in this figure legend, the reader is referred to the web version of this article.)

is $\frac{4}{3}$ times larger than for AAT_{30} (51 949). The linear-scaling regime is thus reached for AAT_{30} and AAT_{40} . The deviations from ideal linear-scaling behavior in Fig. 6 can also be explained from the fact that the four calculations were restarted 1, 3, 6, and 6 times, respectively.

In Table 4, we show weak scalability results for the different systems $\{AAT_{10}, AAT_{20}, AAT_{30}, AAT_{40}\}$ of increasing size, defining the weak scalability efficiency as $E_{ws} = F_j P_i T_i / (F_i P_j T_j)$ where F_i , P_i , and T_i denote the FLOPs, number of processors and TTS for system i , respectively. We achieve a 83.1% weak scaling efficiency for AAT_{40} relative to AAT_{10} despite having to restart the AAT_{40} calculation 6 times.

Each fragment calculation requires access to the Fock matrix and the MO coefficients. For AAT_{40} this corresponds to 9.6 GB of data. The current scheme stores the data locally on the node which means that each MPI rank has less memory available for the AAT_{40} calculation than for AAT_{10} where this data only takes up 0.6 GB. This reduction in available memory results in more tiling and less efficient code which, together with 6 hardware failures, explains the non-ideal weak scalability. A better strategy is to store the required data in parallel distributed memory and retrieve it using one-sided MPI communication. This scheme will be operational shortly.

Table 4

Weak scalability results on Titan for AATs of different size using 3738–14952 nodes. The weak scaling efficiency E_{ws} is given relative to AAT_{10} and the last column denotes the number of times a calculation was restarted. The EFLOPs column denotes the accumulated number of EFLOPs performed during the entire simulation.

| System | # nodes | EFLOPs | TTS (s) | E_{ws} (%) | restarted |
|------------|---------|--------|---------|--------------|-----------|
| AAT_{10} | 3738 | 4.08 | 47570 | | 1 |
| AAT_{20} | 7476 | 9.41 | 60430 | 90.8 | 1 |
| AAT_{30} | 11214 | 15.0 | 71180 | 81.9 | 10 |
| AAT_{40} | 14952 | 19.4 | 68060 | 83.1 | 6 |

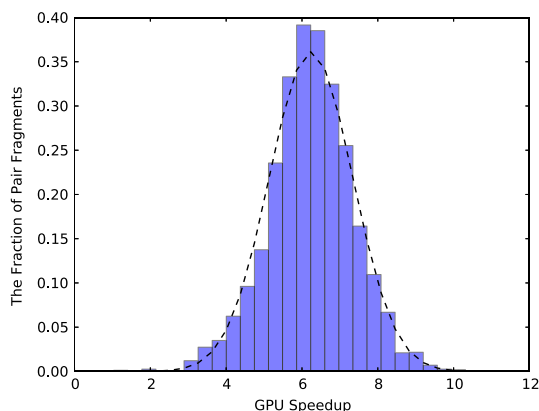


Fig. 7. A histogram of GPU speedup for the individual pair fragments in AAT_4 . The dotted line is the normal distribution using a standard deviation of 1.1 and a mean of 6.2.

The weak scaling attribute arises from the linear scaling features of the DEC algorithm and ensures that we may treat molecular systems significantly larger than the conventional implementation. With its 24 440 basis functions and 91 280 auxiliary functions the AAT_{40} RI-MP2 energy calculation is 2.5 times larger than the calculation of Katouda and Nakajima [16] using the K computer. The AAT_{40} calculation was finished within 19 h on Titan, using 14952 out of 18 688 Titan nodes. In principle, DEC could easily be applied to larger molecular systems using larger basis sets, but the prerequisite HF calculation and orbital localization are currently limiting the size of the systems that may be treated. We are working on addressing these limitations.

In a conventional calculation the fitting coefficients C_{ai}^c are written to disk and read in as needed. However, for AAT_{40} this would require 49 TB of data (3400 valence orbitals, 19 680 unoccupied orbitals and 91 280 auxiliary functions) and put substantial strain on the file system. Alternatively, the fitting coefficients may be stored in parallel distributed memory, which again reduces the size of the operating memory. The DEC scheme eliminates this I/O and memory bottleneck. In a DEC calculation each fragment constructs the part of the fitting coefficients it needs, and stores in the reported calculation a maximum of 28 GB distributed among the nodes in the slot. It has been a design decision to limit the use of I/O despite this being a prominently used technique in quantum chemistry. The I/O is replaced by recalculation and parallel distributed memory storage, which makes the code portable and removes possible bottleneck issues in terms of disk requirements.

The speedup we have obtained through our use of GPUs may be estimated by performing an additional calculation without using the GPUs. For this purpose we chose the AAT_4 system. Fig. 7 displays a histogram of the GPU speedups for the individual pair fragments in the AAT_4 calculation. The maximum GPU speedup achieved is

10.3 while the average is 6.5, and the minimum speedup is 1.03. The general picture is that the GPU speedup is larger for larger fragments. This effectively reduces the inhomogeneity of the timings for the fragment calculations. The smallest speedup of 1.03 is achieved for the smallest fragment which takes 6.9 s using a single node, while the time for the largest fragment is reduced from 14 h and 51 min to 2 h and 0 min using 16 nodes. Since the distribution of fragment size for the larger AATs is similar to the one for AAT_4 , the GPU performance for the larger AATs is similar to the ones obtained in the AAT_4 calculation.

We conclude that, unlike the conventional formulation, the DEC scheme is asymptotically linear scaling. Furthermore, the DEC scheme eliminates the I/O and memory bottleneck of the conventional approach. The linear scaling algorithm and the three levels of parallelization in our DEC implementation ensure strong and weak scalability. The hybrid cross-platform parallel implementation is well suited for achieving performance portability on current and future supercomputers.

6. Conclusions and perspectives

In the presented work, we have applied our recently developed DEC strategy using the lowest member of the CC hierarchy, the MP2 model, and in combination with the RI approximation demonstrated that DEC-RI-MP2 calculations may be carried out in a massively parallel manner. The combination of being *both* linearly scaling *and* massively parallel allows our DEC-RI-MP2 method to be applied to very large molecular systems. Our DEC-RI-MP2 implementation exhibits weak and strong scalability that ensures performance portability of the DEC-RI-MP2 code to the next generations of supercomputers. The largest calculations were carried out on a system comprising 2440 atoms, 6800 correlated electrons, 24 440 basis functions, and 91 280 auxiliary functions and using 14952 out of 18 688 Titan nodes. The presented calculation is 2.5 times larger than the largest conventional RI-MP2 calculation [16]. As DEC-RI-MP2 offers a full control of accuracy, it may serve as a supplement to standard DFT calculations and may become the method of choice for calculations on large molecular systems both with respect to the interpretation of experimental results and for reliable predictions of new structures and phenomena in many areas of molecular sciences. Our DEC strategy may also be applied to molecular gradients [103,104] and higher members of the CC hierarchy and we are currently working on carrying out CCSD and CCSD(T) [105] calculations on large molecular systems using the DEC strategy.

The capabilities of our DEC strategy have been demonstrated here by carrying out DEC-RI-MP2 calculations of interaction energies of AATs using a cc-pVDZ basis set. To bring the calculation of interaction energies to the next level of accuracy, an extended basis set and a higher member of the CC hierarchy, e.g. CCSD(T), have to be used. Furthermore, to remove the basis set error, the DEC-CC methods have to be extended to include explicit electron-correlation corrections. We are currently also working along these lines.

The possibility of carrying out calculations using the DEC-CC hierarchy may be the start of a new era for hybrid, ONIOM-like, approaches [106]. In these approaches, methods of different quality are applied to different parts of a very large system, depending on the chemical importance of a given part of the system. Taking as an example an enzyme in solution, at the current stage of development of the hybrid approaches, an active site of an enzyme is typically treated with DFT, the backbone part of the enzyme with molecular mechanics (MM) or DFT, and the solvent surrounding the enzyme with MM. The DEC-CC hierarchy will make it possible to treat the active site with DEC-CCSD(T) and the backbone part with DEC-RI-MP2, leaving only the solvent part to an HF or MM

treatment. As the protein backbone has been suggested to make important contributions to enzymatic catalysis [107], the possibility of addressing *both* the active site *and* the backbone part with quantum-mechanical correlated wave function methods may shift the modeling and understanding of enzymatic reactions to a new level.

The availability of the DEC-CCSD(T) method will also enable the possibility of obtaining results for large molecular systems against which both DFT functionals, MM force fields, and other local correlation methods could be benchmarked. The DFT functionals and MM force fields are often benchmarked for small molecular systems, for which conventional CCSD(T) results are available. However, conclusions about the accuracy of the DFT functionals and MM force fields drawn from these benchmark studies on small systems do not necessarily carry over to large molecular systems.

Summarizing, the DEC-RI-MP2 massively parallel calculations reported here have been carried out on the Titan supercomputer at Oak Ridge Leadership Computing Facility utilizing both CPUs and GPUs and have shown strong and weak scalability. We have thus shown that the DEC strategy may effectively be used to remove the scaling wall for calculating the RI-MP2 correlation energy. We have also recently performed DEC calculations on other supercomputers and testing facilities in Europe and USA, including Piz Daint, Curie, and Vesta. The DEC program has been compiled and run successfully on all the aforementioned supercomputer architectures proving DEC to be cross-platform and easily portable.

Acknowledgments

This research used resources of the Oak Ridge Leadership Computing Facility at Oak Ridge National Laboratory, which is supported by the Office of Science of the Department of Energy under Contract DE-AC05-00OR22725. The DEC code has been ported to and developed on Titan as part of an Innovative and Novel Computational Impact on Theory and Experiment (INCITE) grant [108–110] and through a Center for Accelerated Application Readiness (CAAR) [111] program. The research leading to these results has received funding from the European Research Council under the European Unions Seventh Framework Programme (FP/2007–2013)/ERC Grant Agreement No. 291371. DB acknowledges the Marie Curie Individual Fellowship funding for “DECOS”, project number 657514. We thank Bobby Sumpter and Jacek Jakowski for useful discussions regarding the AATs.

References

- [1] C. Møller, M.S. Plesset, *Phys. Rev.* 46 (7) (1934) 618.
- [2] G. Purvis, R.J. Bartlett, *J. Chem. Phys.* 76 (1982) 1910.
- [3] K. Raghavachari, G.W. Trucks, J.A. Pople, M. Head-Gordon, *Chem. Phys. Lett.* 157 (1989) 479.
- [4] T. Helgaker, P. Jørgensen, J. Olsen, *Molecular Electronic Structure Theory*, first ed., Wiley, Chichester, England, 2000.
- [5] M. Ziolkowski, B. Jansik, T. Kjærgaard, P. Jørgensen, *J. Chem. Phys.* 133 (2010) 014107. <http://dx.doi.org/10.1063/1.3456535>.
- [6] K. Kristensen, M. Ziolkowski, B. Jansik, T. Kjærgaard, P. Jørgensen, *J. Chem. Theory Comput.* 7 (2011) 1677. <http://dx.doi.org/10.1021/ct200114k>.
- [7] P. Ettenhuber, P. Baudin, T. Kjærgaard, P. Jørgensen, K. Kristensen, *J. Chem. Phys.* 144 (16) (2016). <http://dx.doi.org/10.1063/1.4947019>. URL <http://scitation.aip.org/content/aip/journal/jcp/144/16/10.1063/1.4947019>.
- [8] J.L. Whitten, *J. Chem. Phys.* 58 (10) (1973) 4496–4501. <http://dx.doi.org/10.1063/1.1679012>. URL <http://scitation.aip.org/content/aip/journal/jcp/58/10/10.1063/1.1679012>.
- [9] B.I. Dunlap, J. W.D. Connolly, J.R. Sabin, *J. Chem. Phys.* 71 (8) (1979) 3396–3402.
- [10] B.I. Dunlap, J. W.D. Connolly, J.R. Sabin, *J. Chem. Phys.* 71 (1979) 4993–4999.
- [11] C. Van Alsenoy, *J. Comput. Chem.* 9 (6) (1988) 620–626. <http://dx.doi.org/10.1002/jcc.540090607>.
- [12] O. Vahtras, J. Almlöf, M. Feyereisen, *Chem. Phys. Lett.* 213 (1993) 514.
- [13] M. Feyereisen, G. Fitzgerald, A. Komornicki, *Chem. Phys. Lett.* 208 (1993) 359.
- [14] D.E. Bernholdt, R.J. Harrison, *Chem. Phys. Lett.* 250 (56) (1996) 477–484. [http://dx.doi.org/10.1016/0009-2614\(96\)00054-1](http://dx.doi.org/10.1016/0009-2614(96)00054-1). URL <http://www.science-direct.com/science/article/pii/S0009261496000541>.
- [15] M. Katouda, S. Nagase, *Int. J. Quantum Chem.* 109 (2009) 2121. <http://dx.doi.org/10.1002/qua.22068>.
- [16] M. Katouda, T. Nakajima, *J. Chem. Theory Comput.* 9 (12) (2013) 5373–5380. <http://dx.doi.org/10.1021/ct400795v>.
- [17] L. Vogt, R. Olivares-Amaya, S. Kermes, Y. Shao, C. Amador-Bedolla, A. Aspuru-Guzik, *J. Phys. Chem. A* 112 (10) (2008) 2049–2057. <http://dx.doi.org/10.1021/jp0776762>. URL <http://www.scopus.com/inward/record.url?eid=2-s2.0-47049115273&partnerID=40&md5=2b2a2f1b42fc00a19c8e4225c65ad394>, cited By 67.
- [18] S.A. Maurer, J. Kussmann, C. Ochsenfeld, *J. Chem. Phys.* 141 (5) (2014). <http://dx.doi.org/10.1063/1.4891797>. URL <http://scitation.aip.org/content/aip/journal/jcp/141/5/10.1063/1.4891797>.
- [19] A.F. Izmaylov, G.E. Scuseria, *J. Chem. Phys.* 10 (2008) 3421–3429. <http://dx.doi.org/10.1039/B803274M>.
- [20] T. Nakajima, K. Hirao, *Chem. Phys. Lett.* 427 (13) (2006) 225–229. <http://dx.doi.org/10.1016/j.cplett.2006.06.059>. URL <http://www.sciencedirect.com/science/article/pii/S0009261406009122>.
- [21] R. Kendall, H. Frchtl, *Theoret. Chem. Accounts* 97 (1–4) (1997) 158–163. URL <http://www.scopus.com/inward/record.url?eid=2-s2.0-0031285828&partnerID=40&md5=3f6bb10774ab8f909f3c588a2cfc3bc7>, cited By 142.
- [22] D. Cremer, *WIRES Comput. Mol. Sci.* 1 (4) (2011) 509–530. <http://dx.doi.org/10.1002/wcms.58>. URL <http://onlinelibrary.wiley.com/doi/10.1002/wcms.58/abstract>.
- [23] H. Koch, A. Sánchez de Merás, T.B. Pedersen, *J. Chem. Phys.* 118 (21) (2003) 9481–9484. <http://dx.doi.org/10.1063/1.1578621>.
- [24] F. Aquilante, R. Lindh, T.B. Pedersen, *J. Chem. Phys.* 127 (11) (2007) 114107. <http://dx.doi.org/10.1063/1.2777146>. URL <http://scitation.aip.org/content/aip/journal/jcp/127/11/10.1063/1.2777146>.
- [25] F. Aquilante, L. Gagliardi, T.B. Pedersen, R. Lindh, *J. Chem. Phys.* 130 (15) (2009). <http://dx.doi.org/10.1063/1.3116784>. URL <http://scitation.aip.org/content/aip/journal/jcp/130/15/10.1063/1.3116784>.
- [26] P. Pulay, *Chem. Phys. Lett.* 100 (1983) 151.
- [27] S. Saebø, P. Pulay, *Ann. Rev. Phys. Chem.* 44 (1) (1993) 213–236. <http://dx.doi.org/10.1146/annurev.pc.44.100193.001241>.
- [28] P.Y. Ayala, G.E. Scuseria, *J. Chem. Phys.* 110 (1999) 3660.
- [29] G.E. Scuseria, P.Y. Ayala, *J. Chem. Phys.* 111 (1999) 8330.
- [30] D.S. Lambrecht, B. Doser, C. Ochsenfeld, *J. Chem. Phys.* 123 (18) (2005) 184102.
- [31] C. Hampel, H.-J. Werner, *J. Chem. Phys.* 104 (1996) 6286.
- [32] M. Schütz, G. Hetzer, H.-J. Werner, *J. Chem. Phys.* 111 (13) (1999) 5691–5705. <http://dx.doi.org/10.1063/1.479957>.
- [33] G. Hetzer, M. Schütz, H. Stoll, H.-J. Werner, *J. Chem. Phys.* 113 (21) (2000) 9443–9455.
- [34] J.E. Subotnik, A. Sodt, M. Head-Gordon, *J. Chem. Phys.* 125 (7) (2006) 074116.
- [35] J. Friedrich, M. Dolg, *J. Chem. Theory Comput.* 5 (2) (2009) 287–294. <http://dx.doi.org/10.1021/ct800355e>.
- [36] F. Neese, F. Wennmohs, A. Hansen, *J. Chem. Phys.* 130 (2009) 114108.
- [37] F. Neese, A. Hansen, D.G. Liakos, *J. Chem. Phys.* 131 (2009) 064103.
- [38] W. Li, P. Piecuch, *J. Phys. Chem. A* 114 (2010) 8644.
- [39] H.-J. Werner, M. Schütz, *J. Chem. Phys.* 135 (2011) 144116.
- [40] Y. Kurashige, J. Yang, G.K.-L. Chan, F.R. Manby, *J. Chem. Phys.* 136 (12) (2012) 124106.
- [41] C. Riplinger, F. Neese, *J. Chem. Phys.* 138 (2013) 034106.
- [42] Y. Guo, W. Li, D. Yuan, S. Li, *Sci. China Chem.* 57 (10) (2014) 1393–1398.
- [43] Y. Guo, W. Li, S. Li, *J. Phys. Chem. A* 118 (39) (2014) 8996–9004. <http://dx.doi.org/10.1021/jp501976x>.
- [44] P. Pinski, C. Riplinger, E.F. Valeev, F. Neese, *J. Chem. Phys.* 143 (3) (2015) 034108.
- [45] K. Kristensen, T. Kjærgaard, I.-M. Høyvik, P. Ettenhuber, P. Jørgensen, B. Jansik, S. Reine, J. Jakowski, *Mol. Phys.* 111 (2013) 1196. <http://dx.doi.org/10.1080/00268976.2013.783941>.
- [46] P. Baudin, P. Ettenhuber, S. Reine, K. Kristensen, T. Kjærgaard, *J. Chem. Phys.* 144 (5) (2016) 054102. <http://dx.doi.org/10.1063/1.4940732>.
- [47] H.-J. Werner, F.R. Manby, P.J. Knowles, *J. Chem. Phys.* 118 (18) (2003) 8149–8160.
- [48] H.-J. Werner, G. Knizia, C. Krause, M. Schwiik, M. Dornbach, *J. Chem. Theory Comput.* 11 (2) (2015) 484–507.
- [49] S. Li, J. Shen, W. Li, Y. Jiang, *J. Chem. Phys.* 125 (7) (2006) 074109.
- [50] H. Stoll, *Chem. Phys. Lett.* 191 (1992) 548.
- [51] M. Kobayashi, Y. Imamura, H. Nakai, *J. Chem. Phys.* 127 (7) (2007) 074103. <http://dx.doi.org/10.1063/1.2761878>.
- [52] M. Katouda, M. Kobayashi, H. Nakai, S. Nagase, *J. Comput. Chem.* 32 (2011) 2756.
- [53] T. Ishikawa, K. Kuwata, *Chem. Phys. Lett.* 474 (2009) 195.
- [54] Y. Mochizuki, K. Yamashita, T. Murase, T. Nakano, K. Fukuzawa, K. Takematsu, H. Watanabe, S. Tanaka, *Chem. Phys. Lett.* 457 (46) (2008) 396–403. <http://dx.doi.org/10.1016/j.cplett.2008.03.090>.

- [55] V. Deev, M.A. Collins, *J. Chem. Phys.* 122 (15) (2005) 154102.
- [56] X. He, J. Z.H. Zhang, *J. Chem. Phys.* 124 (18) (2006). <http://dx.doi.org/10.1063/1.2194535>. URL <http://scitation.aip.org/content/aip/journal/jcp/124/18/10.1063/1.2194535>.
- [57] W. Li, S. Li, Y. Jiang, *J. Phys. Chem. A* 111 (11) (2007) 2193–2199. <http://dx.doi.org/10.1021/jp067721q>. PMID: 17388268.
- [58] A.P. Rahalkar, M. Katouda, S.R. Gadre, S. Nagase, *J. Comput. Chem.* 31 (13) (2010) 2405–2418.
- [59] H.-A. Le, H.-J. Tan, J.F. Ouyang, R.P.A. Bettens, *J. Chem. Theory Comput.* 8 (2) (2012) 469–478. <http://dx.doi.org/10.1021/ct200783n>. PMID: 26596597.
- [60] S. Li, W. Li, J. Ma, *Acc. Chem. Res.* 47 (9) (2014) 2712–2720. <http://dx.doi.org/10.1021/ar500038z>. PMID: 24873495.
- [61] J. Almlöf, *Chem. Phys. Lett.* 181 (1991) 319.
- [62] M. Häser, *Theor. Chim. Acta* 87 (1993) 147.
- [63] B. Doser, D.S. Lambrecht, J. Kussmann, C. Ochsenfeld, *J. Chem. Phys.* 130 (6) (2009) 064107.
- [64] S.A. Maurer, D.S. Lambrecht, J. Kussmann, C. Ochsenfeld, *J. Chem. Phys.* 138 (1) (2013) 014101. <http://dx.doi.org/10.1063/1.4770502>. URL <http://scitation.aip.org/content/aip/journal/jcp/138/1/10.1063/1.4770502>.
- [65] B. Doser, J. Zienau, L. Clin, D.S. Lambrecht, C. Ochsenfeld, *Z. Phys. Chem.* 224 (3) (2010) 397.
- [66] M. Ziolkowski, B. Jansík, P. Jørgensen, J. Olsen, *J. Chem. Phys.* 131 (2009) 124112.
- [67] B. Jansík, S. Høst, K. Kristensen, P. Jørgensen, *J. Chem. Phys.* 134 (19) (2011) 194104.
- [68] I.-M. Høyvik, B. Jansík, P. Jørgensen, *J. Chem. Phys.* 137 (22) (2012) 224114.
- [69] I.-M. Høyvik, B. Jansík, P. Jørgensen, *J. Chem. Theory Comput.* 8 (2012) 3137.
- [70] I.-M. Høyvik, B. Jansík, P. Jørgensen, *J. Comput. Chem.* 34 (17) (2013) 1456–1462.
- [71] I.-M. Høyvik, K. Kristensen, T. Kjærsgaard, P. Jørgensen, *Theor. Chem. Acc.* 133 (1) (2013) 1417.
- [72] S.F. Boys, *Rev. Modern Phys.* 32 (2) (1960) 296–299.
- [73] J.M. Foster, S.F. Boys, *Rev. Modern Phys.* 32 (1960) 300.
- [74] C. Edmiston, K. Ruedenberg, *Rev. Modern Phys.* 35 (1963) 457.
- [75] C. Edmiston, K. Ruedenberg, *J. Chem. Phys.* 43 (10) (1965) S97–S116.
- [76] V. Magnasco, A. Perico, *J. Chem. Phys.* 47 (3) (1967) 971–981.
- [77] J. Pipek, P.G. Mezey, *J. Chem. Phys.* 90 (1989) 4916.
- [78] J. Pipek, *Int. J. Quantum Chem.* 36 (1989) 487.
- [79] D. Maynau, S. Evangelisti, N. Guihéry, C.J. Calzado, J.-P. Malrieu, *J. Chem. Phys.* 116 (2002) 10060.
- [80] J.E. Subotnik, A.D. Dutoi, M. Head-Gordon, *J. Chem. Phys.* 123 (2005) 114108.
- [81] F. Aquilante, T.B. Pedersen, A.S. de Merás, H. Koch, J. Chem. Phys. 125 (17) (2006) 174101.
- [82] C. Zhang, S. Li, *J. Chem. Phys.* 141 (24) (2014) 244106.
- [83] I.-M. Høyvik, P. Jørgensen, *Chem. Rev.* 116 (5) (2016) 3306–3327. <http://dx.doi.org/10.1021/acs.chemrev.5b00492>. PMID: 26855066.
- [84] E. Schwegler, M. Challacombe, *J. Chem. Phys.* 105 (7) (1996) 2726.
- [85] E. Schwegler, M. Challacombe, M. Head-Gordon, *J. Chem. Phys.* 106 (23) (1997) 9708.
- [86] M. Challacombe, E. Schwegler, *J. Chem. Phys.* 106 (13) (1997) 5526.
- [87] C. Ochsenfeld, C.A. White, M. Head-Gordon, *J. Chem. Phys.* 109 (5) (1998) 1663.
- [88] C.A. White, B.G. Johnson, P.M.W. Gill, M. Head-Gordon, *Chem. Phys. Lett.* 230 (1–2) (1994) 8.
- [89] M.C. Strain, G.E. Scuseria, M.J. Frisch, *Science* 271 (1996) 51.
- [90] P. Salek, S. Høst, L. Thøgersen, P. Jørgensen, P. Manninen, J. Olsen, B. Jansík, S. Reine, F. Pawłowski, E. Tellgren, T. Helgaker, S. Coriani, *J. Chem. Phys.* 126 (11) (2007) 114110.
- [91] S. Goedecker, *Rev. Modern Phys.* 71 (4) (1999) 1085. <http://dx.doi.org/10.1103/RevModPhys.71.1085>.
- [92] S. Goedecker, G.E. Scuseria, *Comput. Sci. Eng.* 5 (4) (2003) 14.
- [93] A.P. Rendell, *Chem. Phys. Lett.* 229 (3) (1994) 204–210. [http://dx.doi.org/10.1016/0009-2614\(94\)01053-6](http://dx.doi.org/10.1016/0009-2614(94)01053-6). URL <http://www.sciencedirect.com/science/article/pii/0009261494010536>.
- [94] E. Rudberg, E.H. Rubensson, P. Saek, *J. Chem. Phys.* 128 (18) (2008). <http://dx.doi.org/10.1063/1.2918357>. URL <http://scitation.aip.org/content/aip/journal/jcp/128/18/10.1063/1.2918357>.
- [95] I.-M. Høyvik, K. Kristensen, B. Jansík, P. Jørgensen, *J. Chem. Phys.* 136 (2012) 014105. <http://dx.doi.org/10.1063/1.3667266>.
- [96] B. Sumpter, V. Meunier, A. Vazquez-Mayagoitia, R. Castellano, *Int. J. Quantum Chem.* 107 (2007) 2233. <http://dx.doi.org/10.1002/qua.21411>.
- [97] B. Sumpter, V. Meunier, E. Valeev, A.J. Lampkins, H. Li, R.K. Castellano, *J. Phys. Chem. C* 111 (2007) 18912. <http://dx.doi.org/10.1021/jp076329p>.
- [98] F. Weigend, A. Köhn, C. Hättig, *J. Chem. Phys.* 116 (2002) 3175. <http://dx.doi.org/10.1063/1.1445115>.
- [99] S.F. Boys, F. Bernardi, *Mol. Phys.* 19 (1970) 553. <http://dx.doi.org/10.1080/00268977000101561>.
- [100] J. Dongarra, K. London, S. Moore, P. Mucci, D. Terpstra, *Conference on Linux Clusters: The HPC Revolution*, Linux Clusters Institute, Urbana, Illinois, 2002.
- [101] LSDALTON, a linear-scaling molecular electronic structure program, Release Dalton2016, 2016. <http://daltonprogram.org>.
- [102] K. Aidas, C. Angeli, K.L. Bak, V. Bakken, R. Bast, L. Boman, O. Christiansen, R. Cimraglia, S. Coriani, P. Dahle, E.K. Dalskov, U. Ekström, T. Enevoldsen, J.J. Eriksen, P. Ettenhuber, B. Fernández, L. Ferrighi, H. Fliegl, L. Frediani, K. Hald, A. Halkier, C. Hättig, H. Heiberg, T. Helgaker, A.C. Hennum, H. Hettema, E. Hjertenaes, S. Høst, I.-M. Høyvik, M.F. Izzi, B. Jansík, H.J.A. Jensen, D. Jonsson, P. Jørgensen, J. Kauczor, S. Kirpekar, T. Kjærsgaard, W. Klopper, S. Knecht, R. Kobayashi, K. Koch, J. Kongsted, A. Krapp, K. Kristensen, A. Ligabue, O.B. Lutnæs, J.I. Melo, K.V. Mikkelsen, R.H. Myhre, C. Neiss, C.B. Nielsen, P. Norman, J. Olsen, J.M.H. Olsen, A. Osted, M.J. Packer, F. Pawłowski, T.B. Pedersen, P.F. Provasi, S. Reine, Z. Rinkevicius, T.A. Ruden, K. Ruud, V. Rybkin, P. Salek, C.C.M. Samson, A.S. de Merás, T. Saue, S.P.A. Sauer, B. Schimmelpfennig, K. Snegov, A.H. Steindal, K.O. Sylvester-Hvid, P.R. Taylor, A.M. Teale, E.I. Tellgren, D.P. Tew, A.J. Thorvaldsen, L. Thøgersen, O. Vahtras, M.A. Watson, D.J.D. Wilson, M. Ziolkowski, H. Ågren, *WIREs Comput. Mol. Sci.* 4 (2013) 269. <http://dx.doi.org/10.1002/wcms.1172>.
- [103] K. Kristensen, P. Jørgensen, B. Jansík, T. Kjærsgaard, S. Reine, *J. Chem. Phys.* 137 (2012) 114102.
- [104] D. Bykov, K. Kristensen, T. Kjærsgaard, *J. Chem. Phys.* 145 (2) (2016). <http://dx.doi.org/10.1063/1.4956454>. URL <http://scitation.aip.org/content/aip/journal/jcp/145/2/10.1063/1.4956454>.
- [105] J.J. Eriksen, P. Baudin, P. Ettenhuber, K. Kristensen, T. Kjærsgaard, P. Jørgensen, *J. Chem. Theory Comput.* 11 (7) (2015) 2984–2993. <http://dx.doi.org/10.1021/acs.jctc.5b00086>.
- [106] T. Vreven, K.S. Byun, I. Komáromi, S. Dapprich, J.A. Montgomery, K. Morokuma, M.J. Frisch, *J. Chem. Theory Comput.* 2 (3) (2006) 815–826. <http://dx.doi.org/10.1021/ct050289g>.
- [107] G.A. Cisneros, M. Wang, P. Silinski, M.C. Fitzgerald, W. Yang, *Biochemistry* 43 (22) (2004) 6885–6892. <http://dx.doi.org/10.1021/bi049943p>.
- [108] The innovative and novel computational impact on theory and experiment (INCITE) program 2014. <https://www.olcf.ornl.gov/leadership-science/2014-incite-projects/>.
- [109] The innovative and novel computational impact on theory and experiment (INCITE) program 2015. <https://www.olcf.ornl.gov/leadership-science/2015-incite-projects/>.
- [110] The innovative and novel computational impact on theory and experiment (INCITE) program 2016. <https://www.olcf.ornl.gov/leadership-science/2016-incite-projects/>.
- [111] Center for accelerated application readiness (CAAR) <https://www.olcf.ornl.gov/caar>.

B.6 LoFEx — A local framework for calculating excitation energies: Illustrations using RI-CC2 linear response theory

P. Baudin, and K. Kristensen

J. Chem. Phys. **144**, 224106 (2016).

Major contributions: original idea, code implementation (RI-CC2 residual and linear transformation, eigenvalue solver, and LoFEx structure), production of the data, and writing process.

LoFEx — A local framework for calculating excitation energies: Illustrations using RI-CC2 linear response theory

Pablo Baudin^{a)} and Kasper Kristensen

qLEAP Center for Theoretical Chemistry, Department of Chemistry, Aarhus University, Langelandsgade 140, DK-8000 Aarhus C, Denmark

(Received 11 March 2016; accepted 24 May 2016; published online 10 June 2016)

We present a local framework for the calculation of coupled cluster excitation energies of large molecules (LoFEx). The method utilizes time-dependent Hartree-Fock information about the transitions of interest through the concept of natural transition orbitals (NTOs). The NTOs are used in combination with localized occupied and virtual Hartree-Fock orbitals to generate a reduced excitation orbital space (XOS) specific to each transition where a standard coupled cluster calculation is carried out. Each XOS is optimized to ensure that the excitation energies are determined to a predefined precision. We apply LoFEx in combination with the RI-CC2 model to calculate the lowest excitation energies of a set of medium-sized organic molecules. The results demonstrate the black-box nature of the LoFEx approach and show that significant computational savings can be gained without affecting the accuracy of CC2 excitation energies. *Published by AIP Publishing.* [<http://dx.doi.org/10.1063/1.4953360>]

I. INTRODUCTION

Coupled cluster (CC) theory^{1,2} is considered one of the greatest successes of electronic structure theory for the determination of accurate energies and molecular properties of systems dominated by a single configuration. Its strength relies on the hierarchy of CC models that provides a fast and systematic convergence towards the full configuration interaction (FCI) results. The main problem of CC is its computational cost and in particular its steep scaling with the system size. The dynamic correlation effects described by CC theory are spatially local and the steep scaling of the models can be attributed to the use of canonical molecular orbitals (CMOs) that are highly delocalized. This issue prevents a straightforward application of CC theory to large molecules and approximate CC models have to be developed.

The need for accurate and reliable methods for the calculation of excitation energies of large molecular systems can be seen from the number of attempts to do so in the last decade. All recently developed methods try to take advantage of the locality of correlation effects and electronic transitions. The concept of natural transition orbitals (NTOs)³ was, for example, used in the incremental scheme devised by Mata and Stoll⁴ where they used a mixed occupied orbital space composed of NTOs and localized molecular orbitals (LMOs). The virtual orbitals were left intact, and they relied on a many-body expansion of the excitation energies with a fragmentation of the occupied molecular orbital space to reduce the cost of the equation-of-motion coupled cluster singles and doubles (EOM-CCSD) model.

Other local CC methods focus on reformulations of the second-order approximate coupled cluster singles and doubles (CC2) model.⁵ The CC2 model has proven to be a good compromise between accuracy and computational cost for

the calculation of frequency-dependent molecular properties and its reformulation using density fitting techniques (e.g., the resolution of the identity, RI-CC2) has significantly extended the application range of the method.^{6,7} To further reduce the cost of the CC2 model, Helmich and Hättig proposed a local version of CC2 for excitation energies where they used orbital-specific virtuals (OSVs) and pair natural orbitals (PNOs) to reduce the dimension of the virtual orbital space.⁸ Along the same lines, the local CC implementation of Kats, Korona, and Schütz uses information from the coupled cluster singles (CCS) model to select the relevant occupied LMOs to describe each transition, combined with projected atomic orbitals (PAOs) for the virtual space. This strategy was first applied to the CCSD model and involved local approximations in both the singles and the doubles amplitudes,⁹ while the singles amplitudes were left intact in their local CC2 implementation.¹⁰ In a more recent work,¹¹ they proposed a multistate implementation relying on a Laplace transformation of the orbital energy denominators which resulted in an improved description of the CC2 excitation spectrum.

The multi-level coupled cluster theory of Myhre *et al.*^{12,13} is another CC-based method employing a different strategy. In their methods, the orbital space is partitioned based on chemical intuition and different CC models are used to treat different parts of the molecule. In this way, high accuracy (CCSD, CC3)^{14,15} can be achieved at a reduced cost by treating the less important part of the system with CCS and CC2 models.

In this paper, we present a local framework for calculating excitation energies (LoFEx) at the CC level of theory with emphasis on the RI-CC2 model. The overall goal is to enable the calculation of accurate excitation energies of large molecular systems by maintaining the CC error control with a computational cost that can compete against time-dependent density functional theory (TD-DFT).

^{a)}pablo.baudin@chem.au.dk

In the same way as for most local CC models, the strategy used by LoFEx is to reduce the dimension of the orbital space in which the CC equations have to be solved. As we show in Section II B, this is done by considering a mixed orbital space composed of NTOs and LMOs for *both* the occupied and virtual orbital spaces. Information about the main characteristics of the electronic transition is included in the orbital space through the NTOs, while the LMOs enable a compact description of correlation effects at the CC level. In order to reduce the dimension of the mixed NTO/LMO space for the correlated calculation, the LoFEx method considers only the LMOs in the vicinity of the NTOs. The size of the orbital space is optimized in a black-box manner such that the computed excitation energies reproduce the conventional CC results to a predefined accuracy (cf. Section II C). We note that restricting both the occupied and the virtual orbital spaces to a (small) fraction of the total orbital space is a fundamental requirement for the calculation of excitation energies of (very) large molecules. LoFEx differs from the aforementioned local schemes for calculating excitation energies since localized orthogonal virtual orbitals are used, the local excitation space of occupied and virtual orbitals is optimized dynamically, and no many-body expansion of the excitation energy is performed (as is done in the incremental scheme).

We present numerical RI-CC2 results for the lowest transitions in a set of organic molecules and analyse the convergence of excitation energies with the size of the mixed NTO/LMO space in Section III B. The errors and the cost-reduction of the black-box LoFEx procedure when compared to standard RI-CC2 implementations are investigated in Section III C.

II. THEORETICAL FOUNDATIONS OF LoFEx

Over the last few decades, many theoretical methods and tools have been developed to calculate excitation energies and analyse electronic transitions. More recently, the focus has been directed towards developing algorithms with lower computational costs. In this section, we present some of those concepts and describe how we have combined them to develop the LoFEx procedure.

A. The RI-CC2 model for excitation energies

In this paper, we target excitation energies calculated at the CC2 level of theory. The CC2 model was introduced by Christiansen *et al.*⁵ as an intermediate model between the CCS and CCSD models in the CC hierarchy for the calculation of frequency-dependent properties. The CC2 amplitude equations in the absence of external perturbations are given by

$$\Omega_{\mu_1} = \langle \mu_1 | \hat{H} + [\hat{H}, T_2] | \text{HF} \rangle = 0, \quad (1)$$

$$\Omega_{\mu_2} = \langle \mu_2 | \hat{H} + [F, T_2] | \text{HF} \rangle = 0, \quad (2)$$

where $\{|\text{HF}\rangle, |\mu_1\rangle, |\mu_2\rangle\}$ denote the Hartree-Fock (HF) ground state and the set of singles and doubles excitation manifolds. F is the Fock operator and \hat{H} is a similarity transformed Hamiltonian,

$$\hat{H} = \exp(-T_1) H \exp(T_1), \quad (3)$$

where $T_i = \sum_{\mu_i} t_{\mu_i} \tau_{\mu_i}$ is a cluster operator, t_{μ_i} is a cluster amplitude, τ_{μ_i} is an excitation operator, and i denotes the excitation level. In the CC2 model, the doubles amplitudes are only correct through first order in the fluctuation potential ($\Phi = H - F$). This approximation leads to a particularly simple form of the doubles amplitudes, which for closed shell systems reads

$$t_{ij}^{ab} = \frac{1}{(1 + \delta_{ij}\delta_{ab})} \frac{\tilde{g}_{aibj}}{\epsilon_i - \epsilon_a + \epsilon_j - \epsilon_b}, \quad (4)$$

where i, j (a, b) denote occupied (virtual) CMOs, ϵ_p is the energy associated with orbital p of unspecified occupancy, and \tilde{g}_{aibj} is a T_1 -transformed two-electron repulsion integral in Mulliken notation.¹⁶ This simple form of the doubles amplitudes can lead to a CCS-like formulation of the CC2 equations where the doubles amplitudes are calculated on-the-fly. In order to take full advantage of this formulation and avoid the storage of any four-index quantity (amplitudes or integrals), Hättig and Weigend used the resolution of the identity approximation for the two-electron integrals.⁶ Batches of doubles amplitudes are then contracted on-the-fly with three-center integrals to form intermediates that are used in the CC2 vector function. As shown in Ref. 6, this strategy can be generalized to the calculation of excitation energies at the RI-CC2 level. CC excitation energies are usually obtained as eigenvalues of the CC Jacobian matrix. However, to avoid storing four-index quantities also in the excitation energy part of the calculation, an effective CC2 Jacobian has to be considered,

$$\mathbf{A}^{\text{eff}}(\omega) \mathbf{b} = \omega \mathbf{b}, \quad (5)$$

$$A_{\mu_1\nu_1}^{\text{eff}}(\omega) = A_{\mu_1\nu_1} - \sum_{\gamma_2} \frac{A_{\mu_1\gamma_2} A_{\gamma_2\nu_1}}{\epsilon_{\gamma_2} - \omega}, \quad (6)$$

where ω is the excitation energy of interest, \mathbf{b} is a singles excitation vector, and $A_{\mu_i\nu_j} = \partial\Omega_{\mu_i}/\partial t_{\nu_j}$ is an element of the full CC2 Jacobian. The non-linearity in the excitation energy ω introduced by the effective Jacobian in Eq. (6) implies that a standard subspace diagonalization procedure cannot be employed to obtain the RI-CC2 excitation energies. In practice, we construct the effective Jacobian with an initial guess for the eigenvalue ω . It is then diagonalized using standard Davidson techniques,¹⁷⁻¹⁹ and the optimized eigenvalue is used to build a new effective Jacobian until self-consistency is reached. This process is repeated for each excitation of interest.⁷

B. A mixed NTO/LMO space

In order to provide a compact description of electronic transitions, it is important to work with an optimal orbital space both for occupied and virtual orbitals. LoFEx is therefore relying on a mixed orbital representation composed of the most important pair of NTOs, while the rest of the orbital space is localized. The dominant pair of NTOs provides a compact description of the main characteristics of the transition, while the LMOs enable an efficient description

of electron correlation effects. In this section, we detail the generation of the mixed NTO/LMO space.

NTOs are usually generated by singular value decomposition (SVD) of the transition density matrix (b_{ai}^{CCS}) between the HF ground state and an excited state obtained from the CCS model,³

$$b_{ai}^{\text{CCS}} = \langle \text{CCS} | \tau_{ai} | \text{HF} \rangle. \quad (7)$$

We note for later that NTOs can also be generated at the correlated level by performing an SVD of the singles excitation vector (b_{ai}^{CC}) only. Our current pilot implementation also generates NTOs from time-dependent Hartree-Fock theory (TDHF). The TDHF transition density matrix in the CMO basis can be expressed as²⁰

$$\tilde{b}_{ai} = \frac{X_{ai} + Y_{ai}}{|X_{ai} + Y_{ai}|} \sqrt{X_{ai}^2 + Y_{ai}^2}, \quad (8)$$

where \mathbf{X} and \mathbf{Y} are solutions of the TDHF equation for a given excitation energy $\tilde{\omega}$,

$$\begin{pmatrix} \mathbf{A} & \mathbf{B} \\ \mathbf{B} & \mathbf{A} \end{pmatrix} \begin{pmatrix} \mathbf{X} \\ \mathbf{Y} \end{pmatrix} = \tilde{\omega} \begin{pmatrix} \mathbf{1} & \mathbf{0} \\ \mathbf{0} & -\mathbf{1} \end{pmatrix} \begin{pmatrix} \mathbf{X} \\ \mathbf{Y} \end{pmatrix}. \quad (9)$$

The transformation matrices from the CMO basis to NTOs are then obtained by solving the following eigenvalue equations:

$$\tilde{\mathbf{b}}^* \tilde{\mathbf{b}} \mathbf{u}_k = \lambda_k \mathbf{u}_k, \quad k = 1, 2, \dots, N_o, \quad (10)$$

$$\tilde{\mathbf{b}} \tilde{\mathbf{b}}^* \mathbf{v}_k = \lambda'_k \mathbf{v}_k, \quad k = 1, 2, \dots, N_v, \quad (11)$$

where N_o is the number of occupied valence orbitals (in order to prevent the core and valence spaces from mixing), while N_v is the number of virtual orbitals. Finally, unitary matrices transforming to the NTO basis are given by

$$\mathbf{U} = (\mathbf{u}_1, \mathbf{u}_2, \dots, \mathbf{u}_{N_o}), \quad (12)$$

$$\mathbf{V} = (\mathbf{v}_1, \mathbf{v}_2, \dots, \mathbf{v}_{N_v}). \quad (13)$$

for occupied and virtual orbitals, respectively. Note also that $\lambda_k \equiv \lambda'_k$ for $k = 1, 2, \dots, N_o$, and that $\lambda'_k = 0$ for $k = N_o + 1, \dots, N_v$, assuming $N_o \leq N_v$. The first N_o eigenvalues give information about the importance of a given pair of occupied-virtual NTOs for the description of the transition represented by $\tilde{\mathbf{b}}$. For excited states dominated by single-electron replacements—which we are targeting in this paper—this procedure results in one occupied-virtual pair of NTOs with a singular value very close to one, while the remaining NTOs have much smaller singular values and thus provide little information about the electronic transition. We therefore choose to keep only the dominant pair of NTOs, while the rest of the orbital space is localized to enable a compact description of electron correlation effects in the CC part of the calculation. Different localization techniques have been investigated, including Boys localization^{21,22} and minimization of the second power of the second²³ and fourth²⁴ moments of the orbitals. No significant differences in the results presented in Section III were observed and we have therefore chosen a minimization of the second power of the second moment of the orbitals which is known to provide a good compromise between computational cost and spatial locality.²⁵ It is also important to emphasize that the use of NTOs makes the orbital space specific to a given transition,

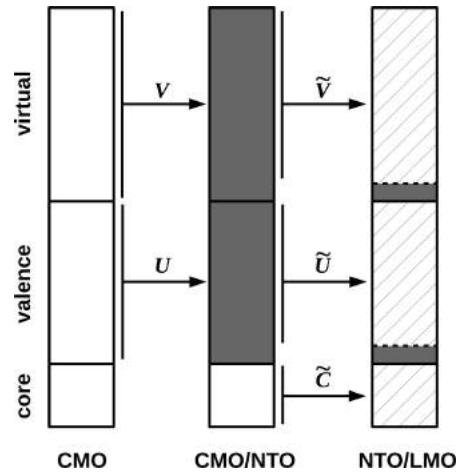


FIG. 1. Schematic representation of the generation of the mixed orbital space. \mathbf{U} and \mathbf{V} represent the valence and virtual transformation matrices [Eqs. (12) and (13)], while \mathbf{C} , $\tilde{\mathbf{U}}$, and $\tilde{\mathbf{V}}$ are transformation matrices to the local basis for core, valence, and virtual orbitals, respectively, excluding the dominant pair of NTOs. White: canonical molecular orbitals (CMOs); gray: natural transition orbitals (NTOs); stripes: Localized molecular orbitals (LMOs).

the one associated with the transition density matrix used to generate the set of NTOs. A different mixed orbital space should thus be constructed for each transition of interest. The generation of the mixed orbital space is summarized in Fig. 1.

C. Space optimization procedure

Once the full orbital space has been transformed to the mixed orbital space to enable an efficient description of the transition process, we need to build and optimize a reduced excitation orbital space (XOS) where the RI-CC2 calculation is carried out to provide the target excitation energy to a predefined accuracy. The main character of the excitation is described by the dominant pair of NTOs already included in the mixed orbital space. The XOS should thus be constructed by considering the dominant NTOs as well as a reduced set of important LMOs. We therefore setup a priority list of all LMOs ordered based on their estimated importance for the description of correlation effects in the vicinity of the NTOs. The importance of a given LMO p (occupied or virtual) is evaluated by the effective distance \tilde{r}_p given by

$$\tilde{r}_p = \min_A \left(\frac{r_{Ap}}{Q_A^{\text{NTO,o}}}, \frac{r_{Ap}}{Q_A^{\text{NTO,v}}} \right), \quad (14)$$

where index A denotes atomic centers, r_{Ap} corresponds to the distance between the center of charge of a local orbital p and atomic center A , and $Q_A^{\text{NTO,o}}$ and $Q_A^{\text{NTO,v}}$ are the Löwdin atomic charges of the occupied and virtual NTOs on center A , respectively. The Löwdin atomic charges of the NTOs (with values between 0 and 1) are used to modify the r_{Ap} distance in Eq. (14) as an attempt to quantify the distance

between the LMOs and the NTOs, even in the case where the NTOs are delocalized over several atomic centers. The smaller the modified distance \tilde{r}_p is, the more important orbital p is expected to be.

A first guess for the XOS (XOS₁) is constructed by including the NTOs as well as a given number of LMOs from the priority list defined by Eq. (14). The standard RI-CC2 amplitude and Jacobian eigenvalue equations are then solved as described in Section II A, except that the excitation manifold is restricted to XOS₁ instead of the full orbital space. For simplicity, the Fock matrix is diagonalized in XOS₁ to solve the RI-CC2 equations in a pseudo-canonical basis. Because of the restriction on the orbital space, the ground state correlation energy associated with the RI-CC2 amplitudes is meaningless and therefore not calculated. However, the excitation energy obtained by diagonalization of the Jacobian in XOS₁ corresponds to a first estimate of the exact RI-CC2 value (in the full orbital space). The quality of this estimate is of course strongly dependent on the size of XOS₁ and on the nature of the excitation.

In order to provide accurate excitation energies in a black-box manner, an optimization of the XOS is required. To this end, XOS₂ is constructed by including more orbitals based on the priority list defined by Eq. (14). The correlated calculation is then carried out in XOS₂ (solution of the RI-CC2 amplitude and Jacobian eigenvalue equations), and the new excitation energy is compared to the previous one. The orbital space is considered converged when the difference between two subsequent excitation energies is smaller than a given threshold (τ_{XOS}). The whole procedure is described step by step in Algorithm 1 and summarized schematically in Fig. 2. Default values for the main LoFEx threshold (τ_{XOS}) and the number of orbitals added to the XOS in each iteration will be discussed in Section III.

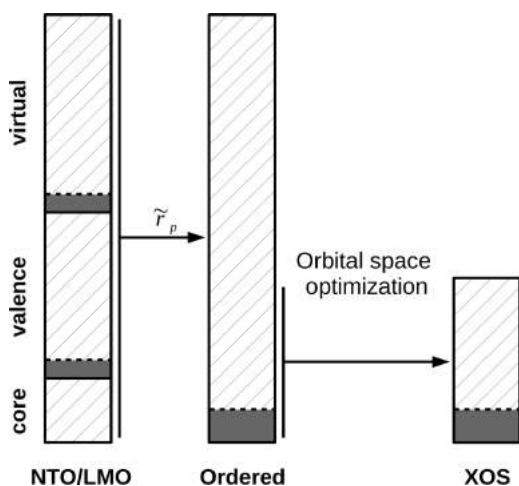


FIG. 2. Schematic representation of the generation of the excitation orbital space (XOS) in LoFEx. The orbitals in the mixed orbital space (left box) are reordered (middle box) according to the measure in Eq. (14), and the XOS (right box) used for the calculation of CC excitation energies is optimized as detailed in Algorithm 1. Gray: natural transition orbitals (NTOs); stripes: Localized molecular orbitals (LMOs).

A couple technical complications arise from the simple procedure described so far. The first issue concerns the computation of several excitation energies. The Davidson algorithm usually employed for such eigenvalue problems converges to the lowest excitation energies present in the subspace.^{17–19} However, if one is interested in the two lowest transitions for a given system, the mixed orbital spaces in LoFEx will be different for each transition, and consequently, the XOSs for the two transitions will also be different and might not even overlap. This means that in the calculation of the second excitation energy, depending on the size of the XOS, the second transition might correspond to the first or the second Jacobian eigenvalue.

In order to circumvent this issue, we employ a projection strategy where, for a given transition k , all previously optimized excitation vectors $\{\mathbf{b}_{\text{opt}}^1, \mathbf{b}_{\text{opt}}^2, \dots, \mathbf{b}_{\text{opt}}^{k-1}\}$ are projected out of the Davidson subspace. This prevents the optimized vector for transition k from collapsing into one of the previous solutions. Because the previously optimized excitation vectors are determined in different XOSs, they need to be transformed to the current mixed orbital space and projected onto the current XOS. As a consequence, the set of previously optimized vectors is usually not orthonormal in the current XOS and a given trial vector \mathbf{b}^i in the Davidson algorithm needs to be orthonormalized with respect to the previous excitation vectors using

$$\mathbf{b}^i \leftarrow (\mathbf{1} - \mathbf{P})\mathbf{b}^i, \quad (15)$$

$$\mathbf{P} = \sum_{j=1}^{k-1} \sum_{l=1}^{k-1} \mathbf{b}_{\text{opt}}^j [\mathbf{S}^{-1}]_{jl} (\mathbf{b}_{\text{opt}}^l)^T, \quad (16)$$

$$S_{jl} = (\mathbf{b}_{\text{opt}}^j)^T \mathbf{b}_{\text{opt}}^l, \quad (17)$$

where all quantities are expressed in the current mixed orbital space as well as restricted to the current XOS. Because of the difference in dimensions between the different XOSs, a given excitation vector might have only very small components in the current XOS (e.g., if the current and old transitions occur in different extremities of the molecular system). In such a case the excitation vector is discarded from the set of $k - 1$ previous vectors to avoid problems in the inversion of the overlap matrix \mathbf{S} .

One possible complication is that the lowest state in the Davidson subspace (after projection) might not have any resemblance with the TDHF state used to calculate NTOs (e.g., in cases where the TDHF and CC2 spectra differ significantly). The current mixed orbital space is then ill-suited to describe the CC2 transition of interest. This issue can be fixed by recalculating NTOs from the optimized CC2 singles excitation vector (\mathbf{b}^{CC2}) obtained in the current XOS. This is done whenever

$$|\tilde{\mathbf{b}}^T \mathbf{b}^{\text{CC2}}| < \tau_{\text{overlap}}, \quad (18)$$

where $\tilde{\mathbf{b}}$ is the last starting guess (usually from TDHF) and τ_{overlap} is fixed to 0.5 for normalized vectors. A new mixed orbital space is then generated using CC2 NTOs and the optimization procedure is restarted as shown in step 12 of Algorithm 1.

ALGORITHM 1. LoFEx pseudo-algorithm, where τ_{XOS} is the main threshold controlling the accuracy of the final excitation energies.

```

1: Solve TDHF problem for the  $n$  target excitation energies:  $\tilde{\omega}_1, \dots, \tilde{\omega}_n$ .
2: for state  $i = 1, n$  do
3:   Generate mixed orbital space using  $\tilde{\mathbf{b}}_i$  (cf. Fig. 1).
4:   Build  $\text{XOS}_1$  based on distance measure [Eq. (14)].
5:   Solve RI-CC2 amplitude and Jacobian equations in  $\text{XOS}_1$  and get  $\omega_i^{(1)}$ .
6:    $j \leftarrow 1$ 
7:   repeat
8:      $j \leftarrow j + 1$ 
9:     Increase orbital space based on distance measure [Eq. (14)] and get  $\text{XOS}_j$ .
10:    Solve RI-CC2 amplitude and Jacobian equations in  $\text{XOS}_j$  and get  $\omega_i^{(j)}$ .
11:    until  $|\omega_i^{(j)} - \omega_i^{(j-1)}| < \tau_{\text{XOS}}$ 
12:    if  $|\tilde{\mathbf{b}}_i^\dagger \mathbf{b}_i^{\text{CC2}}| < \tau_{\text{overlap}}$  then  $\tilde{\mathbf{b}}_i \leftarrow \mathbf{b}_i^{\text{CC2}}$  and go to step 3.
13:    Store optimized excitation energy,  $\omega_i \leftarrow \omega_i^{(j)}$ .
14: end for

```

A second issue concerns the number of atomic orbitals (AOs) needed to describe the molecular orbitals of the XOS. Indeed, both local orbitals and NTOs are constructed as linear combinations of AOs and have in principle small but non-zero coefficients on atoms far from their center of charge. As a consequence, even a small XOS would result in many two-electron integrals to be calculated in the AO basis and would destroy the performance of the method. We therefore reduce the number of AOs $\{\chi_\mu\}$ involved in the construction of a given MO ϕ_p ,

$$\phi_p = \sum_{\mu} \chi_{\mu} c_{\mu p}, \quad (19)$$

by introducing a modified MO $\tilde{\phi}_p$ according to

$$\tilde{\phi}_p = \sum_{\bar{\mu}} \chi_{\bar{\mu}} \tilde{c}_{\bar{\mu} p}, \quad (20)$$

where the summation over AO indices, $\bar{\mu}$, has been restricted to a subset of AOs $\{\chi_{\bar{\mu}}\}$. This restriction is done based on the Löwdin charges of orbital p and the coefficients $\tilde{c}_{\bar{\mu} p}$ are determined such that $\tilde{\phi}_p$ resembles the true MO ϕ_p as much as possible in a least square sense. The details about this procedure are described in Ref. 26 in the context of the divide-expand-consolidate local CC framework. Similarly, in connection with the RI approximation only a subset of auxiliary basis functions are considered, as described in Ref. 27.

III. NUMERICAL ILLUSTRATIONS

In this section, we present proof of concept calculations to support the theoretical foundations developed in Section II. We first investigate the convergence of excitation energies with the size of the XOS and then proceed to the application of the LoFEx algorithm as a black-box method.

A. Molecules and computational details

In Section III B we consider the following test molecules which have been optimized at the RI-MP2²⁸/cc-pVTZ(cc-pVTZ-RI) level of theory:

- caprylic acid,
- lauric acid,
- palmitic acid,
- 15-oxopentadecnoic acid (15-OPDA), and
- Dec-1,3,5,7,9-pentaene (C₁₀H₁₂).

For the application of LoFEx in Sections III C and III D, the above set is augmented with the following molecules:

- prostacyclin,
- an α -helix composed of 8 glycine residues (α -Gly₈),
- leupeptin,
- latanoprost,
- metenkephalin, and
- Phenothiazine-isoalloxazine dyad (dyad).

Those larger molecules were optimized at the RI-MP2/cc-pVDZ(cc-pVDZ-RI) level of theory. All geometry optimizations were performed using the ORCA program²⁹ and Cartesian coordinates are available in the supplementary material.³⁰

For the computation of vertical singlet excitation energies, the cc-pVDZ(cc-pVDZ-RI) basis sets were used on the hydrogen atoms, while diffuse functions were added to the other atoms via the aug-cc-pVDZ(aug-cc-pVDZ-RI) basis sets.^{31–33} We denote this combination of basis sets with a prime (aug-cc-pVDZ'). For the calculations on the dyad system in Section III D, the cc-pVDZ(cc-pVDZ-RI) basis sets were used without adding diffuse functions. The frozen core approximation was used in all calculations. The LoFEx algorithm as described in Section II has been implemented in a local version of the LSD program.^{34,35} The RI-CC2 algorithm used in LoFEx relies on a self-consistent Davidson algorithm⁷ where the norm of the residual is converged below $\tau_{\text{residual}} = 10^{-4}$ a.u. and the self-consistent energy threshold is set to $\tau_{\text{exc}} = 10^{-4}$ a.u. (≈ 2.7 meV). This last parameter should not be confused with the main LoFEx threshold, τ_{XOS} which will be specified in the following investigation. In practical applications of LoFEx, it is of course important to have $\tau_{\text{XOS}} \geq \tau_{\text{exc}}$.

B. Convergence of excitation energies

1. Saturated fatty acids

For analysis purposes, we consider the lowest transition in a set of saturated fatty acids with a chain of 8 (caprylic acid), 12 (lauric acid), and 16 (palmitic acid) carbon atoms. Fatty acids are simple systems, for which the lowest excitation is known to be localized on the carboxyl group. It is therefore a typical case where a canonical CC calculation of the excitation energy is unnecessarily expensive, since most of the carbon chain does not affect the transition. In order to confirm this statement, we examined the convergence of the lowest excitation energy with the size of the XOS in LoFEx. A fixed number of orbitals were added to the XOS in each LoFEx iteration based on the priority list defined by Eq. (14) and the convergence threshold for the excitation energy (τ_{XOS}) was set to zero, such that the full orbital space is included in the last iteration, which therefore provides the target RI-CC2 excitation energy.

In Fig. 3, we have plotted the dominant pair of TDHF NTOs for the lowest transition of the caprylic, lauric,

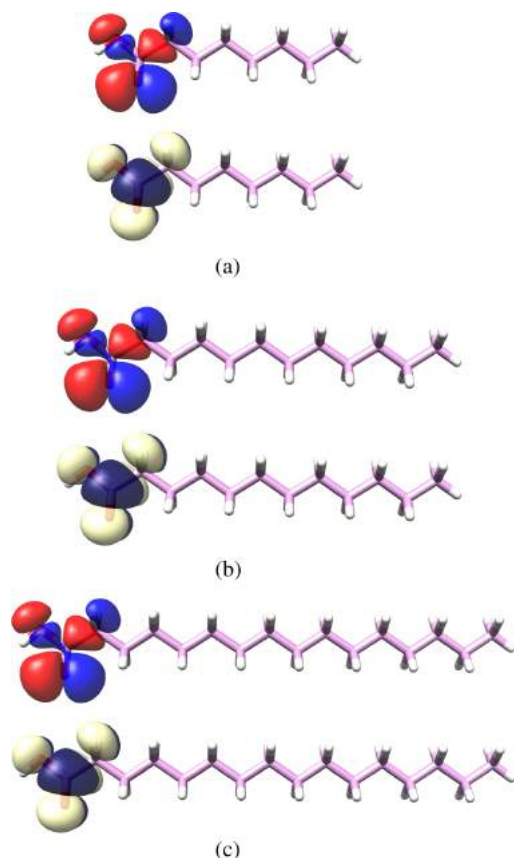


FIG. 3. Occupied (top) and virtual (bottom) TDHF natural transition orbitals (NTOs) for the lowest transition of saturated fatty acids using the aug-cc-pVDZ' basis set. The contour plot value was set to 0.02 a.u.^{36,37} (a) Caprylic acid. (b) Lauric acid. (c) Palmitic acid.

and palmitic acids. These plots clearly support our initial expectation that — at least at the TDHF level — the transition of interest is localized on the carboxyl group and the carbon chain has no important effects on the main characteristics of the electronic transition. This is confirmed at the RI-CC2 level by the plots presented in Fig. 4, which illustrate the effects of the size of the XOS on the excitation energy when MOs are included based on the priority list defined by Eq. (14). It shows a fast and smooth convergence towards the standard RI-CC2 excitation energy. In particular, the error in the excitation energy is below 0.01 eV for all three systems already when

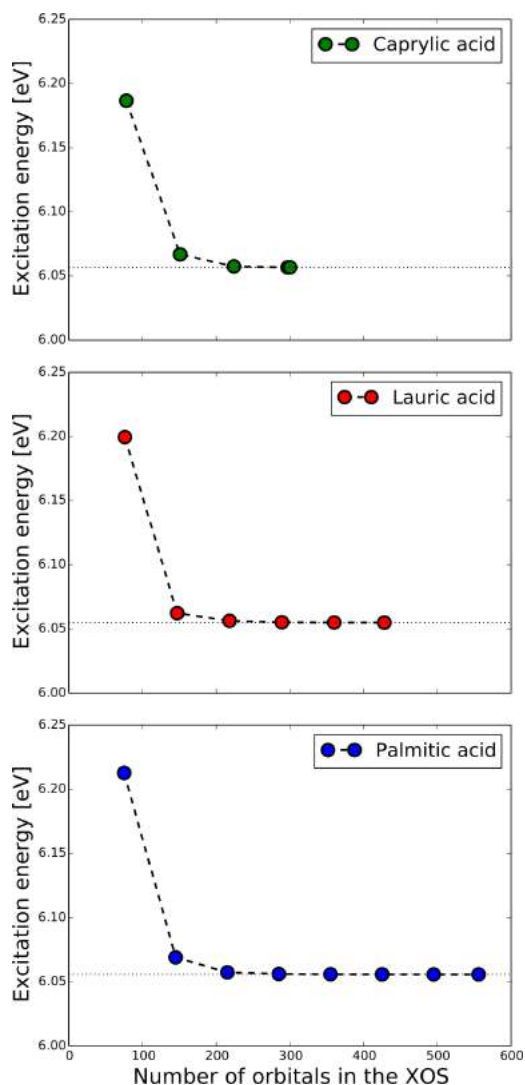


FIG. 4. Convergence of the lowest excitation energy of the caprylic, lauric, and palmitic fatty acids using the aug-cc-pVDZ' basis as a function of the size of the excitation orbital space (XOS) when MOs are included based on the priority list defined by Eq. (14). The last points of the curves and the dotted horizontal lines correspond to the reference RI-CC2 values (complete orbital space).

less than 230 MOs are included in the orbital space (third point in the curves). This demonstrates that a significant amount of computational resources can be saved for such small but simple systems.

2. 15-oxopentadecanoic acid (15-OPDA)

As a complement to this preliminary investigation, we now consider the three lowest excitation energies of the 15-oxopentadecanoic acid (15-OPDA). By looking at the dominant TDHF NTOs of the three transitions in Fig. 5, it is seen that the lowest and third transitions of 15-OPDA are localized on the aldehyde group, while the second lowest transition occurs on the carboxyl group at the other end of the carbon chain. This system is thus a good candidate to test the projection strategy presented in Section II C. The same analysis as before is performed by including a fixed number of orbitals to the XOS until the complete orbital space is included, and this is done independently for the three transitions of interest.

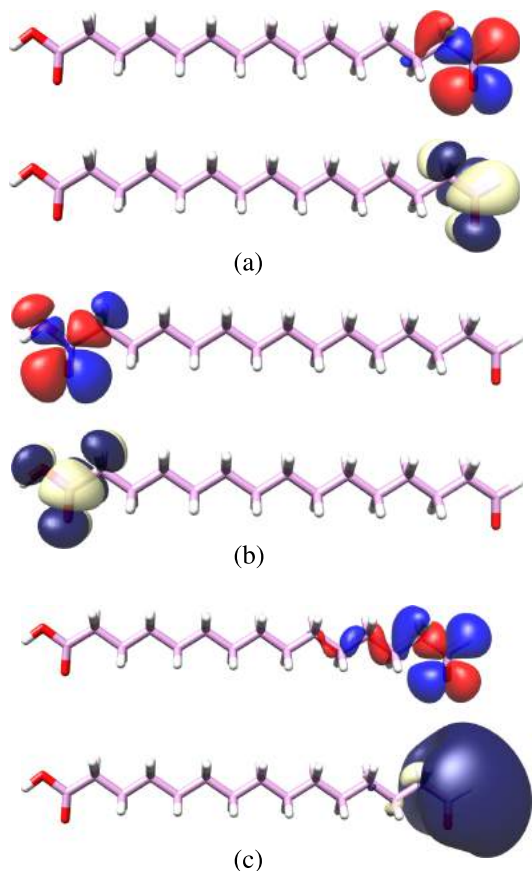


FIG. 5. Occupied (top) and virtual (bottom) TDHF natural transition orbitals (NTOs) for the three lowest transitions of 15-oxopentadecanoic acid (15-OPDA) using the aug-cc-pVDZ' basis set. The contour plot value was set to 0.02 a.u.^{36,37} (a) Dominant pair of NTOs for S_1 . (b) Dominant pair of NTOs for S_2 . (c) Dominant pair of NTOs for S_3 .

The challenge of computing several excitation energies can be exemplified as follows: when computing the second lowest transition on the carboxyl group of 15-OPDA, the first XOS (XOS_1) will not include any component of the lowest excitation vector on the aldehyde group. The standard Davidson procedure would therefore provide the excitation energy of interest (the second lowest for the whole system) by converging to the lowest Jacobian eigenvalue. However, if the XOS corresponds to the complete orbital space, the lowest eigenvalue obtained with the standard Davidson procedure would most likely be the lowest transition on the aldehyde group. The projection strategy described in Section II C is therefore necessary to ensure that the excitation vector is not collapsing to the lowest transition as the XOS is increased.

In Fig. 6, we have plotted the three lowest excitation energies of 15-OPDA against the size of the XOS. It is important to emphasize that the three excitation energies on a specific vertical line in Fig. 6 are determined in different and independent XOSs that contain the same amount of orbitals. The curves in Fig. 6 show a smooth convergence behaviour for all three excitation energies without ever collapsing to another transition which shows that the projection strategy presented in Section II C is enough to ensure convergence to the desired excitation energies. Fig. 6 also shows that the two lowest excitation energies of 15-OPDA converge as fast as the lowest excitation energy of the fatty acids in Fig. 4, while the convergence of the third excitation energy is significantly slower. This is due to the more diffuse character of the third transition (cf. Fig. 5(c)) which is rather poorly described in the small aug-cc-pVDZ' basis.

3. Dec-1,3,5,7,9-pentaene ($C_{10}H_{12}$)

Electronic transitions are not always as local as for the systems treated so far. In some interesting cases, the excitation

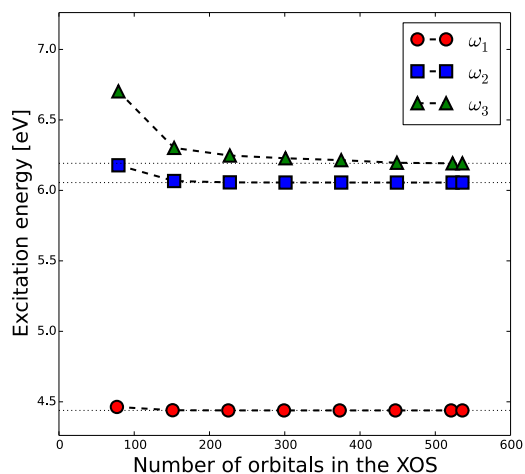


FIG. 6. Convergence of the three lowest excitation energies of the 15-oxopentadecanoic acid (15-OPDA) using the aug-cc-pVDZ' basis as a function of the size of the excitation orbital space (XOS) when MOs are included based on the priority list defined by Eq. (14). The last points of the curves and the dotted horizontal lines correspond to the reference RI-CC2 values (complete orbital space).

can be spread over a large part of the molecule, for example, due to electronic delocalization in conjugated systems or in the case of charge-transfer (CT) transitions. Such examples would necessarily require a larger XOS and in some special cases the complete orbital space needs to be included. To illustrate further the impact of the character of the transition on the size of the XOS, we have applied LoFEx to the $C_{10}H_{12}$ conjugated molecule. The TDHF NTOs plotted in Fig. 7 show that the first transition of $C_{10}H_{12}$ is delocalized over the whole system. Fig. 8 represents the decay of the lowest excitation energy of $C_{10}H_{12}$ with the size of the XOS. As expected, the convergence is stable but much slower than for the systems analyzed previously. For this small molecule, the complete orbital space has to be included in the XOS to reproduce the standard RI-CC2 result, but we can expect that for larger systems, even if the NTOs are delocalized over a part of the molecule, computational savings should still be possible by ignoring all parts of the system not affected by the transition. In short, $C_{10}H_{12}$ represents a worst case scenario for LoFEx and no computational savings can be obtained. Nonetheless, as we shall see in Section III C, the standard RI-CC2 excitation energy is still obtained by the black-box LoFEx algorithm.

4. Convergence behaviour

Finally, we note that, for all examples treated in this section, the excitation energies are systematically lowered when the dimension of the XOS increases. This behaviour is also usually observed in basis set convergence studies of excitation energies,^{38,39} and can be partly explained by Cauchy's interlacing theorem.^{40,41} Part of Cauchy's theorem states that, for a symmetric matrix, the eigenvalues $\omega_k^{B_1}$ obtained with a basis $\{B_1\}$ will always be larger than the corresponding eigenvalues $\omega_k^{B_2}$ obtained with a basis $\{B_2\}$ when $\{B_1\} \subset \{B_2\}$ (i.e., $\omega_k^{B_1} \geq \omega_k^{B_2}$ for each eigenvalue k). This is for example the case in the configuration interaction (CI) excitation energy problem where a symmetric matrix has to be diagonalized. However, it does not strictly hold in CC theory, partly because the Jacobian matrix is not Hermitian and therefore the eigenvalue problem is not ensured to have (real) solutions, but also because the Jacobian matrix depends on the CC amplitudes which are different from one basis to another meaning that the Jacobian in the basis $\{B_1\}$ is not a true submatrix of the Jacobian in the $\{B_2\}$ basis. In spite

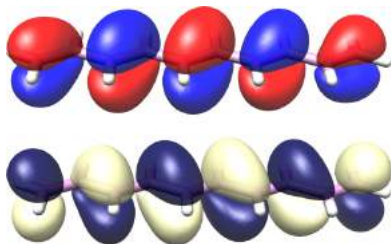


FIG. 7. Occupied (top) and virtual (bottom) TDHF natural transition orbitals (NTOs) for the lowest transition of dec-1,3,5,7,9-pentane ($C_{10}H_{12}$) using the aug-cc-pVDZ' basis set. The contour plot value was set to 0.02 a.u.^{36,37}

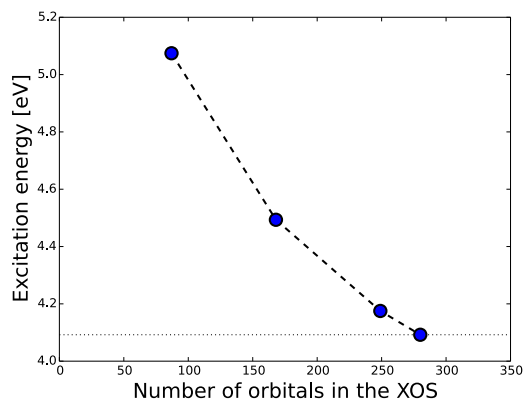


FIG. 8. Convergence of the lowest excitation energy of dec-1,3,5,7,9-pentane ($C_{10}H_{12}$) using the aug-cc-pVDZ' basis as a function of the size of the excitation orbital space (XOS) when MOs are included based on the priority list defined by Eq. (14). The last point of the curve and the dotted horizontal line correspond to the reference RI-CC2 value (complete orbital space).

of these formal differences between CI and CC, we have always observed that the energies are lowered when the XOS is increased, indicating that in practice, Cauchy's theorem effectively holds also for the CC Jacobian. This feature is important in the context of LoFEx since it lowers the risk of premature convergence when the excitation energies of two subsequent XOSs are compared (step 11 in Algorithm 1).

C. LoFEx as a black-box method

It has now been demonstrated with simple examples that the method described in Section II can lead to significant savings. In this section we apply LoFEx as a black-box method and provide default parameters for the optimization procedure that result in accurate excitation energies using a reduced orbital space. The main challenge here is to find the number of orbitals to add to the XOS between two iterations, such that it is large enough to avoid premature convergence and small enough to prevent the XOS from becoming unnecessarily large. This quantity needs to be conservative as the convergence rate of the excitation energies with the size of the XOS is strongly dependent on the nature of the transitions and the chemical structure of the molecules and premature convergence could in principle occur in some difficult cases. In this investigation, the number of orbitals added to the XOS in each LoFEx iteration was set to ten times the average number of MOs per atom (i.e., $10 \times N_{MO}/N_{atom}$) and the main LoFEx threshold was chosen to be $\tau_{XOS} = 0.02$ eV. The number of orbitals added has been chosen based on a series of tests and seems like a conservative choice but more extensive testing of LoFEx will tell if this value is optimal. The LoFEx threshold (τ_{XOS}) is more of a tunable parameter and depends on the required accuracy. A value of 0.02 eV is conservative and is expected to provide excitation energies of standard CC2 quality (CC2 is known to result in excitation energies where the typical errors are an order of magnitude larger).^{6,38,39,42}

In Table I we report the RI-CC2-LoFEx excitation energies as well as measures of the size of the converged XOS and the number of LoFEx iterations (the number of different XOSs considered) for all molecules presented in Section III A. Speed-ups of LoFEx compared to canonical RI-CC2 implementations are also reported. For calculations containing more than one transition, the current RI-CC2 implementation in the LSD program does not allow for fair comparisons. Speed-ups are therefore not reported for those cases.

Comparison with canonical RI-CC2 energies — available in the supplementary material³⁰ — results in errors in the LoFEx excitation energies below 0.01 eV for all molecules. This indicates that the LoFEx parameters chosen above are conservative enough to provide excitation energies of CC2 quality and to avoid false convergence. Concerning the size of the optimized XOS and the reduction in computational cost, one can see from Table I that it is strongly dependent on the nature of the electronic transition and on the size of the molecular system. However, even when the full orbital space has to be included in the XOS (e.g., S_1 of prostacyclin), the last RI-CC2 calculation will in general be time-dominating and the overall cost is of the same order as for canonical RI-CC2 calculations (for $C_{10}H_{12}$ with a speed-up of 0.43, the system is so small that the full calculation is very fast anyway). On the other hand, significant savings are usually obtained when the LoFEx algorithm converges in only two or three iterations. For example, a LoFEx calculation of the lowest transition of metenkephalin provides a speed-up of almost 60, which is already very large, but even larger speed-ups are expected for larger molecules with local transitions. Comparison of the size of the XOS in Table I with the convergence of the excitation energies represented in Figs. 4 and 6 shows that the black-box method often provides too large XOS. This is

due to the structure of the algorithm where the penultimate step is actually converged but requires an additional iteration to check for convergence. This is also the reason for the exceptionally low errors.

D. A difficult case: The phenothiazine-isoalloxazine dyad

As reported by Kats and Schütz in Ref. 11, the few lowest transitions of the phenothiazine-isoalloxazine dyad are particularly difficult to describe at the CC2 level and especially with local approximations. The problem originates from the very poor starting guess that non-correlated methods (CCS/TDHF) provide for the CC2 calculation in that particular case. This observation could indicate that CC2 is not appropriate for describing the electronic spectrum of this molecule and that larger basis sets (double-zeta basis sets were used) as well as higher level models (CCSD or CC3) might provide significantly different results. However, it is interesting to see how the LoFEx method is performing with such a difficult case. In particular, one of the lowest transitions of the dyad is known to exhibit a CT character which is challenging for many computational methods and in particular for TD-DFT.

The five lowest excitation energies of the dyad have been calculated using LoFEx and are reported in Table I. We note that the error in the excitation energies is as low as for the other systems (below 0.01 eV) but that due to the complexity of the transition, the full molecular orbital space has to be included in the XOS for all but the first transition. It is also important to note that for those states (S_2, S_3, S_4 , and S_5), CC2 NTOs were calculated in the course of the calculation because the overlap with the starting guess was below $\tau_{\text{overlap}} = 0.5$ [cf.

TABLE I. Excitation energies from RI-CC2-LoFEx (ω_{LoFEx}) and size of the XOS given by the fraction of the complete set of MOs and AOs included in the XOS. The number of iterations used in LoFEx (number of different XOSs considered) as well as speed-ups compared to canonical RI-CC2 calculations is also reported. All the calculations have been done using the aug-cc-pVDZ' basis set (except for the dyad which uses cc-pVDZ) and the frozen core approximation. The main LoFEx threshold was set to $\tau_{\text{XOS}} = 0.02$ eV.

| System | State | ω_{LoFEx}^a | % MOs | % AOs | No. iterations | Speed-up |
|----------------------------|-------|---------------------------|-------|-------|----------------|----------|
| Caprylic acid | S_1 | 6.06 | 82.3 | 94.8 | 2 | 1.11 |
| Lauric acid | S_1 | 6.05 | 83.9 | 96.2 | 3 | 3.49 |
| Palmitic acid | S_1 | 6.06 | 63.5 | 72.6 | 3 | 4.55 |
| 15-OPDA | S_1 | 4.44 | 46.1 | 57.0 | 2 | ... |
| | S_2 | 6.06 | 46.5 | 52.3 | 2 | ... |
| | S_3 | 6.19 | 100 | 100 | 5 | ... |
| $C_{10}H_{12}$ | S_1 | 4.09 | 100 | 100 | 3 | 0.43 |
| Prostacyclin | S_1 | 4.98 | 92.3 | 99.6 | 5 | 0.98 |
| α -Gly ₈ | S_1 | 5.42 | 71.6 | 93.4 | 4 | 1.81 |
| Leupeptin | S_1 | 4.27 | 46.7 | 91.0 | 3 | 7.08 |
| Latanoprost | S_1 | 5.08 | 44.7 | 58.5 | 3 | 8.12 |
| Metenkephalin | S_1 | 4.78 | 42.3 | 48.9 | 3 | 58.9 |
| Dyad | S_1 | 3.10 | 82.3 | 88.7 | 4 | ... |
| | S_2 | 3.47 | 100 | 100 | 8 ^b | ... |
| | S_3 | 3.51 | 100 | 100 | 6 ^b | ... |
| | S_4 | 3.71 | 100 | 100 | 6 ^b | ... |
| | S_5 | 4.06 | 100 | 100 | 6 ^b | ... |

^aAll errors in the LoFEx excitation energies with respect to canonical RI-CC2 values are below 0.01 eV.

^bExtra iterations due to the calculation of CC2 NTOs.

Eq. (18) and the associated discussion]. This did not occur for any of the other molecules in Table 1 and it is a confirmation of the difference between the optimized TDHF and CC2 states. In general, we have observed that the use of CC2 NTOs does not reduce the size of the optimized XOS which is why CC2 NTOs are only used when the TDHF NTOs do not represent properly the transition of interest. With the geometry of the dyad used in this paper (which is different from the one used in Ref. 11), the CT transition corresponds to the fourth excitation energy and is properly described with LoFEx. However, with the parameters used in the black-box algorithm, it does require that the XOS contains the full orbital space, and consequently, no savings are obtained.

Even though the full orbital space is included for most of the transitions of the dyad, this application of LoFEx shows that the method provides correct CC2 results even for difficult cases such as CT transitions. We also note that significant savings are expected if the dyad is considered in a larger environment (e.g., including solvent).

IV. CONCLUSION AND PERSPECTIVES

We have introduced the LoFEx approach for the calculation of vertical CC excitation energies where the CC amplitude and Jacobian eigenvalue equations are solved in a transition-specific reduced orbital space (the XOS) composed of NTOs and LMOs. The method can be used as a black-box where the error in the excitation energies is controlled by a single parameter (τ_{XOS}). LoFEx was tested on a set of molecules, including small and simple systems as well as larger and more real-life compounds. It was demonstrated at the RI-CC2 level that significant savings can be obtained without loss of accuracy. The computational cost of the method is dominated by the last RI-CC2 calculation using the largest XOS and is expected to be constant with the system size for a given type of transition. For large enough systems, and in particular when the excitation of interest is local compared to the size of the molecule, the cost of the method will be dominated by the underlying TDHF calculation on the full system, resulting in excitation energies of CC2 quality with a computational cost comparable to TD-DFT.

LoFEx relies on TDHF to provide a qualitatively correct description of the excitation process, i.e., the main characteristics of the transition should be described by the NTOs built from the TDHF transition density matrix. If the TDHF and CC2 spectra are significantly different, CC2 NTOs are constructed in the course of the calculation. This results in a more appropriate mixed orbital space which improves the description of the CC2 spectrum. We have shown that LoFEx can handle the description of complex electronic spectra exemplified with the phenothiazine-isoalloxazine dyad molecule for which the CT transition was described properly. This was however achieved without cost-reduction and a more elaborate algorithm is required to achieve that goal. Future works will thus be focused on the development of a more efficient RI-CC2 algorithm and on improving the orbital space optimization procedure together with more extensive testing of LoFEx. The calculation of transition moments and oscillator strengths will also be investigated.

The LoFEx procedure can in principle be straightforwardly applied to more accurate CC models (CCSD, CC3, etc.). However, the size of the XOS needed for a proper description of most transitions would probably prevent most practical applications without introducing further approximations on the underlying CC models. The dependence on the NTOs could also be an issue if CCSD or CC3 are used to describe doubles dominated transitions, and a generalization of the LoFEx strategy would be necessary.

LoFEx is conceptually and practically simple and can be seen as a general framework to select and optimize the orbital spaces needed to provide accurate descriptions of electronic transitions. For a given XOS of orthogonal occupied and virtual orbitals provided by the LoFEx scheme, any single reference CC code can be applied. We could, for instance, imagine combinations with PNO algorithms to further reduce the cost of the solution of the CC equations.⁸ Another possibility is to combine LoFEx with hybrid quantum mechanics and molecular mechanics (QM/MM) techniques, like the polarizable-embedding approach,^{43,44} where a large quantum mechanical part could be treated by LoFEx, while the environment effects would be described at the molecular mechanics level.

ACKNOWLEDGMENTS

The research leading to these results has received funding from the European Research Council under the European Union's Seventh Framework Programme (No. FP/2007-2013)/ERC Grant Agreement No. 291371.

The numerical results presented in this work were performed at the Centre for Scientific Computing, Aarhus (<http://phys.au.dk/forskning/cscaa/>).

This research also used resources of the Oak Ridge Leadership Computing Facility at Oak Ridge National Laboratory, which is supported by the Office of Science of the Department of Energy under Contract No. DE-AC05-00OR22725.

¹R. J. Bartlett and M. Musiał, *Rev. Mod. Phys.* **79**, 291 (2007).

²I. Shavitt and R. J. Bartlett, *Many-Body Methods in Chemistry and Physics: Many-Body Perturbation Theory and Coupled-Cluster Theory* (Cambridge University Press, Cambridge, UK, 2009).

³R. L. Martin, *J. Chem. Phys.* **118**, 4775 (2003).

⁴R. A. Mata and H. Stoll, *J. Chem. Phys.* **134**, 034122 (2011).

⁵O. Christiansen, H. Koch, and P. Jørgensen, *Chem. Phys. Lett.* **243**, 409 (1995).

⁶C. Hättig and F. Weigend, *J. Chem. Phys.* **113**, 5154 (2000).

⁷P. Baudin, J. Sánchez Marín, I. García Cuesta, and A. M. J. Sánchez de Merás, *J. Chem. Phys.* **140**, 104111 (2014).

⁸B. Helmich and C. Hättig, *J. Chem. Phys.* **139**, 084114 (2013).

⁹T. Korona and H.-J. Werner, *J. Chem. Phys.* **118**, 3006 (2003).

¹⁰D. Kats, T. Korona, and M. Schütz, *J. Chem. Phys.* **125**, 104106 (2006).

¹¹D. Kats and M. Schütz, *J. Chem. Phys.* **131**, 124117 (2009).

¹²R. H. Myhre, A. M. J. Sánchez de Merás, and H. Koch, *Mol. Phys.* **111**, 1109 (2013).

¹³R. H. Myhre, A. M. J. Sánchez de Merás, and H. Koch, *J. Chem. Phys.* **141**, 224105 (2014).

¹⁴H. Koch, H. J. A. Jensen, P. Jørgensen, and T. Helgaker, *J. Chem. Phys.* **93**, 3345 (1990).

¹⁵O. Christiansen, H. Koch, and P. Jørgensen, *J. Chem. Phys.* **103**, 7429 (1995).

¹⁶T. Helgaker, P. Jørgensen, and J. Olsen, *Molecular Electronic Structure Theory*, 1st ed. (Wiley, Chichester, England, 2000), pp. 37–38.

- ¹⁷E. R. Davidson, *J. Comput. Phys.* **17**, 87 (1975).
- ¹⁸E. R. Davidson, *Comput. Phys. Commun.* **53**, 49 (1989).
- ¹⁹C. W. Murray, S. C. Racine, and E. R. Davidson, *J. Comput. Phys.* **103**, 382 (1992).
- ²⁰T. Etienne, *J. Chem. Phys.* **142**, 244103 (2015).
- ²¹S. F. Boys, *Rev. Mod. Phys.* **32**, 296 (1960).
- ²²J. M. Foster and S. F. Boys, *Rev. Mod. Phys.* **32**, 300 (1960).
- ²³B. Jansík, S. Høst, K. Kristensen, and P. Jørgensen, *J. Chem. Phys.* **134**, 194104 (2011).
- ²⁴I.-M. Høyvik, B. Jansík, and P. Jørgensen, *J. Chem. Phys.* **137**, 224114 (2012).
- ²⁵I.-M. Høyvik and P. Jørgensen, *Chem. Rev.* **116**, 3306 (2016).
- ²⁶P. Ettenhuber, P. Baudin, T. Kjærgaard, P. Jørgensen, and K. Kristensen, *J. Chem. Phys.* **144**, 164116 (2016).
- ²⁷P. Baudin, P. Ettenhuber, S. Reine, K. Kristensen, and T. Kjærgaard, *J. Chem. Phys.* **144**, 054102 (2016).
- ²⁸M. Feyereisen, G. Fitzgerald, and A. Komornicki, *Chem. Phys. Lett.* **208**, 359 (1993).
- ²⁹F. Neese, *Wiley Interdiscip. Rev.: Comput. Mol. Sci.* **2**, 73 (2012).
- ³⁰See supplementary material at <http://dx.doi.org/10.1063/1.4953360> for molecular geometries and reference excitation energies.
- ³¹T. Dunning, Jr., *J. Chem. Phys.* **90**, 1007 (1989).
- ³²R. Kendall, T. Dunning, Jr., and R. Harrison, *J. Chem. Phys.* **96**, 6769 (1992).
- ³³F. Weigend, A. Köhn, and C. Hättig, *J. Chem. Phys.* **116**, 3175 (2002).
- ³⁴K. Aidas, C. Angeli, K. L. Bak, V. Bakken, R. Bast, L. Boman, O. Christiansen, R. Cimiraglia, S. Coriani, P. Dahle, E. K. Dalskov, U. Ekström, T. Enevoldsen, J. J. Eriksen, P. Ettenhuber, B. Fernández, L. Ferrighi, H. Fliegler, L. Frediani, K. Hald, A. Halkier, C. Hättig, H. Heiberg, T. Helgaker, A. C. Hennum, H. Hettema, E. Hjertenaes, S. Høst, I.-M. Høyvik, M. F. Iozzi, B. Jansík, H. J. A. Jensen, D. Jonsson, P. Jørgensen, J. Kauczor, S. Kirpekar, T. Kjærgaard, W. Klopper, S. Knecht, R. Kobayashi, H. Koch, J. Kongsted, A. Krapp, K. Kristensen, A. Ligabue, O. B. Lutnaes, J. I. Melo, K. V. Mikkelsen, R. H. Myhre, C. Neiss, C. B. Nielsen, P. Norman, J. Olsen, J. M. H. Olsen, A. Osted, M. J. Packer, F. Pawłowski, T. B. Pedersen, P. F. Provasi, S. Reine, Z. Rinkevicius, T. A. Ruden, K. Ruud, V. V. Rybkin, P. Salek, C. C. M. Samson, A. M. J. Sánchez de Merás, T. Saue, S. P. A. Sauer, B. Schimmelpfennig, K. Snegov, A. H. Steindal, K. O. Sylvester-Hvid, P. R. Taylor, A. M. Teale, E. I. Tellgren, D. P. Tew, A. J. Thorvaldsen, L. Thøgersen, O. Vahtras, M. A. Watson, D. J. D. Wilson, M. Ziolkowski, and H. Ågren, *Wiley Interdiscip. Rev.: Comput. Mol. Sci.* **4**, 269 (2014).
- ³⁵See <http://daltonprogram.org> for LSDalton, a linear-scaling molecular electronic structure program, Release Dalton2016, 2015.
- ³⁶E. F. Pettersen, T. D. Goddard, C. C. Huang, G. S. Couch, D. M. Greenblatt, E. C. Meng, and T. E. Ferrin, *J. Comput. Chem.* **25**, 1605 (2004).
- ³⁷Molecular graphics (structures and NTO plots) were performed with the UCSF Chimera package. Chimera is developed by the Resource for Biocomputing, Visualization, and Informatics at the University of California, San Francisco (supported by NIGMS P41-GM103311).
- ³⁸M. R. Silva-Junior, S. P. A. Sauer, M. Schreiber, and W. Thiel, *Mol. Phys.* **108**, 453 (2010).
- ³⁹R. Send, V. R. I. Kaila, and D. Sundholm, *J. Chem. Theory Comput.* **7**, 2473 (2011).
- ⁴⁰T. Helgaker, P. Jørgensen, and J. Olsen, in *Molecular Electronic Structure Theory*, 1st ed. (Wiley, Chichester, England, 2000), Chap. 4.
- ⁴¹B. N. Parlett, *The Symmetric Eigenvalue Problem* (Prentice-Hall, 1980).
- ⁴²H. Koch, O. Christiansen, P. Jørgensen, and J. Olsen, *Chem. Phys. Lett.* **244**, 75 (1995).
- ⁴³K. Snegov, T. Schwabe, J. Kongsted, and O. Christiansen, *J. Chem. Phys.* **134**, 104108 (2011).
- ⁴⁴T. Schwabe, K. Snegov, J. M. Haugaard Olsen, J. Kongsted, O. Christiansen, and C. Hättig, *J. Chem. Theory Comput.* **8**, 3274 (2012).

B.7 A local framework for calculating coupled cluster singles and doubles excitation energies (LoFEx-CCSD)

P. Baudin, D. Bykov, D. Liakh, P. Ettelhuber, and K. Kristensen.

Mol. Phys. [MQM2016](#), 1 (2017).

Major contribution: writing process.

Proportional contributions: original idea, and code implementation (eigenvalue solver, and LoFEx structure).

MQM2016

A local framework for calculating coupled cluster singles and doubles excitation energies (LoFEx-CCSD)

Pablo Baudin^a, Dmytro Bykov^a, Dmitry Liakh^b, Patrick Ettenhuber^a and Kasper Kristensen^a

^aqLEAP Center for Theoretical Chemistry, Department of Chemistry, Aarhus University, Aarhus C, Denmark; ^bScientific Computing Group, National Center for Computational Sciences, Oak Ridge National Laboratory, Oak Ridge, TN, USA

ABSTRACT

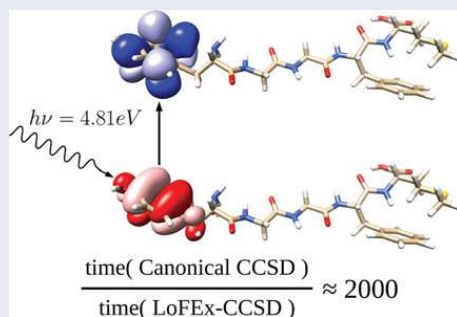
The recently developed Local Framework for calculating Excitation energies (LoFEx) is extended to the coupled cluster singles and doubles (CCSD) model. In the new scheme, a standard CCSD excitation energy calculation is carried out within a reduced excitation orbital space (XOS), which is composed of localised molecular orbitals and natural transition orbitals determined from time-dependent Hartree–Fock theory. The presented algorithm uses a series of reduced second-order approximate coupled cluster singles and doubles (CC2) calculations to optimise the XOS in a black-box manner. This ensures that the requested CCSD excitation energies have been determined to a predefined accuracy compared to a conventional CCSD calculation. We present numerical LoFEx-CCSD results for a set of medium-sized organic molecules, which illustrate the black-box nature of the approach and the computational savings obtained for transitions that are local compared to the size of the molecule. In fact, for such local transitions, the LoFEx-CCSD scheme can be applied to molecular systems where a conventional CCSD implementation is intractable.

ARTICLE HISTORY

Received 13 October 2016
Accepted 25 January 2017

KEYWORDS

Excitation energies; large molecules; coupled cluster theory; CCSD; local correlation



1. Introduction

Molecular properties form a direct link between fundamental quantum mechanical equations and experimental measurements. The development of accurate theoretical methods for determining molecular properties is thus of great importance for the advancement of molecular sciences. Coupled cluster (CC) theory [1,2] is considered the method of choice for high accuracy calculations on small molecular systems dominated by a single configuration. For ground state energies and static properties, one often considers a CC hierarchy of wave function models—MP2 [3] (second-order Møller-Plesset perturbation theory), CCSD [4] (coupled cluster singles

and doubles), CCSD(T) [5] (coupled cluster singles and doubles with perturbative triples), etc.—in which the accuracy of the calculated properties is systematically improved. For frequency-dependent molecular properties, including excitation energies, one often relies on response theory [6–10] and the CC response hierarchy containing the CC2 [11] (second-order approximate coupled cluster singles and doubles), CCSD [12], CC3 [13] (approximate coupled cluster singles, doubles, and triples), etc. models has proven to be successful [14]. Other CC models have been designed for the calculation of frequency-dependent properties, mainly based on the equation-of-motion (EOM) formalism [15–18]. For second-order models we mention the

CONTACT Pablo Baudin  pablo.baudin@chem.au.dk

© 2017 Informa UK Limited, trading as Taylor & Francis Group

EOM-MBPT2 [19,20] and the algebraic diagrammatic construction (ADC(2)) [21] models. A series of triples corrected models have also been designed for the calculation of excitation energies [22–25].

In conventional implementations, the computational scalings of the CC2, CCSD and CC3 models are N^5 , N^6 and N^7 , respectively, where N is a measure of the size of the system. These scalings inhibit the practical applications of the CC models to large molecular systems of interest in contemporary molecular sciences. The correlated CC calculation primarily describes local electron correlation effects, such as the short-ranged electron–electron repulsion effects (the Coulomb hole in the wave function) and dispersion effects. The steep scaling of the CC methods—both with respect to time and memory requirements—stems from the fact that conventional CC implementations are expressed in terms of the highly nonlocal canonical molecular orbitals (CMOs), which makes a local description of electron correlation effects impossible. Due to the scaling problems of the CC models, many practical applications today use time-dependent density functional theory (TDDFT), which can be applied to rather large molecular systems. Although DFT calculations have lower computational costs and often provide useful insights, it is well known that DFT has several limitations [26], including the description of doubly excited states, Rydberg states, and charge-transfer excitations in extended systems [27].

As an alternative to TDDFT calculations, several CC approaches for calculating excitation energies with reduced costs have been suggested. The most common strategy, pioneered by Pulay and Saebø for ground state energies [28,29], consists in reducing the number of wave function parameters by generating a localised orbital space. The occupied orbitals are localised and kept orthogonal, while the virtual space is transformed to non-orthogonal projected atomic orbitals (PAOs) [30–33] or pair natural orbitals (PNOs) [34–36]. An alternative approach proposed in the context of the incremental scheme is based on a many-body expansion of the CCSD excitation energies [37]. Furthermore, in multi-level CC theory [38–40] the orbital space is partitioned based on chemical intuition, and different CC models are used to treat different parts of the molecule to achieve a reduced cost by treating the less important part of the system with the less demanding CC models.

We have recently introduced a local framework for calculating excitation energies (LoFEx) at the CC2 level of theory [41]. In the LoFEx scheme the occupied and virtual CMOs are transformed into a mixed orthogonal orbital space composed of natural transition orbitals [42] (NTOs) and localised molecular orbitals [43,44] (LMOs) for both the occupied and virtual orbital spaces. For

transitions dominated by single-electron replacements (which are targeted in this paper) the mixed orbital space contains the dominant pair of occupied-virtual NTOs, while the remaining orbitals are localised. Conceptually, the NTOs contain information about the main character of the electronic transition, while the LMOs allow for an efficient description of correlation effects. An excitation orbital space (XOS) is then constructed from the mixed orbital space by considering the dominant pair of NTOs as well as a reduced number of LMOs in the vicinity of the NTOs. The XOS is optimised in a black-box manner to ensure that the excitation energy is calculated to the desired precision compared to a conventional CC calculation. The goal of the present paper is to generalise the LoFEx algorithm to CC models beyond the CC2 model. Specifically, we show that the XOS optimisation may be performed at a lower level of theory than the target CC model, exemplified here by CC2-based optimisation to target CCSD excitation energies.

In Section 2, we present an extension of the LoFEx procedure to the next level of the CC response hierarchy by devising an algorithm for calculating CCSD excitation energies [12]. The resulting model is a hybrid approach where the XOS is determined in a black-box manner by a series of CC2 calculations, while a single CCSD calculation is carried out in the final XOS. The algorithm is designed such that the optimised XOS is as small as possible, while ensuring that the CCSD excitation energy is determined to the predefined accuracy. Numerical results are presented and discussed in Section 3 to support the theoretical foundations of the LoFEx-CCSD model. We also note that the present work is a precursor for developing a LoFEx scheme for the next member of the CC response hierarchy, i.e. the CC3 model [13].

2. Theory

In Section 2.1, we summarise the determination of excitation energies at the CCSD level of theory, while Section 2.2 is dedicated to the introduction of the new LoFEx-CCSD algorithm.

2.1. The CCSD model for excitation energies

The CCSD ground state amplitude equations in the absence of external perturbations are given by [4],

$$\begin{aligned}\Omega_{\mu_1} &= \langle \mu_1 | \exp(-T) H \exp(T) | \text{HF} \rangle = 0, \\ \Omega_{\mu_2} &= \langle \mu_2 | \exp(-T) H \exp(T) | \text{HF} \rangle = 0,\end{aligned}\quad (1)$$

where $\{|\text{HF}\rangle, |\mu_1\rangle, |\mu_2\rangle\}$ denote the Hartree–Fock (HF) ground state and the singles and doubles excitation manifolds. The cluster operator is given by $T = T_1 + T_2 + \dots$, where $T_i = \sum_{\mu_i} t_{\mu_i} \tau_{\mu_i}$ denotes a cluster operator where t_{μ_i} is a cluster amplitude, τ_{μ_i} is an excitation operator and i denotes the excitation level. H is the usual non-relativistic molecular electronic Hamiltonian.

In CC response theory, CCSD excitation energies ω are determined by solving the CCSD Jacobian eigenvalue problem [12,45], which may be written in the form,

$$\mathbf{A}\mathbf{b} = \omega\mathbf{b} \quad (2)$$

where the Jacobian is given by,

$$A_{\mu_i\nu_j} = \frac{\partial \Omega_{\mu_i}}{\partial t_{\nu_j}}, \\ = \langle \mu_i | \exp(-T)[H, \tau_{\nu_j}] \exp(T) | \text{HF} \rangle \quad (3)$$

We note that the CCSD Jacobian is nonsymmetric and that it depends on the ground state amplitudes.

In a conventional CCSD calculation, the formal procedure for determining excitation energies after the HF CMOs have been determined is thus to (i) solve Equation (1) to determine the CCSD ground state amplitudes, (ii) use these amplitudes to determine the CCSD Jacobian according to Equation (3) and (iii) obtain the requested excitation energies by solving the eigenvalue equation in (2). The CCSD amplitude equations in (1) are non-linear and are usually solved using a direct inversion of the iterative subspace (DIIS) [46], in our implementation the conjugate residual with optimal trial vectors (CROP) [47,48] method is used since it can often be less memory intensive. The solution of the eigenvalue problem in Equation (2) on the other hand is usually performed via a subspace method such as the Davidson procedure [49] generalised to nonsymmetric matrices [50]. Both of these procedures are iterative and scale as N^6 with the system size which prevents their application to large molecular systems.

2.2. The LoFEx-CCSD model

For the determination of CCSD excitation energies that correspond to transitions localised in space, it is possible to reduce the scaling of the procedure described in Section 2.1 such that it becomes independent of the system size. This is achieved in the LoFEx-CCSD model that we describe in the remainder of this section.

In the LoFEx scheme, a mixed orbital space containing a combination of NTOs [42] and LMOs is used to reduce the dimensions of the CC problems in Equations

(1) and (2). NTOs can be generated from time-dependent Hartree-Fock theory (TDHF) by performing a singular-value-decomposition (SVD) of the TDHF transition density matrix \mathbf{b} (see Refs. [41,51] for details). The transformation matrices \mathbf{U} and \mathbf{V} required to obtain occupied valence and virtual NTOs, respectively, are then obtained by solving the following eigenvalue equations:

$$\tilde{\mathbf{b}}^\dagger \tilde{\mathbf{b}} \mathbf{u}_k = \lambda_k \mathbf{u}_k, \quad k = 1, 2, \dots, N_o, \quad (4)$$

$$\tilde{\mathbf{b}} \tilde{\mathbf{b}}^\dagger \mathbf{v}_k = \lambda'_k \mathbf{v}_k, \quad k = 1, 2, \dots, N_v, \quad (5)$$

$$\mathbf{U} = (\mathbf{u}_1, \mathbf{u}_2, \dots, \mathbf{u}_{N_o}), \quad (6)$$

$$\mathbf{V} = (\mathbf{v}_1, \mathbf{v}_2, \dots, \mathbf{v}_{N_v}), \quad (7)$$

where N_o (N_v) is the number of valence (virtual) orbitals. Assuming $N_o \leq N_v$, it follows that $\lambda_k \equiv \lambda'_k$ for $k = 1, 2, \dots, N_o$, while $\lambda'_k = 0$ for $k = N_o + 1, \dots, N_v$. The singular values λ_k can be interpreted as a measure of the importance of each pair of NTOs for the description of the transition represented by $\tilde{\mathbf{b}}$ [42].

In this paper we consider transitions dominated by single-electron replacements. In such cases, the SVD of the TDHF density matrix results in one occupied-virtual pair of NTOs with a singular value very close to one, while the remaining NTOs with much smaller singular values yield little information about the electronic transition. We therefore keep only the dominant pair of NTOs, which represents the main character of the transition, while the rest of the orbital space is localised to enable a compact description of electron correlation effects in the CC part of the calculation. For the orbital localisation we minimise the second power of the second moment of the orbitals [43], since this localisation strategy is known to provide a good compromise between computational cost and spatial locality [44]. We stress that the use of NTOs makes the orbital space specific to a given transition, and a different mixed orbital space should thus be constructed for each transition of interest.

For excitations that are local compared to the size of the molecular system under consideration, the generation of a mixed NTO/LMO space, as described above, can lead to significant computational savings by truncating the LMO space. Such a truncated orbital space containing the dominant pair of NTOs and a subset of the LMOs is denoted the excitation orbital space (XOS). The main task of the black-box LoFEx algorithm is to ensure that the XOS is large enough to result in accurate excitation energies while remaining as small as possible such that significant computational savings are obtained. To achieve this goal we first define an effective distance

measure \tilde{r}_p given by,

$$\tilde{r}_p = \min_A \left(\frac{r_{Ap}}{Q_A^{\text{NTO,o}}}, \frac{r_{Ap}}{Q_A^{\text{NTO,v}}} \right) \quad (8)$$

where $Q_A^{\text{NTO,o}}$ and $Q_A^{\text{NTO,v}}$ are the Löwdin atomic charges for atom A of the occupied and virtual NTOs, respectively, while r_{Ap} is the distance from the centre of charge of the p th LMO to atom A . The scaling of the distance by the inverse Löwdin atomic charge (values between 0 and 1) enables the definition of an effective distance measure, also when the NTOs are distributed across several atomic centres. The LMOs are ordered according to the distance measure in Equation (8), and the size of the XOS is increased until the excitation energy of interest has been determined to a predefined accuracy (τ_{XOS}). The LoFEx algorithm is depicted schematically in Figure 1 and it may be summarised by the following main steps:

- (1) Carry out a HF ground state calculation on the whole system to generate a set of occupied and virtual CMOs.
- (2) Carry out a TDHF calculation on the whole system and generate NTOs by performing an SVD of the TDHF transition density matrix \mathbf{b} .
- (3) Generate LMOs by localising all orbitals, except the dominant pair of NTOs.
- (4) Order the LMOs according to the measure in Equation (8).
- (5) Determine the optimised XOS:
 - (a) Choose a subset of orbitals from the ordered list (defining $\text{XOS}^{(1)}$) and calculate excitation energy $\omega^{(1)}$ for this set of orbitals, i.e. solve Equations (1) and (2) in $\text{XOS}^{(1)}$.
 - (b) Add a new set of orbitals from the ordered list of LMOs to the existing $\text{XOS}^{(1)}$ to generate $\text{XOS}^{(2)}$. Calculate excitation energy $\omega^{(2)}$ in the new space ($\text{XOS}^{(2)}$) and compare to $\omega^{(1)}$.
 - (c) Continue this procedure until the change in excitation energy for two subsequent calculations (i.e. $|\omega^{(n)} - \omega^{(n-1)}| < \tau_{\text{XOS}}$).

Again, it should be emphasised that steps 2–5 of the outlined procedure are applied to each transition of interest separately. A more detailed description of the LoFEx algorithm, including the treatment of several excited states and reduction of the atomic orbital space used to expand the molecular orbitals (MOs), is given in Ref. [41].

From a conceptual point of view, it should be noted that the Fock matrix entering the CC equations (as a part of the Hamiltonian) has been determined in a HF

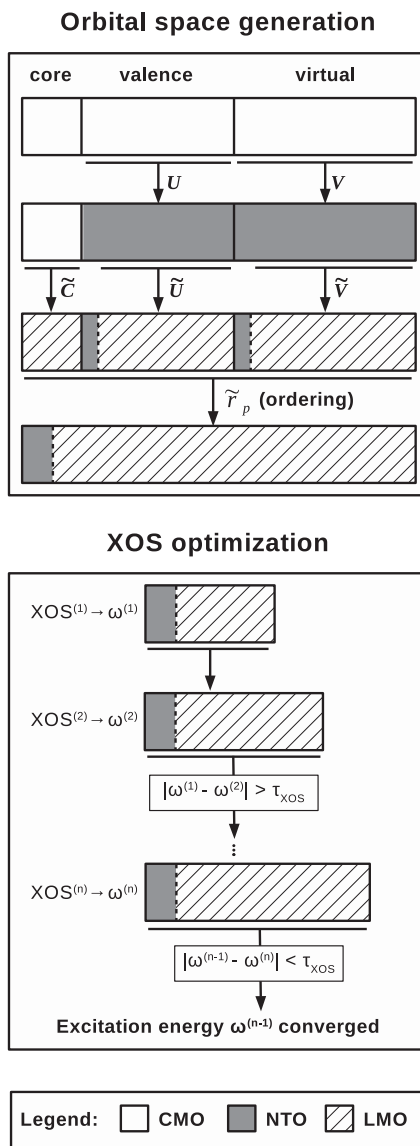


Figure 1. Illustration of the LoFEx procedure. Top: Generation of the mixed molecular orbital space; starting from canonical molecular orbitals (CMOs), U and V represent the valence and virtual transformation matrices to the natural transition orbital (NTO) space, while \tilde{C} , \tilde{U} , and \tilde{V} are transformation matrices to the local basis (LMO) for core, valence, and virtual orbitals, respectively, excluding the dominant pair of NTOs. \tilde{r}_p is the effective distance measure given by Equation (8). Bottom: Determination of the excitation orbital space (XOS), where $\omega^{(i)}$ is the excitation energy corresponding to the i th excitation orbital space ($\text{XOS}^{(i)}$) and τ_{XOS} is the main LoFEx threshold.

calculation on the *total* molecular system and thus contains information about long-range electronic interactions among all electrons in the molecule. Thus, even though a CC calculation within a given XOS involves only the dominant pair of NTOs and subset of LMOs, long-range electronic interactions to the part of the molecule outside the XOS are still included in an indirect manner via the Fock matrix. Concerning the computational effort, it can be expected that the cost of the complete LoFEx calculation will be dominated by the underlying TDHF calculation on the full system for large systems if the excitation of interest is local compared to the size of the molecule. In fact, for such a case, the CC part of the LoFEx calculation is independent on the size of the total molecule. This implies that highly accurate excitation energies of CC quality can be obtained with a computational cost comparable to TDDFT.

Any CC model can in principle be used to calculate excitation energies in step 5 above. However, it is possible to obtain additional computational savings for the CCSD model (and for higher level CC models) by noting that the calculation in the final XOS is carried out only to verify that the previous calculation was indeed converged (see Figure 1). Thus, the penultimate CC calculation is already accurate enough with respect to τ_{XOS} , while being much cheaper than the final XOS calculation due to the sixth-order scaling of the CCSD model. It is therefore possible to devise a LoFEx-CCSD scheme, where the XOS optimisation procedure in Figure 1 is carried out using the cheaper CC2 model to determine the penultimate XOS ($\text{XOS}^{(n-1)}$ in Figure 1), followed by a single CCSD calculation in $\text{XOS}^{(n)}$. This new LoFEx-CCSD model can be summarised as follows (a superscript has been added to emphasise the model used to calculate the excitation energy):

- (1) CC2 optimisation:
 - CC2 calculation in $\text{XOS}^{(1)}$ to calculate $\omega_{\text{CC2}}^{(1)}$.
 - CC2 calculation in $\text{XOS}^{(2)}$ to calculate $\omega_{\text{CC2}}^{(2)}$.
 - ...
 - CC2 calculation in $\text{XOS}^{(n-1)}$ to calculate $\omega_{\text{CC2}}^{(n-1)}$.
 - CC2 calculation in $\text{XOS}^{(n)}$ to calculate $\omega_{\text{CC2}}^{(n)}$, concluding that $|\omega_{\text{CC2}}^{(n)} - \omega_{\text{CC2}}^{(n-1)}| < \tau_{\text{XOS}}$.
- (2) CCSD calculation in $\text{XOS}^{(n)}$ to calculate $\omega_{\text{CCSD}}^{(n)}$, which is the target excitation energy of the calculation.

The CC2 and CCSD calculations in LoFEx scale with the fifth and sixth powers of the size of the XOS, respectively. Avoiding the CCSD calculation in $\text{XOS}^{(n)}$ with such a hybrid procedure is thus expected to reduce the

computational effort tremendously. The capacity of the LoFEx-CCSD model to result in excitation energies of CCSD quality relies on the single assumption that the CC2 model provides a good description of the CCSD electronic transitions. From a theoretical point of view, this assumption is supported by the fact that the CC2 model may be obtained from the CCSD working equations by keeping only the terms of the CCSD doubles equations that are first-order in a Møller–Plesset perturbation expansion, while the singles equations are retained in their original form [11]. This approximation of the CCSD doubles equations in the CC2 model leads to the well-known fact that the CC2 model cannot be used to accurately describe electronic transitions dominated by more than one-electron replacements. For that reason, and because we rely on TDHF NTOs, the LoFEx-CCSD procedure can only be expected to work properly when applied to transitions dominated by one-electron replacements.

3. Results

In this section, we present proof-of-concept calculations to assess the validity of the LoFEx-CCSD model introduced in Section 2.2. Two main questions have to be addressed; (i) does the LoFEx-CCSD scheme result in excitation energies of CCSD quality? (ii) Is it computationally more efficient than a conventional implementation of the CCSD model?

3.1. Computational details

We consider the following molecules, which are depicted in Figure 2:

- Caprylic acid
- Lauric acid
- Palmitic acid
- 15-Oxopentadecanoic acid (15-OPDA)
- Prostacyclin
- An α -helix composed of 8 glycine residues (α -Gly₈)
- Leupeptin
- Latanoprost
- Met-enkephalin

The geometries have been optimised at the RI-MP2 [53] level of theory using the ORCA program [54]. The basis sets used for the geometry optimisations and the Cartesian coordinates are given in Ref. [41] and its supporting information.

We consider calculations of the lowest vertical singlet excitation energy using the cc-pVDZ and aug-cc-pVDZ

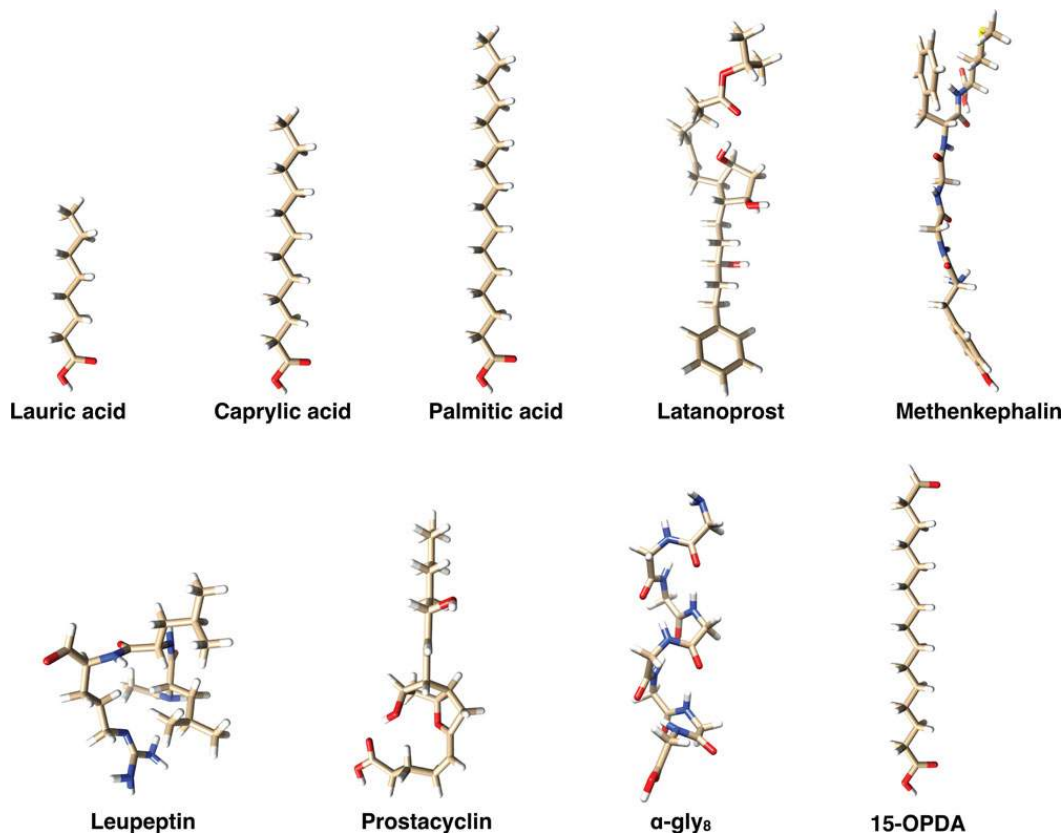


Figure 2. Three-dimensional stick representation of the molecules used in this study [52].

basis sets [55,56] where the prime indicates that diffuse functions have been removed from the hydrogen atoms. Ideally, basis sets of triple- ζ quality or better should be used for CCSD excitation energies; however, the use of the smaller basis sets of double- ζ quality for these proof-of-concept calculations allows us to carry out the full (conventional) CCSD calculations for most of the medium-sized molecules in Figure 2, which would not be possible using larger basis sets. For the CC2 calculations that are used to determine the XOS according to the strategy outlined in Section 2.2, we have used density fitting techniques, i.e. the resolution of the identity, RI-CC2 model [57]. For these calculations, the cc-pVDZ-RI and aug-cc-pVDZ-RI' basis sets [58] were used in combination with the cc-pVDZ and aug-cc-pVDZ' regular basis sets. The frozen core approximation was used in all calculations.

A pilot implementation of the LoFEx-CCSD model described in Section 2.2 has been introduced in a local version of the LSDALTON program [59]. The

parameters defining the XOS optimisation procedure in Figure 1 (bottom) were set as in Ref. [41], i.e. the main LoFEx threshold $\tau_{\text{XOS}} = 0.02$ eV, and the number of orbitals added to the XOS in each expansion step was set to 10 times the average number of MOs per atom. Since this is a conservative choice for the expansion step, we expect CCSD excitation energies with errors of ≈ 0.02 eV or below compared to a full CCSD calculation. We do note that τ_{XOS} is a tunable parameter which can be chosen according to the desired accuracy. The full CCSD calculations were carried out using the Turbomole program package [60].

3.2. Results for the LoFEx-CCSD model

In Tables 1 and 2 we present the results of the LoFEx-CCSD model for the molecules presented in Figure 2 using the cc-pVDZ and aug-cc-pVDZ' basis sets, respectively. We give the lowest excitation energy ω calculated using LoFEx and the absolute error $\delta\omega$ compared to a full

Table 1. Results from the LoFEx-CCSD model using the cc-pVDZ basis. Excitation energies ω (eV); errors compared to full CCSD calculation (eV); number of MOs in LoFEx $XOS^{(n-1)}$ and full calculations, and estimated speed-ups of the most expensive O^2V^4 scaling step of the CCSD part of the calculation.

| System | ω | $\delta\omega$ | #MOs (LoFEx) | #MOs (full) | Speed-up |
|----------------------------|----------|----------------|--------------|-------------|----------|
| Caprylic acid | 6.11 | 0.00 | 93 | 210 | 113 |
| Lauric acid | 6.10 | 0.00 | 91 | 302 | 1074 |
| Palmitic acid | 6.10 | 0.00 | 91 | 394 | 5191 |
| 15-OPDA | 4.45 | 0.00 | 90 | 374 | 4561 |
| Prostacyclin | 5.99 | 0.00 | 190 | 485 | 232 |
| α -Gly ₈ | 5.58 | 0.00 | 211 | 559 | 368 |
| Leupeptin | 4.31 | 0.01 | 94 | 580 | 50259 |
| Latanoprost | 5.12 | 0.00 | 185 | 603 | 1181 |
| Met-enkephalin | 4.94 | - | 202 | 695 | 1758 |

Table 2. Results from the LoFEx-CCSD model using the aug-cc-pVDZ' basis. Excitation energies ω (eV); errors compared to full CCSD calculation (eV); number of MOs in LoFEx $XOS^{(n-1)}$ and full calculations, and estimated speed-ups of the most expensive O^2V^4 scaling step of the CCSD part of the calculation.

| System | ω | $\delta\omega$ | #MOs (LoFEx) | #MOs (full) | Speed-up |
|----------------------------|----------|----------------|--------------|-------------|----------|
| Caprylic acid | 6.04 | 0.02 | 126 | 300 | 155 |
| Lauric acid | 6.02 | 0.00 | 241 | 428 | 27 |
| Palmitic acid | 6.02 | 0.00 | 237 | 556 | 156 |
| 15-OPDA | 4.38 | 0.00 | 125 | 536 | 6511 |
| Prostacyclin | 5.39 | 0.00 | 525 | 710 | 6 |
| α -Gly ₈ | 5.54 | - | 461 | 856 | 40 |
| Leupeptin | 4.23 | - | 266 | 850 | 1059 |
| Latanoprost | 5.02 | - | 264 | 882 | 1394 |
| Met-enkephalin | 4.81 | - | 298 | 1055 | 2021 |

CCSD calculation. For the largest molecules, the steep scaling of the standard CCSD model prevented the calculation of the reference excitation energies, and $\delta\omega$ is therefore not listed for these cases. In addition, we give the number of MOs in the LoFEx ($XOS^{(n-1)}$) and full calculations. Since our LoFEx-CCSD scheme is a pilot implementation, we do not report explicit timings. However, in order to get an idea of the potential computational savings that can be obtained using LoFEx, we report estimated speed-ups for the CCSD calculations in $XOS^{(n-1)}$ compared to the full CCSD calculations. The most expensive step of the CCSD algorithm scales as O^2V^4 for both the ground state [4,61] and excitation energy [12,62] calculations, where O and V denote the number of occupied and virtual orbitals, respectively. The estimated speed-up in the last column of Tables 1 and 2 is thus calculated as the ratio between O^2V^4 for the full system and O^2V^4 for $XOS^{(n-1)}$. We note that such speed-ups can only be taken as a rough estimate for the computational savings since the accumulated time spent in the CC2 calculations during the XOS optimisation has been omitted. However, due to the difference between the CCSD and CC2 computational requirements, the CCSD step in $XOS^{(n-1)}$ is

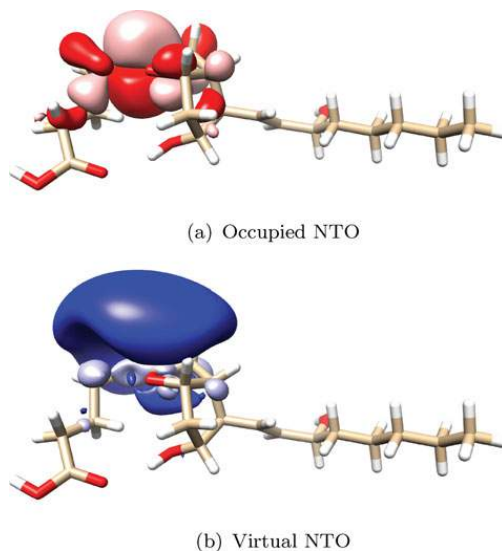


Figure 3. Occupied (a) and virtual (b) TDHF natural transition orbitals (NTOs) for the lowest transition of prostacyclin using the aug-cc-pVDZ' basis set. The contour plot value was set to 0.02 a.u. [52]. (a) Occupied NTO. (b) Virtual NTO.

expected to require more computational efforts than the CC2 calculations in the XOS optimisation.

It is evident from Tables 1 and 2 that the errors of the LoFEx-CCSD scheme compared to a full CCSD calculation are of the order of the LoFEx threshold $\tau_{XOS} = 0.02$ eV or below. This demonstrates that, at least for the systems and transitions considered here, it is sufficient to carry out the black-box XOS optimisation at the CC2 level of theory and calculate the CCSD excitation energy only in the penultimate XOS .

Due to the sixth-order scaling of CCSD calculations, large estimated speed-ups are obtained when the XOS is reduced significantly compared to the full calculation. The most extreme case is for leupeptin in a cc-pVDZ basis where the number of MOs is reduced by a factor 6, resulting in an estimated speed-up of around 50,000. It is also clear that the speed-up depends very much on the locality of the transition. For example, prostacyclin and met-enkephalin in the aug-cc-pVDZ' basis are associated with speed-ups of 6 and 2021, respectively, indicating that the considered transition for met-enkephalin is much more local than the one for prostacyclin. This difference may be rationalised from the NTOs for the lowest transitions of prostacyclin and met-enkephalin, which are plotted in Figures 3 and 4, respectively. It is seen that the NTOs for met-enkephalin are very local compared to the size of the molecule, while the NTOs for prostacyclin are significantly more diffuse (in particular the virtual NTO).

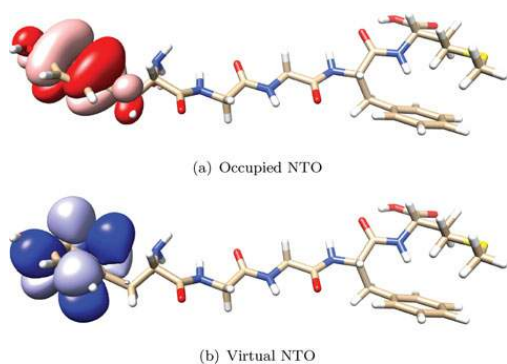


Figure 4. Occupied (a) and virtual (b) TDHF natural transition orbitals (NTOs) for the lowest transition of met-enkephalin using the aug-cc-pVDZ' basis set. The contour plot value was set to 0.02 a.u. [52]. (a) Occupied NTO. (b) Virtual NTO.

The more diffuse character of the prostacyclin transition thus requires more important coupling effects from the LMOs in the vicinity of the NTOs. These coupling effects are included dynamically by the LoFEx optimisation procedure and lead to a significantly larger XOS (298 MOs for met-enkephalin compared to 525 MOs for prostacyclin). The differences in the total size of the molecules and in the locality of the transitions thus explain the large variation in the estimated speed-ups for met-enkephalin and prostacyclin.

Regarding the effect of the basis set on the transitions, as expected, the diffuse functions in the aug-cc-pVDZ' basis bring the excitation energies down by roughly 0.1 eV (see Tables 1 and 2). For prostacyclin, however, the lowest excitation energy goes down by 0.6 eV (from 5.99 to 5.39 eV). This change in the energy is due to a reordering of the spectrum in which the diffuse state corresponding to the NTOs in Figure 3 is stabilised by the aug-cc-pVDZ' basis and become the lowest excited state. This effect is also reflected in the XOS optimisation procedure where two additional steps are required for the lowest transition of prostacyclin in the aug-cc-pVDZ' basis compared to the cc-pVDZ basis.

Finally, let us comment on the strengths and weaknesses of the LoFEx scheme. The quality of the results obtained from a LoFEx-CCSD calculation of excitation energies relies on the assumption that the XOS determined at the CC2 level is well adapted to describe the electronic transition at the CCSD level. In other words, it is assumed that the CC2 model describes properly all the important effects of the targeted CCSD transitions. In addition, if the transition is nonlocal—i.e. it involves significant changes in the electron density in all regions of

a large molecule—then the XOS of a LoFEx-CCSD calculation will include the full MO space and thus be as expensive as a standard CCSD calculation plus the small overhead due to the TDHF and CC2 parts of the LoFEx scheme. However, significant computational savings can be obtained if the excitation is local compared to the size of the total molecular system. This is illustrated by the estimated speed-ups in Tables 1 and 2, but also by the fact that some of the calculations could not be carried out using a conventional CCSD implementation (e.g. met-enkephalin), while the LoFEx scheme allows us to determine excitation energies of CCSD quality for all of the considered molecules. Furthermore, we note that the estimated speed-ups are in agreement with the actual speed-ups presented in Ref. [41] for the CC2 model (i.e. larger speed-ups are obtained) since we are now considering a higher scaling model and since the time-dominating step is now performed in an even smaller XOS.

4. Conclusion and perspectives

We have generalised our recently developed LoFEx approach to enable the determination of CCSD excitation energies for large molecular systems at a low computational cost, provided that the transitions of interest are local in space. In LoFEx, the CC amplitude and Jacobian eigenvalue equations are solved in a transition-specific excitation orbital space (the XOS) composed of the dominant pair of NTOs and a reduced set of LMOs. The XOS is optimised in a black-box manner to ensure that the requested excitation energies are determined to a predefined accuracy compared to a full CC calculation.

Our new LoFEx-CCSD algorithm is a hybrid scheme where the XOS is determined dynamically by carrying out a sequence of CC2 calculations of increasing size, while only one CCSD calculation is carried out in the optimised XOS. The XOS used for the CCSD calculation is chosen to be as small as possible to reduce the computational effort, while still ensuring that the CCSD excitation energy is determined to the predefined precision (0.02 eV in the present work, but it is a tunable parameter set by the user).

If the transition is nonlocal, the LoFEx-CCSD scheme reproduces the standard CCSD calculation and thus do not lead to computational savings. However, large computational savings can be obtained if the excitation is local compared to the size of the total molecular system, and, for these cases, CCSD excitation energies that are out of reach using a conventional implementation can be determined using the LoFEx-CCSD scheme. In fact, if the transition of interest is sufficiently local, the calculations of LoFEx-CCSD excitation energies is only limited by the prerequisite TDHF calculation. Thus, for such local transitions, the presented scheme yields excitation energies of

CCSD quality with a computational cost comparable to TDDFT.

One significant advantage of the LoFEx strategy is that once the mixed orbital space has been defined, any CC implementation can be used to optimise the XOS and calculate the final excitation energies. Indeed, the XOS, defines a subset of orthogonal occupied and virtual orbitals to which is associated a set of atomic functions. If the Fock matrix in the XOS is diagonalised, pseudo-canonical orbitals are obtained and a standard canonical implementation of CC can be used in that space. As a consequence, LoFEx could also be straightforwardly combined with other local approaches relying on, e.g. PNOs or PAOs, to further reduce the computational cost of LoFEx. As mentioned previously, we will also consider extending the LoFEx procedure to the CC3 model and to the calculation of transition strengths.

Acknowledgments

The research leading to these results has received funding from the European Research Council under the European Unions Seventh Framework Programme (FP/2007-2013)/ERC Grant Agreement no. 291371.

DB acknowledges the Marie Curie Individual Fellowship funding for 'DECOS', project number 657514.

This research used resources of the Oak Ridge Leadership Computing Facility at the Oak Ridge National Laboratory, which is supported by the Office of Science of the U.S. Department of Energy under Contract No. DE-AC05-00OR22725.


Disclosure statement

No potential conflict of interest was reported by the authors.

Funding

European Research Council: European Unions Seventh Framework Programme (FP/2007-2013) [Grant Number 291371]; Marie Curie Individual Fellowship, Project Number 657514; Office of Science of the U.S. Department of Energy [Grant Number DE-AC05-00OR22725].

ORCID

Pablo Baudin  <http://orcid.org/0000-0001-7233-645X>

References

- [1] J. Čížek, *J. Chem. Phys.* **45**(11), 4256 (1966).
- [2] I. Shavitt and R.J. Bartlett, *Many-Body Methods in Chemistry and Physics: Many-Body Perturbation Theory and Coupled-Cluster Theory* (Cambridge University Press, Cambridge, 2009).
- [3] C. Møller and M.S. Plesset, *Phys. Rev.* **46**(7), 618 (1934).
- [4] G.D. Purvis and R.J. Bartlett, *J. Chem. Phys.* **76**(1982), 1910 (1982).
- [5] K. Raghavachari, G.W. Trucks, J.A. Pople, and M. Head-Gordon, *Chem. Phys. Lett.* **157**(6), 479 (1989).
- [6] H.J. Monkhorst, *Int. J. Quantum Chem.* **12**(S11), 421 (1977).
- [7] E. Dalgaard and H.J. Monkhorst, *Phys. Rev. A* **28**(3), 1217 (1983).
- [8] J. Olsen and P. Jørgensen, *J. Chem. Phys.* **82**(7), 3235 (1985).
- [9] H. Koch and P. Jørgensen, *J. Chem. Phys.* **93**(5), 3333 (1990).
- [10] A.E. Kondo, P. Piecuch, and J. Paldus, *J. Chem. Phys.* **104**(21), 8566 (1996).
- [11] O. Christiansen, H. Koch, and P. Jørgensen, *Chem. Phys. Lett.* **243**(5-6), 409 (1995).
- [12] H. Koch, H.J.A. Jensen, P. Jørgensen, and T. Helgaker, *J. Chem. Phys.* **93**(5), 3345 (1990).
- [13] O. Christiansen, H. Koch, and P. Jørgensen, *J. Chem. Phys.* **103**(17), 7429 (1995).
- [14] T. Helgaker, S. Coriani, P. Jørgensen, K. Kristensen, J. Olsen, and K. Ruud, *Chem. Rev.* **112**(1), 543 (2012).
- [15] K. Emrich, *Nucl. Phys. A* **351**(3), 397 (1981).
- [16] H. Sekino and R.J. Bartlett, *Int. J. Quantum Chem.* **26**(S18), 255 (1984).
- [17] J.F. Stanton and R.J. Bartlett, *J. Chem. Phys.* **98**(9), 7029 (1993).
- [18] A.I. Krylov, *Annu. Rev. Phys. Chem.* **59**(1), 433 (2008).
- [19] J.F. Stanton and J. Gauss, *J. Chem. Phys.* **103**(3), 1064 (1995).
- [20] S.R. Gwaltney, M. Nooijen, and R.J. Bartlett, *Chem. Phys. Lett.* **248**(3-4), 189 (1996).
- [21] J. Schirmer, *Phys. Rev. A* **26**(5), 2395 (1982).
- [22] O. Christiansen, H. Koch, and P. Jørgensen, *J. Chem. Phys.* **105**(4), 1451 (1996).
- [23] J.D. Watts and R.J. Bartlett, *Chem. Phys. Lett.* **233**(1-2), 81 (1995).
- [24] J.D. Watts and R.J. Bartlett, *Chem. Phys. Lett.* **258**(5-6), 581 (1996).
- [25] K. Kowalski and P. Piecuch, *J. Chem. Phys.* **120**(4), 1715 (2004).
- [26] A.J. Cohen, W.Y.P. Mori-Sánchez, P. Mori-Sánchez, and W. Yang, *Science* **321**(5890), 792 (2008).
- [27] A. Dreuw and M. Head-Gordon, *J. Am. Chem. Soc.* **126**(5), 4007 (2004).
- [28] P. Pulay, *Chem. Phys. Lett.* **100**(2), 151 (1983).
- [29] S. Sæbø and P. Pulay, *Chem. Phys. Lett.* **113**(1), 13 (1985).
- [30] T.D. Crawford and R.A. King, *Chem. Phys. Lett.* **366**(5-6), 611 (2002).
- [31] T. Korona and H.J. Werner, *J. Chem. Phys.* **118**(7), 3006 (2003).
- [32] D. Kats, T. Korona, and M. Schütz, *J. Chem. Phys.* **125**(10), 104106 (2006).
- [33] D. Kats and M. Schütz, *J. Chem. Phys.* **131**(12), 124117 (2009).
- [34] B. Helmich and C. Hättig, *J. Chem. Phys.* **135**(21), 214106 (2011).
- [35] B. Helmich and C. Hättig, *J. Chem. Phys.* **139**(8), 084114 (2013).
- [36] A.K. Dutta, F. Neese, and R. Izsák, *J. Chem. Phys.* **145**(3), 034102 (2016).
- [37] R.A. Mata and H. Stoll, *J. Chem. Phys.* **134**(3), 034122 (2011).

- [38] R.H. Myhre, A.M.J. Sánchez de Merás, and H. Koch, *Mol. Phys.* **111**(February 2016), 1109 (2013).
- [39] R.H. Myhre, A.M.J. Sánchez de Merás, and H. Koch, *J. Chem. Phys.* **141**(22), 224105 (2014).
- [40] R.H. Myhre and H. Koch, *J. Chem. Phys.* **145**(4), 044111 (2016).
- [41] P. Baudin and K. Kristensen, *J. Chem. Phys.* **144**(22), 224106 (2016).
- [42] R.L. Martin, *J. Chem. Phys.* **118**(11), 4775 (2003).
- [43] B. Jansík, S. Høst, K. Kristensen, and P. Jørgensen, *J. Chem. Phys.* **134**(2011), 194104 (2011).
- [44] I.M. Høyvik and P. Jørgensen, *Chem. Rev.* **116**, 3306 (2016).
- [45] O. Christiansen, P. Jørgensen, and C. Hättig, *Int. J. Quantum Chem.* **68**, 1 (1998).
- [46] P. Pulay, *Chem. Phys. Lett.* **73**(2), 393 (1980).
- [47] P. Eitenhuber and P. Jørgensen, *J. Chem. Theory Comput.* **11**(4), 1518 (2015).
- [48] M. Ziolkowski, V. Weijo, P. Jørgensen, and J. Olsen, *J. Chem. Phys.* **128**(20) (2008).
- [49] E.R. Davidson, *J. Comput. Phys.* **17**(1), 87 (1975).
- [50] K. Hirao and H. Nakatsuji, *J. Comput. Phys.* **45**(2), 246 (1982).
- [51] T. Etienne, *J. Chem. Phys.* **142**(24), 244103 (2015).
- [52] E.F. Pettersen, T.D. Goddard, C.C. Huang, G.S. Couch, D.M. Greenblatt, E.C. Meng and T.E. Ferrin, *J. Comput. Phys.* **25**(13), 1605 (2004); Molecular graphics (Structures and NTO plots) were performed with the UCSF Chimera package. Chimera is developed by the Resource for Biocomputing, Visualization, and Informatics at the University of California, San Francisco (supported by NIGMS P41-GM103311).
- [53] M. Feyereisen, G. Fitzgerald, and A. Komornicki, *Chem. Phys. Lett.* **208**(5-6), 359 (1993).
- [54] F. Neese, *WIREs Comput. Mol. Sci.* **2**, 73 (2012); F. Neese, F. Wennmohs, U. Becker, D. Bykov, D. Ganyushin, A. Hansen, R. Izsak, D.G. Liakos, C. Kollmar, S. Kossmann, D.A. Pantazis, T. Petrenko, C. Reimann, C. Riplinger, M. Roemelt, B. Sandhöfer, I. Schapiro, K. Sivalingam, and B. Wezislá, MPI CEC, Mülheim a.d. Ruhr, Ger. (2015).
- [55] T. Dunning Jr, *J. Chem. Phys.* **90**, 1007 (1989).
- [56] R. Kendall, T. Dunning Jr, and R.J. Harrison, *J. Chem. Phys.* **96**, 6769 (1992).
- [57] C. Hättig and F. Weigend, *J. Chem. Phys.* **113**(13), 5154 (2000).
- [58] C. Hättig and A. Köhn, *J. Chem. Phys.* **117**(15), 6939 (2002).
- [59] K. Aidas, C. Angeli, K.L. Bak, V. Bakken, R. Bast, L. Boman, O. Christiansen, R. Cimraglia, S. Coriani, P. Dahle, E.K. Dalskov, U. Ekström, T. Enevoldsen, J.J. Erikson, P. Eitenhuber, B. Fernández, L. Ferrighi, H. Fliegel, L. Frediani, K. Hald, A. Halkier, C. Hättig, H. Heiberg, T. Helgaker, A.C. Hennum, H. Hettema, E. Hjertenaes, S. Høst, I.M. Høyvik, M.F. Iozzi, B. Jansík, H.J.A. Jensen, D. Jonsson, P. Jørgensen, J. Kauczor, S. Kirpekar, T. Kjærgaard, W. Klopper, S. Knecht, R. Kobayashi, H. Koch, J. Kongsted, A. Krapp, K. Kristensen, A. Ligabue, O.B. Lutnaes, J.I. Melo, K.V. Mikkelsen, R.H. Myhre, C. Neiss, C.B. Nielsen, P. Norman, J. Olsen, J.M.H. Olsen, A. Osted, M.J. Packer, F. Pawłowski, T.B. Pedersen, P.F. Provasi, S. Reine, Z. Rinkevicius, T.a. Ruden, K. Ruud, V.V. Rybkin, P. Sałek, C.C.M. Samson, A.M.J. Sánchez de Merás, T. Saue, S.P.A. Sauer, B. Schimmelpennig, K. Sneskov, A.H. Steindal, K.O. Sylvester-Hvid, P.R. Taylor, A.M. Teale, E.I. Tellgren, D.P. Tew, A.J. Thorvaldsen, L. Thøgersen, O. Vahtras, M.a. Watson, D.J.D. Wilson, M. Ziolkowski, and H. Ågren, *WIREs Comput. Mol. Sci.* **4**(3), 269 (2014); LSDalton, a linear-scaling molecular electronic structure program, Release Dalton2016 (2015), see <http://daltonprogram.org>.
- [60] F. Furche, R. Ahlrichs, C. Hättig, W. Klopper, M. Sierka, and F. Weigend, *WIREs Comput. Mol. Sci.* **4**(2), 91 (2014); TURBOMOLE V6.2 2010, a development of University of Karlsruhe and Forschungszentrum Karlsruhe GmbH, 1989-2007, TURBOMOLE GmbH, since 2007; available from <http://www.turbomole.com>.
- [61] T. Helgaker, P. Jørgensen, and J. Olsen, *Molecular Electronic-Structure Theory*, 1st ed. (John Wiley & Sons, Ltd, Chichester, 2000).
- [62] O. Christiansen, H. Koch, A. Halkier, P. Jørgensen, T. Helgaker, and A.M.J. Sánchez de Merás, *J. Chem. Phys.* **105**(16), 6921 (1996).

B.8 CC2 oscillator strengths within the local framework for calculating excitation energies (LoFEx)

P. Baudin, T. Kjærgaard, and K. Kristensen.

Manuscript submitted to *J. Chem. Phys.* 1 (2017).

Major contributions: original idea, code implementation (RI-CC2 routines, eigenvalue solver, and LoFEx structure), production of the data, and writing process.

CC2 oscillator strengths within the local framework for calculating excitation energies (LoFEx)

Pablo Baudin,^{1, a)} Thomas Kjærgaard,¹ and Kasper Kristensen¹

qLEAP Center for Theoretical Chemistry, Department of Chemistry, Aarhus University, Langelandsgade 140, DK-8000 Aarhus C, Denmark

(Dated: 25 January 2017)

In a recent work [Baudin and Kristensen, *J. Chem. Phys.* **144**, 224106 (2016)], we introduced a local framework for calculating excitation energies (LoFEx), based on second-order approximated coupled cluster (CC2) linear-response theory. LoFEx is a black-box method in which a reduced excitation orbital space (XOS) is optimized to provide coupled cluster (CC) excitation energies at a reduced computational cost. In this article, we present an extension of the LoFEx algorithm to the calculation of CC2 oscillator strengths. Two different strategies are suggested, in which the size of the XOS is determined based on the excitation energy or the oscillator strength of the targeted transitions. The two strategies are applied to a set of medium-sized organic molecules in order to assess both the accuracy and the computational cost of the methods. The results show that CC2 excitation energies and oscillator strengths can be calculated at a reduced computational cost, provided that the targeted transitions are local compared to the size of the molecule. To illustrate the potential of LoFEx for large molecules, both strategies have been successfully applied to the lowest transition of the bivalirudin molecule (4255 basis functions) and compared with time-dependent density functional theory.

I. INTRODUCTION

High-accuracy calculations of electronic absorption spectra can be performed using coupled cluster (CC) response theory¹⁻³ via the computation of excitation energies and oscillator strengths. CC theory is well established as the method of choice for describing the electronic structure of molecules with a ground-state dominated by a single electronic configuration. However, the high-accuracy of CC models comes with a high computational cost and for that reason standard CC calculations of excitation energies and oscillator strengths have been limited to rather small molecules. Less reliable computational models like time-dependent density functional theory (TDDFT) are thus extensively used for the simulation of electronic spectra of medium-sized and large molecules.⁴ We note that the equation-of-motion (EOM) CC formalism is closely related to CC response theory and is often used in the same context.⁵⁻⁷ While EOM and response techniques are identical for the calculation of CC excitation energies, we have chosen to consider CC response theory in this work since it results in size-intensive transition moments, in contrast to EOM-CC theory.⁸

The computational scaling of CC methods with the system size is associated with the usage of canonical Hartree-Fock (HF) orbitals which are generally delocalized in space, while CC theory describes local phenomena (electron correlation effects).⁹ In the last decades, a lot of efforts have been dedicated to the design of low-scaling CC models, primarily for the computation of ground-state energies.⁹⁻¹⁸ More recently, several groups turned their attention to the calculation of excitation en-

ergies and molecular properties using local approximations. The combination of local occupied orbitals with non-orthogonal virtual orbitals (*e.g.* projected atomic orbitals (PAOs) or pair natural orbitals (PNOs)) is widely used to reduce the total number of wave function parameters and it has been applied to the calculation of excitation energies,¹⁹⁻²⁶ transition strengths,^{23,27} and other molecular properties.^{23,27-30} The incremental scheme in which the quantities of interest are expanded in a many-body series has also been applied to the calculation of CC excitation energies³¹ and dipole polarizabilities.³² Another recent development is the multilevel CC theory in which different CC models are used to treat different parts of the system.³³⁻³⁵ In this context, we can also mention the reduced virtual space³⁶ and ONIOM strategies.^{37,38}

In a recent publication,³⁹ we have introduced a new strategy for the calculation of CC excitation energies at a reduced computational cost, in which we focused on the second-order approximated CC singles and doubles (CC2) model. In our local framework for calculating excitation energies (LoFEx), the locality of correlation effects is used to generate a state-specific mixed orbital space composed of the dominant pair of natural transition orbitals (NTOs), obtained from time-dependent Hartree-Fock (TDHF) theory, and localized molecular orbitals (LMOs). This mixed orbital space is well adapted to describe the targeted electronic transition and can be significantly reduced (by discarding a subset of least relevant LMOs in a black-box manner) without affecting the accuracy of the calculated excitation energy. In this way, important computational savings are possible for local transitions in large molecular systems.

In Section II, we briefly summarize how excitation energies and oscillator strengths can be computed at the CC2 level of theory. The LoFEx algorithm for excitation energies is then summarized in Section III, in which we

^{a)} pablo.baudin@chem.au.dk

also suggest two different strategies for computing oscillator strengths within LoFEx. In Section IV, these strategies are compared when applied to the lowest electronic transitions of a set of medium-sized organic molecules. We also present results for a large molecule (bivalirudin) and compare the accuracy and computational efforts of LoFEx with TDDFT/CAM-B3LYP calculations.

II. THE RI-CC2 MODEL FOR OSCILLATOR STRENGTHS

The CC2 model was introduced by Christiansen *et al.*⁴⁰ as an intermediate model between the CCS and CCSD models in the CC hierarchy for the calculation of frequency-dependent properties. CC2 is therefore the first model of the CC hierarchy to include correlation effects and thus constitutes an appropriate starting point for LoFEx. In this section, we summarize how CC2 excitation energies and oscillator strengths can be obtained from response theory.

The CC2 ground-state amplitudes are obtained as solution of the following non-linear equations,⁴⁰

$$\Omega_{\mu_1} = \langle \mu_1 | \hat{H} + [\hat{H}, T_2] | \text{HF} \rangle = 0, \quad (1)$$

$$\Omega_{\mu_2} = \langle \mu_2 | \hat{H} + [F, T_2] | \text{HF} \rangle = 0, \quad (2)$$

where $\{|\text{HF}\rangle, |\mu_1\rangle, |\mu_2\rangle\}$ denote the Hartree-Fock (HF) ground-state and the set of singles and doubles excitation manifolds. F is the Fock operator and \hat{H} is a similarity (T_1)-transformed Hamiltonian,

$$\hat{H} = \exp(-T_1)H \exp(T_1), \quad (3)$$

where $T_i = \sum_{\mu_i} t_{\mu_i} \tau_{\mu_i}$ is a cluster operator, t_{μ_i} is a cluster amplitude, τ_{μ_i} is an excitation operator, and i denotes the excitation level. The T_1 -transformation of the Hamiltonian in Eq. (3) can be transferred to the second-quantization elementary operators, which effectively corresponds to a modification of the molecular orbital (MO) transformation matrices \mathbf{C} with the singles amplitudes,^{41,42}

$$\begin{aligned} X_{\alpha i} &= C_{\alpha i} & X_{\alpha a} &= C_{\alpha a} - \sum_i C_{\alpha i} t_i^a \\ Y_{\alpha i} &= C_{\alpha i} + \sum_a C_{\alpha a} t_i^a & Y_{\alpha a} &= C_{\alpha a} \end{aligned} \quad (4)$$

A two-electron T_1 -transformed integral in the Mulliken notation can now be expressed as,

$$(pq|\hat{r}s) = \sum_{\alpha\beta\gamma\delta} X_{\alpha p} Y_{\beta q} X_{\gamma r} Y_{\delta s} (\alpha\beta|\gamma\delta), \quad (5)$$

where we have used the following convention to denote orbitals:

- Atomic orbitals (AOs): $\alpha, \beta, \gamma \dots$
- MOs of unspecified occupancy: $p, q, r \dots$
- Occupied MOs: $i, j, k \dots$

- Virtual MOs: $a, b, c \dots$

Since only closed-shell molecules are targeted in this work, all MOs are considered spin-free.

In the CC2 model, the doubles amplitudes are only correct through first-order in the fluctuation potential ($\Phi = H - F$). This approximation leads to a closed-form of the doubles amplitudes,

$$t_{ij}^{ab} = \frac{(ai|\hat{b}j)}{\epsilon_i - \epsilon_a + \epsilon_j - \epsilon_b}, \quad (6)$$

where ϵ_p denotes the orbital energy associated with orbital p . The CC2 equations can then be formulated in a CCS-like manner in which the doubles amplitudes are calculated on-the-fly. In order to take full advantage of this formulation and avoid the storage of any four-index quantity (amplitudes or integrals), Hättig and Weigend used the resolution-of-the-identity (RI) approximation for the two-electron integrals^{43,44} both in the optimization of the CC2 ground-state and excitation amplitudes.⁴⁵ This strategy was later generalized to the calculation of transition strengths and excited-state first-order properties.⁴⁶

In CC response theory, excitation energies and transition strengths from the ground-state (0) to an excited-state (m) are obtained from the poles and residues of the linear-response function, respectively.⁴⁷ The poles of the CC linear-response function correspond to the eigenvalues of the non-symmetric Jacobian matrix,

$$A_{\mu_i \nu_j} = \partial \Omega_{\mu_i} / \partial t_{\nu_j}, \quad (7)$$

while electric dipole transition strengths are given by,

$$S_{0m}^{V^i V^j} = T_{0m}^{V^i} T_{m0}^{V^j}, \quad (8)$$

$$T_{0m}^{V^j} = \sum_{pq} [D_{pq}^{\eta}(\mathbf{R}) + D_{pq}^{\xi}(\bar{\mathbf{M}})] \hat{V}_{pq}^j, \quad (9)$$

$$T_{m0}^{V^i} = \sum_{pq} D_{pq}^{\xi}(\mathbf{L}) \hat{V}_{pq}^i, \quad (10)$$

where \hat{V}_{pq}^j is a Cartesian component ($j = x, y, z$) of the T_1 -transformed electric dipole integrals in the length gauge and D_{pq}^{η} and D_{pq}^{ξ} are one-electron density matrices (see Appendix A). \mathbf{R} and \mathbf{L} are the right and left Jacobian eigenvectors following the normalization condition $\mathbf{LR} = 1$ and $\bar{\mathbf{M}}$ are the transition moment Lagrangian multipliers. In addition, the ground-state Lagrangian multipliers $\bar{\mathbf{t}}$ are required for the calculation of the one-electron density matrices. As for the CC2 ground-state amplitudes, the CC2 excitation amplitudes and the Lagrange multipliers can be obtained without storing any four-index quantity by considering an effective Jacobian matrix,^{45,46}

$$A_{\mu_1 \nu_1}^{\text{eff}}(\omega) = A_{\mu_1 \nu_1} - \sum_{\gamma_2} \frac{A_{\mu_1 \gamma_2} A_{\gamma_2 \nu_1}}{\epsilon_{\gamma_2} - \omega}, \quad (11)$$

where ω is an excitation energy and $\epsilon_{aibj} = \epsilon_a - \epsilon_i + \epsilon_b - \epsilon_j$. Using the effective Jacobian, the response equations to be solved become,

$$\mathbf{A}^{\text{eff}}(\omega)\mathbf{R}_1 = \omega\mathbf{R}_1, \quad (12)$$

$$\mathbf{L}_1\mathbf{A}^{\text{eff}}(\omega) = \mathbf{L}_1\omega, \quad (13)$$

$$\bar{\mathbf{t}}_1\mathbf{A}^{\text{eff}}(0) = -\boldsymbol{\eta}_1^{\text{eff}}, \quad (14)$$

$$\bar{\mathbf{M}}_1(\mathbf{A}^{\text{eff}}(-\omega) + \omega\mathbf{1}) = -\bar{\mathbf{m}}_1^{\text{eff}}, \quad (15)$$

where the subscript 1 denotes the singles part of a vector, and $\boldsymbol{\eta}_1^{\text{eff}}$ and $\bar{\mathbf{m}}_1^{\text{eff}}$ are the effective right-hand-sides of the linear equations for the ground-state and transition moments Lagrange multipliers, respectively. Once Eqs. (12) to (15) have been solved, the one-electron density matrices D_{pq}^η and D_{pq}^ϵ can be calculated and contracted with \hat{V}_{pq}^j to get the right and left transition dipole moments as well as transition strengths. All doubles quantities can be constructed on-the-fly whenever needed using the RI approximation for the two-electron integrals. In Appendix A we collect all the working equations required to calculate CC2 transition moments in a canonical MO basis. The equations are given here for completeness but should be equivalent to the ones in Ref. 46. (A few typos were present in the original paper and are corrected in Appendix A).

When studying electronic transitions, one often consider oscillator strengths instead of the transition strengths given by Eq. (8). Oscillator strengths in the length gauge are straightforwardly obtained as,

$$f_{0m} = \frac{2}{3}\omega_m \sum_{j=x,y,z} S_{0m}^{V^j}, \quad (16)$$

where ω_m is the excitation energy for a transition from the ground-state to the m -th excited-state. The calculation of excitation energies and oscillator strengths at the CC2 level has been implemented in a local version of the LSDALTON program^{48,49} following the strategy presented in Refs. 45 and 46.

III. EXCITATION ENERGIES AND OSCILLATOR STRENGTHS WITHIN LOFEX

In a previous publication³⁹ we have introduced the LoFEx algorithm as a framework to calculate CC2 excitation energies of large molecules. In this section, we summarize the LoFEx procedure and extend it to the computation of CC2 oscillator strengths.

A. Excitation energies

In LoFEx a transition-specific orbital space is constructed based on the solutions of the TDHF problem for the whole molecule and starting from HF canonical molecular orbitals (CMOs). First, NTOs are obtained by

performing a singular-value-decomposition (SVD) of the TDHF transition density matrix, $\tilde{\mathbf{b}}$, for each transition of interest,^{39,50,51}

$$\tilde{\mathbf{b}}^\dagger\tilde{\mathbf{b}}\mathbf{u}_k = \lambda_k\mathbf{u}_k, \quad k = 1, 2, \dots, N_o, \quad (17)$$

$$\tilde{\mathbf{b}}\tilde{\mathbf{b}}^\dagger\mathbf{v}_k = \lambda'_k\mathbf{v}_k, \quad k = 1, 2, \dots, N_v, \quad (18)$$

which leads to the transformation matrices from CMOs to NTOs for the occupied and virtual spaces, respectively,

$$\mathbf{U} = (\mathbf{u}_1, \mathbf{u}_2, \dots, \mathbf{u}_{N_o}), \quad (19)$$

$$\mathbf{V} = (\mathbf{v}_1, \mathbf{v}_2, \dots, \mathbf{v}_{N_v}), \quad (20)$$

Where N_o (N_v) is the number of occupied valence (virtual) orbitals. Assuming $N_o \leq N_v$, it follows that $\lambda_k \equiv \lambda'_k$ for $k = 1, 2, \dots, N_o$, while $\lambda'_k = 0$ for $k = N_o + 1, \dots, N_v$. The relevance of a given pair of NTOs (k) in the electronic transition associated with the density matrix $\tilde{\mathbf{b}}$ can be evaluated through its singular value $\sqrt{\lambda_k}$.^{50,52} For singles-dominated transitions, one pair of NTOs (with singular value close to one) dominates the transition, while the other NTOs are far less important to describe the process and thus have much smaller singular values. In LoFEx we therefore keep the dominant pair of NTOs intact, while the remaining orbitals are localized using the square of the second central moment of the orbitals as a localization function.^{53,54} This procedure (summarized in the upper part of Fig. 1) results in a mixed orbital space composed of orthogonal NTOs and localized molecular orbitals (LMOs) that is adapted to the description of a specific electronic transition. Core orbitals are not considered in the generation of NTOs and are localized independently to avoid mixing between core and valence spaces.

In this mixed orbital space, the dominant pair of NTOs is expected to describe the main character of the targeted electronic transition, while the LMOs enable an efficient description of correlation effects. In order to reduce the computational cost of the CC calculation, a subspace of the mixed NTO/LMO space is then constructed by considering the most relevant orbitals based on an effective distance \tilde{r}_p given by,

$$\tilde{r}_p = \min_A \left(\frac{r_{Ap}}{Q_A^{\text{NTO},o}}, \frac{r_{Ap}}{Q_A^{\text{NTO},v}} \right), \quad (21)$$

where index A denotes atomic centers, r_{Ap} corresponds to the distance between the center of charge of a local orbital p and atomic center A , and $Q_A^{\text{NTO},o}$ and $Q_A^{\text{NTO},v}$ are the Löwdin atomic charges of the occupied and virtual NTOs on center A , respectively. The resulting reduced space is denoted the excitation orbital space (XOS). The inactive Fock matrix can then be diagonalized in the XOS to obtain a set of pseudo-canonical orbitals. CC excitation energies (and eventually oscillator strengths) can then be calculated in the XOS using standard canonical implementations, as described in Section II and Appendix A for the CC2 model.

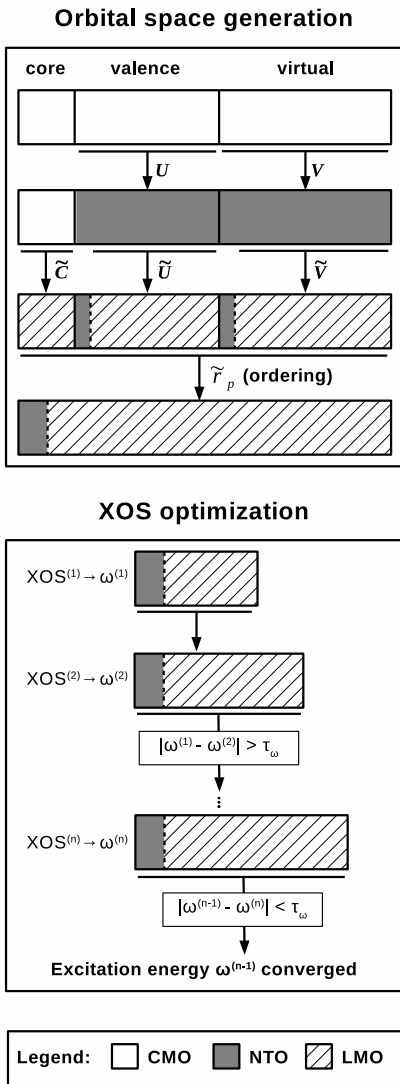


FIG. 1. Schematic representation of the original LoFEx procedure. \mathbf{U} and \mathbf{V} represent the transformation matrices from canonical molecular orbitals (CMOs in white) to natural transition orbitals (NTOs in grey) for the valence and virtual spaces, respectively. $\tilde{\mathbf{C}}$, $\tilde{\mathbf{U}}$, and $\tilde{\mathbf{V}}$ represent the transformation matrices to local molecular orbitals (LMOs in stripes) for core, valence, and virtual orbitals, respectively, excluding the dominant pair of NTOs. \tilde{r}_p is the effective distance measure given by Eq. (21), $\omega^{(i)}$ is the excitation energy corresponding to the i -th excitation orbital space ($\text{XOS}^{(i)}$) and τ_ω is the LoFEx excitation energy threshold.

In order to preserve the black-box feature of CC theory, the XOS is optimized as depicted in the lower part of Fig. 1, *i.e.*, a first guess for the XOS ($\text{XOS}^{(1)}$) is built and the CC problems are solved in that space to provide the excitation energy $\omega^{(1)}$, the XOS is then extended based on the list defined by Eq. (21) until the difference between the last two excitation energies is smaller than the LoFEx excitation energy threshold τ_ω , ($|\omega^{(n-1)} - \omega^{(n)}| < \tau_\omega$). We have shown in Ref. 39 (where τ_ω was denoted τ_{XOS}), that this procedure can result in significant speed-ups compared to standard CC2 implementations without loss of accuracy.

B. Oscillator strengths

For the calculation of oscillator strengths with LoFEx, we consider the following strategies:

1. The XOS is optimized solely based on the excitation energy (as described in Fig. 1 and Ref. 39) and the oscillator strength is only calculated once in the optimized XOS ($\text{XOS}^{(n-1)}$).
2. Both excitation energies and oscillator strengths are calculated in each LoFEx iteration and only the oscillator strength is checked for convergence. In other words, the XOS is considered converged when, $|f^{(n)} - f^{(n-1)}| < \tau_f$, where τ_f is the LoFEx oscillator strength threshold.

Note that in the XOS optimization, the last step (step n) is necessary to check that step $n-1$ was already converged. The calculation of oscillator strengths in point 1 is therefore done in the penultimate XOS to ensure minimal computational efforts.

In the following section, we will refer to point 1 as the standard-LoFEx strategy, while point 2 is denoted the spectrum strategy. Indeed, in point 2 the oscillator strength threshold τ_f has a different purpose than the excitation energy threshold τ_ω . Checking only the oscillator strength for convergence is expected to provide a balanced description of the transitions in the sense that transitions with large oscillator strengths should be well described, while weak transitions (with $f \simeq 0$) are expected to converge in minimal XOSs and lead to less accurate excitation energies, while using less computational resources. The standard-LoFEx strategy is thus preferred if accurate excitation energies are requested for all transitions, while the spectrum strategy is more appropriate if one is only interested in transitions with a significant oscillator strengths.

IV. RESULTS

In this section we present numerical results for excitation energies and oscillator strengths using the standard- and spectrum-LoFEx strategies introduced in Section III.

For that purpose, we consider the following set of medium-sized organic molecules,

- caprylic acid,
- lauric acid,
- palmitic acid,
- 15-oxopentadecanoic acid (15-OPDA),
- prostacyclin,
- an α -helix composed of 8 glycine residues (α -Gly₈),
- leupeptin,
- latanoprost,
- met-enkephalin, and
- 11-cis-retinal.

The molecular geometry for 11-cis-retinal was obtained from Ref. 26, while for the other systems, the Cartesian coordinates as well as details regarding the optimization of the structures are available in Ref. 39 and its supporting information. All the calculations presented in this section have been performed with a local version of the LSDalton program,^{48,49} using the correlation consistent aug-cc-pVDZ' basis set^{55,56} with the corresponding auxiliary basis, aug-cc-pVDZ-RI' for the RI approximation.⁵⁷ The prime in the basis set notation indicates that diffuse functions have been removed on the hydrogen atoms.

The parameters used in the following investigation have been set to the same default values as in Ref. 39, *i.e.*, the LoFEx excitation energy threshold was set to $\tau_\omega = 0.02$ eV and the number of orbitals added to the XOS in each LoFEx iteration corresponds to ten times the average number of orbitals per atom. For the spectrum-LoFEx strategy we have chosen $\tau_f = 0.001$.

A. Calculation of oscillator strengths within LoFEx

In Table I we report the LoFEx excitation energies and oscillator strengths for the lowest electronic transitions of the molecules presented above when using the standard-LoFEx strategy. Absolute errors in the excitation energies and the oscillator strengths as well as speed-ups compared to conventional CC2 implementations are also reported. Since in the standard-LoFEx strategy, the oscillator strength is only calculated in the converged (penultimate) XOS, we report excitation energies corresponding to both the expanded (step n) and converged (step $n - 1$) XOSs. We note that, as demonstrated in Ref. 39, the excitation energies in the expanded steps are "overconverged" (all errors are well below 0.02 eV), while in the penultimate steps the errors in the excitation energies are of the order of the LoFEx excitation energy threshold (0.02 eV). For the oscillator strengths, the absolute errors are equal or below 0.005 and are strongly

correlated with the intensity of the transitions (larger oscillator strengths correspond to larger errors), except for 11-cis-retinal which include the complete orbital space.

Regarding the speed-ups of the standard-LoFEx algorithm compared to a conventional (multi-state) CC2 implementation, it is found that the state-specific approach of LoFEx remains advantageous in most cases, even for the computation of several transitions. This is of course strongly dependent on the character of the transitions and on the size of the molecule, *e.g.* in the case of 15-OPDA, the two lowest transitions are rather local and converge in only two LoFEx iterations but the third transition has a more delocalized character³⁹ and requires almost the complete orbital space to be included in the XOS which limits significantly the obtained speed-up (1.52). Another less favorable case for LoFEx is the lowest transition of 11-cis-retinal. Both the excitation energy and the oscillator strength are perfectly recovered by LoFEx. However, the complete orbital space is required in order to determine the excitation energy to the desired precision, and the oscillator strength thus also has to be calculated in the complete orbital space, which results in a "speed-up" of 0.61. This behaviour can be understood by looking at the dominant pair of NTOs in Fig. 2, which shows that the transition is basically affecting the whole molecule, preventing any computational savings using LoFEx. This should be put in contrast with the performance of LoFEx for the met-enkephalin molecule, where both the excitation energy and the oscillator strength are well described with only 3 LoFEx iterations, resulting in a significant speed-up (34). It should be emphasized that the gain in terms of computational efforts for met-enkephalin is much greater than the computational overhead observed for 11-cis-retinal. These two examples demonstrate that LoFEx is designed to ensure error control and accuracy of the results, while computational savings are transition and system dependent.

With the idea of producing electronic spectra of CC2 quality at a reduced computational cost, we now turn our attention to the spectrum-LoFEx strategy. In electronic spectra, it is important to provide a good description of the transitions with large oscillator strengths and, for that purpose, the standard-LoFEx strategy might be inappropriate since it converges the XOS based on the excitation energies and not on the oscillator strengths. In Table II we report the LoFEx excitation energies and oscillator strengths for the lowest electronic transitions of the molecules presented above when the spectrum-LoFEx strategy is used with $\tau_f = 0.001$. Absolute errors in the excitation energies and the oscillator strengths as well as speed-ups compared to conventional CC2 implementations are also reported. Since in the spectrum-LoFEx strategy, the oscillator strengths and excitation energies are calculated in each LoFEx iteration, we only report the values corresponding to the most accurate results, *i.e.*, the ones from the expanded XOS (step n). Note also that, while in the standard-LoFEx procedure at least two

TABLE I. Comparison of standard-LoFEx ($\tau_\omega = 0.02$ eV) and conventional CC2 excitation energies and oscillator strengths. The LoFEx excitation energies are given in eV for the largest XOS (step n) and for the converged XOS (step $n - 1$), while oscillator strengths are only reported for the converged XOS. Absolute errors are given for both excitation energies and oscillator strengths. Finally, the number of iterations in the XOS optimization (n) as well as speed-ups of LoFEx compared to conventional CC2 algorithms are also reported.

| System | State | No. iter. (n) | $\omega^{(n)}$ | $\delta\omega^{(n)}$ | $\omega^{(n-1)}$ | $\delta\omega^{(n-1)}$ | $f^{(n-1)}$ | $\delta f^{(n-1)}$ | Speed-up |
|----------------|----------------|-------------------|----------------|----------------------|-------------------|------------------------|--------------------|--------------------|----------|
| Caprylic acid | S ₁ | 2 | 6.06 | 0.00 | 6.07 | 0.01 | 0.000 | 0.000 | 0.72 |
| | S ₂ | 3 | 6.83 | 0.00 | 6.83 | 0.00 | 0.066 | 0.003 | |
| Lauric acid | S ₁ | 3 | 6.05 | 0.00 | 6.06 | 0.00 | 0.000 | 0.000 | 1.29 |
| | S ₂ | 3 | 6.81 | 0.00 | 6.82 | 0.01 | 0.065 | 0.005 | |
| Palmitic acid | S ₁ | 3 | 6.06 | 0.00 | 6.06 | 0.00 | 0.000 | 0.000 | 4.07 |
| | S ₂ | 3 | 6.81 | 0.01 | 6.83 | 0.03 | 0.065 | 0.005 | |
| 15-OPDA | S ₁ | 2 | 4.44 | 0.00 | 4.45 | 0.01 | 0.000 | 0.000 | 1.52 |
| | S ₂ | 2 | 6.06 | 0.00 | 6.08 | 0.02 | 0.000 | 0.000 | |
| | S ₃ | 5 | 6.19 | 0.00 | 6.19 | 0.00 | 0.040 | 0.001 | |
| Prostacyclin | S ₁ | 5 | 4.98 | 0.00 | 4.99 | 0.01 | 0.005 | 0.000 | 1.16 |
| α -glys | S ₁ | 4 | 5.43 | 0.00 | 5.43 | 0.00 | 0.001 | 0.000 | 2.46 |
| | S ₂ | 4 | 5.73 | 0.00 | 5.73 | 0.01 | 0.003 | 0.001 | |
| Leupeptin | S ₁ | 3 | 4.27 | 0.01 | 4.28 | 0.01 | 0.001 | 0.000 | 3.37 |
| Latanoprost | S ₁ | 3 | 5.08 | 0.00 | 5.08 | 0.01 | 0.001 | 0.000 | 16.8 |
| Met-enkephalin | S ₁ | 3 | 4.78 | 0.00 | 4.79 | 0.01 | 0.024 | 0.002 | 34.0 |
| 11-cis-retinal | S ₁ | 5 | 2.14 | 0.00 | 2.14 ^a | 0.00 ^a | 1.384 ^a | 0.000 ^a | 0.61 |

^a The full molecule was included in step n which was not yet converged, so in this case, $\omega^{(n-1)}$ and $f^{(n-1)}$ are effectively calculated in XOS^(n).

TABLE II. Comparison of spectrum-LoFEx ($\tau_f = 0.001$) and conventional CC2 excitation energies and oscillator strengths. The LoFEx excitation energies and the corresponding absolute errors are given in eV. We also report the oscillator strengths and corresponding absolute errors as well as the number of iterations used in the XOS optimization (n) and the speed-ups of LoFEx compared to conventional CC2 algorithms.

| System | State | No. iter. (n) | $\omega^{(n)}$ | $\delta\omega^{(n)}$ | $f^{(n)}$ | $\delta f^{(n)}$ | Speed-up |
|----------------|----------------|-------------------|----------------|----------------------|-----------|------------------|----------|
| Caprylic acid | S ₁ | 1 | 6.07 | 0.01 | 0.000 | 0.000 | 0.65 |
| | S ₂ | 3 | 6.82 | 0.00 | 0.069 | 0.000 | |
| Lauric acid | S ₁ | 1 | 6.08 | 0.02 | 0.000 | 0.000 | 0.79 |
| | S ₂ | 4 | 6.81 | 0.00 | 0.070 | 0.000 | |
| Palmitic acid | S ₁ | 1 | 6.09 | 0.04 | 0.000 | 0.000 | 0.88 |
| | S ₂ | 5 | 6.80 | 0.00 | 0.070 | 0.000 | |
| 15-OPDA | S ₁ | 1 | 4.45 | 0.01 | 0.000 | 0.000 | 0.97 |
| | S ₂ | 1 | 6.08 | 0.02 | 0.000 | 0.000 | |
| | S ₃ | 5 | 6.19 | 0.00 | 0.040 | 0.001 | |
| Prostacyclin | S ₁ | 5 | 4.98 | 0.00 | 0.005 | 0.000 | 0.71 |
| α -glys | S ₁ | 2 | 5.46 | 0.03 | 0.001 | 0.000 | 11.1 |
| | S ₂ | 2 | 5.76 | 0.04 | 0.004 | 0.002 | |
| Leupeptin | S ₁ | 1 | 4.30 | 0.04 | 0.000 | 0.001 | 69.0 |
| Latanoprost | S ₁ | 3 | 5.07 | 0.00 | 0.001 | 0.000 | 9.31 |
| Met-enkephalin | S ₁ | 4 | 4.78 | 0.00 | 0.022 | 0.000 | 5.01 |
| 11-cis-retinal | S ₁ | 5 | 2.14 | 0.00 | 1.384 | 0.000 | 0.42 |

steps are necessary to check the convergence of excitation energies ($n \geq 2$), in the spectrum strategy we consider that the first step can be directly converged if $f^{(1)} < \tau_f$.

From Table II, we see that for the strongest transitions (with $f > 0.01$) the errors in both the excitation energies and the oscillator strengths are very satisfactory. As expected, for weaker transitions, larger errors occur in the excitation energies (up to 0.04 eV) which is related to the fact that only the oscillator strengths are used to

converge the XOS. For example, for the lowest transition of leupeptin ($f = 0.001$ and $\delta\omega = 0.04$), the weak character of the transition leads to a converged XOS in the first iteration and a significant speed-up (69.0) is observed. However, the results in Table II also show that, even if some computational time is saved on the weakest transitions, more time has to be dedicated to the stronger ones since larger XOSs are required to achieved the desired accuracy and since the oscillator strengths have to be calcu-

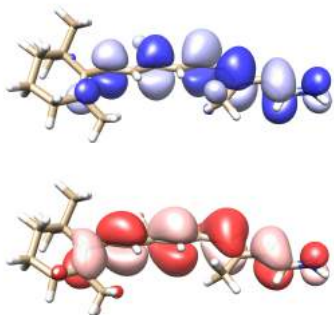


FIG. 2. Stick representation of the 11-cis-retinal molecule. Natural transition orbitals for the lowest transition are represented with a contour value of 0.02 a.u. (bottom: occupied NTO, top: virtual NTO).⁵⁸

lated in each LoFEx iteration. As a consequence, less impressive speed-ups are observed for the spectrum-LoFEx strategy (except for α -gly₈ and leupeptin). However, as for the standard-LoFEx strategy in Table I we note that the potential speed-ups are much larger than the additional overhead present in the less favorable cases.

Comparing Tables I and II we note that for all the transitions with $f > 0.01$, the number of required iterations with the spectrum strategy is always larger or equal to the number of iterations used in the standard-LoFEx strategy. In accordance with Ref. 27, this suggests that a fine-tuned description of (strong) oscillator strengths requires larger orbital spaces than the excitation energy alone. Finally, we note that both the accuracy and the computational savings are driven by the main LoFEx threshold (τ_f for the spectrum strategy) and that in practical applications of LoFEx, τ_f could of course be increased to reduce the computational efforts at the expense of obtaining slightly less accurate oscillator strengths.

B. Large-scale application: the bivalirudin molecule

In order to demonstrate the potential of LoFEx for large molecules, we apply both the standard and spectrum strategies for the calculation of the lowest excitation energy and the corresponding oscillator strength of the bivalirudin molecule (see Fig. 3). Bivalirudin is a synthetic polypeptide containing 20 residues. The structure used in this paper was obtained from the ChemSpider database,⁵⁹ hydrogen atoms were added and the geometry was relaxed at the molecular mechanics level (MMFF94⁶⁰ force field) using Avogadro.^{61,62} The Cartesian coordinates of the optimized structure are available as supplementary material. The calculations have been

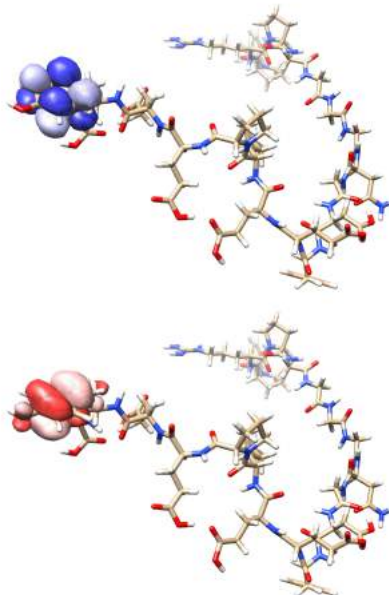


FIG. 3. Stick representation of the bivalirudin molecule. Natural transition orbitals for the lowest transition are represented with a contour value of 0.02 a.u. (bottom: occupied NTO, top: virtual NTO).⁵⁸

performed using the cc-pVDZ and aug-cc-pVDZ' basis sets which (for the whole molecule) contain 2860 and 4255 basis functions, respectively.

One of the goals of LoFEx is to provide CC results with a computational cost that can compete with TDDFT. In order to evaluate this feature for the bivalirudin calculations, we have performed TDDFT/CAM-B3LYP^{63–65} calculations using the same basis sets and targeting the same transition as for the LoFEx calculations. We note that for a fair comparison, the density-fitting^{43,66,67} approximation for the Coulomb integrals was used in both the TDDFT calculations and in the TDHF part of LoFEx. We have also performed the LoFEx calculations without density-fitting in the TDHF part and verified that the final LoFEx-CC2 results were not affected by this approximation (to the desired precision). Note, that the calculations in Section IV A were performed without using density-fitting in the TDHF part of LoFEx. In Table III, we report timings for LoFEx as well as for the TDDFT calculations. For LoFEx, we also report the fraction of the time (in %) spent in the CC part of the calculations denoted T_{CC}/tot . All the calculations reported in Table III were performed on Dell C6220 II compute-nodes, with 2 ten-core Intel E5-2680 v2 CPUs @ 2.8 GHz

TABLE III. LoFEx CC2 calculations of excitation energies and oscillator strengths for the lowest transition of the bivalirudin molecule. For standard-LoFEx, $\tau_\omega = 0.02$ eV and we report values for $\omega^{(n)}$ and $f^{(n-1)}$, while for spectrum-LoFEx, $\tau_f = 0.001$ and we report values for $\omega^{(n)}$ and $f^{(n)}$. For comparison TDDFT/CAM-B3LYP results are also reported. Timings are given in hours for all calculations and the fraction of time spent in the CC part of the LoFEx calculations is given in % as $T_{CC/tot}$.

| Basis set | method | No. iter. (n) | ω | f | Time (hours) | $T_{CC/tot}$ |
|--------------|----------------|-------------------|----------|-------|------------------|--------------|
| cc-pVDZ | standard-LoFEx | 3 | 4.98 | 0.030 | 7 | 3.2 |
| | spectrum-LoFEx | 4 | 4.98 | 0.029 | 8 | 15 |
| | CAM-B3LYP | — | 5.14 | 0.034 | 13 | — |
| aug-cc-pVDZ' | standard-LoFEx | 3 | 4.82 | 0.028 | 157 ^a | 1.4 |
| | spectrum-LoFEx | 4 | 4.82 | 0.026 | 164 ^a | 5.5 |
| | CAM-B3LYP | — | 5.01 | 0.029 | 205 ^a | — |

^a For the aug-cc-pVDZ' results, the TDDFT calculation and the TDHF parts of the LoFEx calculations were performed in parallel using 6 compute-nodes. Timings for those parts was therefore scaled by the number of nodes.

and 128 GB of memory.

Regarding the computational efforts in LoFEx, the values for $T_{CC/tot}$ in Table III indicates that only a few percents of the time is spent in the CC2 part of the calculations. In the best case, for the standard-LoFEx/aug-cc-pVDZ' result only 1.4 % is spent in the CC2 algorithm, while 15 % are used in the spectrum-LoFEx/cc-pVDZ calculation. Of course, for a given type of transition, the larger the molecule, the smaller $T_{CC/tot}$ would be. This indicates that, as expected, LoFEx effectively enables CC calculations of excitation energies and oscillator strengths at roughly the cost of a TDHF calculation, provided that the transition of interest is local compared to the size of the molecule. In fact, the LoFEx calculations are between 1.2 and 1.9 times faster than the corresponding TDDFT/CAM-B3LYP calculations.

In Table III, we also report the excitation energies and oscillator strengths obtained with the different methods (TDDFT and LoFEx). Both LoFEx strategies give the same excitation energies for which a red-shift of 0.16 eV is observed when adding diffuse functions in the basis set. The TDDFT numbers lie 0.16 and 0.19 eV higher than the CC2 excitation energies for the cc-pVDZ and aug-cc-pVDZ' basis sets, respectively, which shows reasonably good agreement between the two methods. As expected, the values for the oscillator strengths are slightly more dependent on the choice of the LoFEx strategy. Since CC2 reference numbers are out of reach, one should consider the results of the spectrum-LoFEx strategy to be superior (it takes one more iteration to converge). The TDDFT oscillator strengths are slightly higher for both basis sets but still very close to the CC2 results.

V. CONCLUSION

In this paper we have presented an extension of the LoFEx algorithm to the computation of oscillator strengths using CC2 linear-response theory. In LoFEx, a state-specific mixed orbital space is generated from a TDHF calculation on the whole molecule by considering

the dominant pair of NTOs, while the remaining orbitals are localized. A reduced excitation orbital space (XOS), is then determined in a black-box manner for each electronic transition. Two different strategies have been suggested for the computation of oscillator strengths within LoFEx: a standard strategy in which the XOS is optimized solely based on the CC2 excitation energy, while the oscillator strength is only calculated in the converged (penultimate) XOS, and a spectrum strategy which performs the XOS optimization directly based on the oscillator strength. The first approach is designed to provide accurate excitation energies for all targeted transitions, while the second strategy is dedicated to the calculation of electronic spectra, such that strong transitions are described accurately, while less computational efforts are spent on weak and forbidden transitions.

Both strategies have shown promising results in terms of accuracy when applied to a set of medium-sized organic molecules. Significant computational savings with respect to conventional CC2 implementations are obtained whenever the considered transitions are local compared to the size of the molecule. However, we note that for the strongest transition investigated in this work (S_1 of 11-cis-retinal), no computational savings could be obtained due to the delocalized electronic structure of the molecule. Many spectroscopically interesting chromophores have a delocalized electronic structure,⁶⁸ and for such species, little or no computational savings would be obtained using LoFEx. In order to extend the applicability of LoFEx, it might therefore be necessary to further reduce the size of the XOS by considering, *e.g.*, pair natural orbitals (PNOs),^{24,26} or improved NTOs. This issue will be addressed in future publications. Nonetheless, the current LoFEx algorithm could be applied successfully to the bivalirudin molecule with 4255 basis functions, demonstrating that for transitions that are local compared to the size of the molecule, LoFEx can provide CC2 excitation energies and oscillator strengths at a computational cost competing with that of TDDFT.

SUPPLEMENTARY MATERIAL

See supplementary material for the Cartesian coordinates of the molecular geometry of bivalirudin.

ACKNOWLEDGMENTS

The research leading to these results has received funding from the European Research Council under the European Unions Seventh Framework Programme (FP/2007-2013)/ERC Grant Agreement no. 291371.

The numerical results presented in this work were performed at the Centre for Scientific Computing, Aarhus (<http://phys.au.dk/forskning/cscaa/>).

This research used resources of the Oak Ridge Leadership Computing Facility at the Oak Ridge National Laboratory, which is supported by the Office of Science of the U.S. Department of Energy under Contract No. DE-AC05-00OR22725.

Appendix A: Working equations for CC2 transition moments

In this appendix we summarize the working equations of the CC2 model for the calculation of excitation energies and (ground-state to excited-state) transition moments for closed-shell molecules. For the derivation of those equations we have considered spin-free canonical orbitals and the following biorthonormal basis,⁴²

$$\langle ij^{ab} | = \langle \text{HF} | E_{jb} E_{ia}, \quad (\text{A1a})$$

$$| ij^{ab} \rangle = E_{ai} E_{bj} | \text{HF} \rangle, \quad (\text{A1b})$$

$$\langle \tilde{ij}^{ab} | = \frac{1}{1 + \delta_{ai,bj}} \left(\frac{1}{3} \langle ij^{ab} | + \frac{1}{6} \langle j^i | \right), \quad (\text{A1c})$$

$$\langle \tilde{ij}^{ab} | \langle \tilde{kl}^{cd} \rangle = \delta_{aibj,ckdl}, \quad (\text{A1d})$$

where E_{ai} is a singlet excitation operator in second-quantization. The singles and doubles cluster operators are then defined as follows,

$$T_1 = \sum_{ai} t_i^a E_{ai}, \quad (\text{A2})$$

$$T_2 = \frac{1}{2} \sum_{aibj} t_{ij}^{ab} E_{ai} E_{bj}. \quad (\text{A3})$$

In the following section we only provide the CC2 working equations, for the details regarding the algorithm and the use of the RI approximation for the two-electron repulsion integrals, we refer to Refs. 45 and 46.

1. Overview

The computation of transition moments from CC2 linear-response theory can be performed as follows (all the intermediate quantities are given in the following sections),

1. Determine the ground-state singles amplitudes t_i^a from Eq. (1) and using Table V (left).
2. Determine the ground-state singles Lagrangian multipliers \tilde{t}_i^a from Eq. (14) and using Table VI (left) with $\omega = 0$ and with the right-hand-side from Eq. (A22).
3. Determine the “right” singles excitation amplitudes R_i^a from Eq. (12) and using Table V (right).
4. Determine the “left” singles excitation amplitudes L_i^a from Eq. (13) and using Table VI (left).
5. Check that right and left excitation energies agree to the desired precision and normalize the excitation vectors using Eqs. (A25) and (A26),

$$\sum_{ai} L_i^a R_i^a + \frac{1}{2} \sum_{aibj} L_{ij}^{ab} R_{ij}^{ab} = 1 \quad (\text{A4})$$

6. Determine the transition moment Lagrangian multipliers M_i^a from Eq. (15) and using Table VI (left). The right-hand-side has to be computed beforehand from Table VI (right) which requires the optimized right excitation amplitudes and the ground-state Lagrangian multipliers. The corresponding doubles quantities are computed on-the-fly from Eqs. (A25), (A27) and (A30).
7. Compute the one-particle density matrices given in Appendix A5 using the doubles quantities in Appendix A4.
8. The density matrices can then be contracted with electric dipole moment T_1 -transformed integrals to get the transition strengths as in Eqs. (8) to (10).

2. Integrals and Fock matrices

We write two-electron repulsion integrals in the Mulliken notation as,

$$(pq|rs) = \sum_{\alpha\beta\gamma\delta} C_{\alpha p} C_{\beta q} C_{\gamma r} C_{\delta s} (\alpha\beta|\gamma\delta) \quad (\text{A5})$$

where the $C_{\alpha p}$ are Hartree-Fock canonical MO coefficients.

A general inactive Fock matrix is given by

$$F_{pq} = h_{pq} + \sum_i [2(pq|ii) - (pi|i q)] = \delta_{pq} \epsilon_p \quad (\text{A6})$$

$$h_{pq} = \sum_{\alpha\beta} C_{\alpha p} C_{\beta q} h_{\alpha\beta} \quad (\text{A7})$$

where we have introduced the one-electron integrals h_{pq} and Hartree-Fock orbital energies $\epsilon_p, \epsilon_q, \dots$

We consider integrals transformed with the singles ground-state amplitudes,

$$(pq|\hat{r}s) = \sum_{\alpha\beta\gamma\delta} X_{\alpha p} Y_{\beta q} X_{\gamma r} Y_{\delta s} (\alpha\beta|\gamma\delta) \quad (\text{A8})$$

$$\hat{h}_{pq} = \sum_{\alpha\beta} X_{\alpha p} Y_{\beta q} h_{\alpha\beta} \quad (\text{A9})$$

$$\begin{aligned} X_{\alpha i} &= C_{\alpha i} & X_{\alpha a} &= C_{\alpha a} - \sum_i C_{\alpha i} t_i^a \\ Y_{\alpha i} &= C_{\alpha i} + \sum_a C_{\alpha a} t_i^a & Y_{\alpha a} &= C_{\alpha a} \end{aligned} \quad (\text{A10})$$

We also have integrals transformed with a general “right” singles vector, b_i^a ,

$$(pq|\bar{r}s) = P_{qs}^{pr} \sum_{\alpha\beta\gamma\delta} (\bar{X}_{\alpha p} Y_{\beta q} + X_{\alpha p} \bar{Y}_{\beta q}) X_{\gamma r} Y_{\delta s} (\alpha\beta|\gamma\delta) \quad (\text{A11})$$

$$P_{qs}^{pr} f_{qs}^{pr} = f_{qs}^{pr} + f_{sq}^{rp} \quad (\text{A12})$$

$$\bar{h}_{pq} = \sum_{\alpha\beta} (\bar{X}_{\alpha p} Y_{\beta q} + X_{\alpha p} \bar{Y}_{\beta q}) h_{\alpha\beta} \quad (\text{A13})$$

$$\begin{aligned} \bar{X}_{\alpha i} &= 0 & \bar{X}_{\alpha a} &= -\sum_i C_{\alpha i} b_i^a \\ \bar{Y}_{\alpha i} &= \sum_a C_{\alpha a} b_i^a & \bar{Y}_{\alpha a} &= 0 \end{aligned} \quad (\text{A14})$$

where, depending on the context, b_i^a may correspond to the trial right excitation amplitudes or the optimized right excitation amplitudes R_i^a .

Similarly, we consider integrals transformed with a general “left” singles vector, \bar{b}_i^a ,

$$(pq|\check{r}s) = P_{qs}^{pr} \sum_{\alpha\beta\gamma\delta} (\check{X}_{\alpha p} Y_{\beta q} + X_{\alpha p} \check{Y}_{\beta q}) X_{\gamma r} Y_{\delta s} (\alpha\beta|\gamma\delta) \quad (\text{A15})$$

$$\begin{aligned} \check{X}_{\alpha i} &= \sum_a X_{\alpha a} \bar{b}_i^a & \check{X}_{\alpha a} &= 0 \\ \check{Y}_{\alpha i} &= 0 & \check{Y}_{\alpha a} &= -\sum_i Y_{\alpha i} \bar{b}_i^a \end{aligned} \quad (\text{A16})$$

where, depending on the context, \bar{b}_i^a may correspond to the trial left excitation amplitudes, the optimized left excitation amplitudes L_i^a , the ground-state Lagrangian multipliers \bar{t}_i^a , or the transition moment Lagrangian multipliers \bar{M}_i^a .

Finally, we also introduce the following one-index transformed integrals,

$$(\widetilde{ia|jb}) = -P_{ij}^{ab} \left(\sum_{ck} \bar{t}_k^c R_k^c (ka|jb) + \sum_{ck} \bar{t}_k^c R_k^c (ic|jb) \right). \quad (\text{A17})$$

Expressions for the different blocks of the T_1 -transformed and “right”-transformed Fock matrices are given in Table IV.

3. Linear-transformed vectors and right-hand-sides

In Table V we gather the working equations for the ground-state singles residual,

$$\Omega_{ai} = \Omega_{ai}^0 + \Omega_{ai}^G + \Omega_{ai}^H + \Omega_{ai}^I + \Omega_{ai}^J = 0, \quad (\text{A18})$$

and for a “right” linear-transformed vector,

$$\sigma_{ai} = \sum_{bj} \mathbf{A}_{ai,bj}^{\text{eff}}(\omega) b_j^b = \sigma_{ai}^0 + \sigma_{ai}^G + \sigma_{ai}^H + \sigma_{ai}^I + \sigma_{ai}^J, \quad (\text{A19})$$

while Table VI contains the working equations for a “left” linear-transformed vector,

$$\bar{\sigma}_{ai} = \sum_{bj} \bar{b}_j^b \mathbf{A}_{bj,ai}^{\text{eff}}(\omega) = \bar{\sigma}_{ai}^0 + \bar{\sigma}_{ai}^G + \bar{\sigma}_{ai}^H + \bar{\sigma}_{ai}^I + \bar{\sigma}_{ai}^J, \quad (\text{A20})$$

and for the effective right-hand-side of the transition moment Lagrangian multipliers,

$$\bar{m}_{ai}^{\text{eff}} = \bar{m}_{ai}^{\text{eff},0} + \bar{m}_{ai}^{\text{eff},G} + \bar{m}_{ai}^{\text{eff},H} + \bar{m}_{ai}^{\text{eff},I} + \bar{m}_{ai}^{\text{eff},J}. \quad (\text{A21})$$

The effective right-hand-side for the ground-state Lagrangian multipliers is given by,

$$\eta_{ai}^{\text{eff}} = 2\hat{F}_{ia} + \sum_{ckd} \bar{\eta}_{ki}^{cd} (ck|\hat{d}a) - \sum_{ckl} \bar{\eta}_{kl}^{ca} (ck|\hat{i}l), \quad (\text{A22})$$

$$\bar{\eta}_{ij}^{ab} = 2 \frac{2(ia|jb) - (ib|ja)}{\epsilon_i - \epsilon_a + \epsilon_j - \epsilon_b}. \quad (\text{A23})$$

4. Doubles quantities

All doubles quantities can be calculated on-the-fly from the corresponding singles which are kept in memory. We consider the ground-state doubles amplitudes,

$$t_{ij}^{ab} = \frac{(ai|\hat{b}j)}{\epsilon_i - \epsilon_a + \epsilon_j - \epsilon_b}, \quad (\text{A24})$$

the right doubles excitation amplitudes,

$$R_{ij}^{ab} = \frac{(ai|\bar{b}j)}{\epsilon_i - \epsilon_a + \epsilon_j - \epsilon_b + \omega}, \quad (\text{A25})$$

the left doubles excitation amplitudes,

$$L_{ij}^{ab} = \frac{2(ia|\check{b}j) - (ib|\check{j}a) + P_{ij}^{ab} [2L_i^a \hat{F}_{jb} - L_j^a \hat{F}_{ib}]}{\epsilon_i - \epsilon_a + \epsilon_j - \epsilon_b + \omega}, \quad (\text{A26})$$

the ground-state doubles Lagrangian multipliers,

$$\bar{t}_{ij}^{ab} = \bar{\eta}_{ij}^{ab} + \frac{2(ia|\check{b}j) - (ib|\check{j}a) + P_{ij}^{ab} [2\bar{t}_i^a \hat{F}_{jb} - \bar{t}_j^a \hat{F}_{ib}]}{\epsilon_i - \epsilon_a + \epsilon_j - \epsilon_b}, \quad (\text{A27})$$

and the transition moment doubles Lagrangian multipliers,

$$\bar{M}_{ij}^{ab} = F_{ij}^{ab} + \frac{2(ia|\check{b}j) - (ib|\check{j}a) + P_{ij}^{ab} [2\bar{M}_i^a \hat{F}_{jb} - \bar{M}_j^a \hat{F}_{ib}]}{\epsilon_i - \epsilon_a + \epsilon_j - \epsilon_b - \omega}. \quad (\text{A28})$$

TABLE IV. Inactive transformed Fock matrices.

| | |
|---|--|
| $\hat{F}_{pq} = \hat{h}_{pq} + \sum_i [2(pq ii) - (pi iq)]$ | $\bar{F}_{pq} = \bar{h}_{pq} + \sum_i [2(pq ii) - (pi iq)]$ |
| $\hat{F}_{ij} = \sum_{ck} [2(ij kc) - (ic kj)]t_k^c + \epsilon_i \delta_{ij}$ | $\bar{F}_{ij} = \sum_{kc} [2(ij kc) - (ic kj)]R_k^c + \sum_b R_j^b \hat{F}_{ib}$ |
| $\hat{F}_{ia} = \sum_{ck} [2(ia kc) - (ic ka)]t_k^c$ | $\bar{F}_{ia} = \sum_{kc} [2(ia kc) - (ic ka)]R_k^c$ |
| $\hat{F}_{ai} = \sum_{ck} [2(ai kc) - (ac ki)]t_k^c + (\epsilon_a - \epsilon_i)t_i^a$ | $\bar{F}_{ai} = \sum_{kc} [2(ai kc) - (ac ki)]R_k^c + \sum_b R_j^b \hat{F}_{ab} - \sum_j R_j^a \hat{F}_{ji}$ |
| $\hat{F}_{ab} = \sum_{ck} [2(ab kc) - (ac kb)]t_k^c + \epsilon_a \delta_{ab}$ | $\bar{F}_{ab} = \sum_{kc} [2(ab kc) - (ac kb)]R_k^c - \sum_j R_j^a \hat{F}_{jb}$ |

TABLE V. CC2 working equations for the ground-state residual Ω_{ai} and a “right” linear-transformed vector σ_{ai} .

| Terms | Ω_{ai} | $\sigma_{ai} = \mathbf{A}_{ai, bj}^{\text{eff}}(\omega)b_j^b$ |
|-------|--|---|
| 0 | $(\epsilon_a - \epsilon_i)t_i^a$ | $\sum_b E_{ab}b_i^b - \sum_j E_{ji}b_j^a$ |
| G | $+\sum_{cdk} \tilde{t}_{ik}^{dc}(kc ad)$ | $+\sum_{cdk} \tilde{b}_{ik}^{dc}(kc ad)$ |
| H | $-\sum_{ckl} \tilde{t}_{ik}^{cc}(kc li)$ | $-\sum_{ckl} \tilde{b}_{ik}^{cc}(kc li)$ |
| I | $+\sum_{ck} \tilde{t}_{ik}^{ac} \hat{F}_{kc}$ | $+\sum_{ck} [\tilde{b}_{ik}^{ac} \hat{F}_{kc} + \tilde{t}_{ik}^{ac} \bar{F}_{kc}]$ |
| J | $+\sum_{ck} [2(kc ai) - (ki ac)]t_k^c$ | $+\sum_{ck} [2(kc ai) - (ki ac)]b_k^c$ |
| | $\tilde{t}_{ij}^{ab} = \frac{2(ai bj) - (bi aj)}{\epsilon_i - \epsilon_a + \epsilon_j - \epsilon_b}$ | $\tilde{b}_{ij}^{ab} = \frac{2(ai bj) - (bi aj)}{\epsilon_i - \epsilon_a + \epsilon_j - \epsilon_b + \omega}$ |
| | | $E_{ji} = \hat{F}_{ji} + \sum_{cdk} \tilde{t}_{ik}^{dc}(kc jd)$ |
| | | $E_{ab} = \hat{F}_{ab} - \sum_{ckl} \tilde{t}_{ik}^{ac}(kc lb)$ |

Where $\tilde{\eta}_{ij}^{ab}$ and F_{ij}^{ab} have been defined in Eq. (A23) and Table VI (right), respectively. The ground-states doubles amplitudes and the doubles excitation amplitudes are often used in the form,

$$\tilde{t}_{ij}^{ab} = 2t_{ij}^{ab} - t_{ij}^{ba}, \quad (\text{A29})$$

$$\tilde{R}_{ij}^{ab} = 2R_{ij}^{ab} - R_{ij}^{ba}. \quad (\text{A30})$$

5. One-particle density matrices

The CC2 transition moments are calculated from the following one-particle density matrices,

$$D_{ij}^{\xi}(\mathbf{X}) = -\sum_{abk} X_{jk}^{ab} t_{ik}^{ab} \quad (\text{A31})$$

$$D_{ia}^{\xi}(\mathbf{X}) = \sum_{ck} X_k^c \tilde{t}_{ik}^{ac} \quad (\text{A32})$$

$$D_{ai}^{\xi}(\mathbf{X}) = X_i^a \quad (\text{A33})$$

$$D_{ab}^{\xi}(\mathbf{X}) = \sum_{ijc} X_{ij}^{ac} t_{ij}^{bc} \quad (\text{A34})$$

where \mathbf{X} denotes either the “left” excitation amplitudes \mathbf{L} or the transition moment Lagrangian multipliers $\bar{\mathbf{M}}$.

TABLE VI. CC2 working equations for a “left” linear-transformed vector $\bar{\sigma}_{ai}$ and the right-hand-side of the transition moment Lagrangian multipliers equation $\bar{m}_{ai}^{\text{eff}}$.

| Terms | $\bar{\sigma}_{ai} = \bar{t}_{bj,ai}^{\text{eff}}(\omega)$ | $\bar{m}_{ai}^{\text{eff}}$ |
|-------|--|--|
| 0 | $\sum_b E_{ba} \bar{b}_i^b - \sum_j E_{ij} \bar{b}_j^a$ | $\sum_b \bar{E}_{ba} \bar{t}_i^b - \sum_j \bar{E}_{ij} \bar{t}_j^a$ |
| G | $+\sum_{cdk} \bar{b}_{ik}^{dc}(ck da)$ | $+\sum_{cdk} [\bar{F}_{ik}^{dc}(ck da) + \bar{t}_{ik}^{dc}(ck da)]$ |
| H | $-\sum_{ckl} \bar{b}_{lk}^{ac}(ck il)$ | $-\sum_{ckl} [\bar{F}_{lk}^{ac}(ck il) + \bar{t}_{lk}^{ac}(ck il)]$ |
| I | $+\sum_{ck} [2(kc ia) - (ka ic)] C_k^c$ | $+\sum_{ck} [2(kc ia) - (ka ic)] \bar{C}_k^c$ |
| J | $+\sum_{ck} [2(ck ia) - (ca ik)] \bar{b}_k^c$ | $+\sum_{ck} [2(ck ia) - (ca ik)] \bar{t}_k^c$ |
| | $\bar{b}_{ij}^{ab} = \frac{2(ia jb) - (ib ja) + P_{ij}^{ab} [2\bar{t}_{jb}^a - \bar{b}_j^a \bar{F}_{ib}]}{\epsilon_i - \epsilon_a + \epsilon_j - \epsilon_b + \omega}$ | $\bar{F}_{ij}^{ab} = \frac{2(\widehat{ia jb}) - (\widehat{ib ja}) + P_{ij}^{ab} [2\bar{t}_{jb}^a - \bar{t}_j^a \bar{F}_{ib}]}{\epsilon_i - \epsilon_a + \epsilon_j - \epsilon_b - \omega}$ |
| | $\bar{C}_i^a = \sum_{bj} \bar{t}_{ij}^{ab} \bar{b}_j^b$ | $\bar{C}_i^a = \sum_{bj} \bar{R}_{ij}^{ab} \bar{t}_j^b$ |
| | $E_{ij} = \hat{F}_{ij} + \sum_{cdk} \bar{t}_{jk}^{dc}(kc id)$ | $\bar{E}_{ij} = \bar{F}_{ij} + \sum_{cdk} \bar{R}_{jk}^{dc}(kc id)$ |
| | $E_{ba} = \hat{F}_{ba} - \sum_{ckl} \bar{t}_{lk}^{bc}(kc la)$ | $\bar{E}_{ba} = \bar{F}_{ba} - \sum_{ckl} \bar{R}_{lk}^{bc}(kc la)$ |

Finally, we have,

$$D_{ij}^n(\mathbf{R}) = - \sum_a \bar{t}_{ij}^a R_i^a - \sum_{abk} \bar{t}_{jk}^{ab} R_{ik}^{ab} \quad (\text{A35})$$

$$D_{ia}^n(\mathbf{R}) = 2R_i^a + \sum_{ck} \bar{t}_k^c \bar{R}_{ik}^{ac} - \sum_b \left(\sum_{kjc} \bar{t}_{kj}^{bc} t_{kj}^{ac} \right) R_i^b - \sum_j \left(\sum_{cbk} \bar{t}_{jk}^{cb} t_{ik}^{cb} \right) R_j^a \quad (\text{A36})$$

$$D_{ai}^n(\mathbf{R}) = 0 \quad (\text{A37})$$

$$D_{ab}^n(\mathbf{R}) = \sum_i \bar{t}_{ai} R_i^b + \sum_{ijc} \bar{t}_{ij}^{ac} R_{ij}^{bc}. \quad (\text{A38})$$

- ¹H. Koch, O. Christiansen, P. Jørgensen, and J. Olsen, *Chem. Phys. Lett.* **244**, 75 (1995).
- ²O. Christiansen, H. Koch, P. Jørgensen, and J. Olsen, *Chem. Phys. Lett.* **256**, 185 (1996).
- ³O. Christiansen, A. Halkier, H. Koch, P. Jørgensen, and T. Helgaker, *J. Chem. Phys.* **108**, 2801 (1998).
- ⁴L. González, D. Escudero, and L. Serrano-Andrés, *ChemPhysChem* **13**, 28 (2012).
- ⁵J. F. Stanton and R. J. Bartlett, *J. Chem. Phys.* **98**, 7029 (1993).
- ⁶J. D. Watts and R. J. Bartlett, *Chem. Phys. Lett.* **233**, 81 (1995).
- ⁷S. R. Gwaltney, M. Nooijen, and R. J. Bartlett, *Chem. Phys. Lett.* **248**, 189 (1996).
- ⁸H. Koch, R. Kobayashi, A. M. J. Sánchez de Merás, and P. Jørgensen, *J. Chem. Phys.* **100**, 4393 (1994).
- ⁹S. Sæbø and P. Pulay, *Annu. Rev. Phys. Chem.* **44**, 213 (1993).
- ¹⁰H.-J. Werner and M. Schutz, *J. Chem. Phys.* **135**, 144116 (2011).
- ¹¹J. Yang, G. K.-L. Chan, F. R. Manby, M. Schütz, and H.-J. Werner, *J. Chem. Phys.* **136**, 144105 (2012).
- ¹²C. Riplinger, B. Sandhoefer, A. Hansen, and F. Neese, *J. Chem. Phys.* **139**, 134101 (2013).
- ¹³J. J. Eriksen, P. Baudin, P. Ettenhuber, K. Kristensen, T. Kjærsgaard, and P. Jørgensen, *J. Chem. Theory Comput.* **11**, 2984 (2015).
- ¹⁴H.-J. Werner, G. Knizia, C. Krause, M. Schwilk, and M. Dornbach, *J. Chem. Theory Comput.* **11**, 484 (2015).
- ¹⁵C. Riplinger, P. Pinski, U. Becker, E. F. Valeev, and F. Neese, *J. Chem. Phys.* **144**, 024109 (2016).
- ¹⁶W. Li, Z. Ni, and S. Li, *Mol. Phys.* **114**, 1447 (2016).
- ¹⁷P. R. Nagy, G. Samu, and M. Kállay, *J. Chem. Theory Comput.* **12**, 4897 (2016).
- ¹⁸J. Friedrich, *J. Chem. Theory Comput.* **8**, 1597 (2012).
- ¹⁹T. D. Crawford and R. A. King, *Chem. Phys. Lett.* **366**, 611 (2002).
- ²⁰T. Korona and H.-J. Werner, *J. Chem. Phys.* **118**, 3006 (2003).
- ²¹D. Kats, T. Korona, and M. Schütz, *J. Chem. Phys.* **125**, 104106 (2006).
- ²²D. Kats and M. Schütz, *J. Chem. Phys.* **131**, 124117 (2009).
- ²³D. Kats and M. Schütz, *Zeitschrift für Phys. Chemie* **224**, 601 (2010).
- ²⁴B. Helmich and C. Hättig, *J. Chem. Phys.* **139**, 084114 (2013).
- ²⁵B. Helmich and C. Hättig, *Comput. Theor. Chem.* **1040-1041**, 35 (2014).
- ²⁶A. K. Dutta, F. Neese, and R. Izsák, *J. Chem. Phys.* **145**, 034102 (2016).
- ²⁷D. Kats, T. Korona, and M. Schutz, *J. Chem. Phys.* **127**, 064107 (2007).
- ²⁸T. D. Crawford, in *Recent Progress in Coupled Cluster Methods: Theory and Applications*, Vol. 53, edited by P. Čárský, J. Paldus, and J. Pittner (Springer Netherlands, Dordrecht, 2010) Chap. 2, pp. 37–55.
- ²⁹N. J. Russ and T. D. Crawford, *Phys. Chem. Chem. Phys.* **10**, 3345 (2008).
- ³⁰H. R. McAlexander and T. D. Crawford, *J. Chem. Theory Comput.* **12**, 209 (2016).
- ³¹R. A. Mata and H. Stoll, *J. Chem. Phys.* **134**, 034122 (2011).
- ³²J. Friedrich, H. R. McAlexander, A. Kumar, and T. D. Crawford, *Phys. Chem. Chem. Phys.* **17**, 14284 (2015).
- ³³R. H. Myhre, A. M. J. Sánchez de Merás, and H. Koch, *Mol. Phys.* **111**, 1109 (2013).
- ³⁴R. H. Myhre, A. M. J. Sánchez de Merás, and H. Koch, *J. Chem. Phys.* **141**, 224105 (2014).
- ³⁵R. H. Myhre and H. Koch, *J. Chem. Phys.* **145**, 044111 (2016).
- ³⁶R. Send, V. R. I. Kaila, and D. Sundholm, *J. Chem. Theory Comput.* **7**, 2473 (2011).

- ³⁷M. Caricato, T. Vreven, G. W. Trucks, and M. J. Frisch, *J. Chem. Phys.* **133**, 054104 (2010).
- ³⁸M. Caricato, T. Vreven, G. W. Trucks, and M. J. Frisch, *J. Chem. Theory Comput.* **7**, 180 (2011).
- ³⁹P. Baudin and K. Kristensen, *J. Chem. Phys.* **144**, 224106 (2016).
- ⁴⁰O. Christiansen, H. Koch, and P. Jørgensen, *Chem. Phys. Lett.* **243**, 409 (1995).
- ⁴¹H. Koch, O. Christiansen, R. Kobayashi, P. Jørgensen, and T. Helgaker, *Chem. Phys. Lett.* **228**, 233 (1994).
- ⁴²T. Helgaker, P. Jørgensen, and J. Olsen, *Molecular Electronic-Structure Theory*, 1st ed. (John Wiley & Sons, Ltd, Chichester, UK, 2000).
- ⁴³J. L. Whitten, *J. Chem. Phys.* **58**, 4496 (1973).
- ⁴⁴M. Feyereisen, G. Fitzgerald, and A. Komornicki, *Chem. Phys. Lett.* **208**, 359 (1993).
- ⁴⁵C. Hättig and F. Weigend, *J. Chem. Phys.* **113**, 5154 (2000).
- ⁴⁶C. Hättig and A. Köhn, *J. Chem. Phys.* **117**, 6939 (2002).
- ⁴⁷O. Christiansen, P. Jørgensen, and C. Hättig, *Int. J. Quantum Chem.* **68**, 1 (1998).
- ⁴⁸K. Aidas, C. Angeli, K. L. Bak, V. Bakken, R. Bast, L. Boman, O. Christiansen, R. Cimraglia, S. Coriani, P. Dahle, E. K. Dalskov, U. Ekström, T. Enevoldsen, J. J. Eriksen, P. Ettenhuber, B. Fernández, L. Ferrighi, H. Fliegl, L. Frediani, K. Hald, A. Halkier, C. Hättig, H. Heiberg, T. Helgaker, A. C. Hennum, H. Hetttema, E. Hjertenaes, S. Høst, I.-M. Høyvik, M. F. Iozzi, B. Jansík, H. J. A. Jensen, D. Jonsson, P. Jørgensen, J. Kauczor, S. Kirpekar, T. Kjærgaard, W. Klopper, S. Knecht, R. Kobayashi, H. Koch, J. Kongsted, A. Krapp, K. Kristensen, A. Ligabue, O. B. Lutnaes, J. I. Melo, K. V. Mikkelsen, R. H. Myhre, C. Neiss, C. B. Nielsen, P. Norman, J. Olsen, J. M. H. Olsen, A. Osted, M. J. Packer, F. Pawłowski, T. B. Pedersen, P. F. Provasi, S. Reine, Z. Rinkevicius, T. a. Ruden, K. Ruud, V. V. Rybkin, P. Salek, C. C. M. Samson, A. M. J. Sánchez de Merás, T. Saue, S. P. A. Sauer, B. Schimmelpennig, K. Sneskov, A. H. Steindal, K. O. Sylvester-Hvid, P. R. Taylor, A. M. Teale, E. I. Tellgren, D. P. Tew, A. J. Thorvaldsen, L. Thøgersen, O. Vahtras, M. a. Watson, D. J. D. Wilson, M. Ziolkowski, and H. Ågren, *WIREs Comput. Mol. Sci.* **4**, 269 (2014).
- ⁴⁹“Lsdalton, a linear-scaling molecular electronic structure program, release dalton2016 (2015), see <http://daltonprogram.org>.”
- ⁵⁰A. V. Luzanov, A. A. Sukhorukov, and V. E. Umanski, *Theor. Exp. Chem.* **10**, 354 (1976).
- ⁵¹T. Etienne, *J. Chem. Phys.* **142**, 244103 (2015).
- ⁵²R. L. Martin, *J. Chem. Phys.* **118**, 4775 (2003).
- ⁵³B. Jansík, S. Høst, K. Kristensen, and P. Jørgensen, *J. Chem. Phys.* **134**, 194104 (2011).
- ⁵⁴I.-M. Høyvik, B. Jansík, and P. Jørgensen, *J. Chem. Theory Comput.* **8**, 3137 (2012).
- ⁵⁵T. Dunning Jr., *J. Chem. Phys.* **90**, 1007 (1989).
- ⁵⁶R. Kendall, T. Dunning Jr., and R. Harrison, *J. Chem. Phys.* **96**, 6769 (1992).
- ⁵⁷F. Weigend, A. Köhn, and C. Hättig, *J. Chem. Phys.* **116**, 3175 (2002).
- ⁵⁸E. F. Pettersen, T. D. Goddard, C. C. Huang, G. S. Couch, D. M. Greenblatt, E. C. Meng, and T. E. Ferrin, *J. Comput. Phys.* **25**, 1605 (2004).
- ⁵⁹ChemSpider page for bivalirudin: CSID:10482069, <http://www.chemspider.com/Chemical-Structure.10482069.html> (accessed 11:56, Nov 21, 2016).
- ⁶⁰T. a. Halgren, *J. Comput. Chem.* **17**, 490 (1996).
- ⁶¹M. D. Hanwell, D. E. Curtis, D. C. Lonie, T. Vandermeersch, E. Zurek, and G. R. Hutchison, *J. Cheminform.* **4**, 1 (2012).
- ⁶²Avogadro: an open-source molecular builder and visualization tool. Version 1.1.1. <http://avogadro.openmolecules.net/>.
- ⁶³E. Runge and E. K. U. Gross, *Phys. Rev. Lett.* **52**, 997 (1984).
- ⁶⁴M. E. Casida, *Recent Advances in Density Functional Methods, Part I*, 155 (1995).
- ⁶⁵T. Yanai, D. P. Tew, and N. C. Handy, *Chem. Phys. Lett.* **393**, 51 (2004).
- ⁶⁶E. J. Baerends, D. Ellis, and P. Ros, *Chem. Phys.* **2**, 41 (1973).
- ⁶⁷S. Reine, E. Tellgren, A. Krapp, T. Kjærgaard, T. Helgaker, B. Jansík, S. Høst, and P. Salek, **129**, 104101 (2008).
- ⁶⁸D. Jacquemin, I. Duchemin, and X. Blase, *J. Chem. Theory Comput.* **11**, 5340 (2015).

B.9 Simplified Natural transition Orbital Framework for Large-scale coupled-cluster Excitation energy calculations (SNOFLE_x)

P. Baudin, and K. Kristensen.

Manuscript in preparation, (2017).

Major contributions: writing process, and theoretical discussions.

Minor contribution: code implementation (RI-CC2 routines, eigenvalue solver, and LoFEx structure, also used in this context).

Simplified Natural transition Orbital Framework for Large-scale coupled-cluster Excitation energy calculations (SNOFLE_x)

Pablo Baudin¹ and Kasper Kristensen^{1, a)}

qLEAP Center for Theoretical Chemistry, Department of Chemistry, Aarhus University, Langelandsgade 140, DK-8000 Aarhus C, Denmark

(Dated: 26 January 2017)

We present a new method for calculating coupled cluster (CC) excitation energies at a reduced computational cost. It relies on correlated natural transition orbitals (NTOs), denoted CIS(D')-NTOs, which are obtained by diagonalizing generalized hole and particle density matrices obtained from configuration interaction singles (CIS) information and additional terms that represent correlation effects. The determination of the CIS(D')-NTOs formally scales cubically with the size of the system. A transition-specific reduced orbital space is determined based on the eigenvalues of the CIS(D')-NTOs, and a standard CC calculation of excitation energies is then performed in that reduced orbital space. The new method denoted SNOFLE_x (Simplified Natural transition Orbital Framework for Large-scale coupled-cluster Excitation energy calculations) is tested by calculating second-order approximate CC singles and doubles (CC2) excitation energies for a set of organic molecules. It is shown that SNOFLE_x generally yields excitation energies of CC2 quality at a significantly reduced computational cost, even for relatively small systems and delocalized electronic transitions. SNOFLE_x is also applied to solvated formamide containing an increasing number of water molecules to illustrate that the method can be applied to large molecular systems (up to 4836 basis functions).

I. INTRODUCTION

Nowadays, coupled cluster (CC) theory,^{1,2} together with the response function³⁻⁷ or the equation-of-motion⁸⁻¹¹ formalisms, is well established as the method of choice for the calculation of electronic transition properties of molecules dominated by a single electronic configuration. However, the steep computational scaling with system size of CC theory limits its application to molecules with a few tens of atoms. For the calculation of transition properties of large molecules, more affordable but less reliable methods, such as time-dependent density-functional-theory (TDDFT), are generally preferred.¹² The limitations of DFT methods are well known,^{13,14} and it is therefore very important to provide more robust alternatives for large scale calculations of transition properties.

The steep computational scaling of CC theory can be attributed to the use of highly delocalized canonical Hartree-Fock (HF) orbitals, while the correlation effects described at the CC level are of local nature.^{15,16} For the calculation of CC ground state energies, many methods have been developed to take advantage of the locality of correlation effects to reduce the cost of CC calculations, and some efficient linear-scaling algorithms are now available.¹⁷⁻²¹ We note that the ground state correlation energy is a size-extensive quantity, and by definition, CC algorithms that target size-extensive properties have to scale at least linearly with the system size. The key to achieving a reduction in computational cost without affecting significantly the accuracy of the calculated quantities is to formulate the CC equations in a basis

where the inherent locality of electron correlation can be efficiently exploited. While local and orthogonal occupied orbitals are universally used,²²⁻²⁵ the virtual space can be described by local orthogonal virtual orbitals,²⁵⁻²⁷ or non-orthogonal alternatives such as projected atomic orbitals (PAOs),²⁸ orbital-specific virtuals (OSVs),²⁹ or pair-natural orbitals (PNOs).³⁰⁻³²

More recently, some attention has also been given to the calculation of excitation energies and other frequency-dependent properties. In this context it is important to realize that electronic transition properties are size-intensive. For local electronic transitions, it should therefore be possible to devise a procedure where the computational cost depends only on the character of the electronic transition but not on the system size. However, electronic transitions may involve changes in the electronic density of the entire molecule, and it is therefore not straightforward to use the same locality approximations in calculations of transition properties as for the ground state energy.

In the design of approximated CC methods for excitation energy calculations, the size-intensivity of electronic transitions has often been ignored. Instead, the local approximations for ground state calculations have been extended to take into account the potential delocalized character of electronic transitions by relying on information from low level calculations (typically from the configuration interaction singles (CIS) model).³³⁻⁴¹ Such strategies allow for a more uniform description of size-intensive and size-extensive properties but it limits significantly the potential computational savings. On the other hand, some approaches have been designed specifically for the calculation of size-intensive properties and cannot be used to obtain, e.g. correlation energies.⁴²⁻⁴⁷ Finally, computational savings can be obtained by simply truncating the virtual orbital space in the canonical

^{a)} kasperk@chem.au.dk

orbital basis.^{48,49}

In a previous publication, we have introduced a local framework for calculating CC excitation energies (LoFEx),⁴⁷ which provides a general approach to calculate excitation energies at a reduced computational cost. The orbital space in the LoFEx approach is a mixed space containing natural transition orbitals (NTOs) and localized molecular orbitals (LMOs). A subset of this mixed orbital space is then optimized in a black-box manner to ensure error control on the calculated quantities. In Ref. 47, it was shown that a very compact description of electronic transitions could be obtained for transitions that are localized to a small part of the molecular system considered. However, as mentioned above, electronic transition are not necessarily local, and for transitions that are delocalized over a large part of the molecule, no computational savings can be obtained with LoFEx.

In this paper we investigate alternative orbital spaces that are not relying on LMOs and can be used to efficiently describe all types of transitions (including delocalized transitions) and avoid the need for an optimization of the reduced orbital space. The new orbital spaces are made of generalized NTOs that include correlation effects and an optimal reduced orbital space can be obtained based solely on the NTO eigenvalues as described in Section II. The new method entitled SNOFLEx (Simplified Natural transition Orbital Framework for Large-scale coupled-cluster Excitation energy calculations) is tested on a set of 22 spectroscopically interesting medium-sized molecules to calculate excitation energies at the second-order approximated CC singles and doubles (CC2) level (Section III). Significant speed-ups can be achieved even for the smallest systems and the most delocalized transitions. We also calculate excitation energies of solvated formamide clusters of increasing size to illustrate the capabilities of the new method.

II. THEORY

Our overall goal is to reduce the computational cost of CC response calculations by employing a reduced set of orthogonal molecular orbitals (MOs). In this work we consider excitation energies calculated using the CC2 model introduced by Christiansen et al.,⁵⁰ where the resolution-of-the-identity (RI) approximation is used for the two-electron repulsion integrals, as introduced by Hättig and Weigend.⁵¹ We refer to Refs. 50,51 for a detailed description of the CC2 model and focus here on the generation of orthogonal MO spaces adapted to describe electronic transitions.

Throughout the paper we consider closed-shell molecules and spin-free orbitals using the following index convention:

- i, j, k, l : Occupied canonical MOs
- a, b, c, d : Virtual canonical MOs

- I, J, K, L : Occupied MOs in the CIS-NTO basis
- A, B, C, D : Virtual MOs in the CIS-NTO basis
- p : MOs of unspecified nature and occupation
- $\alpha, \beta, \gamma, \delta$: Atomic orbitals

In Section II A, we introduce the concept of NTOs at the CIS level and summarize the generation of a CIS-NTO/LMO mixed orbital space similar to the one introduced in Ref. 47. In Sections II B and II C we generalized the concept of NTOs to include correlation effects at the CC2, and CIS(D)⁵² levels of theory, while an approximation to CIS(D)-NTOs is introduced in Section II D.

A. CIS-NTOs and mixed orbital space

NTOs are usually obtained from a singular-value-decomposition (SVD) of one-particle transition density matrices (TDM).^{53,54} At the CIS level, the TDM associated to a given electronic transition is obtained from the following eigenvalue problem,⁵⁵

$$(\mathbf{H}^{\text{CIS}} - E_{\text{HF}}\mathbf{1})\mathbf{R}^{\text{CIS}} = \omega^{\text{CIS}}\mathbf{R}^{\text{CIS}}. \quad (1)$$

where \mathbf{H}^{CIS} is the CIS Hamiltonian, E_{HF} is the HF ground-state energy, and the eigenvalue ω^{CIS} is the excitation energy associated to the TDM or excitation vector \mathbf{R}^{CIS} . An SVD of \mathbf{R}^{CIS} is equivalent to the diagonalization of the following hole and particle density matrices,

$$X_{ij}^{\text{CIS}} = \sum_a R_{ai}^{\text{CIS}} R_{aj}^{\text{CIS}} \quad (2a)$$

$$Y_{ab}^{\text{CIS}} = \sum_i R_{ai}^{\text{CIS}} R_{bi}^{\text{CIS}}. \quad (2b)$$

CIS-NTOs are thus obtained from,

$$\mathbf{X}^{\text{CIS}}\mathbf{U}^{\text{CIS}} = \boldsymbol{\lambda}^{\text{CIS}}\mathbf{U}^{\text{CIS}} \quad (3a)$$

$$\mathbf{Y}^{\text{CIS}}\mathbf{V}^{\text{CIS}} = \tilde{\boldsymbol{\lambda}}^{\text{CIS}}\mathbf{V}^{\text{CIS}} \quad (3b)$$

where $\boldsymbol{\lambda}^{\text{CIS}}$ and $\tilde{\boldsymbol{\lambda}}^{\text{CIS}}$ are diagonal matrices with eigenvalues λ_p^{CIS} and $\tilde{\lambda}_p^{\text{CIS}}$ on the diagonal. The $\mathbf{U}^{\text{CIS}}/\mathbf{V}^{\text{CIS}}$ matrices represent the transformation from the occupied/virtual canonical MO basis to the occupied/virtual CIS-NTO basis. In the following discussion it is assumed that the eigenvalues in Eqs. (3) are numbered in order of decreasing magnitude and that the number of virtual orbitals is larger than the number of occupied orbitals, ($V > O$), which is the case in all practical applications. In order to simplify the following discussion we note that for a real matrix \mathbf{B} of dimension (m, n) , the number of *a priori* non-zero singular values of \mathbf{B} is given by its rank, such that we have,

$$\text{rank}(\mathbf{B}^T\mathbf{B}) = \text{rank}(\mathbf{B}\mathbf{B}^T) = \text{rank}(\mathbf{B}) \leq \min(m, n) \quad (4)$$

Thus, from Eqs. (2) it follows that

$$\text{rank}(\mathbf{X}^{\text{CIS}}) = \text{rank}(\mathbf{R}^{\text{CIS}}) \leq O \quad (5a)$$

$$\text{rank}(\mathbf{Y}^{\text{CIS}}) = \text{rank}(\mathbf{R}^{\text{CIS}}) \leq O \quad (5b)$$

which implies that the last $(V - O)$ eigenvalues of \mathbf{Y}^{CIS} are zero. Furthermore, the first O virtual eigenvalues $\bar{\lambda}_p^{\text{CIS}}$ equals the occupied eigenvalues λ_p^{CIS} , i.e.,⁵⁴

$$\bar{\lambda}_p^{\text{CIS}} = \lambda_p^{\text{CIS}} \quad (1 \leq p \leq O) \quad (6a)$$

$$\bar{\lambda}_p^{\text{CIS}} = 0 \quad (O < p \leq V) \quad (6b)$$

We also note that normalization of the CIS excitation vector is equivalent to requiring the sum of the eigenvalues to equal one,

$$\sum_p \lambda_p^{\text{CIS}} = 1 \quad (7)$$

The magnitude of the eigenvalues λ_p^{CIS} can be related to the importance of a given pair of CIS-NTOs to describe the transition of interest at the CIS level of theory. It would thus be convenient to choose a subset of CIS-NTOs based on their eigenvalues and then carry out a correlated CC calculation within this reduced orbital space in order to decrease the computational effort of the CC calculation. However, such a strategy is not useful in practice since it discards *at least* all the virtual CIS-NTOs with zero eigenvalue which ultimately results in too large errors in the subsequent CC calculation. In Ref. 47, this issue was alleviated by generating a mixed orbital space in which the dominant pair of NTOs was kept unaltered since they represent the main characteristic of the transition (for single-replacement dominated transitions), while the remaining orbitals were localized to enable an efficient description of correlation effects. The importance of a given LMO p to describe the considered transition was then evaluated through an effective distance measure, \tilde{r}_p ,

$$\tilde{r}_p = \min_A \left(\frac{r_{Ap}}{Q_A^{\text{CIS-NTO,o}}}, \frac{r_{Ap}}{Q_A^{\text{CIS-NTO,v}}} \right) \quad (8)$$

where index A denotes atomic centers, r_{Ap} corresponds to the distance between the center of charge of a local orbital p and atomic center A , and $Q_A^{\text{CIS-NTO,o}}$ and $Q_A^{\text{CIS-NTO,v}}$ are the Löwdin atomic charges (with values between 0 and 1) of the dominating occupied and virtual NTOs on center A , respectively. The \tilde{r}_p distance measure is thus small if the center of orbital p is close to an atom where one (or both) of the CIS-NTOs have a large Löwdin charge. Using this measure, the LMOs are listed according to their \tilde{r}_p values, and the LMOs with small \tilde{r}_p values are assumed to be most important for describing the electronic transition of interest. The mixed orbital space was then used in LoFEx to reduce the computational cost of the CC2 model for excitation energies. This strategy is successful when applied to transitions that are

local compared to the size of the considered molecule. However, for molecules with a more delocalized electronic structure, no computational savings could be achieved.⁴⁷ We note that in Ref. 47, time-dependent HF (TDHF)-NTOs were used instead of CIS-NTOs but this difference has very minor effects on the final orbital space since the TDHF and CIS methods are closely related.⁵⁶

In the following sections we generalized the concept of NTOs to include correlation effects with the objective of calculating accurate CC excitation energies within a reduced orbital space of correlated NTOs.

B. CC2-NTOs

In order to add the effects of CC2 doubles excitations in the NTOs, we consider the following generalized hole and particle density matrices at the CC2 level of theory,

$$X_{ij}^{\text{CC2}} = \sum_a R_{ai}^{\text{CC2}} R_{aj}^{\text{CC2}} + \frac{1}{2} \sum_{abk} R_{aibk}^{\text{CC2}} R_{ajbk}^{\text{CC2}} \quad (9a)$$

$$Y_{ab}^{\text{CC2}} = \sum_i R_{ai}^{\text{CC2}} R_{bi}^{\text{CC2}} + \frac{1}{2} \sum_{ijc} R_{aicj}^{\text{CC2}} R_{bicj}^{\text{CC2}} \quad (9b)$$

where R_{ai}^{CC2} and R_{abij}^{CC2} are the singles and doubles components of the solution vector of the right CC2 eigenvalue problem,⁵⁰

$$\mathbf{A}\mathbf{R}^{\text{CC2}} = \omega^{\text{CC2}}\mathbf{R}^{\text{CC2}}, \quad (10)$$

and \mathbf{A} and ω^{CC2} are the CC2 Jacobian and CC2 excitation energy, respectively. In analogy with Eqs. (3) for the CIS density matrices, the CC2-NTOs are obtained by diagonalizing \mathbf{X}^{CC2} and \mathbf{Y}^{CC2} ,

$$\mathbf{X}^{\text{CC2}}\mathbf{U}^{\text{CC2}} = \boldsymbol{\lambda}^{\text{CC2}}\mathbf{U}^{\text{CC2}} \quad (11a)$$

$$\mathbf{Y}^{\text{CC2}}\mathbf{V}^{\text{CC2}} = \tilde{\boldsymbol{\lambda}}^{\text{CC2}}\mathbf{V}^{\text{CC2}} \quad (11b)$$

For the following analysis, it is convenient to interpret the total \mathbf{R}^{CC2} eigenvector entering Eq. (9a) as a matrix \mathbf{R}^X with a singles block of dimension (V, O) and elements $R_{a,i}^{\text{CC2}}$ and a doubles block of dimension (V^2O, O) and elements $\frac{1}{\sqrt{2}}R_{bja,i}^{\text{CC2}}$ (see Fig. 1, left). This enables us to write the \mathbf{X}^{CC2} matrix in Eq. (9a) as,

$$\mathbf{X}^{\text{CC2}} = (\mathbf{R}^X)^T \mathbf{R}^X \quad (12)$$

Similarly, we consider a matrix \mathbf{R}^Y with a singles block of dimension (V, O) and elements $R_{a,i}^{\text{CC2}}$ and a doubles block of dimension (V, O^2V) and elements $\frac{1}{\sqrt{2}}R_{a,ibj}^{\text{CC2}}$ (see Fig. 1, right) and write the \mathbf{Y}^{CC2} matrix in Eq. (9b) as,

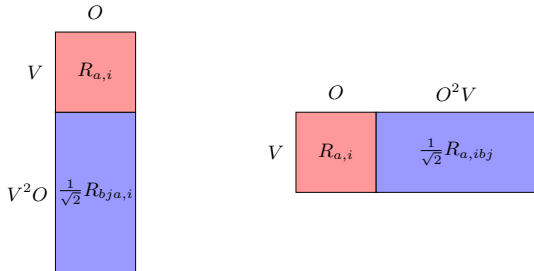
$$\mathbf{Y}^{\text{CC2}} = \mathbf{R}^Y (\mathbf{R}^Y)^T \quad (13)$$

Using the general identity in Eq. (4) and the dimensions of the \mathbf{R}^X and \mathbf{R}^Y matrices it then follows that

$$\text{rank}(\mathbf{X}^{\text{CC2}}) \leq \min(V + V^2O, O) = O \quad (14a)$$

$$\text{rank}(\mathbf{Y}^{\text{CC2}}) \leq \min(V, O + O^2V) = V \quad (14b)$$

FIG. 1: Representation of the \mathbf{R}^X (left) and \mathbf{R}^Y (right) matrices used to calculate generalized transition density matrices.



This should be put in contrast with the ranks of the CIS density matrices in Eqs. (5). Comparing Eqs. (2) and (9) we thus see that the inclusion of the doubles excitation vector component enables the existence of nonzero eigenvalues for all of the CC2-NTOs generated by di-

agonalization of \mathbf{X}^{CC2} and \mathbf{Y}^{CC2} . We also note that, in contrast with the CIS case in Eq. (6), the occupied and virtual CC2-NTO eigenvalues are generally different, $\lambda_p^{\text{CC2}} \neq \bar{\lambda}_p^{\text{CC2}}$.

The generation of the CC2-NTOs requires the determination of the CC2 excitation vector for the full molecular system, and the CC2-NTOs are therefore primarily of analytical interest whenever CC2 excitation energies are targeted. It is thus instructive to look at the explicit expression for the CC2 doubles excitation vector in order to consider approximations in Sections II C and II D that could be invoked in practical calculations of CC2 excitation energies. From Ref. 51, the CC2 doubles excitation vector is given by,

$$R_{aibj}^{\text{CC2}} = \frac{(ai|\bar{b}j)^{\text{CC2}}}{\epsilon_i - \epsilon_a + \epsilon_j - \epsilon_b + \omega^{\text{CC2}}} \quad (15)$$

where the transformed integrals are written as,

$$(ai|\bar{b}j)^{\text{CC2}} = P_{ij}^{ab} \sum_{\alpha\beta\gamma\delta} (\bar{\Lambda}_{\alpha a}^{\text{CC2}} \Lambda_{\beta i}^{\text{CC2}} + \Lambda_{\alpha a}^{\text{CC2}} \bar{\Lambda}_{\beta i}^{\text{CC2}}) \Lambda_{\gamma b}^{\text{CC2}} \Lambda_{\delta j}^{\text{CC2}} (\alpha\beta|\gamma\delta) \quad (16)$$

with

$$P_{ij}^{ab} f_{aibj} = f_{aibj} + f_{bjai} \quad (17)$$

and

$$\bar{\Lambda}_{\alpha a}^{\text{CC2}} = - \sum_i C_{\alpha i} R_{ai}^{\text{CC2}} \quad (18a)$$

$$\bar{\Lambda}_{\alpha i}^{\text{CC2}} = \sum_a C_{\alpha a} R_{ai}^{\text{CC2}} \quad (18b)$$

$$\Lambda_{\alpha a}^{\text{CC2}} = C_{\alpha a} - \sum_i C_{\alpha i} t_{ai} \quad (18c)$$

$$\Lambda_{\alpha i}^{\text{CC2}} = C_{\alpha i} + \sum_a C_{\alpha a} t_{ai} \quad (18d)$$

where \mathbf{C} is the standard (canonical) MO coefficient matrix and t_{ai} are the ground state CC2 singles amplitudes, while ϵ_i and ϵ_a represent occupied and virtual orbital energies, respectively. The expensive part of the CC2-NTO procedure is the calculation of the doubles excitation vector components R_{aibj}^{CC2} in Eqs. (15) and their contraction in Eqs. (9), both of which scale as $\mathcal{O}(N^5)$ where N is a measure of the size of the molecular system. In particular, the determination of R_{aibj}^{CC2} requires the iterative solution of both the ground state CC2 equations (to determine t_{ai}) and the subsequent iterative solution of the CC2 eigenvalue problem in Eq. (10).

C. CIS(D)-NTOs

As a first approximation to the CC2-NTOs, we consider NTOs generated from the simpler CIS(D) model.⁵² In Eq. (15), this effectively corresponds to setting the ground state singles amplitudes to zero ($t_i^e = 0$) and using the CIS excitation energy and excitation vector instead of the corresponding CC2 quantities. Thus, within the CIS(D) model, the $R_{aibj}^{\text{CIS(D)}}$ amplitudes may be determined in a non-iterative $\mathcal{O}(N^5)$ process according to

$$R_{aibj}^{\text{CIS(D)}} = \frac{(ai|\bar{b}j)^{\text{CIS}}}{\epsilon_i - \epsilon_a + \epsilon_j - \epsilon_b + \omega^{\text{CIS}}} \quad (19)$$

where the transformed integrals are given by,

$$(ai|\bar{b}j)^{\text{CIS}} = P_{ij}^{ab} \sum_{\alpha\beta\gamma\delta} (\bar{\Lambda}_{\alpha a}^{\text{CIS}} C_{\beta i} + C_{\alpha a} \bar{\Lambda}_{\beta i}^{\text{CIS}}) C_{\gamma b} C_{\delta j} (\alpha\beta|\gamma\delta) \quad (20)$$

$$\bar{\Lambda}_{\alpha a}^{\text{CIS}} = - \sum_i C_{\alpha i} R_{ai}^{\text{CIS}} \quad (21a)$$

$$\bar{\Lambda}_{\alpha i}^{\text{CIS}} = \sum_a C_{\alpha a} R_{ai}^{\text{CIS}} \quad (21b)$$

The CIS(D)-NTOs are then obtained by diagonalizing the CIS(D) hole and particle density matrices, which are

constructed analogously to Eqs. (9),

$$X_{ij}^{\text{CIS(D)}} = \sum_a R_{ai}^{\text{CIS}} R_{aj}^{\text{CIS}} + \frac{1}{2} \sum_{abk} R_{aibk}^{\text{CIS(D)}} R_{ajbk}^{\text{CIS(D)}} \quad (22a)$$

$$Y_{ab}^{\text{CIS(D)}} = \sum_i R_{ai}^{\text{CIS}} R_{bi}^{\text{CIS}} + \frac{1}{2} \sum_{ijc} R_{aicj}^{\text{CIS(D)}} R_{bicj}^{\text{CIS(D)}} \quad (22b)$$

D. CIS(D')-NTOs

While the generation of \mathbf{X} and \mathbf{Y} according to Eqs. (22) rather than Eqs. (9) represents a significant reduction in terms of computational effort, it is still an $\mathcal{O}(N^5)$ process. We now propose that the generation of correlated NTOs can be simplified even further to reduce the computational scaling by using CIS information to approximate the doubles terms in Eqs. (22). The resulting orbitals are denoted CIS(D')-NTOs, since they represent an approximation to the CIS(D)-NTOs.

The occupied and virtual CIS-NTO bases are defined by the \mathbf{U}^{CIS} and \mathbf{V}^{CIS} transformation matrices, respectively, [see Eq. (3)]. We consider two mixed bases—one where the occupied orbitals are canonical and the virtual orbitals are expressed in the CIS-NTO basis, and vice versa—leading to the following approximate doubles vectors

$$R_{AiBj}^{\text{CIS(D)'}} = \frac{(A\bar{i}|Bj)^{\text{CIS}}}{\epsilon_i - F_{AA} + \epsilon_j - F_{BB} + \omega^{\text{CIS}}} \quad (23a)$$

$$R_{aIbJ}^{\text{CIS(D)'}} = \frac{(a\bar{I}|bJ)^{\text{CIS}}}{F_{II} - \epsilon_a + F_{JJ} - \epsilon_b + \omega^{\text{CIS}}} \quad (23b)$$

where we have used capital letters to denote the CIS-NTO basis. We have made the approximation to use diagonal Fock matrix elements in the CIS-NTO basis. The use of Eqs. (23) alone does not reduce the computational effort compared to CIS(D). However, from Eqs. (2), (3), and (6) we note that the CIS excitation vector in the CIS-NTO basis is of dimension (V, O) and has the following simple form,

$$\mathbf{R}^{\text{CIS}} = \begin{pmatrix} \sqrt{\boldsymbol{\lambda}^{\text{CIS}}} \\ \mathbf{0} \end{pmatrix} \quad (24)$$

where $\sqrt{\boldsymbol{\lambda}^{\text{CIS}}}$ is a diagonal square matrix of dimension (O, O) with diagonal elements $\sqrt{\lambda_p}$. From Eqs. (20) and (21) it thus follows that, in the CIS-NTO basis, only elements of the $\boldsymbol{\Lambda}^{\text{CIS}}$ matrix associated with sizable CIS-NTO eigenvalues will contribute significantly to the doubles vectors in Eqs. (23). Using Eq. (7) we therefore define a subset of Z important CIS-NTOs for which the eigenvalues add up to one minus some threshold τ' ,

$$\min_Z \left(\sum_{p=1}^Z \lambda_p^{\text{CIS}} \right) > 1 - \tau' \quad (25)$$

where p refers to either occupied ($p = I$) or virtual ($p = A$) CIS-NTOs. Our basic assumption is now that

the subset of CIS-NTOs defined by Eq. (25) is sufficient to generate a reasonable approximation to the CIS(D) density matrices in Eq. (22). We thus use the doubles excitation vectors in the mixed canonical/CIS-NTO basis defined by Eqs. (23) to define the following CIS(D') hole and particle density matrices,

$$X_{ij}^{\text{CIS(D)'}} = \sum_a R_{ai}^{\text{CIS}} R_{aj}^{\text{CIS}} + \frac{1}{2} \sum_{A'B'k} R_{A'iB'k}^{\text{CIS(D)'}} R_{A'jB'k}^{\text{CIS(D)'}} \quad (26a)$$

$$Y_{ab}^{\text{CIS(D)'}} = \sum_i R_{ai}^{\text{CIS}} R_{bi}^{\text{CIS}} + \frac{1}{2} \sum_{I'J'c} R_{aI'cJ'}^{\text{CIS(D)'}} R_{bI'cJ'}^{\text{CIS(D)'}} \quad (26b)$$

where the prime indicates that the summations run only over the subset of Z CIS-NTOs defined by Eq. (25), while the summations in the canonical basis run over the full set of orbitals.

The generation of CC2-NTOs and CIS(D)-NTOs are iterative and non-iterative $\mathcal{O}(N^5)$ processes, respectively. An algorithm for generating CIS(D')-NTOs using the RI approximation is given in Appendix A where it is shown that the generation of CIS(D')-NTOs has a formal $\mathcal{O}(N^3)$ scaling behaviour (assuming that the reduced dimension Z is independent of system size for a given type of electronic transition). It follows that CIS(D')-NTOs can be calculated for much larger molecular systems than CC2-NTOs or CIS(D)-NTOs. We thus propose to use CIS(D')-NTOs to reduce the computational cost and thereby extend the application range of CC excitation energy calculations in terms of the following procedure:

1. Solve the CIS eigenvalue problem in Eq. (1) and determine CIS-NTOs according to Eqs. (3).
2. Choose a τ' threshold to define a subset of CIS-NTOs according to Eq. (25).
3. Construct CIS(D')-NTOs by diagonalizing the density matrices calculated from Eqs. (26),

$$\mathbf{X}^{\text{CIS(D)'}} \mathbf{U}^{\text{CIS(D)'}} = \boldsymbol{\lambda}^{\text{CIS(D)'}} \mathbf{U}^{\text{CIS(D)'}} \quad (27a)$$

$$\mathbf{Y}^{\text{CIS(D)'}} \mathbf{V}^{\text{CIS(D)'}} = \tilde{\boldsymbol{\lambda}}^{\text{CIS(D)'}} \mathbf{V}^{\text{CIS(D)'}} \quad (27b)$$

4. Scale the CIS(D') density matrix eigenvalues, such that they add up to one (equivalent to normalizing the CIS(D') excitation vectors),

$$\sum_p \lambda_p^{\text{CIS(D)'}} = \sum_p \tilde{\lambda}_p^{\text{CIS(D)'}} = 1 \quad (28)$$

5. Choose a subset of occupied and virtual CIS(D')-NTOs defined as in Eq. (25) but from CIS(D')-NTO eigenvalues,

$$\min_{Z_o} \left(\sum_{p=1}^{Z_o} \lambda_p^{\text{CIS(D)'}} \right) > 1 - \tau' \quad (29a)$$

$$\min_{Z_v} \left(\sum_{p=1}^{Z_v} \tilde{\lambda}_p^{\text{CIS(D)'}} \right) > 1 - \tau' \quad (29b)$$

This subset of orbitals containing Z_o occupied CIS(D')-NTOs and Z_v virtual CIS(D')-NTOs is denoted the excitation orbital space (XOS).

6. For the chosen CC model (CC2 in this work), determine the CC excitation energy associated to the targeted transition by solving the CC ground state amplitude equations and the CC eigenvalue problem, both of which are solved using only the CIS(D')-NTOs within the XOS.

We denote the approach defined by these six steps as the Simplified Natural transition Orbital Framework for Large-scale coupled-cluster Excitation energy calculations (SNOFLE_x). We emphasize that the SNOFLE_x procedure should be applied to each electronic transition of interest.

In analogy with Eqs. (14) for CC2, the ranks of the CIS(D') density matrices obey the following equations,

$$\text{rank}(\mathbf{X}^{\text{CIS(D')}}) \leq \min(O, V + OZ^2) = O \quad (30a)$$

$$\text{rank}(\mathbf{Y}^{\text{CIS(D')}}) \leq \min(V, O + Z^2V) = V \quad (30b)$$

and, in general, the eigenvalues of all CIS(D')-NTOs are thus nonzero. The importance of having nonzero eigenvalues for all NTOs can now be understood from the SNOFLE_x procedure above. Indeed, the nonzero eigenvalues are required to ensure a smooth convergence to the target CC excitation energies with decreasing values of τ' —i.e., the full CC calculation is reproduced in the limit where $\tau' \rightarrow 0$, since $Z_o \rightarrow O$ and $Z_v \rightarrow V$.

It should be noted that the use of CIS(D')-NTOs implies that only single-replacement dominated electronic transitions that are described at the CIS level of theory can be addressed. However, many transitions of interest in typical organic and biological molecules are of this type. Furthermore, for the CC2 model, which is the target model in the present study, single-replacement dominated transitions are correct through second order in the fluctuation potential, while double-replacement dominated transitions are correct only to zeroth order.⁵⁷ The CC2 model thus provides accurate results only for transitions dominated by single-electron replacements. The fact that our CIS(D')-NTOs can be generated only for such transitions is therefore not a severe limitation from a practical point of view.

In practice we transform the CIS(D')-NTOs within the given XOS to a pseudo-canonical basis by diagonalizing the occupied-occupied and virtual-virtual subblocks of the Fock matrix. In this way, a standard CC code may be used for the ground state and excitation energy calculations in the sixth step above. We also note that the number of atomic orbitals and auxiliary functions used to express the MOs in the XOS can be reduced by removing orbital tails using the least squares fitting procedure, which is detailed in Appendix B of Ref. 58.

In summary, we have described four different sets of orthogonal MOs that may be prioritized according to their expected importance for describing a given electronic

excitation process: the CIS-NTO/LMO mixed orbital space, CC2-NTOs, CIS(D)-NTOs, and CIS(D')-NTOs. The NTOs are defined by the unitary transformation matrices that diagonalize the hole and particle density matrices in Eqs. (2), (9), (22), and (26) for the CIS, CC2, CIS(D), and CIS(D') models, respectively. When defining a reduced orbital space (the XOS), the CC2-NTOs, CIS(D)-NTOs, and CIS(D')-NTOs may be prioritized according to their eigenvalues, while the orbitals of the CIS-NTO/LMO mixed orbital space can be prioritized using the measure in Eq. (8).

III. RESULTS

In this section we present numerical results and investigate the quality of the different orbital spaces introduced in the previous section for the calculation of excitation energies. We consider the lowest CC2 excitation energy for the following molecules:

- The twenty molecules from **XLI** to **LX** in the test set presented in Ref. 59 (depicted in Scheme 3 of that paper).
- 11-cis-retinal using the geometry from Ref. 60.
- Met-enkephalin using the geometry from Ref. 47.
- Molecular clusters of solvated formamide containing up to 144 water molecules. The structures were obtained by modification of a single snapshot taken from Ref. 61 and are available in the supporting information.

All calculations have been performed with a local version of the LSDalton program,^{62,63} using the frozen core approximation. The correlation consistent aug-cc-pVDZ' and aug-cc-pVTZ' basis sets^{64,65} were used with the corresponding auxiliary basis sets aug-cc-pVDZ-RI' and aug-cc-pVTZ-RI' for the RI approximation.⁶⁶ The prime in the basis set notation indicates that diffuse functions have been removed from the hydrogen atoms.

In Section III A we perform a comparison of the four different orbital spaces described in Section II for two selected molecules that represent a local (met-enkephalin) and a delocalized (11-cis-retinal) electronic transition. In Section III B we apply the SNOFLE_x method to a test set composed of molecules **XLI** to **LX**, 11-cis-retinal, and met-enkephalin. The calculated excitation energies and computational timings are compared to full CC2 calculations. In Section III C we demonstrate the potential of SNOFLE_x by applying it to solvated formamide with an increasing number of water molecules.

A. Comparison of NTOs

In this section, we consider the lowest electronic transitions in met-enkephalin and 11-cis-retinal, which are depicted in Figs. 2 and 3 together with the dominant pair

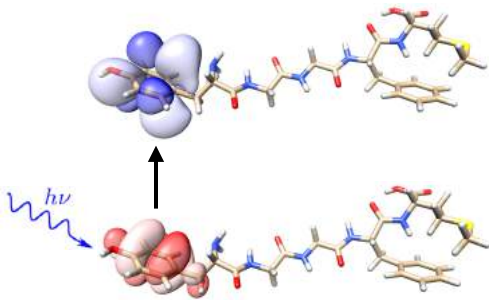


FIG. 2: Illustration of lowest electronic transition in met-enkephalin in terms of the dominant occupied (red, bottom) and virtual (blue, top) CIS-NTOs (aug-cc-pVDZ' basis). The contour plot value was set to 0.02 a.u.^{67,68}

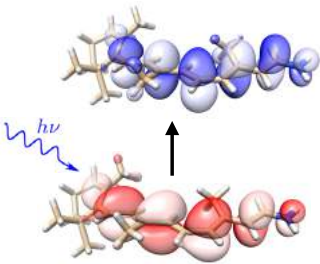


FIG. 3: Illustration of lowest electronic transition in 11-cis-retinal in terms of the dominant occupied (red, bottom) and virtual (blue, top) CIS-NTOs (aug-cc-pVDZ' basis). The contour plot value was set to 0.02 a.u.^{67,68}

of CIS-NTOs corresponding to the lowest electronic transition. For met-enkephalin, it is clear that the transition is localized in a relatively small region of the molecule, while the transition in 11-cis-retinal involves almost the entire molecule. The met-enkephalin and 11-cis-retinal cases are therefore prototypes of a local and a delocalized transition, respectively.

We have carried out CC2 calculations within restricted XOSs using the four different sets of orbitals described in Section II, i.e., the CIS-NTO/LMO, CC2-NTO, CIS(D)-NTO, and CIS(D')-NTO orbital spaces using $\tau' = 10^{-4}$ for the generation of CIS(D')-NTOs. For a given XOS we simply solve the CC2 ground state amplitude equation and CC2 eigenvalue equation using only the subset of orbitals within the XOS. The orbitals are prioritized as described in section II, and the dimension of the XOS is increased until the full CC2 calculation is reproduced. In Figs. 4 and 5 we present the lowest CC2 excitation energies and associated errors for the met-enkephalin and 11-cis-retinal molecules as a function of the number of MOs included in the XOS. For a given XOS, errors compared to full CC2 calculation arise since (i) the ground state amplitude equations and (ii) the CC2 eigenvalue

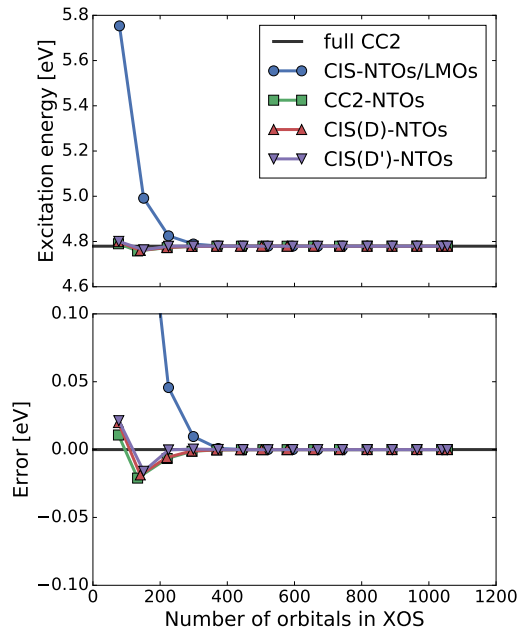


FIG. 4: Calculated CC2/aug-cc-pVDZ' excitation energy (top) and error (bottom) as a function of the size of the excitation orbital space (XOS) for met-enkephalin (aug-cc-pVDZ' basis) using different choices of orbital spaces.

problem in Eq. (10) are solved in the restricted XOS. We note that the (i)-errors affects the (ii)-errors indirectly, since the Jacobian matrix \mathbf{A} in Eq. (10) is determined from ground state amplitudes.⁵⁰ All in all, the complex interplay of these two error sources ultimately leads to the errors observed in Figs. 4 and 5.

The CIS-NTO/LMO mixed space behaves markedly different for the two molecules. For met-enkephalin the excitation energy error is below 0.1 eV when about 200 orbitals have been included in the XOS based on eq. (8) [see Fig. 4 (bottom)], while almost 500 orbitals are required to achieve the same accuracy for 11-cis-retinal [see Fig. 5 (bottom)]. This behaviour is expected based on the localities of the two transitions. For the local transition in met-enkephalin (Fig. 2), the use of LMOs enables a significant reduction of the XOS, since a large region of the molecule is unaffected by the transition. On the other hand, for the delocalized transition in 11-cis-retinal (Fig. 3), the transition induces changes in the electronic structure throughout the molecular system and the use of LMOs offers very modest reductions of the XOS. These two examples clearly show the strength and weaknesses of the CIS-NTO/LMO approach introduced in Ref. 47, i.e., significant computational savings are possible for local transitions, while a delocalized transition essentially requires the full molecular CC calculation to be carried

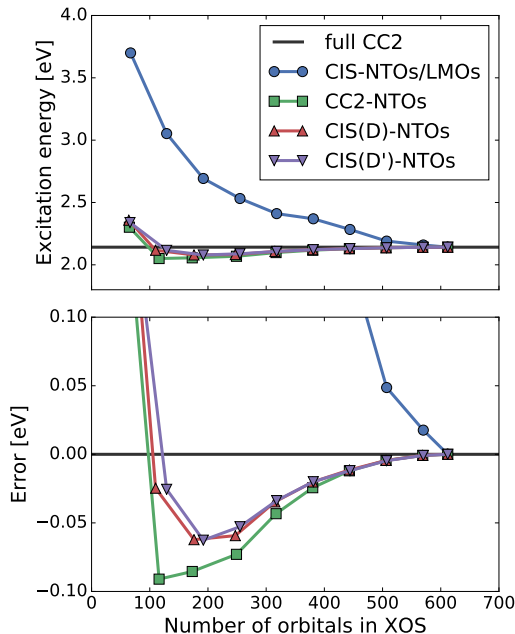


FIG. 5: Calculated CC2/aug-cc-pVDZ' excitation energy (top) and error (bottom) as a function of the size of the excitation orbital space (XOS) for 11-cis-retinal (aug-cc-pVDZ' basis) using different choices of orbital spaces.

out.

From Figs. 4 and 5 it is seen that the calculations using CC2-, CIS(D)-, or CIS(D')-NTOs exhibit much smaller errors than the calculations using the CIS-NTO/LMO mixed space. For the delocalized transition in Fig. 5, the use of either CC2-, CIS(D)-, or CIS(D')-NTOs allow for errors below 0.1 eV with only around 100 orbitals in the XOS, and, even for the local transition in Fig. 4, the use of either CC2-, CIS(D)-, or CIS(D')-NTOs leads to much smaller errors than the CIS-NTO/LMO mixed space for a given size of the XOS.

The results in Figs. 4 and 5 obtained using the CC2-, CIS(D)-, and CIS(D')-NTOs are very similar, indicating that all three sets of NTOs contain information about the basic correlation effects. This is a very important result, since the CIS(D')-NTOs are much cheaper to generate than the CIS(D)- and CC2-NTOs (see Section II and appendix A). We note that both negative and positive errors occur, and it is notable that in many cases the CIS(D')-NTOs yield smaller absolute errors than the CIS(D)- and CC2-NTOs. This can happen due to a cancellation of the error sources (i) and (ii) mentioned above.

In summary, the met-enkephalin and 11-cis-retinal results presented here indicate that the CIS(D')-NTOs can be used to generate a reduced orbital space that may significantly lower the computational cost of CC2 calcu-

lations for both local and delocalized transitions.

B. Performance of SNOFLEx for test set

In this section we use the test set of 22 molecules presented at the beginning of this section to compare the accuracy and computational cost of the SNOFLEx procedure described in Section II D with conventional (canonical) CC2 calculations. In Tables I and II, we report a statistical analysis of the lowest excitation energies for the considered test set using the aug-cc-pVDZ' and aug-cc-pVTZ' basis sets. In order to evaluate the convergence of the excitation energies with the size of the XOS, we have performed calculations using $\tau' = 10^{-3}$, 10^{-4} , and 10^{-5} . For each transition, a conventional CC2 calculation (using the complete orbital space) has been performed to serve as a reference in the statistical analysis. We report the individual errors in the excitation energies, $\Delta_i = \omega_i^{\text{SNOFLEx}} - \omega_i^{\text{ref}}$, along with the mean absolute error,

$$\bar{\Delta}_{\text{abs}} = \frac{1}{n} \sum_{i=1}^n |\Delta_i|, \quad (31)$$

the maximum absolute error,

$$\Delta_{\text{max}} = \max_i |\Delta_i|, \quad (32)$$

the mean error,

$$\bar{\Delta} = \frac{1}{n} \sum_{i=1}^n \Delta_i, \quad (33)$$

and the standard deviation,

$$\Delta_{\text{std}} = \sqrt{\frac{1}{n-1} \sum_{i=1}^n (\Delta_i - \bar{\Delta})^2}. \quad (34)$$

where $n = 22$ is the number of molecules in the test set.

From Tables I and II, we see that the excitation energies obtained with SNOFLEx are very well behaved. For example, using $\tau' = 10^{-4}$, accurate results are obtained compared to a conventional CC2 calculation, with a mean absolute error of $\bar{\Delta}_{\text{abs}} = 0.01$ eV for both aug-cc-pVDZ' and aug-cc-pVTZ' basis sets. However, the maximum absolute errors and the standard deviations are slightly larger in the aug-cc-pVTZ' basis (e.g., $\Delta_{\text{max}} = 0.02$ eV and $\Delta_{\text{max}} = 0.05$ eV in the aug-cc-pVDZ' and aug-cc-pVTZ' basis sets, respectively). Overall, these results indicate that SNOFLEx with $\tau' = 10^{-4}$ provides excitation energies of CC2 quality and it is therefore the threshold that we recommend in practical applications.

In contrast, the results obtained with $\tau' = 10^{-3}$ are significantly less accurate. The mean absolute errors ($\bar{\Delta}_{\text{abs}} = 0.11$ eV and $\bar{\Delta}_{\text{abs}} = 0.09$ eV in the aug-cc-pVDZ' and aug-cc-pVTZ' basis sets, respectively) and the maximum absolute errors ($\bar{\Delta}_{\text{abs}} = 0.28$ eV and $\bar{\Delta}_{\text{abs}} = 0.23$

TABLE I: Statistical analysis of the lowest excitation energy from SNOFLEx calculations compared to conventional CC2 calculations using the aug-cc-pVDZ' basis set. The error (Δ) is reported in eV for each transition together with the reference excitation energy ω^{ref} . Three different values of τ' have been used and are specified in parenthesis in the header of the relevant columns. The mean absolute error ($\bar{\Delta}_{\text{abs}}$), the maximum absolute error (Δ_{max}), the mean error ($\bar{\Delta}$), and the standard deviation (Δ_{std}) are also reported.

| Molecule | $\Delta(10^{-3})$ | $\Delta(10^{-4})$ | $\Delta(10^{-5})$ | ω^{ref} |
|-----------------------------|-------------------|-------------------|-------------------|-----------------------|
| XLI | 0.13 | 0.01 | -0.00 | 4.80 |
| XLII | 0.19 | 0.02 | -0.00 | 4.48 |
| XLIII | 0.07 | 0.00 | -0.00 | 4.06 |
| XLIV | 0.10 | -0.00 | -0.00 | 2.42 |
| XLV | 0.07 | -0.00 | -0.00 | 3.70 |
| XLVI | 0.11 | 0.00 | -0.00 | 2.92 |
| XLVII | 0.05 | -0.00 | -0.00 | 2.52 |
| XLVIII | 0.11 | 0.01 | -0.00 | 3.60 |
| XLIX | 0.21 | 0.00 | -0.00 | 3.94 |
| L | 0.05 | -0.01 | -0.00 | 3.81 |
| LI | 0.04 | -0.00 | -0.00 | 2.10 |
| LII | 0.05 | -0.01 | 0.00 | 2.67 |
| LIII | 0.07 | -0.01 | 0.00 | 2.93 |
| LIV | 0.07 | 0.01 | -0.00 | 2.45 |
| LV | 0.06 | 0.01 | -0.00 | 2.33 |
| LVI | 0.13 | -0.02 | -0.00 | 3.78 |
| LVII | 0.07 | -0.02 | -0.00 | 3.37 |
| LVIII | 0.21 | 0.01 | -0.00 | 3.44 |
| LIX | 0.28 | -0.02 | -0.01 | 2.67 |
| LX | 0.14 | 0.00 | -0.00 | 3.85 |
| 11-cis-retinal | 0.00 | -0.01 | -0.01 | 2.14 |
| met-enkephalin | 0.14 | -0.00 | 0.00 | 4.78 |
| $\bar{\Delta}_{\text{abs}}$ | 0.11 | 0.01 | 0.00 | — |
| Δ_{max} | 0.28 | 0.02 | 0.01 | — |
| $\bar{\Delta}$ | 0.11 | -0.00 | -0.00 | — |
| Δ_{std} | 0.07 | 0.01 | 0.00 | — |

TABLE II: Statistical analysis of the lowest excitation energy from SNOFLEx calculations compared to conventional CC2 calculations using the aug-cc-pVTZ' basis set. The error (Δ) is reported in eV for each transition together with the reference excitation energy ω^{ref} . Three different values of τ' have been used and are specified in parenthesis in the header of the relevant columns. The mean absolute error ($\bar{\Delta}_{\text{abs}}$), the maximum absolute error (Δ_{max}), the mean error ($\bar{\Delta}$), and the standard deviation (Δ_{std}) are also reported.

| Molecule | $\Delta(10^{-3})$ | $\Delta(10^{-4})$ | $\Delta(10^{-5})$ | ω^{ref} |
|-----------------------------|-------------------|-------------------|-------------------|-----------------------|
| XLI | 0.12 | 0.00 | -0.00 | 4.77 |
| XLII | 0.18 | 0.01 | -0.00 | 4.45 |
| XLIII | 0.05 | -0.01 | -0.00 | 4.04 |
| XLIV | 0.09 | -0.01 | -0.00 | 2.42 |
| XLV | 0.07 | -0.01 | -0.00 | 3.67 |
| XLVI | 0.11 | -0.00 | -0.00 | 2.90 |
| XLVII | 0.03 | -0.01 | -0.00 | 2.51 |
| XLVIII | 0.09 | 0.01 | -0.00 | 3.57 |
| XLIX | 0.20 | -0.01 | -0.01 | 3.93 |
| L | 0.02 | -0.02 | -0.00 | 3.78 |
| LI | 0.02 | -0.01 | -0.00 | 2.08 |
| LII | 0.03 | -0.02 | -0.00 | 2.65 |
| LIII | 0.05 | -0.02 | -0.00 | 2.92 |
| LIV | 0.06 | -0.00 | -0.00 | 2.42 |
| LV | 0.05 | 0.00 | -0.00 | 2.32 |
| LVI | 0.12 | -0.02 | -0.00 | 3.77 |
| LVII | 0.04 | -0.04 | -0.01 | 3.37 |
| LVIII | 0.17 | -0.01 | -0.01 | 3.44 |
| LIX | 0.23 | -0.05 | -0.02 | 2.66 |
| LX | 0.13 | 0.00 | -0.00 | 3.83 |
| 11-cis-retinal | -0.03 | -0.03 | -0.01 | 2.12 |
| met-enkephalin | 0.13 | -0.01 | -0.00 | 4.76 |
| $\bar{\Delta}_{\text{abs}}$ | 0.09 | 0.01 | 0.00 | — |
| Δ_{max} | 0.23 | 0.05 | 0.02 | — |
| $\bar{\Delta}$ | 0.09 | -0.01 | -0.00 | — |
| Δ_{std} | 0.07 | 0.02 | 0.00 | — |

TABLE III: Speed-ups of SNOFLE_x calculations compared to full calculations ($T_{\text{full}}/T_{\text{SNOFLE}_x}$ for the molecules in the test set using the aug-cc-pVDZ' basis and different values of τ' .

| Molecule | $\tau' = 10^{-3}$ | $\tau' = 10^{-4}$ | $\tau' = 10^{-5}$ |
|-------------------|-------------------|-------------------|-------------------|
| XLI | 1.5 | 1.1 | 0.9 |
| XLII | 2.1 | 1.4 | 0.8 |
| XLIII | 1.5 | 1.3 | 1.0 |
| XLIV | 2.0 | 1.2 | 0.9 |
| XLV | 1.5 | 1.1 | 1.0 |
| XLVI | 1.6 | 1.1 | 1.0 |
| XLVII | 1.8 | 1.0 | 0.9 |
| XLVIII | 3.8 | 2.0 | 1.3 |
| XLIX | 1.5 | 1.2 | 1.0 |
| L | 3.2 | 1.9 | 1.3 |
| LI | 2.8 | 1.5 | 1.0 |
| LII | 2.2 | 1.7 | 1.2 |
| LIII | 2.8 | 1.7 | 1.3 |
| LIV | 2.1 | 1.3 | 1.0 |
| LV | 2.1 | 1.3 | 1.0 |
| LVI | 3.5 | 2.0 | 1.3 |
| LVII | 3.1 | 1.4 | 1.0 |
| LVIII | 3.0 | 1.8 | 1.3 |
| LIX | 2.6 | 1.3 | 1.3 |
| LX | 3.3 | 1.9 | 1.3 |
| 11-cis-retinal | 2.9 | 1.9 | 1.4 |
| met-enkephalin | 96.2 | 54.7 | 33.5 |
| Max. | 96.2 | 54.7 | 33.5 |
| Min. | 1.5 | 1.0 | 0.8 |
| Mean ^a | 2.4 | 1.5 | 1.1 |

^a Met-enkephalin was excluded from the test set

eV) indicate that the results obtained with $\tau' = 10^{-3}$ can have errors as large as the typical deviations of CC2 excitation energies from FCI results.^{48,69,70} SNOFLE_x with $\tau' = 10^{-3}$ should thus only be used for very preliminary investigations.

Finally, when SNOFLE_x is applied with $\tau' = 10^{-5}$, very accurate results are obtained with virtually no errors compared to conventional CC2 results, ($\bar{\Delta}_{\text{abs}} = 0.00$ eV with both aug-cc-pVDZ' and aug-cc-pVTZ' basis sets). Such calculations can thus be performed to confirm the quality of the SNOFLE_x results obtained with $\tau' = 10^{-4}$. In the following, we will refer to the τ' values of 10^{-3} , 10^{-4} and 10^{-5} as *loose*, *standard*, and *tight*, respectively.

It is also interesting to note that the conventional CC2 results for molecules XLI to LX in Tables I and II differ from the aug-cc-pVTZ results in Ref. 59 by at most 0.03 eV and 0.004 eV for the aug-cc-pVDZ' and aug-cc-pVTZ' basis sets, respectively. It is thus seen that the removal of diffuse basis functions on hydrogen atoms has a negligible effect on the calculated excitation energies, but also that the aug-cc-pVDZ' basis is sufficient to obtain a good description of the considered transitions. Triple- ζ quality basis sets and higher are however generally needed to describe higher lying excited states.⁴⁸

In order to analyze the computational cost of SNOFLE_x compared to conventional CC2 calculations, we have reported speed-ups in Tables III and IV for all the molecules in the test set with the loose, standard, and tight thresholds, as described previously. The speed-ups

TABLE IV: Speed-ups of SNOFLE_x calculations compared to full calculations ($T_{\text{full}}/T_{\text{SNOFLE}_x}$ for the molecules in the test set using the aug-cc-pVTZ' basis and different values of τ' .

| Molecule | $\tau' = 10^{-3}$ | $\tau' = 10^{-4}$ | $\tau' = 10^{-5}$ |
|-------------------|-------------------|-------------------|-------------------|
| XLI | 1.3 | 1.1 | 0.9 |
| XLII | 1.9 | 1.4 | 1.1 |
| XLIII | 1.7 | 1.4 | 1.1 |
| XLIV | 1.8 | 1.3 | 0.9 |
| XLV | 1.4 | 1.1 | 1.0 |
| XLVI | 1.5 | 1.2 | 1.0 |
| XLVII | 1.6 | 1.1 | 1.0 |
| XLVIII | 3.6 | 1.9 | 1.3 |
| XLIX | 1.3 | 1.1 | 1.0 |
| L | 3.0 | 1.9 | 1.2 |
| LI | 2.4 | 1.5 | 1.1 |
| LII | 2.2 | 1.5 | 1.2 |
| LIII | 2.4 | 1.7 | 1.3 |
| LIV | 2.1 | 1.4 | 1.1 |
| LV | 2.0 | 1.3 | 1.0 |
| LVI | 2.4 | 1.7 | 1.2 |
| LVII | 2.5 | 1.3 | 0.9 |
| LVIII | 2.5 | 1.6 | 1.3 |
| LIX | 2.0 | 1.5 | 1.1 |
| LX | 3.1 | 2.0 | 1.4 |
| 11-cis-retinal | 2.5 | 1.9 | 1.4 |
| met-enkephalin | 63.2 | 27.9 | 10.9 |
| Max. | 63.2 | 27.9 | 10.9 |
| Min. | 1.3 | 1.1 | 0.9 |
| Mean ^a | 2.2 | 1.5 | 1.1 |

^a Met-enkephalin was excluded from the test set

are calculated from,

$$\text{speed-up} = \frac{T_{\text{full}}}{T_{\text{SNOFLE}_x}}, \quad (35)$$

where T_{full} corresponds to the time spent in the correlation part of a conventional CC2 calculation, (i.e., determination of the CC2 ground state amplitudes and solution of the Jacobian eigenvalue problem in the complete canonical basis), while T_{SNOFLE_x} corresponds to the sum of the time spent in the generation of the CIS(D')-NTOs (Section II C and appendix A) and the time spent in the calculation of the CC2 excitation energies using the same algorithms as for the conventional calculation but in the restricted XOS determined by τ' .

The test set used in this discussion consists of 21 medium-sized chromophores with highly delocalized electronic structures—which represent difficult but very interesting targets for approximated CC methods—as well as the met-enkephalin molecule with a well localized transition (see Fig. 2). From Tables III and IV, we see that—for the chromophores only—an average speed-up of 1.5 is observed for both the aug-cc-pVDZ' and aug-cc-pVTZ' basis sets, with the standard threshold. This is already quite impressive due to the limited size and the delocalized character of the considered systems. The speed-ups are of course larger (smaller) for the loose (tight) threshold. We note that even with the tight threshold, only very few transitions lead to an effective *slow-down*, which is then due to the overhead used for the generation of the CIS(D')-NTOs. Finally, the results for met-enkephalin demonstrate that huge speed-ups are observed when

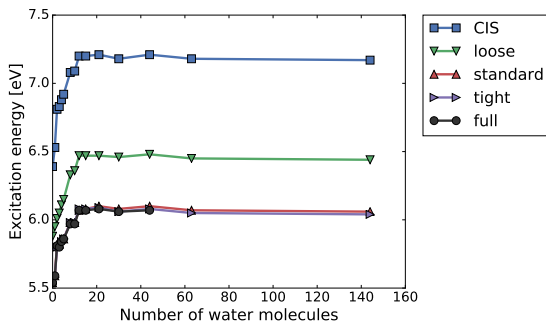


FIG. 6: Lowest excitation energy of a series of solvated formamide with an increasing number of water molecules using the aug-cc-pVDZ’ basis set. CC2-SNOFLEx results are reported using the **loose**, **standard**, and **tight** thresholds. For comparison the conventional **CIS** and CC2 (**full**) results are also reported.

the transition of interested is local (54.7 and 27.9 with the standard threshold for the aug-cc-pVDZ’ and aug-cc-pVTZ’ basis sets, respectively).

All in all, the results presented in Tables I to IV, are very encouraging, both in terms of accuracy and computational savings.

C. Formamide-water clusters

In order to investigate the potential of SNOFLEx for large molecular systems, we now consider the lowest excitation energy in a series of solvated formamide clusters with an increasing number of water molecules. All the calculations have been performed using the aug-cc-pVDZ’ basis set and the SNOFLEx strategy has been applied with the loose, standard, and tight thresholds for clusters including up to 144 water molecules (4836 basis functions). Reference calculations using a conventional CC2 implementation have also been performed for clusters including up to 44 water molecules (1536 basis functions).

In Fig. 6, we have plotted the convergence of the excitation energy as a function of the number of water molecules included in the cluster using the loose, standard, and tight SNOFLEx thresholds. The excitation energies obtained with conventional CIS and CC2 algorithms are also reported. Fig. 6 shows that the solvation effects results in a blueshift of $\simeq 0.8$ eV at the CIS level, while the blueshift is lowered to around 0.5 eV at the CC2 level. Most of the solvation effects are already included with only 12 water molecules and adding more waters results in small oscillations of around 0.03 eV, which are already relatively well described without correlation effects (CIS curve in Fig. 6). We note that the observed solvatochromatic shift is consistent with Ref. 61, but that a conformational sampling is required to obtain reliable results.

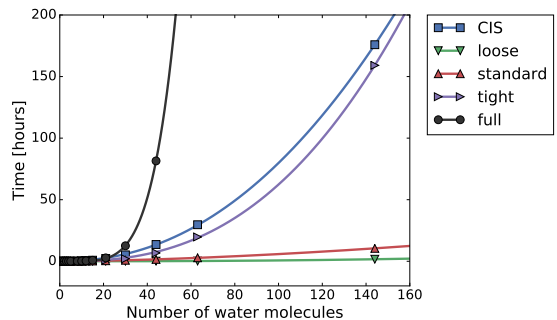


FIG. 7: Computational wall-time spent in the calculation of the lowest excitation energy of a series of formamide-water clusters of increasing size using the aug-cc-pVDZ’ basis set. **CIS**: time spent in the HF ground state and CIS excitation energy calculations (prior the SNOFLEx or full CC2 calculation).

Loose/standard/tight: time spent in the correlated part of the SNOFLEx algorithm (generation of the CIS(D’)-NTOs and solution of the CC2 equations in the XOS). **Full**: solution of the CC2 equations in the full canonical basis. All calculations were performed on a single IBM iDataPlex dx360 M4 compute-node, with 2 octocore Intel E5-2670 CPUs @ 2.67 GHz and 64 GB memory.

Regarding the accuracy of the SNOFLEx calculations, as described in Section III B, the results obtained with the standard and tight thresholds are effectively of CC2 quality, while the loose threshold leads to much larger errors ($\simeq 0.4$ eV). However, it is notable that the main correlation effect (i.e., a lowering of the blueshift compared to the CIS result) is described reasonably well already with the loose threshold.

In order to analyze the performance of the SNOFLEx strategy compared to a conventional algorithm, we have reported timings for the CIS and the correlated parts of the calculations in Fig. 7. For SNOFLEx, the time plotted includes the generation of the CIS(D’)-NTOs and the solution of the CC2 equations in the restricted XOS, while only the time for the solution of the CC2 equations is considered for the full calculation. Fig. 7 shows that the SNOFLEx calculations (with all three thresholds) are systematically faster than the conventional CC2 calculations. For example, for the cluster containing 44 water molecules, the correlated part of the standard SNOFLEx calculation is 53 times faster than the correlated part of a conventional CC2 calculation. Furthermore, the SNOFLEx calculations can be carried out for molecular systems that are out of reach of conventional CC2 code (4836 basis functions).

While the correlated part generally dominates conventional CC2 calculations (“full” curve in Fig. 7), this is not the case for SNOFLEx. The time spent in the correlated part of the calculations with the loose and standard thresholds is in fact negligible compared with time spent in the CIS optimization. Thus, with the standard threshold, CC2 excitation energies are effectively obtained with

the computational cost of a CIS calculation. With the tight threshold, however, the time spent in the correlated part of the calculation is similar to the time spent in the CIS optimization, and it therefore represents a significant part of the total time. Nonetheless, Fig. 7 shows that even with the tight threshold, huge savings are obtained compared to conventional CC2 calculations.

IV. CONCLUSION

In this work we have introduced a new method for the calculation of CC excitation energies on large molecules entitled SNOFLEx. It relies on a generalization of the concept of NTOs to include correlation effects. The correlated NTOs denoted as CIS(D')-NTOS are obtained based on an approximation to the CIS(D) model and their generation formally scales cubically with the system size. Once the CIS(D')-NTOs have been generated, a conventional CC excitation energy calculation can be performed in a reduced orbital space obtained by discarding a subset of occupied and virtual CIS(D')-NTOs with low eigenvalues. We have introduced the loose, standard, and tight thresholds to generate the reduced orbital space, which ultimately define the precision of a SNOFLEx calculation compared to a conventional CC2 calculation.

The SNOFLEx algorithm has been tested for the calculation of CC2 excitation energies on a set of 22 medium-sized molecules resulting in a mean absolute error of 0.01 eV with the standard threshold. Even though the molecules considered were of limited size, significant computational savings were systematically obtained. These results have been confirmed by applying SNOFLEx to a series of formamide-water clusters of increasing size (up to 4836 basis functions) which indicates that our new scheme allows CC2 excitation energies to be determined at the cost of a CIS calculation and thus further extend the capabilities of the CC2 model.

One of the main advantages of SNOFLEx compared to other reduced scaling methods for the calculation of CC excitation energies is that it does not rely explicitly on local approximations. Computational savings are therefore obtained for both local and delocalized electronic transitions. The computational savings and the precision of the calculated excitation energies are defined through a single threshold via the concept of CIS(D')-NTOs. This also implies that only electronic transitions that are described at the CIS level of theory can be addressed (single-replacement dominated transitions). However, these include most transitions of interest in typical organic and biological molecules. We also note that the presented developments are not specific to the CC2 model, and more accurate CC models might also benefit from using the SNOFLEx scheme.

Appendix A: Algorithm for generating CIS(D') density matrices

In this appendix we present an algorithm for calculating the CIS(D') density matrices in Eqs. (26). First, we note that the double-electron integrals entering the evaluation of the doubles excitation vectors in Eqs. (23) may be written as,

$$(A\bar{i}|Bj)^{\text{CIS}} = (\bar{A}i|Bj) + (A\bar{i}|Bj) + (Ai|\bar{B}j) + (Ai|B\bar{j}) \quad (\text{A1a})$$

$$(a\bar{I}|bJ)^{\text{CIS}} = (\bar{a}I|bJ) + (a\bar{I}|bJ) + (aI|\bar{b}J) + (aI|b\bar{J}) \quad (\text{A1b})$$

where we have suppressed the CIS superscript on the right-hand side of the equation and the barred indices are transformed with the $\bar{\Lambda}^{\text{CIS}}$ matrices in Eqs. (21), while the non-barred indices refer to standard MOs in the canonical basis (lowercase) or in the CIS-NTO basis (uppercase), e.g.,

$$(\bar{A}i|Bj) = \sum_{\alpha\beta\gamma\delta} \bar{\Lambda}_{\alpha A}^{\text{CIS}} C_{\beta i} C_{\gamma B} C_{\delta j} (\alpha\beta|\gamma\delta). \quad (\text{A2})$$

We employ the RI approximation to reduced the cost of the generation of four-center integrals in Eq. (A1). For example, the integral in Eq. (A2) may be written as,

$$(\bar{A}i|Bj) = \sum_{\tilde{\Gamma}} (\bar{A}i|\tilde{\Gamma})(\tilde{\Gamma}|Bj) \quad (\text{A3})$$

Here, $|\tilde{\Gamma}\rangle$ is a Löwdin orthonormalized auxiliary basis function,

$$|\tilde{\Gamma}\rangle = \sum_{\Gamma} (\mathbf{S}^{-1/2})_{\Gamma\tilde{\Gamma}} |\Gamma\rangle \quad (\text{A4})$$

where $|\Gamma\rangle$ is an auxiliary basis function and \mathbf{S} is the associated overlap matrix. It then follows that the doubles excitation vectors in Eqs. (23) may be written as,

$$R_{A\bar{i}Bj}^{\text{CIS(D}'')} = \frac{\sum_{\tilde{\Gamma}} P_{ij}^{AB} [(\bar{A}i|\tilde{\Gamma})(\tilde{\Gamma}|Bj) + (A\bar{i}|\tilde{\Gamma})(\tilde{\Gamma}|Bj)]}{\epsilon_i - F_{AA} + \epsilon_j - F_{BB} + \omega^{\text{CIS}}} \quad (\text{A5a})$$

$$R_{a\bar{I}bJ}^{\text{CIS(D}'')} = \frac{\sum_{\tilde{\Gamma}} P_{IJ}^{ab} [(a\bar{I}|\tilde{\Gamma})(\tilde{\Gamma}|bJ) + (a\bar{I}|\tilde{\Gamma})(\tilde{\Gamma}|bJ)]}{F_{II} - \epsilon_a + F_{JJ} - \epsilon_b + \omega^{\text{CIS}}} \quad (\text{A5b})$$

where the action of the permutation operator is defined in Eq. (17). From Eqs. (A5) we see that the following integrals are required to evaluate the doubles contributions to the hole density matrix in Eq. (26a),

- $(\tilde{\Gamma}|A'i), (\tilde{\Gamma}|A'\bar{i}), (\tilde{\Gamma}|\bar{A}'i)$

while the particle density matrix in Eq. (26b) can be determined using the following integrals,

- $(\tilde{\Gamma}|aI'), (\tilde{\Gamma}|\bar{a}I'), (\tilde{\Gamma}|a\bar{I}')$

We recall that the primed indices denote a subset of orbitals of dimension Z as defined by Eq. (25). In the following analysis, we assume that Z is independent of the system size for a given type of electronic transition.

In our current implementation we first calculate the six integrals listed above and store them in memory, but they

TABLE V: Generation of two-electron RI integrals required for constructing CIS(D') hole and particle density matrices. Batching of integrals and reordering of tensors have been omitted for clarity.

| Step | Operation | Prefactor | Scaling |
|------|--|-----------|------------------------------------|
| 1 | Calculate integrals $(\Gamma \alpha\beta)$ | | $\mathcal{O}(N_\Gamma N_\alpha^2)$ |
| 2 | $(\Gamma A'\beta) \leftarrow \sum_\alpha C_{\alpha A'}(\Gamma \alpha\beta)$ $(\Gamma A'\bar{\beta}) \leftarrow \sum_\alpha \bar{\Lambda}_{\alpha A'}^{\text{CIS}}(\Gamma \alpha\beta)$ $(\Gamma \alpha I') \leftarrow \sum_\beta C_{\beta I'}(\Gamma \alpha\beta)$ $(\Gamma \alpha \bar{I}') \leftarrow \sum_\beta \bar{\Lambda}_{\beta I'}^{\text{CIS}}(\Gamma \alpha\beta)$ | Z | $\mathcal{O}(N_\Gamma N_\alpha^2)$ |
| 3 | $(\Gamma A'i) \leftarrow \sum_\beta C_{\beta i}(\Gamma A'\beta)$ $(\Gamma A'\bar{i}) \leftarrow \sum_\beta \bar{\Lambda}_{\beta i}^{\text{CIS}}(\Gamma A'\beta)$ $(\Gamma \bar{A}'i) \leftarrow \sum_\beta C_{\beta i}(\Gamma A'\beta)$ | Z | $\mathcal{O}(N_\Gamma N_\alpha O)$ |
| 4 | $(\Gamma aI') \leftarrow \sum_\alpha C_{\alpha a}(\Gamma \alpha I')$ $(\Gamma \bar{a}I') \leftarrow \sum_\alpha \bar{\Lambda}_{\alpha a}^{\text{CIS}}(\Gamma \alpha I')$ $(\Gamma a\bar{I}') \leftarrow \sum_\alpha C_{\alpha a}(\Gamma \alpha \bar{I}')$ | Z | $\mathcal{O}(N_\Gamma N_\alpha V)$ |
| 5 | $(\tilde{\Gamma} A'i) \leftarrow \sum_\Gamma (\mathbf{S}^{-1/2})_{\Gamma\tilde{\Gamma}}(\Gamma A'i)$ $(\tilde{\Gamma} A'\bar{i}) \leftarrow \sum_\Gamma (\mathbf{S}^{-1/2})_{\Gamma\tilde{\Gamma}}(\Gamma A'\bar{i})$ $(\tilde{\Gamma} \bar{A}'i) \leftarrow \sum_\Gamma (\mathbf{S}^{-1/2})_{\Gamma\tilde{\Gamma}}(\Gamma \bar{A}'i)$ | Z | $\mathcal{O}(N_\Gamma^2 O)$ |
| 6 | $(\tilde{\Gamma} aI') \leftarrow \sum_\Gamma (\mathbf{S}^{-1/2})_{\Gamma\tilde{\Gamma}}(\Gamma aI')$ $(\tilde{\Gamma} \bar{a}I') \leftarrow \sum_\Gamma (\mathbf{S}^{-1/2})_{\Gamma\tilde{\Gamma}}(\Gamma \bar{a}I')$ $(\tilde{\Gamma} a\bar{I}') \leftarrow \sum_\Gamma (\mathbf{S}^{-1/2})_{\Gamma\tilde{\Gamma}}(\Gamma a\bar{I}')$ | Z | $\mathcal{O}(N_\Gamma^2 V)$ |

could of course be written to disk if necessary. The construction of the integrals is detailed in Table V. The first step is the construction of the $(\Gamma|\alpha\beta)$ integrals, which formally scales as $\mathcal{O}(N_\Gamma N_\alpha^2)$ where N_α and N_Γ denote the number of atomic and auxiliary basis functions, respectively. However, this scaling is effectively only quadratic with system size if efficient integral screening techniques are employed. In step 2, one of the AO indices is transformed to a reduced MO index of dimension Z , which is generally much smaller than the occupied and virtual dimensions. It is therefore very important that this reduced index is transformed first, and these steps scale as $\mathcal{O}(N_\Gamma N_\alpha^2)$. In step 3(4), the second AO index is transformed to an occupied (virtual) index leading to a formal scaling of $\mathcal{O}(N_\Gamma N_\alpha O)$ ($\mathcal{O}(N_\Gamma N_\alpha V)$). Finally, in steps 5 and 6 the auxiliary index is transformed with the $\mathbf{S}^{-1/2}$ matrix to provide the desired three-center integrals listed above. This last steps scales as $\mathcal{O}(N_\Gamma^2 O)$ or $\mathcal{O}(N_\Gamma^2 V)$ depending on the type of integrals. Since the reduced dimension Z is considered to be independent of the system size, the generation of the integrals in Table V thus scales cubically with the system size.

Once the integrals have been generated from Table V, the density matrices can be evaluated according to Eq. (26). The algorithm for the hole and particle density matrices are given in Algorithms 1 and 2, respectively. It is seen that these algorithms formally are $\mathcal{O}(N^3)$ scaling, assuming again that the reduced dimension Z is independent of system size.

All in all, we conclude that the generation of the hole and particle density matrices—according to Table V and

Algorithms 1 and 2—scales cubically with the size of the molecular system for a given type of electronic transition. The prefactor depends on the dimension of the reduced set of orbitals, Z , which depends on the requested precision (τ') and the type of electronic transition under consideration.

```

1:  $X_{ij}^{\text{CIS}(\text{D}')} = \sum_a R_{ai}^{\text{CIS}} R_{aj}^{\text{CIS}}$ 
2: for  $A' = 1, Z$  do
3:   for  $B' = 1, Z$  do
4:     for  $k = 1, O$  do
5:       for  $l = 1, O$  do
6:         for  $\tilde{\Gamma} = 1, N_{\Gamma}$  do
7:            $(A'|\bar{l}|B'k)_+ = P_{ik}^{A'B'}[(\bar{A}l|\tilde{\Gamma})(\tilde{\Gamma}|B'k) + (\bar{A}l|\tilde{\Gamma})(\tilde{\Gamma}|B'k)]$ 
8:         end for  $\tilde{\Gamma}$ 
9:          $R_{A'lB'k} = (A'|\bar{l}|B'k)/(e_l - F_{A'A'} + \epsilon_k - F_{B'B'} + \omega^{\text{CIS}})$ 
10:       end for  $l$ 
11:     for  $i = 1, O$  do
12:       for  $j = 1, O$  do
13:          $X_{ij}^{\text{CIS}(\text{D}')}_+ = \frac{1}{2}R_{A'iB'k}R_{A'jB'k}$ 
14:       end for  $j$ 
15:     end for  $i$ 
16:   end for  $k$ 
17: end for  $B'$ 
18: end for  $A'$ 

```

ALG. 1: Construction of the hole density matrix, $\mathbf{X}^{\text{CIS}(\text{D}')}$. The necessary two-electron integrals have been determined using Table V.

```

1:  $Y_{ab}^{\text{CIS}(\text{D}')} = \sum_i R_{ai}^{\text{CIS}} R_{bi}^{\text{CIS}}$ 
2: for  $I' = 1, Z$  do
3:   for  $J' = 1, Z$  do
4:     for  $c = 1, V$  do
5:       for  $d = 1, V$  do
6:         for  $\tilde{\Gamma} = 1, N_{\Gamma}$  do
7:            $(dI'|\bar{c}J')_+ = P_{I'J'}^{dc}[(\bar{d}I'|\tilde{\Gamma})(\tilde{\Gamma}|cJ') + (d\bar{I}|\tilde{\Gamma})(\tilde{\Gamma}|cJ')]$ 
8:         end for  $\tilde{\Gamma}$ 
9:          $R_{dI'cJ'} = (dI'|\bar{c}J')/(F_{I'I'} - \epsilon_d + F_{J'J'} - \epsilon_c + \omega^{\text{CIS}})$ 
10:       end for  $d$ 
11:     for  $a = 1, V$  do
12:       for  $b = 1, V$  do
13:          $Y_{ab}^{\text{CIS}(\text{D}')}_+ = \frac{1}{2}R_{aI'cJ'}R_{bI'cJ'}$ 
14:       end for  $b$ 
15:     end for  $a$ 
16:   end for  $c$ 
17: end for  $J'$ 
18: end for  $I'$ 

```

ALG. 2: Construction of the particle density matrix, $\mathbf{Y}^{\text{CIS}(\text{D}')}$. The necessary two-electron integrals have been determined using Table V.

- ¹J. Čížek, *J. Chem. Phys.* **45**, 4256 (1966).
- ²I. Shavitt and R. J. Bartlett, *Many-Body Methods in Chemistry and Physics: Many-Body Perturbation Theory and Coupled-Cluster Theory* (Cambridge University Press, Cambridge, UK, 2009).
- ³H. J. Monkhorst, *Int. J. Quantum Chem.* **12**, 421 (1977).
- ⁴E. Dalggaard and H. J. Monkhorst, *Phys. Rev. A* **28**, 1217 (1983).
- ⁵J. Olsen and P. Jørgensen, *J. Chem. Phys.* **82**, 3235 (1985).
- ⁶H. Koch and P. Jørgensen, *J. Chem. Phys.* **93**, 3333 (1990).
- ⁷A. E. Kondo, P. Piecuch, and J. Paldus, *J. Chem. Phys.* **104**, 8566 (1996).
- ⁸K. Emrich, *Nucl. Phys. A* **351**, 397 (1981).
- ⁹H. Sekino and R. J. Bartlett, *Int. J. Quantum Chem.* **26**, 255 (1984).
- ¹⁰J. F. Stanton and R. J. Bartlett, *J. Chem. Phys.* **98**, 7029 (1993).
- ¹¹A. I. Krylov, *Annu. Rev. Phys. Chem.* **59**, 433 (2008).
- ¹²L. González, D. Escudero, and L. Serrano-Andrés, *ChemPhysChem* **13**, 28 (2012).
- ¹³A. J. Cohen, P. Mori-Sanchez, and W. Yang, *Science* **321**, 792 (2008).
- ¹⁴A. Dreuw and M. Head-Gordon, *J. Am. Chem. Soc.* **126**, 4007 (2004).
- ¹⁵R. K. Nesbet, *Adv. Chem. Phys.* **IX**, 321 (1965).
- ¹⁶S. Sæbø and P. Pulay, *Annu. Rev. Phys. Chem.* **44**, 213 (1993).
- ¹⁷C. Riplinger, P. Pinski, U. Becker, E. F. Valeev, and F. Neese, *J. Chem. Phys.* **144**, 024109 (2016).
- ¹⁸H.-J. Werner, G. Knizia, C. Krause, M. Schwilk, and M. Dornbach, *J. Chem. Theory Comput.* **11**, 484 (2015).
- ¹⁹Z. Rolik, L. Szegedy, I. Ladjászki, B. Ladóczki, and M. Kállay, *J. Chem. Phys.* **139**, 094105 (2013).
- ²⁰P. R. Nagy, G. Samu, and M. Kállay, *J. Chem. Theory Comput.* **12**, 4897 (2016).
- ²¹T. Kjærgaard, *J. Chem. Phys.* **146**, 044103 (2017).

- ²²J. Pipek and P. G. Mezey, *J. Chem. Phys.* **90**, 4916 (1989).
- ²³S. F. Boys, *Rev. Mod. Phys.* **32**, 296 (1960).
- ²⁴C. Edmiston and K. Ruedenberg, *Rev. Mod. Phys.* **35**, 457 (1963).
- ²⁵B. Jansík, S. Høst, K. Kristensen, and P. Jørgensen, *J. Chem. Phys.* **134**, 194104 (2011).
- ²⁶I.-M. Høyvik, B. Jansík, and P. Jørgensen, *J. Chem. Phys.* **137**, 224114 (2012).
- ²⁷I.-M. Høyvik and P. Jørgensen, *Chem. Rev.* **116**, 3306 (2016).
- ²⁸P. Pulay, *Chem. Phys. Lett.* **100**, 151 (1983).
- ²⁹J. Yang, Y. Kurashige, F. R. Manby, and G. K.-L. Chan, *J. Chem. Phys.* **134**, 044123 (2011).
- ³⁰P.-O. Löwdin, *Phys. Rev.* **97**, 1474 (1955).
- ³¹C. Edmiston, *J. Chem. Phys.* **45**, 1833 (1966).
- ³²F. Neese, F. Wennmohs, and A. Hansen, *J. Chem. Phys.* **130**, 114108 (2009).
- ³³T. D. Crawford and R. A. King, *Chem. Phys. Lett.* **366**, 611 (2002).
- ³⁴T. Korona and H.-J. Werner, *J. Chem. Phys.* **118**, 3006 (2003).
- ³⁵D. Kats, T. Korona, and M. Schütz, *J. Chem. Phys.* **125**, 104106 (2006).
- ³⁶D. Kats, T. Korona, and M. Schütz, *J. Chem. Phys.* **127**, 064107 (2007).
- ³⁷D. Kats and M. Schütz, *J. Chem. Phys.* **131**, 124117 (2009).
- ³⁸B. Helmich and C. Hättig, *J. Chem. Phys.* **139**, 084114 (2013).
- ³⁹B. Helmich and C. Hättig, *Comput. Theor. Chem.* **1040-1041**, 35 (2014).
- ⁴⁰T. D. Crawford, in *Recent Progress in Coupled Cluster Methods: Theory and Applications*, Vol. 53, edited by P. Čársky, J. Paldus, and J. Pittner (Springer Netherlands, Dordrecht, 2010) Chap. 2, pp. 37–55.
- ⁴¹R. A. Mata and H. Stoll, *J. Chem. Phys.* **134**, 034122 (2011).
- ⁴²R. H. Myhre, A. M. J. Sánchez de Merás, and H. Koch, *Mol. Phys.* **111**, 1109 (2013).
- ⁴³R. H. Myhre, A. M. J. Sánchez de Merás, and H. Koch, *J. Chem. Phys.* **141**, 224105 (2014).
- ⁴⁴R. H. Myhre and H. Koch, *J. Chem. Phys.* **145**, 044111 (2016).
- ⁴⁵M. Caricato, T. Vreven, G. W. Trucks, and M. J. Frisch, *J. Chem. Phys.* **133**, 054104 (2010).
- ⁴⁶M. Caricato, T. Vreven, G. W. Trucks, and M. J. Frisch, *J. Chem. Theory Comput.* **7**, 180 (2011).
- ⁴⁷P. Baudin and K. Kristensen, *J. Chem. Phys.* **144**, 224106 (2016).
- ⁴⁸R. Send, V. R. I. Kaila, and D. Sundholm, *J. Chem. Theory Comput.* **7**, 2473 (2011).
- ⁴⁹A. Kumar and T. D. Crawford, *J. Phys. Chem. A Article*, ASAP (2017).
- ⁵⁰O. Christiansen, H. Koch, and P. Jørgensen, *Chem. Phys. Lett.* **243**, 409 (1995).
- ⁵¹C. Hättig and F. Weigend, *J. Chem. Phys.* **113**, 5154 (2000).
- ⁵²M. Head-Gordon, R. J. Rico, M. Oumi, and T. J. Lee, *Chem. Phys. Lett.* **219**, 21 (1994).
- ⁵³A. V. Luzanov, A. A. Sukhorukov, and V. E. Umanskii, *Theor. Exp. Chem.* **10**, 354 (1976).
- ⁵⁴R. L. Martin, *J. Chem. Phys.* **118**, 4775 (2003).
- ⁵⁵J. B. Foresman, M. Head-Gordon, J. a. Pople, and M. J. Frisch, *J. Phys. Chem.* **96**, 135 (1992).
- ⁵⁶C. M. Isborn, N. Luehr, I. S. Ufimtsev, and T. J. Martínez, *J. Chem. Theory Comput.* **7**, 1814 (2011).
- ⁵⁷K. Hald, P. Jørgensen, J. Olsen, and M. Jaszuński, *J. Chem. Phys.* **115**, 671 (2001).
- ⁵⁸P. Ettenhuber, P. Baudin, T. Kjærgaard, P. Jørgensen, and K. Kristensen, *J. Chem. Phys.* **144**, 164116 (2016).
- ⁵⁹D. Jacquemin, I. Duchemin, and X. Blase, *J. Chem. Theory Comput.* **11**, 5340 (2015).
- ⁶⁰A. K. Dutta, F. Neese, and R. Izsák, *J. Chem. Phys.* **145**, 034102 (2016).
- ⁶¹K. Sneskov, T. Schwabe, J. Kongsted, and O. Christiansen, *J. Chem. Phys.* **134**, 104108 (2011).
- ⁶²“LSDalton, a linear-scaling molecular electronic structure program, Release Dalton2016 (2015), see <http://daltonprogram.org>.”
- ⁶³K. Aidas, C. Angeli, K. L. Bak, V. Bakken, R. Bast, L. Boman, O. Christiansen, R. Cimraglia, S. Coriani, P. Dahle, E. K. Dalskov, U. Ekström, T. Enevoldsen, J. J. Eriksen, P. Ettenhuber, B. Fernández, L. Ferrighi, H. Fliegl, L. Frediani, K. Hald, A. Halkier, C. Hättig, H. Heiberg, T. Helgaker, A. C. Hennum, H. Hettema, E. Hjertenaes, S. Høst, I.-M. Høyvik, M. F. Iozzi, B. Jansík, H. J. A. Jensen, D. Jonsson, P. Jørgensen, J. Kauczor, S. Kirpekar, T. Kjærgaard, W. Klopper, S. Knecht, R. Kobayashi, H. Koch, J. Kongsted, A. Krapp, K. Kristensen, A. Ligabue, O. B. Lutnaes, J. I. Melo, K. V. Mikkelsen, R. H. Myhre, C. Neiss, C. B. Nielsen, P. Norman, J. Olsen, J. M. H. Olsen, A. Osted, M. J. Packer, F. Pawłowski, T. B. Pedersen, P. F. Provasi, S. Reine, Z. Rinkevicius, T. a. Ruden, K. Ruud, V. V. Rybkin, P. Salek, C. C. M. Samson, A. M. J. Sánchez de Merás, T. Saue, S. P. A. Sauer, B. Schimmelpfennig, K. Sneskov, A. H. Steindal, K. O. Sylvester-Hvid, P. R. Taylor, A. M. Teale, E. I. Tellgren, D. P. Tew, A. J. Thorvaldsen, L. Thøgersen, O. Vahtras, M. a. Watson, D. J. D. Wilson, M. Ziolkowski, and H. Ågren, *WIREs Comput. Mol. Sci.* **4**, 269 (2014).
- ⁶⁴T. Dunning Jr., *J. Chem. Phys.* **90**, 1007 (1989).
- ⁶⁵R. Kendall, T. Dunning Jr., and R. J. Harrison, *J. Chem. Phys.* **96**, 6769 (1992).
- ⁶⁶F. Weigend, A. Köhn, and C. Hättig, *J. Chem. Phys.* **116**, 3175 (2002).
- ⁶⁷E. F. Pettersen, T. D. Goddard, C. C. Huang, G. S. Couch, D. M. Greenblatt, E. C. Meng, and T. E. Ferrin, *J. Comput. Phys.* **25**, 1605 (2004).
- ⁶⁸Molecular graphics (Structures and NTO plots) were performed with the UCSF Chimera package. Chimera is developed by the Resource for Biocomputing, Visualization, and Informatics at the University of California, San Francisco (supported by NIGMS P41-GM103311).
- ⁶⁹M. R. Silva-Junior, S. P. A. Sauer, M. Schreiber, and W. Thiel, *Mol. Phys.* **108**, 453 (2010).
- ⁷⁰H. Koch, O. Christiansen, P. Jørgensen, and J. Olsen, *Chem. Phys. Lett.* **244**, 75 (1995).

PhD Thesis

COUPLED CLUSTER THEORY FOR LARGE MOLECULES

Pablo Baudin

This thesis describes the development of local approximations to coupled cluster (CC) theory for large molecules. Two different methods are presented, the divide-expand-consolidate scheme (DEC), for the calculation of ground state energies, and a local framework denoted LoFEx, for the calculation of electronic excitation energies and oscillator strengths. After an introduction to the relevant notions of electronic-structure theory, the principal aspects of DEC and LoFEx are summarized. For comparison, a selected review of the state-of-the-art is presented for each domain. This thesis should serve as an introduction to the work developed and presented in the scientific articles collected as appendices.

The DEC scheme has been applied successfully to the calculation of MP2, CCSD and CCSD(T) ground state energies. The intrinsic structure of DEC allows for a linear-scaling (with system size) and massively parallel implementation of CC theory. Applications to large molecules have been reported at the DEC-MP2 level but some limitations remain and prevent efficient and accurate large-scale applications of the DEC-CCSD and DEC-CCSD(T) models.

Regarding the calculation of electronic transition properties of large molecules, LoFEx has been introduced and applied to the CC2 and CCSD models. The black-box character of LoFEx has been demonstrated on medium-sized molecules and significant computational savings can be obtained depending on the character of the transition and on the size of the system. LoFEx has also been applied to large molecules with a computational cost competing with the most commonly used method (TDDFT), while maintaining CC accuracy. Finally, a new strategy has been proposed to overcome the main limitations of LoFEx and enable computational savings for all kinds of electronic transitions.

The development of CC theory for large molecules is still in its infancy, especially regarding the calculation of frequency-dependent molecular properties. Many challenges remain to be solved and some of the ideas presented in this thesis will hopefully open the door to more innovative and creative solutions.